

Blood Pressure and Brain Structure in Early Adulthood

Dissertation

zur Erlangung des akademischen Grades

Dr. rer. med.

an der Medizinischen Fakultät
der Universität Leipzig

eingereicht von Herma Lina Schaare, M. Sc.,
geboren am 16. Januar 1989
in Darlinghurst, Australien

angefertigt am Max-Planck-Institut für Kognitions- und Neurowissenschaften,
Leipzig
Abteilung Neurologie

betreut von Prof. Dr. med. Arno Villringer

Beschluss über die Verleihung des Doktorgrades vom: 08. September 2020

Table of Contents

List of Abbreviations.....	v
List of Tables.....	vii
List of Figures.....	viii
1 Introduction	1
1.1 Hypertension and the Brain	1
1.2 Hypertension	3
1.2.1 Epidemiology.....	3
1.2.1.1 Impact of hypertension and high blood pressure on global health	3
1.2.1.2 Impact of hypertension and high blood pressure in Germany.....	3
1.2.2 Classification of blood pressure.....	3
1.2.2.1 Definition of hypertension in Germany	4
1.2.2.2 Definition of hypertension in the United States	4
1.2.3 Etiology and pathogenesis.....	5
1.2.3.1 Etiology of secondary hypertension	5
1.2.3.2 Pathogenesis of essential hypertension.....	5
1.2.4 Regulation and pathophysiology	6
1.2.4.1 Medium-to long-term regulation	6
1.2.4.2 Short-term regulation	7
1.2.4.3 Neuroanatomy of central blood pressure control	8
1.3 Hypertension-Related Brain Injury.....	9
1.3.1 Symptomatic cardio- and cerebrovascular disease	9
1.3.2 Cognitive decline.....	9
1.3.2.1 Midlife blood pressure	10
1.3.2.2 Late-life blood pressure	10
1.3.2.3 Oldest old blood pressure.....	11
1.3.2.4 Early life blood pressure	11
1.3.3 Asymptomatic cardio- and cerebrovascular disease	12
1.3.3.1 Neuroimaging markers	13
1.3.3.1.1 Cerebral white matter	13
1.3.3.1.2 Cerebral gray matter	14
1.3.3.1.3 Cerebral blood flow.....	15
1.3.4 Impact of blood pressure lowering therapy on the brain	15
1.3.5 Interim summary	17
1.4 A Mind-Brain-Body Approach to Essential Hypertension.....	18

1.4.1	Blood pressure and stress	19
1.4.2	Blood pressure reactivity and psychological stressors	19
1.4.3	Brain correlates of blood pressure reactivity to psychological stressors	20
2	Aims of the Thesis and Rationale for Experimental Work	23
3	Experimental Work	26
3.1	Studies 1 & 2: The MPI-Leipzig Mind-Brain-Body database	26
	Study 1: A Mind-Brain-Body Dataset of MRI, EEG, Cognition, Emotion, and Peripheral Physiology in Young and Old Adults. Babayan...Schaare et al., Scientific Data (2019)	26
	Study 2: A Functional Connectome Phenotyping Dataset Including Cognitive State and Personality Measures. Mendes...Schaare et al., Scientific Data (2019)	26
3.1.1	Materials and methods	26
3.1.1.1	Participants	26
3.1.1.2	Study inclusion.....	26
3.1.1.3	Procedure	27
3.1.1.3.1	Psychological assessment	28
3.1.1.3.2	Physiological data.....	29
3.1.1.3.3	Data processing, sharing and security	30
3.1.1.3.4	Quality assessment	31
3.2	Study 3: Association of Peripheral Blood Pressure with Gray Matter Volume in 19- to 40-Year-Old Adults. Schaare et al., Neurology (2019)	32
3.2.1	Materials and methods.....	32
3.2.1.1	Participants	32
3.2.1.2	Blood pressure measurements	33
3.2.1.3	Neuroimaging.....	34
3.2.1.3.1	Additional preprocessing steps for MP2RAGE images	34
3.2.1.4	Data processing and statistical analysis	35
3.2.1.4.1	Blood pressure classification.....	35
3.2.1.4.2	Voxel-based morphometry: Association of regional GMV and blood pressure within each sample	35
3.2.1.4.3	Image-based meta-analysis: Association of regional GMV and blood pressure across samples	36
3.2.1.4.4	IBMA of regions of interest (ROI): Association of regional GMV and blood pressure across samples in hippocampus and amygdala	36
3.2.1.4.5	Volumetry: Association of total brain volumes and blood pressure within the pooled sample	37
3.2.1.5	Data sharing.....	37
3.2.2	Results	37

3.2.2.1	Sample characteristics	37
3.2.2.2	VBM: Association of regional GMV and blood pressure within each sample	39
3.2.2.3	IBMA: Association of regional GMV and blood pressure across samples	40
3.2.2.3.1	Meta-analytic parametric relations between GMV and blood pressure	40
3.2.2.3.2	Meta-analytic differences in regional GMV between blood pressure categories	43
3.2.2.3.3	Meta-analytic differences in regional hippocampal and amygdalar volumes between blood pressure categories	45
3.2.2.3.4	Meta-analytic positive relations between GMV and blood pressure	46
3.2.2.4	Volumetry in pooled sample: Association of total brain volumes and blood pressure	46
3.2.2.5	Supplementary analysis of first blood pressure reading	46
3.2.3	Discussion	47
3.3	Study 4: The Age-Dependent Relationship Between Resting Heart Rate Variability and Functional Brain Connectivity. Kumral, Schaare et al., NeuroImage (2019)	52
3.4	Study 5: Acute Psychosocial Stress Alters Thalamic Network Centrality. Reinelt, Uhlig...Schaare et al., NeuroImage (2019)	53
3.5	Study 6: Neural Control of Vascular Reactions: Impact of Emotion and Attention. Okon-Singer...Schaare et al., Journal of Neuroscience (2014)	54
4	General Discussion and Outlook	56
5	Summary / Zusammenfassung der Arbeit.....	61
6	References.....	68
7	Appendix	I
7.1	Supplementary Materials of Study 3.....	I
7.2	Published Articles of Studies 1-6	VIII
7.2.1	A Mind-Brain-Body Dataset of MRI, EEG, Cognition, Emotion, and Peripheral Physiology in Young and Old Adults. Babayan et al., Scientific Data (2019)	VIII
7.2.2	A Functional Connectome Phenotyping Dataset Including Cognitive State and Personality Measures. Mendes et al., Scientific Data (2019).....	IX
7.2.3	Association of Peripheral Blood Pressure with Gray Matter Volume in 19- to 40-Year-Old Adults. Schaare et al., Neurology (2019)	X
7.2.4	The Age-Dependent Relationship Between Resting Heart Rate Variability and Functional Brain Connectivity. Kumral et al., NeuroImage (2019)	XI
7.2.5	Acute Psychosocial Stress Alters Thalamic Network Centrality. Reinelt, Uhlig et al., NeuroImage (2019)	XII

7.2.6 Neural Control of Vascular Reactions: Impact of Emotion and Attention. Okon-Singer et al., Journal of Neuroscience (2014).....	XIII
Erklärung über die eigenständige Abfassung der Arbeit.....	XIV
Lebenslauf.....	XV
Publikationen.....	XVII
Danksagung.....	XIX

List of Abbreviations

ACE: Angiotensin-Converting Enzyme

AD: Alzheimer's Disease

ANOVA: Analysis of Variance

BMI: Body Mass Index

BP: Blood Pressure

CARDIA: Coronary Artery Risk Development in Young Adults

CAN: Central Autonomic Network

CBF: Cerebral Blood Flow

CSF: Cerebrospinal Fluid

CVD: Cardio- and Cerebrovascular Disease

DARTEL: Diffeomorphic Anatomical Registration Using Exponentiated Lie Algebra

DBP: Diastolic Blood Pressure

ECG: Electrocardiography

EEG: Electroencephalography

FA: Flip Angle

FLAIR: Fluid-Attenuated Inversion Recovery

fMRI: Functional Magnetic Resonance Imaging

FOV: Field of View

FWE: Family-Wise Error

GLM: General Linear Model

GMV: Gray Matter Volume

HRV: Heart Rate Variability

HTN: Hypertension

IBMA: Image-Based Meta-Analysis

ICA: Independent Component Analysis

LEMON: Leipzig Study for Mind-Body-Emotion Interactions

mmHg: Millimeter of Mercury

MPI CBS: Max Planck Institute for Human Cognitive and Brain Sciences

MPILMBB: MPI-Leipzig Mind-Brain-Body database

MP2RAGE: Magnetization-Prepared 2 Rapid Acquisition Gradient Echoes

MRI: Magnetic Resonance Imaging
N&C: Neuroanatomy and Connectivity protocol
PET: Positron Emission Tomography
RAAS: Renin-Angiotensin-Aldosterone System
ROI: Region of Interest
rs: Resting-State
SBP: Systolic Blood Pressure
SDM: Seed-Based *d* Mapping
SPRINT: Systolic Blood Pressure Intervention Trial
TE: Echo Time
TI: Inversion Time
TIV: Total Intracranial Volume
TR: Repetition Time
TSST: Trier Social Stress Test
VBM: Voxel-Based Morphometry
WMH: White Matter Hyperintensities

List of Tables

Table 1 - Definitions and classification of office blood pressure levels (mmHg) according to the European guidelines for the management of arterial hypertension (Mancia et al., 2013; Williams et al., 2018)	4
Table 2 - Neuroanatomy & Connectivity protocol. Overview of data acquisition	28
Table 3 – Characteristics by blood pressure category	38
Table 4 – Characteristics by sample	39
Table 5 – Image-based meta-analysis results of regional gray matter volume differences associated with blood pressure.	41
Supplementary Table 1 – List of exclusion criteria for each study from which the samples were drawn	I
Supplementary Table 2 – Positive image-based meta-analysis results of regional gray matter volume differences associated with blood pressure	II
Supplementary Table 3 – Image-based meta-analysis results of regional gray matter volume differences associated with first systolic blood pressure	IV

List of Figures

Figure 1 – LEMON study. Overview of data acquisition.....	27
Figure 2 – Flow chart with inclusion procedure for the study samples.....	33
Figure 3 – Associations between gray matter volume and blood pressure within each sample ..	40
Figure 4 – Meta-analytic differences in gray matter volume between blood pressure categories	44
Figure 5 – Meta-analytic differences in volumes of hippocampus and amygdala (Region-of-Interest analysis)	45
Figure 6 – Overview of main results	64
Supplementary Figure 1 – Meta-analytic positive differences in gray matter volume between blood pressure categories	VI
Supplementary Figure 2 – Associations between gray matter volume and first systolic blood pressure reading.....	VII

1 Introduction

1.1 Hypertension and the Brain

High blood pressure, or hypertension, is the single most important risk factor for stroke, dementia and other cardio- and cerebrovascular diseases worldwide (Forouzanfar et al., 2016; Lim et al., 2012). In globally aging populations, the detrimental effects of high blood pressure and related illness impose a huge financial and socio-political burden on societies that will become continuously difficult to bear in the future. While the damaging effects of high blood pressure on the human organism are well known (Forouzanfar et al., 2017), the primary causes of chronic blood pressure elevations and the levels at which adverse blood pressure effects manifest, are still unclear. For the rising number of people with hypertension, effective treatment options are available to lower blood pressure levels and slow down disease progression. However, the global burden of high blood pressure can only be substantially reduced by suspending primary blood pressure elevations and preventing the development of chronically high blood pressure in the first place (Olsen et al., 2016). In this respect, the relationship between high blood pressure and the brain is of particular interest, as will be outlined in the course of this thesis.

The brain is an established target for the adverse effects of hypertension, which reflects in the high prevalence of brain damage and dementia in hypertensive patients (Iadecola et al., 2016; Rapsomaniki et al., 2014). In middle and older ages, hypertension has been shown to impair cerebral blood flow, perfusion and autoregulation (Beason-Held, Moghekar, Zonderman, Kraut, & Resnick, 2007; Hajjar, Zhao, Alsop, & Novak, 2010; Iadecola et al., 2016; Jennings et al., 2005; Muller, Van Der Graaf, Visseren, Mali, & Geerlings, 2012) and to result in irreversible white matter lesions and gray matter atrophy, which can be assessed with magnetic resonance imaging (Iadecola et al., 2016; Jagust et al., 2008; Tzourio, Laurent, & Debette, 2014). Some studies imply a continuous effect of blood pressure on adverse brain outcomes – irrespective of any cut-off threshold – however, evidence for this hypothesis is still sparse (Forouzanfar et al., 2017; Rapsomaniki et al., 2014).

Other knowledge gaps yet to be closed revolve around the mechanisms which initiate primary elevations of blood pressure and precede the manifestation of hypertension. In this respect, the central nervous system has a pivotal role as the primary initiator of blood pressure regulation on the one hand and the link between bodily signals and mental processes on the other hand (Benarroch, 1993; Critchley & Harrison, 2013). This is due to the fact that additionally to homeostatic blood pressure control, several subcortical and cortical centers determine when and how an organism reacts to internal and external

demands (Critchley & Harrison, 2013). Interactions between psychological, neural, and somatic processes can be observed in particularly challenging situations, such as psychosocial stress in humans, which demand for example enhanced peripheral blood pressure reactivity (Lang, Davis, & Öhman, 2000). Or in cardiovascular responses to experimental stressors which are also risk factors for subsequent cardiovascular disease (Esler, 2017; Matthews et al., 2004). Importantly, some brain regions that are involved in the regulation of stress and emotions are also involved in blood pressure control (i.e. neuro-vegetative) (Critchley & Harrison, 2013; Gianaros & Sheu, 2009). Under physiological conditions, blood pressure fluctuations prompt cerebrovascular mechanisms that instantly adapt to maintain constant cerebral blood flow (e.g. rising systemic blood pressure leading to arteriolar constriction, also known as cerebral autoregulation). When sustained in the long-term, these initially adaptive mechanisms, however, will lead to progressive morphological changes in the arteries, such as arteriolar hyalinosis, increased intima-media-thickness and atherosclerosis, that will eventually cause neural tissue damage, visible as cortical atrophy and white matter lesions (Gorelick et al., 2011; Iadecola, 2013; Iadecola et al., 2016; Tzourio et al., 2014). It has been suggested that damage to regions of neuro-vegetative integration may impair their function, which would facilitate mind-brain-body dysregulation and thus cause vascular pathophysiology over time (Jennings & Zanstra, 2009).

In this thesis, I examined the interrelation of blood pressure and the brain within a neuro-vegetative approach. I will present empirical studies which ground on a big database that provides detailed assessments of brain-body dynamics in relation to individual psychological profiles during aging. In a joint data collection effort, my colleagues and I acquired this database to establish a framework in which research hypotheses on mind-brain-body interactions can be tested (studies 1 and 2). Using these data in combination with other large datasets, I conducted the core study of my experimental work: an image-based meta-analysis study on the relationship between sub-hypertensive blood pressure and brain structure in young adults – a critical population which has been neglected in previous research on vascular brain burden (study 3). In addition, we investigated (i) how parasympathetic regulation of the heart relates to brain structure and function during aging (study 4), and (ii) how acute psychosocial stress affects brain connectivity (study 5). To delineate the neural signatures of vascular regulation to emotional distress, we also conducted a mechanistic study with simultaneous acquisition of brain activity and blood pressure, with the aim to contribute to the understanding of blood pressure control and its putative trajectory via dysregulation to essential hypertension (study 6).

1.2 Hypertension

1.2.1 Epidemiology

1.2.1.1 Impact of hypertension and high blood pressure on global health

Arterial hypertension is highly prevalent and the leading single risk factor for death and disability worldwide (Forouzanfar et al., 2016; Lim et al., 2012). In 2015, the global prevalence of hypertension was around 22%, affecting 1.13 billion adults (NCD Risk Factor Collaboration (NCD-RisC), 2016). This number is expected to increase with growth and aging of the world population (Forouzanfar et al., 2016; Olsen et al., 2016). In 2015, high systolic blood pressure accounted for 10.7 million deaths worldwide, in addition to 211.8 million disability-adjusted life-years (Forouzanfar et al., 2016). Between 1990-2015, the leading risks for global disability-adjusted life-years shifted from 1) childhood undernutrition, 2) unsafe water, 3) high blood pressure, to 1) high blood pressure, 2) smoking, 3) high fasting plasma glucose, emphasizing the increasing importance of vascular, metabolic and behavioral risk factors for global health (Forouzanfar et al., 2016).

1.2.1.2 Impact of hypertension and high blood pressure in Germany

Similar to the global trends, hypertension strongly impacts public health also in Germany, where every third adult can be considered hypertensive (Neuhauser, Adler, Rosario, Diederichs, & Ellert, 2015). In people aged 65 years and older, prevalence of hypertension is as high as 70% (Neuhauser et al., 2015). Diseases of the circulatory system are among the largest contributors to German health costs, adding up to 46436 million € or 13.7% of total health costs in 2015 (Statistisches Bundesamt (Destatis), 2018). This includes 10102 million € of direct costs spent on management of hypertension alone (Statistisches Bundesamt (Destatis), 2018). In addition, substantial indirect costs accumulate from secondary diseases that can be attributed to hypertension, including ischemic heart disease (6788 million €) and cerebrovascular disease (9917 million €) (Statistisches Bundesamt (Destatis), 2018). Adequate management of hypertension is thus a national and global challenge in face of demographic changes that will have dramatic societal and financial consequences, if not successfully managed.

1.2.2 Classification of blood pressure

The classification of blood pressure into categories is an important tool for diagnosis and treatment of hypertension. However, there are no standardized guidelines for the classification and management of high blood pressure around the world. Even within Western societies, there is no accepted consensus that is valid for all countries. Management practices are under continuous discussion and research is being carried out

to provide new evidence for their updates. In the following, I will summarize the current guidelines for Germany, Europe and the United States of America.

1.2.2.1 Definition of hypertension in Germany

In Germany, evaluation of blood pressure levels follows the European guidelines for the management of arterial hypertension (Mancia et al., 2013; Williams et al., 2018). The current diagnostic thresholds for blood pressure classification are listed in Table 1 and define hypertension as “blood pressure higher than 140/90 mmHg”. There was an update on the guidelines in 2018, but the diagnostic categories remained unchanged (see section Definition of hypertension in the United States).

Table 1 - Definitions and classification of office blood pressure levels (mmHg) according to the European guidelines for the management of arterial hypertension (Mancia et al., 2013; Williams et al., 2018)

Category	Systolic (mmHg)		Diastolic (mmHg)
Optimal	<120	and	<80
Normal	120-129	and/or	80-84
High normal	130-139	and/or	85-89
Grade I hypertension	140-159	and/or	90-99
Grade II hypertension	160-179	and/or	100-109
Grade III hypertension	≥180	and/or	≥110
Isolated systolic hypertension	≥140	and	<90

1.2.2.2 Definition of hypertension in the United States

In 2017, the American College of Cardiology and the American Heart Association updated their guidelines and changed the blood pressure categories vigorously (Whelton et al., 2017). The previous category of pre-hypertension was renamed to stage I hypertension (systolic blood pressure [SBP] 130-139 mmHg or diastolic blood pressure [DBP] 80-89 mmHg). In response to the updated classification system, the prevalence of US adults with hypertension increased from 32% to 46%, which led to continued discussions about their implications for hypertension management and healthcare systems until today. The rigorous update was motivated by the illuminating results of the randomized clinical Systolic Blood Pressure Intervention Trial (SPRINT) (SPRINT Research Group, 2015). The study compared intensive blood pressure treatment to an SBP goal below 120 mmHg with conventional therapy that targeted blood pressure levels below 140 mmHg in over 9000 participants aged 50 years and older. The results showed that mortality of

cardiovascular events decreased by 27% in the intensive treatment group, which led to premature termination of the trial, allowing all participants access to the favorable intensive therapy (SPRINT Research Group, 2015). Follow-up analyses investigated the risk of dementia in SPRINT participants 5 years after termination of the trial. While the results are not as clear as for cardiovascular events, there was a small effect for a lower risk of incident dementia or mild cognitive impairment in the intensive treatment group (Williamson et al., 2019).

One year after the publication of this new classification system, the European Society of Cardiology and the European Society of Hypertension updated the European guidelines for the management of hypertension, but refrained from aligning the definition of blood pressure categories to the new US guidelines (Williams et al., 2018). Nevertheless, they also advocate for lowering to blood pressure values <130/80 mmHg in most patients to reduce cardio- and cerebrovascular disease (CVD) and mortality risks, which is consistent with the therapeutic targets in the 2017 US guidelines (Volpe, Gallo, Battistoni, & Tocci, 2019).

1.2.3 Etiology and pathogenesis

High blood pressure is defined as either primary or secondary hypertension based on the underlying etiological factors (Williams et al., 2018).

1.2.3.1 *Etiology of secondary hypertension*

Causes involved in secondary hypertension are identifiable and most commonly due to renal and endocrine diseases. Hypertension is also highly prevalent in patients with (other) cardiovascular risk factors, such as diabetes mellitus, chronic kidney disease, and obesity. Other conditions such as pregnancy, as well as obstructive sleep apnea can also initiate the chronic elevation of peripheral blood pressure.

1.2.3.2 *Pathogenesis of essential hypertension*

The etiological factors of initial blood pressure elevations in primary or essential hypertension are unclear; however, decades of research suggest that the presence of a unique undiscovered underlying cause is unlikely. Instead, the pathogenesis of essential hypertension may involve multifactorial risk factors that are either fixed or modifiable (Carretero & Oparil, 2000; Williams et al., 2018). Most hypertensive patients also have other cardiovascular risk factors which include genetic factors (e.g. family history of essential hypertension), unhealthy lifestyle and sympathetic hyperactivity (Carretero & Oparil, 2000). Modifiable risk factors that are common among adults with hypertension include smoking, dyslipidemia, glucose intolerance, overweight or obesity, low physical activity, and unhealthy diet, which is characterized by high intake of salt and alcohol and

low intake of potassium (Carretero & Oparil, 2000; Forouzanfar et al., 2016; Whelton et al., 2017; Williams et al., 2018). Epidemiological studies investigated the influences of psychosocial factors in the pathogenesis of essential hypertension and associated loneliness, occupational stress (incl. unemployment), and poor sleep quality with increased incidence of hypertension (Cuffee, Ogedegbe, Williams, Ogedegbe, & Schoenthaler, 2014; Steptoe & Kivimäki, 2013). Chronic stress has long been suggested to play a causal role in essential hypertension and CVD, but strong evidence from population-based studies remains to be established (Steptoe & Kivimäki, 2013). Mechanistic studies, however, provide evidence that chronic stress is indeed implicated in essential hypertension via sympathetic pathways (Esler et al., 2008). The role of stress in the development of high blood pressure will be reviewed in detail below (section Blood pressure and stress).

In sum, the pathogenic relationship between hypertension and other CVD risk factors presumably involves complex interactions of genetic, biological, behavioral, social and environmental markers which can be conceptualized in a mind-brain-body framework, as will be outlined in the following sections.

1.2.4 Regulation and pathophysiology

Blood pressure is determined by the product of cardiac output and total peripheral resistance. Hence, blood pressure elevations either result from increased pump activity of the heart, from increased resistance in blood vessels or from their combination (Klinke & Silbernagl, 1996; Vaitl, 2001). Cardiac output and total peripheral resistance thus reflect the primary physiological mechanisms underlying any hypertension. Nonetheless, blood pressure regulation is complex and involves processes that operate on different time scales to keep blood pressure constant. As described below, in the short-term, these processes mainly influence heart activity and vessel diameter (Klinke & Silbernagl, 1996; Vaitl, 2001). In the longer-term, the regulation operates on the blood volume (Klinke & Silbernagl, 1996; Vaitl, 2001). Imbalances in both short and long regulation processes may have implications for the development of hypertension and cardiovascular disease (Rau & Elbert, 2001; Vaitl, 2001).

1.2.4.1 *Medium-to long-term regulation*

Over longer time scales, homeostatic blood pressure regulation mainly influences the fluid balance in the circulatory system. When blood pressure levels and consequently renal blood flow decrease, the renin-angiotensin-aldosterone system (RAAS) begins to counteract: The kidneys secrete the enzyme renin which converts the peptide hormone angiotensinogen to angiotensin I. The angiotensin-converting enzyme (ACE)

subsequently converts angiotensin I to elevate plasma concentrations of the potent vasoconstrictor angiotensin II. Angiotensin II directly causes blood vessels to narrow, thereby increasing blood pressure. Sympathetic activity enhances the release of renin, which additionally contributes to this mechanism. Angiotensin II also stimulates the release of the steroid hormone aldosterone from the adrenal cortex. Both angiotensin II and aldosterone influence the reabsorption of sodium and excretion of potassium in the kidneys, which indirectly influences water retention and decreases water excretion, resulting in increased blood volume and thus blood pressure. Dysregulation of the RAAS may secondarily contribute to the development and progression of cardiovascular disease, such as hypertension. The RAAS is of particular clinical relevance due to its target function of many antihypertensive drugs that pharmacologically influence its components, such as ACE-inhibitors, angiotensin-receptor-blockers or aldosterone antagonists.

1.2.4.2 Short-term regulation

In the short-term range, a feedback loop, the baroreflex, serves to maintain homeostasis and keep blood pressure constant. It has parasympathetic and sympathetic components that operate with every cardiac cycle, which describes the evolution of a heartbeat from its generation to the next beat. The cardiac cycle consists primarily of two distinct, mechanically defined phases: During systole, the myocardium contracts to eventually eject blood from the ventricles into the circulatory system. During diastole, in turn, the myocardium relaxes, and the ventricles fill with blood again. The frequency of the cardiac cycle, the heart rate, differs inter-individually and it adapts – both rapidly and in a long-term manner – to internal and external demands. With every systole and consecutive arterial pressure changes, specific stretch- and pressure-sensitive receptors within the walls of major arteries, so-called arterial baroreceptors, signal the pressure's amplitude and temporal dynamics to nuclei of the lower brainstem and primary cortical regions for neuro-vegetative integration (see section Neuroanatomy of central blood pressure control). If baroreceptor signaling indicates pressure increases, the baroreflex operates twofold: On the one hand, it reduces cardiac output by decelerating the heart rate and on the other hand, it leads to dilation of blood vessels which reduces arterial resistance. Both mechanisms result in a rapid decrease of blood pressure to counteract sudden elevations. Baroreceptors can lose their sensitivity, due to for example atherosclerotic processes, which impairs the blood pressure regulating function of the baroreflex. It has been suggested that baroreceptor insensitivity could be a pathogenically important mechanism leading to long-lasting blood pressure elevations in hypertension (Dworkin et al., 1994; Rau & Elbert, 2001).

1.2.4.3 Neuroanatomy of central blood pressure control

As described above, major aspects of blood pressure regulation are provided by renal function. Nevertheless, parasympathetic and sympathetic activity that is elemental for homeostatic and allostatic blood pressure regulation is directed by central nervous system control networks (Critchley & Harrison, 2013). They are formed by several brain regions located in the brainstem, in the subcortex and in the neocortex, as specified in the following section.

With every heartbeat, arterial baroreceptors signal the arterial pressure's amplitude and temporal dynamics to nuclei of the lower brainstem. Most notably, the vagus nerve and the glossopharyngeal nerve convey baroreceptor signals to the nucleus tractus solitarius in the medulla oblongata. These afferents are part of a feedback loop (baroreflex), which has parasympathetic and sympathetic components. Visceral information further ascends via other brainstem nuclei and the mesencephalic periaqueductal grey to amygdala and thalamus, where signals are relayed to anterior cingulate cortex and insula as the primary cortical regions for neuro-vegetative integration. In turn, these higher-level brain structures modulate homeostasis and adapt autonomic activity to environmental demands via efferent pathways to brainstem nuclei. Neuroimaging studies have identified these regions in a network that is not only implicated in the regulation of blood pressure or other autonomic functions, but also in the regulation of affect, cognition and stress (Babo-Rebelo, Wolpert, Adam, Hasboun, & Tallon-Baudry, 2016; Gould van Praag et al., 2017; Sakaki et al., 2016). This Central Autonomic Network (CAN) supports visceromotor and neuroendocrine responses that are critical for goal-directed behavior, adaptability, and health (Benarroch, 1993; Hagemann, Waldstein, & Thayer, 2003). In response to psychological upheaval, the CAN, which receives multiple inputs, initiates behavioral, endocrine and autonomic reactions, such as activation of the hypothalamic-pituitary-adrenal axis. Lesions or seizures in the CAN result in diffuse autonomic manifestations, including myocardial infarction and cardiac arrhythmias even in the absence of CVD (Benarroch, 1993). It has further been suggested that complex neurochemical aspects of the CAN have diagnostic and therapeutic implications for various medical conditions, including panic disorders, obesity and hypertension (Benarroch, 1993). More details on implications of the CAN in essential hypertension will follow below (section 1.4.3 Brain correlates of blood pressure reactivity to psychological stressors).

1.3 Hypertension-Related Brain Injury

1.3.1 Symptomatic cardio- and cerebrovascular disease

Manifestation of hypertension dramatically increases the risk of premature death and concomitant symptomatic disease, such as stroke, vascular dementia and other CVD (Iadecola et al., 2016). In 2015, elevated SBP of at least 110 mmHg was the leading global contributor to mortality and disability burden (Forouzanfar et al., 2017). In middle-aged and older participants, each increment of 20 mmHg for SBP or 10 DBP mmHg has been estimated to double the rate of dying from stroke or ischemic heart disease, starting as low as 115/75 mmHg (Prospective Studies Collaboration, 2002). The largest number of worldwide SBP-associated deaths per year were caused by ischemic heart disease (4.9 million), hemorrhagic stroke (2.0 million) and ischemic stroke (1.5 million) (Forouzanfar et al., 2017). Elevated blood pressure is related to the incidence of several clinical manifestations in major organs, including heart disease (e.g. heart failure, myocardial infarction, angina, atrial fibrillation, sudden death), peripheral artery disease (e.g. atherosclerosis), chronic renal disease, stroke (e.g. ischemic stroke, transient ischemic attack, macro- and microscopic cerebral infarcts, hemorrhagic stroke, subarachnoid and intracerebral hemorrhage), as well as dementia (e.g. vascular dementia, mixed pathology dementia, mild cognitive impairment) (Forouzanfar et al., 2017; Iadecola et al., 2016; Prospective Studies Collaboration, 2002; Rapsomaniki et al., 2014; Veglio et al., 2009). Yet, global age-adjusted rates of stroke, coronary heart disease, and mortality have declined in the last decades (but note the strong divergence between higher and lower income countries, Forouzanfar et al., 2017; Krishnamurthi et al., 2013; Roth et al., 2017). Major contributors to these trends are improved blood pressure control and primary prevention through risk factor reduction. However, these trends seem to level off in younger generations, suggesting that control of blood pressure is still inadequate, that age-specific effects in primary prevention require more scrutiny and that the increase of other lifestyle-related risk factors, such as metabolic risk factors, could negate the benefits of hypertension management (Carretero & Oparil, 2000; Koton et al., 2019; Prospective Studies Collaboration, 2002).

1.3.2 Cognitive decline

Most of the above-mentioned hypertension-associated diseases do not occur in isolation and often share the same risk factors with their underlying pathophysiology. For example, larger lesion volumes and a greater number of macroscopic cerebral infarcts are associated with an increased likelihood of dementia (Gorelick et al., 2011). These interactions are important to consider in the evaluation of CVD risk factors. Aging is another major factor in the development of vascular diseases that is difficult to disentangle

from vascular pathogenesis in advanced stages. Consequently, the impact of hypertension on the brain strongly depends on when blood pressure is measured in life. This has been best observed in the association between hypertension and cognitive function: High blood pressure in middle age is a risk factor for dementia later in life, but this association cannot be found robustly when the blood pressure measurement is taken at older ages (see below). Below, I will outline the evidence of vascular influence on dementia and cognitive (dys-) function across the lifespan.

Blood pressure effects on cognition across the lifespan have mainly been investigated in cross-sectional and longitudinal study designs within and across three age groups (Gąsecki, Kwarciany, Nyka, & Narkiewicz, 2013; Iadecola et al., 2016): middle-age (40-64 years), old age (65-84 years) and oldest old (≥ 85 years). Few studies also investigated the relationship between blood pressure and cognitive function in young adults (<40 years).

1.3.2.1 Midlife blood pressure

Most consistent relationships have been found between cognitive decline and high blood pressure or hypertension in middle-age. Midlife hypertension, in particular, is a predictor for cognitive decline in late-life and has been associated with risk of dementia, including late-onset Alzheimer's disease (AD, Iadecola et al., 2016; Norton, Matthews, Barnes, Yaffe, & Brayne, 2014; Power et al., 2016). Even in the absence of fully developed dementia, many middle-aged hypertensive individuals develop cognitive problems later in life, including deficits in attention, memory and abstract reasoning (for review see Waldstein, Manuck, Ryan, & Muldoon, 1991). Clinical longitudinal studies investigated the effects of high blood pressure or hypertension on cognitive function with consistent findings that higher blood pressure relates to lower cognitive scores, on global measures of cognition (M. F. Elias, Wolf, D'Agostino, Cobb, & White, 1993; P. K. Elias, Elias, Robbins, & Budge, 2004; Launer, 1995), as well as specific cognitive domains, such as (verbal) memory (Chen, Henderson, Stolwyk, Dennerstein, & Szoeki, 2015; M. F. Elias et al., 1993; P. K. Elias et al., 2004; Yaffe et al., 2014), processing speed (Chen et al., 2015; Yaffe et al., 2014), and executive functions and attention (M. F. Elias et al., 1993; P. K. Elias et al., 2004; Yaffe et al., 2014).

1.3.2.2 Late-life blood pressure

Most cross-sectional studies on the associations between hypertension and cognition have been conducted in old aged participants, where a high prevalence of hypertension can be expected. Those studies, however, have provided mixed results, showing that the relationship between hypertension or high blood pressure and cognition can have negative, positive, u-shaped or no associations (Iadecola et al., 2016). Longitudinal study

designs in this age group did not show a clearer picture, possibly due to the diffuse pathologies that present themselves in late life. Iadecola et al.'s (2016) review on this topic concludes that methodological aspects, such as differences in study design, cognitive domains assessed, adjustment for confounds (e.g. medication), and sex differences, could explain the inconsistency of results. Notably, risk factors for vascular cognitive impairment are the same as for stroke and likely also for AD (Gorelick et al., 2011). Neuropathology in later life is thus often a mixture of AD and microvascular brain damage resulting in heterogeneous and complex patterns of cognitive impairment that may warrant closer examination (Gorelick et al., 2011; Iadecola et al., 2016).

1.3.2.3 *Oldest old blood pressure*

Interestingly, cross-sectional and longitudinal studies in the oldest old have found that higher blood pressure relates to *better* cognitive abilities in this age group (Harrison et al., 2015; Qiu, Winblad, & Fratiglioni, 2009). Not many large-scale longitudinal studies investigated the oldest old, however, those that exist showed that SBP/DBP \geq 130/85 predicts better global cognitive abilities in follow-up times between 3-5 years (Harrison et al., 2015). This paradoxical effect might be explained by survival bias, according to which people who were exposed to higher blood pressure earlier in their lives would not be included in those studies of oldest old due to premature disease, disability or death. Another explanation for these effects could be that the onset of dementia and other debilitating diseases is often accompanied by decreases in blood pressure (Harrison et al., 2015; Qiu et al., 2009).

1.3.2.4 *Early life blood pressure*

The pioneering study for effects of vascular risk factors in younger ages, is the Coronary Artery Risk Development in Young Adults (CARDIA) study. Recent results of a sample with a mean age of 25 years at baseline showed that higher SBP over a 25-years-follow-up was associated with worse cognitive performance in the domains of verbal memory, processing speed and executive function (Yaffe et al., 2014). Other results from the same study, however, showed that higher SBP *reactivity* at baseline was associated with better cognitive performance in middle-age (Yano et al., 2016). The association between early life blood pressure and cognition in midlife thus warrants more research to draw substantial conclusions. Blood pressure reactivity, on the other hand, has been suggested as a risk factor in the development of hypertension which will be outlined below (section Blood pressure reactivity and psychological stressors).

In general terms, it can be concluded that the risk of blood pressure-related cognitive deficits increases with aging, but evidence for this mainly stems from studies following

middle-aged hypertensives to late life. Neuropsychological tests emphasized executive functions and memory as the cognitive domains which show greatest impairments related to hypertension. Interactions with exposure effects of vascular pathogenesis and pathophysiology must be considered. Finally, to assess the full scope of their impact, blood pressure should be assessed several decades before onset of cognitive decline or symptomatic brain injury.

1.3.3 Asymptomatic cardio- and cerebrovascular disease

Importantly, even in the absence of symptomatic disease, elevated blood pressure is associated with often undetected asymptomatic neural changes well before overt clinical symptoms occur. These signs of silent cerebrovascular disease are highly prevalent in older people. It has been estimated that for one symptomatic stroke, there are approximately 10 silent brain infarcts (Leary & Saver, 2003). In older populations without apparent stroke, 1 in 5 adults presents with silent brain infarctions (Gupta et al., 2016). Hypertension and other vascular risk factors impact the incidence and progression of asymptomatic CVD as well as symptomatic stroke and dementia severely (Gupta et al., 2016; Iadecola et al., 2016; Rapsomaniki et al., 2014). Deleterious effects of hypertension mainly target the cerebral (and peripheral) vasculature, where blood pressure elevations promote vascular stiffening, endothelial failure, and dysfunction of the blood-brain barrier, among other mechanisms that lead to insidious vascular brain damage (Iadecola et al., 2016; Laurent & Boutouyrie, 2015; Sierra, Coca, & Schiffrin, 2011). Elevated blood pressure causes stress on vessel walls which induces adaptive structural and functional changes to protect the vessels and contribute to changes in cerebral blood flow (CBF), including: (1) vascular hypertrophic remodeling of the smooth muscle cells reducing the vessel lumen, (2) the deposition of fibrous proteins in the vessel walls, (3) increases of vascular stiffness, and (4) microvascular rarefaction (i.e. loss of microvessels). In advanced stages, these processes deteriorate vascular muscle contractility, impair cerebrovascular function and disturb cerebral autoregulation. Ultimately, these processes lead to hypoperfusion, disruption of the blood-brain-barrier, ischemic and hemorrhagic stroke and white and gray matter injury. The majority of silent CVD represents manifestations of cerebral small vessel disease, arising from pathology in the perforating cerebral arterioles and capillaries in the cerebral white and deep gray matter (Pantoni, 2010). Small and large vessel disease result in progression of arteriosclerosis and atherosclerosis, which impair CBF and promote thrombogenesis. Other pathological alterations include endothelium-dependent mechanisms, which are critical in regulating microvascular flow, may play a role in the effects of hypertension on reducing CBF, promoting atherosclerosis and amyloid beta accumulation. Hypertension can also

attenuate the local increase in CBF induced by neural activity (i.e. neurovascular coupling). The resulting mismatch between energy demands and blood flow delivery likely contributes to the cognitive decline in hypertension (Iadecola, 2013). Chronic blood pressure elevations thus induce adaptive changes to reduce stress on cerebral vessels and protect them from damaging arterial pressure fluctuations. Over time, these structural changes in addition to impaired vascular regulatory processes, lead to reductions in CBF that can eventually expose sensitive subcortical white matter regions to insufficient perfusion. Critical factors that are involved in these alterations are angiotensin II-dependent vascular oxidative stress, endothelial cell and blood-brain-barrier alterations (especially in small vessel disease), as well as exacerbated amyloid beta accumulation (Iadecola, 2013). The latter suggests an interactive effect of hypertension and AD pathology, which is to some extent corroborated by neurohistological evidence relating raised midlife blood pressure with lower post-mortem brain weight, increased numbers of hippocampal neurofibrillary tangles, and higher numbers of hippocampal and cortical neuritic plaques (Petrovitch et al., 2000).

1.3.3.1 Neuroimaging markers

The development of magnetic resonance imaging (MRI) has had a significant impact on the study of covert brain injury in humans. Neuroimaging features of asymptomatic structural brain damage include acute lacunar or small subcortical infarcts or hemorrhages, lacunes, white matter hyperintensities, visible perivascular spaces (Virchow-Robin spaces), microbleeds, microinfarcts, and brain atrophy, that can be evaluated in-vivo with structural MRI (Muller et al., 2014; Smith et al., 2017; Wardlaw, Smith, & Dichgans, 2013). In addition, advanced neuroimaging methods can reveal other forms of asymptomatic CVD that are not visible to the naked eye. These include altered white matter integrity and disrupted axonal connections, increased brain water content, altered myelination, and focal thinning of the cortical gray matter (Wardlaw et al., 2013). While these features do not present with overt clinical symptoms, they have an important role in the progression of CVD and the pathogenesis of cognitive decline and functional loss in the elderly. With hypertension being the primary risk factor for vascular brain damage, a multitude of neuroimaging studies investigated the pathophysiological relationship between elevated blood pressure and subtle brain injury. Key evidence from this field of research will be outlined below.

1.3.3.1.1 Cerebral white matter

The most common manifestations of cerebral small vessel disease and brain aging in structural MRI are detectable in the white matter. On T2/FLAIR sequences, the affected regions present themselves with increased signal intensity and are hence commonly

known as white matter hyperintensities (WMH). WMH are highly prevalent in the general population, especially in advanced age. In individuals older than 80 years, the prevalence of some degree of WMH is more than 90% (DeBette & Markus, 2010), but already middle-aged people (55-64 years) have been shown to present WMH with a prevalence of up to 66% (Smith et al., 2017). There is a well-established relation between WMH and future risk of symptomatic CVD, as well as with hypertension. Greater WMH burden is associated with a 2- to 3-fold increased risk of stroke and dementia (DeBette & Markus, 2010). High blood pressure is the most important modifiable risk factor for development of WMH and relates both to increased incidence and progression of WMH (DeBette et al., 2011; Muller et al., 2014; Verhaaren et al., 2013). Clinical trials have shown that WMH progression can be reduced with antihypertensive treatment (see section Impact of blood pressure lowering therapy on the brain). Other neuroimaging markers measured by diffusion-weighted imaging, such as fractional anisotropy or mean diffusivity, have been applied to detect even more subtle alterations in white matter microstructure. Both measures have been associated with high blood pressure (Maillard et al., 2012; Salat et al., 2012) and arterial stiffness (Maillard et al., 2016). Maillard et al. (2012) showed that higher SBP was linearly associated with decreased fractional anisotropy and increased mean diffusivity in regions including the anterior corpus callosum, the inferior fronto-occipital fasciculi, and the connection fibers between the thalamus and the superior frontal gyrus in young and middle-aged individuals between 19 and 63 years (median age = 39 years). WMH are also associated with cognitive decline, sensorimotor dysfunction, depression and global functional decline. They can thus be considered a nonspecific marker of brain aging. Depending on the spatial location of WMH, however, specific behavioral outcomes can be predicted (Lampe et al., 2017).

1.3.3.1.2 Cerebral gray matter

Cerebral atrophy is associated with both aging and hypertension. Neuroimaging correlates of atrophy include reduced volumes of global and regional gray matter, as well as thickness of the cortex. Many early studies investigated how hypertension relates to total brain volumes, including total intracranial volume, as well as total volumes of white matter, gray matter and cerebrospinal fluid (Beauchet et al., 2013; Firbank et al., 2007; Gąsecki et al., 2013). Other studies aimed to identify spatial specificity of hypertension effects by applying region-of-interest analyses or voxel/vertex-based analyses. These studies observed regional cortical thinning and regional brain volume reductions primarily in the medial temporal and frontal lobes of middle-aged and older people with vascular risk factors (Beauchet et al., 2013; den Heijer et al., 2005; Gianaros, Greer, Ryan, & Jennings, 2006; Hajjar et al., 2010; Leritz et al., 2011; Power et al., 2016; Raz et al., 2005; Raz, Rodrigue,

Kennedy, & Acker, 2007). A recent meta-analysis found that hippocampal volumes, in particular, were consistently associated with hypertension (Beauchet et al., 2013; Bender, Daugherty, & Raz, 2013). Frontal and medial temporal regions have been proposed to be especially sensitive to effects of pulsation, hypoperfusion and ischemia, which often result from the consequences of increasing peripheral pressure (Beauchet et al., 2013; Iadecola et al., 2016).

1.3.3.1.3 Cerebral blood flow

In addition to above mentioned structural changes of vascular origin, some functional neuroimaging studies revealed alterations of CBF in hypertension. Compared to age-matched controls, hypertensives show a decrease in total resting CBF (Beason-Held et al., 2007; Muller et al., 2012). Regional investigations comparing hypertensives with controls, found decreases of resting CBF in subcortical, medial cortical, and limited frontal and temporal areas (Beason-Held et al., 2007). In a continuous arterial spin labeling study with a breathing challenge, Hajjar et al. (2010) found that higher mean systolic blood pressure and hypertension were associated with lower cerebral vasoreactivity in frontal, temporal and parietal lobes. In quantitative positron emission tomography (PET) during cognitive demand (working memory task compared to a sensorimotor control task), hypertensives showed a pattern of dampened amplitudes of CBF responses that also spread over greater areas as in normotensives (Jennings et al., 2005). Dampened resting CBF responses were found specifically in posterior parietal areas and thalamic areas. Interestingly, increases in hippocampal blood flow activation were observed in hypertensives who performed well in the task. A similar increase was found in frontal brain areas, suggesting that compensatory activation of additional brain areas may be supportive to maintain certain levels of memory performance in hypertension. Jennings (2003) suggested that peripheral blood pressure elevations cause autoregulatory adjustment of CBF, as well as structural cerebrovascular alterations, such as remodeling and rarefaction, which subsequently impair vasodilation to support active brain regions during cognitive demand. In early stages, this would induce compensatory blood flow adjustments to preserve functional performance levels. Some mixed results in line with this hypothesis, corroborate that blood pressure of pre-hypertensive middle-aged participants relates to cognitive performance and to CBF alterations similar to those observed in manifest hypertension (Jennings, Heim, et al., 2017; Jennings, Muldoon, et al., 2017; Launer et al., 2015).

1.3.4 Impact of blood pressure lowering therapy on the brain

Lowering blood pressure, by lifestyle or pharmacological interventions, has been significantly related to reduced occurrences of stroke, heart failure, coronary events, and

death making it a primary intervention target to decrease cardiovascular risk (Whelton et al., 2017; Williams et al., 2018). However, it remains to be clarified whether the damaging effects of hypertension on the brain are reversible or improvable with antihypertensive therapy. If essential hypertension is solely dependent on vascular pathophysiology, treatment that reduces blood pressure levels and ameliorates vascular function should also improve CBF and cognitive function, and halt brain structural changes.

Several clinical trials over the last 30 years have failed to provide direct conclusive evidence about antihypertensive therapy to protect cognition (Williams et al., 2018). Only three of these trials included neuroimaging sub-samples to investigate the effect of blood pressure on MRI markers associated with hypertension (mainly WMH) and found mixed results (Dufouil et al., 2005; Weber et al., 2012; Williamson et al., 2014). The PRoFESS trial found no differences between treatment group (Weber et al., 2012). PROGRESS found significant slowing of WMH volume progression between treatment groups (Dufouil et al., 2005). And the ACCORD sub-study MIND concluded that total brain volume declined more with intensive vs. standard treatment (Williamson et al., 2014). Recent results of SPRINT-MIND, the MRI sub-study of the SPRINT trial, showed that WMH volume increases over 4 years of follow-up were significantly smaller in the intensive treatment group (increase of 0.92 cm³ compared to 1.45 cm³, mean group difference of 0.54 cm³). However, total brain volume (sum of gray and white matter volumes) decreased more in the intensive treatment group (decrease of -30.6 cm³ compared to -26.9 cm³, mean group difference of -3.7 cm³) (Kjeldsen, Narkiewicz, Burnier, & Oparil, 2018). Williamson et al. (2019) just published results from 5 years follow-up of this trial that show a small effect for lower risk of incident dementia or mild cognitive impairment in the intensive treatment arm.

The primary aim of these clinical studies was to test for any beneficial effect of blood pressure lowering therapy on cognition and the brain. Some epidemiological studies, however, investigated whether any potentially pathological brain correlates differentiate treated from untreated or poorly controlled hypertensives. For example, participants from the Rotterdam Study with uncontrolled untreated hypertension had significantly more WMH progression within 3.5 years than participants with treated hypertension, whose blood pressure levels remained in the hypertensive range (difference [95% confidence interval], 0.12 [0.00; 0.23] mL/y) (Verhaaren et al., 2013). In a small intervention study of previously unmedicated hypertensive patients with a follow-up after one year, Jennings et al. (2012) found significant reductions in regional gray matter volume in mid-temporal areas, entorhinal cortex and thalamus over the follow-up period despite successful lowering of blood pressure of approximately 22 mmHg systolic and 18 mmHg diastolic.

Some studies also investigated the effects of antihypertensive treatment on cerebral perfusion. In the SMART-MR study, untreated hypertension, poorly controlled hypertension, and high blood pressure levels were associated with a decline in parenchymal CBF (i.e. total CBF per 100 ml brain parenchymal volume) relative to normotensive controls (Muller et al., 2012). The largest declines were found for poorly controlled and untreated hypertension. Analyses by class of antihypertensive medication showed that all hypertensive patients declined in parenchymal CBF, independent of the drug category they were using or if they took any antihypertensives at all. An exception was that the change in parenchymal CBF did not significantly differ from zero in hypertensives using angiotensin receptor blockers. Whether this is due to a specific pharmacological effect of angiotensin (Nagata, Kawabe, & Ikeda, 2010; Zhang, Witkowski, Fu, Claassen, & Levine, 2007) or potentially due to low power (N=42) needs to be tested in future studies. A sub-study of the Baltimore Longitudinal Study of Aging with PET data from 14 treated hypertensives and 14 healthy controls, found that hypertensives, relative to controls, showed greater linear decline of regional CBF over seven years in areas of the prefrontal, anterior cingulate, occipitotemporal, and posterior occipital cortex (Beason-Held et al., 2007). Over time, healthy controls also showed linear CBF increases in motor, superior temporal and hippocampal regions which were not observed to the same extent in hypertensives. The authors interpret this finding as a lack in the hypertensive group to preserve brain function.

Taken together, results from clinical trials to test for beneficial effects of antihypertensive treatment on the brain and cognition are conflicting. Successful lowering of blood pressure decelerates but does not entirely halt or reverse the progression of WMH or silent brain injury, such as dysfunctional cerebral perfusion. Notably, there is no evidence, yet, that hypertension treatment attenuates the progression of gray matter changes (Jennings et al., 2012; Kjeldsen et al., 2018). If successful antihypertensive therapy does not reduce the progression of brain injury, this may be due to already present irreversible vascular damage (i.e., atherosclerosis) or other factors that are not entirely dependent on blood pressure levels. Both possibilities may be involved in the initiation of the adverse effects of essential hypertension.

1.3.5 Interim summary

In sum, mid- and late-life hypertension is related to sub-clinical functional (Beason-Held et al., 2007; Hajjar et al., 2010; Jennings et al., 2005; Muller et al., 2012) and structural cerebrovascular changes (Debette et al., 2011; den Heijer et al., 2005; Hajjar et al., 2010; Launer et al., 2015; Leritz et al., 2011; Maillard et al., 2012; Muller et al., 2014; Power et al., 2016; Raz et al., 2005). Specifically, these include signs of brain damage such as

global brain atrophy (Firbank et al., 2007; Power et al., 2016), white matter injury (Maillard et al., 2012; Muller et al., 2014; Verhaaren et al., 2013) and gray matter reductions (Gianaros et al., 2006; Leritz et al., 2011; Maillard et al., 2012). Especially hippocampal and frontal regions seem to be sensitive areas where gray matter reductions have been repeatedly shown (Beauchet et al., 2013; Bender et al., 2013; Power et al., 2016; Raz et al., 2007). It is important to note that structural and functional neuroimaging correlates of hypertension have been investigated primarily in middle-aged and older individuals with manifest hypertension and often under the influence of blood pressure lowering medication. With respect to the evidence pointing towards the presence of pathophysiological mechanisms even in the early stages of blood pressure elevations, interactions with age, high blood pressure exposure and treatment effects should be expected but are rarely accounted for. It is thus unclear how elevated blood pressure and other vascular risk factors in younger ages relate to brain health in later life. Furthermore, it has been assumed that vascular brain injury typically arises over years of manifest vascular disease, such as hypertension and atherosclerosis. This assumption has been challenged by increasing evidence showing that *asymptomatic* CVD is highly prevalent in the general aging population and increases the risk for stroke, dementia and cognitive decline far below recent thresholds which have been defined as “clinically relevant” for vascular disease. More research is needed to comprehend how trajectories of blood pressure and brain injury are intertwined with respect to their multi-etiological contexts.

1.4 A Mind-Brain-Body Approach to Essential Hypertension

We have seen that while consequences of hypertension on the brain and other organs are well documented, the primary causes of initial blood pressure elevations in essential hypertension remain elusive. Above, I also reviewed that current research suggests that pathogenesis of essential hypertension is multi-etiological and consists of biological, social and psychological interactions. Investigations of such mind-brain-body interactions are for example common in psychophysiological experiments or in research of psychological consequences of somatic illness, such as depressive symptoms after stroke or a cancer diagnosis (Linden, Vodermaier, MacKenzie, & Greig, 2012; Robinson & Jorge, 2016). How mental factors contribute to bodily diseases, however, has received comparably less scientific recognition. Stress and emotional processing are prominent mechanisms in which bodily signals shape behavior and thoughts and may have negative consequences on both mental and somatic health. In this vein, this section will be about evidence that shows how the brain is not only a target for adverse effects of hypertension, but also putatively a key figure in a mind-brain-body framework of the development of essential hypertension.

1.4.1 Blood pressure and stress

The idea that stress leads to hypertension and heart disease is often encountered in common knowledge realms, but the scientific foundation in support of this claim has been inconclusive over many years of research. Stress is a difficult concept to define and to operationalize. In the interest of the research area at hand, many different definitions of stress have been proposed. Despite these challenges, a line of research has been conducted to date which suggests that cardiovascular disease and hypertension are, in fact, caused by chronic mental distress (Esler, 2017; Esler et al., 2008). Over several years, Esler and colleagues, among others, investigated (often invasively) the link between the sympathetic nervous system, mental stress (and affective disorders), and cardiovascular disease (Esler, 2017; Esler et al., 2008). The primary outcomes in these studies have been heart disease of sudden onset which typically follow acute emotional upheaval, such as cardiac arrhythmias, myocardial infarction or Takotsubo myopathy (also known as “broken heart syndrome”). These studies also suggest adverse cardiovascular consequences in the presence of chronic psychological stress, such as affective disorders (i.e. depressive and anxiety disorders) which often co-occur with cardiovascular disease (Cohen, Edmondson, & Kronish, 2015; Hamer, Batty, Stamatakis, & Kivimaki, 2010). Neural mechanisms, particularly sympathetic activity, are critical in the linkage between stress responses of psychological symptoms and cardiovascular disease. Increased noradrenaline synthesis rate of brainstem neurons projecting to the hypothalamus and amygdala, the co-release of adrenaline in sympathetic nerves (which is not observed in healthy individuals) and persistent sympathetic nerve firing patterns in skeletal muscle vasculature are, among others, putative biomarkers of stress exposure, which are all present in patients with essential hypertension (Esler et al., 2008; Macefield, James, & Henderson, 2013). Acute and chronic psychological distress therefore induces signatures of enhanced sympathetic nervous outflow which are crucial in the development of coronary heart disease, atherosclerosis and essential hypertension.

1.4.2 Blood pressure reactivity and psychological stressors

Another predictor for subsequent cardiovascular disease has been found in cardiovascular reactivity to experimentally induced stressors. Psychophysiological studies most often assessed cardiovascular reactivity as a change in heart rate or blood pressure from a given baseline. To evoke cardiovascular responses in the laboratory, stressors are commonly operationalized by physiological (e.g. cold-pressor test, isometric exercise) or psychological (e.g. mental arithmetic, delivering free speeches on personal topics, effortful cognitive demand such as Stroop task) challenges (Krantz & Manuck, 1984; Rose et al., 2004). Several studies found that stressor-evoked cardiovascular reactivity predicts

premature development of hypertension and other precursors of CVD, as well as accelerated progression of atherosclerosis (Chida & Steptoe, 2010; Krantz & Manuck, 1984; Treiber et al., 2003). Especially stressor-evoked blood pressure reactivity has been associated with prospective CVD and cardiovascular events in clinical and epidemiological studies (Chida & Steptoe, 2010; Treiber et al., 2003). For example, in more than 4100 young, normotensive adults from the longitudinal CARDIA study, enhanced blood pressure reactivity during the cold-pressor test and during cognitive tasks involving executive functions, predicted earlier onset of hypertension during a 13 years follow-up period (Matthews et al., 2004; but cf. Yano et al., 2016). Panaite et al. (2015) concluded from their meta-analytic comparison that in addition to reactivity, cardiovascular recovery might play an equally important role in the prediction of future CVD events. In sum, these studies suggest that certain patterns of blood pressure reactivity in normotension relate to the subsequent development of hypertension and other precursors of CVD and thus precede elevations in blood pressure levels.

1.4.3 Brain correlates of blood pressure reactivity to psychological stressors

Although there are plenty of studies linking adverse effects of blood pressure reactivity to cardiovascular events, only recently research aimed to understand 'neuro-vegetative coupling' or the neurobiological pathways that couple the central nervous system processing of acute stressors with the peripheral expression of cardiovascular reactions implicated in CVD risk (Gianaros & Sheu, 2009). Non-invasive investigations of neural activity and vascular responses in humans have been methodologically challenging in the past. Due to technical developments in the last 20 years, however, concurrent acquisition of peripheral physiological signals, like heart rate and blood pressure, and neuroimaging markers became possible (Gray et al., 2009). These methodological advances enabled studies to investigate how experimental stressors modulate behavioral, neural and autonomic activity simultaneously. One of the first brain imaging studies to relate blood pressure reactivity with neural activation used positron emission tomography to investigate whether changes in regional CBF correlated with blood pressure changes evoked by a frustrating mental arithmetic task and an isometric handgrip task, respectively (Critchley, Corfield, Chandler, Mathias, & Dolan, 2000). Results showed that increased stressor-evoked mean arterial pressure correlated with increased resting CBF to the postcentral gyrus, anterior cingulate cortex, insula and cerebellum; and with decreased resting CBF primarily to prefrontal and medial temporal regions (Critchley et al., 2000). This study provided the first human neuroimaging evidence for the involvement of areas previously implicated in cognitive and emotional behaviors in the representation of peripheral autonomic states.

Until today, however, technical difficulties related to the MRI environment complicate the continuous, simultaneous acquisition of some autonomic markers during functional MRI. For example, the beat-to-beat acquisition of blood pressure has been difficult to achieve in the scanner environment and was circumvented by using intermittent blood pressure recordings immediately before and after experimental blocks in the first fMRI studies in this realm. These early studies were therefore limited to testing neuro-vegetative coupling associated with longer-lasting “stress periods” over several minutes. More recent techniques, however, on which we build in study 6 of this dissertation, allow for simultaneous recording of blood pressure during fMRI which matches neural activity following brief stimulation events more closely to blood pressure changes (in seconds range) (Gray et al., 2009; Okon-Singer et al., 2014). While pioneering these new methods to investigate neuro-vegetative coupling, these studies became especially relevant as they showed that individual differences of brain function and structure covary with stressor-evoked blood pressure changes (Gianaros & Sheu, 2009; Okon-Singer et al., 2014). In a series of studies by Gianaros et al., non-hypertensive adults, performed a Stroop color-word-interference task during fMRI with intermittent blood pressure acquisition (Gianaros et al., 2005; Gianaros, Jennings, Sheu, Derbyshire, & Matthews, 2007; Gianaros et al., 2008). A meta-analytic summary of these studies showed that exaggerated blood pressure reactivity in response to the task correlated with increased activation in brain regions such as cingulate cortex, amygdala, insula, and prefrontal areas (Gianaros & Sheu, 2009). Even in young, non-hypertensive adults within their twenties, greater stressor-evoked blood pressure reactivity correlated with increased activation of and functional connectivity within cortico-limbic and CAN regions (Gianaros et al., 2008; Okon-Singer et al., 2014), as well as with reduced gray matter volume in the amygdala and medial frontal areas (Gianaros et al., 2008). Another recent study of 20-year-old women found that systolic blood pressure reactivity in response to a frustrating mental arithmetic task correlated with lower hippocampus volume in the following year (Trotman, Gianaros, Veldhuijzen van Zanten, Williams, & Ginty, 2018). In this study, other cardiovascular reactivity parameters also related to lower amygdala volume.

What can be concluded from these studies is the outline of a higher-order functional network of cortico-limbic regions, including the cingulate/medial frontal cortex, insula and amygdala, which integrates the processing of psychological stressors with regulatory cardiovascular responses to mobilize hemodynamic and metabolic support for adaptive behaviors. Activity within this neuro-vegetative coupling network linearly relates to the expression of stressor-evoked blood pressure reactivity independent of hypertension. Neural activation patterns which relate to the initiation of vascular responses that

repeatedly exceed hemodynamic and metabolic demands, may serve as a mechanistic link between excessive stress-related cardiovascular reactivity and prospective hypertension and CVD.

2 Aims of the Thesis and Rationale for Experimental Work

The rationale for the experimental work of this thesis grounds on the following assumptions. As outlined above, there is a substantial impact of high blood pressure on general health, cognition, brain structure and brain function. Some studies point to a continuous, linear relation between high blood pressure and adverse brain outcomes – irrespective of any cut-off threshold – which presents before overt clinical symptoms occur. However, evidence from neuroimaging studies which test continuous associations of blood pressure on brain structure and function independent of vascular disease or other confounding factors is sparse. In addition, maladaptive reactivity and regulation of blood pressure in younger age, prior to manifestation of hypertension, may determine the development and progression of cognitive decline and brain damage during aging. In this respect, a combination of neural, autonomic and psychological processes seems to interact and putatively underlies the factors driving initial blood pressure elevations and pathogenesis of essential hypertension. Thus, the motivation for this thesis was to approach the question of how blood pressure and other vascular risk factors relate to brain structure and function from a mind-brain-body perspective and by that contribute to the understanding of the complex interrelation between the brain, blood pressure control and hypertension.

We approached this first by a large data collection effort to build a multimodal database, which we made available for public use, that provides a suitable framework for investigations of multifactorial mind-brain-body interactions in young and old age (studies 1 and 2). This database is a key aspect of my experimental work and forms the core of the empirical studies of this thesis. Using this new database, the main study of my experimental work aimed to investigate if blood pressure relates to impaired brain structure in younger adults at sub-hypertensive levels (study 3). Two related studies from this database aimed to elucidate the relationship between intrinsic functional brain connectivity and other vascular risk factors (heart rate variability in study 4; acute psychosocial stress in study 5). The final study presented here aimed to understand neural control of blood pressure regulation and investigated which brain areas are involved in the cognitive modulation of blood pressure reactivity to negative emotions (study 6).

Rationale of studies 1 & 2 (key work for data acquisition):

The first studies included in this thesis are a data collection effort, that is openly available for researchers around the world, with the aim to provide a large database for in-depth investigations of mind-brain-body interactions. To achieve a holistic picture of healthy aging and the development of civilization diseases, it is vital to consider a multi-etiological

research approach. The *MPI-Leipzig Mind-Brain-Body database* (MPILMBB) was designed to provide such a framework by deeply phenotyping younger and older participants. Using multimodal state-of-the-art methods, comprehensive individual physiological and psychological profiles were assessed that allow a multitude of investigations to illuminate how mind, brain and body interact across the lifespan, which may inform clinical research. The database also provided a basis for the empirical studies of this thesis.

Rationale of study 3 (main study using the database of studies 1 & 2):

The third study was set out to determine the relevance of blood pressure for brain structural integrity of young adults without diagnosed hypertension. As introduced above, asymptomatic brain changes related to vascular risk factors, including high blood pressure, are visible in MRI long before symptomatic disease manifests. This suggests continuous detrimental effects of blood pressure on the brain. However, this was only investigated in middle and older age where participants have been exposed to vascular risk factors for years before assessment. Little is known about the effects of elevated blood pressure on brain structure in young adulthood where prevalence of vascular risk factors is typically low. We conducted a meta-analytic MRI study to investigate how sub-hypertensive blood pressure levels relate to gray matter volume of adults below 40 years of age.

Rationale of study 4 & 5 (related studies using the database of studies 1 & 2):

Studies 4 and 5 show different applications of the MPILMBB database in the field of mind-brain-body investigations.

Heart-brain interactions have critical implications for mental and physical health and have previously been shown to relate to structure and function in cortical midline and limbic areas. In study 4, we investigated how the relation between parasympathetic cardio-regulation and brain structure and function varied across the human lifespan. Since heart rate variability decreases with age, we hypothesized that structural and functional neural correlates of heart rate variability are age dependent. Our study combined measures of resting heart rate variability, structural brain MRI and resting-state functional brain connectivity to test their interrelation and dependence on age in a large sample of healthy adults.

Study 5 aimed to describe the neural correlates of acute psychosocial stress. While psychophysiological responses to acute stress have been shown in many previous studies, it is less well defined how the brain is directly implicated in stress reactivity. Using resting-state fMRI, we investigated how both stress reactivity and recovery (up to 90 min

after stress onset) are reflected in whole-brain functional connectivity changes and how these changes relate to other measures of stress in healthy young men. We hypothesized that immediate stress induces effects on whole-brain network topology. In addition, the study aimed to explore the association between neural stress reactivity and (i) subjective stress ratings, (ii) autonomic (i.e. heart rate variability) and (iii) endocrine (i.e. cortisol) stress measures, respectively.

Rationale of study 6 (using the mind-brain-body approach to understand blood pressure control):

Finally, considering that emotional processing is a substantial factor in the development of hypertension and cerebrovascular disease, this field of research offers good prospects for future investigations. Previous studies investigated neural activation and blood pressure reactivity in response to cognitive demand or physiological stress in young adults. However, the interplay of cognitive, neural and vascular factors in the context of emotional processing are less well defined. Thus, in study 6 we set out to investigate the neural correlates of blood pressure reactivity to negative emotions. Our aims were (i) to identify neural processes involved in blood pressure responses to emotional stimuli, and (ii) to elucidate how attention modulates these neural processes and the associated blood pressure response in young adults. We hypothesized that, in the low attentional load condition of a perceptual load task, negative pictures would deteriorate task performance, activate regions implicated in emotion processing (amygdala, anterior insula, orbitofrontal cortex, visual areas) and transiently decrease blood pressure (Dan-Glauser & Gross, 2011; Minati et al., 2009). In the high load condition (reduced attention) these reactions were hypothesized to be attenuated. Finally, we expected activations related to enhanced perceptual load in frontoparietal and primary visual regions.

3 Experimental Work

3.1 Studies 1 & 2: The MPI-Leipzig Mind-Brain-Body database

Study 1: A Mind-Brain-Body Dataset of MRI, EEG, Cognition, Emotion, and Peripheral Physiology in Young and Old Adults. Babayan...Schaare et al., *Scientific Data* (2019)

Study 2: A Functional Connectome Phenotyping Dataset Including Cognitive State and Personality Measures. Mendes...Schaare et al., *Scientific Data* (2019)

The basis for the studies of this thesis is a large data acquisition effort to create a database which allows for testing mind-body-emotion interactions in a comprehensive manner. The database is built upon two complementary data acquisition protocols – on a partially overlapping cohort of participants – which vary in their study designs and methodological foci. The datasets have been peer-reviewed and published as data articles (Babayan et al., 2019; Mendes et al., 2019). Dataset 1, the “Leipzig Study for Mind-Body-Emotion Interactions” (LEMON), was designed to assess a wide range of neural, psychological and psychophysiological markers that allow to test mind-brain-body interactions in young and older adults (n=227) (Babayan et al., 2019). Dataset 2, the “Neuroanatomy and Connectivity protocol (N&C), focused on a detailed assessment of the functional connectome, by including one hour of resting-state fMRI, and cognitive and personality measures in adults between 20-75 years of age (n=194) (Mendes et al., 2019). Overall, 109 participants completed both protocols. The protocols are described in detail elsewhere (Babayan et al., 2019; Mendes et al., 2019), however an overview of the procedures and measures included in the database is given below.

3.1.1 Materials and methods

3.1.1.1 *Participants*

The total sample of the LEMON study included in total 227 younger (N=153, 25.1±3.1 years, range 20–35 years, 45 female) and older (N=74, 67.6±4.7 years, range 59–77 years, 37 female) German-speaking participants. The N&C protocol included 194 adults between 20-75 years of age (34±16 years, 94 female). Overall, 109 participants completed both studies. The studies were approved by the ethics committee at the medical faculty of Leipzig University (reference numbers 154/13-ff for LEMON, 097/15-ff for N&C).

3.1.1.2 *Study inclusion*

Study eligibility of prospective participants for both protocols was prescreened in a semi-structured telephone interview. Individuals who did not meet any exclusion criteria, such

as history of cardiovascular disease, psychiatric illness, or neurological disease, were invited to an information event about the study procedures which was followed by a second, individual screening for study eligibility by a physician.

3.1.1.3 Procedure

LEMON

Participants completed two assessment days which lasted around four hours each (Figure 1). On the first assessment day, a cognitive test profile, MRI, blood pressure and anthropometric measurements and a blood sample were acquired. On the second assessment day, we acquired resting-state EEG and participants completed a psychological assessment including an emotion and personality test battery as well as a psychiatric interview. Participants were also invited for follow-up experiments, where additional behavioral and psychological measures were assessed depending on the experiments' aims.

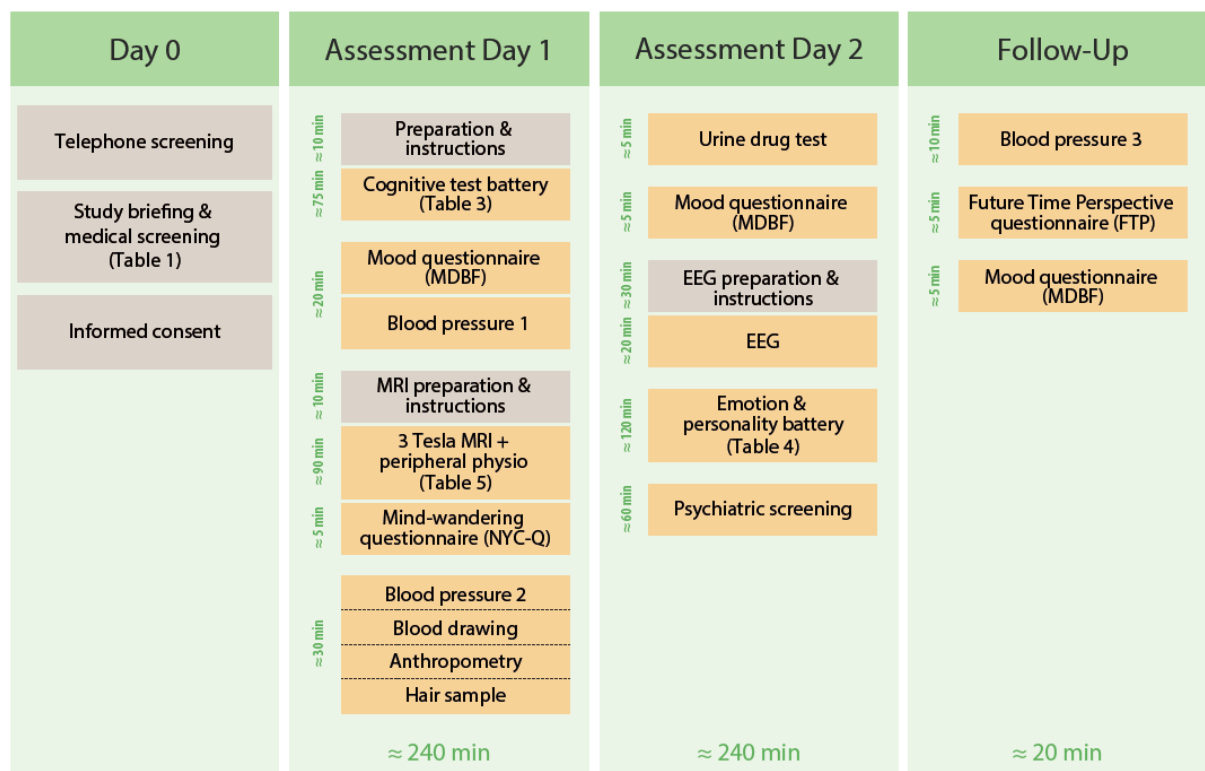


Figure 1 – LEMON study. Overview of data acquisition

N&C

In the N&C study, participants completed five assessment days (Table 2). The first day consisted of the completion of a set of questionnaires at the Max Planck Institute for Human Cognitive and Brain Sciences (MPI CBS). The second day required the completion of a set of online questionnaires which the participants could do at home at their

convenience, On the third day, participants underwent neuroimaging at the Clinic for Cognitive Neurology at the University of Leipzig Medical Center and completed several experimental paradigms and another set of questionnaires. The fourth day included more online questionnaires that could be completed at home. On the fifth and final assessment day, a set of questionnaires and tasks was administered at the MPI CBS. Within each set, the order of questionnaires and tasks was randomized across participants.

Table 2 - Neuroanatomy & Connectivity protocol. Overview of data acquisition

Uni Clinic= Day Clinic for Cognitive Neurology, University of Leipzig. **ACS**=Attention Control Scale, **AMAS**=Abbreviated Math Anxiety Scale, **ASR**=Adult Self Report, **AUT**=Alternative Uses Task, **BCQ**=Body Consciousness Questionnaire, **BDI**=Beck Depression Inventar-II, **BIS/BAS**=Behavioral Inhibition and Approach System, **BP**=Boredom Proneness Scale, **CAQ**=Creative Achievement Questionnaire, **CCPT**=Conjunctive Continuous Performance Task, **ESS**=Epworth Sleepiness Scale, **ETS**=Emotional task switching; **FBI**=Facebook Intensity Scale, **FFMQ**=Five Facets of Mindfulness Questionnaire, **Gold-MSI**=Goldsmiths Musical Sophistication Index, **HADS**=Hospital Anxiety and Depression Scale, **IAT**=Internet Addiction Test, **IMIS**=Involuntary Musical Imagery Scale, **MCQ-30**=Metacognition Questionnaire, **MGIQ**=Multi-Gender Identity Questionnaire, **MMI**=Multimedia Multitasking Index, **MPU**=Mobile Phone Usage, **NEO PI-R**=NEO Personality Inventory-Revised, **NYC-Q_postscan**=New York Cognition Questionnaire after scan, **Oddball**=Adaptive Visual and Auditory Oddball Target Detection Task, **PSSI**=Personality Style and Disorder Inventory, **RAT**=Remote Associates Test, **SCS**=Brief Self-Control Scale, **SD3**=Short Dark Triad, **S-D-MW**=Spontaneous and Deliberate Mind-Wandering, **SDS**=Social Desirability Scale-17; **SE**=Self-Esteem Scale, **Short-NYC-Q_inscan1-4**=Short Version of the New York Cognition Questionnaire in scanner, **Short-NYC-Q_postETS**=Short Version of the New York Cognition Questionnaire after tasks, **SYN**=Synesthesia Color Picker Test, **TCIA**=Test of Creative Imagery Abilities, **TPS**=Tuckman Procrastination Scale, **UPPS-P**=UPPS-P Impulsive Behavior Scale, **VISQ**=Varieties of Inner Speech Questionnaire.

Day 1 (MPI CBS)	Day 2 (Home)	Day 3 (Uni Clinic)	Day 4 (Home)	Day 5 (MPI CBS)
ASR	ACS	Scanning session	AMAS	BIS/BAS
God-MSI	BDI		NEO PI-R	CAQ
IAT	BP	FBI		MCQ-30
IMIS	ESS	S-D=MW		BCQ
MGIQ	HADS	Short-NYC-Q_inscan1-4		FFMQ
SCS	MMI	Short-NYC-Q_postETS		RAT
SD3	MPU	NYC-Q_postscan		SYN
SE	PSSI	ETS		AUT
TPS		CCPT		TCIA
VISQ		Oddball		
UPPS-P				
SDS				

3.1.1.3.1 Psychological assessment

LEMON

The psychological assessment of the study included a wide range of psychological constructs which were measured with common psychometric instruments (details in Babayan et al., 2019). The cognitive test battery included six tests assessing verbal learning, memory capacity, alertness, interference, working memory, executive function, verbal crystallized intelligence, fluid intelligence, and verbal fluency. The emotion and

personality test battery assessed the following constructs in 21 questionnaires: big five personality factors, impulsivity, approach and inhibition behavior, emotion regulation, perceived social support, coping, optimism, pessimism, perceived chronic stress, eating behavior, emotional intelligence, trait anxiety, trait anger, alexithymia, mood, individual anticipation of time left to live, as well as content and form of self-generated thoughts. While these instruments mainly cover sub- or non-clinical manifestations of psychological constructs, we also assessed past and present psychiatric symptoms with the Standardized Clinical Interview for Diagnostic and Statistical Manual of Mental Disorders (DSM-IV) axis I disorders (SCID-I). Furthermore, we screened for depressive symptoms, borderline personality symptoms, and alcohol abuse. Substance abuse was also tested by an in-vitro urine drug test to exclude substance abuse at the time point of testing.

N&C

The psychological assessment in N&C was more extensive than the one in LEMON and included a broad set of 42 state and trait questionnaires and tasks which covered constructs of personality and habitual behaviors, mind-wandering and mindfulness, synesthesia, cognitive control and sustained attention, and creativity. An overview of all measures is given in Table 2.

3.1.1.3.2 Physiological data

LEMON

The LEMON study acquired a large dataset of structural and resting-state (rs) functional MRI at the 3 Tesla MAGNETOM Verio scanner (Siemens, Erlangen, Germany) located at the Clinic for Cognitive Neurology at the University of Leipzig Medical Center. The imaging protocol lasted approximately 70 minutes and included the following scans in fixed order: 1) gradient echo fieldmap scan for distortion correction in rs-fMRI, 2) a pair of spin echo images with reversed phase encoding direction for distortion correction in rs-fMRI, 3) a 15-min rs-fMRI scan, 4) a second pair of spin echo images with reversed phase encoding direction, 5) quantitative and weighted T1 Magnetization-Prepared 2 Rapid Acquisition Gradient Echoes (MP2RAGE) images, 6) a T2-weighted image, 7) a Fluid-attenuated inversion recovery (FLAIR) scan, 8) a diffusion-weighted imaging (DWI) scan, 9) a pair of spin echo images with reversed phase encoding for distortion correction in DWI, 10) T2*/susceptibility-weighted imaging (SWI) scan. During the acquisition of rs-fMRI, continuous beat-to-beat blood pressure, electrocardiography (ECG), pulse, and respiration were recorded non-invasively with MR-compatible devices. We also recorded a 16-min rs-EEG with a 62-channel active electrode setup. The EEG session comprised a total of 16 interleaved eyes-closed and eyes-open blocks (8 each), each 60 s long. Additional measures included three seated resting blood pressure recordings,

anthropometry measures (including body weight and height to calculate BMI, as well as waist and hip measurements to calculate the waist-to-hip ratio), a hair sample and a peripheral blood sample with direct laboratory analysis of common blood markers.

N&C

The physiological assessment in N&C consisted of a session of MRI including a T1-weighted structural scan, one hour of rs-fMRI separated in four scans, and scans for distortion correction. The scanning protocols were equivalent to the sequences of LEMON (see above).

3.1.1.3.3 Data processing, sharing and security

To protect participants' identities and other sensitive information, data of both protocols were pseudonymized by allocating study IDs to all data. The public database was arranged in the BIDS format for standardized data management (Gorgolewski et al., 2016). Further pseudonymization was achieved by binning participants' age at study entry into five-year bins (cutoff values for binning were 20.0, 25.0, 30.0 and so forth). Data were shared in raw and partly in preprocessed form for some measures, such as MRI, EEG, psychological assessment. We report most data from the psychological tests as aggregated scores, where applicable (i.e. sub-scale scores instead of raw item values). For MRI, rs-fMRI and T1 scans were preprocessed and shared. The preprocessing of the rs-fMRI data was implemented in Nipype and comprised the following steps: (i) discarding the first five EPI volumes to allow for signal equilibration and steady state, (ii) 3D motion correction (FSL MCFLIRT), (iii) distortion correction (FSL FUGUE), (iv) rigid-body coregistration of unwarped temporal mean image to the individual's anatomical image (FreeSurfer *bbregister*), (v) denoising (Nipype *rapidart* and *aCompCor*), (vi) band-pass filtering between 0.01-0.1 Hz (FSL), mean-centering, as well as variance normalization of the denoised time series (*Nitime*), (vii) spatial normalization to MNI152 2 mm standard space via transformation parameters derived during structural preprocessing (ANTs *SyN*). The preprocessing of the T1 MP2RAGE data was also implemented in Nipype and included following steps: The background of the uniform T1-weighted image was removed using CBS Tools, and the masked image was used for cortical surface reconstruction using FreeSurfer's full version of *recon-all*. A brain mask was created based on the FreeSurfer segmentation results. Diffeomorphic nonlinear registration as implemented in ANTs *SyN* algorithm was used to compute a spatial transformation between the individual's T1-weighted image and the MNI152 1mm standard space. To remove identifying information from the structural MRI scans, a mask for defacing was created from the MP2RAGE images using CBS Tools. This mask was subsequently applied to all T1 scans. The raw EEG data used for preprocessing was downsampled from 2500 Hz to 250 Hz, bandpass

filtered within 1-45 Hz (8th order, Butterworth filter) and split into eyes-open and eyes-closed conditions for the subsequent analyses.

3.1.1.3.4 Quality assessment

We performed detailed quality control of all data before their inclusion in the database and provide its outcomes for public use. First, all data were manually checked for missing or corrupt data. For behavioral data, we provide descriptive statistics, reliability estimates and density plots of data distributions to assess their usability and facilitate the evaluation of the data. We visually inspected the quality of preprocessed MRI images in reports which we created using the mriqc package, implemented in Python. Mriqc creates a report for each individual scan based on different parameters like motion, coregistration, and temporal signal-to-noise (tSNR). Overall, the quality of the data was very good and only eight participants were excluded from preprocessing of LEMON MRI data due to errors during data acquisition (ghosting artifact N= 2, incomplete scan N=1), anatomical preprocessing (N=4) or functional preprocessing (N=1). Quality assessment of EEG data included visual inspection and removal of outlier channels showing poor signal quality and data intervals containing extreme signal shifts, as well as ICA-based rejection of components reflecting eye movement, eye blinks or heartbeat-related artefacts.

3.2 Study 3: Association of Peripheral Blood Pressure with Gray Matter Volume in 19- to 40-Year-Old Adults. Schaare et al., *Neurology* (2019)

This is the main study of my experimental work which builds on data from the MPILMBB database (study 1 and 2), in addition to other large datasets (see below). The article has been published in a peer-reviewed journal (Schaare et al., *Neurology*, 2019), thus large excerpts of the text below is kept in the original form of the article as it was approved by the reviewing experts. The objective of the study was to test whether varying levels of blood pressure relate to gray matter volume (GMV) differences between young adults.

3.2.1 Materials and methods

We applied voxel-based morphometry (VBM) to four independent datasets including young adults aged between 19-40 years without previous diagnosis of hypertension (HTN) or any other severe, chronic or acute disease. Results from each dataset were combined in image-based meta-analyses (IBMA) for well-powered, cumulative evaluation of findings across study differences (i.e. recruitment procedure, inclusion criteria and data acquisition, Supplementary Table 1, Figure 2).

3.2.1.1 *Participants*

We included cross-sectional data of 423 young participants from four samples. The samples were drawn from larger studies that were conducted in Leipzig, Germany, between 2010-2015: 1. Leipzig Study for Mind-Body-Emotion Interactions (LEMON) (Babayán et al., 2019), 2. Neural Consequences of Stress Study (NeCoS) (Reinelt et al., 2019), 3. Neuroanatomy and Connectivity Protocol (N&C) (Mendes et al., 2019), 4. Leipzig Research Centre for Civilization Diseases (LIFE) (Loeffler et al., 2015). The objective of LEMON was to cross-sectionally investigate mind-brain-body-emotion interactions in a younger (20-35 years) and an older (59-77 years) group of 228 healthy volunteers. NeCoS aimed to investigate neural correlates of acute psychosocial stress in 79 young (18-35 years), healthy, non-smoking men. The study protocol for the baseline assessment of participants in NeCoS was adapted from the LEMON protocol. In N&C, 194 healthy volunteers between 20-75 years of age participated in one session of MRI and completed an extensive assessment of cognitive and personality measures. This dataset aimed to relate intrinsic functional brain connectivity with cognitive faculties, self-generated mental experience, and personality features. The LIFE-study is a population-based dataset in the city of Leipzig, Germany, with the objective to investigate the development of major modern diseases. Overall, 10000 participants were randomly drawn from the local population of whom 2667 underwent MRI and detailed screening. With dementia being one of the key scientific topics in this study, most participants in the MRI-subcohort were

adults above the age of 60 years. The exact inclusion procedure and numbers for the current investigation is depicted in Figure 2. Inclusion criteria for our study were age between 19-40 years, availability of high-resolution structural T1-weighted MRI and ≥ 1 blood pressure measurements. Participants were excluded in case of previously diagnosed HTN, intake of antihypertensive drugs or severe diseases (Supplementary Table 1). The studies were in agreement with the Declaration of Helsinki and approved by the ethics committee of the medical faculty at the University of Leipzig, Germany (ethics reference numbers study 1: 154/13-ff, study 2: 385/14-ff, study 3: 097/15-ff, study 4: 263-2009-14122009). Before entering the studies, participants gave written informed consent.

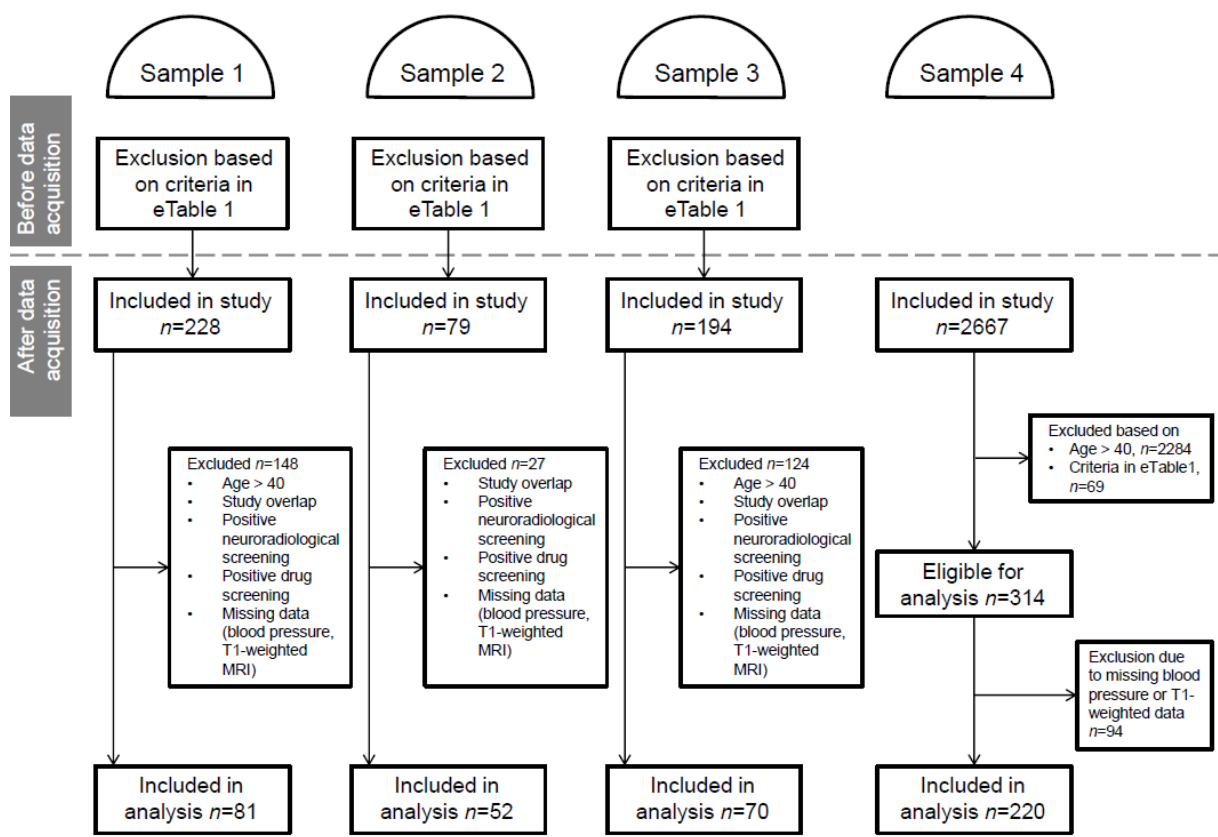


Figure 2 – Flow chart with inclusion procedure for the study samples

Sample 1: Leipzig Study for Mind-Body-Emotion Interactions. Sample 2: Neural Consequences of Stress Study. 3: Neuroanatomy and Connectivity Protocol. 4: Leipzig Research Centre for Civilization Diseases (MRI-subcohort).

3.2.1.2 Blood pressure measurements

Systolic (SBP) and diastolic blood pressure (DBP) were measured at varying times of day using an automatic oscillometric blood pressure monitor (OMRON M500 (samples 1-3), 705IT (sample 4), OMRON Medizintechnik, Mannheim, Germany) after a seated resting period of 5 min. In sample 1, three measurements were taken from participants' left arms on three separate occasions within two weeks. In sample 2, two measurements were taken from participants' left arms on two separate occasions on the same day. In sample 3, blood

pressure was measured once before participants underwent MRI. In sample 4, the procedure consisted of three consecutive blood pressure measurements, taken from the right arm in intervals of 3 minutes. In each sample, all available measurements per participant were averaged to one systolic and one diastolic blood pressure value. These averages were used for classification of blood pressure.

3.2.1.3 Neuroimaging

MRI was performed at the same 3 Tesla MAGNETOM Verio Scanner (Siemens, Erlangen, Germany) for all studies with a 32-channel head coil. Whole-brain 3D T1-weighted volumes with a resolution of 1 mm³ isotropic were acquired for the assessment of brain structure. T1-weighted images in sample 4 were acquired with a standard MPRAGE protocol (inversion time TI=900 ms, repetition time TR=2300 ms, echo time TE=2.98 ms, flip angle FA=9°, field of view FOV=256x240x176 mm³, voxel size=1x1x1 mm³), while T1-weighted images in samples 1-3 resulted from an MP2RAGE protocol (TI1=700 ms, TI2=2500 ms, TR=5000 ms, TE=2.92 ms, FA1=4°, FA2=5°, FOV=256x240x176 mm³, voxel size=1x1x1 mm³). Gray and white matter contrast are comparable for the two sequence protocols (Marques et al., 2010; Streitbürger et al., 2014), but additional preprocessing steps were performed for MP2RAGE T1-weighted images (see section Additional preprocessing steps for MP2RAGE images). FLAIR images were acquired in all samples for radiological examination for incidental findings and for Fazekas scale ratings for WMH (Table 3, Table 4).

3.2.1.3.1 Additional preprocessing steps for MP2RAGE images

Before segmentation, T1-weighted images acquired with an MP2RAGE sequence were additionally masked to remove noise signal outside of the brain (following the procedure described in (Streitbürger et al., 2014): a binarized brain mask was created from the second inversion-contrast volume by setting voxels with intensities of less than 10% of the maximum signal to zero. Any holes in the mask were filled. For the final image, the mask was multiplied with the T1-weighted volume which eliminated background noise but preserved signals from the brain and other tissues. All of these steps were performed with tools in FSL 5.0 (Jenkinson, Beckmann, Behrens, Woolrich, & Smith, 2012, www.fmrib.ox.ac.uk/fsl). T1-weighted images from MP2RAGE are free of magnetic field inhomogeneity (they are also named *uniform*). Thus, a correction for this bias was omitted and only applied to MPRAGE images. Bias correction for MPRAGE images followed the default settings within SPM12's *segment* batch. All other processing steps were identical for the pulse sequences.

3.2.1.4 Data processing and statistical analysis

3.2.1.4.1 Blood pressure classification

For statistical analyses, all available blood pressure measurements per participant were averaged to one mean SBP and DBP, respectively. Based on these averages, we categorized blood pressure according to the European guidelines for the management of arterial hypertension (Mancia et al., 2013): *category 1* (SBP<120 mmHg and DBP<80 mmHg), *category 2* (SBP 120-129 mmHg or DBP 80-84 mmHg), *category 3* (SBP 130-139 mmHg or DBP 85-89 mmHg) and *category 4* (SBP≥140 mmHg or DBP≥90 mmHg).

3.2.1.4.2 Voxel-based morphometry: Association of regional GMV and blood pressure within each sample

For each of the four samples, 3 Tesla high-resolution T1-weighted 3D whole-brain images were processed by using voxel-based morphometry (VBM) and the diffeomorphic anatomical registration using exponentiated lie algebra (DARTEL) method (Ashburner, 2007; Ashburner & Friston, 2000) within SPM12 (12.6685, Wellcome Trust Centre for Neuroimaging, UCL, London, UK; <http://www.fil.ion.ucl.ac.uk/spm12/>) running under Matlab 9.0.0 (R2016a, MathWorks, Natick, MA, USA). In short, processing of GMV probabilities included segmentation into tissue types, sample-specific DARTEL template creation, modulation of grey matter voxels to preserve tissue properties, normalization to MNI space, and 8 mm full-width-at-half-maximum Gaussian smoothing. Voxel-wise general linear models (GLM) were performed to relate blood pressure and GMV within each sample: We tested for a continuous relationship between GMV and SBP or DBP, in separate models, with a multiple linear regression *t*-contrast. The overall effect of blood pressure category on GMV was tested with an Analysis of Variance (ANOVA) *F*-contrast. The general linear model for this whole-brain analysis included a factor for blood pressure as variable of interest (levels: (1) category 4, (2) category 3, (3) category 2, (4) category 1). To assess differences in GMV between blood pressure categories, the following pairwise *t*-comparisons were tested: (a) category 4 vs. category 1, (b) category 3 vs. category 1, (c) category 2 vs. category 1. Each *t*-contrast was tested in negative and positive direction (i.e. category A<category B and category A>category B). All analyses included total intracranial volume (TIV), sex and age as covariates. The influence of BMI did not significantly contribute to the models and was thus not included as covariate in the analyses. We considered a sample eligible for image-based meta-analysis if its *F*-contrast effects exceeded an uncorrected peak-level threshold of $p<0.001$. Effects within each sample were explored at cluster-level $p<0.05$ with family-wise error correction for multiple comparisons.

3.2.1.4.3 Image-based meta-analysis: Association of regional GMV and blood pressure across samples

To evaluate cumulative results from all samples while considering their heterogeneities, we combined the VBM outcome of each sample in an image-based meta-analysis (IBMA). The meta-analysis was performed with Anisotropic Effect-Size Signed Differential Mapping (AES-SDM) implemented in the SDM software package using default parameters (Radua et al., 2012, <http://www.sdmproject.com/>, <http://www.sdmproject.com/software/tutorial.pdf>). Meta-analyses were performed on the unthresholded *t*-maps with SDM software using default parameters (Radua et al., 2012). For each sample and *t*-contrast, unthresholded whole-brain *t*-statistic maps were converted to Hedges' *g* effect size maps and variance maps. To assess weighted mean differences in grey matter across all samples, a meta-analytic model was set up for each voxel. Within this random-effects model, samples are weighted by their sample size, within-study variance and between-study heterogeneity. The result is a mean map of *z*-values which are quotients of the mean effect-sizes and their standard errors. Since these *z*-values are not normally distributed, null distributions were estimated empirically by Monte Carlo randomizations. Voxels in the mean map were randomly permuted within a software-implemented grey matter mask to create null distributions for the assessment of critical *z*-values. We applied 50 permutations, while statistical stability has been shown from 20 permutations on (Radua et al., 2012). Statistical significance of mean effect size maps was evaluated according to validated thresholds of high meta-analytic sensitivity and specificity (Radua et al., 2012): voxel threshold= $p < 0.005$, peak height threshold= $\text{SDM-Z} > 1.0$ and cluster extent threshold= $k \geq 10$ voxels. Anatomy toolbox (Eickhoff et al., 2007, version 2.2 for SPM8) was used to automatically label significant clusters in all analyses. Nilearn (Abraham et al., 2014, version 0.2.6, <https://nilearn.github.io/index.html>) was used to visualize statistical brain maps. Exploratory IBMA for positive associations were performed in analogy to negative associations as described above.

3.2.1.4.4 IBMA of regions of interest (ROI): Association of regional GMV and blood pressure across samples in hippocampus and amygdala

With the meta-analysis approach, we also tested if specific regions of interest (ROI) that included bilateral hippocampus and bilateral amygdala differed in their volumes related to SBP, DBP and between blood pressure categories, respectively. Separate IBMAs were calculated within binary atlas-defined masks for bilateral hippocampus and bilateral amygdala that were retrieved from the latest available version of the Anatomy toolbox (Eickhoff et al., 2007, version 2.2 for SPM8). The statistical thresholds were defined as $p < 0.05$, $\text{SDM-Z} > 1.0$ and $k \geq 1$ voxels. Peak voxels' effect sizes were extracted with SDM

software's *Extract* option and plotted as forest plots (Figure 4) with R (3.2.3, R Core Team, 2015, Vienna, Austria; <https://www.R-project.org/>) and the package *rmeta* (2.16).

3.2.1.4.5 Volumetry: Association of total brain volumes and blood pressure within the pooled sample

In addition to VBM and IBMA, we explored if total brain volumes (average volume over all voxels within a region) differed between blood pressure categories. Specifically, we tested if estimated total intracranial volume, total grey matter volume, total white matter volume, total amount of WMH, total CSF volume, total left and right hippocampal and amygdalar volume differed between blood pressure categories. WMH was assessed by Fazekas scale ratings from FLAIR images (Fazekas, Chawluk, Alavi, Hurtig, & Zimmerman, 1987). For these comparisons within the total sample, we defined correlation models (for SBP and DBP as independent variable, respectively) and ANOVA models for blood pressure category as independent variable. The models included the respective volume as dependent variable, as well as TIV (where applicable), sex, age, and sample (where applicable) as covariates. We considered p -values < 0.05 as significant. The analyses were performed with R (3.2.3, R Core Team, 2015, Vienna, Austria; <https://www.R-project.org/>).

3.2.1.5 Data sharing

Results (i.e. unthresholded whole-brain statistical maps) from VBM analyses of each sample and from all IBMAs can be found online in the public repository NeuroVault for detailed, interactive inspection (<http://neurovault.org/collections/FDWHFSYZ/>). Raw data of samples 1-3 available from <https://www.openfmri.org/dataset/ds000221/>.

3.2.2 Results

3.2.2.1 Sample characteristics

The characteristics of the total sample by blood pressure category are reported in Table 3. The total sample included 423 participants between 19-40 years of whom 177 were women (42%). Mean (SD) age was 27.7 (5.3) years. SBP, DBP, and BMI differed significantly between blood pressure categories (all $p < 0.001$). A significant effect of sex yielded that men were more frequent in higher blood pressure categories (all $p < 0.001$).

Table 3 – Characteristics by blood pressure category

Characteristics of the total sample by blood pressure categories. Column *p* specifies significant results of comparisons between blood pressure categories: empty cells = $p > 0.05$. Column Pairwise comparisons specifies significant post-hoc comparisons for: 2=category 1 vs. 2, 3=category 1 vs. 3, 4=category 1 vs. 4. ***= $p < 0.001$, **= $p < 0.01$, *= $p < 0.05$. Definition of blood pressure categories: category 1 (SBP<120 mmHg and DBP<80 mmHg), category 2 (SBP 120-129 mmHg or DBP 80-84 mmHg), category 3 (SBP 130-139 mmHg or DBP 85-89 mmHg) and category 4 (SBP≥140 mmHg or DBP≥90 mmHg).

	Total		Category 1		Category 2		Category 3		Category 4		<i>p</i>	Pairwise comparisons
n (%)	423 (100%)		175 (41%)		121 (29%)		80 (19%)		47 (11%)			
Women [n (%)]	177 (42%)		117 (67%)		40 (33%)		11 (14%)		9 (19%)		***	2***, 3***, 4***
Age (mean years, SD)	27.66	5.27	27.61	5.53	27.30	4.95	28.01	5.24	28.21	5.23		
Range (min-max years)	19-40		19-40		20-40		20-40		20-39			
Systolic Blood Pressure (mean mmHg, SD)	123.2	12.19	111.91	5.44	123.99	3.62	134.57	3.48	143.56	7.76	***	2***, 3***, 4***
Diastolic Blood Pressure (mean mmHg, SD)	73.38	8.49	67.67	5.81	73.64	5.77	78.79	6.46	84.75	8.26	***	2***, 3***, 4***
Body Mass Index (mean kg/m ² , SD)	23.48	3.25	22.60	2.74	23.45	3.23	24.22	3.42	25.59	3.62	***	2*, 3**, 4***
Missing values [n (%)]	13 (3%)		5 (3%)		4 (3%)		1 (1%)		3 (6%)			
Range (min-max kg/m ²)	17.96-36.93											
Smoking status: [n (%)]												
non-smoker	273 (65%)		113 (65%)		78 (64%)		53 (66%)		29 (62%)			
occasional smoker	57 (13%)		23 (13%)		17 (14%)		13 (16%)		4 (9%)			
smoker	73 (17%)		29 (17%)		21 (17%)		13 (16%)		10 (21%)			
missing values	20 (5%)		10 (6%)		5 (4%)		1 (1%)		4 (9%)			
Fazekas score [n (%)]												
0	303 (72%)		123 (70%)		85 (70%)		59 (74%)		36 (77%)			
1	72 (17%)		39 (22%)		16 (13%)		10 (13%)		7 (15%)			
2	0 (0%)		0 (0%)		0 (0%)		0 (0%)		0 (0%)			
3	0 (0%)		0 (0%)		0 (0%)		0 (0%)		0 (0%)			
Missing values	48 (11%)		13 (7%)		20 (17%)		11 (14%)		4 (9%)			
Total intracranial volume (mean ml, SD)	1450.05	137.39	1400.49	127.47	1457.43	142.07	1508.05	116.23	1516.90	126.29		
Grey matter volume (mean ml, SD)	777.41	88.69	748.55	79.50	784.29	90.41	809.72	87.36	812.16	86.47		
White matter volume (mean ml, SD)	449.79	55.74	435.84	53.56	452.75	55.93	464.19	53.34	469.58	55.52		
Cerebrospinal fluid volume (mean ml, SD)	222.86	56.60	216.09	54.57	220.40	59.53	234.14	54.14	235.16	57.34		
Hippocampal volume, left (mean ml, SD)	3.90	0.45	3.77	0.41	3.93	0.46	4.06	0.43	4.09	0.43		
Hippocampal volume, right (mean ml, SD)	3.97	0.43	3.83	0.40	4.00	0.44	4.12	0.40	4.14	0.39		
Amygdalar volume, left (ml)	1.68	0.19	1.62	0.18	1.68	0.19	1.75	0.18	1.75	0.18		
Amygdalar volume, right (ml)	1.50	0.16	1.45	0.15	1.51	0.17	1.56	0.16	1.57	0.15		

Table 4 shows differences in characteristics between the four included samples. The samples differed significantly in almost all characteristic variables, specifically regarding sex, age, SBP, DBP, smoking status, and brain volumes (all $p < 0.001$).

Table 4 – Characteristics by sample

Characteristics of the study samples. Column *p* specifies significant results of comparisons between samples: empty cells = $p > 0.05$. Column Pairwise comparisons specifies significant post-hoc comparisons between samples: *** = $p < 0.001$, ** = $p < 0.01$, * = $p < 0.05$.

	Total	Sample 1	Sample 2	Sample 3	Sample 4	<i>p</i>	Pairwise comparisons
n	423	81	52	70	220		
Women [n (%)]	177 (42%)	37 (46%)	0 (0%)	43 (61%)	97 (44%)	***	1 vs. 2***, 2 vs. 3***, 2 vs. 4***, 3 vs. 4*
Age (mean years, SD)	27.66 5.27	24.36 3.07	25.77 2.44	26.54 4.82	29.69 5.65	***	1 vs. 3*, 1 vs. 4***, 2 vs. 4***, 3 vs. 4***
Range (min-max years)	19-40	20-35	21-31	20-40	19-40		
Systolic Blood Pressure (mean mmHg, SD)	123.2 12.19	121.8 12.02	128.4 9.80	128.4 12.16	120.8 11.95	***	1 vs. 2**, 1 vs. 3***, 2 vs. 4***, 3 vs. 4***
Diastolic Blood Pressure (mean mmHg, SD)	73.38 8.49	73.27 6.77	75.68 8.03	79.91 7.65	70.80 8.20	***	1 vs. 3***, 1 vs. 4*, 2 vs. 3**, 2 vs. 4***, 3 vs. 4***
Blood Pressure Category [n (%)]						***	1 vs. 2*, 1 vs. 3**, 2 vs. 4***, 3 vs. 4***
Category 1 (SBP < 120 mmHg and DBP < 80 mmHg)	175 (41%)	38 (47%)	10 (19%)	15 (21%)	112 (51%)		
Category 2 (SBP 120-139 mmHg or DBP 80-84 mmHg)	121 (29%)	23 (28%)	21 (40%)	19 (27%)	58 (26%)		
Category 3 (SBP 130-139 mmHg or DBP 85-89 mmHg)	80 (19%)	13 (16%)	12 (23%)	21 (30%)	34 (15%)		
Category 4 (SBP ≥ 140 mmHg or DBP ≥ 90 mmHg)	47 (11%)	7 (9%)	9 (17%)	15 (21%)	16 (7%)		
Body Mass Index (mean kg/m ² , SD)	23.48 3.25	23.14 3.06	23.02 2.47	23.17 3.58	23.79 3.38		
Missing values [n (%)]	13 (3%)	0 (0%)	0 (0%)	12 (17%)	1 (0%)		
Range (min-max kg/m ²)	17.96-36.93	18.0-34.5	17.96-28.85	18.1-36.88	18.55-36.93		
Smoking status [n (%)]						***	1 vs. 2***, 1 vs. 4***, 2 vs. 3***, 2 vs. 4***, 3 vs. 4*
non-smoker	273 (65%)	57 (70%)	52 (100%)	40 (57%)	124 (56%)		
occasional smoker	57 (13%)	16 (20%)	0 (0%)	11 (16%)	30 (14%)		
smoker	73 (17%)	5 (6%)	0 (0%)	6 (9%)	62 (28%)		
missing values	20 (5%)	3 (4%)	0 (0%)	13 (19%)	4 (2%)		
Fazekas score [n (%)]							
0	303 (72%)	60 (74%)	15 (29%)	49 (70%)	179 (81%)		
1	72 (17%)	14 (17%)	4 (8%)	16 (23%)	38 (17%)		
2	0 (0%)	0 (0%)	0 (0%)	0 (0%)	0 (0%)		
3	0 (0%)	0 (0%)	0 (0%)	0 (0%)	0 (0%)		
Missing values	48 (11%)	7 (9%)	33 (63%)	5 (7%)	3 (1%)		
Total intracranial volume (mean ml, SD)	1450.05 137.39	1448.41 138.07	1553.45 100.05	1424.99 127.14	1434.19 137.82	***	1 vs. 2***, 2 vs. 3***, 2 vs. 4***
Grey matter volume (mean ml, SD)	777.41 88.69	829.38 74.94	880.24 59.62	805.25 64.19	725.11 66.89	***	1 vs. 2***, 1 vs. 3*, 1 vs. 4***, 2 vs. 3***, 2 vs. 4***, 3 vs. 4***
White matter volume (mean ml, SD)	449.79 55.74	430.85 49.28	467.25 40.38	420.51 46.23	461.95 58.48	***	1 vs. 2***, 1 vs. 4***, 2 vs. 3***, 3 vs. 4***
Cerebrospinal fluid volume (mean ml, SD)	222.86 56.60	188.19 42.88	205.97 36.83	199.22 48.70	247.13 56.18	***	1 vs. 4***, 2 vs. 4***, 3 vs. 4***

3.2.2.2 VBM: Association of regional GMV and blood pressure within each sample

Figure 3 shows differences in regional GMV between blood pressure categories for each of the four samples tested with an ANOVA *F*-contrast. Results show significant clusters of various extents that were distributed heterogeneously between the samples. Exploration of sample-specific effects showed a cluster in the left posterior insula for the *F*-contrast (peak MNI coordinates [-38,-24,24], $F=11.35$, cluster size $k=1239$) as well as clusters in left inferior frontal gyrus ([-42,34,0], $T=4.99$, $k=2039$) and in right anterior cingulate cortex ([14,34,14], $T=4.44$, $k=2086$) for the contrast blood pressure category 4<1 in sample 1. In sample 2, the contrast blood pressure category 4<1 yielded a cluster in left planum polare ([-44,-22,-3], $T=10.70$, $k=1151$) and the contrast blood pressure category 2<1 yielded a trend for a cluster in left middle temporal gyrus ($p=0.059$, [-54,-28,-9], $T=5.41$, $k=683$). Furthermore, there was a negative association between DBP and a cluster in left middle temporal gyrus in sample 2 ([-57,-45,6], $T=6.03$, $k=1180$). All other comparisons yielded no suprathreshold voxels (all $p_{FWE} > 0.05$). The statistical maps for sample-specific effects can be inspected on NeuroVault (<http://neurovault.org/collections/FDWHFSYZ/>).

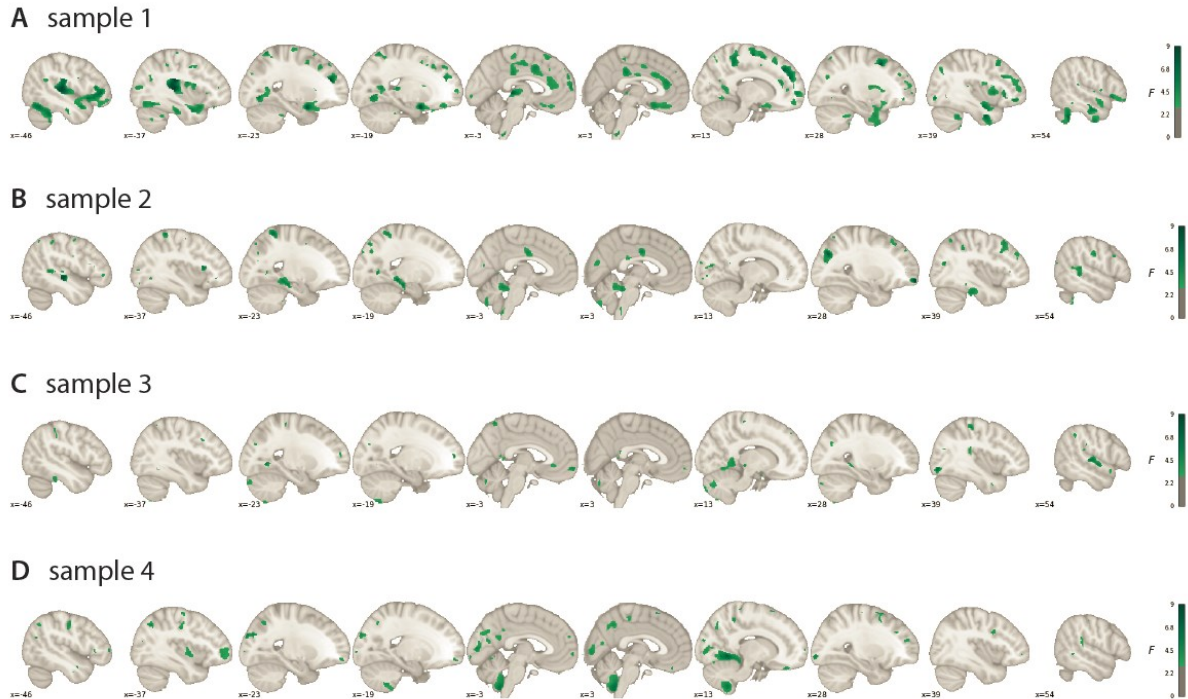


Figure 3 – Associations between gray matter volume and blood pressure within each sample

Sagittal views of VBM F -contrast results showing the overall effect of BP category on gray matter volume per sample. Each sample is represented in one row (A-D). Slice order runs from left hemisphere (left-hand side of the plot) to right hemisphere (right-hand side of the plot). Color bars represent F -values (uncorrected). Sample sizes: sample 1 $n = 81$; sample 2 $n = 52$; sample 3 $n = 70$; sample 4 $n = 220$. 3D-volumetric results of these analyses can be inspected in detail on <http://neurovault.org/collections/FDWHFSYZ/>.

3.2.2.3 IBMA: Association of regional GMV and blood pressure across samples

3.2.2.3.1 Meta-analytic parametric relations between GMV and blood pressure

As expected, increases in SBP and DBP were associated with lower GMV. Specifically, higher SBP related to lower GMV in right paracentral/cingulate areas ([8,-30,56], $\text{SDM-Z} = -3.859$, $k=288$), bilateral inferior frontal gyrus (IFG, left: [-40,30,0], $\text{SDM-Z} = -3.590$, $k=49$; right: [-40,30,0], $\text{SDM-Z} = -3.394$, $k=16$), bilateral sensorimotor cortex (left: [-58,-20,24], $\text{SDM-Z} = -3.290$, $k=146$; right: [48,0,48], $\text{SDM-Z} = -3.196$, $k=127$), bilateral superior temporal gyrus (left: [-52,-10,6], $\text{SDM-Z} = -3.268$, $k=78$; right: [64,-42,12], $\text{SDM-Z} = -3.192$, $k=42$), bilateral cuneus cortex (left: [-8,-76,18], $\text{SDM-Z} = -3.019$, $k=27$; right: [10,-68,26], $\text{SDM-Z} = 2.937$, $k=18$), and right thalamus ([8,-28,2], $\text{SDM-Z} = -2.977$, $k=45$; Figure 4A, Table 5). Increases in DBP were related to lower GMV in bilateral anterior insula (left: [-36,26,6], $\text{SDM-Z} = -3.876$, $k=266$; right: [34,10,8], $\text{SDM-Z} = -3.139$, $k=100$), frontal regions ([-26,24,54], $\text{SDM-Z} = -3.820$, $k=62$), right midcingulate cortex ([4,-34,50], $\text{SDM-Z} = -3.545$, $k=246$), bilateral inferior parietal areas (left: [-46,-26,48], $\text{SDM-Z} = -3.239$, $k=59$; right: [44,-44,50], $\text{SDM-Z} = -3.188$, $k=18$), and right superior temporal gyrus ([60,2,-12], $\text{SDM-Z} = 2.991$, $k=35$; Figure 4B, Table 5).

Table 5 – Image-based meta-analysis results of regional gray matter volume differences associated with blood pressure. Image-based meta-analysis results of significant clusters yielding lower gray matter volume for the respective contrast of interest. Columns indicate cluster-specific MNI coordinates of peak voxels, meta-analytic SDM-Z-value, meta-analytic p-value, number of voxels in cluster and anatomical label of the peak voxel. Anatomical labels were assigned using SPM's Anatomy toolbox. Q and I² are measures of meta-analytic heterogeneity. Voxel threshold was set to p<0.005, peak height threshold was set to SDM-Z>1.0 and cluster extent threshold was set to k≥10 voxels as recommended by Radua et al. (2012). Final voxel size was 2 x 2 x 2 mm³. MNI: Montreal Neurological Institute. SDM: Seed-based d Mapping. SBP: Systolic blood pressure. DBP: Diastolic blood pressure.

	MNI (x/y/z)	SDM- Z	P	k	Peak Description	Q	I ²
<i>Negative Correlation with Systolic Blood Pressure</i>	8,-30,56	-3.859	0.000	288	Right paracentral lobule	0.000	0.0
	-40,30,0	-3.590	0.000	49	Left inferior frontal gyrus (p. triangularis)	0.053	0.0
	36,6,34	-3.394	0.000	16	Right inferior frontal gyrus (p. opercularis)	0.000	0.0
	10,2,40	-3.325	0.001	45	Right midcingulate cortex	0.000	0.0
	-58,-20,24	-3.290	0.001	146	Left postcentral gyrus	0.000	0.0
	-52,-10,6	-3.268	0.001	78	Left superior temporal gyrus	0.000	0.0
	48,32,10	-3.204	0.001	27	Right inferior frontal gyrus (p. triangularis)	0.000	0.0
	48,0,48	-3.196	0.001	127	Right precentral gyrus	0.000	0.0
	64,-42,12	-3.192	0.001	42	Right superior temporal gyrus	0.000	0.0
	6,8,-18	-3.110	0.001	40	Right subgenual cingulate cortex	0.000	0.0
	50,8,28	-3.045	0.002	26	Right inferior frontal gyrus (p. opercularis)	0.000	0.0
	-8,-76,18	-3.019	0.002	27	Left cuneus cortex	0.175	0.0
	8,-28,2	-2.977	0.002	45	Right thalamus	0.000	0.0
	10,-68,26	-2.937	0.002	18	Right cuneus cortex	0.000	0.0
	58,4,-8	-2.934	0.002	32	Right temporal pole	0.000	0.0
	-28,10,60	-2.896	0.003	19	Left middle frontal gyrus	0.000	0.0
	-52,-12,42	-2.860	0.003	10	Left postcentral gyrus	0.116	0.0
<i>Negative Correlation with Diastolic Blood Pressure</i>	-36,26,6	-3.876	0.000	266	Left insula	0.000	0.0
	-26,24,54	-3.820	0.000	62	Left middle frontal gyrus	0.000	0.0
	4,-34,50	-3.545	0.000	246	Right midcingulate cortex	0.000	0.0
	-60,-24,14	-3.462	0.000	90	Left supramarginal gyrus	0.000	0.0
	-46,-26,48	-3.239	0.001	59	Left inferior parietal lobule	0.000	0.0
	44,-44,50	-3.188	0.001	18	Right inferior parietal lobule	0.257	0.0
	36,8,32	-3.180	0.001	25	Right inferior frontal gyrus (p. opercularis)	0.000	0.0
	34,10,8	-3.139	0.001	100	Right insula	0.000	0.0
	28,14,60	-3.069	0.001	12	Right superior frontal gyrus	0.000	0.0
	62,-44,16	-2.991	0.002	35	Right superior temporal gyrus	0.000	0.0
	-38,14,-20	-2.983	0.002	30	Left temporal pole	0.000	0.0
	60,2,-12	-2.862	0.003	13	Right superior temporal gyrus	0.189	0.0
	-38,40,32	-2.845	0.003	14	Left middle frontal gyrus	0.000	0.0
	30,28,0	-2.796	0.003	14	Right insula	0.000	0.0
	-36,8,10	-2.788	0.003	24	Left insula	0.000	0.0
	-58,-46,30	-2.750	0.004	11	Left supramarginal gyrus	0.000	0.0
	-34,32,32	-2.734	0.004	11	Left middle frontal gyrus	0.201	0.0

Category 4 (SBP \geq 140 mmHg or DBP \geq 90 mmHg) < Category 1 (SBP<120 mmHg and DBP<80 mmHg)

-52,28,12	-3.473	0.000	107	Left inferior frontal gyrus (p. triangularis)	0.324	3.9
-48,-4,4	-3.322	0.000	93	Left rolandic operculum	0.297	1.8
18,-52,-48	-3.097	0.001	40	Right cerebellum, hemispheric lobule VIIIb	0.000	0.0
40,30,26	-3.093	0.001	10	Right inferior frontal gyrus (p. triangularis)	0.000	0.0
48,32,10	-3.064	0.001	48	Right inferior frontal gyrus (p. triangularis)	0.000	0.0
-38,48,-16	-3.014	0.001	40	Left inferior frontal gyrus (p. orbitalis)	0.000	0.0
-54,-12,42	-2.940	0.002	30	Left postcentral gyrus	0.000	0.0
-8,-76,18	-2.936	0.002	14	Left cuneus	0.000	0.0
-16,-36,-18	-2.872	0.002	24	Left cerebellum, hemispheric lobule V	0.000	0.0
12,-42,48	-2.854	0.002	11	Right midcingulate cortex	0.000	0.0
-12,-50,-56	-2.849	0.002	30	Left cerebellum, hemispheric lobule IX	0.325	4.0
10,-52,18	-2.836	0.002	21	Right precuneus	0.000	0.0
64,-44,14	-2.824	0.002	26	Right superior temporal gyrus	0.000	0.0
10,-66,28	-2.821	0.002	56	Right precuneus	0.000	0.0
6,-28,50	-2.792	0.003	16	Right midcingulate cortex	0.025	0.0
18,-54,22	-2.765	0.003	15	Right precuneus	0.000	0.0

Category 3 (SBP 130-139 mmHg or DBP 85-89 mmHg) < Category 1

36,6,34	-3.474	0.000	179	Right inferior frontal gyrus (p. opercularis)	0.000	0.0
6,-28,54	-3.119	0.000	179	Right posterior-medial frontal gyrus	0.127	0.0
48,-50,20	-2.917	0.000	74	Right middle temporal gyrus	0.000	0.0
-60,-20,36	-2.857	0.000	205	Left postcentral gyrus	0.000	0.0
-40,30,2	-2.598	0.000	24	Left inferior frontal gyrus (p. triangularis)	0.000	0.0
36,8,-18	-2.523	0.001	123	N/A (Right insula)	0.000	0.0
42,-74,12	-2.454	0.001	25	Right middle occipital gyrus	0.200	0.0
-62,-42,28	-2.433	0.001	41	Left supramarginal gyrus	0.000	0.0
20,-32,6	-2.384	0.001	133	Right thalamus	0.000	0.0
-10,36,-6	-2.384	0.001	102	Left anterior cingulate cortex	0.000	0.0
28,-94,-4	-2.373	0.001	14	Right inferior occipital gyrus	0.000	0.0
-12,-32,0	-2.264	0.002	133	Left thalamus	0.237	0.0
-56,-64,16	-2.222	0.002	28	Left middle temporal gyrus	0.050	0.0
-40,8,30	-2.197	0.002	82	Left precentral gyrus	0.000	0.0
-12,-54,14	-2.187	0.002	20	Left precuneus	0.000	0.0

Category 2 (SBP 120-129 mmHg or DBP 80-84 mmHg) < Category 1

-54,-10,14	-3.407	0.000	230	Left rolandic operculum	0.016	0.0
30,-96,-8	-3.290	0.000	102	Right inferior occipital gyrus	0.038	0.0
-34,-16,-30	-3.164	0.000	133	Left fusiform gyrus	0.000	0.0
-8,-54,22	-3.084	0.000	433	Left precuneus	0.000	0.0
54,-24,32	-2.968	0.000	31	Right supramarginal gyrus	0.019	0.0
-46,28,0	-2.942	0.000	41	Left inferior frontal gyrus (p. triangularis)	0.000	0.0
-64,-20,30	-2.939	0.000	227	Left postcentral gyrus	0.000	0.0
-62,-42,34	-2.876	0.000	68	Left supramarginal gyrus	0.000	0.0
-36,-64,42	-2.827	0.001	30	Left angular gyrus	0.000	0.0
18,-72,54	-2.804	0.001	40	Right superior parietal lobule	0.083	0.0
46,-74,12	-2.734	0.001	26	Right middle temporal gyrus	0.000	0.0

8,-18,46	-2.647	0.001	32	Right midcingulate cortex	0.000	0.0
56,-32,12	-2.470	0.002	52	Right superior temporal gyrus	0.000	0.0
28,-72,-38	-2.413	0.002	23	Right cerebellum, crus I	0.000	0.0
-62,-22,-30	-2.403	0.003	11	N/A (Left inferior temporal gyrus)	0.000	0.0

3.2.2.3.2 Meta-analytic differences in regional GMV between blood pressure categories
 Meta-analytic results for category 4 (highest blood pressure) compared to category 1 (lowest blood pressure) yielded lower regional GMV in frontal, cerebellar, parietal, occipital, and cingulate regions (Figure 4C). Table 5 describes the specific regions with lower GMV, including bilateral IFG (left: [-52,-28,12], SDM-Z=-3.473, $k=107$; right: [40,30,26], SDM-Z=-3.093, $k=10$), right midcingulate cortex ([12,-42,48], SDM-Z=-2.854, $k=11$), and right precuneus ([10,-52,18], SDM-Z=-2.836, $k=21$). We also compared GMV of individuals at sub-hypertensive levels (category 3 and 2, respectively) to GMV of individuals in category 1. Figure 4D shows meta-analysis results for the comparison between category 3 and category 1. Compared to category 1, category 3 was associated with lower GMV in bilateral IFG (left: [-40,30,2], SDM-Z=-2.598, $k=24$; right: [36,6,34], SDM-Z=-3.474, $k=179$), sensorimotor cortices (left: [-60,-20,36], SDM-Z=-2.857, $k=205$; right: [6,-28,54], SDM-Z=-3.119, $k=179$), bilateral middle temporal gyrus (left: [-56,-64,16], SDM-Z=-2.222, $k=28$; right: [48,-50,20], SDM-Z=-3.119, $k=179$), right insula ([36,8,-18], SDM-Z=-2.523, $k=123$), right occipital regions ([42,-74,12], SDM-Z=-2.454, $k=25$), left parietal ([-60,-20,36], SDM-Z=-2.857, $k=205$), bilateral thalamus (left: [-12,-32,0], SDM-Z=-2.264, $k=133$; right: [20,-32,6], SDM-Z=-2.384, $k=133$), left anterior cingulate cortex ([-10,36,-6], SDM-Z=-2.384, $k=102$), and left precuneus ([-12,-54,14], SDM-Z=-2.187, $k=20$; Table 5).

Figure 4E illustrates brain regions that yielded meta-analytic GMV decreases for category 2 compared to category 1. These include left frontal regions ([-54,-10,14], SDM-Z=-3.407, $k=230$), right inferior occipital gyrus ([30,-96,-8], SDM-Z=-3.290, $k=102$), bilateral temporal regions (left: [-34,-16,-30], SDM-Z=-3.164, $k=133$; right: [46,-74,12], SDM-Z=-2.734, $k=26$), left precuneus ([-8,-54,22], SDM-Z=-3.084, $k=433$) and inferior parietal regions (supramarginal, [54,-24,32], SDM-Z=-2.968, $k=31$, and angular gyri, [-36,-64,42], SDM-Z=-2.827, $k=30$), as well as midcingulate cortex ([8,-18,46], SDM-Z=-2.647, $k=32$; Table 5).

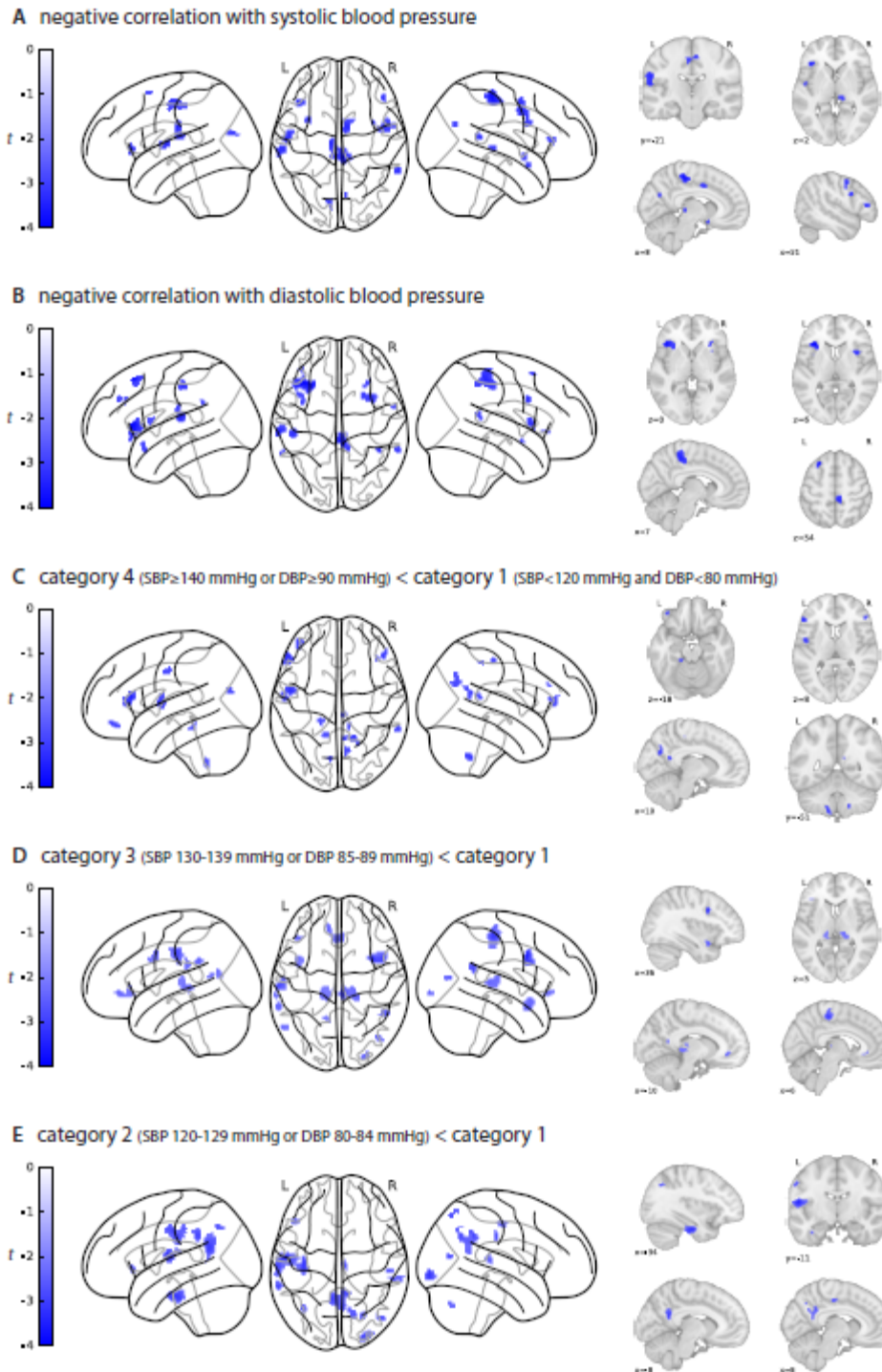


Figure 4 – Meta-analytic differences in gray matter volume between blood pressure categories
 Glass brain views of image-based meta-analysis results for the blood pressure category contrasts of interest with relevant slice views below (A-E). A and B depict associations between higher SBP/DBP, respectively, and lower gray matter volume, i.e. negative correlations. Blue clusters indicate meta-analytic grey matter volume differences for the given contrast at a voxel threshold of $p < 0.005$ with peak height threshold of $\text{SDM-Z} < -1.0$ and cluster extent threshold of $k \geq 10$ (validated for high meta-analytic sensitivity and specificity, Radua et al. 2012). Color bars represent SDM-Z values. 3D-volumetric results of these analyses can be inspected in detail on <http://neurovault.org/collections/FDWHFSYZ/>. SDM: Seed-based d Mapping. SBP: Systolic blood pressure. DBP: Diastolic blood pressure. L: Left hemisphere. R: Right hemisphere.

3.2.2.3.3 Meta-analytic differences in regional hippocampal and amygdalar volumes between blood pressure categories

In this IBMA ROI comparison, SBP was negatively correlated with bilateral posterior medial hippocampal volume (Figure 5). DBP negatively correlated with left hippocampal volume and right anterior hippocampal volume. Furthermore, all higher blood pressure categories were associated with lower regional hippocampal volume when compared to the lowest blood pressure category 1 (Figure 5). Compared to category 1 and across samples, blood pressure category 4 was predominantly associated with lower left medial posterior hippocampus volume and category 3 with lower bilateral posterior and left medial hippocampus volume. Smaller volume associated with category 2 was predominantly located in left lateral anterior hippocampus. Category 4 vs. category 1 and the correlation with SBP and DBP also yielded significantly lower regional volume in bilateral amygdala, respectively. Effect sizes highly varied across samples (Figure 5).

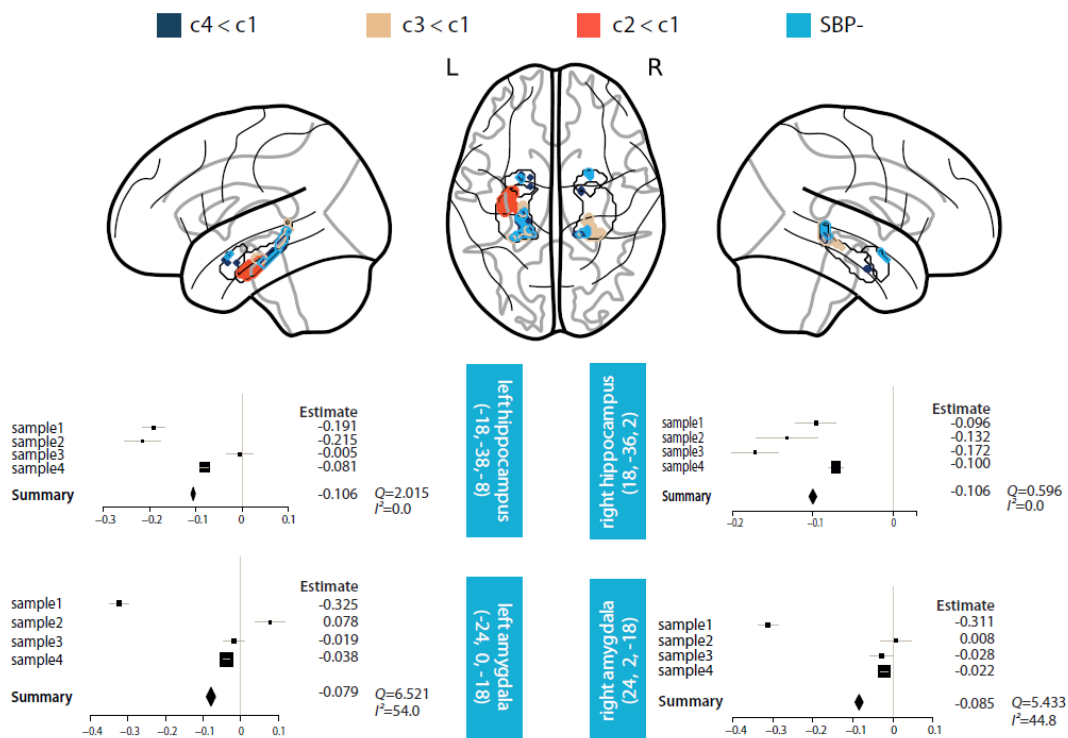


Figure 5 – Meta-analytic differences in volumes of hippocampus and amygdala (Region-of-Interest analysis)

Upper part of plot: Glass brain views of image-based meta-analysis ROI results for the blood pressure category contrasts of interest in bilateral hippocampus and amygdala masks. Voxel threshold was set to $p < 0.05$ with a peak height threshold of $\text{SDM-Z} < -1.0$ and a cluster extent threshold of $k \geq 1$. Lower part of plot: Exemplary forest plots of sample-specific peak voxels' effect sizes for the negative correlation with SBP in the respective ROI. The box sizes are determined by each sample's weight. Light blue boxes include ROI name and MNI coordinates of the peak voxel. Q and I^2 are measures of meta-analytic heterogeneity. Definition of blood pressure categories: *category 1* (SBP < 120 mmHg and DBP < 80 mmHg), *category 2* (SBP 120-129 mmHg or DBP 80-84 mmHg), *category 3* (SBP 130-139 mmHg or DBP 85-89 mmHg) and *category 4* (SBP \geq 140 mmHg or DBP \geq 90 mmHg). SBP-: negative correlation with SBP. ROI: Region of Interest. SDM: Seed-based d Mapping. MNI: Montreal Neurological Institute. SBP: Systolic blood pressure. DBP: Diastolic blood pressure. L: Left hemisphere. R: Right hemisphere.

3.2.2.3.4 Meta-analytic positive relations between GMV and blood pressure

Exploratory analyses also revealed positive associations between blood pressure and GMV (Supplementary Figure 1, Supplementary Table 2, NeuroVault maps). However, the cumulative positive effects are comparably weaker than the cumulative negative results (negative: 17 out of 34 clusters from parametric analyses with $\text{SDM-Z} > 3.0$; positive: 0 out of 28 clusters from parametric analyses with $\text{SDM-Z} > 3.0$), they show greater heterogeneity across studies (negative: maximum $I^2 = 4.0$; positive: maximum $I^2 = 56.3$) and they seem to appear primarily in regions where standard preprocessing of brain tissue is suboptimal (e.g. in cerebellum/inferior occipital regions (Diedrichsen, 2006)). We therefore regard these findings as overall questionable. By also providing the results as statistical maps on NeuroVault, future investigations can use the data for reliability analyses of potential positive associations.

3.2.2.4 *Volumetry in pooled sample: Association of total brain volumes and blood pressure*

None of the volumetric brain measures (TIV, total GMV, total white matter volume, total CSF volume, total hippocampal, total amygdalar volume and total WMH) were significantly associated with SBP or DBP in the correlation models, nor with blood pressure categories in the ANOVA models (all $p > 0.05$, Table 3).

3.2.2.5 *Supplementary analysis of first blood pressure reading*

Intra-individual blood pressure variation and white coat hypertension are important to consider when measuring blood pressure (Pickering et al., 2005). For the meta-analyses, we had reasoned that the most accurate and generalizable basis for estimation of individual blood pressure is the inclusion of all available blood pressure readings within each sample for each participant (i.e. following the intention of the blood pressure measurement in each included study). Since blood pressure measurement protocols differed between the study samples, this approach resulted in the inclusion of blood pressure values from different numbers of blood pressure measurements: in samples 1, 2 and 4, ≥ 2 blood pressure readings were taken in varying time intervals and averaged for analyses ($n = 353$). In sample 3, only one blood pressure reading was available and used for analyses ($n = 70$). We accounted for sample differences by employing random-effects models in IBMA (Higgins & Green, 2011; Radua et al., 2012). Alternatively, by analyzing the first blood pressure reading only, an important difference between the studies would be eliminated, while a potential white coat effect would be possibly emphasized. Followingly, we recalculated one crucial parametric analysis with only the first systolic

blood pressure reading in each study. We chose to reanalyze this contrast since it had the largest difference between the first and average blood pressure readings (note that even in this case the readings overall correlated strongly, Supplementary Figure 2C).

The results of this analysis and the results of the previous analysis (with averaged SBP measurements, as reported above) are presented in Supplementary Table 3 and Supplementary Figure 2A-B for comparison. The results are strikingly similar: for the analysis based on just the first blood pressure reading, several clusters even showed stronger statistical results.

3.2.3 Discussion

In this image-based meta-analysis of four previously unpublished independent samples, we found that elevated, sub-hypertensive blood pressure was correlated with lower GMV in several brain regions, including parietal, frontal, and subcortical structures in young adults (<40 years). These regions are consistent with the lower regional GMV observed in middle-aged and older individuals with HTN (Beauchet et al., 2013; den Heijer et al., 2005; Hajjar et al., 2010; Leritz et al., 2011; Power et al., 2016; Raz et al., 2005). Our results show that blood pressure-associated gray matter alterations emerge earlier in adulthood than previously assumed and continuously across the range of blood pressure.

Interestingly, we found that blood pressure was associated with lower hippocampal volume. In older individuals, the hippocampal formation and surrounding structures are known to be affected by HTN (Beauchet et al., 2013; den Heijer et al., 2005; Petrovitch et al., 2000; Power et al., 2016; Raz et al., 2005). In a meta-analytic evaluation of HTN-effects on total GMV and on hippocampal volume, lower volumes across studies were only consistently found for the hippocampus (Beauchet et al., 2013). In analogy to those findings, our results showed that hippocampal volume was affected by higher blood pressure in a considerably younger sample. It should be mentioned that the effects in hippocampus only exceeded statistical thresholds in ROI analyses, similar to previous reports of lower hippocampal volume in older samples with manifest HTN that were all ROI-based (Beauchet et al., 2013; den Heijer et al., 2005; Power et al., 2016; Raz et al., 2005). As potential pathophysiological explanations it has been proposed that medial temporal (and frontal regions) might be especially sensitive to effects of pulsation, hypoperfusion and ischemia, which often result from increasing pressure (Beauchet et al., 2013; Iadecola et al., 2016).

We furthermore observed negative correlations between amygdalar and thalamic volumes and blood pressure, notably already below levels which are currently regarded as hypertensive. Amygdalar and thalamic nuclei are substantially involved in blood pressure

regulation as they receive baroreceptor afferent signals via the brainstem and mesencephalic nuclei, relaying these signals to primary cortical regions of neuro-vegetative integration, such as anterior cingulate cortex and insula (Critchley & Harrison, 2013). It has been shown that lower amygdalar volume correlates with increased blood pressure-reactivity during cognitive demand among young normotensive adults (Gianaros et al., 2008). Previous studies have reported lower thalamic volume in HTN (Power et al., 2016), heart failure (Woo, Macey, Fonarow, Hamilton, & Harper, 2003), asymptomatic carotid stenosis (Avelar et al., 2015), and aging (Lorio et al., 2014). Higher SBP has also been related to higher mean diffusivity of white matter thalamic radiations (Maillard et al., 2012). Our results are in line with accumulating evidence of amygdalar and thalamic involvement in cardiovascular (dys-) regulation but may also reflect early pathology in these regions. For example, occurrence of neurofibrillary tangles in thalamus has also been reported in the earliest stages of AD neuropathology (Braak & Braak, 1991).

Beyond subcortical structures, we found lower volumes in cortical regions: cingulate volume and insular volume were markedly lower with higher DBP in the meta-analysis results and in the individual analyses of sample 1. As noted above, these regions constitute primary cortical sites of afferent neuro-vegetative integration and modulate homeostasis via efferents to brainstem nuclei (Critchley & Harrison, 2013). Lesions in cingulate cortex and insula result in altered cardiovascular regulation, increased sympathetic tone (Critchley et al., 2003; Oppenheimer, Kedem, & Martin, 1996) and myocardial injury (Krause et al., 2017). Both regions are also critical for the appraisal and regulation of emotion and stress (Critchley & Harrison, 2013). Thus, structural alterations in these regions may contribute to insidious blood pressure elevations via sympathetic pathways. However, based on our data we can only speculate about the involvement of such mechanisms for our results.

Frontal and parietal volumes were affected in all our statistical comparisons. The precuneus cortex, especially, was associated with lower GMV in blood pressure categories 4, 3, and 2 compared to category 1. Our results of lower blood pressure-related GMV in regions such as hippocampal, frontal and parietal areas highlight specific brain regions which are known to be vulnerable to putative vascular or neurodegenerative damage mechanisms (Beauchet et al., 2013; den Heijer et al., 2005; Dickerson et al., 2011; Hajjar et al., 2010; Leritz et al., 2011; Petrovitch et al., 2000; Power et al., 2016; Raz et al., 2005). Raised midlife blood pressure is not only known to be a major risk factor for vascular dementia, but some reports suggest a link between HTN and AD-type pathophysiology (Iadecola et al., 2016; Norton et al., 2014). For example in neuropathological studies, raised midlife blood pressure has been associated with lower post-mortem brain weight,

increased numbers of hippocampal neurofibrillary tangles, and higher numbers of hippocampal and cortical neuritic plaques (Petrovitch et al., 2000). Similarly, a potential pathophysiological link between HTN and AD has been supported by noninvasive MRI studies: regions referred to as AD-signature regions (including inferior parietal, precuneus cortices, and medial temporal structures) have been associated with cortical thinning years before clinical AD-symptoms arise (Dickerson et al., 2011) and with brain volume reductions predicted by increasing blood pressure from middle to older age (Power et al., 2016). In light of these previous results, our findings of lower blood pressure-related GMV in AD-signature regions may be indicative of a link to AD-pathology at an even earlier age; however, this cannot be causally inferred from our cross-sectional data. In the study by Power et al. (2016), blood pressure also predicted volume loss in non-AD-typical brain regions, such as frontal lobe and subcortical gray matter, which may relate to other (than AD-related) pathophysiological mechanisms. A similar pattern seems to be reflected in our findings of lower GMV related to higher blood pressure in non-AD-typical regions.

Some previous studies did not find relations between HTN and lower brain volumes, but associated HTN with other forms of structural or functional brain alterations, such as white matter injury (Allan et al., 2015) or reduced cerebral perfusion (Muller et al., 2010). A key aspect of diverging results is the heterogeneity of methods used to assess brain volumes. Earlier investigations of blood pressure effects on brain tissues have applied manual or automated volumetric methods to quantify total brain volumes in pre-selected ROIs (Debette et al., 2011; den Heijer et al., 2005; Raz et al., 2005). The focus of this study was to employ computational anatomy methods to assess *regional gray matter differences across the whole brain*. We found significant differences between blood pressure groups using VBM but not in the analysis of total brain volumes. This supports the view that VBM is a sensitive measure to quantify regional morphological differences (Kennedy et al., 2009) which might be undetected from the analysis of total brain volumes alone. In addition, we employed random-effects IBMA which results in effects that are consistent across studies and that may otherwise be neglected at sub-threshold. Investigating effects of blood pressure on regional vs. total brain volumes at all stages of health and disease thus warrants further research with standardized methods to identify neuropathological mechanisms.

Our data, however, do not allow inference on causality between lower brain volumes and HTN, which likely involves complex interactions of different pathophysiological mechanisms that still need to be fully elucidated. It is assumed that vascular stiffness, endothelial failure and a dysfunctional blood-brain barrier are precursors of cerebral small and large vessel disease that reduce cerebral blood flow, disturb autoregulatory

adjustment and decrease vasomotor reactivity, which may impair perivascular central nervous waste clearance systems (Iadecola et al., 2016). These mechanisms have also been suggested to potentially underlie the epidemiological connection between vascular risk factors, such as HTN, and AD (Iadecola et al., 2016). The similarities between our findings and AD-signature regions (see above) would also be consistent with this putative link. Consequently, demyelination, apoptosis and intoxication of neurons and glial cells, as well as gray and white matter necrosis accumulate and may be reflected in neuroimaging on a macroscopic scale. Lower GMV assessed by VBM, as reported in our study, can thus arise from neuronal loss, but also from alterations of glial cells or composition of microstructural or metabolic tissue properties (Tardif et al., 2017). Our findings point to an early effect of such mechanisms on gray matter integrity which is present in the absence of overt disease, such as HTN, and in young age. Indicators of early atherosclerosis in major peripheral arteries can already be detected in youth (Strong et al., 1999). Recently, arterial stiffness has also been associated with white matter and gray matter alterations among adults between 24 and 76 years of age (Maillard et al., 2016). Thus, already early and subtle vascular changes, deficient cerebral perfusion and impaired perivascular clearance systems may initiate and sustain neuropathology from early to late adulthood.

The cross-sectional design of our four study samples limits the interpretation frame for the results presented. Causality between blood pressure and potential brain damage cannot be assessed with these data but is crucial for implications of early signs of cerebrovascular disease. Furthermore, the study samples differed regarding recruitment, sex distribution, sample size, prevalence of high blood pressure, and data acquisition methods (blood pressure and MRI) which might not represent the general population or standard acquisition protocols: similar to German prevalence (Neuhauser et al., 2015), men had higher blood pressure in our study. We thus included sex as covariate in all our analyses to adjust for sex effects. We did not perform separate analyses for men and women given that one of the four samples included only men. However, the topic of sex differences in brain structure related to blood pressure is a very interesting open question for future investigations.

In sample 3, only one blood pressure measurement was recorded which could be biased due to white coat hypertension or blood pressure variability. Practice guidelines recommend an average of ≥ 2 seated readings obtained on ≥ 2 occasions to provide a more accurate estimate of an individual's blood pressure level (Chobanian et al., 2003; Mancia et al., 2013; Whelton et al., 2017). By combining the samples in random-effects IBMA, we considered the limitations of each sample and accounted for within- and between-sample heterogeneity and evaluated effects cumulatively. Moreover, this approach enabled us to

investigate the expected small effects of blood pressure-related gray matter alterations in a well-powered total sample of over 400 young adults. To further ensure that the results are not substantially influenced by the heterogeneity of blood pressure measurements across studies, we recalculated the parametric SBP analysis (Figure 4A) with only the first SBP reading in each study. The results of this additional analysis are strikingly similar to the results reported here (Supplementary Figure 2). HTN is also the most important risk factor for WM damage (Debette et al., 2011; Iadecola et al., 2016) and sub-clinical white matter injury in relation to elevated blood pressure levels has recently been reported in 19- to 63-year-old adults (Maillard et al., 2012). As our study included only gray matter measures, we cannot assess mediating effects of WM injury on GMV differences. We did not observe any significant differences in Fazekas scores for WMH between blood pressure categories, likely due to the lower sensitivity and poorer specificity as a proxy for vascular disease in a sub-clinical sample of young adults with (mostly) normal blood pressure.

Our study shows that blood pressure-related brain alterations may occur in early adulthood and at blood pressure levels below current thresholds for manifest HTN. Contrary to assumptions that blood pressure-related brain damage arises over years of manifest disease our data suggest that subtle pressure-related GM alterations can be observed in young adults without previously diagnosed HTN. Considering our results, large-scale cohort studies should investigate whether sub-hypertensive blood pressure and related brain changes in early adulthood increase the risk for subsequent development of CVD later in life. Gaining insights whether and how the brain is globally affected by vascular changes or if these are specific to susceptible regions could help identifying neuroimaging biomarkers for the earliest stages of CVD. Such data would provide evidence for future guidelines to formulate informed recommendations for blood pressure-management in young adults, which are critical for the prevention of CVD. Lifestyle interventions and neurobehavioral therapy have recently been suggested to benefit CVD prevention (Grossman et al., 2017). Our results highlight the importance of taking blood pressure levels as a continuous measure into consideration which could help initiate such early preventive measures.

3.3 Study 4: The Age-Dependent Relationship Between Resting Heart Rate Variability and Functional Brain Connectivity. Kumral, Schaare et al., NeuroImage (2019)

Heart rate variability (HRV), is known to be an indicator of parasympathetic cardiovascular regulation, which typically decreases with age (De Meersman & Stein, 2007; Umetani, Singer, McCraty, & Atkinson, 1998). By using the MPILMBB database (Babayan et al., 2019; Mendes et al., 2019), we were able to investigate the relationship between HRV and the brain across the lifespan. In this study we hypothesized that the relationship between HRV and brain structure and function is age dependent. The study has been published as a peer-reviewed article and can be reviewed in its entirety elsewhere (Kumral et al., 2019). In brief, 388 healthy participants of three age groups (140 younger: 26.0 ± 4.2 years, 119 middle-aged: 46.3 ± 6.2 years, 129 older: 66.9 ± 4.7 years) underwent resting ECG recordings, T1-weighted MRI and resting-state fMRI at 3T as part of the LEMON or LIFE protocol, respectively (see studies 1, 2 and 3 for details on the protocols). We derived gray matter volume and resting-state functional connectivity (i.e. eigenvector centrality, seed-based functional connectivity) and related those measures to resting HRV, quantified as the root mean square of successive differences (RMSSD). In line with previous studies, we found that resting HRV decreased with age. There were no statistically significant effects for age groups between HRV and gray matter volumes. However, in whole-brain functional connectivity analyses, we found an age-dependent association between resting HRV and eigenvector centrality in the bilateral ventromedial prefrontal cortex ($p_{FWE}=0.005$, peak MNI coordinates: [0, 57, -6], $k=62$, $F=10.79$). Post-hoc two-sample t-tests revealed that this effect was stronger in the young age group compared to the middle and old age groups, respectively (young>old: $p_{FWE}<0.001$, [0, 57, -6], $k=131$, $T=4.51$; young>middle: $p_{FWE}=0.005$, [3, 45, -6], $k=85$, $T=4.13$). We furthermore explored the underlying HRV-related whole-brain network by using this ventromedial prefrontal cortex cluster in seed-based functional connectivity analyses. This analysis yielded a stronger relation between HRV-related ventromedial prefrontal cortex connectivity and a cortico-cerebellar network in younger but not in middle-aged or older adults (ANOVA: $p_{FWE}=0.049$, [33, -42, -45], $k=46$, $F=15.19$; young>old: $p_{FWE}=0.032$, [33, -42, -45], $k=67$, $T=4.66$; young>middle: $p_{FWE}<0.001$, [33, -42, -45], $k=189$, $T=5.08$). Across all age groups, HRV was positively correlated with eigenvector centrality in the bilateral posterior cingulate cortex/precuneus ($p_{FWE}=0.005$, MNI coordinates: [0, -54, 36], $k=204$, $T=5.39$). Our results indicate that the decrease of HRV with age is accompanied by changes in functional connectivity along the cortical midline in healthy adults between 20 and 80 years of age. Our main findings are correlations between resting HRV and functional connectivity in the posterior cingulate

cortex across all age groups and in the ventromedial prefrontal cortex in young but not in middle-aged or older participants. The findings support the view that the well-known HRV decrease with age may have a functional brain network correlate along the cortical midline. Consistent with the role of these areas in affective, cognitive, and autonomic regulation (Benarroch, 1993; Thayer, Åhs, Fredrikson, Sollers, & Wager, 2012), these results provide a comprehensive picture of the differential effect of aging on heart-brain interactions. This extends our knowledge of brain-body interactions and their changes over the lifespan and emphasizes the importance of parasympathetic cardio-regulation in healthy aging.

3.4 Study 5: Acute Psychosocial Stress Alters Thalamic Network Centrality.

Reinelt, Uhlig...Schaare et al., *NeuroImage* (2019)

Stress triggers a broad range of psychophysiological responses, which are controlled by the brain, and has implications in the development of high blood pressure (McEwen & Gianaros, 2011). In this study, we investigated how acute psychosocial stress is reflected in whole-brain network topology. It builds on the MPILMBB database (Babayán et al., 2019; Mendes et al., 2019) and extends it by an additional testing day, where a psychosocial stress experiment, structural and resting-state fMRI and subjective, autonomic, and endocrine measures of stress were assessed throughout the experiment. The study has been published as a peer-reviewed article and can be reviewed in its entirety elsewhere (Reinelt et al., 2019). In brief, in this randomized study 67 young men (age range=18-35 years) participated in the Trier Social Stress Test (TSST, $n=33$, mean age=25.45 years) or a placebo TSST as control ($n=34$, mean age=26.18 years). The experimental procedure included 15 timepoints at which saliva and subjective experience samples were collected, 14 timepoints at which blood samples were collected by an intravenous catheter, two rs-fMRI scans and one anatomical MRI scan before the intervention, as well as four rs-fMRI scans and one anatomical MRI scan after the intervention. Heart rate was recorded throughout the entire duration of the experimental procedure. The main results of the study are as follows. First, the intervention group showed an immediate, stress-driven increase in eigenvector centrality in a sub-cortical cluster peaking in the thalamus ($p_{FWE}=0.011$, peak MNI coordinates: [-6, -26, 2], $k=335$, $T=4.14$). The interaction effect of timepoint by group overlapped with the thalamus cluster and showed an extension to bilateral putamen and caudate nucleus ($p_{FWE}< 0.001$, [-26, 12, -6], $k=545$, $T=5.24$; $p_{FWE}< 0.001$, [28, 14, -8], $k=1336$, $T=4.5$). The thalamic cluster was used as a seed in an exploratory whole-brain analysis which showed its connections to widespread brain regions, including parietal and temporal regions; the latter comprising

bilateral hippocampus and amygdala. Second, the stress-related EC increase was more pronounced in participants who also showed stronger stress-related changes in subjective (visual analog scale) as well as – to a lesser extent – autonomic (HRV), and endocrine (saliva cortisol) measures. Third, and diverging from our hypotheses, the stress-driven elevation of eigenvector centrality did not recover within 105 min after stress onset. Eigenvector centrality values did decrease at 50 min after stressor onset but then increased again (at least) until the 105 min after stressor onset. Our results show that thalamic areas are central for information processing after stress exposure and underlie stress-related connectivity changes across the whole brain. The thalamus has been implicated in various mechanisms and conditions, ranging from homeostasis, emotion and motivation to post-traumatic stress disorder and psychopathology (Critchley & Harrison, 2013; Giraldo-Chica & Woodward, 2017; Greicius et al., 2007; Yin et al., 2011). Thalamic connectivity may generally provide an interface for the stress response in the rest of the body and in the mind.

3.5 Study 6: Neural Control of Vascular Reactions: Impact of Emotion and Attention. Okon-Singer...Schaare et al., *Journal of Neuroscience* (2014)

The study has been published as a peer-reviewed article and can be reviewed in its entirety elsewhere (Okon-Singer et al., 2014). In brief, this study investigated neural mechanisms involved in blood pressure regulation of aversive information. In the context of human evolution, cardiovascular reactivity to threatening stimuli was an adaptive response to facilitate sensorimotor behavior designed for fight-or-flight reactions (Lang et al., 2000). However, such reactions are frequently inappropriate for the mostly psychosocial challenges faced in the modernized world. Thus, an additional aim of the study was to identify potential cognitive ways to modulate emotion-related neural and blood pressure responses by allocation of attentional resources. Twenty-four healthy adults (11 females; age=24.75±2.49 years) participated in an affective perceptual load task that manipulated attention to negative/neutral distractor pictures (Okon-Singer, Tzelgov, & Henik, 2007). In the task, participants discriminated a target letter among few (low attentional load) or many (high attentional load) distractor letters, whereas they were asked to ignore simultaneously presented distractor pictures that were either aversive or neutral. This paradigm allows for the direct investigation of executive attentional effects on emotional processing. Participants performed the task while fMRI was collected simultaneously with continuous recording of peripheral blood pressure. A parametric

modulation analysis examined the impact of attention and emotion on the relation between neural activation and blood pressure reactivity during the task. When attention was available for processing the distractor pictures, negative pictures resulted in behavioral interference, neural activation in brain regions previously related to emotion, a transient decrease of blood pressure, and a positive correlation between blood pressure response and activation in a network including prefrontal and parietal regions, the amygdala, caudate, and mid-brain. These effects were modulated by attention: behavioral and neural responses to negative distractor pictures (compared with neutral pictures) were smaller or diminished, as was the negative blood pressure response when the central task involved high perceptual load. Furthermore, comparing high and low load revealed enhanced activation in frontoparietal regions implicated in attention control. Our results fit theories emphasizing the role of attention in the control of behavioral and neural reactions to irrelevant emotional distracting information (Iordan, Dolcos, & Dolcos, 2013; Okon-Singer, Lichtenstein-Vidne, & Cohen, 2013). Our findings furthermore extend the function of attention to the control of autonomous reactions associated with negative emotions by showing altered blood pressure reactions to emotional stimuli, which is consistent with the effect of emotion regulation on autonomic reactions (Dan-Glauser & Gross, 2011). The latter being of potential clinical relevance as it may provide a basis for establishing preventive strategies for individuals at risk of developing hypertension.

4 General Discussion and Outlook

The aim of this thesis was to narrow the knowledge gap of the complex interrelation between the brain, blood pressure control and hypertension. This was achieved by (i) the construction of a publicly available database to promote investigations on mind-brain-body dynamics during aging (studies 1 and 2) (Babayán et al., 2019; Mendes et al., 2019), (ii) using this database in addition to other large datasets to conduct an image-based meta-analysis on the relevance of blood pressure for brain structural integrity in young adults at sub-hypertensive blood pressure levels (study 3) (Schaare et al., 2019), (iii) using the database to examine the relationship between intrinsic functional brain connectivity and other vascular risk factors (heart rate variability in study 4 (Kumral et al., 2019); acute psychosocial stress in study 5 (Reinelt et al., 2019)), (iv) and by delineating the neural signatures of blood pressure regulation to emotional distress (study 6) (Okon-Singer et al., 2014).

In study 3, we assessed how blood pressure relates to brain structure in non-hypertensive adults below 40 years of age (Schaare et al., 2019). By using structural MRI at 3 Tesla in 423 young adults, we showed that higher blood pressure, below the hypertensive threshold of 140/90 mmHg, was associated with lower gray matter volumes in regions that have previously been shown to relate to hypertension in older individuals or cardiovascular dysregulation, such as hippocampus, amygdala, thalamus, frontal and parietal structures (e.g. precuneus). The results of this study show that brain structure is associated with blood pressure in young age and in ranges that are typically considered “normal”.

Studies 4 and 5 showed that intrinsic functional connectivity of neuro-vegetative brain regions relates to vascular risk factors: In study 4, we found that the well-known decrease of HRV with age has a functional brain network correlate in the posterior cingulate cortex and in the ventromedial prefrontal cortex. Whereas in study 5, we showed that thalamic areas are central for information processing after psychosocial stress exposure and underlie stress-related connectivity changes across the whole brain.

To gain a better understanding of the mechanisms underlying the brain’s role in blood pressure control, in study 6, we assessed how the brain integrates blood pressure reactivity to emotional stimuli and how these processes can be modulated by executive attention (Okon-Singer et al., 2014). The main results were a positive correlation between blood pressure response and activation in a network including prefrontal and parietal regions, the amygdala, caudate, and mid-brain. As expected, the effects were modulated by attention yielding smaller or diminished neural, behavioral and vascular responses when attentional load was high.

Overall, our results show that blood pressure is strongly intertwined with brain processes (Schaare et al., 2019) that control and regulate autonomic responses (Kumral et al., 2019; Reinelt et al., 2019). In combination with other recent studies, our findings contribute to a better understanding of the underlying mechanisms driving initial blood pressure elevations (Gianaros et al., 2017; Okon-Singer et al., 2014). Identifying pathological pathways to blood pressure elevations is a major goal for the prevention of hypertension and adverse secondary effects of elevated blood pressure.

Besides genetic and biological aspects, current research suggests that the etiology of essential hypertension is crucially dependent on lifestyle factors. For example psychosocial factors, such as work conditions, mental health, living situation, social support, and sleep have been shown to increase the risk of hypertension (Cuffee et al., 2014). Psychiatric conditions, including depression and anxiety disorders, show a high co-occurrence with hypertension and cardiovascular disease (Cohen et al., 2015; Hamer et al., 2010). Others argue that chronic psychological stress is in fact a cause of essential hypertension (Esler et al., 2008). As we showed in studies 5 and 6, acute psychosocial stress or aversive stimulation lead to rapid autonomic, endocrine, and neural changes in CAN regions among others. The CAN, a network of cortico-limbic and subcortical brain regions, is the primary integrator of neuro-vegetative coupling and regulates bodily responses in service of adaptive behaviors (Benarroch, 1993; Critchley & Harrison, 2013; Gianaros & Sheu, 2009). These same regions have been found in neuroimaging studies of blood pressure reactivity in response to stress or emotions, which implies their involvement in the mediation of blood pressure reactivity to psychosocial stressors (Critchley et al., 2000; Gianaros & Sheu, 2009; Gianaros et al., 2008, 2017; Okon-Singer et al., 2014). Individual differences in such neural and vascular response patterns to stressful or emotional demand, in turn, may relate to the development of hypertension and heart disease (Gianaros & Sheu, 2009). Macefield and colleagues (2013) demonstrated that repetitive mental stress, as observed in panic disorder and essential hypertension, drives hyperactivity of the sympathetic nervous system which is coupled with brain activity in regions including midbrain, anterior insula, posterior cingulate and precuneus. It has thus been proposed that the development of essential hypertension can be regarded as a consequence of repetitive stressor-related blood pressure reactivity which is orchestrated by autonomic brain regions (Esler et al., 2008; Jennings & Zanstra, 2009; Rau & Elbert, 2001). In this view, a loop of neural processes drives chronic blood pressure increases and vascular pathology as follows: (i) repetitive psychosocial stress prompts enhanced reactivity of blood pressure and in neuro-vegetative networks; (ii) over time this leads to hyperactivity of the sympathetic nervous system, renin-angiotensin mechanisms and sub-

clinical vascular damage, all of which interfere with regulatory functions; (iii) followingly, these changes result in enhanced blood pressure reactivity to a magnitude of stress which required lower reactivity previously.

Support for this 'neurogenic' hypothesis of essential hypertension comes from studies which compared neuropsychological performance and neuroimaging patterns between young, normotensive individuals at genetic risk for essential hypertension and controls. The risk for essential hypertension is hereditary. Compared to healthy controls, stressor-evoked vascular reactivity is larger and follows a distinct pattern in patients with hypertension and in individuals at risk for hypertension (Armario et al., 2003; Falkner, Onesti, Angelakos, Fernandes, & Langman, 1979; Fredrikson & Matthews, 1990; Kaushik, Mahajan, Rajesh, & Kaushik, 2004). The latter also show a slowed autonomic recovery from experimental stressors (Schneider, Jacobs, Gevirtz, & O'Connor, 2003). Individuals at genetic risk for essential hypertension may also present cognitive and neural alterations, but more studies are needed to draw conclusive evidence from this research. In this otherwise healthy, young, normotensive population, subtle deficits in cognitive function, including memory, attention and verbal learning, have been reported compared to controls without parental history of hypertension (Haley et al., 2008). In fMRI, family history of hypertension was also associated with decreased working memory task-related activation in the posterior cingulate cortex, right inferior parietal lobule and right temporal gyrus (Haley et al., 2008). In animal models of neurogenic hypertension, lesions to the amygdala of rats with a genetic predisposition to develop hypertension decreased cardiovascular reactivity (Galeno, Van Hoesen, & Brody, 1984) and prevented the development of hypertension induced by stress (Fukumori, Nishigori, Goshima, & Kubo, 2004), highlighting a significant role of the amygdala and potentially of connected neuro-vegetative brain regions in the pathogenesis of essential hypertension.

A contributing effect to this vicious circle of neurogenic hypertension is a paradoxical phenomenon that higher blood pressure relates to positive behavioral effects. Previously, moderating effects of blood pressure have been described in pain perception experiments, where participants with higher blood pressure exhibit decreased pain sensitivity (hypoalgesia) than participants with lower blood pressure (Ghione, Rosa, Mezzasalma, & Panattoni, 1988). Similarly, some hypertensives report less distress in general and better quality of life (Berendes, Meyer, Hulpke-Wette, & Herrmann-Lingen, 2013; Hassoun et al., 2015; Nyklíček, Vingerhoets, & Van Heck, 2001). Positive associations in situations of high blood pressure levels (e.g. in a stressful work environment or during an important test) could positively reinforce individuals to increase blood pressure levels to achieve better performance, which would accelerate vascular pathology (Rau & Elbert, 2001).

Some interesting perspectives on the question if essential hypertension really is a consequence of lifestyle choices, have been gained in the 1980s by studying populations which strongly diverge from the prototypical modern, stress-prone, sedentary lifestyle. It has been described that villages in rural parts of Papua New Guinea do not show elevations of blood pressure with age and in fact stay far below 120/80 mmHg (King et al., 1985). Similarly, a 30-year follow-up study with Italian nuns in a secluded order showed that the nuns' blood pressure stayed stable and below DBP of 90 mmHg, whereas blood pressure of the control group from the same region rose as expected (Timio et al., 1997, 1988). In the general population, some modifiable lifestyle-related vascular risk factors have been reduced in the last decades (e.g. smoking), while others have increased in incidence and time of exposure (e.g. high BMI) (Forouzanfar et al., 2016; Neuhauser et al., 2015). A sedentary lifestyle is often also accompanied with increased BMI. Blood pressure and weight are tightly interrelated with blood pressure levels increasing linearly with increases in BMI. Therefore, primary prevention strategies for hypertension must include prevention of weight gain. With respect to the consequences of modifiable vascular risk factors for the brain, Kharabian et al. (2018) found differential profiles of structural gray matter networks depending on the vascular risk factor. Understanding the presumably varying impact of different vascular risk factors on diseases of the brain will be informative for targeted interventions. These examples demonstrate that our behaviors have a great impact on vascular disease risk and that lifestyle-targeted interventions may indeed qualify for the prevention of elevated blood pressure; primarily by managing stress regulation and preventing obesity.

How to design targeted interventions in early stages of vascular disease is a further relevant clinical issue in the population under investigation in this thesis. Most participants in our studies did not exceed blood pressure levels which would be categorized as stage I hypertension. Questions of how, when and to which target to treat blood pressure need to be addressed for young adults at risk of vascular disease progression. Lifestyle interventions have a beneficial effect on CVD prevention (Grossman et al., 2017), but their efficacy in the prevention of brain injury warrants further research. Blood pressure regulation and hypertension are examples of mind-body-emotion interactions and can now be tested in a suitable framework by using the MPILMBB database that we established. With the MPILMBB database, we have provided a large dataset of deeply phenotyped individuals that can be used to identify biological, medical and psychological biomarkers of brain diseases. Individualized profiles might prove useful to identify people at increased risk which should be monitored more closely. In the case of hypertension, such profiles could evaluate unmodifiable (e.g. genetic or environmental risks, high blood pressure

reactivity) and modifiable (e.g. physical inactivity, unhealthy diet) factors that are known to be implicated in chronic blood pressure elevations. The European cardiological society recommends such a risk score system for the management of patients with vascular risk factors (Williams et al., 2018). The results presented in this thesis, in addition to other research that demonstrates premature adverse effects of elevated blood pressure or hypertension, speak in favor of extending current clinical practices to initiate earlier interventions in order to delay initial blood pressure increases.

5 Summary / Zusammenfassung der Arbeit

Dissertation zur Erlangung des akademischen Grades Dr. rer. med.

Blood Pressure and Brain Structure in Early Adulthood

eingereicht von Herma Lina Schaare, M.Sc.

angefertigt am Max-Planck-Institut für Kognitions- und Neurowissenschaften,
Leipzig
Abteilung Neurologie

betreut von Prof. Dr. med. Arno Villringer

Dezember 2019

High blood pressure (BP) at or above levels of systolic 140 mmHg or diastolic 90 mmHg, or hypertension (HTN), affects 1.13 billion adults worldwide and is the leading single risk factor for disability, cardio- and cerebrovascular diseases and death (Forouzanfar et al., 2016; Lim et al., 2012; NCD Risk Factor Collaboration (NCD-RisC), 2016). The brain is a primary target for the adverse effects of high BP and often undetected asymptomatic neural changes can be detected well before overt clinical symptoms occur. Mid- and late-life HTN in particular has been related to sub-clinical brain damage, including white matter lesions, gray matter atrophy and functional cerebrovascular changes (Beauchet et al., 2013; Hajjar et al., 2010; Maillard et al., 2012; Muller et al., 2014; Power et al., 2016; Raz et al., 2005). Crucially, signs of silent cerebrovascular disease are highly prevalent in the general aging population (Gupta et al., 2016; Leary & Saver, 2003). Deleterious effects of HTN mainly target the cerebral (and peripheral) vasculature, where BP elevations promote vascular stiffening, endothelial failure, and dysfunction of the blood-brain barrier, among other mechanisms that lead to insidious vascular brain damage (Iadecola et al., 2016;

Laurent & Boutouyrie, 2015; Sierra et al., 2011). Some studies imply a continuous effect of BP on adverse brain outcomes – irrespective of any cut-off threshold for HTN – however, evidence for this hypothesis is still sparse (Forouzanfar et al., 2017; Rapsomaniki et al., 2014).

Which mechanisms initiate primary BP elevations also remains unclear. The brain has a pivotal role in BP regulation on the one hand and linking bodily signals with mental processes on the other hand. Importantly, some brain regions that are involved in the regulation of stress and emotions are also involved in BP control (Critchley & Harrison, 2013; Gianaros & Sheu, 2009). These functions have been mapped onto structures including particularly the insula, cingulate cortex and amygdala (Critchley & Harrison, 2013; Gianaros & Sheu, 2009). It has been suggested that damage to these regions would facilitate dysregulation of affective, cognitive and autonomic (mind-brain-body) processes and thus cause vascular pathophysiology over time (Jennings & Zanstra, 2009). Inversely, maladaptive reactivity and regulation of BP in younger age, prior to manifestation of HTN, may contribute to the development and progression of cardio- and cerebrovascular disease during aging (Matthews et al., 2004).

In this thesis, I investigated the interrelation of BP and the brain in six published studies. The studies build on the assumption that a combination of psychological (mind), neural (brain), and autonomic (body) processes seems to interact and putatively underlies the factors driving pathogenesis of essential HTN and insidious brain changes. My collaborators and I approached this research framework by first establishing a public database which allows to study mind-brain-body interactions comprehensively (studies 1 and 2). This led to the main study of my thesis (study 3) which explored associations between sub-hypertensive BP and brain structure in young adults. Further collaborations studied relations between brain function and other vascular risk factors (parasympathetic cardioregulation and stress) using the database (studies 4 and 5) and neural signatures of BP regulation to emotional distress (study 6).

Studies 1 & 2: The MPI-Leipzig Mind-Brain-Body database (key work for data acquisition)

Study 1: A mind-brain-body dataset of MRI, EEG, cognition, emotion, and peripheral physiology in young and old adults. Babayan...Schaare et al., Scientific Data (2019)

Study 2: A functional connectome phenotyping dataset including cognitive state and personality measures. Mendes...Schaare et al., Scientific Data (2019)

The experimental work presented in this thesis grounds on a large data acquisition effort which resulted in the establishment of the publicly available MPI-Leipzig Mind-Brain-Body

database (MPILMBB) (Babayan et al., 2019; Mendes et al., 2019). This big database provides detailed assessments of brain-body dynamics in relation to individual psychological profiles during aging and thus a framework in which mind-brain-body can be tested in a comprehensive manner. It consists of two datasets which were acquired with partly overlapping protocols and participants: Dataset 1, the LEMON study (N=227), was designed to assess a wide range of neural, psychological and psychophysiological markers that allow to test mind-brain-body interactions in young (N=153, 25.1±3.1 years, range 20–35 years, 45 female) and older adults (N=74, 67.6±4.7 years, range 59–77 years, 37 female) (Babayan et al., 2019). The two-day assessment included multimodal structural MRI at 3 Tesla, 15 minutes of resting-state fMRI with continuous acquisition of BP, ECG, pulse and respiration, 62-channel resting-state EEG, anthropometrics, blood and urine samples, as well as psychiatric screenings, six cognitive tests and 21 psychometric questionnaires related to personality traits, emotions, eating behaviors and addiction. Dataset 2, the neuroanatomy and connectivity protocol, focused on a detailed assessment of the functional connectome, by including one hour of resting-state fMRI, and cognitive and personality measures in adults between 20-75 years of age (N=194, 34±16 years, 94 female) (Mendes et al., 2019). Specifically, the five-day assessment included a broad set of state and trait psychological phenotypes measured by 31 questionnaires, seven tasks, and four sessions of mind-wandering during scanning. Overall, 109 participants completed both protocols.

Study 3: Association of peripheral blood pressure with gray matter volume in 19- to 40-year-old adults. Schaare et al., *Neurology* (2019). (main study using the database of studies 1 & 2)

Using the MPILMBB database in combination with other large datasets, I conducted the main study of my experimental work: The aim of study 3 was to test whether subtle structural brain changes already occur in early adulthood where confounding effects are minimal, and at BP levels below the current diagnostic threshold for HTN (SBP/DBP≥140/90 mmHg). We hypothesized that higher BP would relate to lower regional gray matter volume (GMV) – independent of any threshold – and that this would predominantly affect frontal and medial temporal lobes, including amygdala and hippocampus.

We tested this hypothesis using four cross-sectional datasets from Leipzig, Germany, in a total sample of 423 adults between 19 and 40 years of age without previous diagnosis of HTN (mean age 27.7±5.3 years, 177 women, mean SBP/DBP 123.2/73.4±12.2/8.5 mmHg). To derive whole-brain regional GMV that could be related to resting BP levels, we

conducted high-resolution structural 3 Tesla T1-weighted MRI and performed voxel-based morphometry (VBM) on each dataset, separately. Next, we combined the VBM outcomes of each dataset in image-based meta-analyses (IBMA) to evaluate the cumulative results across datasets. Resting BP was analyzed both as a continuous measure and as a discrete measure including four categories: (1) SBP<120 and DBP<80 mm Hg, (2) SBP 120–129 or DBP 80–84 mm Hg, (3) SBP 130–139 or DBP 85–89 mm Hg, (4) SBP≥140 or DBP≥90 mm Hg. Results showed consistently lower GMV in those individuals with higher BP (Figure 6). Strikingly, already BP levels within the *normal* range were related to lower GMV in several regions known to be affected by HTN in older ages (e.g. hippocampus, Figure 6). Specifically, IBMA yielded: (a) regional GMV decreased linearly as peripheral BP increased; (b) significantly decreased GMV with higher BP when comparing individuals in sub-hypertensive categories 3 and 2, respectively, to those in category 1; (c) lower BP-related GMV was found in regions including hippocampus, amygdala, thalamus, frontal and parietal structures (e.g. precuneus).

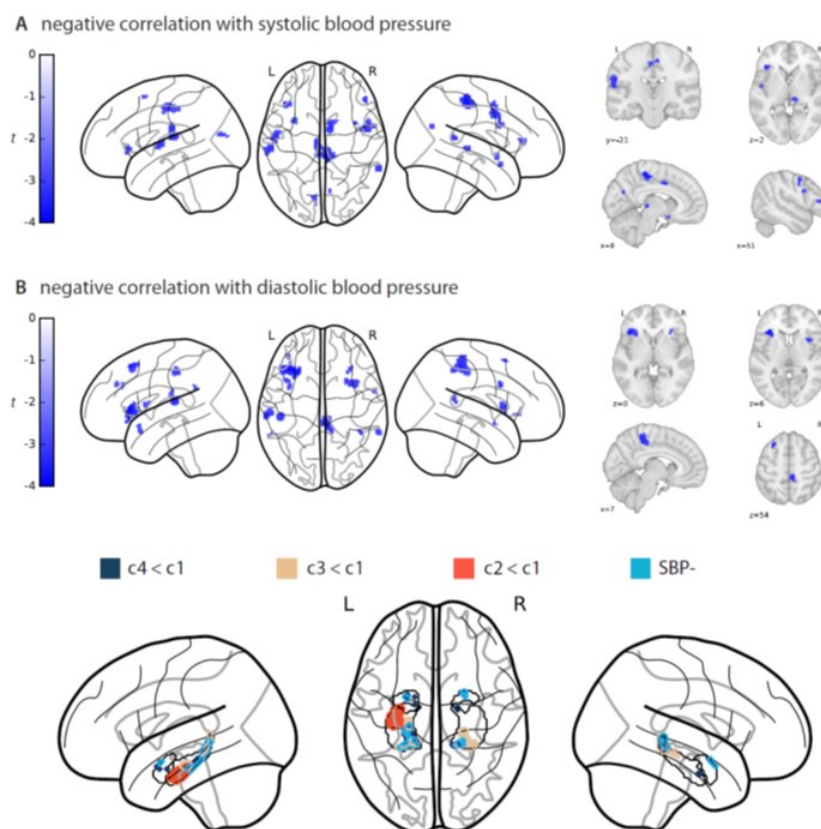


Figure 6 – Overview of main results

Glass brain view of image-based meta-analysis results for the association between systolic (A) and diastolic (B) blood pressure and gray matter volume with relevant slice views on the right-hand side. Bottom: Glass brain views of image-based meta-analysis ROI results for the blood pressure category contrasts of interest in bilateral hippocampus and amygdala masks. Definition of blood pressure categories: c1 (SBP<120 mmHg and DBP<80 mmHg), c2 (SBP 120-129 mmHg or DBP 80-84 mmHg), c3 (SBP 130-139 mmHg or DBP 85-89 mmHg) and c4 (SBP≥140 mmHg or DBP≥90 mmHg). L: Left hemisphere. R: Right hemisphere.

Thus, in this study, we found that BP-associated gray matter alterations emerge earlier in adulthood than previously assumed and continuously across the range of BP. The affected brain regions predominantly include parietal, frontal, and subcortical structures (e.g. hippocampus), which have been consistently associated with gray matter damage in middle-aged and older individuals with HTN (Beauchet et al., 2013; den Heijer et al., 2005; Hajjar et al., 2010; Leritz et al., 2011; Power et al., 2016; Raz et al., 2005). The causes of brain damage in HTN involve complex interactions of different pathophysiological mechanisms that still need to be fully elucidated. Medial temporal and frontal regions might be especially sensitive to effects of pulsation, hypoperfusion and ischemia, which often result from increasing pressure (Beauchet et al., 2013; Iadecola et al., 2016). It is assumed that vascular stiffness, endothelial failure and a dysfunctional blood-brain barrier are precursors of cerebral small and large vessel disease that reduce cerebral blood flow, disturb autoregulatory adjustment and decrease vasomotor reactivity, which may impair perivascular central nervous waste clearance systems (Iadecola et al., 2016). Consequently, demyelination, apoptosis and intoxication of neurons and glial cells, as well as gray and white matter necrosis accumulate and can be observed with neuroimaging on a macroscopic scale. Further, our results yielded lower GMV in amygdala, thalamus, insula, cingulate regions, which are central structures in affective, cognitive, and autonomic control (Benarroch, 1993; Critchley & Harrison, 2013). Presumably, structural alterations in these regions may contribute to cardiovascular dysregulation and BP elevations via sympathetic pathways (Esler et al., 2008; Macefield et al., 2013). Whether our results reflect any of such mechanisms putatively leading to vascular or neurodegenerative damage remains speculative. Neither do our cross-sectional data allow inference on causality between lower brain volumes and raised BP.

In sum, insidious BP increases might reflect progression of pathophysiological mechanisms that remain asymptomatic in early-life and manifest as overt disease in mid- or late-life. Our study points to an early effect of elevated BP on brain alterations that occur in early adulthood, at BP levels below current diagnostic thresholds for HTN and in the absence of overt disease, such as HTN.

Studies 4 & 5: Other vascular risk factors and functional brain connectivity (related studies using the database of studies 1 & 2)

Study 4: The age-dependent relationship between resting heart rate variability and functional brain connectivity. Kumral, Schaare et al., NeuroImage (2019)

Study 5: Acute psychosocial stress alters thalamic network centrality. Reinelt, Uhlig...Schaare et al., NeuroImage (2019)

In two further studies, we investigated the relationship between other vascular risk factors and functional brain connectivity using the MPILMBB database. In study 4 (Kumral et al., 2019), we assessed how parasympathetic regulation of the heart (i.e. heart rate variability) – a proxy for autonomic function which decreases during aging – relates to brain structure (i.e. VBM) and function (i.e. eigenvector centrality and seed-based functional connectivity) across three age groups (N=140 younger: 26.0±4.2 years, N=119 middle-aged: 46.3±6.2 years, N=129 older: 66.9±4.7 years). We found correlations between resting HRV and functional connectivity in the posterior cingulate cortex across all age groups and in the ventromedial prefrontal cortex in young participants only. These results illustrate a differential effect of aging on heart-brain interactions in cortical midline structures which have been implicated in autonomic, cognitive and affective regulation.

As stress is a likely contributing factor in the development of HTN and various other mental and somatic conditions, in study 5 (Reinelt et al., 2019), we investigated how acute psychosocial stress (i.e. Trier Social Stress Test) affects brain connectivity (i.e. eigenvector centrality and seed-based functional connectivity) in 67 young men (18-35 years, mean age_{TSSST}=25.45, mean age_{Control}=26.18). Following the stress intervention, whole-brain analyses yielded increased centrality in thalamus, which also was linearly associated with stress-related changes in subjective, as well as autonomic (HRV), and endocrine (saliva cortisol) measures. These elevations of centrality and saliva cortisol concentrations persisted during recovery until 105 min after stress onset, suggesting that thalamic connectivity is essential in the central and peripheral processing of acute psychosocial stress and its aftermath. Both studies exemplify the interconnectedness of mind, brain and body pathways and emphasize its significance for a better understanding of vascular risk factors.

Study 6: Neural control of vascular reactions: impact of emotion and attention. Okon-Singer...Schaare et al., Journal of Neuroscience (2014). (using the mind-brain-body approach to understand blood pressure control)

In the final study included in this thesis, we simultaneously recorded brain activity and BP to gain a better understanding of the mechanisms underlying the brain's role in BP control. Twenty-four healthy adults (11 females; age=24.75±2.49 years) participated in an affective perceptual load task that manipulated executive attention to aversive or neutral distractor pictures during fMRI with continuous BP acquisition (Okon-Singer et al., 2014). The main result of study 6 was a positive correlation between BP response and activation in a network including prefrontal and parietal regions, the amygdala, caudate, and mid-brain. As expected, the effects were modulated by attention yielding smaller or diminished

neural, behavioral and vascular responses when attentional load was high. The findings match theories emphasizing the role of attentional control in neural and behavioral reactions to aversive distractors and extend it to the control of autonomous reactions to emotional distress with potential clinical relevance.

Overall, the studies in this thesis demonstrate that BP is strongly intertwined with brain processes (Schaare et al., 2019) which control and regulate autonomic responses (Kumral et al., 2019; Reinelt et al., 2019) and indicate premature vascular brain damage. In addition to other recent studies, our findings contribute to a better understanding of the underlying mechanisms driving initial BP elevations (Gianaros et al., 2017; Okon-Singer et al., 2014). Our research speaks in favor of extending clinical practices to initiate earlier interventions to suspend primary BP elevations and prevent secondary diseases.

6 References

- Abraham, A., Pedregosa, F., Eickenberg, M., Gervais, P., Mueller, A., Kossaifi, J., ... Varoquaux, G. (2014). Machine learning for neuroimaging with scikit-learn. *Frontiers in Neuroinformatics*, 8(February), 14. <https://doi.org/10.3389/fninf.2014.00014>
- Allan, C., Zsoldos, E., Filippini, N., Sexton, C., Topiwala, A., Valkanova, V., ... Kivimäki, M. (2015). Life-time hypertension as a predictor of brain structure in older adults: a prospective cohort study. *The British Journal of Psychiatry: The Journal of Mental Science*, 206(4), 308–315. <https://doi.org/10.1192/bjp.bp.114.153536>
- Armario, P., del Rey, R. H., Martin-Baranera, M., Almendros, M. C., Ceresuela, L. M., & Pardell, H. (2003). Blood pressure reactivity to mental stress task as a determinant of sustained hypertension after 5 years of follow-up. *Journal of Human Hypertension*, 17(3), 181–186. <https://doi.org/10.1038/sj.jhh.1001530>
- Ashburner, J. (2007). A fast diffeomorphic image registration algorithm. *NeuroImage*, 38(1), 95–113. <https://doi.org/10.1016/j.neuroimage.2007.07.007>
- Ashburner, J., & Friston, K. J. (2000). Voxel-based morphometry--the methods. *NeuroImage*, 11(6 Pt 1), 805–821. <https://doi.org/10.1006/nimg.2000.0582>
- Avelar, W. M., D'Abreu, A., Coan, A. C., Lima, F. O., Guimarães, R., Yassuda, C. L., ... Cendes, F. (2015). Asymptomatic carotid stenosis is associated with gray and white matter damage. *International Journal of Stroke*, 10(8), 1197–1203. <https://doi.org/10.1111/ijss.12574>
- Babayan, A., Erbey, M., Kumral, D., Reinelt, J. D., Reiter, A. M. F., Röbbing, J., ... Villringer, A. (2019). A mind-brain-body dataset of MRI, EEG, cognition, emotion, and peripheral physiology in young and old adults. *Scientific Data*, 6(1), 180308. <https://doi.org/10.1038/sdata.2018.308>
- Babo-Rebelo, M., Wolpert, N., Adam, C., Hasboun, D., & Tallon-Baudry, C. (2016). Is the cardiac monitoring function related to the self in both the default network and right anterior insula? *Philosophical Transactions of the Royal Society B: Biological Sciences*, 371(1708), 20160004. <https://doi.org/10.1098/rstb.2016.0004>
- Beason-Held, L. L., Moghekar, A., Zonderman, A. B., Kraut, M. A., & Resnick, S. M. (2007). Longitudinal Changes in Cerebral Blood Flow in the Older Hypertensive Brain. *Stroke*, 38(6), 1766–1773. <https://doi.org/10.1161/STROKEAHA.106.477109>
- Beauchet, O., Celle, S., Roche, F., Bartha, R., Montero-Odasso, M., Allali, G., & Annweiler, C. (2013). Blood pressure levels and brain volume reduction: a systematic review and meta-analysis. *Journal of Hypertension*, 31(8), 1502–1516. <https://doi.org/10.1097/HJH.0b013e32836184b5>
- Benarroch, E. E. (1993). The Central Autonomic Network: Functional Organization, Dysfunction, and Perspective. *Mayo Clinic Proceedings*, 68(10), 988–1001. [https://doi.org/10.1016/S0025-6196\(12\)62272-1](https://doi.org/10.1016/S0025-6196(12)62272-1)
- Bender, A. R. A., Daugherty, A. M. A., & Raz, N. (2013). Vascular risk moderates associations between hippocampal subfield volumes and memory. *Journal of Cognitive Neuroscience*, 25(11), 1851–1862. https://doi.org/10.1162/jocn_a_00435
- Berendes, A., Meyer, T., Hulpke-Wette, M., & Herrmann-Lingen, C. (2013). Association of elevated blood pressure with low distress and good quality of life: results from the nationwide representative German Health Interview and Examination. *Psychosomatic Medicine*, 75(4), 422–428. <https://doi.org/10.1097/PSY.0b013e31828ef0c2>
- Braak, H., & Braak, E. (1991). Neuropathological staging of Alzheimer-related changes. *Acta Neuropathol*, 82, 239–259. <https://doi.org/10.1007/BF00308809>
- Carretero, O. A., & Oparil, S. (2000). Essential hypertension. Part I: definition and etiology. *Circulation*, 101(3), 329–335. <https://doi.org/10.1161/01.cir.101.3.329>
- Chen, K. H. M., Henderson, V. W., Stolwyk, R. J., Dennerstein, L., & Szoek, C. (2015). Prehypertension in midlife is associated with worse cognition a decade later in middle-aged and older women. *Age and Ageing*, 44(3), 439–445. <https://doi.org/10.1093/ageing/afv026>
- Chida, Y., & Steptoe, A. (2010). Greater cardiovascular responses to laboratory mental stress are associated with poor subsequent cardiovascular risk status: A meta-analysis of prospective evidence. *Hypertension*, 55(4), 1026–1032. <https://doi.org/10.1161/HYPERTENSIONAHA.109.146621>
- Chobanian, A. V., Bakris, G. L., Black, H. R., Cushman, W. C., Green, L. A., Izzo, J. L., ... Roccella, E. J. (2003). Seventh report of the Joint National Committee on Prevention, Detection, Evaluation, and Treatment of High Blood Pressure. *Hypertension*, 42(6), 1206–1252. <https://doi.org/10.1161/01.HYP.0000107251.49515.c2>
- Cohen, B. E., Edmondson, D., & Kronish, I. M. (2015). State of the art review: Depression, stress, anxiety, and cardiovascular disease. *American Journal of Hypertension*. <https://doi.org/10.1093/ajh/hpv047>

- Critchley, H. D., Corfield, D., Chandler, M., Mathias, C., & Dolan, R. (2000). Cerebral correlates of autonomic cardiovascular arousal: a functional neuroimaging investigation in humans. *The Journal of Physiology*, *523*(1), 259–270. <https://doi.org/10.1111/j.1469-7793.2000.t011-1-00259.x>
- Critchley, H. D., & Harrison, N. a. (2013). Visceral influences on brain and behavior. *Neuron*, *77*(4), 624–638. <https://doi.org/10.1016/j.neuron.2013.02.008>
- Critchley, H. D., Mathias, C. J., Josephs, O., O’Doherty, J., Zanini, S., Dewar, B. K., ... Dolan, R. J. (2003). Human cingulate cortex and autonomic control: Converging neuroimaging and clinical evidence. *Brain*, *126*(10), 2139–2152. <https://doi.org/10.1093/brain/awg216>
- Cuffee, Y., Ogedegbe, C., Williams, N. J., Ogedegbe, G., & Schoenthaler, A. (2014). Psychosocial Risk Factors for Hypertension: an Update of the Literature. *Current Hypertension Reports*. <https://doi.org/10.1007/s11906-014-0483-3>
- Dan-Glauser, E. S., & Gross, J. J. (2011). The temporal dynamics of two response-focused forms of emotion regulation: experiential, expressive, and autonomic consequences. *Psychophysiology*, *48*(9), 1309–1322. <https://doi.org/10.1111/j.1469-8986.2011.01191.x>
- De Meersman, R. E., & Stein, P. K. (2007). Vagal modulation and aging. *Biological Psychology*, *74*(2), 165–173. <https://doi.org/10.1016/j.biopsycho.2006.04.008>
- Debette, S., & Markus, H. S. (2010). The clinical importance of white matter hyperintensities on brain magnetic resonance imaging: systematic review and meta-analysis. *BMJ*, *341*(jul26 1), c3666–c3666. <https://doi.org/10.1136/bmj.c3666>
- Debette, S., Seshadri, S., Beiser, A., Au, R., Himali, J. J., Palumbo, C., ... DeCarli, C. (2011). Midlife vascular risk factor exposure accelerates structural brain aging and cognitive decline. *Neurology*, *77*(5), 461–468. <https://doi.org/10.1212/WNL.0b013e318227b227>
- den Heijer, T., Launer, L. J., Prins, N. D., van Dijk, E. J., Vermeer, S. E., Hofman, A., ... Breteler, M. M. B. (2005). Association between blood pressure, white matter lesions, and atrophy of the medial temporal lobe. *Neurology*, *64*(2), 263–267. <https://doi.org/10.1212/01.WNL.0000149641.55751.2E>
- Dickerson, B. C., Stoub, T. R., Shah, R. C., Sperling, R. A., Killiany, R. J., Albert, M. S., ... Detoleto-Morrell, L. (2011). Alzheimer-signature MRI biomarker predicts AD dementia in cognitively normal adults. *Neurology*, *76*(16), 1395–1402. <https://doi.org/10.1212/WNL.0b013e3182166e96>
- Diedrichsen, J. (2006). A spatially unbiased atlas template of the human cerebellum. *NeuroImage*, *33*(1), 127–138. <https://doi.org/10.1016/j.neuroimage.2006.05.056>
- Dufouil, C., Chalmers, J., Coskun, O., Besançon, V., Bousser, M.-G., Guillon, P., ... PROGRESS MRI Substudy Investigators. (2005). Effects of blood pressure lowering on cerebral white matter hyperintensities in patients with stroke: the PROGRESS (Perindopril Protection Against Recurrent Stroke Study) Magnetic Resonance Imaging Substudy. *Circulation*, *112*(11), 1644–1650. <https://doi.org/10.1161/CIRCULATIONAHA.104.501163>
- Dworkin, B. R., Elbert, T., Rau, H., Birbaumer, N., Pauli, P., Droste, C., & Brunia, C. H. (1994). Central effects of baroreceptor activation in humans: attenuation of skeletal reflexes and pain perception. *Proceedings of the National Academy of Sciences*, *91*(14), 6329–6333. <https://doi.org/10.1073/pnas.91.14.6329>
- Eickhoff, S. B., Paus, T., Caspers, S., Grosbras, M.-H., Evans, A. C., Zilles, K., & Amunts, K. (2007). Assignment of functional activations to probabilistic cytoarchitectonic areas revisited. *NeuroImage*, *36*(3), 511–521. <https://doi.org/10.1016/j.neuroimage.2007.03.060>
- Elias, M. F., Wolf, P. A., D’Agostino, R. B., Cobb, J., & White, L. R. (1993). Untreated Blood Pressure Level Is Inversely Related to Cognitive Functioning: The Framingham Study. *American Journal of Epidemiology*, *138*(6), 353–364. <https://doi.org/10.1093/oxfordjournals.aje.a116868>
- Elias, P. K., Elias, M. F., Robbins, M. A., & Budge, M. M. (2004). Blood pressure-related cognitive decline: Does age make a difference? *Hypertension*, *44*(5), 631–636. <https://doi.org/10.1161/01.HYP.0000145858.07252.99>
- Esler, M. (2017). Mental stress and human cardiovascular disease. *Neuroscience and Biobehavioral Reviews*. <https://doi.org/10.1016/j.neubiorev.2016.10.011>
- Esler, M., Eikelis, N., Schlaich, M., Lambert, G., Alvarenga, M., Dawood, T., ... Lambert, E. (2008). Chronic mental stress is a cause of essential hypertension: presence of biological markers of stress. *Clinical and Experimental Pharmacology & Physiology*, *35*(4), 498–502. <https://doi.org/10.1111/j.1440-1681.2008.04904.x>
- Falkner, B., Onesti, G., Angelakos, E. T., Fernandes, M., & Langman, C. (1979). Cardiovascular response to mental stress in normal adolescents with hypertensive parents: Hemodynamics and mental stress in adolescents. *Hypertension*, *1*(1), 23–30. <https://doi.org/10.1161/01.HYP.1.1.23>

- Fazekas, F., Chawluk, J., Alavi, A., Hurtig, H., & Zimmerman, R. (1987). MR signal abnormalities at 1.5 T in Alzheimer's dementia and normal aging. *American Journal of Roentgenology*, *149*(2), 351–356. <https://doi.org/10.2214/ajr.149.2.351>
- Firbank, M. J., Wiseman, R. M., Burton, E. J., Saxby, B. K., O'Brien, J. T., & Ford, G. A. (2007). Brain atrophy and white matter hyperintensity change in older adults and relationship to blood pressure: Brain atrophy, WMH change and blood pressure. *Journal of Neurology*, *254*(6), 713–721. <https://doi.org/10.1007/s00415-006-0238-4>
- Forouzanfar, M. H., Afshin, A., Alexander, L. T., Anderson, H. R., Bhutta, Z. A., Biryukov, S., ... Murray, C. J. L. (2016). Global, regional, and national comparative risk assessment of 79 behavioural, environmental and occupational, and metabolic risks or clusters of risks, 1990–2015: a systematic analysis for the Global Burden of Disease Study 2015. *The Lancet*, *388*(10053), 1659–1724. [https://doi.org/10.1016/S0140-6736\(16\)31679-8](https://doi.org/10.1016/S0140-6736(16)31679-8)
- Forouzanfar, M. H., Liu, P., Roth, G. A., Ng, M., Biryukov, S., Marczak, L., ... MH, F. (2017). Global Burden of Hypertension and Systolic Blood Pressure of at Least 110 to 115 mm Hg, 1990-2015. *JAMA*, *317*(2), 827–838. <https://doi.org/10.1001/JAMA.2016.19043>
- Fredrikson, M., & Matthews, K. A. (1990). Cardiovascular Responses to Behavioral Stress and Hypertension: A Meta-Analytic Review. *Annals of Behavioral Medicine*, *12*(1), 30–39. https://doi.org/10.1207/s15324796abm1201_3
- Fukumori, R., Nishigori, Y., Goshima, Y., & Kubo, T. (2004). Contribution of the medial amygdaloid nucleus to the development of hypertension in spontaneously hypertensive rats. *Neuroscience Letters*, *365*(2), 128–131. <https://doi.org/10.1016/j.neulet.2004.04.066>
- Galeno, T. M., Van Hoesen, G. W., & Brody, M. J. (1984). Central amygdaloid nucleus lesion attenuates exaggerated hemodynamic responses to noise stress in the spontaneously hypertensive rat. *Brain Research*, *291*(2), 249–259. [https://doi.org/10.1016/0006-8993\(84\)91257-5](https://doi.org/10.1016/0006-8993(84)91257-5)
- Gąsecki, D., Kwarciany, M., Nyka, W., & Narkiewicz, K. (2013). Hypertension, Brain Damage and Cognitive Decline. *Current Hypertension Reports*, *15*(6), 547–558. <https://doi.org/10.1007/s11906-013-0398-4>
- Ghione, S., Rosa, C., Mezzasalma, L., & Panattoni, E. (1988). Arterial hypertension is associated with hypalgesia in humans. *Hypertension*, *12*, 491–497. <https://doi.org/10.1161/01.HYP.12.5.491>
- Gianaros, P. J., Derbyshire, S. W. G., May, J. C., Siegle, G. J., Gamalo, M. A., & Jennings, J. R. (2005). Anterior cingulate activity correlates with blood pressure during stress. *Psychophysiology*, *42*(6), 627–635. <https://doi.org/10.1111/j.1469-8986.2005.00366.x>
- Gianaros, P. J., Greer, P. J., Ryan, C. M., & Jennings, J. R. (2006). Higher blood pressure predicts lower regional grey matter volume: Consequences on short-term information processing. *NeuroImage*, *31*(2), 754–765. <https://doi.org/10.1016/j.neuroimage.2006.01.003>
- Gianaros, P. J., Jennings, J. R., Sheu, L. K., Derbyshire, S. W. G., & Matthews, K. a. (2007). Heightened functional neural activation to psychological stress covaries with exaggerated blood pressure reactivity. *Hypertension*, *49*(1), 134–140. <https://doi.org/10.1161/01.HYP.0000250984.14992.64>
- Gianaros, P. J., & Sheu, L. K. (2009). A review of neuroimaging studies of stressor-evoked blood pressure reactivity: emerging evidence for a brain-body pathway to coronary heart disease risk. *NeuroImage*, *47*(3), 922–936. <https://doi.org/10.1016/j.neuroimage.2009.04.073>
- Gianaros, P. J., Sheu, L. K., Matthews, K. a, Jennings, J. R., Manuck, S. B., & Hariri, A. R. (2008). Individual differences in stressor-evoked blood pressure reactivity vary with activation, volume, and functional connectivity of the amygdala. *Journal of Neuroscience*, *28*(4), 990–999. <https://doi.org/10.1523/JNEUROSCI.3606-07.2008>
- Gianaros, P. J., Sheu, L. K., Uyar, F., Koushik, J., Jennings, J. R., Wager, T. D., ... Verstynen, T. D. (2017). A brain phenotype for stressor-evoked blood pressure reactivity. *Journal of the American Heart Association*, *6*(9). <https://doi.org/10.1161/JAHA.117.006053>
- Giraldo-Chica, M., & Woodward, N. D. (2017). Review of thalamocortical resting-state fMRI studies in schizophrenia. *Schizophrenia Research*, *180*, 58–63. <https://doi.org/10.1016/j.schres.2016.08.005>
- Gorelick, P. B., Scuteri, A., Black, S. E., Decarli, C., Greenberg, S. M., Iadecola, C., ... Seshadri, S. (2011). Vascular contributions to cognitive impairment and dementia: A statement for healthcare professionals from the American Heart Association/American Stroke Association. *Stroke*, *42*(9), 2672–2713. <https://doi.org/10.1161/STR.0b013e3182299496>
- Gorgolewski, K. J., Auer, T., Calhoun, V. D., Craddock, R. C., Das, S., Duff, E. P., ... Milham, M. P. (2016). The brain imaging data structure, a format for organizing and describing outputs of neuroimaging experiments. *Scientific Data*, *3*, 160044. <https://doi.org/10.1038/sdata.2016.44>
- Gould van Praag, C. D., Garfinkel, S. N., Sparasci, O., Mees, A., Philippides, A. O., Ware, M., ... Critchley, H. D.

- (2017). Mind-wandering and alterations to default mode network connectivity when listening to naturalistic versus artificial sounds. *Scientific Reports*, 7(1), 45273. <https://doi.org/10.1038/srep45273>
- Gray, M. A., Minati, L., Harrison, N. A., Gianaros, P. J., Napadow, V., & Critchley, H. D. (2009). Physiological recordings: basic concepts and implementation during functional magnetic resonance imaging. *NeuroImage*, 47(3), 1105–1115. <https://doi.org/10.1016/j.neuroimage.2009.05.033>
- Greicius, M. D., Flores, B. H., Menon, V., Glover, G. H., Solvason, H. B., Kenna, H., ... Schatzberg, A. F. (2007). Resting-State Functional Connectivity in Major Depression: Abnormally Increased Contributions from Subgenual Cingulate Cortex and Thalamus. *Biological Psychiatry*, 62(5), 429–437. <https://doi.org/10.1016/j.biopsych.2006.09.020>
- Grossman, D. C., Bibbins-Domingo, K., Curry, S. J., Barry, M. J., Davidson, K. W., Doubeni, C. A., ... Tseng, C.-W. (2017). Behavioral Counseling to Promote a Healthful Diet and Physical Activity for Cardiovascular Disease Prevention in Adults Without Cardiovascular Risk Factors. *JAMA*, 318(2), 167. <https://doi.org/10.1001/jama.2017.7171>
- Gupta, A., Giambone, A. E., Gialdini, G., Finn, C., Delgado, D., Gutierrez, J., ... Kamel, H. (2016). Silent Brain Infarction and Risk of Future Stroke A Systematic Review and Meta-Analysis, 719–725. <https://doi.org/10.1161/STROKEAHA.115.011889>
- Hagemann, D., Waldstein, S. R., & Thayer, J. F. (2003). Central and autonomic nervous system integration in emotion. *Brain and Cognition*, 52(1), 79–87. [https://doi.org/10.1016/S0278-2626\(03\)00011-3](https://doi.org/10.1016/S0278-2626(03)00011-3)
- Hajjar, I., Zhao, P., Alsop, D., & Novak, V. (2010). Hypertension and cerebral vasoreactivity: a continuous arterial spin labeling magnetic resonance imaging study. *Hypertension*, 56(5), 859–864. <https://doi.org/10.1161/HYPERTENSIONAHA.110.160002>
- Haley, A. P., Gunstad, J., Cohen, R. A., Jerskey, B. A., Mulligan, R. C., & Sweet, L. H. (2008). Neural Correlates of Visuospatial Working Memory in Healthy Young Adults at Risk for Hypertension. *Brain Imaging and Behavior*, 2(3), 192–199. <https://doi.org/10.1007/s11682-008-9025-4>
- Hamer, M., Batty, G. D., Stamatakis, E., & Kivimaki, M. (2010). The combined influence of hypertension and common mental disorder on all-cause and cardiovascular disease mortality. *Journal of Hypertension*, 28(12), 2401–2406. <https://doi.org/10.1097/HJH.0b013e32833e9d7c>
- Harrison, S. L., Stephan, B. C. M., Siervo, M., Granic, A., Davies, K., Wesnes, K. A., ... Jagger, C. (2015). Is there an association between metabolic syndrome and cognitive function in very old adults? the newcastle 85+ study. *Journal of the American Geriatrics Society*, 63(4), 667–675. <https://doi.org/10.1111/jgs.13358>
- Hassoun, L., Herrmann-Lingen, C., Hapke, U., Neuhauser, H., Scheidt-Nave, C., & Meyer, T. (2015). Association between chronic stress and blood pressure: findings from the German Health Interview and Examination Survey for Adults 2008-2011. *Psychosomatic Medicine*, 77(5), 575–582. <https://doi.org/10.1097/PSY.0000000000000183>
- Higgins, J. P. T., & Green, S. (Eds.). (2011). *Cochrane Handbook for Systematic Reviews of Interventions Version 5.1.0 [updated March 2011]*. The Cochrane Collaboration. Retrieved from <http://handbook.cochrane.org>
- Iadecola, C. (2013). The Pathobiology of Vascular Dementia. *Neuron*, 80(4), 844–866. <https://doi.org/10.1016/j.neuron.2013.10.008>
- Iadecola, C., Yaffe, K., Biller, J., Bratzke, L. C., Faraci, F. M., Gorelick, P. B., ... Zeki Al Hazzouri, A. (2016). Impact of hypertension on cognitive function: a scientific statement from the American Heart Association. *Hypertension*, 68, e67–e94. <https://doi.org/10.1161/HYP.0000000000000053>
- Iordan, A. D., Dolcos, S., & Dolcos, F. (2013). Neural signatures of the response to emotional distraction: a review of evidence from brain imaging investigations. *Frontiers in Human Neuroscience*, 7. <https://doi.org/10.3389/fnhum.2013.00200>
- Jagust, W. J., Zheng, L., Harvey, D. J., Mack, W. J., Vinters, H. V., Weiner, M. W., ... Chui, H. C. (2008). Neuropathological basis of magnetic resonance images in aging and dementia. *Annals of Neurology*, 63(1), 72–80. <https://doi.org/10.1002/ana.21296>
- Jenkinson, M., Beckmann, C. F., Behrens, T. E. J., Woolrich, M. W., & Smith, S. M. (2012). FSL. *NeuroImage*, 62(2), 782–790. <https://doi.org/10.1016/j.neuroimage.2011.09.015>
- Jennings, J. R., Heim, A. F., Sheu, L. K., Muldoon, M. F., Ryan, C., Gach, H. M., ... Gianaros, P. J. (2017). Brain Regional Blood Flow and Working Memory Performance Predict Change in Blood Pressure Over 2 Years. *Hypertension*, 70(6), 1132–1141. <https://doi.org/10.1161/HYPERTENSIONAHA.117.09978>
- Jennings, J. R., Mendelson, D. N., Muldoon, M. F., Ryan, C. M., Gianaros, P. J., Raz, N., & Aizenstein, H. (2012).

- Regional grey matter shrinks in hypertensive individuals despite successful lowering of blood pressure. *Journal of Human Hypertension*, 26(5), 295–305. <https://doi.org/10.1038/jhh.2011.31>
- Jennings, J. R., Muldoon, M. F., Ryan, C., Gach, H. M., Heim, A., Sheu, L. K., & Gianaros, P. J. (2017). Prehypertensive blood pressures and regional cerebral blood flow independently relate to cognitive performance in midlife. *Journal of the American Heart Association*, 6(3), e004856. <https://doi.org/10.1161/JAHA.116.004856>
- Jennings, J. R., Muldoon, M. F., Ryan, C., Price, J. C., Greer, P., Sutton-Tyrrell, K., ... Meltzer, C. C. (2005). Reduced cerebral blood flow response and compensation among patients with untreated hypertension. *Neurology*, 64(8), 1358–1365. <https://doi.org/10.1212/01.WNL.0000158283.28251.3C>
- Jennings, J. R., & Zanstra, Y. (2009). Is the brain the essential in hypertension? *NeuroImage*, 47(3), 914–921. <https://doi.org/10.1016/j.neuroimage.2009.04.072>
- Kaushik, R. M., Mahajan, S. K., Rajesh, V., & Kaushik, R. (2004). Stress profile in essential hypertension. *Hypertension Research*, 27(9), 619–624. <https://doi.org/10.1291/hypres.27.619>
- Kennedy, K. M., Erickson, K. I., Rodrigue, K. M., Voss, M. W., Colcombe, S. J., Kramer, A. F., ... Raz, N. (2009). Age-related differences in regional brain volumes: A comparison of optimized voxel-based morphometry to manual volumetry. *Neurobiology of Aging*, 30(10), 1657–1676. <https://doi.org/10.1016/j.neurobiolaging.2007.12.020>
- Kharabian Masouleh, S., Beyer, F., Lampe, L., Loeffler, M., Luck, T., Riedel-Heller, S. G., ... Witte, A. V. (2018). Gray matter structural networks are associated with cardiovascular risk factors in healthy older adults. *Journal of Cerebral Blood Flow and Metabolism*, 38(2), 360–372. <https://doi.org/10.1177/0271678X17729111>
- King, H., Collins, A., King, L. F., Heywood, P., Alpers, M., Coventry, J., & Zimmet, P. (1985). Blood pressure in Papua New Guinea: A survey of two highland villages in the Asaro Valley. *Journal of Epidemiology and Community Health*, 39(3), 215–219. <https://doi.org/10.1136/jech.39.3.215>
- Kjeldsen, S. E., Narkiewicz, K., Burnier, M., & Oparil, S. (2018). Intensive blood pressure lowering prevents mild cognitive impairment and possible dementia and slows development of white matter lesions in brain: the SPRINT Memory and Cognition IN Decreased Hypertension (SPRINT MIND) study. *Blood Pressure*, 27(5), 247–248. <https://doi.org/10.1080/08037051.2018.1507621>
- Klinke, R., & Silbernagl, S. (1996). *Lehrbuch der Physiologie*. Stuttgart [u.a.]: Thieme.
- Koton, S., Sang, Y., Schneider, A. L. C., Rosamond, W. D., Gottesman, R. F., & Coresh, J. (2019). Trends in Stroke Incidence Rates in Older US Adults. *JAMA Neurology*. <https://doi.org/10.1001/jamaneurol.2019.3258>
- Krantz, D. S., & Manuck, S. B. (1984). Acute psychophysiological reactivity and risk of cardiovascular disease: A review and methodologic critique. *Psychological Bulletin*, 96(3), 435–464. <https://doi.org/10.1037/0033-2909.96.3.435>
- Krause, T., Werner, K., Fiebach, J. B., Villringer, K., Piper, S. K., Haeusler, K. G., ... Nolte, C. H. (2017). Stroke in right dorsal anterior insular cortex Is related to myocardial injury. *Annals of Neurology*, 81(4), 502–511. <https://doi.org/10.1002/ana.24906>
- Krishnamurthi, R. V., Feigin, V. L., Forouzanfar, M. H., Mensah, G. A., Connor, M., Bennett, D. A., ... Murray, C. (2013). Global and regional burden of first-ever ischaemic and haemorrhagic stroke during 1990–2010: findings from the Global Burden of Disease Study 2010. *The Lancet Global Health*, 1(5), e259–e281. [https://doi.org/10.1016/S2214-109X\(13\)70089-5](https://doi.org/10.1016/S2214-109X(13)70089-5)
- Kumral, D., Schaare, H. L., Beyer, F., Reinelt, J., Uhlig, M., Liem, F., ... Gaebler, M. (2019). The age-dependent relationship between resting heart rate variability and functional brain connectivity. *NeuroImage*, 185, 521–533. <https://doi.org/10.1016/j.neuroimage.2018.10.027>
- Lampe, L., Kharabian-Masouleh, S., Kynast, J., Arelin, K., Steele, C. J., Löffler, M., ... Bazin, P.-L. (2017). Lesion location matters: The relationships between white matter hyperintensities on cognition in the healthy elderly. *Journal of Cerebral Blood Flow & Metabolism*, 0271678X1774050. <https://doi.org/10.1177/0271678X17740501>
- Lang, P. J., Davis, M., & Öhman, A. (2000). Fear and anxiety: animal models and human cognitive psychophysiology. *Journal of Affective Disorders*, 61(3), 137–159. [https://doi.org/10.1016/S0165-0327\(00\)00343-8](https://doi.org/10.1016/S0165-0327(00)00343-8)
- Launer, L. J. (1995). The Association Between Midlife Blood Pressure Levels and Late-Life Cognitive Function. *Jama*, 274(23), 1846. <https://doi.org/10.1001/jama.1995.03530230032026>
- Launer, L. J., Lewis, C. E., Schreiner, P. J., Sidney, S., Battapady, H., Jacobs, D. R., ... Bryan, R. N. (2015). Vascular factors and multiple measures of early brain health: CARDIA brain MRI study. *PLoS ONE*, 10(3), e0122138. <https://doi.org/10.1371/journal.pone.0122138>
- Laurent, S., & Boutouyrie, P. (2015). The Structural Factor of Hypertension: Large and Small Artery Alterations.

- Leary, M. C., & Saver, J. L. (2003). Annual Incidence of First Silent Stroke in the United States: A Preliminary Estimate. *Cerebrovascular Diseases*, *16*(3), 280–285. <https://doi.org/10.1159/000071128>
- Leritz, E. C., Salat, D. H., Williams, V. J., Schnyer, D. M., Rudolph, J. L., Lipsitz, L., ... Milberg, W. P. (2011). Thickness of the human cerebral cortex is associated with metrics of cerebrovascular health in a normative sample of community dwelling older adults. *NeuroImage*, *54*(4), 2659–2671. <https://doi.org/10.1016/j.neuroimage.2010.10.050>
- Lim, S. S., Vos, T., Flaxman, A. D., Danaei, G., Shibuya, K., Adair-Rohani, H., ... Ezzati, M. (2012). A comparative risk assessment of burden of disease and injury attributable to 67 risk factors and risk factor clusters in 21 regions, 1990–2010: A systematic analysis for the Global Burden of Disease Study 2010. *The Lancet*, *380*(9859), 2224–2260. [https://doi.org/10.1016/S0140-6736\(12\)61766-8](https://doi.org/10.1016/S0140-6736(12)61766-8)
- Linden, W., Vodermaier, A., MacKenzie, R., & Greig, D. (2012). Anxiety and depression after cancer diagnosis: Prevalence rates by cancer type, gender, and age. *Journal of Affective Disorders*, *141*(2), 343–351. <https://doi.org/https://doi.org/10.1016/j.jad.2012.03.025>
- Loeffler, M., Engel, C., Ahnert, P., Alfermann, D., Arelin, K., Baber, R., ... Thiery, J. (2015). The LIFE-Adult-Study: objectives and design of a population-based cohort study with 10,000 deeply phenotyped adults in Germany. *BMC Public Health*, *15*, 691. <https://doi.org/10.1186/s12889-015-1983-z>
- Lorio, S., Lutti, A., Kherif, F., Ruef, A., Dukart, J., Chowdhury, R., ... Draganski, B. (2014). Disentangling in vivo the effects of iron content and atrophy on the ageing human brain. *NeuroImage*, *103*, 280–289. <https://doi.org/10.1016/j.neuroimage.2014.09.044>
- Macefield, V. G., James, C., & Henderson, L. a. (2013). Identification of sites of sympathetic outflow at rest and during emotional arousal: concurrent recordings of sympathetic nerve activity and fMRI of the brain. *International Journal of Psychophysiology: Official Journal of the International Organization of Psychophysiology*, *89*(3), 451–459. <https://doi.org/10.1016/j.ijpsycho.2013.06.002>
- Maillard, P., Mitchell, G. F., Himali, J. J., Beiser, A., Tsao, C. W., Pase, M. P., ... DeCarli, C. (2016). Effects of Arterial Stiffness on Brain Integrity in Young Adults From the Framingham Heart Study. *Stroke*, *47*(4), 1030–1036. <https://doi.org/10.1161/STROKEAHA.116.012949>
- Maillard, P., Seshadri, S., Beiser, A., Himali, J. J., Au, R., Fletcher, E., ... DeCarli, C. (2012). Effects of systolic blood pressure on white-matter integrity in young adults in the Framingham Heart Study: a cross-sectional study. *The Lancet. Neurology*, *11*(12), 1039–1047. [https://doi.org/10.1016/S1474-4422\(12\)70241-7](https://doi.org/10.1016/S1474-4422(12)70241-7)
- Mancia, G., Fagard, R., Narkiewicz, K., Redon, J., Zanchetti, A., Böhm, M., ... Wood, D. A. (2013). 2013 ESH/ESC Guidelines for the management of arterial hypertension. *European Heart Journal*, *34*(28), 2159–2219. <https://doi.org/10.1093/eurheartj/ehf151>
- Marques, J. P., Kober, T., Krueger, G., van der Zwaag, W., Van de Moortele, P.-F., & Gruetter, R. (2010). MP2RAGE, a self bias-field corrected sequence for improved segmentation and T1-mapping at high field. *NeuroImage*, *49*(2), 1271–1281. <https://doi.org/10.1016/j.neuroimage.2009.10.002>
- Matthews, K. A., Katholi, C. R., McCreath, H., Whooley, M. A., Williams, D. R., Zhu, S., & Markovitz, J. H. (2004). Blood pressure reactivity to psychological stress predicts hypertension in the CARDIA study. *Circulation*, *110*(1), 74–78. <https://doi.org/10.1161/01.CIR.0000133415.37578.E4>
- McEwen, B. S., & Gianaros, P. J. (2011). Stress- and allostasis-induced brain plasticity. *Annual Review of Medicine*, *62*, 431–445. <https://doi.org/10.1146/annurev-med-052209-100430>
- Mendes, N., Oligschläger, S., Lauckner, M. E., Golchert, J., Huntenburg, J. M., Falkiewicz, M., ... Margulies, D. S. (2019). A functional connectome phenotyping dataset including cognitive state and personality measures. *Scientific Data*, *6*, 180307. <https://doi.org/10.1038/sdata.2018.307>
- Minati, L., Jones, C. L., Gray, M. A., Medford, N., Harrison, N. A., & Critchley, H. D. (2009). Emotional modulation of visual cortex activity: a functional near-infrared spectroscopy study. *NeuroReport*, *20*(15), 1344–1350. <https://doi.org/10.1097/WNR.0b013e328330c751>
- Muller, M., Sigurdsson, S., Kjartansson, O., Aspelund, T., Lopez, O. L., Jonnson, P. V., ... Launer, L. J. (2014). Joint effect of mid- and late-life blood pressure on the brain: the AGES-Reykjavik study. *Neurology*, *82*(24), 2187–2195. <https://doi.org/10.1212/WNL.0000000000000517>
- Muller, M., Van Der Graaf, Y., Visseren, F. L., Mali, W. P. T. M., & Geerlings, M. I. (2012). Hypertension and longitudinal changes in cerebral blood flow: The SMART-MR study. *Annals of Neurology*, *71*(6), 825–833. <https://doi.org/10.1002/ana.23554>

- Muller, M., van der Graaf, Y., Visseren, F. L., Vlek, A. L., Mali, W. Pt., & Geerlings, M. I. (2010). Blood pressure, cerebral blood flow, and brain volumes. The SMART-MR study. *Journal of Hypertension*, *28*(7), 1498–1505. <https://doi.org/10.1097/HJH.0b013e32833951ef>
- Nagata, R., Kawabe, K., & Ikeda, K. (2010). Olmesartan, an Angiotensin II Receptor Blocker, Restores Cerebral Hypoperfusion in Elderly Patients With Hypertension. *Journal of Stroke and Cerebrovascular Diseases*, *19*(3), 236–240. <https://doi.org/10.1016/j.jstrokecerebrovasdis.2009.08.004>
- NCD Risk Factor Collaboration (NCD-RisC). (2016). Worldwide trends in blood pressure from 1975 to 2015: a pooled analysis of 1479 population-based measurement studies with 19·1 million participants. *The Lancet*, *389*(10064), 634–647. [https://doi.org/10.1016/S0140-6736\(16\)31919-5](https://doi.org/10.1016/S0140-6736(16)31919-5)
- Neuhauser, H. K., Adler, C., Rosario, A. S., Diederichs, C., & Ellert, U. (2015). Hypertension prevalence, awareness, treatment and control in Germany 1998 and 2008–11. *Journal of Human Hypertension*, *29*(August), 1–7. <https://doi.org/10.1038/jhh.2014.82>
- Norton, S., Matthews, F. E., Barnes, D. E., Yaffe, K., & Brayne, C. (2014). Potential for primary prevention of Alzheimer’s disease: An analysis of population-based data. *The Lancet Neurology*, *13*(8), 788–794. [https://doi.org/10.1016/S1474-4422\(14\)70136-X](https://doi.org/10.1016/S1474-4422(14)70136-X)
- Nyklíček, I., Vingerhoets, A. J. J. ., & Van Heck, G. . (2001). Hypertension and appraisal of physical and psychological stressors. *Journal of Psychosomatic Research*, *50*(5), 237–244. [https://doi.org/10.1016/S0022-3999\(01\)00194-5](https://doi.org/10.1016/S0022-3999(01)00194-5)
- Okon-Singer, H., Lichtenstein-Vidne, L., & Cohen, N. (2013). Dynamic modulation of emotional processing. *Biological Psychology*, *92*(3), 480–491. <https://doi.org/10.1016/j.biopsycho.2012.05.010>
- Okon-Singer, H., Mehnert, J., Hoyer, J., Hellrung, L., Schaare, H. L., Dukart, J., & Villringer, A. (2014). Neural Control of Vascular Reactions: Impact of Emotion and Attention. *Journal of Neuroscience*, *34*(12), 4251–4259. <https://doi.org/10.1523/JNEUROSCI.0747-13.2014>
- Okon-Singer, H., Tzelgov, J., & Henik, A. (2007). Distinguishing between automaticity and attention in the processing of emotionally significant stimuli. *Emotion*, *7*(1), 147–157. <https://doi.org/10.1037/1528-3542.7.1.147>
- Olsen, M. H., Angell, S. Y., Asma, S., Boutouyrie, P., Burger, D., Chirinos, J. A., ... Wang, J. G. (2016). A call to action and a lifecourse strategy to address the global burden of raised blood pressure on current and future generations: the Lancet Commission on hypertension. *The Lancet*, *388*(10060), 2665–2712. [https://doi.org/10.1016/S0140-6736\(16\)31134-5](https://doi.org/10.1016/S0140-6736(16)31134-5)
- Oppenheimer, S. M., Kedem, G., & Martin, W. M. (1996). Left-insular cortex lesions perturb cardiac autonomic tone in humans. *Clinical Autonomic Research*, *6*(3), 131–140. <https://doi.org/10.1007/BF02281899>
- Panaite, V., Salomon, K., Jin, A., & Rottenberg, J. (2015). Cardiovascular Recovery From Psychological and Physiological Challenge and Risk for Adverse Cardiovascular Outcomes and All-Cause Mortality. *Psychosomatic Medicine*, *77*(3), 215–226. <https://doi.org/10.1097/PSY.0000000000000171>
- Pantoni, L. (2010). Cerebral small vessel disease: from pathogenesis and clinical characteristics to therapeutic challenges. *The Lancet. Neurology*, *9*(7), 689–701. [https://doi.org/10.1016/S1474-4422\(10\)70104-6](https://doi.org/10.1016/S1474-4422(10)70104-6)
- Petrovitch, H., White, L. R., Izmirlian, G., Ross, G. W., Havlik, R. J., Markesbery, W., ... Launer, L. J. (2000). Midlife blood pressure and neuritic plaques, neurofibrillary tangles, and brain weight at death: the HAAS. *Neurobiology of Aging*, *21*(1), 57–62. [https://doi.org/10.1016/S0197-4580\(00\)00106-8](https://doi.org/10.1016/S0197-4580(00)00106-8)
- Pickering, T. G., Hall, J. E., Appel, L. J., Falkner, B. E., Graves, J., Hill, M. N., ... Roccella, E. J. (2005). Recommendations for Blood Pressure Measurement in Humans and Experimental Animals. *Hypertension*, *45*(1), 142–161. <https://doi.org/10.1161/01.HYP.0000150859.47929.8e>
- Power, M. C., Schneider, A. L. C., Wruck, L., Griswold, M., Coker, L. H., Alonso, A., ... Gottesman, R. F. (2016). Life-course blood pressure in relation to brain volumes. *Alzheimer’s and Dementia*, *12*(8), 890–899. <https://doi.org/10.1016/j.jalz.2016.03.012>
- Prospective Studies Collaboration. (2002). Age-specific relevance of usual blood pressure to vascular mortality: a meta-analysis of individual data for one million adults in 61 prospective studies. *The Lancet*, *360*(9349), 1903–1913. [https://doi.org/10.1016/S0140-6736\(02\)11911-8](https://doi.org/10.1016/S0140-6736(02)11911-8)
- Qiu, C., Winblad, B., & Fratiglioni, L. (2009). Low diastolic pressure and risk of dementia in very old people: A longitudinal study. *Dementia and Geriatric Cognitive Disorders*, *28*(3), 213–219. <https://doi.org/10.1159/000236913>
- Radua, J., Mataix-Cols, D., Phillips, M. L., El-Hage, W., Kronhaus, D. M., Cardoner, N., & Surguladze, S. (2012). A new meta-analytic method for neuroimaging studies that combines reported peak coordinates and statistical parametric maps. *European Psychiatry*, *27*(8), 605–611. <https://doi.org/10.1016/j.eurpsy.2011.04.001>

- Rapsomaniki, E., Timmis, A., George, J., Pujades-Rodriguez, M., Shah, A. D., Denaxas, S., ... Hemingway, H. (2014). Blood pressure and incidence of twelve cardiovascular diseases: lifetime risks, healthy life-years lost, and age-specific associations in 1.25 million people. *Lancet*, *383*(9932), 1899–1911. [https://doi.org/10.1016/S0140-6736\(14\)60685-1](https://doi.org/10.1016/S0140-6736(14)60685-1)
- Rau, H., & Elbert, T. (2001). Psychophysiology of arterial baroreceptors and the etiology of hypertension. *Biological Psychology*, *57*(1–3), 179–201. [https://doi.org/10.1016/S0301-0511\(01\)00094-1](https://doi.org/10.1016/S0301-0511(01)00094-1)
- Raz, N., Lindenberger, U., Rodrigue, K. M., Kennedy, K. M., Head, D., Williamson, A., ... Acker, J. D. (2005). Regional brain changes in aging healthy adults: general trends, individual differences and modifiers. *Cerebral Cortex*, *15*(11), 1676–1689. <https://doi.org/10.1093/cercor/bhi044>
- Raz, N., Rodrigue, K. M., Kennedy, K. M., & Acker, J. D. (2007). Vascular health and longitudinal changes in brain and cognition in middle-aged and older adults. *Neuropsychology*, *21*(2), 149–157. <https://doi.org/10.1037/0894-4105.21.2.149>
- Reinelt, J., Uhlig, M., Müller, K., Lauckner, M. E., Kumral, D., Schaare, H. L., ... Gaebler, M. (2019). Acute psychosocial stress alters thalamic network centrality. *NeuroImage*, *199*, 680–690. <https://doi.org/10.1016/j.neuroimage.2019.06.005>
- Robinson, R. G., & Jorge, R. E. (2016). Post-stroke depression: A review. *American Journal of Psychiatry*, *173*(3), 221–231. <https://doi.org/10.1176/appi.ajp.2015.15030363>
- Rose, K. M., North, K., Arnett, D. K., Ellison, R. C., Hunt, S. C., Lewis, C. E., & Tyroler, H. a. (2004). Blood pressure and pulse responses to three stressors: associations with sociodemographic characteristics and cardiovascular risk factors. *Journal of Human Hypertension*, *18*(5), 333–341. <https://doi.org/10.1038/sj.jhh.1001677>
- Roth, G. A., Johnson, C., Abajobir, A., Abd-Allah, F., Abera, S. F., Abyu, G., ... Murray, C. (2017). Global, Regional, and National Burden of Cardiovascular Diseases for 10 Causes, 1990 to 2015. *Journal of the American College of Cardiology*, *70*(1), 1–25. <https://doi.org/10.1016/j.jacc.2017.04.052>
- Sakaki, M., Yoo, H. J., Nga, L., Lee, T.-H., Thayer, J. F., & Mather, M. (2016). Heart rate variability is associated with amygdala functional connectivity with MPFC across younger and older adults. *NeuroImage*, *139*, 44–52. <https://doi.org/10.1016/j.neuroimage.2016.05.076>
- Salat, D. H., Williams, V. J., Leritz, E. C., Schnyer, D. M., Rudolph, J. L., Lipsitz, L. A., ... Milberg, W. P. (2012). Inter-individual variation in blood pressure is associated with regional white matter integrity in generally healthy older adults. *NeuroImage*, *59*(1), 181–192. <https://doi.org/10.1016/j.neuroimage.2011.07.033>
- Schaare, H. L., Kharabian Masouleh, S., Beyer, F., Kumral, D., Uhlig, M., Reinelt, J. D., ... Villringer, A. (2019). Association of peripheral blood pressure with gray matter volume in 19- to 40-year-old adults. *Neurology*, *92*(8), e758–e773. <https://doi.org/10.1212/wnl.00000000000006947>
- Schneider, G. M., Jacobs, D. W., Gevirtz, R. N., & O'Connor, D. T. (2003). Cardiovascular haemodynamic response to repeated mental stress in normotensive subjects at genetic risk of hypertension: evidence of enhanced reactivity, blunted adaptation, and delayed recovery. *Journal of Human Hypertension*, *17*(12), 829–840. <https://doi.org/10.1038/sj.jhh.1001624>
- Sierra, C., Coca, A., & Schiffrin, E. L. (2011). Vascular mechanisms in the pathogenesis of stroke. *Current Hypertension Reports*, *13*(3), 200–207. <https://doi.org/10.1007/s11906-011-0195-x>
- Smith, E. E., Saposnik, G., Biessels, G. J., Doubal, F. N., Fornage, M., Gorelick, P. B., ... Higashida, R. T. (2017). AHA / ASA Scientific Statement Prevention of Stroke in Patients With Silent Cerebrovascular Disease, 44–71. <https://doi.org/10.1161/STR.0000000000000116>
- SPRINT Research Group. (2015). A Randomized Trial of Intensive versus Standard Blood-Pressure Control. *New England Journal of Medicine*, *373*(22), 2103–2116. <https://doi.org/10.1056/NEJMoa1511939>
- Statistisches Bundesamt (Destatis). (2018). Krankheitskosten: Deutschland, Jahre, Krankheitsdiagnosen (ICD-10). Retrieved April 6, 2018, from <https://www-genesis.destatis.de/genesis/online/data>
- Steptoe, A., & Kivimäki, M. (2013). Stress and Cardiovascular Disease: An Update on Current Knowledge. *Annual Review of Public Health*, *34*(1), 337–354. <https://doi.org/10.1146/annurev-publhealth-031912-114452>
- Streitbürger, D.-P., Pampel, A., Krueger, G., Lepsien, J., Schroeter, M. L., Mueller, K., & Möller, H. E. (2014). Impact of image acquisition on voxel-based-morphometry investigations of age-related structural brain changes. *NeuroImage*, *87*, 170–182. <https://doi.org/10.1016/j.neuroimage.2013.10.051>
- Strong, J. P., Malcom, G. T., McMahan, C. A., Tracy, R. E., Iii, W. P. N., Herderick, E. E., & Cornhill, J. F. (1999). Prevalence and Extent of Atherosclerosis in Adolescents and Young Adults. *JAMA*, *281*(8), 727–735. <https://doi.org/10.1001/jama.281.8.727>

- Tardif, C. L., Steele, C. J., Lampe, L., Bazin, P. L., Ragert, P., Villringer, A., & Gauthier, C. J. (2017). Investigation of the confounding effects of vasculature and metabolism on computational anatomy studies. *NeuroImage*, *149*, 233–243. <https://doi.org/10.1016/j.neuroimage.2017.01.025>
- Thayer, J. F., Åhs, F., Fredrikson, M., Sollers, J. J., & Wager, T. D. (2012). A meta-analysis of heart rate variability and neuroimaging studies: Implications for heart rate variability as a marker of stress and health. *Neuroscience & Biobehavioral Reviews*, *36*(2), 747–756. <https://doi.org/10.1016/j.neubiorev.2011.11.009>
- Timio, M., Lippi, G., Venanzi, S., Gentili, S., Quintaliani, G., Verdura, C., ... Timio, F. (1997). Blood pressure trend and cardiovascular events in nuns in a secluded order: a 30-year follow-up study. *Blood Pressure*, *6*(2), 81–87. <https://doi.org/10.3109/08037059709061804>
- Timio, M., Verdecchia, P., Venanzi, S., Gentili, S., Ronconi, M., Francucci, B., ... Bichisao, E. (1988). Age and blood pressure changes. A 20-year follow-up study in nuns in a secluded order. *Hypertension*, *12*(4), 457–461. <https://doi.org/10.1161/01.HYP.12.4.457>
- Treiber, F. A., Kamarck, T., Schneiderman, N., Sheffield, D., Kapuku, G., & Taylor, T. (2003). Cardiovascular reactivity and development of preclinical and clinical disease states. *Psychosomatic Medicine*, *65*(1), 46–62. <https://doi.org/10.1097/00006842-200301000-00007>
- Trotman, G. P., Gianaros, P. J., Veldhuijzen van Zanten, J. J. C. S., Williams, S. E., & Ginty, A. T. (2018). Increased stressor-evoked cardiovascular reactivity is associated with reduced amygdala and hippocampus volume. *Psychophysiology*, e13277. <https://doi.org/10.1111/psyp.13277>
- Tzourio, C., Laurent, S., & Debette, S. (2014). Is Hypertension Associated With an Accelerated Aging of the Brain? *Hypertension*, *63*(5), 894–903. <https://doi.org/10.1161/HYPERTENSIONAHA.113.00147>
- Umetani, K., Singer, D. H., McCraty, R., & Atkinson, M. (1998). Twenty-Four Hour Time Domain Heart Rate Variability and Heart Rate: Relations to Age and Gender Over Nine Decades. *Journal of the American College of Cardiology*, *31*(3), 593–601. [https://doi.org/10.1016/S0735-1097\(97\)00554-8](https://doi.org/10.1016/S0735-1097(97)00554-8)
- Vaitl, D. (2001). *Hypertonie*. Göttingen [u.a.]: Hogrefe.
- Veglio, F., Paglieri, C., Rabbia, F., Bisbocci, D., Bergui, M., & Cerrato, P. (2009). Hypertension and cerebrovascular damage. *Atherosclerosis*. <https://doi.org/10.1016/j.atherosclerosis.2008.10.028>
- Verhaaren, B. F. J., Vernooij, M. W., de Boer, R., Hofman, A., Niessen, W. J., van der Lugt, A., & Ikram, M. A. (2013). High blood pressure and cerebral white matter lesion progression in the general population. *Hypertension*, *61*(6), 1354–1359. <https://doi.org/10.1161/HYPERTENSIONAHA.111.00430>
- Volpe, M., Gallo, G., Battistoni, A., & Tocci, G. (2019). Implications of Guidelines for Hypertension Management in Europe. *Circulation Research*, *124*(7), 972–974. <https://doi.org/10.1161/CIRCRESAHA.119.314724>
- Waldstein, S. R., Manuck, S. B., Ryan, C. M., & Muldoon, M. F. (1991). Neuropsychological correlates of hypertension: Review and methodologic considerations. *Psychological Bulletin*, *110*(3), 451–468. <https://doi.org/10.1037/0033-2909.110.3.451>
- Wardlaw, J. M., Smith, C., & Dichgans, M. (2013). Mechanisms underlying sporadic cerebral small vessel disease: insights from neuroimaging. *Lancet Neurology*, *12*(5), 70060–70067. [https://doi.org/10.1016/S1474-4422\(13\)70060-7](https://doi.org/10.1016/S1474-4422(13)70060-7).Mechanisms
- Weber, R., Weimar, C., Blatchford, J., Hermansson, K., Wanke, I., Möller-Hartmann, C., ... PRoFESS Imaging Substudy Group. (2012). Telmisartan on Top of Antihypertensive Treatment Does Not Prevent Progression of Cerebral White Matter Lesions in the Prevention Regimen for Effectively Avoiding Second Strokes (PRoFESS) MRI Substudy. *Stroke*, *43*(9), 2336–2342. <https://doi.org/10.1161/STROKEAHA.111.648576>
- Whelton, P. K., Carey, R. M., Aronow, W. S., Casey, D. E., Collins, K. J., Dennison Himmelfarb, C., ... Wright, J. T. (2017). 2017 ACC/AHA/AAPA/ABC/ACPM/AGS/APhA/ASH/ASPC/NMA/PCNA Guideline for the Prevention, Detection, Evaluation, and Management of High Blood Pressure in Adults. *Hypertension*, HYP.0000000000000065. <https://doi.org/10.1161/HYP.0000000000000065>
- Williams, B., Mancia, G., Spiering, W., Agabiti Rosei, E., Azizi, M., Burnier, M., ... Brady, A. (2018). 2018 ESC/ESH Guidelines for the management of arterial hypertension. *European Heart Journal*, *39*(33), 3021–3104. <https://doi.org/10.1093/eurheartj/ehy339>
- Williamson, J. D., Launer, L. J., Bryan, R. N., Coker, L. H., Lazar, R. M., Gerstein, H. C., ... Action to Control Cardiovascular Risk in Diabetes Memory in Diabetes Investigators. (2014). Cognitive Function and Brain Structure in Persons With Type 2 Diabetes Mellitus After Intensive Lowering of Blood Pressure and Lipid Levels. *JAMA Internal Medicine*, *174*(3), 324. <https://doi.org/10.1001/jamainternmed.2013.13656>
- Williamson, J. D., Pajewski, N. M., Auchus, A. P., Bryan, R. N., Chelune, G., Cheung, A. K., ... Wright, C. B. (2019).

Effect of Intensive vs Standard Blood Pressure Control on Probable Dementia: A Randomized Clinical Trial. *JAMA*, 27157, 1–9. <https://doi.org/10.1001/JAMA.2018.21442>

- Woo, M. A., Macey, P. M., Fonarow, G. C., Hamilton, M. A., & Harper, R. M. (2003). Regional brain gray matter loss in heart failure. *Journal of Applied Physiology (Bethesda, Md. : 1985)*, 95(2), 677–684. <https://doi.org/10.1152/jappphysiol.00101.2003>
- Yaffe, K., Vittinghoff, E., Pletcher, M. J., Hoang, T. D., Launer, L. J., Whitmer, R., ... Sidney, S. (2014). Early adult to midlife cardiovascular risk factors and cognitive function. *Circulation*, 129(15), 1560–1567. <https://doi.org/10.1161/CIRCULATIONAHA.113.004798>
- Yano, Y., Ning, H., Reis, J. P., Lewis, C. E., Launer, L. J., Bryan, R. N., ... Liu, K. (2016). Blood Pressure Reactivity to Psychological Stress in Young Adults and Cognition in Midlife: The Coronary Artery Risk Development in Young Adults (CARDIA) Study. *Journal of the American Heart Association*, 5(1). <https://doi.org/10.1161/JAHA.115.002718>
- Yin, Y., Jin, C., Hu, X., Duan, L., Li, Z., Song, M., ... Li, L. (2011). Altered resting-state functional connectivity of thalamus in earthquake-induced posttraumatic stress disorder: A functional magnetic resonance imaging study. *Brain Research*, 1411, 98–107. <https://doi.org/10.1016/j.brainres.2011.07.016>
- Zhang, R., Witkowski, S., Fu, Q., Claassen, J. A. H. R., & Levine, B. D. (2007). Cerebral Hemodynamics After Short- and Long-Term Reduction in Blood Pressure in Mild and Moderate Hypertension. *Hypertension*, 49(5), 1149–1155. <https://doi.org/10.1161/HYPERTENSIONAHA.106.084939>

7 Appendix

7.1 Supplementary Materials of Study 3

Supplementary Table 1 – List of exclusion criteria for each study from which the samples were drawn

Study	Exclusion criteria
Leipzig Study for Mind-Body-Emotion Interactions (sample 1) (Babayan et al., 2019)	<ul style="list-style-type: none"> • Age <20 or 36-58 or >77 • Self-reported diagnosis of hypertension without intake of antihypertensive medication • Any other cardiovascular disease (e.g. heart attack, congenital heart defect) • History of psychiatric diseases that required inpatient treatment for longer than 2 weeks within the last 10 years (e.g. psychosis, attempted suicide, post-traumatic stress disorder) • History of neurological disorders (incl. multiple sclerosis, stroke, epilepsy, brain tumor, meningoencephalitis, severe concussion) • History of malignant diseases • Intake of one of the following medications: <ul style="list-style-type: none"> • Any centrally active drugs (including Hypericum perforatum) • Beta- and alpha-blocker • Cortisol • Any chemotherapeutic or psychopharmacological medication • Positive drug anamnesis (extensive alcohol, MDMA, amphetamines, cocaine, opiates, benzodiazepine, cannabis) • Body Mass Index < 18 or > 30 • Previous participation in any scientific study • Past or present student of Psychology • MRI exclusion criteria including: <ul style="list-style-type: none"> • Any metallic implants, braces, non-removable piercings • Tattoos • Pregnancy • Claustrophobia • Tinnitus • Surgical operation in the last 3 months
Neural Consequences of Stress Study (sample 2) (Reinelt et al., 2019)	<ul style="list-style-type: none"> • Female sex • Age < 20 or >35 • Smoking • Past or present student of Psychology • Excessive alcohol or drug consumption • Regular medication intake • History of cardiovascular or neurological diseases • Body Mass Index > 27 • Positive drug anamnesis (extensive alcohol, MDMA, amphetamines, cocaine, opiates, benzodiazepine, cannabis) • Positive diagnosis in psychiatric screening of axis I disorders • Abnormalities in analysis of blood screening • MRI exclusion criteria including: <ul style="list-style-type: none"> • Any metallic implants, braces, non-removable piercings • Tattoos • Pregnancy • Claustrophobia • Tinnitus • Surgical operation in the last 3 months
Neuroanatomy and Connectivity Protocol (sample 3) (Mendes et al., 2019)	<ul style="list-style-type: none"> • Age < 20 or >75 • History of psychiatric diseases that required inpatient treatment for longer than 2 weeks within the last 10 years (e.g. psychosis, attempted suicide, post-traumatic stress disorder) • History of neurological disorders (incl. multiple sclerosis, stroke, epilepsy, brain tumor, meningoencephalitis, severe concussion) • History of malignant diseases • Intake of one of the following medications: <ul style="list-style-type: none"> • Any centrally active drugs (including Hypericum perforatum) • Beta-and alpha-blocker • Cortisol • Any chemotherapeutic or psychopharmacological medication • Positive drug anamnesis (extensive alcohol, MDMA, amphetamines, cocaine, opiates, benzodiazepine, cannabis) • Body Mass Index <18 or >30

	<ul style="list-style-type: none"> • Extensive testing experience at the Max-Planck-Institute or other academic institution • Past or present student of Psychology • MRI exclusion criteria: <ul style="list-style-type: none"> • Any metallic implants, braces, non-removable piercings • Tattoos • Pregnancy • Claustrophobia • Tinnitus • Surgical operation in the last 3 months
Leipzig Research Centre for Civilization Diseases (sample 4) (Loeffler et al., 2015)	<ul style="list-style-type: none"> • History of neurological disorders (incl. multiple sclerosis, stroke, epilepsy, parkinson's disease, brain tumor) • History of malignant diseases • History of depression • History of cardiovascular disease (e.g. myocardial infarction, coronary heart disease, heart surgery, bypass, catheter, stent) • Hypertension • Intake of anti-hypertensive drugs • Intake of centrally-active drugs • Diabetes (Type I or II) • MRI exclusion criteria: <ul style="list-style-type: none"> • Any metallic implants, braces, non-removable piercings • Tattoos • Pregnancy • Claustrophobia • Tinnitus • Surgical operation in the last 3 months

Supplementary Table 2 – Positive image-based meta-analysis results of regional gray matter volume differences associated with blood pressure

Image-based meta-analysis results of significant clusters yielding higher grey matter volume for the respective contrast of interest. Columns indicate cluster-specific MNI coordinates of peak voxels, meta-analytic SDM-Z-value, meta-analytic p-value, number of voxels in cluster and anatomical label of the peak voxel. Anatomical labels were assigned using SPM's Anatomy toolbox⁸. Q and I² are measures of meta-analytic heterogeneity. Voxel threshold was set to $p < 0.005$, peak height threshold was set to $SDM-Z > 1.0$ and cluster extent threshold was set to $k \geq 10$ voxels as recommended by Radua et al. (2012)⁷. Final voxel size was $2 \times 2 \times 2 \text{ mm}^3$. MNI: Montreal Neurological Institute. SDM: Seed-based d Mapping. SBP: Systolic blood pressure. DBP: Diastolic blood pressure.

	MNI (x/y/z)	SDM- Z	P	k	Peak Description	Q	I ²
<i>Positive Correlation with Systolic Blood Pressure</i>							
	32,-74,-8	2.249	0.000	294	N/A (right occipital cortex)	0.000	0.0
	-50,-10,-18	1.922	0.001	79	Left middle temporal gyrus	0.230	0.0
	12,-74,-4	2.155	0.000	58	Right lingual gyrus	0.000	0.0
	-30,-94,-12	2.325	0.000	50	Left inferior occipital gyrus	0.000	0.0
	26,24,40	2.480	0.000	31	Right middle frontal gyrus	0.000	0.0
	-18,-100,-2	2.044	0.001	32	Left middle occipital gyrus	0.000	0.0
	-48,-72,-36	1.653	0.002	34	Left cerebellum, crus I	0.159	0.0
	56,-26,-18	2.478	0.000	27	Right inferior temporal gyrus	0.200	0.0
	52,-52,-6	1.882	0.001	29	Right inferior temporal gyrus	0.031	0.0
	-34,-82,-8	1.998	0.001	27	Left inferior occipital gyrus	0.374	7.8
	-26,-92,8	2.057	0.001	22	Left middle occipital gyrus	0.040	0.0
	48,0,-22	1.822	0.001	21	Right middle temporal gyrus	0.000	0.0
	-28,-36,-38	1.639	0.003	20	Left cerebellum, hemispheric lobule VI	0.000	0.0
	52,-20,40	1.616	0.003	18	Right postcentral gyrus	0.224	0.0

	48,-44,32	1.761	0.002	14	Right supramarginal gyrus	0.473	14.8
	-36,2,-36	1.763	0.002	13	Left inferior temporal gyrus	0.000	0.0
	40,-66,28	1.722	0.002	10	Right middle occipital gyrus	1.257	51.3
	30,-58,42	1.656	0.002	10	Right angular gyrus	1.432	56.3
<hr/>							
<i>Positive Correlation with Diastolic Blood</i>							
<i>Pressure</i>	30,-88,-22	2.691	0.000	752	N/A (right cerebellum, crus I)	0.046	0.0
	-36,-84,-10	2.294	0.001	235	Left inferior occipital gyrus	0.000	0.0
	-14,-6,20	2.414	0.000	90	Left caudate nucleus	0.103	0.0
	2,-74,-24	1.921	0.002	82	Cerebellum, vermic lobule VII	0.086	0.0
	-26,-90,6	2.350	0.001	37	Left middle occipital gyrus	0.000	0.0
	-54,-46,-8	2.151	0.001	36	Left middle temporal gyrus	0.419	11.0
	18,-2,20	1.996	0.002	28	Right caudate nucleus	0.000	0.0
	42,-60,40	2.035	0.002	17	Right angular gyrus	0.000	0.0
	48,-48,-48	2.057	0.002	12	Right cerebellum, crus II	0.000	0.0
	24,-96,-12	1.884	0.003	10	Right inferior occipital gyrus	0.558	20.3
<hr/>							
<i>Category 4 (SBP\geq140 mmHg or DBP\geq90 mmHg) > Category 1 (SBP<120 mmHg and DBP<80 mmHg)</i>							
	42,-66,26	2.320	0.000	87	Right middle occipital gyrus	0.000	0.0
	12,-2,16	1.927	0.001	71	Right caudate nucleus	0.000	0.0
	48,-44,-12	2.142	0.000	48	Right inferior temporal gyrus	0.000	0.0
	30,-52,46	1.942	0.001	41	Right inferior parietal lobule	0.000	0.0
	28,-78,24	1.907	0.001	33	Right middle occipital gyrus	0.088	0.0
	34,-78,-24	1.716	0.002	35	Right cerebellum, crus I	0.195	0.0
	54,-28,-18	1.857	0.001	22	Right inferior temporal gyrus	0.000	0.0
	-30,-36,64	1.727	0.002	20	Left postcentral gyrus	0.313	3.1
	-56,-30,32	1.732	0.002	19	Left supramarginal gyrus	0.000	0.0
	-20,56,12	1.845	0.001	17	Left superior frontal gyrus	0.000	0.0
	32,-66,34	1.625	0.003	17	Right middle occipital gyrus	0.212	0.0
	24,24,40	1.869	0.001	16	Right middle frontal gyrus	0.000	0.0
	-52,-66,-36	1.807	0.001	14	Left cerebellum, crus I	0.000	0.0
	-36,0,-36	1.938	0.001	12	Left inferior temporal gyrus	0.114	0.0
	-48,-46,20	1.884	0.001	10	Left superior temporal gyrus	0.000	0.0
<hr/>							
<i>Category 3 (SBP 130-139 mmHg or DBP 85-89 mmHg) > Category 1</i>							
	12,-54,-6	3.439	0.000	537	Right lingual gyrus	0.018	0.0
	-8,-56,-42	2.728	0.001	172	Left cerebellum, hemispheric lobule IX	0.000	0.0
	6,-38,24	3.167	0.000	78	N/A (right midcingulate cortex)	0.000	0.0
	-14,-100,-2	2.800	0.001	57	Left calcarine gyrus	0.000	0.0
	-30,-12,56	2.902	0.000	46	Left precentral gyrus	0.000	0.0
	36,4,-38	3.477	0.000	35	Right medial temporal pole	0.000	0.0
	-8,-54,-8	2.378	0.003	41	Left cerebellum, hemispheric lobule IV-V	0.000	0.0

	-28,-46,-20	2.670	0.001	37	Left fusiform gyrus	0.265	0.0
	-54,-10,-4	2.937	0.000	26	Left superior temporal gyrus	0.000	0.0
	58,-54,-24	2.798	0.001	24	Right inferior temporal gyrus	0.000	0.0
	58,6,-22	2.345	0.003	23	Right medial temporal pole	0.000	0.0
	8,-90,30	2.573	0.002	15	Right cuneus	0.000	0.0
	-28,-92,6	2.330	0.004	11	Left middle occipital gyrus	0.000	0.0
<hr/>							
<i>Category 2 (SBP 120-129 mmHg or DBP 80-84 mmHg) > Category 1</i>							
	-46,-48,-36	3.501	0.000	565	Left cerebellum, crus I	0.241	0.0
	-10,-54,-8	2.382	0.001	173	Left cerebellum, hemispheric lobule IV-V	0.000	0.0
	-34,-32,62	2.972	0.000	106	Left postcentral gyrus	0.000	0.0
	-28,-10,56	2.619	0.000	80	Left precentral gyrus	0.000	0.0
	48,-52,-30	2.224	0.002	61	Right cerebellum, crus I	0.243	0.0
	8,-12,64	2.442	0.001	41	Right posterior-medial frontal	0.000	0.0
	8,-80,-46	2.040	0.003	41	Right cerebellum, hemispheric lobule VII	0.351	6.0
	38,-72,26	2.726	0.000	28	Right middle occipital gyrus	0.000	0.0
	-44,36,4	2.557	0.001	29	Left inferior frontal gyrus (p. triangularis)	0.000	0.0
	-24,-44,60	2.246	0.001	27	Left postcentral gyrus	0.000	0.0
	-36,-52,58	2.542	0.001	17	Left superior parietal lobule	0.000	0.0
	20,2,68	2.247	0.001	18	Right superior frontal gyrus	0.000	0.0
	30,-72,-8	2.394	0.001	15	Right fusiform gyrus	0.232	0.0
	20,-66,34	2.122	0.002	15	Right cuneus	0.022	0.0
	6,30,14	2.281	0.001	12	Right anterior cingulate cortex	0.000	0.0
	44,-58,0	2.179	0.002	11	N/A	0.180	0.0

Supplementary Table 3 – Image-based meta-analysis results of regional gray matter volume differences associated with first systolic blood pressure

Image-based meta-analysis results of significant clusters yielding lower grey matter volume for the respective contrast of interest (averaged SBP, first SBP). Columns indicate cluster-specific MNI coordinates of peak voxels, meta-analytic SDM-Z-value, meta-analytic p-value, number of voxels in cluster and anatomical label of the peak voxel. Q- and I²-statistics are estimates of meta-analytic heterogeneity of effects across studies. Anatomical labels were assigned using SPM's Anatomy toolbox⁸. Voxel threshold was set to $p < 0.005$, peak height threshold was set to $SDM-Z > 1.0$ and cluster extent threshold was set to $k \geq 10$ voxels. Final voxel size was $2 \times 2 \times 2 \text{ mm}^3$. MNI: Montreal Neurological Institute. SDM: Seed-based d Mapping.

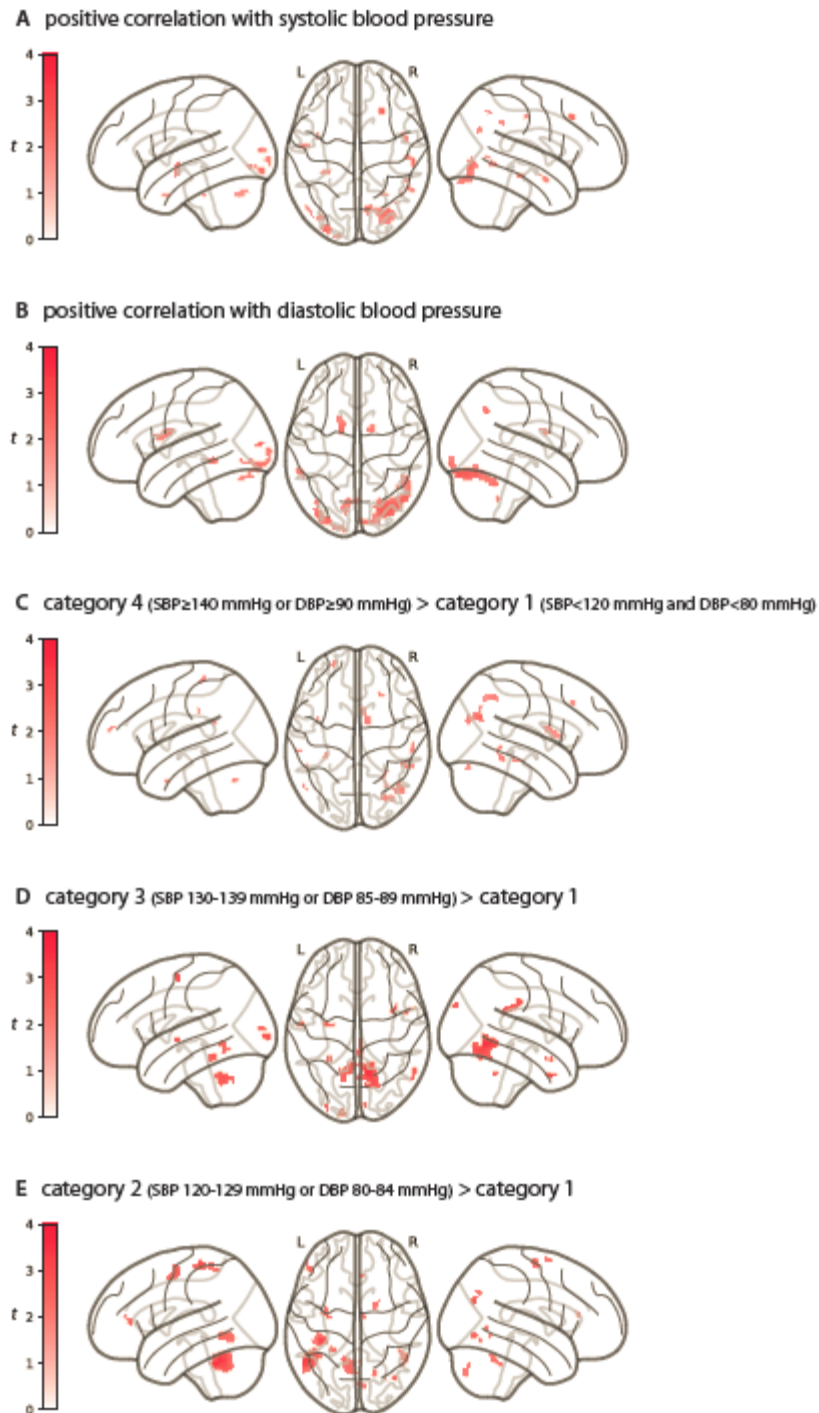
	SDM-						
	MNI (x/y/z)	Z	P	k	Peak Description	Q	I ²
<hr/>							
<i>Negative Correlation with Systolic Blood Pressure</i>	8,-30,56	-3.859	0.000	288	Right paracentral lobule	0.000	0.0
	-40,30,0	-3.590	0.000	49	Left inferior frontal gyrus (p. triangularis)	0.053	0.0
	36,6,34	-3.394	0.000	16	Right inferior frontal gyrus (p. opercularis)	0.000	0.0
	10,2,40	-3.325	0.001	45	Right midcingulate cortex	0.000	0.0
	-58,-20,24	-3.290	0.001	146	Left postcentral gyrus	0.000	0.0

-52,-10,6	-3.268	0.001	78	Left superior temporal gyrus	0.000	0.0
48,32,10	-3.204	0.001	27	Right inferior frontal gyrus (p. triangularis)	0.000	0.0
48,0,48	-3.196	0.001	127	Right precentral gyrus	0.000	0.0
64,-42,12	-3.192	0.001	42	Right superior temporal gyrus	0.000	0.0
6,8,-18	-3.110	0.001	40	Right subgenual cingulate cortex	0.000	0.0
50,8,28	-3.045	0.002	26	Right inferior frontal gyrus (p. opercularis)	0.000	0.0
-8,-76,18	-3.019	0.002	27	Left cuneus cortex	0.175	0.0
8,-28,2	-2.977	0.002	45	Right thalamus	0.000	0.0
10,-68,26	-2.937	0.002	18	Right cuneus cortex	0.000	0.0
58,4,-8	-2.934	0.002	32	Right temporal pole	0.000	0.0
-28,10,60	-2.896	0.003	19	Left middle frontal gyrus	0.000	0.0
-52,-12,42	-2.860	0.003	10	Left postcentral gyrus	0.116	0.0

Negative Correlation with First

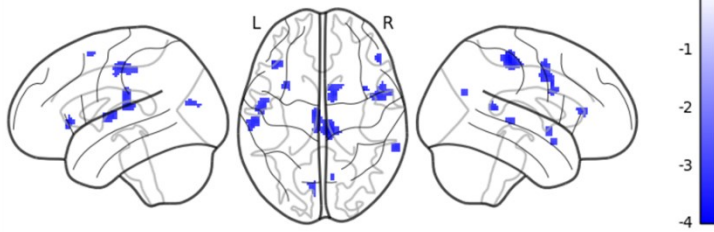
Systolic Blood Pressure

8,-30,56	-4.137	0.000	307	Right paracentral lobule	0.000	0.0
48,0,44	-3.826	0.000	384	Right precentral gyrus	0.000	0.0
-60,-20,24	-3.771	0.000	224	Left postcentral gyrus	0.000	0.0
48,30,12	-3.587	0.000	110	Right inferior frontal gyrus (p. triangularis)	0.000	0.0
14,-30,2	-3.462	0.000	176	Right thalamus	0.000	0.0
10,2,40	-3.382	0.001	44	Right midcingulate cortex	0.000	0.0
-26,24,54	-3.315	0.001	29	Left middle frontal gyrus	0.000	0.0
-42,30,0	-3.308	0.001	28	Left inferior frontal gyrus (p. triangularis)	0.238	0.0
30,-2,62	-3.233	0.001	10	Right superior frontal gyrus	0.000	0.0
64,-44,12	-3.216	0.001	33	Right superior temporal gyrus	0.000	0.0
-54,26,14	-3.203	0.001	26	Left inferior frontal gyrus (p. triangularis)	0.232	0.0
-50,-4,4	-3.196	0.001	60	Left rolandic operculum	0.000	0.0
8,6,-18	-3.075	0.002	35	N/A (Right striatum)	0.000	0.0
-4,34,24	-3.061	0.002	30	Left anterior cingulate cortex	0.000	0.0
-42,4,30	-3.042	0.002	46	Left precentral gyrus	0.000	0.0
58,4,-6	-3.019	0.002	28	Right temporal pole	0.000	0.0
10,-68,26	-2.986	0.002	20	Right cuneus	0.000	0.0
-36,-24,54	-2.974	0.002	14	Left postcentral gyrus	0.000	0.0
-2,-68,18	-2.963	0.003	15	Left calcarine gyrus	0.277	0.1
10,-58,12	-2.947	0.003	25	Right calcarine gyrus	0.000	0.0
-6,-4,36	-2.874	0.004	18	Left midcingulate cortex	0.000	0.0

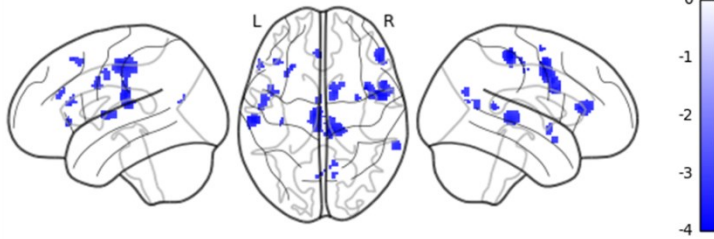


Supplementary Figure 1 – Meta-analytic positive differences in gray matter volume between blood pressure categories
 Glass brain views of image-based meta-analysis results for the blood pressure category contrasts of interest with relevant slice views below (A-E). A and B depict positive correlations between SBP/DBP and gray matter volume, respectively. Red clusters indicate meta-analytic grey matter volume differences for the given contrast at a voxel threshold of $p < 0.005$ with peak height threshold of $\text{SDM-Z} > 1.0$ and cluster extent threshold of $k \geq 10$ (validated for high meta-analytic sensitivity and specificity, Radua et al., 2012). Color bars represent SDM-Z-values. 3D-volumetric results of these analyses can be inspected in detail on <http://neurovault.org/collections/FDWHFSYZ/>. SDM: Seed-based d Mapping. SBP: Systolic blood pressure. DBP: Diastolic blood pressure. L: Left hemisphere. R: Right hemisphere.

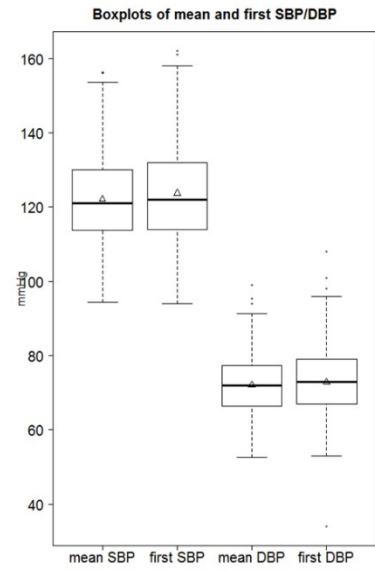
A negative correlation with systolic blood pressure



B negative correlation with 1st systolic blood pressure



C



Supplementary Figure 2 – Associations between gray matter volume and first systolic blood pressure reading

A: Glass brain views of image-based meta-analysis results for the negative correlation between systolic blood pressure and gray matter volume in all four samples ($n=423$). **B:** Glass brain views of image-based meta-analysis results for the negative correlation between first measured systolic blood pressure and gray matter volume in all four samples. Blue clusters indicate meta-analytic gray matter volume differences at a voxel threshold of $p < 0.005$ with peak height threshold of $\text{SDM-Z} < -1.0$ and cluster extent threshold of $k \geq 10$. Color bars represent SDM-Z-values. **C:** Boxplots of mean and first SBP or DBP, respectively, in study samples with ≥ 2 BP readings (samples 1, 2 and 4, $n=353$). Triangles represent the mean. SDM: Seed-based d Mapping. SBP: Systolic blood pressure. DBP: Diastolic blood pressure. L: Left hemisphere. R: Right hemisphere.

7.2 Published Articles of Studies 1-6

7.2.1 A Mind-Brain-Body Dataset of MRI, EEG, Cognition, Emotion, and Peripheral Physiology in Young and Old Adults. Babayan et al., Scientific Data (2019)

www.nature.com/scientificdata

SCIENTIFIC DATA

OPEN Data Descriptor: A mind-brain-body dataset of MRI, EEG, cognition, emotion, and peripheral physiology in young and old adults

Received: 20 June 2018
Accepted: 12 October 2018
Published: 12 February 2019

Anahit Babayan^{1,2}, Miray Erbey^{1,2,3}, Deniz Kumral^{1,2}, Janis D. Reinelt¹, Andrea M. F. Reiter^{1,4,5,6}, Josefin Röbbig⁷, H. Lina Schaare^{1,4}, Marie Uhlig^{1,4}, Alfred Anwander⁷, Pierre-Louis Bazin^{1,8,9}, Annette Horstmann^{1,10}, Leonie Lampe¹, Vadim V. Nikulin¹, Hadas Okon-Singer^{1,11}, Sven Preusser¹, André Pampel¹², Christiane S. Rohr¹, Julia Sacher¹, Angelika Thöne-Otto^{1,13}, Sabrina Trapp¹, Till Nierhaus¹, Denise Altmann¹, Katrin Arelin¹, Maria Blöchl^{1,14}, Edith Bongartz¹, Patric Breig¹, Elena Cesnaite¹, Sufang Chen¹, Roberto Cozani¹⁵, Saskia Czerwonatis¹, Gabriele Dambrauskaitė¹, Maria Dreyer¹, Jessica Enders¹, Melina Engelhardt¹, Marie Michele Fischer¹, Norman Forscheck¹, Johannes Golkert¹⁶, Laura Golz¹, C. Alexandrina Guran¹, Susanna Hedrich¹, Nicole Hentschel¹, Daria I. Hoffmann¹, Julia M. Huntenburg¹⁶, Rebecca Jost¹, Anna Kosatschek¹, Stella Kunzendorf¹, Hannah Lammers¹, Mark E. Lauckner¹⁶, Keyvan Mahjoory¹, Ahmad S. Kanaan¹⁷, Natacha Mendes¹⁶, Ramona Menger¹, Enzo Morino¹, Karina Nätthe¹⁷, Jennifer Neubauer¹, Handan Noyan¹, Sabine Oligschläger¹⁶, Patricia Panczyszyn-Trzewik¹, Dorothee Poehlichen¹, Nadine Putzke¹, Sabrina Roski¹, Marie-Catherine Schaller¹, Anja Schieferbein¹, Benito Schlaak¹, Robert Schmidt¹⁸, Krzysztof J. Gorgolewski¹⁹, Hanna Maria Schmidt¹, Anne Schrimpf¹, Sylvia Stasch¹, Maria Voss¹, Annett Wiedemann¹, Daniel S. Margulies¹⁶, Michael Gaebler^{1,2,20} & Arno Villringer^{1,2}

¹Department of Neurology, Max Planck Institute for Human Cognitive and Brain Sciences, Leipzig, Germany. ²MindBrainBody Institute at the Berlin School of Mind and Brain, Humboldt-Universität Berlin, Berlin, Germany. ³International Max Planck School on the Life Course, Max Planck Institute for Human Development, Berlin, Germany. ⁴International Max Planck Research School NeuroCom, Max Planck Institute for Human Cognitive and Brain Sciences, Leipzig, Germany. ⁵Max Planck Research Group for Cognitive and Affective Control of Behavioral Adaptation, Max Planck Institute for Human Cognitive and Brain Sciences, Leipzig, Germany. ⁶Lifespan Developmental Neuroscience, Technische Universität Dresden, Dresden, Germany. ⁷Department of Neuropsychology, Max Planck Institute for Human Cognitive and Brain Sciences, Leipzig, Germany. ⁸Netherlands Institute for Neuroscience, Amsterdam, Netherlands. ⁹Spinoza Centre for Neuroimaging, Amsterdam, Netherlands. ¹⁰IFB Adiposity Diseases, Leipzig University Medical Center, Leipzig, Germany. ¹¹Department of Psychology, University of Haifa, Haifa, Israel. ¹²Nuclear Magnetic Resonance Group, Max Planck Institute for Human Cognitive and Brain Sciences, Leipzig, Germany. ¹³Day Clinic for Cognitive Neurology, University Hospital Leipzig, Leipzig, Germany. ¹⁴Department of Psychology, University Leipzig, Leipzig, Germany. ¹⁵Database Management, Max Planck Institute for Human Cognitive and Brain Sciences, Leipzig, Germany. ¹⁶Max Planck Research Group for Neuroanatomy & Connectivity, Max Planck Institute for Human Cognitive and Brain Sciences, Leipzig, Germany. ¹⁷Library, Max Planck Institute for Human Cognitive and Brain Sciences, Leipzig, Germany. ¹⁸Institute for Laboratory Medicine, Clinical Chemistry and Molecular Diagnostics (ILM) of the Medical Faculty at the Leipzig University, Leipzig, Germany. ¹⁹Department of Psychology, Stanford University, Stanford, California 94305, USA. ²⁰Leipzig Research Centre for Civilization Diseases LIFE, Leipzig University, Leipzig, Germany. Correspondence and requests for materials should be addressed to A.B. (email: babayan@cbs.mpg.de) or A.V. (email: villringer@cbs.mpg.de)

SCIENTIFIC DATA | 6:180308 | https://doi.org/10.1038/sdata.2018.308

SCIENTIFIC DATA

OPEN

Data Descriptor: A mind-brain-body dataset of MRI, EEG, cognition, emotion, and peripheral physiology in young and old adults

Received: 20 June 2018

Accepted: 12 October 2018

Published: 12 February 2019

Anahit Babayan^{1,2}, Miray Erbey^{1,2,3}, Deniz Kumral^{1,2}, Janis D. Reinelt¹, Andrea M. F. Reiter^{1,4,5,6}, Josefin Röbbing¹, H. Lina Schaare^{1,4}, Marie Uhlig^{1,4}, Alfred Anwander⁷, Pierre-Louis Bazin^{1,8,9}, Annette Horstmann^{1,10}, Leonie Lampe¹, Vadim V. Nikulin¹, Hadas Okon-Singer^{1,11}, Sven Preusser¹, André Pampel¹², Christiane S. Rohr¹, Julia Sacher¹, Angelika Thöne-Otto^{1,13}, Sabrina Trapp¹, Till Nierhaus¹, Denise Altmann¹, Katrin Arelin¹, Maria Blöchl^{4,14}, Edith Bongartz¹, Patric Breig¹, Elena Cesnaite¹, Sufang Chen¹, Roberto Cozatl¹⁵, Saskia Czerwonatis¹, Gabriele Dambrauskaite¹, Maria Dreyer¹, Jessica Enders¹, Melina Engelhardt¹, Marie Michele Fischer¹, Norman Forschack¹, Johannes Golchert¹⁶, Laura Golz¹, C. Alexandrina Guran¹, Susanna Hedrich¹, Nicole Hentschel¹, Daria I. Hoffmann¹, Julia M. Huntenburg¹⁶, Rebecca Jost¹, Anna Kosatschek¹, Stella Kunzendorf¹, Hannah Lammers¹, Mark E. Lauckner¹⁶, Keyvan Mahjoory¹, Ahmad S. Kanaan¹², Natacha Mendes¹⁶, Ramona Menger¹, Enzo Morino¹, Karina Näthe¹⁷, Jennifer Neubauer¹, Handan Noyan¹, Sabine Oligschläger¹⁶, Patricia Panczyszyn-Trzewik¹, Dorothee Poehlchen¹, Nadine Putzke¹, Sabrina Roski¹, Marie-Catherine Schaller¹, Anja Schieferbein¹, Benito Schlaak¹, Robert Schmidt¹⁸, Krzysztof J. Gorgolewski¹⁹, Hanna Maria Schmidt¹, Anne Schrimpf¹, Sylvia Stasch¹, Maria Voss¹, Annett Wiedemann¹, Daniel S. Margulies¹⁶, Michael Gaebler^{1,2,20} & Arno Villringer^{1,2}

¹Department of Neurology, Max Planck Institute for Human Cognitive and Brain Sciences, Leipzig, Germany.

²MindBrainBody Institute at the Berlin School of Mind and Brain, Humboldt-Universität Berlin, Berlin, Germany.

³International Max Planck School on the Life Course, Max Planck Institute for Human Development, Berlin, Germany.

⁴International Max Planck Research School NeuroCom, Max Planck Institute for Human Cognitive and Brain Sciences, Leipzig, Germany.

⁵Max Planck Research Group for Cognitive and Affective Control of Behavioral Adaptation, Max Planck Institute for Human Cognitive and Brain Sciences, Leipzig, Germany.

⁶Lifespan Developmental Neuroscience, Technische Universität Dresden, Dresden, Germany.

⁷Department of Neuropsychology, Max Planck Institute for Human Cognitive and Brain Sciences, Leipzig, Germany.

⁸Netherlands Institute for Neuroscience, Amsterdam, Netherlands.

⁹Spinoza Centre for Neuroimaging, Amsterdam, Netherlands.

¹⁰IFB Adiposity Diseases, Leipzig University Medical Center, Leipzig, Germany.

¹¹Department of Psychology, University of Haifa, Haifa, Israel.

¹²Nuclear Magnetic Resonance Group, Max Planck Institute for Human Cognitive and Brain Sciences, Leipzig, Germany.

¹³Day Clinic for Cognitive Neurology, University Hospital Leipzig, Leipzig, Germany.

¹⁴Department of Psychology, University Leipzig, Leipzig, Germany.

¹⁵Database Management, Max Planck Institute for Human Cognitive and Brain Sciences, Leipzig, Germany.

¹⁶Max Planck Research Group for Neuroanatomy & Connectivity, Max Planck Institute for Human Cognitive and Brain Sciences, Leipzig, Germany.

¹⁷Library, Max Planck Institute for Human Cognitive and Brain Sciences, Leipzig, Germany.

¹⁸Institute for Laboratory Medicine, Clinical Chemistry and Molecular Diagnostics (ILM) of the Medical Faculty at the Leipzig University, Leipzig, Germany.

¹⁹Department of Psychology, Stanford University, Stanford, California 94305, USA.

²⁰Leipzig Research Centre for Civilization Diseases LIFE, Leipzig University, Leipzig, Germany.

Correspondence and requests for materials should be addressed to A.B. (email: babayan@cbs.mpg.de) or A.V. (email: villringer@cbs.mpg.de)

We present a publicly available dataset of 227 healthy participants comprising a young ($N = 153$, 25.1 ± 3.1 years, range 20–35 years, 45 female) and an elderly group ($N = 74$, 67.6 ± 4.7 years, range 59–77 years, 37 female) acquired cross-sectionally in Leipzig, Germany, between 2013 and 2015 to study mind-body-emotion interactions. During a two-day assessment, participants completed MRI at 3 Tesla (resting-state fMRI, quantitative T1 (MP2RAGE), T2-weighted, FLAIR, SWI/QSM, DWI) and a 62-channel EEG experiment at rest. During task-free resting-state fMRI, cardiovascular measures (blood pressure, heart rate, pulse, respiration) were continuously acquired. Anthropometrics, blood samples, and urine drug tests were obtained. Psychiatric symptoms were identified with Standardized Clinical Interview for DSM IV (SCID-I), Hamilton Depression Scale, and Borderline Symptoms List. Psychological assessment comprised 6 cognitive tests as well as 21 questionnaires related to emotional behavior, personality traits and tendencies, eating behavior, and addictive behavior. We provide information on study design, methods, and details of the data. This dataset is part of the larger MPI Leipzig Mind-Brain-Body database.

Design Type(s)	parallel group design • data collection and processing objective
Measurement Type(s)	brain measurement • behavior
Technology Type(s)	magnetic resonance imaging • questionnaire
Factor Type(s)	age • biological sex • handedness
Sample Characteristic(s)	Homo sapiens • brain

Background & Summary

Emotions - intrinsically related to the body - have a huge influence on our behavior¹. The connection between emotions and the body has been acknowledged by “folk psychology”², language metaphors (e.g., “heart-breaking”), and scientists: in classic theories, emotions arise from our perception of bodily changes, which is understood as more³ or less strongly influenced⁴ by cognitive-evaluative processes. Hence, emotions – like other mental processes – depend on interactions between the brain and the rest of the body. While in psychology, a lot of research measured the physiological effects of psychological manipulations, the inverse (body-mind) direction has been less frequently studied⁵. In clinical research, the opposite is true: While psychological changes after physical or somatic illness, such as depressive symptoms after stroke⁶ or a cancer diagnosis^{7–9} have been investigated, mental factors contributing to bodily diseases have received comparatively less scientific recognition. For example, psychological stress has negative influences on somatic and mental health¹⁰ and emotional episodes like depressive symptoms have been discussed as a risk factor for stroke¹¹, coronary heart disease¹² or diabetes¹³.

Informed by these recent studies, we investigate psychological factors that play a key role in the pathogenesis, development, and treatment of somatic diseases in a multi-modular approach. This “mind-body-emotion” approach emphasizes the bi-directionality of brain-body interactions as they underlie mental phenomena and the importance of psychological factors for somatic health and disease. In the “Leipzig Study for Mind-Body-Emotion Interactions” (LEMON), we acquired a large dataset of physiological, psychological, and neuroimaging measures in younger and older healthy adults.

The LEMON dataset provides the following advantages:

1. Subjects underwent an extensive medical and psychological selection procedure: Past and current somatic or mental illnesses as well as current medication status are well-controlled and documented. Careful adherence to selection and “health” criteria is especially important when investigating healthy aging.
2. Psychometric tools to assess cognitive and socio-emotional characteristics are tailored to relate them to bodily and brain measures. The LEMON dataset thereby enables basic research on the healthy interaction between brain, mind, and body – as it is assumed to be altered in somatic and mental illness.
3. LEMON complements data of brain structure and brain function with extensive bodily measures. Measures of peripheral physiology serve a double function of being utilized for removing artifacts from the Magnetic Resonance Imaging (MRI) data (as e.g., the fMRI BOLD signal is also influenced by magnetic field changes induced by peripheral fluctuations¹⁴). However, in addition to explaining psychological variance for themselves, they can be related to cerebral measures to test for fundamental brain-body interactions at rest (e.g., heart rate variability and fMRI data¹⁵).
4. The current study included a broad set of psychological measures to cover individual psychological categories but also their overlap. This is important as psychological categories are sometimes

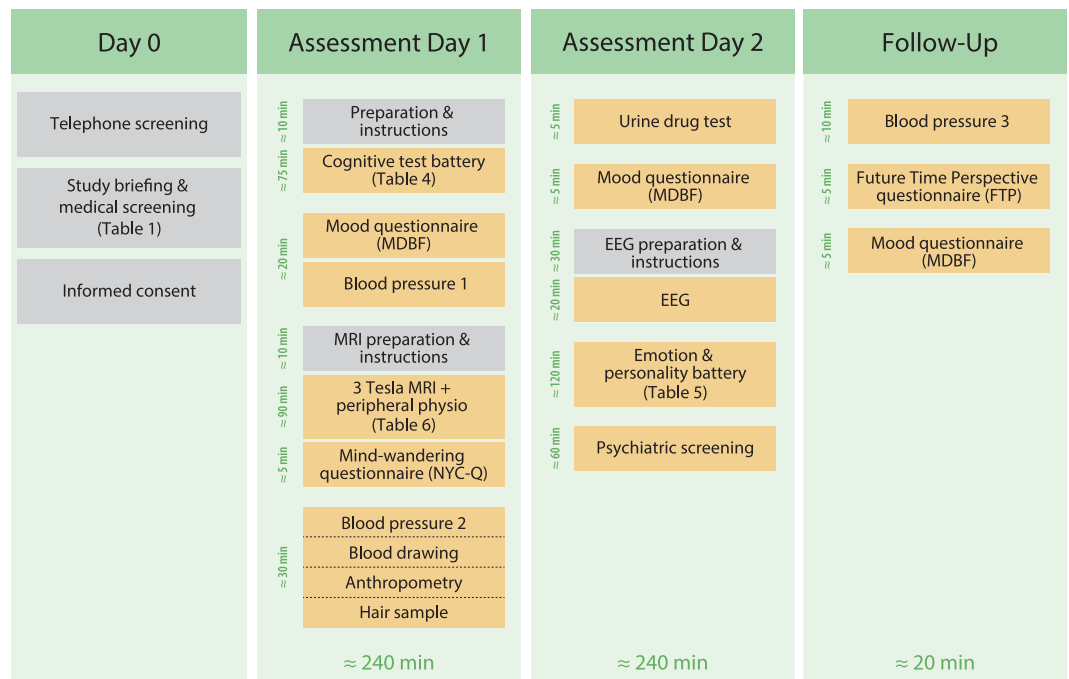


Figure 1. Overview of data acquisition. Measures are listed in their order of acquisition and time duration on each assessment day.

artificially separated, which hinders their comprehensive investigation. This holds true for broader fields like cognition and emotion¹⁶ but also for more specific psychological processes like emotion regulation and value-based decision-making¹⁷. Particularly from a clinical viewpoint, a more integrative approach is beneficial, as risk factors for disease usually do not occur in isolation – and for example mental distress, hypertension, and obesity often co-occur^{18–20}.

In summary, the LEMON dataset is particularly suited to comprehensively relate cognitive and emotional traits or states to physiological characteristics of brain and body. While focusing on fundamental mind-body-emotion interactions in healthy younger and older adults, our data and results may inform clinical research. Here, we present the study's objectives, design, and methods together with available data types, their quality and quantities.

The dataset presented here was acquired as one of two complementary data acquisition protocols on a partially overlapping cohort of participants which constitute the MPI-Leipzig Mind-Brain-Body database. All MRI data of both projects were acquired on the same scanner. Taken in conjunction with the data acquired in the complementary project by Mendes *et al.*²¹, the MPI-Leipzig Mind-Brain-Body (MPILMBB) database aims to enable exploration of individual variance across a wide range of cognitive, emotional, physiological phenotypes in relation to the brain.

Methods

Participants

The total sample included 227 participants in two age groups. The young age group was between 20–35 years old ($N=153$, 45 females, median age=24 years, mean age=25.1 years, standard deviation (SD)=3.1) and the older age group was between 59–77 years old ($N=74$, 37 females, median age=67 years, mean age=67.6 years, SD=4.7). All participants were tested at the Day Clinic for Cognitive Neurology of the University Clinic Leipzig and the Max Planck Institute for Human and Cognitive and Brain Sciences (MPI CBS) in Leipzig, Germany. The study was carried out in accordance with the Declaration of Helsinki and the study protocol was approved by the ethics committee at the medical faculty of the University of Leipzig (reference number 154/13-ff).

Recruitment and Exclusion Criteria

Participants were recruited via public advertisements, leaflets, online advertisements, and information events at the University of Leipzig. Eligibility for the study was determined in two steps that are referred to as Day 0 in Fig. 1. First, we prescreened prospective participants via telephone with a semi-structured interview for study eligibility ($N=695$). Individuals that did not meet any exclusion criteria in the prescreening (Table 1) were invited to MPI CBS to receive detailed information about the study in a

Exclusion criteria via telephone screening: Self-reported
▶ Diagnosis of hypertension without intake of antihypertensive medication
▶ Any other cardiovascular disease (current and/or previous heart attack or congenital heart defect)
▶ History of psychiatric diseases that required inpatient treatment for longer than 2 weeks, within the last 10 years (psychosis, attempted suicide, post-traumatic stress disorder)
▶ History of neurological disorders (multiple sclerosis, stroke, epilepsy, brain tumor, meningoencephalitis, severe concussion)
▶ History of malignant diseases
▶ Intake of one of the following medications (centrally active medication, beta- and alpha-blocker, cortisol, any chemotherapeutic or psychopharmacological medication)
▶ Positive drug anamnesis (extensive alcohol, MDMA, amphetamines, cocaine, opiates, benzodiazepine, cannabis)
▶ MRI exclusion criteria (metallic implants, braces, non-removable piercings, tattoos, pregnancy, claustrophobia, tinnitus, surgical operation in the last 3 months)
▶ Previous participation in any scientific study within the last 10 years
▶ Previous or current enrollment in undergraduate, graduate or postgraduate psychology studies

Table 1. Exclusion criteria.

group briefing. There, they were informed about the study procedure and its measures with a special focus on MRI acquisition and safety. Following the group briefing, the study physician performed a second, individual screening of every participant to ensure that none of the exclusion criteria were fulfilled. Participants who were included in the study provided written informed consent prior to any data acquisition for the study (including agreement to their data being shared anonymously). Participants received monetary compensation for volunteering in the study after the completion of all assessment days. A participant was excluded because of brain pathology after completion of study, thus the total number of included participants became 227.

Procedure

Data acquisition was performed from September 2013 until September 2015 and distributed over four “rounds” (subsamples) with varying time intervals between each round. Round 1 was acquired from 09/2013-12/2013 and included 53 (34 females, young $N = 31$, 17 females, mean age = 24.0, $SD = 2.8$, older $N = 22$, 17 females, mean age = 67.4, $SD = 4.1$, 23.3% of total sample) participants.

Acquisition of round 2 lasted from 02/2014-06/2014 and included 59 (25 females, young $N = 36$, 14 females, mean age = 25.3, $SD = 3.3$, older $N = 23$, 11 females, mean age = 68.9, $SD = 5.2$, 26% of total sample) participants.

In round 3, 58 (23 females, young $N = 29$, 14 females, mean age = 25, $SD = 3.7$, older $N = 29$, 9 females, mean age = 66.6, $SD = 4.6$, 25.6% of total sample) participants were tested between 10/2014 and 03/2015.

Round 4 consisted of 57 young males only (mean age = 25.6, $SD = 2.6$, 25.1% of total sample) and was acquired from 03/2015-09/2015. In round 4 we limited the sample to only male participants, since these participants were included in a follow-up stress experiment (not described here) which only included males (this was due to the attempt to replicate a previous study performed in male soldiers).

The following general study procedure was established. During the process of the study some measures were adapted and are thus not available for the total sample. Table 2 and Table 3 give a detailed overview of all measures and their availability for assessment day 1 and day 2 and Table 4 gives detailed overview of all measures and their availability for follow-up assessment days.

Participants completed two assessment days of approximately 4 hours duration each (Fig. 1). The first assessment day (day 1) included a cognitive test battery, MRI scanning, blood pressure and anthropometric measurements as well as acquisition of a blood sample. On the second assessment day (day 2), we acquired resting-state electroencephalogram (EEG) data and participants completed a psychological assessment including an emotion and personality test battery as well as a psychiatric interview. Participants were also invited for follow-up experiments, of which some measures are included here (3rd occasion of blood pressure, Future Time Perspective questionnaire, Multidimensional Mood State Questionnaire).

A complementary project by Mendes *et al.*²¹ included 194 participants of which 109 participants completed both protocols which enables repeated-measures (e.g., test-retest) analyses. Some data from Mendes *et al.* will be released as part of the study described here (e.g. continuous peripheral physiological recordings during resting-state (rs) fMRI).

Psychological Assessment

Cognitive Test Battery. Cognitive tests were administered by undergraduate psychology students specifically trained in neuropsychological assessment following a standardized protocol. On day 1, participants underwent cognitive testing session of six cognitive tests in a fixed order (cf. Table 5). The subtests (“Alertness”, “Incompatibility”, and “Working Memory”) of the “Test of Attentional

Days	Assessments	Details	n
Participant Enrollment Day 0	Telephone Screening/study and MRI/ Medical briefing	Inclusion	n = 227
		Exclusion	n = 468
Assessment Day 1	Cognitive Test Battery	CVLT	n = 228
		TAP	n = 227
		TMT	n = 227
		WST	n = 227
		LPS-2 (Subtest 3)	n = 227
		RWT	n = 227
	Mood Questionnaire	MDBF (Day 1)	n = 227
	Blood Pressure 1	BP1 (left)	n = 225
		Pulse1 (left)	n = 223
		BP1 (right)	n = 223
		Pulse1 (right)	n = 222
	Peripheral physiological recordings during rs-fMRI	ECG	n = 213
		Blood pressure (beat-to-beat)	n = 143
		Pulse (Photoplethysmography)	n = 143
		Respiration	n = 162
	MRI	Fieldmap for rs-fMRI	n = 226
		Spin echo images with reversed phase encoding direction (2 pairs) for rs-fMRI	n = 226
		rs-fMRI	n = 226
		MP2RAGE	n = 226
		T2-weighted	n = 224
		FLAIR (2D)	n = 110
		FLAIR (3D)	n = 115
		DWI (in first 112 participants)	n = 110
		Spin echo images with reversed phase encoding direction (2 pairs) for DWI (in first 112 participants)	n = 110
		DWI (after 112 participants)	n = 115
		Spin echo images with reversed phase encoding direction (2 pairs) for DWI (after 112 participants)	n = 115
		SWI and QSM	n = 111
	Mind Wandering Questionnaire	NYC-Q	n = 227
	Blood Pressure 2	BP2 (left)	n = 225
		Pulse2 (left)	n = 225
	Peripheral Blood Sample Laboratory Analysis	Electrolytes: Sodium (NA+), Potassium (K), Chloride (Cl-)	n = 217
		Liver: Alanine transaminase (ALAT), asparate transaminase (ASAT), Gamma-glutamyltransferase (GGT)	n = 217
		Kidney: Creatinine	n = 217
		Lipid metabolism: Cholesterol, High density lipoprotein cholesterol (HDL), Low density lipoprotein cholesterol (LDL), triglycerides	n = 217
		Inflammatory mediators: C-reactive protein (CRP)	n = 217
		Thyroid gland: Thyreotropin/ Thyroid-stimulating hormone (TSH)	n = 217
		Glucose (not fasting), Glycated hemoglobin (HbA1c; NSGP/DCCT), Glycated hemoglobin (HbA1c; IFCC)	n = 215
Complete Blood cell Count (CBC) without differential		n = 213	
Prothrombin time (PT) & International normalized ratio (INR)		n = 211	
Frozen Blood Sample		Serum (Frozen Samples)	n = 220
	EDTA full blood (Frozen Aliquots)	n = 217	
	Blood Sample in RNA tubes (Frozen Samples)	n = 211	
Anthropometry	Body weight	n = 227	
	Body height	n = 227	
	Waist and hip circumference	n = 227	
Hair Sample	Hair 4 cm	n = 177	

Table 2. Overview of Measures and Data Availability for Day 0 and Day 1. BP1 = Blood Pressure measured before scan, BP2 = Blood Pressure measured after scan, CVLT = California Verbal Learning Task, DWI = Diffusion-weighted imaging, ECG = Electrocardiography, EDTA full blood = Ethylenediaminetetraacetic acid in full blood, FLAIR (2D) = Fluid-attenuated inversion recovery (2 Dimensional), FLAIR (3D) = Fluid-attenuated inversion recovery (3 Dimensional), LPS-2 (Subtest 3) = Subtest 3 of the “Leistungsprüfsystem 2”, MDBF = Multidimensional Mood State Questionnaire, MP2RAGE = Magnetization-Prepared 2 Rapid Acquisition Gradient Echoes, NYC-Q = New York Cognition Questionnaire, RNA = Ribonucleic acid, rsfMRI = Resting-state Magnetic Resonance Imaging, RWT = Regensburger Wortflüssigkeitstest, SWI = T2*/susceptibility-weighted imaging, QSM = quantitative susceptibility mapping, T2-weighted = Spin-Spin-Relaxation imaging, TAP = Test of Attentional Performance, TMT = Trail Making Test, WST = Wortschatztest.

Performance” (TAP) were administered electronically via computer. An overview of this cognitive testing session is shown in Table 5, and detailed information on all measures is provided in the subsequent section.

California Verbal Learning Task (CVLT): The California Verbal Learning Task (CVLT)²² assesses verbal learning and memory capacity. Participants are acoustically presented with 16 words, which have to be memorized and recalled or recognized several times. By quantifying, the CVLT provides how much information has been acquired over the rounds and — by generating a variety of measures — it can provide information about different learning strategies. The task has two main parts (CVLT-part 1 and CVLT-part 2) and for the second part another free recall takes place after 20 min. During the interval between recall 1 and 2, typically a different non-verbal task is administered, for instance other cognitive tasks. In the present study the TAP-Test (see below) was administered, because the items are not supposed to interfere with verbal learning.

Test of Attentional Performance (TAP): Test of Attentional Performance (TAP)²³ measures different aspects of attentional processing. Here, the TAP version 2.3.1 was used. Three subtests assessed a participant’s capacity of sustained attention (“TAP Alertness”, and “TAP Incompatibility”- i.e. Simon effect) and working memory (“TAP Working Memory”- i.e. 2-back task)²³. Mistakes, omissions, and reaction times in these subtests were recorded as measures of performance.

Trail Making Test (TMT): The Trail Making Test (TMT) measures cognitive flexibility, and it consists of subtest A (TMT-A) and subtest B (TMT-B)²⁴. Participants are asked to quickly and correctly connect circles which are randomly distributed on a piece of paper. In TMT-A, these circles contain numbers from 1 to 25. In TMT-B, numbers and letters have to be connected in alternating and increasing order. The reaction time quantifies visual attention and executive functioning.

Wortschatztest (WST): The Vocabulary Test (Wortschatztest, WST)²⁵ indicates the measurement of verbal intelligence level and the assessment of language comprehension. By determining the vocabulary of a person, the WST allows estimation of his/her crystallized intelligence. It consists of 43 rows with 6 words each. In each row, participants have to identify the one word that actually exists in German.

Subtest 3 of the “Leistungsprüfsystem 2” (LPS-2): Subtest 3 of the Performance Testing System (Leistungsprüfsystem 2, LPS-2)²⁶ measures logical or inferential thinking and quantifies fluid intelligence. In subtest 3, participants are asked to identify the one item in a series of symbols that does not follow the logical rule of that series. The goal is to find as many items as possible within three minutes.

Regensburger Wortflüssigkeitstest (RWT): The Regensburger Word Fluency Test (Regensburger Wortflüssigkeitstest, RWT)²⁷ quantifies the verbal fluency of a person. In the section of “S-Words”, participants have two minutes to name as many valid German words as possible that start with the letter “S”. In the “Animals” section, as many animals as possible should be named within two minutes. The correct number of words quantifies formal lexical (“S-Words”) or categorical-semantic fluency (“Animals”).

Emotion and Personality Test Battery. On day 2, participants were asked to answer electronic version of 18 emotion-related questionnaires (*cf. first 18 sections below*) in a randomized sequence on a computer (LimeSurvey version 2.0)²⁸. The whole questionnaire completion took on average 1.5 hours to 2.5 hours with a short break after 45 min.

Besides those electronic testing session of 18 questionnaires, which were answered on a computer via LimeSurvey, there were pen-and-paper version of three other emotion-related questionnaires (*cf. last 3 sections below*) that were filled out at different time points. The Multidimensional Mood State Questionnaire (*German* MDBF) was answered on each of the two assessment days. After the MRI scanning session, participants filled out the New York Cognition Questionnaire (NYC-Q). The questionnaire of Future Time Perspective (FTP) was assessed during LEMON Rounds 1–3 only at the

Days	Assessments	Details	n
Assessment Day 2	Mood Questionnaire	MDBF (Day 2)	n = 218
	EEG	Raw rs-EEG (Brain Products ActiCaps)	n = 217
		Preprocessed rs-EEG	n = 202
		Digitized EEG channel locations	n = 144
	Drug Test	Multi 8/2 Drogentest	n = 220
	Emotion and Personality Battery	ERQ	n = 220
		CERQ	n = 220
		PSQ	n = 220
		TICS	n = 220
		COPE	n = 219
		LOT-R	n = 220
		STAXI	n = 220
		NEO-FFI	n = 220
		STAI-G-X2	n = 220
		FEV	n = 220
		YFAS	n = 169
		BIS/BAS	n = 220
		UPPS	n = 220
		TAS-26	n = 220
		MARS	n = 208
		F-SozU K-22	n = 220
	MSPSS	n = 220	
	TEIQue-SF	n = 220	
	Psychiatric screening	SCID I	n = 219
HAM-D		n = 218	
AUDIT		n = 219	
BSL-23		n = 169	

Table 3. Overview of Measures and Data Availability for Day 2. AUDIT = Alcohol Use Disorder Identification Test, BIS/BAS = Behavioral Inhibition and Approach System, BSL-23 = Borderline Symptoms List (short version), CERQ = Cognitive Emotion Regulation Questionnaire, COPE = Coping Orientations to Problems Experienced, CVLT = California Verbal Learning Task, DWI = Diffusion-weighted imaging, ECG = Electrocardiography, EDTA full blood = Ethylenediaminetetraacetic acid in full blood, ERQ = Emotion Regulation Questionnaire, F-SoZU K-22 = Social Support Questionnaire, FEV = Eating Behavior, FLAIR (2D) = Fluid-attenuated inversion recovery (2 Dimensional), FLAIR (3D) = Fluid-attenuated inversion recovery (3 Dimensional), FTP = Future Time Perspective Questionnaire, HAM-D = Hamilton Depression scale (HAM-D), LOT-R = Optimism Pessimism Questionnaire-Revised, MARS = Affect Regulation Style, MDBF = Multi-dimensional Mood State Questionnaire, MP2RAGE = Magnetization-Prepared 2 Rapid Acquisition Gradient Echoes, MSPSS = Multidimensional Scale of Perceived Social Support, NEO-FFI = Big-Five of Personality, PSQ = Perceived Stress Questionnaire, RNA = Ribonucleic acid, RsEEG = Resting-state electroencephalogram, STAI-G-X2 = State-Trait Anxiety Inventory (short version), STAXI = State-Trait Anger Expression Inventory, TAS-26 = Toronto-Alexithymia Scale, TEIQue-SF = Emotional Intelligence Questionnaire, TICS = Trier Inventory of Chronic Stress, UPPS = Impulsivity Questionnaires, YFAS = Addicted Eating Behavior.

beginning of a follow-up experiment. An overview of the individual questionnaires can be found in Table 6 (available online only) and a more detailed description is given in the section below.

Big-Five of Personality (NEO-FFI): We used the German adaptation of NEO-Five-Factor Inventory²⁹ to assess Costa and McCrae's Big-Five of Personality Inventory (NEO-FFI)³⁰. The 60 items can be divided into the five factors of "Neuroticism", "Extraversion", "Openness to experience", "Agreeableness", and "Conscientiousness". Answers are given on a 5-point Likert scale ranging from 0 (strong denial) to 4 (strong approval).

Impulsive Behavior Scale (UPPS): We applied the German adaptation (UPPS)³¹ of Impulsive Behavior Scale (UPPS)³² to assess the four sub-dimensions of impulsivity "Urgency", "Premeditation",

Days	Assessments	Details	n	
Follow-up LEMON	Blood Pressure 3	BP3 (left)	n = 159	
	Future Time Perspective Questionnaire	FTP	n = 141	
	Mood Questionnaire	MBDF (Day 3)	n = 159	
Additional data from complimentary project by Mendes <i>et al.</i>	Blood Pressure	BP1 (left)	n = 91	
		Pulse1 (left)	n = 44	
	Peripheral physiological recordings during rs-fMRI of participants in LEMON and Mendes <i>et al.</i> (test-retest sample for LEMON)	ECG	rs-fMRI 1 (AP-run1)	n = 98
			rs-fMRI 2 (PA-run1)	n = 97
			rs-fMRI 3 (AP-run2)	n = 94
			rs-fMRI 4 (PA-run2)	n = 90
		Blood pressure (beat-to-beat)	rs-fMRI 1 (AP-run1)	n = 101
			rs-fMRI 2 (PA-run1)	n = 101
			rs-fMRI 3 (AP-run2)	n = 97
			rs-fMRI 4 (PA-run2)	n = 91
		Pulse (Photoplethysmography)	rs-fMRI 1 (AP-run1)	n = 101
			rs-fMRI 2 (PA-run1)	n = 101
			rs-fMRI 3 (AP-run2)	n = 97
			rs-fMRI 4 (PA-run2)	n = 91
		Respiration	rs-fMRI 1 (AP-run1)	n = 98
			rs-fMRI 2 (PA-run1)	n = 97
			rs-fMRI 3 (AP-run2)	n = 94
			rs-fMRI 4 (PA-run2)	n = 90
	Additional peripheral physiological recordings during rs-fMRI of participants in Mendes <i>et al.</i>	ECG	rs-fMRI 1 (AP-run1)	n = 86
			rs-fMRI 2 (PA-run1)	n = 84
			rs-fMRI 3 (AP-run2)	n = 80
			rs-fMRI 4 (PA-run2)	n = 74
		Blood pressure (beat-to-beat)	rs-fMRI 1 (AP-run1)	n = 79
			rs-fMRI 2 (PA-run1)	n = 76
			rs-fMRI 3 (AP-run2)	n = 74
			rs-fMRI 4 (PA-run2)	n = 67
Pulse (Photoplethys-mography)		rs-fMRI 1 (AP-run1)	n = 79	
		rs-fMRI 2 (PA-run1)	n = 76	
		rs-fMRI 3 (AP-run2)	n = 74	
		rs-fMRI 4 (PA-run2)	n = 67	
Respiration		rs-fMRI 1 (AP-run1)	n = 86	
		rs-fMRI 2 (PA-run1)	n = 84	
		rs-fMRI 3 (AP-run2)	n = 80	
		rs-fMRI 4 (PA-run2)	n = 74	

Table 4. Follow-up assessment days. AP = anterior-posterior phase encoding acquisition (rs-fMRI), BP3 = Blood Pressure measured on follow-up assessment day, FTP = Future Time Perspective Questionnaire, MBDF = Multidimensional Mood State Questionnaire, PA = posterior- anterior phase encoding acquisition (rs-fMRI).

“Perseverance” and “Sensation Seeking”. The 45 items are rated on a 4-point Likert scale ranging from 1 (agree strongly) to 4 (disagree strongly).

Behavioral Inhibition and Approach System (BIS/BAS): The German version³³ of the Behavioral Inhibition and Approach System (BIS/BAS)³⁴ was applied to measure reactivity of the aversive “Behavioral Inhibition” and the appetitive “Behavioral Approach” motivational systems in response to punishment or reward. This measure consists of a BIS subscale and three BAS subscales “Drive”, “Reward Responsiveness”, and “Fun Seeking”, each consisting of 7 items. A total of 24 items are rated on a 4-point Likert-type response format ranging from 1 (does not apply to me at all) to 4 (fully applies to me).

Name	Full Name	Reference	Measured construct
CVLT-part 1	California Verbal Learning Task	Niemann <i>et al.</i> ²²	Verbal learning, memory
TAP Alertness	Test of Attentional Performance: Alertness	Zimmermann & Fimm ²³	Alertness, general wakefulness
TAP Incompatibility	Test of Attentional Performance: Incompatibility	Zimmermann & Fimm ²³	Interference
TAP Working Memory	Test of Attentional Performance: Memory	Zimmermann & Fimm ²³	Working memory
TMT A	Trail Making Test	Reitan ²⁴	Visuomotor speed
TMT B	Trail Making Test	Reitan ²⁴	Executive function
CVLT-part 2	California Verbal Learning Task	Niemann <i>et al.</i> ²²	Verbal learning, memory
WST	Wortschatztest	Schmidt & Metzler ²⁵	Verbal intelligence, crystallized intelligence
LPS-2, subtest 3	Subtest 3 of the "Leistungsprüfsystem 2"	Kreuzpointner <i>et al.</i> ²⁶	Fluid intelligence
RWT S-Words	Regensburger Wortflüssigkeitstest: S-words	Aschenbrenner <i>et al.</i> ²⁷	Verbal fluency
RWT Animals	Regensburger Wortflüssigkeitstest: Animals	Aschenbrenner <i>et al.</i> ²⁷	Verbal fluency

Table 5. Cognitive test battery. These tests are completed in a fixed order on assessment day 1.

Emotion Regulation Questionnaire (ERQ): To measure inter-individual differences in habitual emotion regulation, participants completed the German version³⁵ of the emotion regulation questionnaire (ERQ)³⁶, which has 10 items that are answered on a 7-point Likert-type scale ranging from 1 (strongly disagree) to 7 (strongly agree). Six of the 10 items measure the tendency to use reappraisal for emotion regulation, and the other 4 items assess habitual expressive suppression.

Cognitive Emotion Regulation Questionnaire (CERQ): The Cognitive Emotion Regulation Questionnaire (CERQ) evaluates the cognitive aspects of emotion regulation^{37,38}. It contains nine scales that measure five adaptive (acceptance, positive refocusing, refocusing on planning, positive reappraisal, putting into perspective) and four maladaptive emotion regulation strategies (self blame, rumination, catastrophising, blaming others) on a 5-point Likert scale from 0 (almost never) to 4 (almost always).

Affect Regulation Style (MARS): We used the German version (external official translation, not validated yet) of the Measure of Affect Regulation Style (MARS)³⁹ to evaluate cognitive and behavioral aspects of emotion regulation. The scale consists of six subscales of "Behavioral Distraction", "Cognitive Distraction", "Situation-focused Strategies", "Affect-focused Strategies", "Disengagement", and "Avoidance". Ratings are given on a 7-point Likert scale ranging from 0 (not at all) to 6 (almost always). Since this data refers to the first version of a German validation — a process which is still on-going — the data should be used with caution.

Social Support Questionnaire (F-SozU K-22): Perceived social support was assessed using the German *Fragebogen zur Sozialen Unterstützung*⁴⁰, the 22-item short version Social Support Questionnaire (F-SozU K-22)⁴¹. The scale comprises subscales of "Emotional Support", "Practical support", "Social Integration", "Availability of Trusted Person", and "Satisfaction with Social Support". The 22 items are answered on a 5-point Likert scale ranging from 1 (does not apply at all) to 5 (strongly applies).

Multidimensional Scale of Perceived Social Support (MSPSS): The German version of the Multidimensional Scale of Perceived Social Support (MSPSS)⁴² was used to evaluate the perceived availability of social resources in the area of friends, family and significant others. In addition to the three subscales of the sources of social support, a sum score can be computed. Ratings can be provided on a 7-point Likert scale ranging from 1 (not true at all) to 7 (very true).

Coping Orientations to Problems Experienced (Brief COPE): We used the German adaptation of the 28-item version of Brief COPE Inventory⁴³ to assess participants' Coping Orientations to Problems Experienced (Brief COPE)⁴⁴. The measure consists of four subscales of "Positive Coping", "Active Coping", "Support Coping", and "Evasive Coping". The answers are rated on a 4-point Likert scale ranging from 1 (not at all) to 4 (very much).

Optimism Pessimism Questionnaire-Revised (LOT-R): The German version⁴⁵ of Life Orientation Test-Revised (LOT-R) was used to assess individual differences in generalized optimism versus pessimism⁴⁶. The 10 items are added to an overall optimism score ranging from 0–24, with higher scores representing greater positive expectation. Answers are rated on a 5-point Likert scale ranging from 0 (does not apply at all) to 4 (strongly applies).

Perceived Stress Questionnaire (PSQ): We used the German version⁴⁷ of 20-item short version of the Perceived Stress Questionnaire (PSQ)⁴⁸ in order to assess the perception, appraisal, and processing of stressors during the last two years. The scale contains four subscales of "Worries", "Tension", "Joy", and "Demands". Answers are rated on a 4-point Likert scale from 1 (almost never) to 4 (usually).

Trier Inventory of Chronic Stress (TICS): To assess aspects of chronic stress we applied the German version⁴⁹ of the Trier Inventory of Chronic Stress (TICS)⁵⁰. The 57-item scale comprises nine factors of chronic stress: “Work Overload”, “Social Overload”, “Pressure to Perform”, “Work Discontent”, “Excessive Demands at Work”, “Lack of Social Recognition”, “Social Tension”, “Social Isolation”, and “Chronic Worrying”. Answers are rated on a 5-point Likert scale ranging from 0 (never) to 4 (very often).

Eating Behavior (FEV): The three-factor eating questionnaire (TFEQ)⁵¹, German version Fragebogen zum Essverhalten (FEV)⁵², was used to assess three domains of eating behavior. ‘Cognitive Restraint of Eating’ measures whether eating behavior is under cognitive, rather than physiological control, ‘Disinhibition of Eating’ measures the lack of control over eating, especially in the presence of tempting external cues or situations, and ‘Susceptibility to Hunger’ measures the experience of prominent and disturbing subjective hunger feelings. The 60 items are answered in different response formats ranging from dichotomous scales (applies, does not apply) to 4-point Likert scales from 1 (always) to 4 (never) or 1 (very much) to 4 (not). Item 58-60 are rated by selecting from a list of behavior descriptions.

Addicted Eating Behavior (YFAS): We applied the German version⁵³ of Yale Food Addiction Scale (YFAS)⁵⁴ in order to classify food-dependent eating behavior. Twenty of the total 27 items measure the seven DSM-IV-TR criteria of dependence⁵⁵, two items measure if the eating behavior causes a clinically significant impairment, three items ask for particular foods related to the problematic eating behavior, and three items act as a primer for the other questions. The items are rated either on a 5-point Likert scale from 0 (never) to 4 (four times a week to daily) or dichotomous 0 (never) or 1 (yes).

Emotional Intelligence Questionnaire (TEIQue-SF): The 30-item short version of the Trait Emotional Intelligence Questionnaire (TEIQue-SF)⁵⁶ of German adaptation⁵⁷ was used to measure emotion-related dispositions and self-perception abilities. The scale contains the four subscales of “Well-being”, “Self-control”, “Emotionality”, and “Sociability”, which can be averaged to one “Global Trait Emotional Intelligence” score. Answers are rated in a 7-point Likert format, ranging from 1 (do not agree at all) to 7 (agree completely).

State-Trait Anxiety Inventory (STAI-G-X2): We applied the German version⁵⁸ of the Trait Scale of the State-Trait Anxiety Inventory (STAI-G-X2) short version⁵⁹ for the assessment of a situation-independent general condition of anxiety. This subscale consists of 20 items rated on a 4-point Likert scale ranging from 1 (almost never) to 4 (nearly always).

State-Trait Anger Expression Inventory (STAXI): We used the 44-item German version⁶⁰ of the State-Trait Anger Expression Inventory (STAXI)⁶¹ to measure the habitual experience, expression, and control of anger. We applied the four trait scales “Trait-anger”, the individual anger-disposition, “Anger-in”, the tendency to suppress and non-verbalization of angry feelings, “Anger-out”, the verbal or physical expression of anger towards others or self, and “Anger-control”, which measures the attempt to control anger-expressions. All ratings were ranked rated on a 4-point Likert scale either from 1 (not at all or hardly ever) to 4 (very much or nearly always).

Toronto-Alexithymia Scale (TAS): The German version⁶² of the 26-item Toronto-Alexithymia Scale (TAS)⁶³ was used to measure alexithymia, difficulty experiencing, and expressing emotional states. We applied all three subscales: “difficulty with identifying feelings”, “difficulty with expressing and describing feelings”, and “externally-oriented thinking”. Answers are rated on 5-point Likert scale from 1 (does not apply at all) to 5 (applies completely).

Multidimensional Mood State Questionnaire (MDBF): The 24-item German version of the Multidimensional Mood State Questionnaire (German MDBF)⁶⁴ was completed by the participants on each assessment day. Mood ratings (“happy”, “nervous”, etc.) are ranked on a 5-point Likert scale from 1 (not at all) to 5 (very much). Three subscales can be computed along the dimensions of “good-bad”, “awake-tired”, “calm-nervous”.

Future Time Perspective Questionnaire (FTP): We applied the Future Time Perspective Questionnaire⁶⁵ to assess the individual anticipation of time left to live. Agreement with the statements is ranked on a 7-point Likert scale ranging from 1 (very untrue) to 7 (very true). The mean value indicates the anticipated time horizon.

New York Cognition Questionnaire (NYC-Q): After completion of the scanning session, participants filled out the New York Cognition Questionnaire (NYC-Q)⁶⁶, which measures content and form of self-generated thoughts with 31 statements. The first part “Content of thoughts” is ranked on a Likert scale from 1 (did not describe my thoughts at all) to 9 (completely described my thoughts), while the second part “form of self-generated thoughts” is rated on a scale ranging from 1 (does not characterize my experience at all) to 9 (completely characterizes my experience).

Assessment of Past and Present Psychiatric Symptoms. Standardized Clinical Interview for DSM IV (SCID-I): The LEMON protocol included a broad characterization of present and past psychiatric symptoms in all participants, which was assessed on the second testing day. Participants underwent SCID⁶⁷ — the Standardized Clinical Interview for Diagnostic and Statistical Manual of Mental Disorders (DSM IV) — to identify whether participants (in the past or in the present) met/meet diagnostic criteria

of an Axis I psychiatric disorder according to DSM IV⁶⁸. The SCID I is a semi-structured interview that covers the major DSM-IV Axis I diagnoses. Interviews were either led by a trained psychologist or by a psychology student who had been trained to use the SCID I and supervised by a licensed psychiatrist. Documentation includes full current or history of Axis I diagnosis as well as a column with notes on noteworthy current or past subclinical symptoms beyond full fulfillment of diagnostic criteria (e.g., occasional use of an illegal drug, subclinical symptoms).

Screening of Depressive Symptoms or Borderline Symptomatology (HAM-D and BSL-23): Any reported depressive symptoms were additionally assessed by a trained psychologist or trained research assistant using the Hamilton Depression Scale (HAM-D)⁶⁹. Documentation includes the Hamilton sum score. Note that our psychiatric assessment focused primarily on present or past Axis I disorders. In addition, the Borderline Symptoms List (short version BSL-23)⁷⁰ was applied in 170 participants. This questionnaire is a self-rating instrument for borderline-typical symptomatology. Documentation includes sum scores of the BSL-23 and an additional sum score regarding borderline-typical behaviors. Additionally, participants were asked about their relationship status (“yes”/“no”).

Screening for Alcohol Abuse: We also assessed alcohol consumption during the last 28 days using the Time Line Follow Back Questionnaire⁷¹. Using a calendar, participants self-report retrospectively the number of alcohol units consumed on each day in this period. Documentation includes the number of alcohol units consumed. The Alcohol Use Disorder Identification Test (AUDIT)⁷² questionnaire was administered to screen for any indication of alcohol abuse. We additionally asked for family history of addiction in participants’ 1st to 3rd degree relatives. Documentation includes presence or absence of family history of addiction.

Screening for Substance Abuse: In addition to the semi-structured interview, an in-vitro urine drug screening was performed using the “Multi 8/2 Drogen-Tauchtest” (Diagnostik Nord, Schwerin, Germany) to assess present substance use. The test detects the following substances simultaneously and up to two weeks after their administration: buprenorphine (cut-off 10 ng/mL), amphetamine (cut-off 1000 ng/mL), benzodiazepine (cut-off 300 ng/mL), cocaine (cut-off 300 ng/mL), methamphetamine (cut-off 1000 ng/mL), morphine/heroin (cut-off 300 ng/mL), methadone (cut-off 300 ng/mL), and THC (Marihuana, cut-off 50 ng/mL). Cut-off values of the tests were chosen according to recommendations of the American National Institute on Drug Abuse (NIDA)⁷³. Documentation includes name of the substance detected (if any). The drug screening was performed on the second day of assessments, which was randomly assigned in order for participants not to know the date of the urine drug screening ahead of time. Moreover, it covered more than 1 week presence of any substance in urine, thus covering also assessment day 1.

Physiological data

MRI. Magnetic resonance imaging (MRI) was performed on a 3 Tesla scanner (MAGNETOM Verio, Siemens Healthcare GmbH, Erlangen, Germany) equipped with a 32-channel head coil. Over the course of MRI data acquisition, the scanner remained stable and did not undergo any major maintenance or updates which would systematically affect the quality of data provided here. This is also true in relation to the complementary protocol by Mendes *et al.*, ensuring comparability between the studies.

The imaging protocol lasted approximately 70 min and included the following scans in fixed order: 1) gradient echo fieldmap scan for distortion correction in rs-fMRI^{74,75}, 2) a pair of spin echo images with reversed phase encoding direction for distortion correction in rs-fMRI^{76,77}, 3) rs-fMRI scan, 4) a second pair of spin echo images with reversed phase encoding direction, 5) quantitative and weighted T1 Magnetization-Prepared 2 Rapid Acquisition Gradient Echoes (MP2RAGE)⁷⁸ image, 6) T2-weighted image, 7) Fluid-attenuated inversion recovery (FLAIR) scan, 8) diffusion-weighted imaging (DWI) scan, 9) a pair of spin echo images with reversed phase encoding for distortion correction in DWI, 10) T2*/susceptibility-weighted imaging (SWI) scan.

The data were acquired with a very large coverage using simultaneous multi-slice acquisition to include the brain and the cerebellum. Diffusion data were acquired parallel to the AC-PC line and the volume (149.6 mm height) covered the entire brain including the cerebellum in all participants. The fMRI data were angulated by -15° (backwards) with respect to the AC-PC line. The slice block (147 mm) also covered the entire brain including the full cerebellum. The figures in Supplementary Figure S1 show cross-subject coverage of the fMRI (left) and DWI (right) data normalized to the MNI brain.

During rs-fMRI, electrocardiography (ECG), pulse, beat-to-beat blood pressure and respiration were recorded simultaneously (see section *Continuous peripheral physiological recordings during rs-fMRI*). Before imaging started, participants filled out the first MDBF questionnaire. Once imaging was completed, participants were asked to fill out the New York Cognition Questionnaire (NYC-Q, for details on the questionnaires see section *Emotion and Personality Test Battery*).

Resting-state fMRI (rs-fMRI): A T2*-weighted gradient echo echo planar imaging (EPI) multiband BOLD rs-fMRI scan^{79–81} was acquired to enable functional connectivity analyses. Participants were instructed to remain awake and lie still with their eyes open while looking at a low-contrast fixation cross. Data regarding sleep/wake for the rs-fMRI as such does not exist, but it is assumed that the participants were awake throughout the duration of the scan because they were requested to do so. The sequence parameters were specified as follows: TR = 1400 ms and the total number of volumes = 657 (for more

MRI scan	Sequence parameters	File name (raw, nifti format)	File name (preprocessed, nifti format)
Gradient echo fieldmap for rs-fMRI distortion correction	voxel size = 2.3 mm isotropic, FOV = 202 mm, imaging matrix = 88 × 88, 64 slices with 2.3 mm thickness, TR = 680 ms, TE1 = 5.19 ms, TE2 = 7.65 ms, flip angle = 60°, bandwidth = 389 Hz/pixel, prescan normalization, no partial fourier, duration = 2 min 3 s	acq-GEfmap_run-01_magnitude1, acq-GEfmap_run-01_magnitude2, acq-GEfmap_run-01_phasediff	
Spin echo EPI with reversed phase encoding for rs-fMRI distortion correction	voxel size = 2.3 mm isotropic, FOV = 202 mm, imaging matrix = 88 × 88, 64 slices with 2.3 mm thickness, TR = 2200 ms, TE = 50 ms, flip angle = 90°, echo spacing = 0.67 ms, phase encoding = A >> P / P >> A, bandwidth = 1776 Hz/pixel, partial fourier 6/8, no pre-scan normalization, duration = 29 s each	acq-SEfmapBOLDpost_dir-AP_epi, acq-SEfmapBOLDpost_dir-PA_epi, acq-SEfmapBOLDpre_dir-AP_epi, acq-SEfmapBOLDpre_dir-PA_epi	
Resting-state fMRI (T2*-weighted gradient-echo EPI BOLD)	Axial acquisition orientation, phase encoding = A >> P, voxel size = 2.3 mm isotropic, FOV = 202 mm, imaging matrix = 88 × 88, 64 slices with 2.3 mm thickness, TR = 1400 ms, TE = 30 ms, flip angle = 69°, echo spacing = 0.67 ms, bandwidth = 1776 Hz/pixel, partial fourier 7/8, no pre-scan normalization, multiband acceleration factor = 4, 657 volumes, slice order = interleaved, duration = 15 min 30 s	acq-AP-run-01_bold	task-rest_acq-AP_run-01_native, task-rest_acq-AP_run-01_MNI2mm
Magnetization Prepared 2 Rapid Acquisition Gradient Echoes (MP2RAGE)	Sagittal acquisition orientation, one 3D volume with 176 slices, TR = 5000 ms, TE = 2.92 ms, TI1 = 700 ms, TI2 = 2500 ms, FA1 = 4°, FA2 = 5°, pre-scan normalization, echo spacing = 6.9 ms, bandwidth = 240 Hz/pixel, FOV = 256 mm, voxel size = 1 mm isotropic, GRAPPA acceleration factor 3, slice order = interleaved, duration = 8 min 22 s	acq-mp2rage_T1w, acq-mp2rage_T1map, acq-mp2rage_defacemask, inv-1_mp2rage, inv-2_mp2rage	acq-mp2rage_brain
T2-weighted	Sagittal acquisition orientation, one 3D volume with 176 slices, TR = 3200 ms, TE = 409 ms, FA = variable, pre-scan normalization, echo spacing = 3.42 ms, bandwidth = 751 Hz/pixel, FOV = 256 mm, voxel size = 1 mm isotropic, GRAPPA acceleration factor 2, duration = 4 min 43 s	T2w	
Fluid-attenuated inversion recovery (FLAIR) 2D (scanned in first 112 participants)	Axial acquisition orientation, 28 slices, TR = 10000 ms, TE = 90 ms, TI = 2500 ms, FA = 180°, pre-scan normalization, echo spacing = 9.98 ms, bandwidth = 199 Hz/pixel, FOV = 220 mm, voxel size = 0.9 × 0.9 × 4.0 mm ³ , slice order = interleaved, duration = 4 min 42 s	acq-lowres_FLAIR	
3D SPACE sequence with fluid-attenuated inversion-recovery preparation (introduced after first 112 participants)	Sagittal acquisition orientation, one 3D volume with 192 slices, TR = 5000 ms, TE = 395 ms, TI = 1800 ms, FA = variable, pre-scan normalization, echo spacing = 3.36 ms, bandwidth = 781 Hz/pixel, FOV = 250 mm, voxel size = 1 mm isotropic, GRAPPA acceleration factor 2, duration = 7 min 2 s	acq-highres_FLAIR	
Diffusion-weighted Imaging (DWI, scanned in first 112 participants)	88 axial slices, voxel size = 1.7 mm isotropic, 60 diffusion-encoding gradient directions, b-value of 1000 s/mm ² , 7 non-diffusion-weighted b0 distributed in the sequence, TR = 7000 ms, TE = 80 ms, FA = 90°, bandwidth = 1502 Hz/pixel, echo spacing = 0.78 ms, FOV = 220 mm, voxel dimension = 1.7 mm isotropic, imaging matrix = 128 × 128, acquired with 7/8 partial Fourier encoding and GRAPPA (acceleration factor 2, 32 ref. lines), 60 diffusion-encoding gradient directions, b-value = 1000 s/mm ² , 7 b0 images, raw data filter, fat suppression (strong), advanced shim mode, no prescan normalization, interleaved acquisition, CMRR sequence, monopolar diffusion scheme, SENSE coil combine, multiband acceleration factor 2, phase encoding A >> P, duration = 9 min 27 s	dwi	
Spin echo images with reversed phase encoding for DWI distortion correction (scanned in first 112 participants)	Two volumes with A >> P and P >> A phase encoding, voxel size = 1.7 mm isotropic, 88 axial slices, TR = 7000 ms, TE = 80 ms, FA = 90°, bandwidth = 1502 Hz/pixel, echo spacing 0.78 ms, FOV = 220 mm, voxel dimension = 1.7 mm isotropic, imaging matrix = 128 × 128, acquired with 7/8 partial Fourier encoding and GRAPPA (acceleration factor 2, 32 ref. lines), fat suppression (strong), advanced shim mode, no prescan normalization, interleaved acquisition, CMRR sequence, SENSE coil combine, multiband acceleration factor 2, duration = 1 min 59 s each	acq-SEfmapDWI_dir-AP_epi, acq-SEfmapDWI_dir-PA_epi	
Diffusion-weighted Imaging (DWI, new version introduced after first 112 participants)	88 axial slices, voxel size = 1.7 mm isotropic, 60 diffusion-encoding gradient directions, b-value of 1000 s/mm ² , 7 non-diffusion-weighted b0 distributed in the sequence, TR = 7000 ms, TE = 80 ms, FA = 90°, bandwidth = 1502 Hz/pixel, echo spacing = 0.78 ms, FOV = 220 mm, voxel dimension = 1.7 mm isotropic, imaging matrix = 128 × 128, acquired with 7/8 partial Fourier encoding and GRAPPA (acceleration factor 2, 32 ref. lines), 60 diffusion-encoding gradient directions, b-value = 1000 s/mm ² , 7 b0 images, raw data filter, fat suppression, advanced shim mode, no prescan normalization, interleaved acquisition, CMRR sequence, monopolar diffusion scheme, SENSE coil combine, multiband acceleration factor 2, phase encoding A >> P, duration = 8 min 38 s	dwi	
Spin echo images with reversed phase encoding for DWI distortion correction (new version introduced after first 112 participants)	Two volumes with A >> P and P >> A phase encoding, voxel size = 1.7 mm isotropic, 88 axial slices, TR = 7000 ms, TE = 80 ms, FA = 90°, bandwidth = 1502 Hz/pixel, echo spacing 0.78 ms, FOV = 220 mm, voxel dimension = 1.7 mm isotropic, imaging matrix = 128 × 128, acquired with 7/8 partial Fourier encoding and GRAPPA (acceleration factor 2, 32 ref. lines), fat suppression, advanced shim mode, no prescan normalization, interleaved acquisition, CMRR sequence, SENSE coil combine, multiband acceleration factor 2, duration = 1 min 10 s each	acq-SEfmapDWI_dir-AP_epi, acq-SEfmapDWI_dir-PA_epi	
Gradient echo Susceptibility-weighted data for SWI and QSM estimation (introduced after first 112 participants)	Axial acquisition orientation, one 3D volume with 160 slices, TR = 30 ms, TE = 17.3 ms, FA = 13°, bandwidth = 150 Hz/pixel, FOV = 205 mm, acquired with 6/8 phase partial Fourier and GRAPPA (acceleration factor 2, 24 ref. lines), no prescan normalization, interleaved acquisition, voxel size = 0.8 mm isotropic, duration = 7 min 50 s	acq-phase_GRE, acq-mag_GRE	

Table 7. MRI sequences.

details see Table 7). The total acquisition time for rs-fMRI was 15 min 30 s. To enable correction for geometric distortions in EPI images from rs-fMRI, a gradient echo fieldmap scan and two pairs of spin echo EPI images with reversed phase encoding direction were acquired.

Resting-state fMRI Data Preprocessing: The preprocessing of the rs-fMRI data was implemented in Nipype and the details of it can be found in the complementary project by Mendes *et al.*²¹. The pipeline is

available at https://github.com/NeuroanatomyAndConnectivity/pipelines/tree/master/src/lsd_lemon and comprised the following steps: (i) discarding the first five EPI volumes to allow for signal equilibration and steady state, (ii) 3D motion correction (FSL MCFLIRT)⁸², (iii) distortion correction (FSL FUGUE)⁸³, (iv) rigid-body coregistration of unwarped temporal mean image to the individual's anatomical image (FreeSurfer bbregister)⁸⁴, (v) denoising (Nipype rapidart and aCompCor)⁸⁵, (vi) band-pass filtering between 0.01-0.1 Hz (FSL), mean-centering, as well as variance normalization of the denoised time series (Nitime)⁸⁶, (vii) spatial normalization to MNI152 2 mm standard space via transformation parameters derived during structural preprocessing (ANTs SyN)⁸⁷.

Structural MRI T1 and T2: The MP2RAGE⁷⁸ sequence was acquired for assessment of brain structure with a voxel resolution of 1 mm (isotropic). Resulting T1-weighted images and quantitative T1 maps can be used for analyses of gray and white matter (e.g., cortical thickness, voxel-based morphometry), as well as for the assessment of myelin content^{88,89}. Importantly, these T1-weighted images differ from MPRAGE T1-weighted images as they are uniform and free of other imaging properties (i.e. proton density, T2*) which can affect morphometric measurements⁹⁰. The total acquisition time for MP2RAGE was 8 min 22 s. In addition, a standard T2-weighted volume with 1 mm isotropic resolution was acquired within 4 min 43 s (for details see Table 7).

T1 Data Preprocessing: The preprocessing of the T1 MP2RAGE data was implemented in Nipype and the details of it can be found in the complementary project by Mendes *et al.*²¹. The pipeline is available at https://github.com/NeuroanatomyAndConnectivity/pipelines/tree/master/src/lsd_lemon and comprised the following steps: The background of the uniform T1-weighted image was removed using CBS Tools⁹¹, and the masked image was used for cortical surface reconstruction using FreeSurfer's full version of recon-all^{92,93}. A brain mask was created based on the FreeSurfer segmentation results. Diffeomorphic nonlinear registration as implemented in ANTs SyN algorithm⁸⁷ was used to compute a spatial transformation between the individual's T1-weighted image and the MNI152 1mm standard space. To remove identifying information from the structural MRI scans, a mask for defacing was created from the MP2RAGE images using CBS Tools⁹¹. This mask was subsequently applied to all anatomical scans.

Fluid-Attenuated Inversion Recovery (FLAIR): T2-weighted FLAIR images were used for clinical screening of incidental findings. The scan was changed from a low-resolution 2D FLAIR to a 3D SPACE sequence with fluid-attenuated inversion-recovery preparation after the first 112 participants. Acquisition time for the 2D image was 4 min 42 s and 7 min 2 s for the 3D volume (for details see Table 7).

Diffusion-Weighted Imaging (DWI): We acquired axial whole brain high angular resolution diffusion-weighted images to analyze structural connectivity. The images were acquired with 1.7mm isotropic resolution using a multi-band accelerated sequence^{79,81,94} and an in-plane GRAPPA⁹⁵ (60 diffusion directions, b-value = 1000 s/mm², 7 b0 images, for details see Table 7). The total DWI scanning time was 9 min 27 s. To correct for geometric distortions, two volumes with reversed phase encoding (AP and PA) were acquired after the DWI sequence, lasting 1 min 59 s each. A new version of the DWI sequence (CMRR) with a faster calibration procedure was introduced after the first 112 participants which reduced the scanning time to 8 min 38 s and the time for the two scans with reversed phase encoding to 1 min 10 s each.

Susceptibility-weighted data acquisition: The visualization of magnetic susceptibility tissue differences is most commonly achieved via gradient echo data acquired using a single- or multi-echo spoiled-gradient-recalled-echo (GRE) sequence⁹⁶. The Susceptibility-Weighted Imaging (SWI) technique capitalizes on the contrast inherent in the magnitude and phase images to improve susceptibility contrast by combining both images to enhance contrast between grey-/white-matter and water/fat, in addition to enhancing the contrast of paramagnetic elements exhibiting high densities in the brain (e.g. iron). SWI has a number of applications in the clinical setting including the diagnosis of cerebral vascular pathology and the detection of abnormal accumulation of mineral deposition. On the other hand, Quantitative Susceptibility Mapping (QSM) is a recently established technique that allows the determination of the intrinsic magnetic susceptibility properties of tissues based on signal from the phase image^{97,98}. Susceptibility-weighted data were acquired using a three-dimensional (3D) flow-compensated fast low-angle shot (FLASH) sequence (for parameter details see Table 7) in a sub-sample which was introduced only after 112 participants. High-quality phase maps (i.e. excluding coil-combination pole artifacts) were reconstructed from multi-channel complex signals using an automated, data-driven coil combination method (SVD-ESPIRiT)^{99,100}. Both magnitude and phase images are provided for SWI and QSM calculation which could be achieved using varied techniques^{96,101}. The total time of acquisition was 7 min 50 s.

Continuous Peripheral Physiological Recordings During rs-fMRI. During the 15 min 30 s acquisition of resting-state fMRI, continuous beat-to-beat blood pressure (NIBP), electrocardiography (ECG), pulse, and respiration were recorded non-invasively with MR-compatible devices. Blood pressure and pulse via photoplethysmography were recorded with a BIOPAC MP150 acquisition system (BIOPAC Systems Inc., Goleta, CA, USA) and the acquisition software AcqKnowledge (Version 4.0, BIOPAC Systems Inc., Goleta, CA, USA). In addition to the MP150 main hardware unit, blood

pressure acquisition required the NIBP-MRI module including a CareTaker Bluetooth® transmitter and pulse acquisition required the OXY100C pulse oximeter module with TSD123A finger clip transducer. All data streams were recorded with a sampling frequency of 1000 Hz. A digital input channel recorded triggers from the MR scanner for synchronisation of blood pressure and pulse data with repetition time onsets of rs-fMRI data.

Beat-to-beat blood pressure was detected from the pulse pressure signal at the brachial artery of the left arm with an air-filled pressure-sensitive sensor. The left arm was supported with tape and cushions to ensure optimal signal quality. The pulse pressure signal was transformed into two continuous streams of systolic and diastolic blood pressure through Pulse Decomposition Analysis¹⁰².

Initial calibration for the continuous blood pressure acquisition was achieved with a seated resting blood pressure measurement using an automatic oscillometric blood pressure monitor (OMRON M500, OMRON Medizintechnik Handelsgesellschaft mbH, Mannheim, Germany). Blood pressure data was recorded with a sampling frequency of 512 Hz and resampled in AcqKnowledge to 1000 Hz.

ECG and respiration were recorded with an MR-compatible BrainAmp ExG MR amplifier (Brain Products GmbH, Gilching, Germany) with PowerPack battery, SyncBox synchronization interface and relevant sensors (see below), as well as the acquisition software BrainVision Recorder (Version 1.20).

ECG was measured with three reusable ring electrodes that were taped on the participant's back to reduce artifacts caused by breathing movements of the torso in the magnetic field: the ground electrode was taped at the lumbar region superior to the tailbone (coccyx), the reference electrode was taped at the upper part of the back at the level of the seventh cervical vertebra and the recording electrode was placed on the left-hand side of a participant's back at the level of the tenth rib.

Respiration was measured with an MR-compatible pneumatic-based respiration sensor within a belt that was fastened around the torso of the participants.

After rs-fMRI was acquired, all sensors were removed from the MR chamber and the MRI session continued without peripheral physiological recordings.

The complementary project by Mendes *et al.*²¹ also comprised rs-fMRI scans with continuous peripheral physiological recordings (as described above). The peripheral physiological data of the 194 participants from Mendes *et al.* will be released as part of the study described here. 109 participants completed both protocols which enables repeated-measures (e.g., test-retest) analyses (see Supplementary Table S1).

For all the above mentioned peripheral physiological parameters only raw data is provided. All available data has been included - irrespective of data quality. The data has been cropped and the MRI artifact was removed but peak detection has not been done. Data quality can be eyeballed from the included image file (*.png) for each participant and modality.

EEG. Resting-state EEG (rs-EEG) was obtained in 216 participants who completed the second MDBF just before the EEG recording and underwent the Multi 8/2 drug strip test. The whole experiment session took approximately 1.5 hours (including the 16-minute EEG recording). The raw rs-EEG data with preprocessed rs-EEG and localizer files are openly available.

Resting-state EEG: A 16-min rs-EEG was recorded with a BrainAmp MR plus amplifier in an electrically shielded and sound-attenuated EEG booth using 62-channel (61 scalp electrodes plus 1 electrode recording the VEOG below the right eye) active ActiCAP electrodes (both Brain Products GmbH, Gilching, Germany) attached according to the international standard 10–20 extended localization system, also known as 10–10 system,¹⁰³ and referenced to FCz. The ground was located at the sternum and skin electrode impedance was kept below 5 K Ω . The amplitude resolution was set to 0.1 μ V. EEG was recorded with a bandpass filter between 0.015 Hz and 1 kHz and digitized with a sampling rate of 2500 Hz. The EEG session comprised a total of 16 blocks, each 60 s long, 8 with eyes-closed (EC) and 8 with eyes-open (EO) (EO and EC segments being interleaved), where the recording started with eyes-closed condition. The blocks were introduced using Presentation software (version 16.5, Neurobehavioral Systems Inc., Berkeley, CA, USA). Participants were seated in front of a computer screen and asked to stay awake while fixating eyes on a black cross presented on a white background (during the eyes-open sessions).

Digitized EEG channel locations: Starting from the second round (54th participant), a Polhemus PATRIOT Motion Tracking System (Polhemus, Colchester, VT, USA) localizer was used together with the Brainstorm toolbox¹⁰⁴ to digitize the exact location of each 62 electrode on a participant's head relative to three fiducial points (plus 1 electrode referenced to FCz).

Resting-State EEG Data Preprocessing: Data from 13 participants were excluded due to missing event information, different sampling rate, mismatching header files or insufficient data quality. The raw EEG data from 203 participants used for preprocessing was downsampled from 2500 Hz to 250 Hz, bandpass filtered within 1–45 Hz (8th order, Butterworth filter) and split into EO and EC conditions for the subsequent analyses. Outlier channels were rejected after visual inspection for frequent jumps/shifts in voltage and poor signal quality. Data intervals containing extreme peak-to-peak deflections or large bursts of high frequency activity were identified by visual inspection and removed. Intervals containing traces from eye blinks or eye movements were not removed at this stage. Further data preprocessing was

done in EEGLAB¹⁰⁵ (version 14.1.1b) for MATLAB (Delorme and Makeig, 2004). The dimensionality of the data was reduced using principal component analysis (PCA), by keeping PCs ($N \geq 30$) that explain 95% of the total data variance. Next, independent component analysis¹⁰⁶ (ICA) was performed using the Infomax (runica) algorithm. Components reflecting eye movement, eye blink or heartbeat related artifacts were removed. Retained independent components for EO (mean: 19.7, range: 9–30) and EC (mean: 21.4, range: 14–28) conditions were back-projected to sensor space for further analysis.

Additional Measures. *Seated Resting Blood Pressure:* Blood pressure (BP) was measured using an automatic oscillometric blood pressure monitor (OMRON M500, OMR HEM-7213-D) and a 22–42 cm arm cuff (OMRON HEM-RML30, both OMRON Medizintechnik Handelsgesellschaft mbH, Mannheim, Germany) after a seated resting period of 5 min. The BP measurements took place on three occasions throughout the course of the study: 1) before the MRI session (BP1), 2) after the MRI session (BP2), 3) at the beginning of follow-up experiments (BP3). All BP measurements were recorded at the left arm. Before the MRI session, an additional measurement at the right arm was recorded to rule out pathologic differences between right and left arm measurements. Accompanying pulse measurements at the arm (Pulse1, Pulse2) were saved during BP measurements 1 and 2. As part of the complementary project by Mendes *et al.*²¹, one blood pressure measurement at the left arm was taken from 91 additional participants before a rs-fMRI session that also included continuous peripheral physiological recordings (see section Continuous Peripheral Physiological Recordings During rs-fMRI).

Peripheral Blood Sample Collection and Analysis: A blood sample of approximately 70 ml in total was collected on the first assessment day after acquisition of MRI data. If the blood drawing was not possible on this date, it was acquired on the following assessment days and documented as such. The new date is mentioned in the data files. The blood was collected with four different types of sampling tubes: Serum, EDTA, Citrate and RNA. A portion of the sample was directly sent to the Institute for Laboratory Medicine, Clinical Chemistry and Molecular Diagnostics (ILM) of the Medical Faculty at the Leipzig University; the remaining samples were stored for later use. One serum tube (S-Monovette® 7.5 ml, Sarstedt), one EDTA tube (S-Monovette® 2.7 ml K3E, Sarstedt), and one citrate tube (S-Monovette® 3.0 ml 9NC, Sarstedt) were sent for direct analysis to the ILM. The remaining blood samples were divided into 10 microtainers of 2.0 ml size. Together with three EDTA tubes (S-Monovette® 2.7 ml K3E, Sarstedt) and 2 RNA tubes (Tempus™, Applied Biosystems)—containing stabilization solution—the remaining aliquots were stored at -80°C for later use.

Anthropometry: Classical anthropometric measurements were taken according to standardized procedures by trained medical persons. Body weight was measured using an electronic scale (SECA 813, Seca GmbH & Co KG) with a precision of 0.01 kg. The participants were barefoot, dressed with empty pockets and without outer garments. Body height of barefoot participants was measured using a stadiometer (SECA 216) to the nearest 0.1 cm. During measurement, the body of the participants were erect and centered placing feet together, the heels and the occiput touching the wall. The waist was measured 1 cm above the belly button, and the hip was measured around the widest part of the hip, with all outer garments removed. The waist and the hip were assessed by using an ergonomic circumference measuring tape (SECA 201) to the nearest 0.1 cm.

Hair Sample: To obtain the required amount of hair for the sample the hair had to be a minimum 4 cm long. Participants with colored/dyed hair were also included (as suggested by the analyzing lab), dreadlocked hair was an exclusion criterion. The hair sample was taken from the back of – and as close as possible to – the scalp (posterior vertex position). The strands were carefully placed in aluminum foil and the proximal end was marked. The sample was weighed before being sent to the laboratory. Hair sampling followed the procedure described here: <http://poolux.psychopool.tu-dresden.de/dat/videos/hmd1.mpg>. Hair samples were delivered to Technische Universität Dresden (TU Dresden) laboratory for analysis (lab of Prof. Dr. C. Kirschbaum). However, the results for cortisol and other hormonal measurements contained an unusual high percentage of 0-values (cortisol 13%, progesterone 63%, corticosterone 73%). Therefore hair-derived corticosteroid measurements were deemed unreliable and will not be released.

Code Availability

All code that was implemented for MRI data acquisition and processing pipelines is available online: (https://github.com/NeuroanatomyAndConnectivity/pipelines/tree/v2.0/src/lsc_lemon/). Data handling and computation of summary measures were implemented in Python.

Data Records

Data Security and Data Anonymization Procedures

To protect health information prevent direct identification, the participant were given special LEMON IDs. All the data, whether pen-and-paper, computer administered, as well as LimeSurvey, were saved only with these LEMON IDs. For public data sharing we anonymized them once more these IDs into BIDS 6-digit format (010000). Thus our participants are given now IDs such as sub-010000.

For internal use, the data was first saved on a MPI-CBS in-house local secured network. Later, the data for all participants was stored on our instance of the eXtensible Neuroimaging Archive Toolkit (XNAT 35) v.1.6.5. at the MPI-CBS. Access to the initial project was restricted (via XNAT's private project mode) to members of the Leipzig Study for Mind-Body-Emotion Interactions and Neuroanatomy & Connectivity Group at MPI-CBS for initial curation and quality assessment of data. All data comprised in the MPI-Leipzig Mind-Brain-Body database were derived from MPI-CBS so data import into XNAT was done from our local secured network. A specially customized XNAT uploader was used to upload all participants' data to XNAT.

The native DICOM format was used for MRI data, whilst a standard ASCII (*.csv, *.txt) format was employed to upload all other experimental data such as surveys, test batteries, and demographical data in XNAT also in local secured network. The anonymization measures applied to the MRI data consisted of removal of DICOM header tags containing information which could lead to the identification of test participants as well as the defacing of all structural (NIFTI) scans.

This applied mainly for internal use. For releasing the data publicly, the MRI data in NIFTI files in JavaScript Object Notation (*.json) with (*.tsv) format is stored. More details regarding publicly released data can be found below in Usage Notes section.

MRI Data

All MRI datasets are made available in NIFTI format, and all anatomical scans have been defaced. For more details see Mendes *et al.* The dataset is organized in concordance with the Brain Imaging Data Structure (BIDS) format. This facilitates data analysis, for example with BIDS-Apps¹⁰⁷ (<http://bids-apps.neuroimaging.io>). BIDS-Apps encapsulate standard MRI analysis tools within an application that understands the BIDS format and allows automatic access to relevant data and metadata. The MRI raw and preprocessed data can be found in GWDG (https://ftp.gwdg.de/pub/misc/MPI-Leipzig_Mind-Brain-Body-LEMON/) as well as in *Functional Connectomes Project International Neuroimaging Data-Sharing Initiative/Child Mind Institute* (Data Citation 1) and OpenNeuro repository (Data Citation 2).

EEG Data

The raw rs-EEG data folder contains raw resting state EEG data files (Brain Vision files). The marker codings are S200 for eyes open at rest and S210 for eyes closed at rest.

The preprocessed resting state EEG data folder contains preprocessed EEG (see method section for details) saved in the standard EEGLAB¹⁰⁰ file format (.set and .fdt files). For each participant (N = 203) eyes-closed (EC) and eyes-open (EO) conditions are stored separately thus each having 4 files (2 for EC condition and 2 for EO), with the following naming structure: sub-BIDS condition.fdt (.set) and conditions: eyes closed (EC) or eyes open (EO). This preprocessed data has already been used in another EEG study about non-sinusoidal nature of neuronal oscillations¹⁰⁸.

The digitized EEG channel locations (62) with Polhemus PATRIOT Motion Tracking System are stored in separate folder as MATLAB (.mat) files. The EEG raw and preprocessed data can be found at GWDG (https://ftp.gwdg.de/pub/misc/MPI-Leipzig_Mind-Brain-Body-LEMON/) or *Functional Connectomes Project International Neuroimaging Data-Sharing Initiative/Child Mind Institute* (Data Citation 1).

Emotion and Cognition Test Batteries, Assessments, and Other Protocols

The data from most questionnaires are reported as summary scores. Whenever summary scores do not provide an adequate measure, we report raw item scores, for instance the New York cognition (NYC-Q).

Questionnaires that do not come with summary scores are released as raw item scores, namely: New York Cognition Questionnaire (NYC-Q).

Cognitive test data for the CVLT, LPS, TA P, TMT, WST, RWT and emotion and personality test battery questionnaires such as BIS/BAS, CERQ, COPE, ERQ, FEV, F-SozU K-22, LOT-R, MARS, MSPSS, NEO, PSQ, STAI, STAXI, TAS, TEIQue-SF, TICS, UPPS, FTP, YFAS, as well as MDBF and NYC-Q are available via subject-specific *.csv files. Moreover, for each questionnaire and cognitive test, accompanying specifications and information are given in *.txt file format with item details and Likert scores.

For each participant, the average age across the course of the study was reported which was the same in both supplementary studies of MPI Leipzig Mind-Brain-Body database. For the purpose of anonymity, the mean age was then binned into five year width (5-year bins). Cutoff values for binning were 20.0, 25.0, 30.0 and so forth. A meta file with demographic summary in *.csv format includes: gender, age (5-year bins), handedness, formal education, drug test results on day 2, smoking status, SKID, HAM-D, BLS-23, AUDIT, and relationship status. Separate subject-specific (.csv) files with information given in Text (.txt) file include the results of blood sample, blood pressure (for 3 occasions), and anthropometry.

In addition to this meta file, we include a data availability (.csv) file which includes all the LEMON data available for each specific data acquisition section with subscales (1 = available, 0 = not available).

The data can be accessed via GWDG (https://ftp.gwdg.de/pub/misc/MPI-Leipzig_Mind-Brain-Body-LEMON/), and *Functional Connectomes Project International Neuroimaging Data-Sharing Initiative/Child Mind Institute* (Data Citation 1), or directly at NITRC (<https://www.nitrc.org/projects/mpilmbb>).

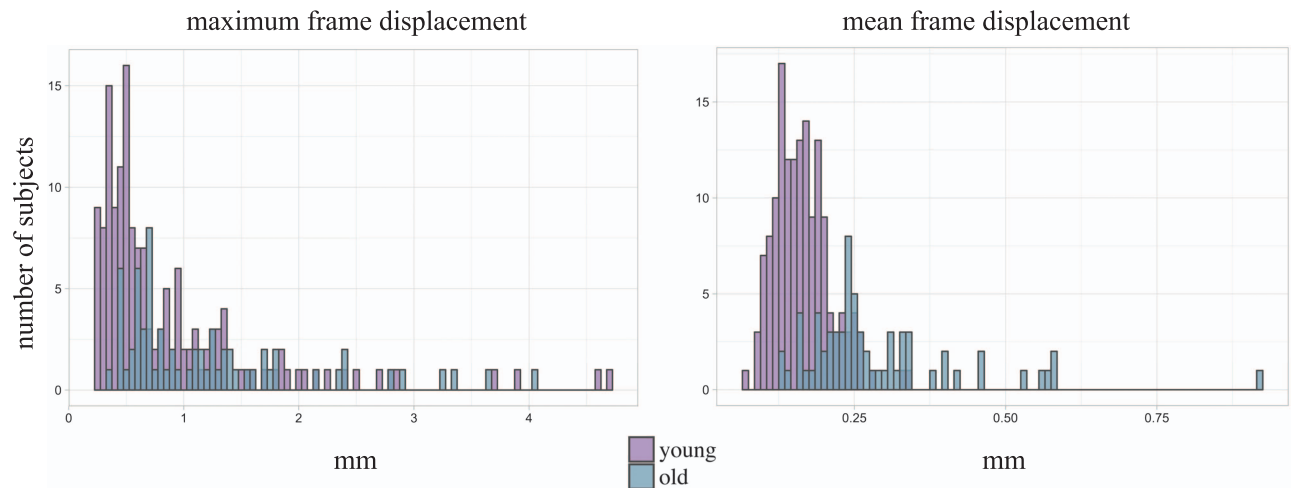


Figure 2. Quality assessment of resting-state fMRI scans. Distribution of motion (maximum and mean framewise displacement).

Technical Validation

Before inclusion in the database, we manually double-checked all datasets for missing or corrupt data. Further quality control of the data was applied to the MRI and behavioral measures, as described below.

MRI Data Quality Assessment

As described in Mendes *et al.*²¹, we assessed the quality of preprocessed resting-state fMRI images using the mriqc package¹⁰⁹, implemented in Python. Mriqc creates a report for each individual scan based on different parameters like motion, coregistration, and temporal signal-to-noise (tSNR). The details of tSNR and fieldmap correction can be found in the previous article of Mendes *et al.*²¹. Resting-state fMRI data from 8 participants were excluded from preprocessing due to errors during data acquisition (ghosting artifact $n=2$, incomplete scan $n=1$), anatomical preprocessing ($n=4$) or functional preprocessing ($n=1$).

We visually inspected the quality assessment reports for each participant. Furthermore, frames with high motion were marked according to the framewise displacement, which was calculated as the sum of the absolute values of the six realignment parameters¹¹⁰. For comparison, all individual-level scores are displayed with respect to the group-level distribution ($N=219$). In Fig. 2, the mean and maximum framewise displacement for all participants ($N=219$), as well as separately for young ($N=152$) and old ($N=67$) participants, are given. Overall, the summary of the motion parameters of our MRI data shows that 91.78% of runs have less than one voxel (2.3 mm) maximum framewise displacement, and mean framewise displacement of 0.202 mm ($SD=0.101$ mm), demonstrating sufficient quality. Mean framewise displacement was 0.165 mm ($SD=0.046$ mm) in young participants and a slightly higher in the elderly group ($M=0.289$, $SD=0.134$).

Behavioral Measures Quality Assessment

We calculated descriptive statistics and reliability estimates of each subscale of the emotion and personality battery to ensure their general usability (see Table 6 (available online only)). Since we used mainly German questionnaires with validated factor structures (besides NYC-Q and MARS, which were translated by a professional translator), we report both the Cronbach's alpha coefficients from the original validation studies of the respective questionnaires as well as the ones calculated from our data in Table 6 (available online only). We did not compute the Cronbach's alpha coefficient for the NYC-Q as the heterogeneity of items within these questionnaires neither describe a unitary phenomenon nor are they designed to be internal consistent¹¹¹. We recommend a factor analytic approach⁶⁶ to derive behavioral scores from this questionnaire. Moreover, for YFAS we calculated the internal consistency based on Kuder-Richardson's alpha coefficient¹¹².

To further facilitate the evaluation of emotion and personality data, we plotted densities of all subscale scores for younger and older participants (see Supplementary Figure S2), which suggest sensible distributions: For example, normal distributions were observed for most personality traits (NEO-FFI), whereas skewed distributions were observed for social support variables (FSozU, MSPSS). Age-group differences observed after conservative Bonferroni correction for multiple comparisons ($\alpha=0.0005$) are in general alignment with previous reports of changes in emotional processing during aging^{113,114}. Significant differences between younger and older adults emerged on 20 of 98 subscales (see

Supplementary Figure S2). These results further underline the value of the LEMON dataset to examine associations of emotions and brain-body functions in healthy aging.

Usage Notes

The public dataset, protocols, and software used in the acquisition and processing of the data are documented, curated, and available for research purposes. The datasets are provided with three different tiers of access. Users are kindly asked to first agree to the terms of data usage, especially for access to behavioral data, which prohibits identifying individuals on these phenotyping data.

The complete LEMON data can be retrieved from the first location (GWDG) under point 1 (a) below. Moreover, with the complementary project by Mendes *et al.* the raw MRI data are currently available from the OpenNeuro and INDI mentioned under point 1 (b) below. All MRI datasets are shared in NIFTI files, and all anatomical scans have been defaced. A standard ASCII (*.csv, *.txt) format was employed to upload all other experimental data such as surveys, test batteries, and demographical data in GWDG, and in NITRC.

1. Complete MPILMBB LEMON Data

a. The complete LEMON Data can be accessed via Gesellschaft für wissenschaftliche Datenverarbeitung mbH Göttingen (GWDG) <https://www.gwdg.de/>. Raw and preprocessed data at this location is accessible through web browser https://ftp.gwdg.de/pub/misc/MPI-Leipzig_Mind-Brain-Body-LEMON/ and a fast FTP connection (ftp://ftp.gwdg.de/pub/misc/MPI-Leipzig_Mind-Brain-Body-LEMON/). In the case the location of the data changes in the future, the location of the dataset can be resolved with PID 21.11101/0000-0007-C379-5 (e.g. <http://hdl.handle.net/21.11101/0000-0007-C379-5>).

b. Additionally, the complete LEMON Data is accessible via Functional Connectomes Project International Neuroimaging Data-Sharing Initiative (INDI) at Child Mind Institute (Data Citation 1).

2. Only MPILMBB LEMON MRI Raw Data

The OpenNeuro.org platform also hosts the raw data (Data Citation 2). The OpenNeuro repository provides API access available via <https://openneuro.org/dataset/api/>. In addition, similar to all other datasets in OpenNeuro, our dataset is available via Amazon Web Services S3 object data store (Data Citation 2).

3. Only MPILMBB Behavioral Data

Additionally, the MPILMBB LEMON behavioral data can be found at Neuroimaging Tools and resources Collaboratory (NITRC): <https://www.nitrc.org/projects/mpilmbb>.

References

- LeDoux, J. E. *The Emotional Brain*. (Touchstone Book, 1996).
- Nummenmaa, L., Glerean, E., Hari, R. & Hietanen, J. K. In Bodily maps of emotions. *Proceedings Natl. Acad. Sci. USA* **111**, 646–651 (2014).
- Schachter, S. & Singer, J. Cognitive, social, and physiological determinants of emotional state. *Psychol. Rev.* **69**, 379–399 (1962).
- James, W. What is an emotion? *Mind* **9**, 188–205 (1884).
- Garfinkel, S. N. & Critchley, H. D. Threat and the body: how the heart supports fear processing. *Trends Cogn. Sci.* **20**, 34–46 (2016).
- House, A. Depression after stroke. *Br. Med. J. (Clin. Res. Ed.)* **294**, 76–78 (1987).
- Linden, W., Vodermaier, A., MacKenzie, R. & Greig, D. Anxiety and depression after cancer diagnosis: Prevalence rates by cancer type, gender, and age. *J. Affect. Disord.* **141**, 343–351 (2012).
- Lu, D. *et al.* Clinical diagnosis of mental disorders immediately before and after cancer diagnosis. *JAMA Oncol* **2**, 1188–1196 (2016).
- Pyter, L. M., Pineros, V., Galang, J. A., McClintock, M. K. & Prendergast, B. J. Peripheral tumors induce depressive-like behaviors and cytokine production and alter HPA regulation. *PNAS* **106**, 9069–9074 (2009).
- Chrousos, G. P. & Gold, P. W. The concepts of stress and stress system disorders: overview of physical and behavioral homeostasis. *JAMA* **267**, 1244–1252 (1992).
- Jonas, B. S. & Mussolino, M. E. Symptoms of depression as a prospective risk factor for stroke. *Psychosom. Med.* **62**, 463–471 (2000).
- Kubzansky, L. D. & Kawachi, I. Going to the heart of the matter: do negative emotions cause coronary heart disease? *J. Psychosom Res.* **48**, 323–337 (2000).
- Golden, S. H. *et al.* Atherosclerosis Risk in Communities study. *Diabetes Care* **27**, 429–435 (2004).
- Glover, G. H., Li, T. Q. & Ress, D. Image-based method for retrospective correction of physiological motion effects in fMRI: RETROICOR. *Magn. Reson. Med.* **44**, 162–167 (2000).
- Thayer, J. F., Åhs, F., Fredrikson, M., Sollers, J. J. & Wager, T. D. A meta-analysis of heart rate variability and neuroimaging studies: implications for heart rate variability as a marker of stress and health. *Neurosci. Biobehav. Rev.* **36**, 747–756 (2012).
- Pessoa, L. Précis on the cognitive-emotional brain. *Behav. Brain. Sci.* **38**, e71 (2015).
- Etkin, A., Büchel, C. & Gross, J. J. The neural bases of emotion regulation. *Nat. Rev. Neurosci.* **16**, 693–700 (2015).
- Djuric, Z. *et al.* Biomarkers of Psychological Stress in Health Disparities Research. *Open Biomark J.* **1**, 7–19 (2008).
- Stepoe, A., Deaton, A. & Stone, A. A. Psychological wellbeing, health and ageing. *Lancet* **385**, 640–648 (2015).
- Baumgart, M. *et al.* Summary of the evidence on modifiable risk factors for cognitive decline and dementia: A population-based perspective. *Alzheimer's & Dementia* **11**, 718–726 (2015).
- Mendes, N. *et al.* A Functional connectome phenotyping dataset including cognitive state and personality measures. *Sci. Data.* **6**:180307, <https://doi.org/10.1038/sdata.2018.307> (2019).
- Niemann, H., Sturm, W., Thöne-Otto, A. I. & Willmes, K. *California Verbal Learning Test (CVLT). German Adaptation. Manual.* (Pearson, 2008).
- Zimmermann, P. & Fimm, V. *Testatterie zur Aufmerksamkeitsprüfung (TAP)*. Version 2.3.1, https://www.psytest.net/index.php?page=TAP-2-2&hl=en_US (Psytest, 2012).

24. Reitan, R. M. *Trail making test A & B*. (Reitan Neuropsychology Laboratory, 1992).
25. Schmidt, K. H. & Metzler, P. *WST: Wortschatztest*. (Beltz, 1992).
26. Kreuzpointner, L., Lukesch, H. & Horn, W. *Leistungsprüfsystem 2. LPS-2. Manual*. (Hogrefe, 2013).
27. Aschenbrenner, S., Tucha, O. & Lange, K. W. *RWT: Regensburger Wortflüssigkeits-Test*. (Hogrefe, 2000).
28. LimeSurvey Project Team / Carsten Schmitz. LimeSurvey: An Open Source survey tool. LimeSurvey version 2.0. LimeSurvey Project Hamburg <http://www.limesurvey.org>, (2012).
29. Borkenau, P. & Ostendorf, F. *NEO-Fünf-Faktoren Inventar nach Costa und McCrae (NEO-FFI). Manual (2. Aufl.)*. (Hogrefe, 2008).
30. Costa, P. T. & McCrae, R. R. *Revised NEO Personality Inventory (NEO PI-R) and NEO Five Factor Inventory (NEO-FFI) Professional Manual*. (Psychological Assessment Resources Inc., 1992).
31. Schmidt, R. E., Gay, P., d'Acromont, M. & Van der Linden, M. A German adaptation of the UPPS Impulsive Behavior Scale: Psychometric properties and factor structure. *Swiss. J. Psychol.* **67**, 107–112 (2008).
32. Whiteside, S. P. & Lynam, D. R. The five factor model and impulsivity: Using a structural model of personality to understand impulsivity. *Pers. Individ. Differ.* **30**, 669–689 (2001).
33. Strobel, A., Beauducel, A., Debener, S. & Brocke, B. Eine deutschsprachige Version des BIS/BAS-Fragebogens von Carver und White. *Zeitschrift für Differentielle und diagnostische Psychologie* **22**, 216–227 (2001).
34. Carver, C. S. & White, T. L. Behavioral inhibition, behavioral activation, and affective responses to impending reward and punishment: the BIS/BAS scales. *J. Pers. Soc. Psychol.* **67**, 319–333 (1994).
35. Ablner, B. & Kessler, H. Emotion Regulation Questionnaire - Eine deutsche Version des ERQ von Gross & John. *Diagnostica* **55**, 144–152 (2009).
36. Gross, J. J. & John, O. P. Individual differences in two emotion regulation processes: implications for affect, relationships, and well-being. *J. Pers. Soc. Psychol.* **85**, 348–362 (2003).
37. Loch, N., Hiller, W. & Witthöft, M. Der cognitive emotion regulation questionnaire (CERQ). *Zeitschrift für Klinische Psychologie und Psychotherapie* **40**, 94–106 (2011).
38. Garnefski, N., Kraaij, V. & Spinhoven, P. Negative life events, cognitive emotion regulation and emotional problems. *Pers. Individ. Dif* **30**, 1311–1327 (2001).
39. Larsen, R. J., Prizmic, Z. Affect regulation. In: Baumeister, R. F. & Vohs, K. D. (Eds) *Handbook of self-regulation: Research, theory, and applications*, 40–61 (Guilford Press, 2004).
40. Fydrich, T., Sommer, G. & Brähler, E. *F-SOZU: Fragebogen zur sozialen Unterstützung*. (Hogrefe, 2007).
41. Fydrich, T., Sommer, G., Menzel, U. & Höll, B. Social Support Questionnaire (short-form; SozU-K-22). *Z. Klin. Psychol. Psychother.* **16**, 434–436 (1987).
42. Zimet, G. D., Dahlem, N. W., Zimet, S. G., & Farley, G. K. The Multidimensional Scale of Perceived Social Support. *J. Pers. Assess.* **52**, 30–41 (1988).
43. Knoll, N., Rieckmann, N. & Schwarzer, R. Coping as a mediator between personality and stress outcomes: A longitudinal study with cataract surgery patients. *Eur. J. Personality* **19**, 229–247 (2005).
44. Carver, C. S. You want to measure coping but your protocol's too long: Consider the Brief COPE. *Int. J. Behav. Med.* **4**, 92–100 (1997).
45. Glaesmer, H., Hoyer, J., Klotsche, J. & Herzberg, P. Y. Die Deutsche Version des Life-Orientierung-Tests (LOT-R) zum dispositionellen Optimismus und Pessimismus. *Zeitschrift für Gesundheitspsychologie* **16**, 26–31 (2008).
46. Scheier, M. F., Carver, C. S. & Bridges, M. W. Distinguishing optimism from neuroticism (and trait anxiety, self-mastery, and self-esteem): A re-evaluation of the Life Orientation Test. *J. Pers. Soc. Psychol.* **67**, 1063–1078 (1994).
47. Fliege, H., Rose, M., Arck, P., Levenstein, S. & Klapp, B. F. Validierung des "Perceived Stress Questionnaire" (PSQ) an einer deutschen Stichprobe. *Diagnostica* **47**, 142–152 (2001).
48. Levenstein, S. *et al.* Development of the Perceived Stress Questionnaire: A new tool for psychosomatic research. *J. Psychosom. Res.* **37**, 19–32 (1993).
49. Schulz, P., Schlotz, W. & Becker, P. *Trierer Inventar zum chronischen Stress: TICS*. (Hogrefe, 2004).
50. Schulz, P. & Schlotz, W. Trierer Inventar zur Erfassung von chronischem Stress (TICS): Skalenkonstruktion, teststatistische Überprüfung und Validierung der Skala Arbeitsüberlastung. *Diagnostica* **45**, 8–19 (1999).
51. Stunkard, A. J. & Messick, S. The three-factor eating questionnaire to measure dietary restraint, disinhibition and hunger. *J. Psychosom. Res.* **29**, 71–83 (1985).
52. Pudiel, D. & Westenhöfer, J. *Fragebogen zum Eßverhalten (FEV)*. (Hogrefe, 1989).
53. Meule, A., Vögele, C. & Kübler, A. Deutsche Übersetzung und Validierung der Yale Food Addiction Scale-German translation and validation of the Yale Food Addiction Scale. *Diagnostica* **58**, 115–126 (2012).
54. Gearhardt, A.N., Corbin, W.R. & Brownell, K.D. Preliminary validation of the Yale Food Addiction Scale. *Appetite* **52**, 430–436 (2009).
55. Saß, H., Wittchen, H. U., Zaudig, M. & Houben, I. *Diagnostische Kriterien. DSM-IV-TR*. (Hogrefe, 2003).
56. Petrides, K. V. & Furnham, A. TEIQue-SF: Trait Emotional Intelligence Questionnaire-Short Form. *J. Appl. Soc. Psychol.* **36**, 552–569 (2006).
57. Freudenthaler, H. H., Neubauer, A. C., Gabler, P. & Scherl, W. G. Testing the Trait Emotional Intelligence Questionnaire (TEIQue) in a German-speaking sample. *Pers. Individ. Differ.* **45**, 673–678 (2008).
58. Laux, L., Glanzmann, P., Schaffner, P. & Spielberger, C.D. *Das State-Trait-Angstinventar*. (Beltz Test, 1981).
59. Spielberger, C. D., Gorsuch, R. L. & Lushene, R. E. *Manual for the State-Trait Anxiety Inventory. Manual for the State-Trait Anxiety Inventory*. (Consulting Psychologists Press, 1970).
60. Schwenkmezger, P., Hodapp, V. & Spielberger, C. D. *Das State-Trait-Ärgerausdrucks-Inventar STAXI*. (Huber, 1992).
61. Spielberger, C. D. *State-Trait Anger Expression Inventory (STAXI). Research edition*. (Psychological Assessment Resources: Odessa, 1988).
62. Kupfer, J., Brosig, B. & Brähler, E. *Toronto-Alexithymie-Skala-26. Deutsche Version (TAS-26)*. (Hogrefe, 2001).
63. Bagby, R. M., Parker, J. D. & Taylor, G. J. The twenty-item Toronto Alexithymia Scale—I. Item selection and cross-validation of the factor structure. *J. Psychosom. Res.* **38**, 23–32 (1994).
64. Steyer, R., Schwenkmezger, P., Notz, P. & Eid, M. *Der Mehrdimensionale Befindlichkeitsfragebogen*. (Hogrefe, 1997).
65. Lang, F. R. & Carstensen, L. L. Time counts: future time perspective, goals, and social relationships. *Psychol. Aging* **17**, 125–139 (2002).
66. Gorgolewski, K. J. *et al.* A correspondence between individual differences in the brain's intrinsic functional architecture and the content and form of self-generated thoughts. *PLoS One* **9**, e97176 (2014).
67. Wittchen, H., Wunderlich, U. & Gruschwitz, S. *SKID-I. Strukturiertes klinisches Interview für DSM-IV; Achse I: Psychische Störungen*. (Hogrefe, 1997).
68. Saß, H., Wittchen, H. U. & Zaudig, M. *Diagnostisches und statistisches Manual psychischer Störungen-DSM-IV*. (Hogrefe: Göttingen, 1996).
69. Hamilton, M. A rating scale for depression. *J. Neurol Neurosurg Psychiatry* **23**, 56–62 (1960).

70. Bohus, M. *et al.* The short version of the Borderline Symptom List (BSL-23): development and initial data on psychometric properties. *Psychopathology* **42**, 32–39 (2008).
71. Sobell, L. C., Sobell, M. B. Timeline Follow Back. A technique for assessing self-reported alcohol consumption. In Litten R. & Allen J. eds. *Measuring alcohol consumption*. 41–72 (Humana Press, 1992).
72. Saunders, J. B., Aasland, O. G., Babor, T. F., De la Fuente, J. R. & Grant, M. Development of the alcohol use disorders identification test (AUDIT): WHO collaborative project on early detection of persons with harmful alcohol consumption - II. *Addiction* **88**, 791–804 (1993).
73. Hawks, R. L. & Chiang, C. N. *Urine testing for drugs of abuse*. (National Institute on Drug Abuse, 1986).
74. Jezzard, P. & Balaban, R. S. Correction for geometric distortion in echo planar images from B0 field variations. *Magn. Reson. Med.* **34**, 65–73 (1995).
75. Reber, P. J., Wong, E. C., Buxton, R.B. & Frank, L.R. Correction of off resonance-related distortion in echo-planar imaging using EPI-based field maps. *Magn. Reson. Med.* **39**, 328–330 (1998).
76. Chang, H. & Fitzpatrick, J. M. A technique for accurate magnetic resonance imaging in the presence of field inhomogeneities. *IEEE Trans. Med. Imaging* **11**, 319–329 (1992).
77. Andersson, J. L., Skare, S. & Ashburner, J. How to correct susceptibility distortions in spin-echo echo-planar images: application to diffusion tensor imaging. *NeuroImage* **20**, 870–888 (2003).
78. Marques, J. P. *et al.* MP2RAGE, a self bias-field corrected sequence for improved segmentation and T1-mapping at high field. *NeuroImage* **49**, 1271–1281 (2010).
79. Xu, J. *et al.* Evaluation of slice accelerations using multiband echo planar imaging at 3T. *NeuroImage* **83**, 991–1001 (2013).
80. Moeller, S. *et al.* Multiband multislice GE-EPI at 7 tesla, with 16-fold acceleration using partial parallel imaging with application to high spatial and temporal whole-brain fMRI. *Magn. Reson. Med.* **63**, 1144–1153 (2010).
81. Feinberg, D. A. *et al.* Multiplexed echo planar imaging for sub-second whole brain fMRI and fast diffusion imaging. *PLoS One* **5**, e15710 (2010).
82. Jenkinson, M., Bannister, P., Brady, M. & Smith, S. Improved optimization for the robust and accurate linear registration and motion correction of brain images. *NeuroImage* **17**, 825–841 (2002).
83. Jenkinson, M., Beckmann, C. F., Behrens, T. E., Woolrich, M. W. & Smith, S. M. Fsl. *NeuroImage* **62**, 782–790 (2012).
84. Greve, D. N. & Fischl, B. Accurate and robust brain image alignment using boundary- based registration. *NeuroImage* **48**, 63–72 (2009).
85. Behzadi, Y., Restom, K., Liao, J. & Liu, T. T. A component based noise correction method (CompCor) for BOLD and perfusion based fMRI. *NeuroImage* **37**, 90–101 (2007).
86. Rokem, A., Trampus, M. & Perez, F. Nitime: time-series analysis for neuroimaging data. in *Proceedings. of the 8th Python in Science Conference 2* 68–75 (Caltech, 2009).
87. Avants, B. B. *et al.* A reproducible evaluation of ANTs similarity metric performance in brain image registration. *NeuroImage* **54**, 2033–2044 (2011).
88. Marques, J. P. & Gruetter, R. New developments and applications of the MP2RAGE sequence-focusing the contrast and high spatial resolution R1 mapping. *PLoS One* **8**, e69294 (2013).
89. Waehnert, M. D. *et al.* A subject-specific framework for in vivo myeloarchitectonic analysis using high resolution quantitative MRI. *Neuroimage* **125**, 94–107 (2016).
90. Lorio, S. *et al.* Neurobiological origin of spurious brain morphological changes: A quantitative MRI study. *Hum. Brain Mapp.* **37**, 1801–1815 (2016).
91. Bazin, P.-L. *et al.* A computational framework for ultra-high resolution cortical segmentation at 7Tesla. *NeuroImage* **93**, 201–209 (2014).
92. Dale, A. M., Fischl, B. & Sereno, M. I. Cortical surface-based analysis: I. Segmentation and surface reconstruction. *NeuroImage* **9**, 179–194 (1999).
93. Fischl, B., Sereno, M. I. & Dale, A. M. Cortical surface-based analysis: II: inflation, flattening, and a surface-based coordinate system. *NeuroImage* **9**, 195–207 (1999).
94. Setsompop, K. *et al.* Blipped-controlled aliasing in parallel imaging for simultaneous multislice echo planar imaging with reduced g-factor penalty. *Magn. Reson. Med.* **67**, 1210–1224 (2012).
95. Griswold, M.A. *et al.* Generalized autocalibrating partially parallel acquisitions (GRAPPA). *Magn. Reson. Med.* **47**, 1202–1210 (2002).
96. Liu, C., Li, W., Tong, K.A., Yeom, K.W. & Kuzminski, S. Susceptibility-weighted imaging and quantitative susceptibility mapping in the brain. *J. Magn. Reson. Imaging* **42**, 23–41 (2015).
97. Haacke, E. M., Mittal, S., Wu, Z., Neelavalli, Z. & Cheng, Y.-CN. Susceptibility-weighted imaging: technical aspects and clinical applications, part 1. *Am. J. Neuroradiol.* **30**, 19–30 (2009).
98. Mittal, S., Wu, Z., Neelavalli, J. & Haacke, E. M. Susceptibility-weighted imaging: technical aspects and clinical applications, part 2. *Am. J. Neuroradiol.* **30**, 232–252 (2009).
99. Uecker, M. *et al.* ESPIRiT - An eigenvalue approach to autocalibrating parallel MRI: Where SENSE meets GRAPPA. *Magn. Reson. Med.* **71**, 990–1001 (2014).
100. Chatnuntawech, I. *et al.* Single-step quantitative susceptibility mapping with variational penalties. *NMR Biomed.* **30**, e3570 (2016).
101. Deistung, A., Schweser, F. & Reichenbach, J. R. Overview of quantitative susceptibility mapping. *NMR Biomed.* **30**, e3569 (2017).
102. Baruch, M. C. Pulse Decomposition Analysis of the digital arterial pulse during hemorrhage simulation. *Nonlinear Biomed. Phys.* **5**, 1–15 (2011).
103. Oostenveld, R. & Praamstra, P. The five percent electrode system for high-resolution EEG and ERP measurements. *Clin. Neurophysiol.* **112**, 713–719 (2001).
104. Tadel, F., Baillet, S., Mosher, J. C., Pantazis, D. & Leahy, R. M. Brainstorm: a user-friendly application for MEG/EEG analysis. *Comput. Intell. Neurosci.* **2011**, 1–13 (2011).
105. Delorme, A. & Makeig, S. EEGLAB: an open source toolbox for analysis of single-trial EEG dynamics. *J. Neurosci. Methods* **134**, 9–21 (2004).
106. Makeig, S., Bell, A. J., Jung, T.-P., Sejnowski, T. J. Independent component analysis of electroencephalographic data. In Touretzky D., Mozer M. & Hasselmo M. Eds. *Advances in Neural Information Processing Systems* **8**, 145–151 (1996).
107. Gorgolewski, K. J. *et al.* BIDS Apps: Improving ease of use, accessibility and reproducibility of neuroimaging data analysis methods. *PLoS Comp. Biol.* **13**, e1005209 (2017).
108. Schaworonk, N. & Nikulin, V. V. Spatial neuronal synchronization and the waveform of oscillations: implications for EEG and MEG. *bioRxiv*, <https://www.biorxiv.org/content/early/2018/08/27/401091> (2018).
109. Esteban, O. *et al.* MRIQC: Advancing the Automatic Prediction of Image Quality in MRI from Unseen Sites. *PLoS One* **12**, e0184661 (2017).

110. Power, J. D., Barnes, K. A., Snyder, A. Z., Schlaggar, B. L. & Petersen, S. E. Spurious but systematic correlations in functional connectivity MRI networks arise from subject motion. *NeuroImage* **59**, 2142–2154 (2012).
111. Streiner, D. L. Starting at the beginning: an introduction to coefficient alpha and internal consistency. *J. Pers. Assess.* **80**, 99–103 (2003).
112. Meule, A. & Gearhardt, A. N. Five years of the Yale Food Addiction Scale: Taking stock and moving forward. *Current Addiction Reports* **1**, 193–205 (2014).
113. Kunzmann, U., Kappes, C. & Wrosch, W. Emotional aging: a discrete emotions perspective. *Front. Psychol* **5**, 308 (2014).
114. Scott, S. B., Sliwinski, M. J. & Blanchard-Fields, F. Age differences in emotional responses to daily stress: The role of timing, severity, and global perceived stress. *Psychol. and Aging* **28**, 4 (2013).

Data Citations

1. *Functional Connectomes Project International Neuroimaging Data-Sharing Initiative* http://doi.org/10.15387/fcp_indi.mpi_lemon (2018).
2. *OpenNeuro* <https://doi.org/10.18112/OPENNEURO.DS000221.V2> (2017).

Acknowledgements

We thank all participants who volunteered to partake in our study. Moreover, we thank Elizabeth Kelly for proofreading the manuscript and Heike Schmidt-Duderstedt for editing tables and figures.

Author Contributions

Conception, design, and preparation of the manuscript (Core LEMON group): Anahit Babayan, Miray Erbey, Andrea M.F. Reiter, Josefin Röbbing, H. Lina Schaare, Deniz Kumral, Janis D. Reinelt, Marie Uhlig, Michael Gaebler, Arno Villringer. Contribution to study design: Alfred Anwander, Pierre-Louis Bazin, Annette Horstmann, Leonie Lampe, Daniel S. Margulies, Hadas Okon-Singer, André Pampel, Christiane S. Rohr, Julia Sacher, Angelika Thöne-Otto, Sabrina Trapp, Roberto Cozatl, Karina Nätthe, Sven Preusser, Anne Schrimpf, Norman Forschack, Till Nierhaus, Krzysztof J. Gorgolewski. Quality control of MRI data: Miray Erbey, Andrea M. F. Reiter, Josefin Röbbing, H. Lina Schaare, Deniz Kumral, Janis D. Reinelt, Marie Uhlig, Michael Gaebler. MRI data preprocessing: Julia M. Huntenburg, Deniz Kumral, H. Lina Schaare, Ahmad S. Kaanan. EEG data quality control and preprocessing: Keyvan Mahjoory, Elena Cesnaite, Vadim V. Nikulin. Behavioral data analyses: Josefin Röbbing, Maria Blöchl. Medical Briefing: Katrin Arelin, Janis D. Reinelt, Anna Kosatschek. Recruiting participants and data acquisition (Core LEMON group, and medical or student assistants): Anahit Babayan, Miray Erbey, Andrea M. F. Reiter, Josefin Röbbing, H. Lina Schaare, Deniz Kumral, Janis D. Reinelt, Marie Uhlig, Michael Gaebler, Denise Altmann, Edith Bongartz, Patric Breig, Sufang Chen, Saskia Czerwonatis, Gabriele Dambrauskaite, Maria Dreyer, Jesica Enders, Melina Engelhardt, Marie Michele Fischer, Johannes Golchert, Laura Golz, C. Alexandrina Guran, Susanna Hedrich, Nicole Hentschel, Daria I. Hoffmann, Rebecca Jost, Stella Kunzendorf, Hannah Lammers, Mark E. Lauckner, Natacha Mendes, Ramona Menger, Enzo Morino, Jennifer Neubauer, Handan Noyan, Sabine Oligschläger, Patricia Panczyszyn-Trzewik, Dorothee Poehlchen, Nadine Putzke, Sabrina Roski, Marie-Catherine Schaller, Anja Schieferbein, Benito Schlaak, Hanna Maria Schmidt, Robert Schmidt, Sylvia Stasch, Maria Voss, Anett Wiedemann. All authors critically reviewed and approved the final version of the manuscript.

Additional Information

Table 6 is only available in the online version of this paper.

Supplementary information accompanies this paper at <http://www.nature.com/sdata>.

Competing interests: The authors declare no competing interests.

How to cite this article: Babayan, A. *et al.* A mind-brain-body dataset of MRI, EEG, cognition, emotion, and peripheral physiology in young and old adults. *Sci. Data.* 6:180308 <https://doi.org/10.1038/sdata.2018.308> (2019).

Publisher's note: Springer Nature remains neutral with regard to jurisdictional claims in published maps and institutional affiliations.



Open Access This article is licensed under a Creative Commons Attribution 4.0 International License, which permits use, sharing, adaptation, distribution and reproduction in any medium or format, as long as you give appropriate credit to the original author(s) and the source, provide a link to the Creative Commons license, and indicate if changes were made. The images or other third party material in this article are included in the article's Creative Commons license, unless indicated otherwise in a credit line to the material. If material is not included in the article's Creative Commons license and your intended use is not permitted by statutory regulation or exceeds the permitted use, you will need to obtain permission directly from the copyright holder. To view a copy of this license, visit <http://creativecommons.org/licenses/by/4.0/>

The Creative Commons Public Domain Dedication waiver <http://creativecommons.org/publicdomain/zero/1.0/> applies to the metadata files made available in this article.

© The Author(s) 2019

7.2.2 A Functional Connectome Phenotyping Dataset Including Cognitive State and Personality Measures. Mendes et al., Scientific Data (2019)

www.nature.com/scientificdata

SCIENTIFIC DATA

OPEN Data Descriptor: A functional connectome phenotyping dataset including cognitive state and personality measures

Received: 27 October 2017
Accepted: 5 November 2018
Published: 12 February 2019

Natacha Mendes¹, Sabine Oligschläger^{1,2,3}, Mark E. Lauckner¹, Johannes Golchert¹, Julia M. Huntenburg^{2,4}, Marcel Falkiewicz¹, Melissa Ellami¹, Sarah Krause¹, Blazej M. Baczkowski^{1,2,3}, Roberto Cozatl⁵, Anastasia Osolianu^{1,6}, Deniz Kumral^{7,8}, Jared Pool¹, Laura Goltz^{9,10}, Maria Dreyer⁷, Philipp Haueis^{2,8}, Rebecca Jost¹, Yelyzaveta Kramarenko¹, Haakon Engen^{11,12}, Katharina Ohmberger^{1,8}, Krzysztof J. Gorgolewski^{1,3}, Nicolas Farrugia^{1,4}, Anahit Babayan⁷, Andrea Reiter^{7,13}, H. Lina Schaare^{2,7}, Janis Reinelt⁷, Josefin Röbbing⁷, Marie Uhlig^{2,7}, Miray Erbey⁷, Michael Gaebler^{7,8}, Jonathan Smallwood^{2,6}, Arno Villringer^{7,8} & Daniel S. Margulies¹

The dataset enables exploration of higher-order cognitive faculties, self-generated mental experience, and personality features in relation to the intrinsic functional architecture of the brain. We provide multimodal magnetic resonance imaging (MRI) data and a broad set of state and trait phenotypic assessments: mind-wandering, personality traits, and cognitive abilities. Specifically, 194 healthy participants (between 20 and 75 years of age) filled out 31 questionnaires, performed 7 tasks, and reported 4 probes of in-scanner mind-wandering. The scanning session included four 15.5-min resting-state functional MRI runs using a multiband EPI sequence and a high-resolution structural scan using a 3D MP2RAGE sequence. This dataset constitutes one part of the MPI-Leipzig Mind-Brain-Body database.

¹Max Planck Research Group for Neuroanatomy & Connectivity, Max Planck Institute for Human Cognitive and Brain Sciences, Leipzig, Germany. ²International Max Planck Research School NeuroCom, Leipzig, Germany. ³Faculty of Biosciences, Pharmacy and Psychology, University Leipzig, Leipzig, Germany. ⁴Neuro-computation and Neuroimaging Unit, Department of Education and Psychology, Freie Universität Berlin, Berlin, Germany. ⁵Database management, Max Planck Institute for Human Cognitive and Brain Sciences, Leipzig, Germany. ⁶Department of Psychology, Technische Universität Dresden, Dresden, Germany. ⁷Department of Neurology, Max Planck Institute for Human Cognitive and Brain Sciences, Leipzig, Germany. ⁸MindBrainBody Institute, Berlin School of Mind and Brain, Humboldt-Universität zu Berlin, Berlin, Germany. ⁹Max Planck Research Group Cognitive and Affective Control of Behavioural Adaptation, Max Planck Institute for Human Cognitive and Brain Sciences, Leipzig, Germany. ¹⁰Universitäre Psychiatrische Kliniken Basel, Switzerland. ¹¹Department of Social Neuroscience, Max Planck Institute for Human Cognitive and Brain Sciences, Leipzig, Germany. ¹²MRC Cognition and Brain Sciences Unit, Cambridge University, Cambridge, UK. ¹³Department of Psychology, Stanford University, Stanford, California 94305, USA. ¹⁴LabSTICC-IMT Atlantique-campus de Brest, Brest, France. ¹⁵Lifespan Developmental Neuroscience, Department of Psychology, Technische Universität Dresden, Dresden, Germany. ¹⁶Department of Psychology, University of York, York, UK. Correspondence and requests for materials should be addressed to N.M. (email: mendes@cbs.mpg.de) or to D.S.M. (email: margulies@cbs.mpg.de)

SCIENTIFIC DATA

OPEN Data Descriptor: A functional connectome phenotyping dataset including cognitive state and personality measures

Received: 27 October 2017

Accepted: 5 November 2018

Published: 12 February 2019

Natacha Mendes¹, Sabine Oligschläger^{1,2,3}, Mark E. Lauckner¹, Johannes Golchert¹, Julia M. Huntenburg^{1,4}, Marcel Falkiewicz¹, Melissa Ellamil¹, Sarah Krause¹, Blazej M. Baczkowski^{1,2,3}, Roberto Cozatl⁵, Anastasia Osoianu^{1,6}, Deniz Kumral^{7,8}, Jared Pool¹, Laura Golz^{9,10}, Maria Dreyer⁷, Philipp Haueis^{1,8}, Rebecca Jost¹, Yelyzaveta Kramarenko¹, Haakon Engen^{11,12}, Katharina Ohrnberger^{1,8}, Krzysztof J. Gorgolewski¹³, Nicolas Farrugia¹⁴, Anahit Babayan⁷, Andrea Reiter^{7,15}, H. Lina Schaare^{2,7}, Janis Reinelt⁷, Josefin Röbbing⁷, Marie Uhlig^{2,7}, Miray Erbey⁷, Michael Gaebler^{7,8}, Jonathan Smallwood¹⁶, Arno Villringer^{7,8} & Daniel S. Margulies¹

The dataset enables exploration of higher-order cognitive faculties, self-generated mental experience, and personality features in relation to the intrinsic functional architecture of the brain. We provide multimodal magnetic resonance imaging (MRI) data and a broad set of state and trait phenotypic assessments: mind-wandering, personality traits, and cognitive abilities. Specifically, 194 healthy participants (between 20 and 75 years of age) filled out 31 questionnaires, performed 7 tasks, and reported 4 probes of in-scanner mind-wandering. The scanning session included four 15.5-min resting-state functional MRI runs using a multiband EPI sequence and a high-resolution structural scan using a 3D MP2RAGE sequence. This dataset constitutes one part of the MPI-Leipzig Mind-Brain-Body database.

¹Max Planck Research Group for Neuroanatomy & Connectivity, Max Planck Institute for Human Cognitive and Brain Sciences, Leipzig, Germany. ²International Max Planck Research School NeuroCom, Leipzig, Germany. ³Faculty of Biosciences, Pharmacy and Psychology, University Leipzig, Leipzig, Germany. ⁴Neurocomputation and Neuroimaging Unit, Department of Education and Psychology, Freie Universität Berlin, Berlin, Germany. ⁵Database management, Max Planck Institute for Human Cognitive and Brain Sciences, Leipzig, Germany. ⁶Department of Psychology, Technische Universität Dresden, Dresden, Germany. ⁷Department of Neurology, Max Planck Institute for Human Cognitive and Brain Sciences, Leipzig, Germany. ⁸MindBrainBody Institute, Berlin School of Mind and Brain, Humboldt-Universität zu Berlin, Berlin, Germany. ⁹Max Planck Research Group Cognitive and Affective Control of Behavioural Adaptation, Max Planck Institute for Human Cognitive and Brain Sciences, Leipzig, Germany. ¹⁰Universitäre Psychiatrische Kliniken Basel, Basel, Switzerland. ¹¹Department of Social Neuroscience, Max Planck Institute for Human Cognitive and Brain Sciences, Leipzig, Germany. ¹²MRC Cognition and Brain Sciences Unit, Cambridge University, Cambridge, UK. ¹³Department of Psychology, Stanford University, Stanford, California 94305, USA. ¹⁴LabSTICC-IMT Atlantique-campus de Brest, Brest, France. ¹⁵Lifespan Developmental Neuroscience, Department of Psychology, Technische Universität Dresden, Dresden, Germany. ¹⁶Department of Psychology, University of York, York, UK. Correspondence and requests for materials should be addressed to N.M. (email: mendes@cbs.mpg.de) or to D.S.M. (email: margulies@cbs.mpg.de)

Design Type(s)	behavioral data analysis objective • data collection and processing objective
Measurement Type(s)	behavior • brain activity measurement
Technology Type(s)	questionnaire • MRI Scanner
Factor Type(s)	biological sex • age
Sample Characteristic(s)	Homo sapiens • brain

Background & Summary

Understanding the unique features of brain organization giving rise to distinct patterns of behavior, cognition, and mental experience remains one of the key research questions in the emerging field of human functional connectomics¹. Functional connectivity has become a prominent method for investigating phenotypic differences across individuals^{2,3}. However, there is ever greater need for validation of findings across independent datasets. The dataset presented here joins several others in contributing to this research agenda^{4–6} (Data Citation 1) and provides an additional resource for cross-site validation studies.

We acquired a wide range of self-reported personality measures as well as features of self-generated mental experience. In addition, a core magnetic resonance imaging (MRI) dataset—including one-hour of resting-state functional MRI (rs-fMRI) data—was acquired on 194 healthy participants. Questionnaires and behavioral measures were acquired over several follow-up sessions.

This dataset constitutes one part of the MPI-Leipzig Mind-Brain-Body (MPILMBB) database, which consists of data from a partially overlapping cohort of participants⁷. The contribution described here enables exploration of individual variance across cognitive and emotional phenotypes in relation to the brain, which is complemented by data regarding physiology, clinical assessment, and anthropometric measures described in our related publication⁷. All MRI data across the MPILMBB were acquired on the same Siemens Verio 3 Tesla MRI scanner.

Methods

Participants

In total, datasets from 194 native German-speaking participants are included (94 female, mean age = 34 years, median age = 27, SD = 16 years; Fig. 1; see Supplementary Table 1 and Supplementary File 1). All participants were scanned on a 3 Tesla magnetic resonance imaging (MRI) scanner (Siemens Magnetom Verio) for the acquisition of one structural and four rs-fMRI scans. In addition, extensive questionnaire and task performance data were acquired from each participant. A subset of participants (N = 109) were also included in a complementary data acquisition.

Recruitment and inclusion criteria. Prospective participants were initially recruited by the Leipzig Study for Mind-Body-Emotion Interactions project. Additional participants were recruited through online and poster advertisements. All participants were prescreened via telephone to determine their eligibility for the current study (Box 1). Participants fulfilling the eligibility criteria (including medical screening for MRI-scanning and neurological history) were invited to Max Planck Institute for Human Cognitive and Brain Sciences (MPI-CBS) where they were screened for past and present psychiatric disorders using the Structured Clinical Interview for DSM-IV (SCID-I⁸). After meeting eligibility criteria, participants received detailed information regarding the study.

All participants fulfilled the MRI safety requirements of the MPI-CBS (Supplementary Table 2), provided written informed consent (including agreement to their data being shared anonymously) prior to their participation in the study. Participants received monetary compensation for their participation. The study protocol was approved by the ethics committee at the medical faculty of the University of Leipzig (097/15-ff).

Data acquisition and protocol overview

Participants were required to complete: 1) four functional MRI scans within one scanning session and, if not previously acquired, one structural scan; 2) a battery of personality and mind-wandering questionnaires spread over five appointments, and 3) a set of cognitive control and sustained attention, synesthesia, and creativity tasks spread over two appointments.

The data acquisition took place over five appointments over a two-year period (see Table 1):

- Day 1: We acquired data on a set of questionnaires that were completed at MPI-CBS (Table 1).
- Day 2: We sent personalized links to participants, who could complete the set of online questionnaires at their convenience (Table 1).

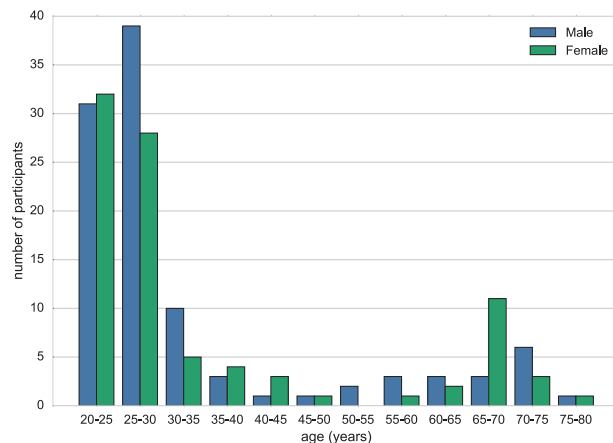


Figure 1. Age distribution. Age distribution (5-year bins) of the participants split by gender.

Box 1 | Exclusion criteria. Exclusion criteria to prospective participants.

Exclusion Criteria

- History of psychiatric diseases that required inpatient treatment for longer than 2 weeks within the last 10 years (e.g., psychosis, attempted suicide, post-traumatic stress disorder);
- History of neurological disorders (incl. multiple sclerosis, stroke, epilepsy, brain tumour, meningoencephalitis, severe concussion);
- History of malignant diseases;
- Intake of one of the following medications:
 - Any centrally active drugs (including *Hypericum perforatum*)
 - Beta- and alpha-blocker
 - Cortisol
 - Any chemotherapeutic or psychopharmacological medication;
- Positive drug anamnesis (extensive alcohol, MDMA, amphetamines, cocaine, opiates, benzodiazepine, cannabis);
- Extensive testing experience at the MPI-CBS or other academic institution;
- Past or present student of Psychology;
- MRI exclusion criteria (see Supplementary Table 2)
 - Any metallic implants, braces, non-removable piercings
 - Tattoos
 - Pregnancy
 - Claustrophobia
 - Tinnitus
 - Surgical operation in the last 3 months

- Day 3: Participants were scanned at the Day Clinic for Cognitive Neurology, University of Leipzig. Before entering the scanner, participants completed a pen-and-paper practice trial of the short version of the New York Cognition Questionnaire⁹. While in the scanner, and immediately after each of the four resting state runs, participants received the computerized version of the same questionnaire. Immediately after the scanning session participants received additional questionnaires and a set of tasks (Table 1).
- Day 4: The Abbreviated Math Anxiety Scale¹⁰ and the NEO Personality Inventory-Revised^{11–13} were completed online at the participant's convenience (Table 1).
- Day 5: We acquired data on a set of questionnaires and tasks that were administered at MPI-CBS. Tasks were conducted using pen-and-paper, computer-administered, as well as Limesurvey (<http://www.limesurvey.org>; version 2.00+) interfaces (Table 1).

Within each set of questionnaires and tasks, the order of presentation of questionnaires and tasks was randomized across participants. If participants failed to complete a given questionnaire it was excluded from data analysis. Due to dropout, not all participants completed the full set of questionnaires and tasks (Table 2).

Day 1 (MPI CBS)	Day 2 (Home)	Day 3 (Uni Clinic)	Day 4 (Home)	Day 5 (MPI CBS)
ASR	ACS	Scanning session	AMAS	BIS/BAS
God-MSI	BDI		NEO PI-R	CAQ
IAT	BP	FBI		MCQ-30
IMIS	ESS	S-D = MW		BCQ
MGIQ	HADS	Short-NYC-Q_inscan1-4		FFMQ
SCS	MMI	Short-NYC-Q_postETS		RAT
SD3	MPU	NYC-Q_postscan		SYN
SE	PSSI	ETS		AUT
TPS		CCPT		TCIA
VISQ		Oddball		
UPPS-P				
SDS				

Table 1. Phases of the data acquisition. Overview of the different phases of the data acquisition. **Note.** **MPI-CBS** = Max Planck Institute for Human Cognitive and Brain Sciences, Leipzig; **Uni Clinic** = Day Clinic for Cognitive Neurology, University of Leipzig. **ACS** = Attention Control Scale, **AMAS** = Abbreviated Math Anxiety Scale, **ASR** = Adult Self Report, **AUT** = Alternative Uses Task, **BCQ** = Body Consciousness Questionnaire, **BDI** = Beck Depression Inventar-II, **BIS/BAS** = Behavioral Inhibition and Approach System, **BP** = Boredom Proneness Scale, **CAQ** = Creative Achievement Questionnaire, **CCPT** = Conjunctive Continuous Performance Task, **ESS** = Epworth Sleepiness Scale, **ETS** = Emotional task switching; **FBI** = Facebook Intensity Scale, **FFMQ** = Five Facets of Mindfulness Questionnaire, **Gold-MSI** = Goldsmiths Musical Sophistication Index, **HADS** = Hospital Anxiety and Depression Scale, **IAT** = Internet Addiction Test, **IMIS** = Involuntary Musical Imagery Scale, **MCQ-30** = Metacognition Questionnaire, **MGIQ** = Multi-Gender Identity Questionnaire, **MMI** = Multimedia Multitasking Index, **MPU** = Mobile Phone Usage, **NEO PI-R** = NEO Personality Inventory-Revised, **NYC-Q_postscan** = New York Cognition Questionnaire after scan, **Oddball** = Adaptive Visual and Auditory Oddball Target Detection Task, **PSSI** = Personality Style and Disorder Inventory, **RAT** = Remote Associates Test, **SCS** = Brief Self-Control Scale, **SD3** = Short Dark Triad, **S-D-MW** = Spontaneous and Deliberate Mind-Wandering, **SDS** = Social Desirability Scale-17; **SE** = Self-Esteem Scale, **Short-NYC-Q_inscan1-4** = Short Version of the New York Cognition Questionnaire in scanner, **Short-NYC-Q_postETS** = Short Version of the New York Cognition Questionnaire after tasks, **SYN** = Synesthesia Color Picker Test, **TCIA** = Test of Creative Imagery Abilities, **TPS** = Tuckman Procrastination Scale, **UPPS-P** = UPPS-P Impulsive Behavior Scale, **VISQ** = Varieties of Inner Speech Questionnaire.

Behavioral measures

Below we provide a short description of the acquired behavioral measures assessing: Personality and habitual behaviors, mind-wandering and mindfulness, synesthesia, cognitive control and sustained attention, and creativity.

Personality and Habitual Behaviors

Abbreviated Math Anxiety Scale (AMAS). The AMAS is a self-report inventory measuring the subjectively experienced level of anxiety in mathematical contexts¹⁰. It consists of nine items, related to the question “How anxious do you feel when ...”, that can be scored on a five-point Likert scale (1 = “not at all” to 5 = “a lot”). We used a German translated version of the original English questionnaire.

Adult Self Report (ASR). The ASR assesses mental problems in adults between 18 and 59 years-old¹⁴. It has four major scales related to the following topics: adaptive functioning, psychological syndromes, DSM-oriented problems, and substance use. Adaptive functioning comprises 36 items in the form of either a three or four-point Likert scale describing the quantity and quality of relationships, education level, and job satisfaction. Comments to open questions are not made openly available. Scales of psychological syndromes, DSM-oriented problems, and substance use comprise 126 items that can be scored on a three-point Likert scale (0 = “does not apply” to 2 = “exactly or does happen often”). Two items were erroneously excluded (i.e., item 56.h “Heart pounding or racing”; item 56.i “Numbness or tingling in body parts”). These affect somatic complaints and internalizing subscales of the psychological syndromes scale. We used the German ASR version¹⁴.

Beck Depression Inventar-II (BDI). The BDI-II measures the severity of various depressive symptoms in adolescents and adults over the two weeks prior to completion of the inventar^{15,16}. It consists of 21 items that require multiple-choice answers that best describe statements about subjectively experienced

Abbreviation	Behavioral Measure	N
Personality and Habitual Behaviors		
AMAS	Abbreviated Math Anxiety Scale ⁹	145
ASR	Adult Self Report adapted from ¹³	213
BDI	Beck Depression Inventar-II ¹⁴⁻¹⁶	210
BIS/BAS	Behavioral Inhibition and Approach System ¹⁷⁻²⁰	288
BCQ	Body Consciousness Questionnaire ²¹	79
BP	Boredom Proneness Scale ²²	209
SCS	Brief Self-Control Scale ^{23,24}	214
ESS	Epworth Sleepiness Scale ^{25,26}	210
FBI	Facebook Intensity Scale ²⁷	180
Gold-MSI	Goldsmiths Musical Sophistication Index ^{28,29}	214
HADS	Hospital Anxiety and Depression Scale ^{30,31}	210
IAT	Internet Addiction Test ³²	214
IMIS	Involuntary Musical Imagery Scale ³³	214
MPU	Mobile Phone Usage	210
MGIQ	Multi-Gender Identity Questionnaire ³⁴	159
MMI	Multimedia Multitasking Index ³⁵	209
NEO PI-R	NEO Personality Inventory-Revised ¹⁰⁻¹²	169
PSSI	Personality Style and Disorder Inventory ³⁶	209
SE	Self-Esteem Scale ³⁸	214
SD3	Short Dark Triad ³⁹	213
SDS	Social Desirability Scale-17 ^{40,96}	214
TPS	Tuckman Procrastination Scale ⁴¹	214
UPPS-P	UPPS-P Impulsive Behavior Scale ^{42,43} , cf. ⁴⁴	214
Mind-Wandering and Mindfulness		
FFMQ	Five Facets of Mindfulness Questionnaire ⁴⁵	79
MCQ-30	Metacognition Questionnaire ^{46,47}	79
NYC-Q_posttasks	New York Cognition Questionnaire ⁴⁸	202
NYC-Q_postscan		188
NYC-Q		
Short-NYC-Q_inscan1	Short Version of the New York Cognition Questionnaire ⁸	175
Short-NYC-Q_inscan2		174
Short-NYC-Q_inscan3		174
Short-NYC-Q_inscan4		170
Short-NYC-Q_postETS		181
Short-NYC-Q_prescan		159
S-D-MW	Spontaneous and Deliberate Mind-Wandering ⁵¹ ; cf. ⁴⁴	214
VISQ	Varieties of Inner Speech Questionnaire ⁵²	214
Synesthesia		
SYN	Synesthesia Color Picker Test (synesthete.org) ⁵³	73
Cognitive Control and Sustained Attention		
Oddball	Adaptive Visual and Auditory Oddball Target Detection Task e.g., ⁵⁴ , cf. ⁵⁵	137
ACS	Attention Control Scale ⁵⁶	210
CCPT	Conjunctive Continuous Performance Task ⁵⁰	169
ETS	Emotional Task Switching ⁴⁹ ; see ⁵⁷	189
Creativity		
AUT	Alternative Uses Task ^{58,59}	77
CAQ	Creative Achievement Questionnaire ⁶⁰	79
RAT	Remote Associates Test cf. ^{61,62}	77
TCIA	Test of Creative Imagery Abilities ⁶³	77

Table 2. Behavioral measures. Overview of data available for each questionnaire and task.

states. The items can be scored on a four-point Likert scale (e.g., 0 = “I do not feel sad.” to 3 = “I am so sad or unhappy that I can’t stand it”). We used the German BDI version¹⁷.

Behavioral Inhibition and Approach System (BIS/BAS). The BIS/BAS¹⁸ measures individual differences in response to two motivational systems: behavioral inhibition and behavioral approach (systems postulated by Gray^{19,20}). It comprises a total of 24 items that can be scored using a four-point Likert-type scale (1 = “not true for me at all” to 4 = “very true for me”). We used the German version of the questionnaire²¹.

Body Consciousness Questionnaire (BCQ). The BCQ assesses three components of body consciousness: private body (e.g., heartbeat perception), public body (perception of outward appearance), and body competence (aspects of the body, e.g., strength)²². The questionnaire consists of 15 items that can be scored on a five-point Likert scale (0 = “extremely uncharacteristic” to 4 = “extremely characteristic”). We used a German translated version of the original English questionnaire.

Boredom Proneness Scale (BP). The BP measures the tendency to experience boredom, in particular the self-reported lack of internal and external stimulation²³. It consists of 28 items that can be scored on a seven-point Likert scale (1 = “total disagreement” to 7 = “total agreement”). We used a German translated version of the original English scale.

Brief Self-Control Scale (SCS). The SCS is a self-report measurement assessing the capacity for self-control²⁴. Self-control was operationalized as the capability to modify or override one’s own response tendencies²⁴. We used the German adaption of the brief SCS²⁵. It consists of 13 items that can be scored on a five-point Likert scale (1 = “do not agree at all” to 5 = “completely agree”).

Epworth Sleepiness Scale (ESS). The ESS measures tendencies of sleepiness in everyday life²⁶. The scale consists of eight items addressing the subjective propensity to fall asleep in different situations. The items can be scored on a four-point Likert scale (0 = “would never doze” to 3 = “high chance of dozing”). We used the German ESS version²⁷.

Facebook Intensity Scale (FBI). The FBI measures the intensity of Facebook usage that incorporates emotional connectedness to the site, its integration into daily activities, membership duration, and the number of friends²⁸. It consists of eight items that can be scored on a five-point Likert scale (1 = “strongly disagree” to 5 = “strongly agree”). Small alterations in the formulation and in the order of presentation of the items were applied—see the *.txt file of this questionnaire. We used a German translated and adapted version of the original English scale.

Goldsmiths Musical Sophistication Index (Gold-MSI). The Gold-MSI measures the level of experience with and understanding of music in community samples²⁹. A subset of 16 items was measured, including the active engagement subscale and the musical training subscales (the item order is explained in the *.txt file of this index). The subscales perceptual abilities, singing abilities, and emotions were not included in the measurement. The items can be scored on a seven-point Likert scale (1 = “completely disagree” to 7 = “completely agree”). We used the German version of the index³⁰.

Hospital Anxiety and Depression Scale (HADS). The HADS measures the severity of depression- and anxiety-related symptoms³¹ for the week prior to completion and can be used to assess subclinical tendencies of depression and anxiety. It consists of 14 items in total that can be scored on a four-point Likert scale (e.g., 1 = “most of the time” to 4 = “never”). We used the German HADS version³².

Internet Addiction Test (IAT). The IAT assesses self-reported excessive use of the Internet³³. The test is comprised of 20 items that can be scored on a six-point Likert scale (0 = “does not apply” to 5 = “always”). We used item three (i.e., “how often do you prefer the excitement of the Internet to intimacy with your partner?”) with a different scale compared to the original one. Therefore, this item was not included in the scoring of the scale. We used a German translated and adapted version of the original English test.

Involuntary Musical Imagery Scale (IMIS). IMIS is a self-report inventory measuring phenomenological properties of the experiential tendency of having involuntary musical imagery, also known as “earworms”³⁴. It measures four facets of involuntary musical imagery: the subjective evaluation of this phenomenon (negative valence), the embodied responses (movement), the personal contemplations (personal reflections), and the constructive properties (help). It consists of 18 items that can be scored on different scales: 14 items can be scored on a five-point Likert scale (1 = “never” to 5 = “always”); two items with different five-point Likert scales (e.g., 1 = “less than 5 seconds” to 5 = “more than a minute”); one item with a six-point Likert scale (1 = “never” to 6 = “almost continuously”). The English questionnaire consists of two parts (A and B) which were combined in the German version (see the respective *.txt file for more details). We used a German translated and adapted version of the original English scale.

Mobile Phone Usage (MPU). This in-house developed collection of items measures various patterns of mobile phone usage, such as e-mail usage as well as the use of social network sites via smartphone. It consists of 19 items with various answer formats. A translated version of the original English questionnaire (see below) was used.

1. Do you own a mobile phone? (yes, no)
2. How often do you have your mobile phone on you?
 - a all the time
 - b most of the day
 - c a few hours a day
3. How many text messages do you send a week (on average)?
4. How many phone calls (using your mobile phone) do you make/take per week (on average)?
5. Do you own a smartphone (iPhone, Android etc. - a multipurpose phone with Internet connection)? (yes, no)
6. Do you have a flat Internet rate? (yes, no)
7. How long have you been using a smartphone [months, years...]?
8. Do you use your smartphone to browse the web? (yes, no)
 - a. How often do you look up facts on your phone in a social situation?
 - i never
 - ii sometimes
 - iii often
9. Do you use your smartphone to check your email? (yes, no)
 - a Do you get a notification each time you get a new email or do you have to check it manually?
 - b If manually, how often?
 - i never
 - ii sometimes
 - iii often
10. Do you use your phone for social networking (Facebook, Twitter, Google+ etc.)?
 - i never
 - ii sometimes
 - iii often

Do you post messages (including tweets) to social networks using your phone (as opposed to just reading)?
11. Do you use your phone for instant messaging (Viber, WhatsApp, Google chat, Facebook Messaging etc.)?
 - i never
 - ii sometimes
 - iii often
12. Do you use your phone to check the news?
 - i never
 - ii sometimes
 - iii often
13. Do you use your phone to take and share pictures?
 - i never
 - ii sometimes
 - iii often
14. In a social situation such as a dinner with friends how often do you have an urge to check your phone (to check the news, Facebook etc.)?
 - i never
 - ii sometimes
 - iii often
 1. How often do you resist this urge due to social pressure?
 - a never
 - b sometimes
 - c often
15. Do you read printed newspapers/magazines?
 - i never
 - ii sometimes
 - iii often
16. How many books do you read a year?

Multi-Gender Identity Questionnaire (MGIQ). The MGIQ used in this study was adapted from the Multi-Gender Identity Questionnaire developed by Joel and colleagues³⁵. The questionnaire assesses:

gender identity, sexual orientation, gender of the preferred sexual partner, preferred form of relationship, and attitudes towards the social construction of gender. The original questionnaire consists of 38 items that can be scored on either a five- or a six-point Likert scale (1 = “always” to 5 = “never”; 1 = “always” to 6 = “does not apply”). Two additional sections—relevance of the MGIQ questions and demographic details—were added to the questionnaire. Please see the respective *.txt file for details on the modifications and additional sections. We used a German translated and adapted version of the original English questionnaire.

Multimedia Multitasking Index (MMI). The MMI measures the extent of simultaneous use of 12 different media types³⁶: computer-based streaming (video, music), non-music audio, computer games, voice calls, instant messaging, text messaging, email, web surfing, and other applications such as Word processing. It consists of a total of 219 items, across the 12 media types, that can be scored on different Likert scales (e.g., 1 = “never” to 4 = “most of the time”; 1 = “more time” to 3 = “same amount of time”). We used a translated version of the original English index.

NEO Personality Inventory-Revised (NEO PI-R). The NEO PI-R assesses the five personality traits: extraversion, agreeableness, conscientiousness, neuroticism, and openness to experience^{11,12}. Moreover, the questionnaire also assesses six underlying facets for each of the five main factors. It consists of 241 items that can be scored on a five-point Likert scale. We used the German version of the inventory¹². Due to a technical error, item 71 (i.e., “I am seldom sad or depressed”) was measured twice; one time instead of item 46 (i.e., “I seldom feel self-conscious when I’m around people”). Thus, item 46 was not taken into account for the summary score of subscale N3. Additionally, item 83 was missing and was therefore not taken into account for creating subscale O5.

Personality Style and Disorder Inventory (PSSI). The PSSI is a self-report measurement assessing 14 personality styles³⁷. These personality styles are conceptualized as non-pathologic, sub-clinical equivalents of personality disorders as described in diagnostic manuals such as the Diagnostic and Statistical Manual of Mental Disorders³⁸. The inventory consists of 140 items that can be scored on a four-point Likert scale (1 = “do not agree” to 4 = “highly agree”).

Self-Esteem Scale (SE). The SE is a self-report scale measuring global self-worth by assessing positive and negative feelings about the self³⁹. It comprises eight items that can be scored on a six-point Likert scale (0 = “does not apply” to 5 = “applies to me”). We used a German translated version of the original English scale.

Short Dark Triad (SD3). The SD3 assesses the following personality traits: machiavellianism, narcissism, and psychopathy in their subclinical manifestations⁴⁰. It consists of 27 items that can be scored on a five-point Likert scale (1 = “strongly disagree” to 5 = “strongly agree”). The questionnaire was retrieved from an online platform (<http://www.midss.org/sites/default/files/d3.pdf>) previous to its publication⁴⁰. Thus, item two of the used questionnaire (i.e., “Generally speaking, people won’t work hard unless they have to”) is different from the published version (i.e., “I like to use clever manipulation to get my way”). We used a German translated version of the original English questionnaire.

Social Desirability Scale-17 (SDS). The SDS is a self-report questionnaire that assesses one’s tendency to seek social approval⁴¹, and it can be used to control for biased answer’s tendencies due to social desirability. We used a German version of the scale⁴¹ consisting of 17 items that can be scored on a five-point Likert scale (1 = “do not agree at all” to 5 = “completely agree”).

Tuckman Procrastination Scale (TPS). The TPS assesses self-reports of procrastination in everyday life, which are related to the tendency to inappropriately delay pending tasks⁴². It consists of 16 items that can be scored on a five-point Likert scale (1 = “does not apply to me at all” to 5 = “applies to me to a great extent”). We used the German version of the scale (TPS-D; https://www.dgps.de/fachgruppen/diff_psy/pdf/instrumente/Prokrastination.pdf).

UPPS-P Impulsive Behavior Scale (UPPS-P). The UPPS-P is a self-report measure of different trait aspects of impulsive behavior^{43,44}. This revised scale⁴⁴ quantifies five distinguishable facets of impulsivity: positive urgency, negative urgency, lack of premeditation, lack of perseverance, and sensation seeking. It consists of 59 items that can be scored on a four-point Likert scale (1 = “strongly agree” to 4 = “strongly disagree”). We used a German translated version of the original English questionnaire cf.⁴⁵.

Mind-Wandering and Mindfulness

Five Facets of Mindfulness Questionnaire (FFMQ). The FFMQ assesses five aspects of mindfulness⁴⁶: observation of internal and external processes, description of internal processes, conscious actions, non-judgement about mental processes, and non-reaction to mental processes. It consists of 39 items that can be scored on a five-point Likert scale (1 = “never or very rarely true” to 5 = “very often or always true”). We used a German translated version of the original English questionnaire.

Metacognition Questionnaire (MCQ-30). The MCQ-30 assesses self-reported attitudes and abilities in relation to: worrying, trust in cognitive abilities, control over thoughts, and cognitive self-consciousness⁴⁷. It consists of 30 items that can be scored on a four-point Likert scale (1 = “do not agree” to 4 = “agree very much”). The order of presentation of the items was done according to Sadeghi and colleagues⁴⁸. We used a German translated version of the original English questionnaire.

New York Cognition Questionnaire (NYC-Q). The NYC-Q is a self-report questionnaire that retrospectively measures thoughts and feelings experienced by a person while doing a specific task or activity just prior to completion⁴⁹. The NYC-Q consists of two parts. The first part measures the content of thoughts (e.g. past related) and feelings with 23 items. The second part measures the form of thoughts (e.g. in the form of images) with 8 items. The items in both parts of the questionnaire can be scored on a nine-point Likert scale (First part: 1 = “completely did not describe my thoughts” to 9 = “completely did describe my thoughts”; Second part: 1 = “completely does not characterize my experience” to 9 = “completely characterize my experience”). We assessed the NYC-Q at two time points: 1) immediately after the scanning session and 2) after both the emotional task switching (ETS)⁵⁰ and conjunctive continuous performance task (CCPT)⁵¹ were completed. For the NYC-Q presented after both ETS and CCPT, the first part of the questionnaire was consistently assessed; while the second part is only available for a subset of participants.

Short Version of the New York Cognition Questionnaire (Short-NYC-Q). The short-NYC-Q⁹ is similar to the NYC-Q⁵⁰, but it only uses 12 items to measure form and content of mind-wandering. The questions can be rated using a digital format of a scale bar, with an answer resolution of 5% increments (0% = “describes my thoughts not at all” - 100% = “describes my thoughts completely”).

Spontaneous and Deliberate Mind-Wandering (S-D-MW). Both spontaneous mind-wandering (S-MW) and deliberate mind-wandering (D-MW) quantify trait-level tendencies to experience spontaneous and deliberate forms of mind-wandering⁵². Each of the scales comprises four items. The D-MW scale captures experiences of intentional mind-wandering, whereas the S-MW scale assesses unintentional occasions of mind-wandering. Although in the original questionnaire the items can be scored on a seven-point Likert scale, we have adopted a five-point Likert scale instead (1 = “almost never” to 5 = “very often”). We used a German translated version of the original English questionnaire cf.⁴⁵.

Varieties of Inner Speech Questionnaire (VISQ). The VISQ measures phenomenological properties of inner speech⁵³. The questionnaire includes 18 items assessing four dimensions of inner speech: dialogic inner speech, the extent to which inner speech involves the voice of others, condensed/expanded inner speech, and evaluative/motivational inner speech⁵³. The items can be scored using a six-point Likert scale (1 = “Certainly does not apply to me” to 6 = “Certainly applies to me”). We used a German translated version of the original English questionnaire.

Synesthesia

Synesthesia Color Picker Test (SYN). The SYN measures the consistency of synesthetic color experiences in response to graphemes (letters and numbers)⁵⁴. Participants assign colors to repeatedly presented graphemes. Digits 0–9 and all letters of the alphabet were randomly repeated three times. Perfect consistency would be reflected in a score of 0. A consistency score of 1 or less indicates the presence of grapheme-color synesthesia.

Cognitive Control and Sustained Attention

Adaptive Visual and Auditory Oddball Target Detection Task (Oddball). This task was designed to estimate the modality specific (visual/auditory) perceptual threshold in relation to content and form of ongoing thoughts that were experienced during the task. Based on a common “oddball” paradigm e.g.⁵⁵, participants had to respond via button press to target stimuli—amplitude modulated gabor patches [visual condition], and sinus tone waves [auditory condition]—that occur infrequently and irregularly within a series of standard stimuli. The task was designed to adapt to the level of the participant’s performance, that is, the better the performance, the lower the deviation between the infrequent and standard stimuli (1-up 2-down staircase procedure). From time to time, participants were interrupted and asked to rate what they had thought about prior to the interruption cf.⁵⁶ by using a visual analogue scale. Visual and auditory conditions appeared to be in two alternating blocks, with 30 deviants per block, 3–7 standard stimuli before each deviant, and 5 thought probes per block. The task had a duration of 60 min.

Attention Control Scale (ACS). The ACS is a self-report inventory constructed to assess individual differences in attentional control⁵⁷. It consists of 20 items that can be scored using a four-point Likert scale (1 = “almost never” to 4 = “always”). We used a German translated version of the original English scale.

Conjunctive Continuous Performance Task (CCPT). The visual variant of the CCPT⁵¹ was used to assess the sustained and selective attention of participants. Participants were instructed to accurately and quickly respond to a target stimuli (red square) that infrequently appeared within a series of other geometrically shaped and colored stimuli (e.g., yellow triangle, blue square, etc.). A 4 × 4 × 4 design with four geometrical forms, four colors, and four interstimulus intervals was used. Each combination was presented five times, resulting in a total of 320 trials. For demonstration purposes, participants fulfilled a practice round consisting of 15 trials. Immediately after finishing the task, participants completed The New York Cognition Questionnaire (NYC-Q)⁴⁹ to assess several dimensions of thoughts and feelings experienced during the task (see above). The entire procedure lasted 15 min.

Emotional Task Switching Task (ETS). The ETS measures cognitive control, more specifically task switching ability and cognitive inhibition^{50,58}. Participants were presented with a series of words and were asked to judge their emotional valence (positive/negative), color (blue/green), or word class (adjective/noun). Participants indicated their response by pressing a button on the left or right side of a word, which corresponded to a congruent forced-choice. There were two blocks with a short pause in between. In total there were 300 trials across the three conditions (i.e., 100 words per category). The order of presentation of the conditions was randomized. The experiment has both N-1 and N-2 trial effects, stemming from either simple task switching (N-1) or task-set inhibition (N-2). The task had a duration of 25 min.

Creativity

Alternative Uses Task (AUT). The AUT is a measure of divergent thinking⁵⁹. Participants were asked to generate novel and creative uses for three items: an umbrella, a car tire, and a water hose. For each of these items, two minutes were given to generate and write down the ideas. Afterwards, participants had to select and mark their top two answers⁶⁰. Three trained judges rated the answers with respect to (i) creative quality and (ii) amount of detail given (elaboration). The interrater reliability was moderate to high (intra-class correlation of 0.74–0.82) for the rated scores. Further, fluency was assessed, which refers to the total number of given answers per subject. Additionally, the statistical rareness of the answers (originality) was calculated by assessing the relative frequency of each answer. To achieve this, semantically similar answers (e.g. “flower pot” and “plant pot” a use for the car tire) were counted as the same answer.

Creative Achievement Questionnaire (CAQ). The CAQ assesses the amount of creative achievements with 96 items in ten different domains⁶¹: visual arts, dance, music, drama, culinary arts, architecture, creative writing, humor, science, and invention. Each domain consists of eight ranked questions (e.g., 0 = “I do not have training or recognized talent in this area” to 7 = “My work has been reviewed in national publications”). We used a German translated version of the original English questionnaire.

Remote Associates Test (RAT). The RAT has mostly been used to operationalize concepts such as creativity or problem solving cf.⁶². The German version of the test consists of 20 word puzzles⁶³, presented in counterbalanced sets of ten. Each word puzzle comprises three stimulus words, which seem to be unrelated. Participants are instructed to find out a unifying fourth word that relates to each of the three words. (e.g., work, alarm, ladder - fire). A total of 40 seconds was given for each puzzle (30 seconds thinking time and ten seconds answering time).

Test of Creative Imagery Abilities (TCIA). The TCIA measures creative imagery abilities with the help of a drawing task⁶⁴. Participants are instructed to complete seven ambiguous figures in a creative way. First, participants are asked to generate and write down ideas for completion of the figures. Second, participants have to select one of their ideas and try to illustrate the figure in a way that represents the chosen idea. Finally, a title for the figure needs to be generated. No time limit is given for completion of the task. The drawings were rated by five trained judges in three different categories: (i) vividness, which describes the level of detail and abstraction of the drawing; (ii) originality, which refers to the creative quality in terms of novel and surprising drawings, and (iii) transformativeness, the level of modification and improvement of the initially generated idea. Interrater reliability for those scores was between acceptable and good (intra-class correlation 0.73–0.76).

Drug screening prior to MRI data acquisition

Each of the participants was instructed not to use illicit drugs within two weeks of the scanning appointment. Participants were also requested to abstain from alcohol and caffeine consumption, as well as nicotine on the night prior to the scanning day and on the day of scanning. Before the beginning of the MRI session, participants' urine was biochemically screened with a MULTI 8/2 strip test (Diagnostik Nord, Schwerin, Germany) for the presence of buprenorphine (cutoff 10 ng/mL), amphetamine (cutoff 1000 ng/mL), benzodiazepine (300 ng/mL), cocaine (cutoff 300 ng/mL), methamphetamine (1000 ng/mL), morphine/heroin (cutoff 300 ng/mL), methadone (cutoff 300 ng/mL), THC (cutoff 50 ng/mL). Cutoff levels are those recommended by the American National Institute on Drug Abuse (NIDA⁶⁵). Participants

provided informed consent on the use of the urine strip test and agreed to its anonymous data sharing, prior to their participation in the study.

MRI data acquisition

All magnetic resonance imaging (MRI) data was acquired using a whole-body 3 Tesla scanner (Magnetom Verio, Siemens Healthcare, Erlangen, Germany) equipped with a 32-channel Siemens head coil at the Day Clinic for Cognitive Neurology, University of Leipzig. For all the MRI data provided here, the scanner remained stable and did not undergo any major maintenance or updates that would systematically affect the quality of the acquired data. For each participant the following scans were obtained: 1) a high-resolution structural scan, 2) four rs-fMRI scans, 3) two gradient echo fieldmaps and, 4) two pairs of spin echo images with reversed phase encoding direction. A low-resolution structural image of each participant was acquired using a FLAIR sequence for clinical screening.

Structural scan. The high-resolution structural image was acquired using a 3D MP2RAGE sequence⁶⁶ with the following parameters: voxel size = 1.0 mm isotropic, FOV = 256 × 240 × 176 mm, TR = 5000 ms, TE = 2.92 ms, TI1 = 700 ms, TI2 = 2500 ms, flip angle 1 = 4°, flip angle 2 = 5°, bandwidth = 240 Hz/Px, GRAPPA acceleration with iPAT factor 3 (32 reference lines), pre-scan normalization, duration = 8.22 min. From the two images produced by the MP2RAGE sequence at different inversion times (inv1 and inv2), a quantitative T1 map (t1map), and a uniform T1-weighted image (t1w) were generated. Importantly, the latter image is purely T1-weighted, whereas standard T1-weighted image, for example acquired with the MPRAGE sequence, also contain contributions of proton density and T2*. It should be taken into account that such differences can affect morphometric measures⁶⁷.

For one participant (010025), the structural scan is MPRAGE instead of MP2RAGE (the T1-weighted image file names contain the sequence type) with voxel size = 1 mm isotropic, FoV = 256 × 240 × 176, TR = 2300 ms, TE = 2.98 ms, TI = 900 ms, flip angle = 9°, bandwidth = 238 Hz/Px.

Resting-state scans. Four rs-fMRI scans were acquired in axial orientation using T2*-weighted gradient-echo echo planar imaging (GE-EPI) with multiband acceleration, sensitive to blood oxygen level-dependent (BOLD) contrast^{68,69}. Sequences were identical across the four runs, with the exception of alternating slice orientation and phase-encoding direction, to vary the spatial distribution of distortions and signal loss. Thus, the y-axis was aligned parallel to the AC-PC axis for runs 1 and 2, and parallel to orbitofrontal cortex for runs 2 and 4. The phase-encoding direction was A–P for runs 1 and 3, and P–A for runs 2 and 4. Further parameters were set as follows for all four runs: voxel size = 2.3 mm isotropic, FOV = 202 × 202 mm², imaging matrix = 88 × 88, 64 slices with 2.3 mm thickness, TR = 1400 ms, TE = 39.4 ms, flip angle = 69°, echo spacing = 0.67 ms, bandwidth = 1776 Hz/Px, partial fourier 7/8, no pre-scan normalization, multiband acceleration factor = 4, 657 volumes, duration = 15 min 30 s. During the resting-state scans, participants were instructed to remain awake with their eyes open and to fixate on a crosshair.

Scans for distortion correction. Two prominent methods exist to correct for geometric distortions in EPI images: fieldmaps, which represent the degree of distortion as calculated from two phase images with different echo times^{70,71}, and reverse phase encoding, in which pairs of “blip-up blip-down” images are acquired with opposite phase encoding direction — thus opposite distortions — and used to model a middle distortion-free image^{72,73}. This dataset contains scans required for both methods to accommodate different preprocessing approaches and facilitate method comparison. Before each pair of resting-state runs with the same y-axis orientation (see above), the following scans were acquired in the same orientation as the subsequent resting-state scans: a pair of spin echo images (voxel size = 2.3 mm isotropic, FOV = 202 × 202 mm², imaging matrix = 88 × 88, 64 slices with 2.3 mm thickness, TR = 2200 ms, TE = 52 ms, flip angle = 90°, echo spacing = 0.67 ms, phase encoding = AP/PA, bandwidth = 1776 Hz/Px, partial fourier 6/8, no pre-scan normalization, duration = 0.20 min each), and a gradient echo fieldmap (voxel size = 2.3 mm isotropic, FOV = 202 × 202 mm², imaging matrix = 88 × 88, 64 slices with 2.3 mm thickness, TR = 680 ms, TE1 = 5.19 ms, TE2 = 7.65 ms, flip angle = 60°, bandwidth = 389 Hz/Px, prescan normalization, no partial fourier, duration = 2.03 min).

Additional scans. 109 subjects also took part in a complementary protocol. Therefore, additional modalities will be available for these subjects. Modalities include high-resolution T2-weighted (108 subjects), diffusion-weighted (109), 3D FLAIR (47), phases and magnitudes of gradient-echo images suitable for Susceptibility-Weighted Imaging (SWI), and Quantitative Susceptibility Mapping (QSM) (45 subjects), as well as an additional 15-minute resting-state scan for all 109 subjects.

MRI data preprocessing

To enhance data usability we provide preprocessed data from 189 subjects (five participants did not have all four resting-state scans available, and were excluded from preprocessing). Data from five participants were further excluded due to failure at the preprocessing stage. The raw MRI data of these subjects are not corrupted, and are therefore available in the main database. Preprocessing pipelines were

implemented using Nipype⁷⁴ and are described in more detail below. All code is openly available (https://github.com/NeuroanatomyAndConnectivity/pipelines/tree/master/src/lsc_lemmon).

Importantly, the preprocessing performed here is just one out of a multitude of possible pipelines that could be conceived for this dataset. The decisions taken at individual processing steps will not be suitable for every application. Users are strongly advised to familiarize themselves with the details of the workflow before adopting the preprocessed data for their study. We also encourage users to subscribe to the mailing list for updates and discussions regarding the preprocessing pipelines used here (http://groups.google.com/group/resting_state_preprocessing).

Structural data. The background of the uniform T1-weighted image was removed using CBS Tools⁷⁵, and the masked image was used for cortical surface reconstruction using FreeSurfer's full version of recon-all^{76,77}. A brain mask was created based on the FreeSurfer segmentation results. Diffeomorphic nonlinear registration as implemented in ANTs SyN algorithm⁷⁸ was used to compute a spatial transformation between the individual's T1-weighted image and the MNI152 1mm standard space.

To remove identifying information from the structural MRI scans, a mask for defacing was created from the MP2RAGE images using CBS Tools⁷⁵. This mask was subsequently applied to all anatomical scans.

Functional data. The first five volumes of each resting-state run were excluded. Transformation parameters for motion correction were obtained by rigid-body realignment to the first volume of the shortened time series using FSL MCFLIRT⁷⁹. The fieldmap images were preprocessed using the `fsl_prepare_fieldmap` script. A temporal mean image of the realigned time series was rigidly registered to the fieldmap magnitude image using FSL FLIRT⁸⁰ and unwarped using FSL FUGUE⁸¹ to estimate transformation parameters for distortion correction. The unwarped temporal mean was rigidly coregistered to the subject's structural scan using FreeSurfer's boundary-based registration algorithm⁸², yielding transformation parameters for coregistration. The spatial transformations from motion correction, distortion correction, and coregistration were then combined and applied to each volume of the original time series in a single interpolation step. The time series were masked using the brain mask created from the structural image (see above). The six motion parameters and their first derivatives were included as nuisance regressors in a general linear model (GLM), along with regressors representing outliers as identified by Nipype's rapidart algorithm (<https://nipype.readthedocs.io/en/latest/interfaces/generated/nipype.algorithms.rapidart.html>), as well as linear and quadratic trends. To remove physiological noise from the residual time series, we followed the aCompCor approach as described by Behzadi and colleagues⁸³. Masks of the white matter and cerebrospinal fluid were created by applying FSL FAST⁸⁴ to the T1-weighted image, thresholding the resulting probability images at 99%, eroding by one voxel and combining them to a single mask. Of the signal of all voxels included in this mask, the first six principal components were included as additional regressors in a second GLM, run on the residual time series from the first GLM. The denoised time series were temporally filtered to a frequency range between 0.01 and 0.1 Hz using FSL, mean centered and variance normalized using Nitime⁸⁵. The fully preprocessed time series of all for runs were temporally concatenated. To facilitate analysis in standard space, the previously derived transformation was used to project the full-length time series into MNI152 2 mm space. The preprocessed data are made available in the subjects' native structural space and MNI standard space, along with the subject's brain mask and all regressors used for denoising.

Data security and data anonymization procedures

Data for all participants was stored on our instance of the eXtensible Neuroimaging Archive Toolkit (XNAT⁸⁶) v.1.6.5. at the MPI-CBS. Access to the initial project was restricted (via XNAT's private project mode) to members of the Neuroanatomy & Connectivity Group at MPI-CBS for initial curation and quality assessment of data. All data comprised in the MPI-Leipzig Mind-Brain-Body database were derived from MPI-CBS so data import into XNAT was done from a local secured network.

A specially customized XNAT uploader was used to upload all participants' data to XNAT. The native DICOM format was used for MRI data, whilst a standard ASCII (*.csv, *.txt) format was employed to upload all other experimental data such as surveys, test batteries, and demographical data.

The anonymization measures applied to the MRI data consisted of removal of DICOM header tags containing information which could lead to the identification of test subjects as well as the defacing of all structural (NIFTI) scans. Specific surveys and test batteries containing sensitive information are only available via the restricted project in XNAT for which access needs to be applied for (see the Usage Notes section below).

Code availability

All code that was implemented for data acquisition and processing is available online (<https://neuroanatomyandconnectivity.github.io/pendata/>). Data handling and computation of summary measures were implemented in Python. The pipeline used for MRI preprocessing is also available (https://github.com/NeuroanatomyAndConnectivity/pipelines/tree/v2.0/src/lsc_lemmon_releasev2.0).

The tasks that the participants received were implemented using the Python package PsychoPy2 Experiment Builder v1.81.03^{87,88}, OpenSesame 0.27.4⁸⁹, and Presentation® software (Version 16.5,

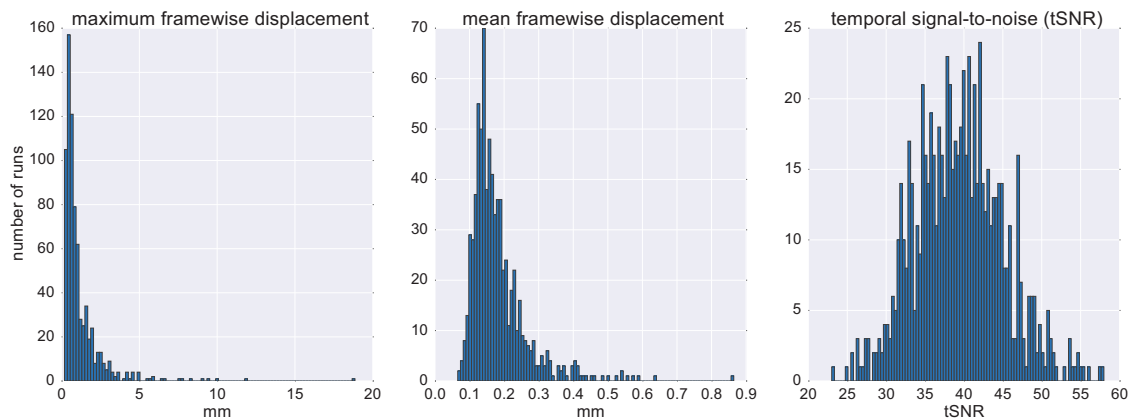


Figure 2. Quality assessment of resting-state fMRI scans. Distribution of motion (maximum and mean framewise displacement).

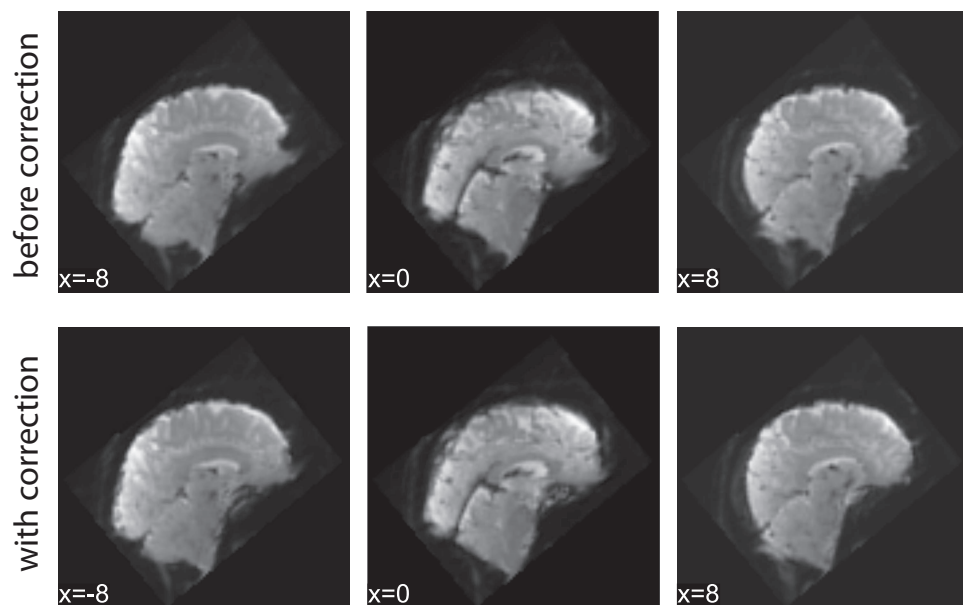


Figure 3. Example impact of fieldmap correction.

Neurobehavioral Systems, Inc., Berkeley, CA, <http://www.neurobs.com>). We provide the respective source codes of the Adaptive Visual and Auditory Oddball Target Detection Task e.g.,⁵⁵; cf.⁵⁶ (Oddball; <https://github.com/NeuroanatomyAndConnectivity/opendata/tree/master/scripts>), Conjunctive Continuous Performance Task⁵¹ (CCPT; <https://github.com/NeuroanatomyAndConnectivity/ConjunctiveContinuousPerformanceTask>), and Emotional Task Switching^{50,58} (ETS; <https://github.com/NeuroanatomyAndConnectivity/opendata/tree/master/scripts>).

Data Records

Survey and task data

Data from all questionnaires are open access, except for two (Facebook Intensity Scale²⁸ and Multi-Gender Identity Questionnaire³⁵). Results of questionnaires are released as summary scores, except for: Multi-Gender Identity Questionnaire³⁵ (MGIQ), Mobile Phone Usage (MPU), Facebook Intensity Scale²⁸ (FBI), New York Cognition Questionnaire⁴⁹ (NYC-Q), and the short version of the New York Cognition Questionnaire⁹ (Short-NYC-Q). Task data for the CCPT⁵¹, ETS^{50,58}, and oddball task e.g.,⁵⁵; cf.⁵⁶ are available via subject-specific .csv files. Accompanying specifications and information for each questionnaire and task are given in .txt file format.

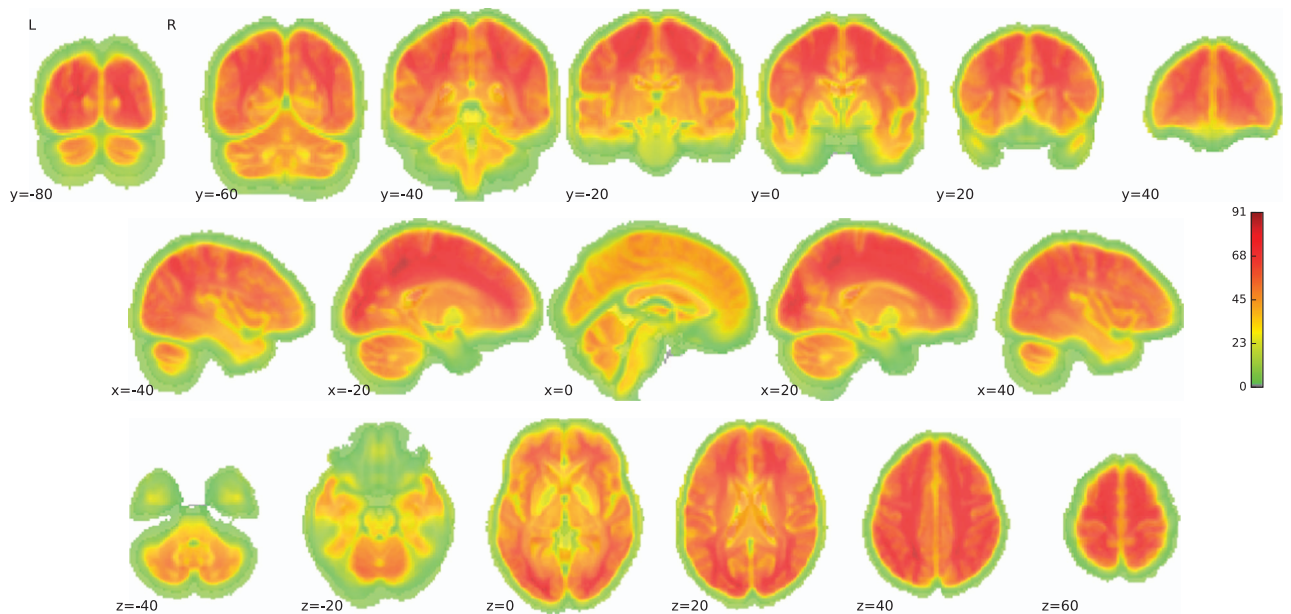


Figure 4. Temporal signal-to-noise (tSNR). Group-level variance in temporal signal-to-noise (tSNR) across the brain. tSNR values are lower in ventral regions including orbitofrontal and temporal cortex.

A basic demographic summary is provided together with general information on data acquisition. The metafile includes gender, age (5-year bins), body mass index, handedness, current or past diagnosed psychiatric disorder(s), result of the drug test on day of scanning, and formal education.

Behavioral and questionnaire data is provided at <https://dataverse.harvard.edu/> through the following link <https://doi.org/10.7910/DVN/VMJ6NV> (Data Citation 2).

MRI data

The dataset is organized in concordance with the Brain Imaging Data Structure (BIDS) format⁹⁰. This facilitates data analysis, for example with BIDS-Apps⁹¹ (<http://bids-apps.neuroimaging.io>). BIDS-Apps encapsulate standard MRI analysis tools within an application that understands the BIDS format and allows to automatically access relevant data and metadata.

MRI data are currently available from three locations:

1. OpenfMRI.org (now renamed to OpenNeuro) platform also hosts the raw data (Data Citation 3)
The OpenfMRI repository provides API access available via <https://openfmri.org/dataset/api/>. In addition, similar to all other datasets in OpenfMRI, our dataset is available via Amazon Web Services S3 object data store under the `s3://openneuro/ds000221/`
2. International Neuroimaging Data-sharing Initiative, INDI (Data Citation 4)
3. Gesellschaft für wissenschaftliche Datenverarbeitung mbH Göttingen (GWDG): <https://www.gwdg.de/>
Raw and preprocessed data at this location is accessible through web browser (https://ftp.gwdg.de/pub/misc/MPI-Leipzig_Mind-Brain-Body/) and a fast FTP connection (ftp://ftp.gwdg.de/pub/misc/MPI-Leipzig_Mind-Brain-Body/). In the case the location of the data changes in the future, the location of the dataset can be resolved with PID 21.11101/0000-0004-2CD6-A (e.g., <https://hdl.handle.net/21.11101/0000-0004-2CD6-A>).

Technical Validation

All datasets were manually assessed for missing or corrupt data (see Supplementary Table 3 and Supplementary File 1). Further quality control of the data was applied to the MRI and behavioral measures, as described below.

MRI data quality assessment

Preprocessed MRI data were assessed for quality using the `mriqc` package⁹² (the code was adapted from <https://github.com/chrisfilo/mriqc> and can be found at https://github.com/NeuroanatomyAndConnectivity/pipelines/tree/master/src/lsc_lemon, release v2.0), implemented in Python. `mriqc` creates a report for each individual scan based on assessment of movement parameters, coregistration, and temporal

Translated Questionnaires	Cronbach's alpha coefficient (α)
Personality and Habitual Behaviors	
Abbreviated Math Anxiety Scale ⁹	$\alpha = 0.92$ (English original: $\alpha = 0.90$)
Body Consciousness Questionnaire ²¹	Private body scale, $\alpha = 0.63$ Public body scale, $\alpha = 0.62$ Body competence scale, $\alpha = 0.62$ Note: Cronbach's α coefficients of the original scales are not available
Boredom Proneness Scale ²²	$\alpha = 0.84$ (English original: $\alpha = 0.79$)
Internet Addiction Test ³²	$\alpha = 0.91$ (item 3 was excluded from the analysis due to different scaling; values for English unavailable)
Involuntary Musical Imagery Scale ³³	Negative valence, $\alpha = 0.88$ for (English original: $\alpha = 0.91$) Movement, $\alpha = 0.92$ (English original: $\alpha = 0.88$) Personal reflections, $\alpha = 0.64$ (English original: $\alpha = 0.76$) Help, $\alpha = 0.90$ (English original: $\alpha = 0.84$)
Multimedia Multitasking Index ³⁵	$\alpha = 0.97$ (English original: not reported)
Self-Esteem Scale ³⁸	$\alpha = 0.88$ (English original: $\alpha = 0.79$ for males; $\alpha = 0.83$ for females)
Short Dark Triad ³⁹	Machiavellianism, $\alpha = 0.68$ (English original: $\alpha = 0.78$) Narcissism, $\alpha = 0.65$ (English original: $\alpha = 0.77$) Psychopathy, $\alpha = 0.59$ for (English original: $\alpha = 0.80$)
UPPS-P Impulsive Behavior Scale ^{42,43} , cf. ⁴⁵	Negative urgency, $\alpha = 0.83$ (English original: $\alpha = 0.90$) Lack of premeditation, $\alpha = 0.75$ (English original: $\alpha = 0.91$) Lack of perseverance, $\alpha = 0.84$ (English original: $\alpha = 0.82$) Sensation seeking, $\alpha = 0.82$ (English original: $\alpha = 0.86$) Positive urgency, $\alpha = 0.90$ (English original: not reported)
Mind-Wandering and Mindfulness	
Five Facets of Mindfulness ⁴⁶	Observing scale, $\alpha = 0.68$ (English original: $\alpha = 0.83$) Describing scale, $\alpha = 0.89$ (English original: $\alpha = 0.91$) Acting with Awareness scale, $\alpha = 0.70$ (English original: $\alpha = 0.87$) Nonjudging scale, $\alpha = 0.87$ (English original: $\alpha = 0.87$) Nonreactivity scale, $\alpha = 0.69$ (English original: $\alpha = 0.75$)
Metacognition Questionnaire ^{46,48}	Cognitive confidence, $\alpha = 0.80$ (English original: $\alpha = 0.93$) Positive beliefs, $\alpha = 0.85$ (English original: $\alpha = 0.92$) Cognitive self-consciousness, $\alpha = 0.85$ (English original: $\alpha = 0.92$) Uncontrollability and danger, $\alpha = 0.80$ (English original: $\alpha = 0.91$) Need to control thoughts, $\alpha = 0.67$ (English original: $\alpha = 0.72$)
Spontaneous and Deliberate Mind-Wandering ⁵¹ , cf. ⁴⁵	Deliberate mind-wandering, $\alpha = 0.81$ (English original: $\alpha = 0.90$) Spontaneous mind-wandering, $\alpha = 0.81$ (English original: $\alpha = 0.88$)
Varieties of Inner Speech Questionnaire ⁵²	Dialogic inner speech, $\alpha = 0.74$ (English original: $\alpha = 0.83$) Condensed inner speech, $\alpha = 0.79$ (English original: $\alpha = 0.83$) Other people in inner speech, $\alpha = 0.86$ (English original: $\alpha = 0.88$) Evaluative inner speech, $\alpha = 0.74$ (English original: $\alpha = 0.80$)
Cognitive Control and Sustained Attention	
Attention Control Scale ⁵⁶	$\alpha = 0.74$ (English original: not reported)
Creativity	
Creative Achievement Questionnaire ⁶⁰	$\alpha = 0.67$ (English original: $\alpha = 0.96$)

Table 3. Reliability of translated questionnaires. Estimated reliability of the English-German translated questionnaires using Cronbach's Alpha coefficient (α). **Note.** Cronbach's alpha coefficient was not computed for the NYC-Q and the Short-NYC-Q, as the heterogeneity of items within these questionnaires do not describe a unitary phenomenon and are not designed to be internally consistent⁹⁴. We recommend a factor analytic approach to derive behavioral scores from these questionnaires (see⁴⁸).

signal-to-noise (tSNR) calculations. For comparison, all individual-level scores are displayed with respect to the group-level distribution. We visually inspected the quality assessment reports for each subject to ensure adequate coregistration and fieldmap correction.

As motion during the resting-state fMRI scan poses a substantial source of noise⁹³, we characterized motion for each run as the mean and maximum framewise displacement (Fig. 2). Overall, the summary of motion parameters demonstrates that the data are largely of sufficient quality, with 89.2% of runs showing less than one voxel (2.3 mm) maximum framewise displacement, and a mean framewise displacement of 0.18 mm (SD = 0.08 mm).

Fieldmap correction provides an approach to correct for distortions due to susceptibility artifacts. While unable to recover signal loss, the correction of such nonlinear distortions improves coregistration between scan types, and group-level alignment⁹⁴. As an example, we present a single dataset, pre- and post-fieldmap correction, in Fig. 3. As expected, fieldmap correction primarily shifted voxels within ventral regions.

Temporal signal-to-noise (tSNR), which is calculated on the voxel-level as the mean signal divided by the standard deviation, offers a general overview of the local differences across the brain. We observed lower tSNR in ventral regions, including the orbitofrontal and temporal cortex (Fig. 4).

Behavioral measures quality assessment

Fifteen questionnaires without a published German version were in-house translated (English-German). To ensure general usability of the translated questionnaires, their reliability was estimated using Cronbach's Alpha coefficient (see Table 3). For comparison, the Cronbach's Alpha coefficients from the original questionnaires are also reported in Table 3.

Internal consistency⁹⁵ of the majority of questionnaires was acceptable, with an average Cronbach's Alpha of 0.78, thus showing that the German translations of those specific questionnaires are reproducible and valid. However, three questionnaires (Short Dark Triad⁴⁰, Body Consciousness Questionnaire²², and the Creative Achievement Questionnaire⁶¹) and four scales (two scales of the Five Facets of Mindfulness Questionnaire⁴⁶, one scale of the Metacognition Questionnaire⁴⁷, and one scale of the Involuntary Musical Imagery Scale³⁴) showed modest reliability, with Cronbach's Alpha coefficient < 0.70, and should be interpreted with caution.

Usage Notes

The MRI dataset can be accessed at <https://openneuro.org>, http://fcon_1000.projects.nitrc.org, or <https://www.gwdg.de/> and the behavioral data is available at <http://www.nitrc.org> (<http://nitrc.org/projects/mpilmbb/>). The following data are publicly available: 1) MRI data (structural and functional), 2) general demographic of the studied population, 3) summary scores and/or indexes of the questionnaires and tasks, and 4) raw scores of the measures that do not possess summary scores and have not been classified as sensitive. All MRI datasets are made available in NIFTI format, and all anatomical scans have been defaced.

The dataset, protocols, and software used in the acquisition and processing of the data are documented, curated, and available for download. For access to the behavioral data, users must first agree to the terms of data usage, which prohibit any usage that aims to identify the individuals based on these phenotypic data.

Additional access to sensitive behavioral measures

Individual behavioral scores and sensitive phenotypic measures may be made available upon request to the corresponding authors. The completion of additional data license and confidentiality forms will be required in advance of further data access.

References

- Kelly, C., Biswal, B. B., Craddock, R. C., Castellanos, F. X. & Milham, M. P. Characterizing variation in the functional connectome: promise and pitfalls. *Trends Cogn. Sci.* **16**, 181–188 (2012).
- Smith, S. M. *et al.* A positive-negative mode of population covariation links brain connectivity, demographics and behavior. *Nat. Neurosci.* **18**, 1565–1567 (2015).
- Vaidya, C. J. & Gordon, E. M. Phenotypic variability in resting-state functional connectivity: current status. *Brain Connect* **3**, 99–120 (2013).
- Nooner, K. B. *et al.* The NKI-Rockland sample: a model for accelerating the pace of discovery science in psychiatry. *Front. Neurosci.* **6**, 152 (2012).
- Holmes, A. J. *et al.* Brain Genomics Superstruct Project initial data release with structural, functional, and behavioral measures. *Sci. Data* **2** (2015).
- Van Essen, D. C. *et al.* The WU-Minn human connectome project: an overview. *NeuroImage* **80**, 62–79 (2013).
- Babayán, A. *et al.* A mind-brain-body dataset of MRI, EEG, cognition, emotion, and peripheral physiology in young and old adults. *Sci. Data*, Accepted.
- Wittchen, H.-U., Kessler, R. C., Zhao, S. & Abelson, J. Reliability and clinical validity of UM-CIDI DSM-III-R generalized anxiety disorder. *J. Psychiatr. Res.* **29**, 95–110 (1995).
- Ruby, F. J., Smallwood, J., Engen, H. & Singer, T. How self-generated thought shapes mood—the relation between mind-wandering and mood depends on the socio-temporal content of thoughts. *PLoS ONE* **8**, e77554 (2013).
- Hopko, D. R., Mahadevan, R., Bare, R. L. & Hunt, M. K. The abbreviated math anxiety scale (AMAS) construction, validity, and reliability. *ASM.* **10**, 178–182 (2003).
- Costa, P. T. & McCrae, R. R. *The NEO Personality Inventory Manual.* (Psychological Assessment Resources, 1985).
- Costa, P. T. & McCrae, R. R. *Revised NEO Personality Inventory (NEO PI-R) and NEP Five-Factor Inventory (NEO-FFI): Professional Manual.* (Psychological Assessment Resources Lutz, FL, 1992).
- Ostendorf, F. & Angleitner, A. *NEO-Persönlichkeitsinventar (revidierte Form, NEO-PI-R) nach Paul T. Costa und Robert R. McCrae.* (Hogrefe, 2004).
- Achenbach, T. M. & Rescorla, L. A. *Manual for the ASEBA Adult Forms & Profiles.* (Research Center for Children, Youth, & Families, University of Vermont: Burlington, VT, USA, 2003).
- Beck, A. T., Steer, R. A. & Brown, G. K. *Manual for the Beck Depression Inventory-II* (San Antonio TX, 1996).
- Beck, A. T., Ward, C. H., Mendelson, M., Mock, J. & ERBAUGH, J. An inventory for measuring depression. *Arch. Gen. Psychiatry* **4**, 561–571 (1961).
- Hautzinger, M., Bailer, M., Worall, H. & Keller, F. *BDI: Beck-Depressions-Inventar Testhandbuch 2.* (Bern Verlag Hans Huber, 1995).
- Carver, C. S. & White, T. L. Behavioral inhibition, behavioral activation, and affective responses to impending reward and punishment: The BIS/BAS Scales. *J. Pers. Soc. Psychol.* **67**, 319 (1994).
- Gray, J. A. Precis of the neuropsychology of anxiety: An enquiry into the functions of the septo-hippocampal system. *Behav. Brain. Sci.* **5**, 469–534 (1982).
- Gray, J. A. *in A Model for Personality*, Pgs 246–276 Eysenck H. J. ed. (Springer Berlin Heidelberg, 1981).
- Strobel, A., Beauducel, A., Debener, S. & Brocke, B. Eine deutschsprachige Version des BIS/BAS-Fragebogens von Carver und White. *Zeitschrift für Differentielle und diagnostische Psychologie* **22**, 216–227 (2001).
- Miller, L. C., Murphy, R. & Buss, A. H. Consciousness of body: private and public. *J. Pers. Soc. Psychol.* **41**, 397 (1981).
- Farmer, R. & Sundberg, N. D. Boredom proneness—the development and correlates of a new scale. *J. Pers. Assess.* **50**, 4–17 (1986).

24. Tangney, J. P., Baumeister, R. F. & Boone, A. L. High self-control predicts good adjustment, less pathology, better grades, and interpersonal success. *J. Pers.* **72**, 271–324 (2004).
25. Bertrams, A. & Dickhäuser, O. Messung dispositioneller Selbstkontroll-Kapazität: Eine deutsche Adaptation der Kurzform der Self-Control Scale (SCS-KD). *Diagnostica* **55**, 2–10 (2009).
26. Johns, M. W. A new method for measuring daytime sleepiness: the Epworth sleepiness scale. *Sleep* **14**, 540–545 (1991).
27. Bloch, K. E., Schoch, O. D., Zhang, J. N. & Russi, E. W. German version of the Epworth sleepiness scale. *Respiration* **66**, 440–447 (1999).
28. Ellison, N. B., Steinfield, C. & Lampe, C. The benefits of Facebook “friends”: Social capital and college students’ use of online social network sites. *J. Comput. Mediat. Commun.* **12**, 1143–1168 (2007).
29. Müllensiefen, D., Gingras, B., Musil, J. & Stewart, L. Measuring the facets of musicality: The Goldsmiths Musical Sophistication Index (Gold-MSI). *Pers. Individ. Dif.* **60**, S35 (2014).
30. Schaal, N. K., Bauer, A.-K. R. & Müllensiefen, D. Der Gold-MSI: replikation und validierung eines fragebogeninstrumentes zur messung musikalischer erfahrungheit anhand einer deutschen stichprobe. *Music. Sci.* **18**, 423–447 (2014).
31. Zigmond, A. S. & Snaith, R. P. The hospital anxiety and depression scale. *Acta Psychiatr. Scand.* **67**, 361–370 (1983).
32. Herrmann-Lingen, C., Buss, U. & Snaith, P. *Hospital Anxiety and Depression Scale-Deutsche Version (HADS-D)*. (Huber, 1995).
33. Young, K. S. Internet addiction: The emergence of a new clinical disorder. *Cyberpsychol. Behav.* **1**, 237–244 (1998).
34. Floridou, G. A., Williamson, V. J., Stewart, L. & Müllensiefen, D. The Involuntary Musical Imagery Scale (IMIS). *Psychomusicology* **25**, 28 (2015).
35. Joel, D., Tarrasch, R., Berman, Z., Mukamel, M. & Ziv, E. Queering gender: studying gender identity in ‘normative’ individuals. *Psychol. Sex* **5**, 291–321 (2014).
36. Ophir, E., Nass, C. & Wagner, A. D. Cognitive control in media multitaskers. *Proc. Natl. Acad. Sci. U.S.A.* **106**, 15583–15587 (2009).
37. Kuhl, J. & Kazén, M. *Persönlichkeits-Stil-und Störungs-Inventar: PSSI; Manual*. (Hogrefe, 2009).
38. American Psychiatric Association. *Diagnostic and statistical manual of mental disorders. 4th edn*, (American Psychiatric Association, 2000).
39. O’malley, P. M. & Bachman, J. G. Self-esteem and education: Sex and cohort comparisons among high school seniors. *J. Pers. Soc. Psychol.* **37**, 1153 (1979).
40. Jones, D. N. & Paulhus, D. L. Introducing the short dark triad (SD3) a brief measure of dark personality traits. *Assessment* **21**, 28–41 (2014).
41. Stöber, J. Die Soziale-Erwünschtheits-Skala-17 (SES-17): Entwicklung und erste Befunde zu Reliabilität und Validität. *Diagnostica* **45**, 173–177 (1999).
42. Tuckman, B. W. The development and concurrent validity of the procrastination scale. *Educ. Psychol. Meas.* **51**, 473–480 (1991).
43. Whiteside, S. P. & Lynam, D. R. The five factor model and impulsivity: Using a structural model of personality to understand impulsivity. *Pers. Individ. Dif.* **30**, 669–689 (2001).
44. Lynam, D. R., Smith, G. T., Whiteside, S. P. & Cyders, M. A. *The UPPS-P: Assessing Five Personality Pathways to Impulsive Behavior*. (West Lafayette, Purdue University, 2006).
45. Golchert, J. *et al.* Individual variation in intentionality in the mind-wandering state is reflected in the integration of the default-mode, fronto-parietal, and limbic networks. *NeuroImage* **146**, 226–235 (2017).
46. Baer, R. A., Smith, G. T., Hopkins, J., Krietemeyer, J. & Toney, L. Using self-report assessment methods to explore facets of mindfulness. *Assessment* **13**, 27–45 (2006).
47. Wells, A. & Cartwright-Hatton, S. A short form of the metacognitions questionnaire: properties of the MCQ-30. *Behav. Res. Ther.* **42**, 385–396 (2004).
48. Sadeghi, H., Hajloo, N., Babayi, K. & Shahri, M. The relationship between metacognition and obsessive beliefs, and procrastination in students of Tabriz and Mohaghegh Ardabili Universities, Iran. *Iran J. Psychiatry Behav. Sci.* **8**, 42 (2014).
49. Gorgolewski, K. J. *et al.* A correspondence between individual differences in the brain’s intrinsic functional architecture and the content and form of self-generated thoughts. *PLoS ONE* **9**, e97176 (2014).
50. Whitmer, A. J. & Banich, M. T. Inhibition versus switching deficits in different forms of rumination. *Psychol. Sci.* **18**, 546–553 (2007).
51. Shalev, L., Ben-Simon, A., Mevorach, C., Cohen, Y. & Tsal, Y. Conjunctive continuous performance task (CCPT)—a pure measure of sustained attention. *Neuropsychologia* **49**, 2584–2591 (2011).
52. Carriere, J. S., Seli, P. & Smilek, D. Wandering in both mind and body: individual differences in mind wandering and inattention predict fidgeting. *Can. J. Exp. Psychol.* **67**, 19 (2013).
53. McCarthy-Jones, S. & Fernyhough, C. The varieties of inner speech: links between quality of inner speech and psychopathological variables in a sample of young adults. *Conscious Cogn.* **20**, 1586–1593 (2011).
54. Eagleman, D. M., Kagan, A. D., Nelson, S. S., Sagaram, D. & Sarma, A. K. A standardized test battery for the study of synesthesia. *J. Neurosci. Methods* **159**, 139–145 (2007).
55. Huettel, S. A. & McCarthy, G. What is odd in the oddball task?: Prefrontal cortex is activated by dynamic changes in response strategy. *Neuropsychologia* **42**, 379–386 (2004).
56. Smallwood, J. *et al.* Representing representation: Integration between the temporal lobe and the posterior cingulate influences the content and form of spontaneous thought. *PLoS ONE* **11**, e0152272 (2016).
57. Derryberry, D. & Reed, M. A. Anxiety-related attentional biases and their regulation by attentional control. *J. Abnorm. Psychol.* **111**, 225 (2002).
58. Hildebrandt, L. K., McCall, C., Engen, H. G. & Singer, T. Cognitive flexibility, heart rate variability, and resilience predict fine-grained regulation of arousal during prolonged threat. *Psychophysiology* **53**, 880–890 (2016).
59. Guilford, J., Christensen, P., Merrifield, P. & Wilson, R. *Alternate Uses: Manual of Instructions and Interpretation*. (Orange, CA: Sheridan Psychological Services, 1978).
60. Silvia, P. J. *et al.* Assessing creativity with divergent thinking tasks: Exploring the reliability and validity of new subjective scoring methods. *Psychol. Aesthet. Creat. Arts* **2**, 68 (2008).
61. Carson, S. H., Peterson, J. B. & Higgins, D. M. Reliability, validity, and factor structure of the creative achievement questionnaire. *Creat. Res. J* **17**, 37–50 (2005).
62. Lee, C. S., Huggins, A. C. & Theriault, D. J. A measure of creativity or intelligence? Examining internal and external structure validity evidence of the Remote Associates Test. *Psychol. Aesthet. Creat. Arts* **8**, 446 (2014).
63. Landmann, N. *et al.* Entwicklung von 130 deutschsprachigen Compound Remote Associate (CRA)-Worträtseln zur Untersuchung kreativer Prozesse im deutschen Sprachraum. *Psychol. Rundsch.* **65**, 200–211 (2014).
64. Jankowska, D. M. & Karwowski, M. Measuring creative imagery abilities. *Front. Psychol.* **6**, 1591 (2015).
65. Hawks, R. L. & Chiang, C. N. *Urine Testing for Drugs of Abuse*. (National Institute on Drug Abuse: Rockville, MD, 1986).
66. Marques, J. P. *et al.* MP2RAGE, a self bias-field corrected sequence for improved segmentation and T 1-mapping at high field. *NeuroImage* **49**, 1271–1281 (2010).

67. Lorio, S. *et al.* Neurobiological origin of spurious brain morphological changes: A quantitative MRI study. *Hum. Brain. Mapp.* **37**, 1801–1815 (2016).
68. Feinberg, D. A. *et al.* Multiplexed echo planar imaging for sub-second whole brain fMRI and fast diffusion imaging. *PLoS ONE* **5**, e15710 (2010).
69. Moeller, S. *et al.* Multiband multislice GE-EPI at 7 tesla, with 16-fold acceleration using partial parallel imaging with application to high spatial and temporal whole-brain fMRI. *Magn. Reson. Med.* **63**, 1144–1153 (2010).
70. Jezzard, P. & Balaban, R. S. Correction for geometric distortion in echo planar images from B0 field variations. *Magn. Reson. Med.* **34**, 65–73 (1995).
71. Reber, P. J., Wong, E. C., Buxton, R. B. & Frank, L. R. Correction of off resonance-related distortion in echo-planar imaging using EPI-based field maps. *Magn. Reson. Med.* **39**, 328–330 (1998).
72. Chang, H. & Fitzpatrick, J. M. A technique for accurate magnetic resonance imaging in the presence of field inhomogeneities. *IEEE Trans. Med. Imag* **11**, 319–329 (1992).
73. Andersson, J. L., Skare, S. & Ashburner, J. How to correct susceptibility distortions in spin-echo echo-planar images: application to diffusion tensor imaging. *NeuroImage* **20**, 870–888 (2003).
74. Gorgolewski, K. *et al.* Nipype: a flexible, lightweight and extensible neuroimaging data processing framework in python. *Front. Neuroinform* **5**, 13 (2011).
75. Bazin, P.-L. *et al.* A computational framework for ultra-high resolution cortical segmentation at 7Tesla. *NeuroImage* **93**, 201–209 (2014).
76. Dale, A. M., Fischl, B. & Sereno, M. I. Cortical surface-based analysis: I. Segmentation and surface reconstruction. *NeuroImage* **9**, 179–194 (1999).
77. Fischl, B., Sereno, M. I. & Dale, A. M. Cortical surface-based analysis: II: inflation, flattening, and a surface-based coordinate system. *NeuroImage* **9**, 195–207 (1999).
78. Avants, B. B. *et al.* A reproducible evaluation of ANTs similarity metric performance in brain image registration. *NeuroImage* **54**, 2033–2044 (2011).
79. Jenkinson, M., Bannister, P., Brady, M. & Smith, S. Improved optimization for the robust and accurate linear registration and motion correction of brain images. *NeuroImage* **17**, 825–841 (2002).
80. Jenkinson, M. & Smith, S. A global optimisation method for robust affine registration of brain images. *Med. Imag. Anal* **5**, 143–156 (2001).
81. Jenkinson, M., Beckmann, C. F., Behrens, T. E., Woolrich, M. W. & Smith, S. M. Fsl. *NeuroImage* **62**, 782–790 (2012).
82. Greve, D. N. & Fischl, B. Accurate and robust brain image alignment using boundary-based registration. *NeuroImage* **48**, 63–72 (2009).
83. Behzadi, Y., Restom, K., Liau, J. & Liu, T. T. A component based noise correction method (CompCor) for BOLD and perfusion based fMRI. *NeuroImage* **37**, 90–101 (2007).
84. Zhang, Y., Brady, M. & Smith, S. Segmentation of brain MR images through a hidden Markov random field model and the expectation-maximization algorithm. *IEEE Trans. Med. Imag* **20**, 45–57 (2001).
85. Rokem, A., Trumpis, M. & Perez, F. In *Proceedings of the 8th Python in Science Conference (SciPy 2009)*, Pgs 68–75 (SciPy Conference, 2009).
86. Marcus, D. S., Olsen, T. R., Ramaratnam, M. & Buckner, R. L. The extensible neuroimaging archive toolkit. *Neuroinformatics* **5**, 11–33 (2007).
87. Peirce, J. W. PsychoPy—psychophysics software in Python. *J. Neurosci. Methods* **162**, 8–13 (2007).
88. Peirce, J. W. Generating stimuli for neuroscience using PsychoPy. *Front. Neuroinform* **2** (2008).
89. Mathôt, S., Schreij, D. & Theeuwes, J. OpenSesame: An open-source, graphical experiment builder for the social sciences. *Behav. Res. Methods* **44**, 314–324 (2012).
90. Gorgolewski, K. J. *et al.* The brain imaging data structure, a format for organizing and describing outputs of neuroimaging experiments. *Sci. Data* **3**, 160044 (2016).
91. Gorgolewski, K. J. *et al.* BIDS Apps: Improving ease of use, accessibility and reproducibility of neuroimaging data analysis methods. *PLoS Comput. Biol.* **13**, e1005209 (2017).
92. Esteban, O. *et al.* MRIQC: Advancing the automatic prediction of image quality in MRI from unseen sites. *PLoS ONE* **12**, e0184661 (2017).
93. Power, J. D. *et al.* Methods to detect, characterize, and remove motion artifact in resting state fMRI. *NeuroImage* **84**, 320–341 (2014).
94. Jezzard, P. Correction of geometric distortion in fMRI data. *NeuroImage* **62**, 648–651 (2012).
95. Streiner, D. L. Starting at the beginning: an introduction to coefficient alpha and internal consistency. *J. Pers. Assess.* **80**, 99–103 (2003).
96. Crowne, D. P. & Marlowe, D. A new scale of social desirability independent of psychopathology. *J. Consult. Psychol.* **24**, 349 (1960).

Data Citations

1. Buckner, R. L., Roffman, J. L. & Smoller, J. W. *Harvard Dataverse* <https://doi.org/10.7910/DVN/25833> (2014).
2. Mendes, N. *et al.* *Harvard Dataverse* <https://doi.org/10.7910/DVN/VMJ6NV> (2018).
3. Mendes, N. *et al.* *OpenNeuro* <https://doi.org/10.18112/OPENNEURO.DS000221.V2> (2017).
4. Margulies, D. *Child Mind Institute* https://doi.org/10.15387/fcp_indi.mpi (2017).

Acknowledgements

This work was partially supported by the Volkswagen Foundation (AZ.: 89 440). We thank Shameem Wagner and Elizabeth Kelly for assistance in the preparation of the manuscript.

Author Contributions

Conception, design, and preparation of the manuscript: D.S.M., J.G., J.M.H., M.E.L., M.F., N.M., S.O. Behavioral data analyses: J.G., M.E.L., S.O. MRI data preprocessing: J.M.H., M.E.L. Quality Control of MRI data: D.S.M., J.G., J.M.H., M.E.L., S.O. Contributions to study design: B.M.B., H.E., J.P., J.S., K.J.G., K.O., N.F. Mobile phone usage questionnaire was developed and provided by: K.J.G. Participant recruitment: A.O., J.G., M.E.L., N.M., P.H., R.J., S.K., Y.K. Data acquisition: D.K., J.G., J.P., L.G., M.D., M.E.L., N.M., S.K., S.O. Data curation: M.F., R.C. Data contributions: A.B., A.R., A.V., D.K., H.L.S., J.R., J.R., M.E., M.G., M.U. All authors provided critical feedback and approval of the manuscript.

Additional Information

Supplementary information accompanies this paper at <http://www.nature.com/sdata>.

Competing interests: The authors declare no competing interests.

How to cite this article: Mendes, N. *et al.* A functional connectome phenotyping dataset including cognitive state and personality measures. *Sci. Data*. 6:180307 <https://doi.org/10.1038/sdata.2018.307> (2019).

Publisher's note: Springer Nature remains neutral with regard to jurisdictional claims in published maps and institutional affiliations.



Open Access This article is licensed under a Creative Commons Attribution 4.0 International License, which permits use, sharing, adaptation, distribution and reproduction in any medium or format, as long as you give appropriate credit to the original author(s) and the source, provide a link to the Creative Commons license, and indicate if changes were made. The images or other third party material in this article are included in the article's Creative Commons license, unless indicated otherwise in a credit line to the material. If material is not included in the article's Creative Commons license and your intended use is not permitted by statutory regulation or exceeds the permitted use, you will need to obtain permission directly from the copyright holder. To view a copy of this license, visit <http://creativecommons.org/licenses/by/4.0/>

The Creative Commons Public Domain Dedication waiver <http://creativecommons.org/publicdomain/zero/1.0/> applies to the metadata files made available in this article.

© The Author(s) 2019

7.2.3 Association of Peripheral Blood Pressure with Gray Matter Volume in 19- to 40-Year-Old Adults. Schaare et al., Neurology (2019)

ARTICLE

Association of peripheral blood pressure with gray matter volume in 19- to 40-year-old adults

H. Lina Schaare, MSc, Shahrzad Kharabian Masouleh, MSc, Frauke Beyer, MSc, Deniz Kumral, MSc, Marie Uhlig, MSc, Janis D. Reinelt, Andrea M.F. Reiter, PhD, Leonie Lampe, MD, Anahit Babayan, PhD, Miray Erbey, MSc, Josefin Roebbig, MSc, Matthias L. Schroeter, MD, PhD, Hadas Okon-Singer, PhD, Karsten Müller, PhD, Natacha Mendes, PhD, Daniel S. Margulies, PhD, A. Veronica Witte, PhD, Michael Gaebler, PhD, and Arno Villringer, MD

Correspondence
H.L. Schaare
schaare@cbs.mpg.de

Neurology® 2019;92:e758-e773. doi:10.1212/WNL.0000000000006947

Abstract

Objective

To test whether elevated blood pressure (BP) relates to gray matter (GM) volume (GMV) changes in young adults who had not previously been diagnosed with hypertension (systolic BP [SBP]/diastolic BP [DBP] $\geq 140/90$ mm Hg).

Methods

We associated BP with GMV from structural 3T T1-weighted MRI of 423 healthy adults between 19 and 40 years of age (mean age 27.7 ± 5.3 years, 177 women, SBP/DBP $123.2/73.4 \pm 12.2/8.5$ mm Hg). Data originated from 4 previously unpublished cross-sectional studies conducted in Leipzig, Germany. We performed voxel-based morphometry on each study separately and combined results in image-based meta-analyses (IBMA) to assess cumulative effects across studies. Resting BP was assigned to 1 of 4 categories: (1) SBP < 120 and DBP < 80 mm Hg, (2) SBP 120–129 or DBP 80–84 mm Hg, (3) SBP 130–139 or DBP 85–89 mm Hg, (4) SBP ≥ 140 or DBP ≥ 90 mm Hg.

Results

IBMA yielded the following results: (1) lower regional GMV was correlated with higher peripheral BP; (2) lower GMV was found with higher BP when comparing individuals in subhypertensive categories 3 and 2, respectively, to those in category 1; (3) lower BP-related GMV was found in regions including hippocampus, amygdala, thalamus, frontal, and parietal structures (e.g., precuneus).

Conclusion

BP $\geq 120/80$ mm Hg was associated with lower GMV in regions that have previously been related to GM decline in older individuals with manifest hypertension. Our study shows that BP-associated GM alterations emerge continuously across the range of BP and earlier in adulthood than previously assumed. This suggests that treating hypertension or maintaining lower BP in early adulthood might be essential for preventing the pathophysiologic cascade of asymptomatic cerebrovascular disease to symptomatic end-organ damage, such as stroke or dementia.

From the Department of Neurology (H.L.S., S.K.M., F.B., D.K., M.U., J.D.R., A.M.F.R., L.L., A.B., M.E., J.R., M.L.S., A.V.W., M.G., A.V.), Max Planck Research Group for Neuroanatomy & Connectivity (N.M., D.S.M.), and Nuclear Magnetic Resonance Group (K.M.), Max Planck Institute for Human Cognitive and Brain Sciences; International Max Planck Research School NeuroCom (M.L.S., M.U.), Leipzig; MindBrainBody Institute at Berlin School of Mind and Brain (D.K., A.B., M.E., M.G., A.V.), Charité & Humboldt Universität zu Berlin; Lifespan Developmental Neuroscience (A.M.F.R.) Technische Universität Dresden; Leipzig Research Centre for Civilization Diseases (LFC) (M.L.S., M.G., A.V.); Clinic for Cognitive Neurology (M.L.S., A.V.) and Collaborative Research Centre 1052 'Obesity Mechanisms' Subproject A1, Faculty of Medicine (F.B., A.V.W., A.V.), University of Leipzig, Germany; Department of Psychology (H.O.-S.) University of Haifa, Israel; and Center for Stroke Research Berlin (A.V.), Charité-Universitätsmedizin Berlin, Germany.

Go to [Neurology.org](https://www.neurology.org) for full disclosures. Funding information and disclosures deemed relevant by the authors, if any, are provided at the end of the article.

e758 Copyright © 2019 American Academy of Neurology

Copyright © 2019 American Academy of Neurology. Unauthorized reproduction of this article is prohibited.

Association of peripheral blood pressure with gray matter volume in 19- to 40-year-old adults

H. Lina Schaare, MSc, Shahrzad Kharabian Masouleh, MSc, Frauke Beyer, MSc, Deniz Kumral, MSc, Marie Uhlig, MSc, Janis D. Reinelt, Andrea M.F. Reiter, PhD, Leonie Lampe, MD, Anahit Babayan, PhD, Miray Erbey, MSc, Josefin Roebbig, MSc, Matthias L. Schroeter, MD, PhD, Hadas Okon-Singer, PhD, Karsten Müller, PhD, Natacha Mendes, PhD, Daniel S. Margulies, PhD, A. Veronica Witte, PhD, Michael Gaebler, PhD, and Arno Villringer, MD

Correspondence

H.L. Schaare
schaare@cbs.mpg.de

Neurology® 2019;92:e758-e773. doi:10.1212/WNL.0000000000006947

Abstract

Objective

To test whether elevated blood pressure (BP) relates to gray matter (GM) volume (GMV) changes in young adults who had not previously been diagnosed with hypertension (systolic BP [SBP]/diastolic BP [DBP] $\geq 140/90$ mm Hg).

Methods

We associated BP with GMV from structural 3T T1-weighted MRI of 423 healthy adults between 19 and 40 years of age (mean age 27.7 ± 5.3 years, 177 women, SBP/DBP $123.2/73.4 \pm 12.2/8.5$ mm Hg). Data originated from 4 previously unpublished cross-sectional studies conducted in Leipzig, Germany. We performed voxel-based morphometry on each study separately and combined results in image-based meta-analyses (IBMA) to assess cumulative effects across studies. Resting BP was assigned to 1 of 4 categories: (1) SBP < 120 and DBP < 80 mm Hg, (2) SBP 120–129 or DBP 80–84 mm Hg, (3) SBP 130–139 or DBP 85–89 mm Hg, (4) SBP ≥ 140 or DBP ≥ 90 mm Hg.

Results

IBMA yielded the following results: (1) lower regional GMV was correlated with higher peripheral BP; (2) lower GMV was found with higher BP when comparing individuals in subhypertensive categories 3 and 2, respectively, to those in category 1; (3) lower BP-related GMV was found in regions including hippocampus, amygdala, thalamus, frontal, and parietal structures (e.g., precuneus).

Conclusion

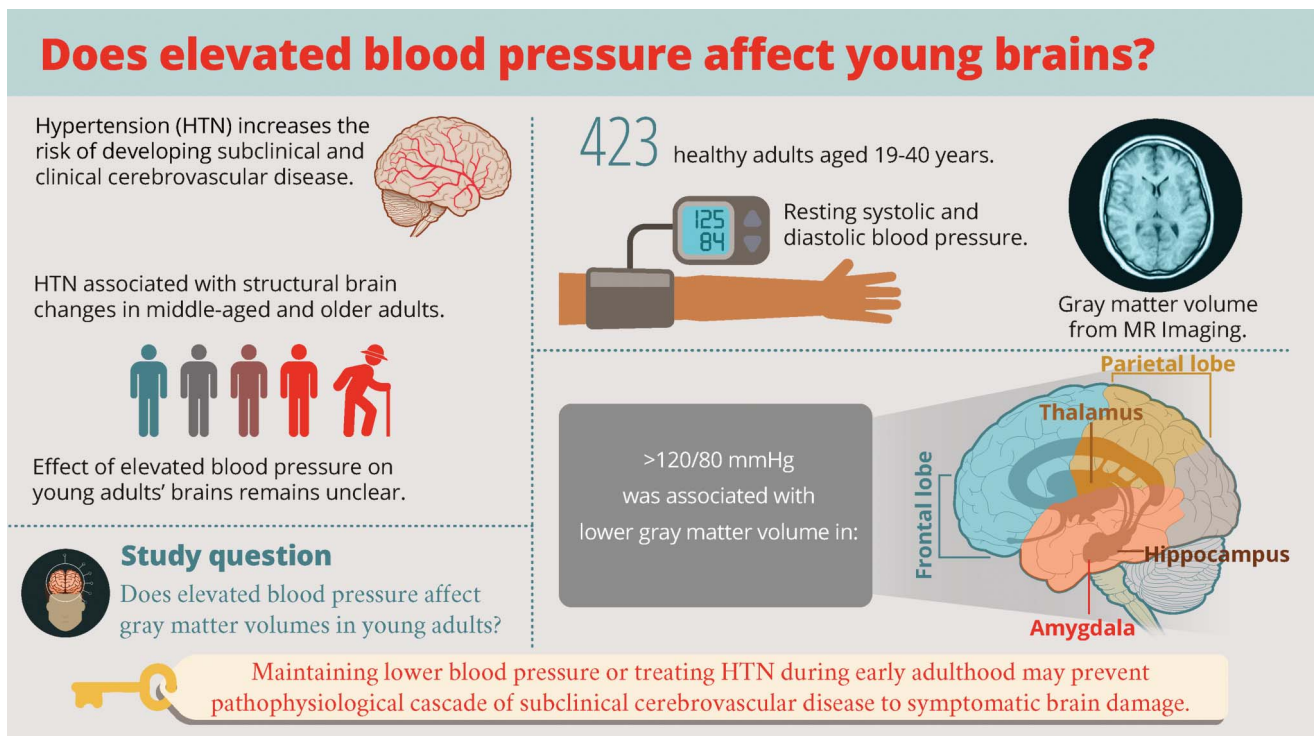
BP $\geq 120/80$ mm Hg was associated with lower GMV in regions that have previously been related to GM decline in older individuals with manifest hypertension. Our study shows that BP-associated GM alterations emerge continuously across the range of BP and earlier in adulthood than previously assumed. This suggests that treating hypertension or maintaining lower BP in early adulthood might be essential for preventing the pathophysiologic cascade of asymptomatic cerebrovascular disease to symptomatic end-organ damage, such as stroke or dementia.

From the Department of Neurology (H.L.S., S.K.M., F.B., D.K., M.U., J.D.R., A.M.F.R., L.L., A.B., M.E., J.R., M.L.S., A.V.W., M.G., A.V.), Max Planck Research Group for Neuroanatomy & Connectivity (N.M., D.S.M.), and Nuclear Magnetic Resonance Group (K.M.), Max Planck Institute for Human Cognitive and Brain Sciences; International Max Planck Research School NeuroCom (H.L.S., M.U.), Leipzig; MindBrainBody Institute at Berlin School of Mind and Brain (D.K., A.B., M.E., M.G., A.V.), Charité & Humboldt Universität zu Berlin; Lifespan Developmental Neuroscience (A.M.F.R.), Technische Universität Dresden; Leipzig Research Centre for Civilization Diseases (LIFE) (M.L.S., M.G., A.V.), Clinic for Cognitive Neurology (M.L.S., A.V.), and Collaborative Research Centre 1052 'Obesity Mechanisms,' Subproject A1, Faculty of Medicine (F.B., A.V.W., A.V.), University of Leipzig, Germany; Department of Psychology (H.O.-S.), University of Haifa, Israel; and Center for Stroke Research Berlin (A.V.), Charité-Universitätsmedizin Berlin, Germany.

Go to [Neurology.org/N](https://www.neurology.org/N) for full disclosures. Funding information and disclosures deemed relevant by the authors, if any, are provided at the end of the article.

Glossary

AD = Alzheimer disease; ANOVA = analysis of variance; BMI = body mass index; BP = blood pressure; CSFV = cerebrospinal fluid volume; CVD = cerebrovascular disease; DBP = diastolic blood pressure; FA = flip angle; FLAIR = fluid-attenuated inversion recovery; FOV = field of view; FWE = family-wise error; GM = gray matter; GMV = gray matter volume; HTN = hypertension; IBMA = image-based meta-analyses; LIFE Study = Leipzig Research Centre for Civilization Diseases Study; ROI = region of interest; SBP = systolic blood pressure; SDM = seed-based *d* mapping; TE = echo time; TI = inversion time; TIV = total intracranial volume; TR = repetition time; VBM = voxel-based morphometry; WM = white matter; WMH = white matter hyperintensities; WMV = white matter volume.



NPub.org/875914 doi: 10.1212/WNL.000000000000694
Copyright © 2019 American Academy of Neurology

Neurology®

Hypertension (HTN) is highly prevalent and the leading single risk factor for global disease burden and overall health loss.^{1,2} The risk for insidious brain damage and symptomatic cerebrovascular disease (CVD) (e.g., stroke and vascular dementia) multiplies with manifestation of HTN.³ Midlife HTN is a major risk factor for late-life cognitive decline and has been associated with risk for dementia, including late-onset Alzheimer disease (AD).³⁻⁵

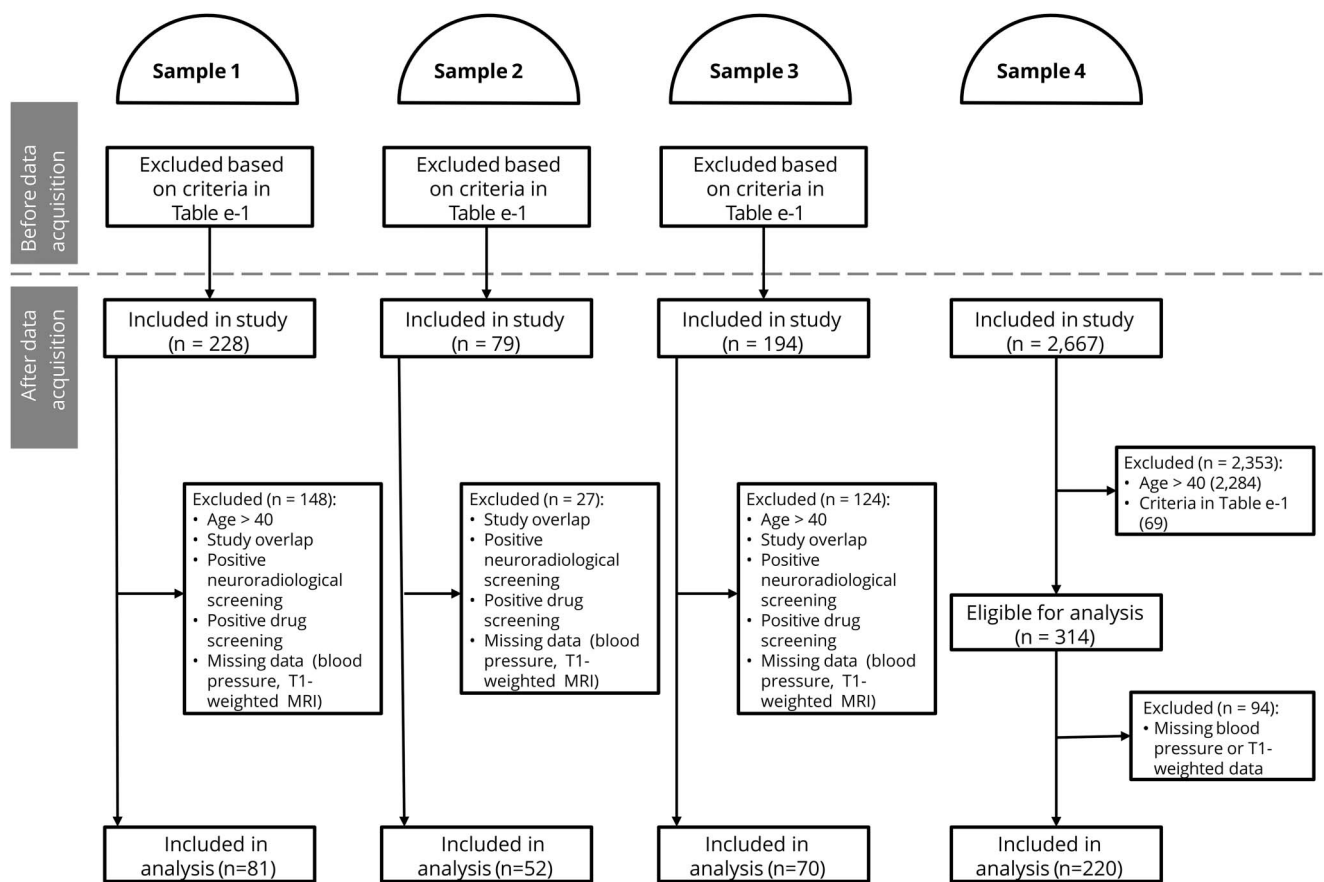
Importantly, HTN is also related to subclinical functional^{6,7} and structural⁵⁻¹⁴ brain changes, or asymptomatic CVD, including brain volume reductions in the medial temporal and frontal lobes.^{5,6,9-11,15} Hippocampal volumes, in particular, have been consistently associated with HTN-related reductions.^{5,9,10,15} Furthermore, computational anatomy has been employed to detect subtle cerebral changes, such as microstructural white matter (WM) alterations¹³ or reductions in regional gray matter

(GM),^{5,11} in middle-aged and older adults with elevated blood pressure (BP).

Recent statements suggest that symptomatic clinical disease, resulting from elevated BP, could be prevented by avoiding primary BP elevations and subclinical target organ damage (including brain damage) in early adulthood and middle age.^{3,16,17} However, effects of elevated BP on adult brains before the age of 40 are unclear. Preliminary evidence from 32 young, normotensive adults showed that BP reactivity correlated with lower amygdala volume.¹⁸

This study aimed to investigate if subtle structural brain changes occur in early adulthood (<40 years) at sub-hypertensive BP levels. We hypothesized that higher BP would relate to lower regional GM volume (GMV) and that this would predominantly affect frontal and medial temporal lobes, including amygdala and hippocampus.

Figure 1 Flow chart with inclusion procedure for the 4 samples



Sample 1: Leipzig Study for Mind–Body–Emotion Interactions. Sample 2: Neural Consequences of Stress Study. Sample 3: Neuroanatomy and Connectivity Protocol. Sample 4: Leipzig Research Centre for Civilization Diseases (MRI subcohort).

Methods

We applied voxel-based morphometry^{19,20} (VBM) to 4 previously unpublished independent datasets including young adults aged between 19 and 40 years without previous diagnosis of HTN or any other severe, chronic, or acute disease. Results from each dataset were combined in image-based meta-analyses (IBMA) for well-powered, cumulative evaluation of findings across study differences (i.e., recruitment procedure, inclusion criteria, and data acquisition, figure 1 and table e-1, doi.org/10.1101/239160).

Participants

We included cross-sectional data of 423 young participants from 4 samples. The samples were drawn from larger studies that were conducted in Leipzig, Germany, between 2010 and 2015: (1) Leipzig Study for Mind–Body–Emotion Interactions (Babayan et al., under review), (2) Neural Consequences of Stress Study (Reinelt et al., in preparation), (3) Neuroanatomy and Connectivity Protocol,²¹ and (4) Leipzig Research Centre for Civilization Diseases Study (LIFE Study).²²

The objective of study 1 was to cross-sectionally investigate mind–brain–body–emotion interactions in a younger (20–35 years) and an older (59–77 years) group of 228 healthy volunteers. Study 2 aimed to investigate neural correlates of acute psychosocial stress in 79 young (18–35 years), healthy, non-smoking men. The study protocol for the baseline assessment of participants in study 2 was adapted from the protocol in study 1. In study 3, 194 healthy volunteers between 20 and 75 years of age participated in 1 session of MRI and completed an extensive assessment of cognitive and personality measures. This dataset aimed to relate intrinsic functional brain connectivity with cognitive faculties, self-generated mental experience, and personality features. Together, studies 1–3 constitute the MPI-Leipzig Mind–Brain–Body database. Study 4 (LIFE Study) is a population-based dataset in Leipzig, Germany, with the objective to investigate the development of major modern diseases. Overall, 10,000 participants were randomly drawn from the local population, of whom 2,667 underwent MRI and detailed screening. With dementia being one of the key scientific topics in this study, most participants in the MRI subcohort were adults older than 60 years. The exact inclusion procedure and numbers for the current investigation are

Table 1 Characteristics by blood pressure (BP) category

	Total	Category 1	Category 2	Category 3	Category 4	p Value	Pairwise comparisons
No. (%)	423 (100)	175 (41)	121 (29)	80 (19)	47 (11)		
Women, n (%)	177 (42)	117 (67)	40 (33)	11 (14)	9 (19)	^a	2, ^a 3, ^a 4 ^a
Age, y, mean (SD)	27.66 (5.27)	27.61 (5.53)	27.30 (4.95)	28.01 (5.24)	28.21 (5.23)		
Range, y, min-max	19-40	19-40	20-40	20-40	20-39		
SBP, mm Hg, mean (SD)	123.2 (12.19)	111.91 (5.44)	123.99 (3.62)	134.57 (3.48)	143.56 (7.76)	^a	2 ^a 3, ^a 4 ^a
DBP, mm Hg, mean (SD)	73.38 (8.49)	67.67 (5.81)	73.64 (5.77)	78.79 (6.46)	84.75 (8.26)	^a	2, ^a 3, ^a 4 ^a
Body mass index, kg/m², mean (SD)	23.48 (3.25)	22.60 (2.74)	23.45 (3.23)	24.22 (3.42)	25.59 (3.62)	^a	2, ^b 3, ^c 4 ^a
Missing values, n (%)	13 (3)	5 (3)	4 (3)	1 (1)	3 (6)		
Range, kg/m², min-max	17.96-36.93						
Smoking status, n (%)							
Nonsmoker	273 (65)	113 (65)	78 (64)	53 (66)	29 (62)		
Occasional smoker	57 (13)	23 (13)	17 (14)	13 (16)	4 (9)		
Smoker	73 (17)	29 (17)	21 (17)	13 (16)	10 (21)		
Missing values	20 (5)	10 (6)	5 (4)	1 (1)	4 (9)		
Fazekas score, n (%)							
0	303 (72)	123 (70)	85 (70)	59 (74)	36 (77)		
1	72 (17)	39 (22)	16 (13)	10 (13)	7 (15)		
2	0 (0)	0 (0)	0 (0)	0 (0)	0 (0)		
3	0 (0)	0 (0)	0 (0)	0 (0)	0 (0)		
Missing values	48 (11)	13 (7)	20 (17)	11 (14)	4 (9)		
Total intracranial volume, mL, mean (SD)	1,450.05 (137.39)	1,400.49 (127.47)	1,457.43 (142.07)	1,508.05 (116.23)	1,516.90 (126.29)		
Gray matter volume, mL, mean (SD)	777.41 (88.69)	748.55 (79.50)	784.29 (90.41)	809.72 (87.36)	812.16 (86.47)		
White matter volume, mL, mean (SD)	449.79 (55.74)	435.84 (53.56)	452.75 (55.93)	464.19 (53.34)	469.58 (55.52)		
CSF volume, mL, mean (SD)	222.86 (56.60)	216.09 (54.57)	220.40 (59.53)	234.14 (54.14)	235.16 (57.34)		
Hippocampal volume, left, mL, mean (SD)	3.90 (0.45)	3.77 (0.41)	3.93 (0.46)	4.06 (0.43)	4.09 (0.43)		
Hippocampal volume, right, mL, mean (SD)	3.97 (0.43)	3.83 (0.40)	4.00 (0.44)	4.12 (0.40)	4.14 (0.39)		
Amygdalar volume, left, mL, mean (SD)	1.68 (0.19)	1.62 (0.18)	1.68 (0.19)	1.75 (0.18)	1.75 (0.18)		
Amygdalar volume, right, mL, mean (SD)	1.50 (0.16)	1.45 (0.15)	1.51 (0.17)	1.56 (0.16)	1.57 (0.15)		

Abbreviations: DBP = diastolic blood pressure; SBP = systolic blood pressure.

The p Value column specifies significant results of comparisons between BP categories: empty cells = $p > 0.05$.

The Pairwise comparisons column specifies significant post hoc comparisons for: 2 = category 1 vs 2, 3 = category 1 vs 3, 4 = category 1 vs 4. ^a $p < 0.001$; ^b $p < 0.05$; ^c $p < 0.01$.

Definition of BP categories: category 1, SBP <120 mm Hg and DBP <80 mm Hg; category 2, SBP 120-129 mm Hg or DBP 80-84 mm Hg; category 3, SBP 130-139 mm Hg or DBP 85-89 mm Hg; and category 4, SBP ≥140 mm Hg or DBP ≥90 mm Hg.

Table 2 Characteristics by sample

	Total	Sample 1	Sample 2	Sample 3	Sample 4	p Value	Pairwise comparisons
No.	423	81	52	70	220		
Women, n (%)	177 (42)	37 (46)	0 (0)	43 (61)	97 (44)	^a	1 vs 2, ^a 2 vs 3, ^a 2 vs 4, ^a 3 vs 4 ^b
Age, y, mean (SD)	27.66 (5.27)	24.36 (3.07)	25.77 (2.44)	26.54 (4.82)	29.69 (5.65)	^a	1 vs 3, ^b 1 vs 4, ^a 2 vs 4, ^a 3 vs 4 ^a
Range, y, min-max	19-40	20-35	21-31	20-40	19-40		
SBP, mm Hg, mean (SD)	123.2 (12.19)	121.8 (12.02)	128.4 (9.80)	128.4 (12.16)	120.8 (11.95)	^a	1 vs 2, ^c 1 vs 3, ^a 2 vs 4, ^a 3 vs 4 ^a
DBP, mm Hg, mean (SD)	73.38 (8.49)	73.27 (6.77)	75.68 (8.03)	79.91 (7.65)	70.80 (8.20)	^a	1 vs 3, ^a 1 vs 4, ^b 2 vs 3, ^c 2 vs 4, ^a 3 vs 4 ^a
BP category, n (%)						^a	1 vs 2, ^b 1 vs 3, ^c 2 vs 4, ^a 3 vs 4 ^a
Category 1 (SBP <120 mm Hg and DBP <80 mm Hg)	175 (41)	38 (47)	10 (19)	15 (21)	112 (51)		
Category 2 (SBP 120-129 mm Hg or DBP 80-84 mm Hg)	121 (29)	23 (28)	21 (40)	19 (27)	58 (26)		
Category 3 (SBP 130-139 mm Hg or DBP 85-89 mm Hg)	80 (19)	13 (16)	12 (23)	21 (30)	34 (15)		
Category 4 (SBP ≥140 mm Hg or DBP ≥90 mm Hg)	47 (11)	7 (9)	9 (17)	15 (21)	16 (7)		
Body mass index, kg/m², mean (SD)	23.48 (3.25)	23.14 (3.06)	23.02 (2.47)	23.17 (3.58)	23.79 (3.38)		
Missing values, n (%)	13 (3)	0 (0)	0 (0)	12 (17)	1 (0)		
Range, kg/m², min-max	17.96-36.93	18.0-34.5	17.96-28.85	18.1-36.88	18.55-36.93		
Smoking status, n (%)						^a	1 vs 2, ^a 1 vs 4, ^a 2 vs 3, ^a 2 vs 4, ^a 3 vs 4 ^b
Nonsmoker	273 (65)	57 (70)	52 (100)	40 (57)	124 (56)		
Occasional smoker	57 (13)	16 (20)	0 (0)	11 (16)	30 (14)		
Smoker	73 (17)	5 (6)	0 (0)	6 (9)	62 (28)		
Missing values	20 (5)	3 (4)	0 (0)	13 (19)	4 (2)		
Fazekas score, n (%)							
0	303 (72)	60 (74)	15 (29)	49 (70)	179 (81)		
1	72 (17)	14 (17)	4 (8)	16 (23)	38 (17)		
2	0 (0)	0 (0)	0 (0)	0 (0)	0 (0)		
3	0 (0)	0 (0)	0 (0)	0 (0)	0 (0)		
Missing values	48 (11)	7 (9)	33 (63)	5 (7)	3 (1)		
Total intracranial volume, mL, mean (SD)	1,450.05 (137.39)	1,448.41 (138.07)	1,553.45 (100.05)	1,424.99 (127.14)	1,434.19 (137.82)	^a	1 vs 2, ^a 2 vs 3, ^a 2 vs 4 ^a
Gray matter volume, mL, mean (SD)	777.41 (88.69)	829.38 (74.94)	880.24 (59.62)	805.25 (64.19)	725.11 (66.89)	^a	1 vs 2, ^a 1 vs 3, ^b 1 vs 4, ^a 2 vs 3, ^a 2 vs 4, ^a 3 vs 4 ^a
White matter volume, mL, mean (SD)	449.79 (55.74)	430.85 (49.28)	467.25 (40.38)	420.51 (46.23)	461.95 (58.48)	^a	1 vs 2, ^a 1 vs 4, ^a 2 vs 3, ^a 3 vs 4 ^a
CSF volume, mL, mean (SD)	222.86 (56.60)	188.19 (42.88)	205.97 (36.83)	199.22 (48.70)	247.13 (56.18)	^a	1 vs 4, ^a 2 vs 4, ^a 3 vs 4 ^a
Hippocampal volume, left, mL, mean (SD)	3.90 (0.45)	4.17 (0.39)	4.42 (0.33)	4.03 (0.35)	3.65 (0.32)	^a	1 vs 2, ^a 1 vs 3, ^b 1 vs 4, ^a 2 vs 3, ^a 2 vs 4, ^a 3 vs 4 ^a

Continued

Table 2 Characteristics by sample (continued)

	Total	Sample 1	Sample 2	Sample 3	Sample 4	p Value	Pairwise comparisons
Hippocampal volume, right, mL, mean (SD)	3.97 (0.43)	4.20 (0.37)	4.43 (0.36)	4.06 (0.36)	3.74 (0.33)	^a	1 vs 2, ^a 1 vs 3, ^a 1 vs 4, ^a 2 vs 3, ^a 2 vs 4, ^a 3 vs 4 ^a
Amygdalar volume, left, mL, mean (SD)	1.68 (0.19)	1.77 (0.18)	1.88 (0.14)	1.71 (0.17)	1.58 (0.15)	^a	1 vs 2, ^a 1 vs 3, ^b 1 vs 4, ^a 2 vs 3, ^a 2 vs 4, ^a 3 vs 4 ^a
Amygdalar volume, right, mL, mean (SD)	1.50 (0.16)	1.58 (0.16)	1.67 (0.14)	1.53 (0.14)	1.43 (0.13)	^a	1 vs 2, ^a 1 vs 3, ^b 1 vs 4, ^a 2 vs 3, ^a 2 vs 4, ^a 3 vs 4 ^a

Abbreviations: BP = blood pressure; DBP = diastolic blood pressure; SBP = systolic blood pressure.

The p Value column specifies significant results of comparisons between samples: empty cells = $p > 0.05$.

The Pairwise comparisons column specifies significant post hoc comparisons between samples: ^a $p < 0.001$, ^b $p < 0.05$, ^c $p < 0.01$.

depicted in figure 1. Inclusion criteria for our study were age between 19 and 40 years, availability of high-resolution structural T1-weighted MRI, and ≥ 1 BP measurements. Participants were excluded in case of previously diagnosed HTN, intake of antihypertensive drugs, or severe diseases (table e-1, doi.org/10.1101/239160).

Standard protocol approvals, registrations, and patient consents

The studies were in agreement with the Declaration of Helsinki and approved by the ethics committee of the medical faculty at the University of Leipzig, Germany (ethics reference numbers: study 1: 154/13-ff; study 2: 385/14-ff; study 3: 097/15-ff; study 4: 263-2009-14122009). Before entering the studies, participants gave written informed consent.

BP measurements

Systolic BP (SBP) and diastolic BP (DBP) were measured at varying times of day using an automatic oscillometric BP monitor (OMRON M500 [samples 1–3], 705IT [sample 4], OMRON Medizintechnik, Mannheim, Germany) after a seated resting period of 5 minutes. In sample 1, 3 measurements were taken from participants' left arms on 3 separate occasions within 2 weeks. In sample 2, 2 measurements were taken from participants' left arms on 2 separate occasions on the same day. In sample 3, BP was measured once before participants underwent MRI. In sample 4, the procedure consisted of 3 consecutive BP measurements, taken from the right arm in intervals of 3 minutes. In each sample, all available measurements per participant were averaged to 1 SBP and 1 DBP value. These averages were used for classification of BP.

Neuroimaging

MRI was performed at the same 3T MAGNETOM Verio Scanner (Siemens, Erlangen, Germany) for all studies with a 32-channel head coil. Whole-brain 3D T1-weighted volumes with a resolution of 1 mm isotropic were acquired for the assessment of brain structure. T1-weighted images in sample 4 were acquired with a standard magnetization-prepared rapid gradient echo protocol (inversion time [TI] 900 ms, repetition time [TR] 2,300 ms, echo time [TE] 2.98 ms, flip angle

[FA] 9°, field of view [FOV] 256 × 240 × 176 mm³, voxel size 1 × 1 × 1 mm³), while T1-weighted images in samples 1–3 resulted from an MP2RAGE protocol (TI1 700 ms, TI2 2,500 ms, TR 5,000 ms, TE 2.92 ms, FA1 4°, FA2 5°, FOV 256 × 240 × 176 mm³, voxel size 1 × 1 × 1 mm³). GM and WM contrast are comparable for the 2 sequence protocols,^{1,2} but additional preprocessing steps were performed for MP2RAGE T1-weighted images (e-Methods, doi.org/10.1101/239160). Fluid-attenuated inversion recovery (FLAIR) images were acquired in all samples for radiologic examination for incidental findings and for Fazekas scale ratings for WM hyperintensities (WMH) (tables 1 and 2).

Data processing and statistical analysis

Details on all analysis methods can be found in the e-Methods (doi.org/10.1101/239160).

BP classification

For statistical analyses, all available BP measurements per participant were averaged to 1 mean SBP and DBP, respectively. Based on these averages, we categorized BP according to the European guidelines for the management of arterial hypertension²³: category 1 (SBP <120 mm Hg and DBP <80 mm Hg), category 2 (SBP 120–129 mm Hg or DBP 80–84 mm Hg), category 3 (SBP 130–139 mm Hg or DBP 85–89 mm Hg), and category 4 (SBP ≥ 140 mm Hg or DBP ≥ 90 mm Hg).

VBM: Association of regional GMV and BP within each sample

For each of the 4 samples, 3T high-resolution T1-weighted 3D whole-brain images were processed using VBM and the diffeomorphic anatomical registration using the exponentiated lie algebra (DARTEL) method^{19,20} within SPM12. Voxel-wise general linear models were performed to relate BP and GMV within each sample: we tested for a continuous relationship between GMV and SBP or DBP, in separate models, with a multiple linear regression *t* contrast. The overall effect of BP category on GMV was tested with an analysis of variance (ANOVA) *F* contrast. To assess differences in GMV between BP categories, the following pairwise *t* comparisons were tested: (1) category 4 vs category 1, (2) category 3 vs category 1, (3) category 2 vs category 1. All

analyses included total intracranial volume (TIV), sex, and age as covariates. The influence of body mass index (BMI) did not significantly contribute to the models and was thus not included as covariate in the analyses. We considered a sample eligible for image-based meta-analysis if its *F* contrast effects exceeded an uncorrected peak-level threshold of $p < 0.001$. Effects within each sample were explored at cluster-level $p < 0.05$ with family-wise error (FWE) correction for multiple comparisons.

IBMA: Association of regional GMV and BP across samples

To evaluate cumulative results from all samples while considering their heterogeneities, we combined the VBM outcome of each sample in IBMA. Meta-analyses were performed on the unthresholded *t* maps with seed-based *d* mapping (SDM) software using default parameters.²⁴ Statistical significance of mean effect size maps was evaluated according to validated thresholds of high meta-analytic sensitivity and specificity²⁴: voxel threshold = $p < 0.005$, peak height threshold = $\text{SDM-Z} > 1.0$, and cluster extent threshold = $k \geq 10$ voxels.

Exploratory IBMA for positive associations were performed in analogy to negative associations as described above.

IBMA of regions of interest (ROI): Association of regional GMV and BP across samples in hippocampus and amygdala

We performed IBMA within atlas-defined masks to test if regional bilateral hippocampal and amygdalar volumes related

to SBP, DBP, and BP categories, respectively. The statistical thresholds were defined as $p < 0.05$, $\text{SDM-Z} > 1.0$, and $k \geq 1$ voxel.

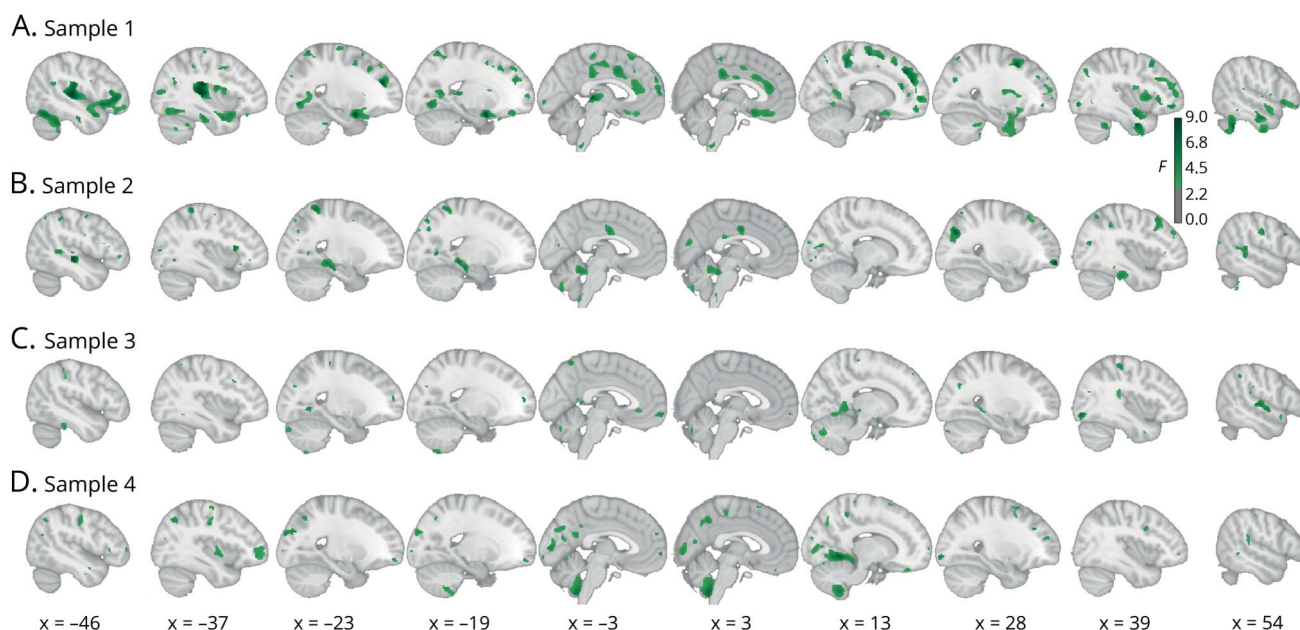
Volumetry: Association of total brain volumes and BP within the pooled sample

In addition to VBM and IBMA, we explored if total brain volumes (average volume over all voxels within a region) differed between BP categories. Specifically, we tested if estimated TIV, total GM volume, total WM volume (WMV), total amount of WMH, total CSF volume (CSFV), total left and right hippocampal, and amygdalar volume differed between BP categories. WMH was assessed by Fazekas scale ratings from FLAIR images.²⁵ For these comparisons within the total sample, we defined correlation models (for SBP and DBP as independent variable, respectively) and ANOVA models for BP category as independent variable. The models included the respective volume as dependent variable, as well as TIV (where applicable), sex, age, and sample (where applicable) as covariates. We considered *p* values < 0.05 as significant. The analyses were performed with R (3.2.3, R Core Team, 2015, Vienna, Austria; R-project.org/).

Data sharing

Results (i.e., unthresholded whole-brain statistical maps) from VBM analyses of each sample and from all IBMAs can be found online in the public repository NeuroVault for detailed, interactive inspection (neurovault.org/collections/FDWHFSYZ/). Raw data of samples 1–3 are available from openfmri.org/dataset/ds000221/.

Figure 2 Associations between gray matter (GM) volume and blood pressure (BP) within each sample



Sagittal views of voxel-based morphometry *F* contrast results show the overall effect of BP category on GM volume per sample. Each sample is represented in 1 row (A–D). Slice order runs from left hemisphere (left-hand side of the plot) to right hemisphere (right-hand side of the plot). Color bars represent *F* values (uncorrected). Sample sizes: sample 1, $n = 81$; sample 2, $n = 52$; sample 3, $n = 70$; sample 4, $n = 220$. 3D volumetric results of these analyses can be inspected in detail on neurovault.org/collections/FDWHFSYZ/.

Results

Sample characteristics

The characteristics of the total sample by BP category are reported in table 1. The total sample included 423 participants between 19 and 40 years of age, of whom 177 were women (42%). Mean (SD) age was 27.7 (5.3) years. SBP, DBP, and BMI differed between BP categories (all $p < 0.001$). An effect of sex yielded that men were more frequent in higher BP categories (all $p < 0.001$).

Table 2 shows differences in characteristics among the 4 included samples. The samples differed in almost all characteristic variables, specifically regarding sex, age, SBP, DBP, smoking status, and brain volumes (all $p < 0.001$).

VBM: Association of regional GMV and BP within each sample

Figure 2 shows differences in regional GMV between BP categories for each of the 4 samples tested with an ANOVA F contrast. Results show significant clusters of various extents that were distributed heterogeneously between the samples. Exploration of sample-specific effects showed a cluster in the left posterior insula for the F contrast (peak Montreal Neurological Institute coordinates $[-38, -24, 24]$, $F = 11.35$, cluster size $k = 1,239$) as well as clusters in left inferior frontal gyrus ($[-42, 34, 0]$, $T = 4.99$, $k = 2,039$) and in right anterior cingulate cortex ($[14, 34, 14]$, $T = 4.44$, $k = 2,086$) for the contrast BP category 4 < 1 in sample 1. In sample 2, the contrast BP category 4 < 1 yielded a cluster in left planum polare ($[-44, -22, -3]$, $T = 10.70$, $k = 1,151$) and the contrast BP category 2 < 1 yielded a trend for a cluster in left middle temporal gyrus ($p_{FWE} = 0.059$, $[-54, -28, -9]$, $T = 5.41$, $k = 683$). Furthermore, higher DBP was associated with a cluster of lower GMV in left middle temporal gyrus in sample 2 ($[-57, -45, 6]$, $T = 6.03$, $k = 1,180$). All other comparisons yielded no suprathreshold voxels (all $p_{FWE} > 0.05$). The statistical maps for sample-specific effects can be inspected on NeuroVault.

IBMA: Association of regional GMV and BP across samples

Meta-analytic parametric relations between lower GMV and higher BP

As expected, increases in systolic and diastolic BP were associated with lower GMV. Specifically, higher SBP related to lower GMV in right paracentral/cingulate areas ($[8, -30, 56]$, $SDM-Z = -3.859$, $k = 288$), bilateral inferior frontal gyrus (IFG, left: $[-40, 30, 0]$, $SDM-Z = -3.590$, $k = 49$; right: $[-40, 30, 0]$, $SDM-Z = -3.394$, $k = 16$), bilateral sensorimotor cortex (left: $[-58, -20, 24]$, $SDM-Z = -3.290$, $k = 146$; right: $[48, 0, 48]$, $SDM-Z = -3.196$, $k = 127$), bilateral superior temporal gyrus (left: $[-52, -10, 6]$, $SDM-Z = -3.268$, $k = 78$; right: $[64, -42, 12]$, $SDM-Z = -3.192$, $k = 42$), bilateral cuneus cortex (left: $[-8, -76, 18]$, $SDM-Z = -3.019$, $k = 27$; right: $[10, -68, 26]$, $SDM-Z = -2.937$, $k = 18$), and right thalamus ($[8, -28, 2]$, $SDM-Z = -2.977$, $k = 45$; figure 3A and table 3). Increases in DBP were related to lower GMV in bilateral

anterior insula (left: $[-36, 26, 6]$, $SDM-Z = -3.876$, $k = 266$; right: $[34, 10, 8]$, $SDM-Z = -3.139$, $k = 100$), frontal regions ($[-26, 24, 54]$, $SDM-Z = -3.820$, $k = 62$), right midcingulate cortex ($[4, -34, 50]$, $SDM-Z = -3.545$, $k = 246$), bilateral inferior parietal areas (left: $[-46, -26, 48]$, $SDM-Z = -3.239$, $k = 59$; right: $[44, -44, 50]$, $SDM-Z = -3.188$, $k = 18$), and right superior temporal gyrus ($[60, 2, -12]$, $SDM-Z = -2.991$, $k = 35$; figure 3B and table 3).

Meta-analytic differences in regional GMV between BP categories

Meta-analytic results for category 4 (highest BP) compared to category 1 (lowest BP) yielded lower regional GMV in frontal, cerebellar, parietal, occipital, and cingulate regions (figure 3C). Table 3 describes the specific regions with lower GMV, including bilateral IFG (left: $[-52, -28, 12]$, $SDM-Z = -3.473$, $k = 107$; right: $[40, 30, 26]$, $SDM-Z = -3.093$, $k = 10$), right midcingulate cortex ($[12, -42, 48]$, $SDM-Z = -2.854$, $k = 11$), and right precuneus ($[10, -52, 18]$, $SDM-Z = -2.836$, $k = 21$).

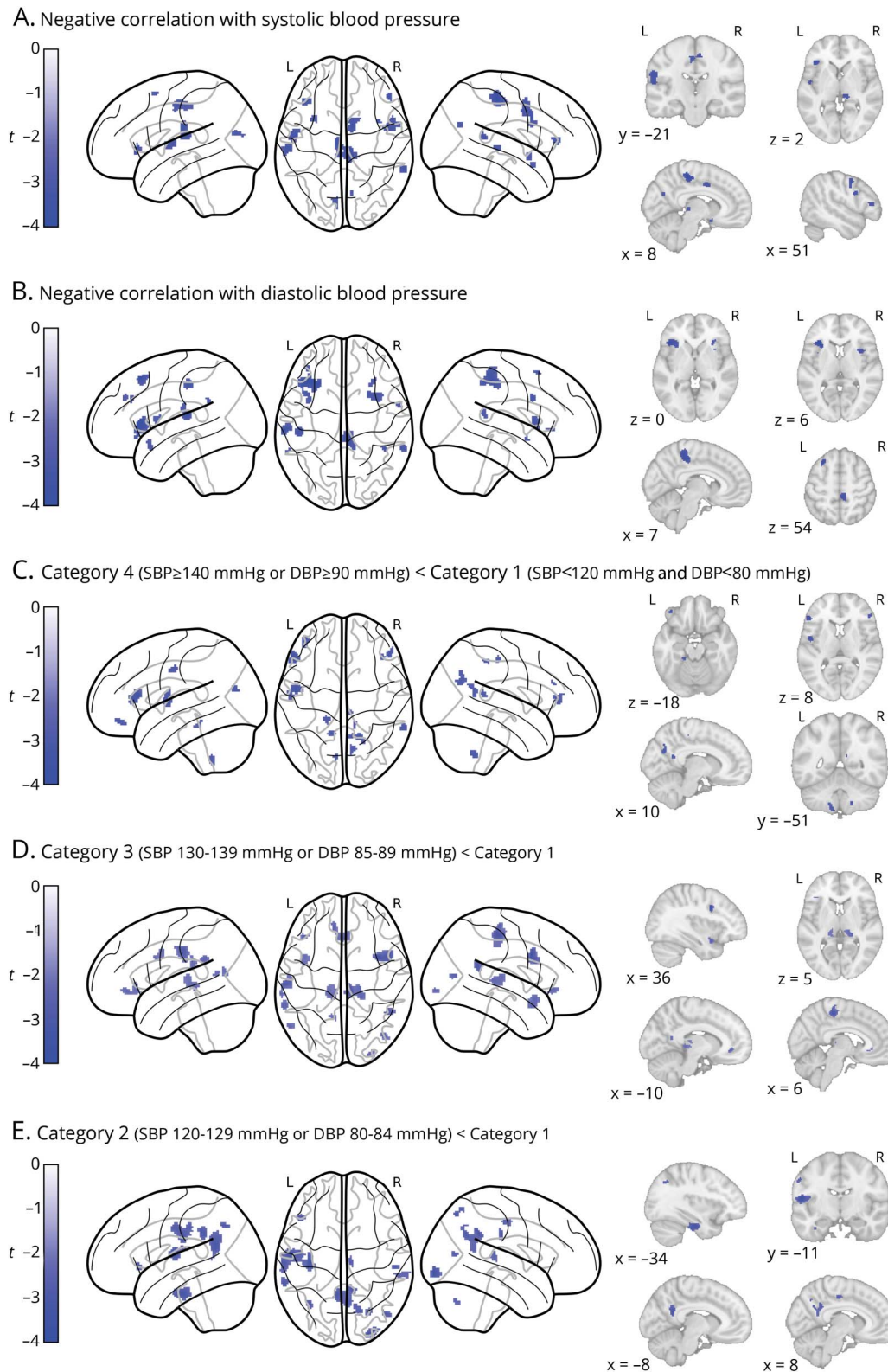
We also compared GMV of individuals at subhypertensive levels (category 3 and 2, respectively) to GMV of individuals in category 1. Figure 3D shows meta-analysis results for the comparison between category 3 and category 1. Compared to category 1, category 3 was associated with lower GMV in bilateral IFG (left: $[-40, 30, 2]$, $SDM-Z = -2.598$, $k = 24$; right: $[36, 6, 34]$, $SDM-Z = -3.474$, $k = 179$), sensorimotor cortices (left: $[-60, -20, 36]$, $SDM-Z = -2.857$, $k = 205$; right: $[6, -28, 54]$, $SDM-Z = -3.119$, $k = 179$), bilateral middle temporal gyrus (left: $[-56, -64, 16]$, $SDM-Z = -2.222$, $k = 28$; right: $[48, -50, 20]$, $SDM-Z = -3.119$, $k = 179$), right insula ($[36, 8, -18]$, $SDM-Z = -2.523$, $k = 123$), right occipital regions ($[42, -74, 12]$, $SDM-Z = -2.454$, $k = 25$), left parietal ($[-60, -20, 36]$, $SDM-Z = -2.857$, $k = 205$), bilateral thalamus (left: $[-12, -32, 0]$, $SDM-Z = -2.264$, $k = 133$; right: $[20, -32, 6]$, $SDM-Z = -2.384$, $k = 133$), left anterior cingulate cortex ($[-10, 36, -6]$, $SDM-Z = -2.384$, $k = 102$), and left precuneus ($[-12, -54, 14]$, $SDM-Z = -2.187$, $k = 20$; table 3).

Figure 3E illustrates brain regions that yielded lower meta-analytic GMV comparing category 2 to category 1. These include left frontal regions ($[-54, -10, 14]$, $SDM-Z = -3.407$, $k = 230$), right inferior occipital gyrus ($[30, -96, -8]$, $SDM-Z = -3.290$, $k = 102$), bilateral temporal regions (left: $[-34, -16, -30]$, $SDM-Z = -3.164$, $k = 133$; right: $[46, -74, 12]$, $SDM-Z = -2.734$, $k = 26$), left precuneus ($[-8, -54, 22]$, $SDM-Z = -3.084$, $k = 433$), and inferior parietal regions (supramarginal, $[54, -24, 32]$, $SDM-Z = -2.968$, $k = 31$, and angular gyri, $[-36, -64, 42]$, $SDM-Z = -2.827$, $k = 30$), as well as midcingulate cortex ($[8, -18, 46]$, $SDM-Z = -2.647$, $k = 32$; table 3).

Meta-analytic differences in regional hippocampal and amygdalar volumes between BP categories

In this IBMA ROI comparison, higher SBP was correlated with lower bilateral posterior medial hippocampal volume (figure 4). Higher DBP was correlated with lower left hippocampal volume and lower right anterior hippocampal

Figure 3 Meta-analytic differences in gray matter (GM) volume between blood pressure (BP) categories



Glass brain views of image-based meta-analysis results for the BP category contrasts of interest with relevant slice views below (A-E). A and B depict associations between higher systolic BP (SBP)/diastolic BP (DBP), respectively, and lower GM volume, i.e., negative correlations. Blue clusters indicate meta-analytic GM volume differences for the given contrast at a voxel threshold of $p < 0.005$ with peak height threshold of seed-based d mapping (SDM) $Z < -1.0$ and cluster extent threshold of $k \geq 10$ (validated for high meta-analytic sensitivity and specificity²⁴). Color bars represent SDM- Z values. 3D volumetric results of these analyses can be inspected in detail on neurovault.org/collections/FDWHFSYZ/. L = left hemisphere; R = right hemisphere.

Table 3 Image-based meta-analysis results of regional gray matter (GM) volume differences associated with blood pressure (BP)

	MNI, x,y,z	SDM-Z	<i>P</i> Value	<i>k</i>	Peak description	<i>Q</i>	<i>I</i> ²
Negative correlation with SBP	8,-30,56	-3.859	0.000	288	Right paracentral lobule	0.000	0.0
	-40,30,0	-3.590	0.000	49	Left inferior frontal gyrus (pars triangularis)	0.053	0.0
	36,6,34	-3.394	0.000	16	Right inferior frontal gyrus (pars opercularis)	0.000	0.0
	10,2,40	-3.325	0.001	45	Right midcingulate cortex	0.000	0.0
	-58,-20,24	-3.290	0.001	146	Left postcentral gyrus	0.000	0.0
	-52,-10,6	-3.268	0.001	78	Left superior temporal gyrus	0.000	0.0
	48,32,10	-3.204	0.001	27	Right inferior frontal gyrus (pars triangularis)	0.000	0.0
	48,0,48	-3.196	0.001	127	Right precentral gyrus	0.000	0.0
	64,-42,12	-3.192	0.001	42	Right superior temporal gyrus	0.000	0.0
	6,8,-18	-3.110	0.001	40	Right subgenual cingulate cortex	0.000	0.0
	50,8,28	-3.045	0.002	26	Right inferior frontal gyrus (pars opercularis)	0.000	0.0
	-8,-76,18	-3.019	0.002	27	Left cuneus cortex	0.175	0.0
	8,-28,2	-2.977	0.002	45	Right thalamus	0.000	0.0
	10,-68,26	-2.937	0.002	18	Right cuneus cortex	0.000	0.0
	58,4,-8	-2.934	0.002	32	Right temporal pole	0.000	0.0
	-28,10,60	-2.896	0.003	19	Left middle frontal gyrus	0.000	0.0
	-52,-12,42	-2.860	0.003	10	Left postcentral gyrus	0.116	0.0
Negative correlation with DBP	-36,26,6	-3.876	0.000	266	Left insula	0.000	0.0
	-26,24,54	-3.820	0.000	62	Left middle frontal gyrus	0.000	0.0
	4,-34,50	-3.545	0.000	246	Right midcingulate cortex	0.000	0.0
	-60,-24,14	-3.462	0.000	90	Left supramarginal gyrus	0.000	0.0
	-46,-26,48	-3.239	0.001	59	Left inferior parietal lobule	0.000	0.0
	44,-44,50	-3.188	0.001	18	Right inferior parietal lobule	0.257	0.0
	36,8,32	-3.180	0.001	25	Right inferior frontal gyrus (pars opercularis)	0.000	0.0
	34,10,8	-3.139	0.001	100	Right insula	0.000	0.0
	28,14,60	-3.069	0.001	12	Right superior frontal gyrus	0.000	0.0
	62,-44,16	-2.991	0.002	35	Right superior temporal gyrus	0.000	0.0
	-38,14,-20	-2.983	0.002	30	Left temporal pole	0.000	0.0
	60,2,-12	-2.862	0.003	13	Right superior temporal gyrus	0.189	0.0
	-38,40,32	-2.845	0.003	14	Left middle frontal gyrus	0.000	0.0
	30,28,0	-2.796	0.003	14	Right insula	0.000	0.0
	-36,8,10	-2.788	0.003	24	Left insula	0.000	0.0
	-58,-46,30	-2.750	0.004	11	Left supramarginal gyrus	0.000	0.0
	-34,32,32	-2.734	0.004	11	Left middle frontal gyrus	0.201	0.0

Continued

Table 3 Image-based meta-analysis results of regional gray matter (GM) volume differences associated with blood pressure (BP) (continued)

	MNI, x,y,z	SDM-Z	P Value	k	Peak description	Q	I ²
Category 4 (SBP ≥140 mm Hg or DBP ≥90 mm Hg) < category 1 (SBP <120 mm Hg and DBP <80 mm Hg)	-52,28,12	-3.473	0.000	107	Left inferior frontal gyrus (pars triangularis)	0.324	3.9
	-48,-4,4	-3.322	0.000	93	Left rolandic operculum	0.297	1.8
	18,-52,-48	-3.097	0.001	40	Right cerebellum, hemispheric lobule VIIIb	0.000	0.0
	40,30,26	-3.093	0.001	10	Right inferior frontal gyrus (pars triangularis)	0.000	0.0
	48,32,10	-3.064	0.001	48	Right inferior frontal gyrus (pars triangularis)	0.000	0.0
	-38,48,-16	-3.014	0.001	40	Left inferior frontal gyrus (pars orbitalis)	0.000	0.0
	-54,-12,42	-2.940	0.002	30	Left postcentral gyrus	0.000	0.0
	-8,-76,18	-2.936	0.002	14	Left cuneus	0.000	0.0
	-16,-36,-18	-2.872	0.002	24	Left cerebellum, hemispheric lobule V	0.000	0.0
	12,-42,48	-2.854	0.002	11	Right midcingulate cortex	0.000	0.0
	-12,-50,-56	-2.849	0.002	30	Left cerebellum, hemispheric lobule IX	0.325	4.0
	10,-52,18	-2.836	0.002	21	Right precuneus	0.000	0.0
	64,-44,14	-2.824	0.002	26	Right superior temporal gyrus	0.000	0.0
	10,-66,28	-2.821	0.002	56	Right precuneus	0.000	0.0
	6,-28,50	-2.792	0.003	16	Right midcingulate cortex	0.025	0.0
	18,-54,22	-2.765	0.003	15	Right precuneus	0.000	0.0
Category 3 (SBP 130-139 mm Hg or DBP 85-89 mm Hg) < category 1	36,6,34	-3.474	0.000	179	Right inferior frontal gyrus (pars opercularis)	0.000	0.0
	6,-28,54	-3.119	0.000	179	Right posterior-medial frontal gyrus	0.127	0.0
	48,-50,20	-2.917	0.000	74	Right middle temporal gyrus	0.000	0.0
	-60,-20,36	-2.857	0.000	205	Left postcentral gyrus	0.000	0.0
	-40,30,2	-2.598	0.000	24	Left inferior frontal gyrus (pars triangularis)	0.000	0.0
	36,8,-18	-2.523	0.001	123	NA (Right insula)	0.000	0.0
	42,-74,12	-2.454	0.001	25	Right middle occipital gyrus	0.200	0.0
	-62,-42,28	-2.433	0.001	41	Left supramarginal gyrus	0.000	0.0
	20,-32,6	-2.384	0.001	133	Right thalamus	0.000	0.0
	-10,36,-6	-2.384	0.001	102	Left anterior cingulate cortex	0.000	0.0
	28,-94,-4	-2.373	0.001	14	Right inferior occipital gyrus	0.000	0.0
	-12,-32,0	-2.264	0.002	133	Left thalamus	0.237	0.0
	-56,-64,16	-2.222	0.002	28	Left middle temporal gyrus	0.050	0.0
	-40,8,30	-2.197	0.002	82	Left precentral gyrus	0.000	0.0
	-12,-54,14	-2.187	0.002	20	Left precuneus	0.000	0.0
Category 2 (SBP 120-129 mm Hg or DBP 80-84 mm Hg) < category 1	-54,-10,14	-3.407	0.000	230	Left rolandic operculum	0.016	0.0
	30,-96,-8	-3.290	0.000	102	Right inferior occipital gyrus	0.038	0.0

Continued

Table 3 Image-based meta-analysis results of regional gray matter (GM) volume differences associated with blood pressure (BP) (continued)

MNI, x,y,z	SDM-Z	<i>p</i> Value	<i>k</i>	Peak description	<i>Q</i>	<i>I</i> ²
-34,-16,-30	-3.164	0.000	133	Left fusiform gyrus	0.000	0.0
-8,-54,22	-3.084	0.000	433	Left precuneus	0.000	0.0
54,-24,32	-2.968	0.000	31	Right supramarginal gyrus	0.019	0.0
-46,28,0	-2.942	0.000	41	Left inferior frontal gyrus (pars triangularis)	0.000	0.0
-64,-20,30	-2.939	0.000	227	Left postcentral gyrus	0.000	0.0
-62,-42,34	-2.876	0.000	68	Left supramarginal gyrus	0.000	0.0
-36,-64,42	-2.827	0.001	30	Left angular gyrus	0.000	0.0
18,-72,54	-2.804	0.001	40	Right superior parietal lobule	0.083	0.0
46,-74,12	-2.734	0.001	26	Right middle temporal gyrus	0.000	0.0
8,-18,46	-2.647	0.001	32	Right midcingulate cortex	0.000	0.0
56,-32,12	-2.470	0.002	52	Right superior temporal gyrus	0.000	0.0
28,-72,-38	-2.413	0.002	23	Right cerebellum, crus I	0.000	0.0
-62,-22,-30	-2.403	0.003	11	NA (Left inferior temporal gyrus)	0.000	0.0

Abbreviations: DBP = diastolic blood pressure; MNI = Montreal Neurologic Institute; SBP = systolic blood pressure; SDM = seed-based *d* mapping. Image-based meta-analysis results of significant clusters yielding lower GM volume for the respective contrast of interest. Columns indicate cluster-specific MNI coordinates of peak voxels, meta-analytic SDM-Z-value, meta-analytic *p* value, number of voxels in cluster, and anatomical label of the peak voxel. Anatomical labels were assigned using SPM's Anatomy toolbox. *Q* and *I*² are measures of meta-analytic heterogeneity. Voxel threshold was set to *p* < 0.005, peak height threshold was set to SDM-Z > 1.0, and cluster extent threshold was set to *k* ≥ 10 voxels as recommended in reference 24. Final voxel size was 2 × 2 × 2 mm³.

volume. Furthermore, all higher BP categories were associated with lower regional hippocampal volume when compared to the lowest BP category 1 (figure 4). Compared to category 1, BP category 4 was predominantly associated with lower left medial posterior hippocampus volume and category 3 with lower bilateral posterior and left medial hippocampus volume across samples. Lower volume comparing categories 2 and 1 was predominantly located in left lateral anterior hippocampus. Category 4 vs category 1 and the associations with higher SBP and DBP also yielded significantly lower regional volume in bilateral amygdala, respectively. Effect sizes highly varied across samples (figure 4).

Meta-analytic relations between higher GMV and higher BP

Exploratory analyses also revealed associations between higher BP and higher GMV (figure e-1, table e-2, doi.org/10.1101/239160, and NeuroVault maps). However, the cumulative positive effects are comparably weaker than the cumulative negative results (table 3, negative: 17 out of 34 clusters from parametric analyses with SDM-Z > 3.0; positive: 0 out of 28 clusters from parametric analyses with SDM-Z > 3.0), they show greater heterogeneity across studies (negative: maximum *I*² = 4.0; positive: maximum *I*² = 56.3), and they seem to appear primarily in regions where standard preprocessing of brain tissue is suboptimal (e.g., in cerebellum/inferior occipital regions²⁶). We therefore regard these findings as questionable overall. By also providing the results as statistical

maps on NeuroVault, future investigations can use the data for reliability analyses of potential positive associations.

Volumetry in pooled sample: Association of total brain volumes and BP

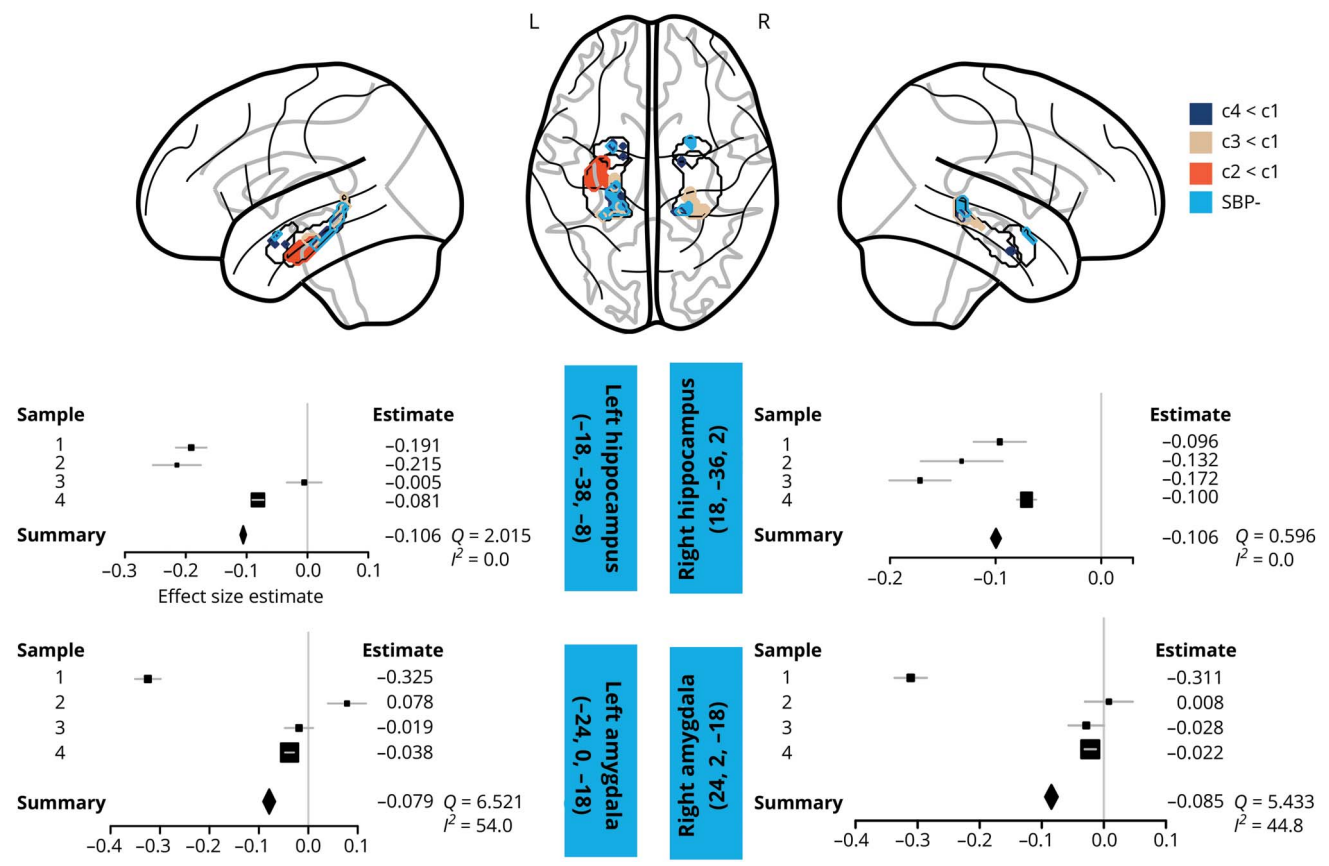
All associations of volumetric brain measures (TIV, total GMV, total WMV, total CSFV, total hippocampal, total amygdalar volume, and total WMH) with SBP or DBP in the correlation models, or with BP categories in the ANOVA models, were below the statistical threshold (all *p* > 0.05, table 1).

Discussion

In this image-based meta-analysis of 4 previously unpublished independent samples, we found that elevated, subhypertensive BP was correlated with lower GMV in several brain regions, including parietal, frontal, and subcortical structures in young adults (<40 years). These regions are consistent with the lower regional GMV observed in middle-aged and older individuals with HTN.^{5,6,9-11,15} Our results show that BP-associated GM alterations emerge earlier in adulthood than previously assumed and continuously across the range of BP.

Interestingly, we found that BP was associated with lower hippocampal volume. In older individuals, the hippocampal formation and surrounding structures are known to be affected by HTN.^{5,8-10,15} In a meta-analytic evaluation of HTN

Figure 4 Meta-analytic differences in volumes of hippocampus and amygdala (region of interest [ROI] analysis)



Upper part of plot: Glass brain views of image-based meta-analysis ROI results for the BP category contrasts of interest in bilateral hippocampus and amygdala masks. Voxel threshold was set to $p < 0.05$ with a peak height threshold of seed-based d mapping (SDM) $Z < -1.0$ and a cluster extent threshold of $k \geq 1$. Lower part of plot: Exemplary forest plots of sample-specific peak voxels' effect sizes for the negative correlation with systolic BP (SBP) in the respective ROI. The box sizes are determined by each sample's weight. Light blue boxes include ROI name and Montreal Neurologic Institute coordinates of the peak voxel. Q and I^2 are measures of meta-analytic heterogeneity. Definition of BP categories: category 1 (SBP < 120 mm Hg and diastolic BP [DBP] < 80 mm Hg), category 2 (SBP 120–129 mm Hg or DBP 80–84 mm Hg), category 3 (SBP 130–139 mm Hg or DBP 85–89 mm Hg), and category 4 (SBP \geq 140 mm Hg or DBP \geq 90 mm Hg). L = left hemisphere; R = right hemisphere; SBP- = negative correlation with SBP.

effects on total GMV and on hippocampal volume, lower volumes across studies were only consistently found for the hippocampus.¹⁵ In analogy to those findings, our results showed that hippocampal volume was affected by higher BP in a considerably younger sample. It should be mentioned that the effects in hippocampus only exceeded statistical thresholds in ROI analyses, similar to previous reports of lower hippocampal volume in older samples with manifest HTN that were all ROI-based.^{5,9,10,15} As potential pathophysiologic explanations, it has been proposed that medial temporal (and frontal regions) might be especially sensitive to effects of pulsation, hypoperfusion, and ischemia, which often result from increasing pressure.^{3,15}

We furthermore observed correlations between lower amygdalar and thalamic volumes and higher BP, notably already below levels that are currently regarded as hypertensive. Amygdalar and thalamic nuclei are substantially involved in BP regulation as they receive baroreceptor afferent signals via the brainstem and mesencephalic nuclei, relaying these signals

to primary cortical regions of viscerosensory integration, such as anterior cingulate cortex and insula.²⁷ It has been shown that lower amygdalar volume correlates with increased BP reactivity during cognitive demand among young normotensive adults.¹⁸ Previous studies have reported lower thalamic volume in HTN,⁵ heart failure,²⁸ asymptomatic carotid stenosis,²⁹ and aging.³⁰ Higher systolic BP has also been related to higher mean diffusivity of WM thalamic radiations.¹³ Our results are in line with accumulating evidence of amygdalar and thalamic involvement in cardiovascular (dys-) regulation but may also reflect early pathology in these regions. For example, occurrence of neurofibrillary tangles in thalamus has also been reported in the earliest stages of AD neuropathology.³¹

Beyond subcortical structures, we found lower volumes in cortical regions: cingulate volume and insular volume were markedly lower with higher DBP in the meta-analysis results and in the individual analyses of sample 1. As noted above, these regions constitute primary cortical sites of afferent viscerosensory integration and modulate homeostasis via

efficients to brainstem nuclei.²⁷ Lesions in cingulate cortex and insula result in altered cardiovascular regulation, increased sympathetic tone,^{32,33} and myocardial injury.³⁴ Both regions are also critical for the appraisal and regulation of emotion and stress.²⁷ Thus, structural alterations in these regions may contribute to insidious BP elevations via sympathetic pathways.

Frontal and parietal volumes were affected in all our statistical comparisons. The precuneus cortex, especially, was associated with lower GMV in BP categories 4, 3, and 2 compared to category 1. Our results of lower BP-related GMV in regions such as hippocampal, frontal, and parietal areas highlight specific brain regions that are known to be vulnerable to putative vascular or neurodegenerative damage mechanisms.^{5,6,8–11,15,35} Raised midlife BP is not only known to be a major risk factor for vascular dementia, but some reports suggest a link between HTN and AD-type pathophysiology.^{3,4} For example, in neuropathologic studies, raised midlife BP has been associated with lower post-mortem brain weight, increased numbers of hippocampal neurofibrillary tangles, and higher numbers of hippocampal and cortical neuritic plaques.⁸ Similarly, a potential pathophysiologic link between HTN and AD has been supported by noninvasive MRI studies: regions referred to as AD-signature regions (including inferior parietal, precuneus cortices, and medial temporal structures) have been associated with cortical thinning years before clinical AD symptoms arise³⁵ and with brain volume reductions predicted by increasing BP from middle to older age.⁵ In light of these previous results, our findings of lower BP-related GMV in AD signature regions may be indicative of a link to AD pathology at an even earlier age; however, this cannot be causally inferred from our cross-sectional data. In the study by Power et al.,⁵ BP also predicted volume loss in non-AD-typical brain regions, such as frontal lobe and subcortical GM, which may relate to other (than AD-related) pathophysiologic mechanisms. A similar pattern seems to be reflected in our findings of lower GMV related to higher BP in non-AD-typical regions.

Some previous studies did not find relations between HTN and lower brain volumes, but associated HTN with other forms of structural or functional brain alterations, such as WM injury³⁶ or reduced cerebral perfusion.³⁷ A key aspect of diverging results is the heterogeneity of methods used to assess brain volumes. Earlier investigations of BP effects on brain tissues have applied manual or automated volumetric methods to quantify total brain volumes in preselected ROIs.^{9,10,12} The focus of this study was to employ computational anatomy methods to assess regional GM differences across the whole brain. We found significant differences between BP groups using VBM but not in the analysis of total brain volumes. This supports the view that VBM is a sensitive measure to quantify regional morphologic differences³⁸ that might be undetected from the analysis of total brain volumes alone. In addition, we employed random-effects IBMA, which results in effects that are consistent across studies and that may otherwise be

neglected at subthreshold. Investigating effects of BP on regional vs total brain volumes at all stages of health and disease thus warrants further research with standardized methods to identify neuropathologic mechanisms.

Our data, however, do not allow inference on causality between lower brain volumes and HTN, which likely involves complex interactions of different pathophysiologic mechanisms that still need to be fully elucidated. It is assumed that vascular stiffness, endothelial failure, and a dysfunctional blood–brain barrier are precursors of cerebral small and large vessel disease that reduce cerebral blood flow, disturb autor-regulatory adjustment, and decrease vasomotor reactivity, which may impair perivascular central nervous waste clearance systems.³ These mechanisms have also been suggested to potentially underlie the epidemiologic connection between vascular risk factors, such as HTN, and AD.³ The similarities between our findings and AD signature regions (see above) would also be consistent with this putative link. Consequently, demyelination, apoptosis, and intoxication of neurons and glial cells, as well as GM and WM necrosis, accumulate and may be reflected in neuroimaging on a macroscopic scale. Lower GMV assessed by VBM, as reported in our study, can thus arise from neuronal loss, but also from alterations of glial cells or composition of microstructural or metabolic tissue properties.³⁹ Our findings point to an early effect of such mechanisms on GM integrity, which is present in the absence of overt disease, such as HTN, and in young age. Indicators of early atherosclerosis in major peripheral arteries can already be detected in youth.⁴⁰ Recently, arterial stiffness has also been associated with WM and GM alterations among adults between 24 and 76 years of age.⁴¹ Thus, early and subtle vascular changes, deficient cerebral perfusion, and impaired perivascular clearance systems may initiate and sustain neuropathology from early to late adulthood.

The cross-sectional design of our 4 study samples limits the interpretation frame for the results presented. Causality between BP and potential brain damage cannot be assessed with these data but is crucial for implications of early signs of cerebrovascular disease. Furthermore, the study samples differed regarding recruitment, sex distribution, sample size, prevalence of high BP, and data acquisition methods (BP and MRI), which might not represent the general population or standard acquisition protocols: similar to German prevalence,⁴² men had higher BP in our study. We thus included sex as covariate in all our analyses to adjust for sex effects. We did not perform separate analyses for men and women given that 1 of the 4 samples included only men. However, the topic of sex differences in brain structure related to BP is an interesting open question for future investigations. In sample 3, only 1 BP measurement was recorded, which could be biased due to white coat hypertension or BP variability. Practice guidelines recommend an average of ≥ 2 seated readings obtained on ≥ 2 occasions to provide a more accurate estimate of an individual's BP level.^{23,43,44} By combining the samples in random-effects IBMA, we considered the limitations of each sample

and accounted for within- and between-sample heterogeneity and evaluated effects cumulatively. Moreover, this approach enabled us to investigate the expected small effects of BP-related GM alterations in a well-powered total sample of over 400 young adults. To further ensure that the results are not substantially influenced by the heterogeneity of BP measurements across studies, we recalculated the parametric SBP analysis (figure 3A) with only the first SBP reading in each study. The results of this additional analysis are strikingly similar to the results reported here (table e-3 and figure e-2, doi.org/10.1101/239160). HTN is also the most important risk factor for WM damage^{3,12} and subclinical WM injury in relation to elevated BP levels has recently been reported in 19- to 63-year-old adults.¹³ As our study included only GM measures, we cannot assess mediating effects of WM injury on GMV differences. We did not observe any significant differences in Fazekas scores for WMH between BP categories, likely due to their lower sensitivity and poorer specificity as a proxy for vascular disease in a subclinical sample of young adults with (mostly) normal BP.

Our study shows that BP-related brain alterations may occur in early adulthood and at BP levels below current thresholds for manifest HTN. Contrary to assumptions that BP-related brain damage arises over years of manifest disease, our data suggest that subtle pressure-related GM alterations can be observed in young adults without previously diagnosed HTN. Considering our results, large-scale cohort studies should investigate whether subhypertensive BP and related brain changes in early adulthood increase the risk for subsequent development of CVD later in life. Gaining insights whether and how the brain is globally affected by vascular changes or if these are specific to susceptible regions could help identify neuroimaging biomarkers for the earliest stages of CVD. Such data would provide evidence for future guidelines to formulate informed recommendations for BP management in young adults, which are critical for the prevention of CVD. Lifestyle interventions and neurobehavioral therapy have recently been suggested to benefit CVD prevention.¹⁷ Our results highlight the importance of taking BP levels as a continuous measure into consideration, which could help initiate such early preventive measures.

Author contributions

Study concept and design: H.L. Schaare, Dr. Villringer. Statistical analysis: H.L. Schaare. Acquisition or interpretation of data: all authors. Drafting of the manuscript: H.L. Schaare, Dr. Villringer. Critical revision of the manuscript: all authors.

Acknowledgment

The authors thank the volunteers for their participation and the researchers, technicians, and students who planned, collected, entered, and curated data used in this article.

Study funding

Max Planck Institute for Human Cognitive and Brain Sciences.

Disclosure

The authors report no disclosures relevant to the manuscript. Go to Neurology.org/N for full disclosures.

Publication history

Received by *Neurology* January 9, 2018. Accepted in final form October 15, 2018.

References

1. Forouzanfar MH, Afshin A, Alexander LT, et al. Global, regional, and national comparative risk assessment of 79 behavioural, environmental and occupational, and metabolic risks or clusters of risks, 1990–2015: a systematic analysis for the Global Burden of Disease Study 2015. *Lancet* 2016;388:1659–1724.
2. NCD Risk Factor Collaboration (NCD-RisC). Worldwide trends in blood pressure from 1975 to 2015: a pooled analysis of 1479 population-based measurement studies with 19.1 million participants. *Lancet* 2016;389:634–647.
3. Iadecola C, Yaffe K, Biller J, et al. Impact of hypertension on cognitive function: a scientific statement from the American Heart Association. *Hypertension* 2016;68:e67–e94.
4. Norton S, Matthews FE, Barnes DE, Yaffe K, Brayne C. Potential for primary prevention of Alzheimer's disease: an analysis of population-based data. *Lancet Neurol* 2014;13:788–794.
5. Power MC, Schneider ALC, Wruck L, et al. Life-course blood pressure in relation to brain volumes. *Alzheimers Dement* 2016;12:890–899.
6. Hajjar L, Zhao P, Alsop D, et al. Association of blood pressure elevation and nocturnal dipping with brain atrophy, perfusion and functional measures in stroke and non-stroke individuals. *Am J Hypertens* 2010;23:17–23.
7. Launer LJ, Lewis CE, Schreiner PJ, et al. Vascular factors and multiple measures of early brain health: CARDIA brain MRI study. *PLoS One* 2015;10:e0122138.
8. Petrovitch H, White LR, Zmirlilian G, et al. Midlife blood pressure and neuritic plaques, neurofibrillary tangles, and brain weight at death: the HAAS. *Neurobiol Aging* 2000;21:57–62.
9. den Heijer T, Launer LJ, Prins ND, et al. Association between blood pressure, white matter lesions, and atrophy of the medial temporal lobe. *Neurology* 2005;64:263–267.
10. Raz N, Lindenberger U, Rodrigue KM, et al. Regional brain changes in aging healthy adults: general trends, individual differences and modifiers. *Cereb Cortex* 2005;15:1676–1689.
11. Leritz EC, Salat DH, Williams VJ, et al. Thickness of the human cerebral cortex is associated with metrics of cerebrovascular health in a normative sample of community dwelling older adults. *Neuroimage* 2011;54:2659–2671.
12. Debette S, Seshadri S, Beiser A, et al. Midlife vascular risk factor exposure accelerates structural brain aging and cognitive decline. *Neurology* 2011;77:461–468.
13. Maillard P, Seshadri S, Beiser A, et al. Effects of systolic blood pressure on white-matter integrity in young adults in the Framingham Heart Study: a cross-sectional study. *Lancet Neurol* 2012;11:1039–1047.
14. Muller M, Sigurdsson S, Kjartansson O, et al. Joint effect of mid- and late-life blood pressure on the brain: the AGES-Reykjavik study. *Neurology* 2014;82:2187–2195.
15. Beauchet O, Celle S, Roche F, et al. Blood pressure levels and brain volume reduction: a systematic review and meta-analysis. *J Hypertens* 2013;31:1502–1516.
16. Olsen MH, Angell SY, Asma S, et al. A call to action and a lifecourse strategy to address the global burden of raised blood pressure on current and future generations: the Lancet Commission on Hypertension. *Lancet* 2016;388:2665–2712.
17. Grossman DC, Bibbins-Domingo K, Curry SJ, et al. Behavioral counseling to promote a healthful diet and physical activity for cardiovascular disease prevention in adults without cardiovascular risk factors. *JAMA* 2017;318:167.
18. Gianaros PJ, Sheu LK, Matthews KA, Jennings JR, Manuck SB, Hariri AR. Individual differences in stressor-evoked blood pressure reactivity vary with activation, volume, and functional connectivity of the amygdala. *J Neurosci* 2008;28:990–999.
19. Ashburner J, Friston KJ. Voxel-based morphometry: the methods. *Neuroimage* 2000;11:805–821.
20. Ashburner J. A fast diffeomorphic image registration algorithm. *Neuroimage* 2007;38:95–113.
21. Mendes N, Oligschlaeger S, Lauckner ME, et al. A functional connectome phenotyping dataset including cognitive state and personality measures. *bioRxiv* 2017. Available at: biorxiv.org/content/early/2017/07/18/164764. Accessed July 19, 2017.
22. Loeffler M, Engel C, Ahnert P, et al. The LIFE-Adult-Study: objectives and design of a population-based cohort study with 10,000 deeply phenotyped adults in Germany. *BMC Public Health* 2015;15:691.
23. Mancia G, Fagard R, Narkiewicz K, et al. 2013 ESH/ESC Guidelines for the management of arterial hypertension. *Eur Heart J* 2013;34:2159–2219.
24. Radau J, Mataix-Cols D, Phillips ML, et al. A new meta-analytic method for neuroimaging studies that combines reported peak coordinates and statistical parametric maps. *Eur Psychiatry* 2012;27:605–611.
25. Fazekas F, Chawluk J, Alavi A, Hurtig H, Zimmerman R. MR signal abnormalities at 1.5 T in Alzheimer's dementia and normal aging. *Am J Roentgenol* 1987;149:351–356.
26. Diedrichsen J. A spatially unbiased atlas template of the human cerebellum. *Neuroimage* 2006;33:127–138.
27. Critchley HD, Harrison NA. Visceral influences on brain and behavior. *Neuron* 2013;77:624–638.

28. Woo MA, Macey PM, Fonarow GC, Hamilton MA, Harper RM. Regional brain gray matter loss in heart failure. *J Appl Physiol* 2003;95:677–684.
29. Avelar WM, D'Abreu A, Coan AC, et al. Asymptomatic carotid stenosis is associated with gray and white matter damage. *Int J Stroke* 2015;10:1197–1203.
30. Lorio S, Lutti A, Kherif F, et al. Disentangling in vivo the effects of iron content and atrophy on the ageing human brain. *Neuroimage* 2014;103:280–289.
31. Braak H, Braak E. Neuropathological staging of Alzheimer-related changes. *Acta Neuropathol* 1991;82:239–259.
32. Critchley HD, Mathias CJ, Josephs O, et al. Human cingulate cortex and autonomic control: converging neuroimaging and clinical evidence. *Brain* 2003;126:2139–2152.
33. Oppenheimer SM, Kedem G, Martin WM. Left-insular cortex lesions perturb cardiac autonomic tone in humans. *Clin Auton Res* 1996;6:131–140.
34. Krause T, Werner K, Fiebach JB, et al. Stroke in right dorsal anterior insular cortex is related to myocardial injury. *Ann Neurol* 2017;81:502–511.
35. Dickerson BC, Stoub TR, Shah RC, et al. Alzheimer-signature MRI biomarker predicts AD dementia in cognitively normal adults. *Neurology* 2011;76:1395–1402.
36. Allan C, Zsoldos E, Filippini N, et al. Life-time hypertension as a predictor of brain structure in older adults: a prospective cohort study. *Br J Psychiatry* 2015;206:308–315.
37. Muller M, van der Graaf Y, Visseren FL, Vlek AL, Mali WP, Geerlings ML. Blood pressure, cerebral blood flow, and brain volumes: The SMART-MR study. *J Hypertens* 2010;28:1498–1505.
38. Kennedy KM, Erickson KI, Rodrigue KM, et al. Age-related differences in regional brain volumes: a comparison of optimized voxel-based morphometry to manual volumetry. *Neurobiol Aging* 2009;30:1657–1676.
39. Tardif CL, Steele CJ, Lampe L, et al. Investigation of the confounding effects of vasculature and metabolism on computational anatomy studies. *Neuroimage* 2017;149:233–243.
40. Strong JP, Malcom GT, McMahan CA, et al. Prevalence and extent of atherosclerosis in adolescents and young adults. *JAMA* 1999;281:727–735.
41. Maillard P, Mitchell GF, Himali JJ, et al. Effects of arterial stiffness on brain integrity in young adults from the Framingham Heart Study. *Stroke* 2016;47:1030–1036.
42. Neuhauser HK, Adler C, Rosario AS, Diederichs C, Ellert U. Hypertension prevalence, awareness, treatment and control in Germany 1998 and 2008–11. *J Hum Hypertens* 2015;29:1–7.
43. Chobanian A V, Bakris GL, Black HR, et al. Seventh report of the Joint National Committee on Prevention, Detection, Evaluation, and Treatment of High Blood Pressure. *Hypertension* 2003;42:1206–1252.
44. Whelton PK, Carey RM, Aronow WS, et al. 2017 ACC/AHA/AAPA/ABC/ACPM/AGS/APhA/ASH/ASPC/NMA/PCNA guideline for the prevention, detection, evaluation, and management of high blood pressure in adults. *Hypertension* 2018;7:1269–1324.

7.2.4 The Age-Dependent Relationship Between Resting Heart Rate Variability and Functional Brain Connectivity. Kumral et al., NeuroImage (2019)

NeuroImage 185 (2019) 521–533



Contents lists available at ScienceDirect

NeuroImage

journal homepage: www.elsevier.com/locate/neuroimage



The age-dependent relationship between resting heart rate variability and functional brain connectivity



D. Kumral^{a,b,*}, H.L. Schaare^{a,c}, F. Beyer^{a,d}, J. Reinelt^a, M. Uhlig^{a,c}, F. Liem^a, L. Lampe^a, A. Babayan^a, A. Reiter^{a,e}, M. Erbey^b, J. Roebbig^a, M. Loeffler^f, M.L. Schroeter^{a,g,h}, D. Husser^h, A.V. Witte^a, A. Villringer^{a,b,d,i,j}, M. Gaebler^{a,b,i}

^a Department of Neurology, Max Planck Institute for Human Cognitive and Brain Sciences, Leipzig, Germany

^b MindBrainBody Institute at the Berlin School of Mind and Brain, Humboldt-Universität zu Berlin, Berlin, Germany

^c International Max Planck Research School NeuroGen, Leipzig, Germany

^d Subprojekt A1, Collaborative Research Centre 1052 "ObesityMechanisms", University of Leipzig, Leipzig, Germany

^e Lifespan Developmental Neuroscience, Technical University of Dresden, Dresden, Germany

^f LIFE – Leipzig Research Center for Civilization Diseases, University of Leipzig, Leipzig, Germany

^g Department of Cognitive Neurology, University of Leipzig, Leipzig, Germany

^h Department of Electrophysiology, Leipzig Heart Centre, University of Leipzig, Leipzig, Germany

ⁱ Center for Stroke Research Berlin, Charité – Universitätsmedizin Berlin, Berlin, Germany

ARTICLE INFO

Keywords

Heart rate variability

Aging

Eigenvector centrality mapping

Brain structure

Voxel-based morphometry

Default mode network

ABSTRACT

Resting heart rate variability (HRV), an index of parasympathetic cardioregulation and an individual trait marker related to mental and physical health, decreases with age. Previous studies have associated resting HRV with structural and functional properties of the brain – mainly in cortical midline and limbic structures. We hypothesized that aging affects the relationship between resting HRV and brain structure and function. In 388 healthy subjects of three age groups (140 younger: 26.0 ± 4.2 years, 119 middle-aged: 46.3 ± 6.2 years, 129 older: 66.9 ± 4.7 years), gray matter volume (GMV, voxel-based morphometry) and resting state functional connectivity (eigenvector centrality mapping and exploratory seed-based functional connectivity) were related to resting HRV, measured as the root mean square of successive differences (RMSSD). Confirming previous findings, resting HRV decreased with age. For HRV-related GMV, there were no statistically significant differences between the age groups, nor similarities across all age groups. In whole-brain functional connectivity analyses, we found an age-dependent association between resting HRV and eigenvector centrality in the bilateral ventromedial prefrontal cortex (vmPPC), driven by the younger adults. Across all age groups, HRV was positively correlated with network centrality in the bilateral posterior cingulate cortex. Seed-based functional connectivity analysis using the vmPPC cluster revealed an HRV-related cortico-cerebellar network in younger but not in middle-aged or older adults. Our results indicate that the decrease of HRV with age is accompanied by changes in functional connectivity along the cortical midline. This extends our knowledge of brain-body interactions and their changes over the lifespan.

1. Introduction

Behavioral and physiological changes that occur with advancing age become manifest in the structure and function of multiple macro- and micro-systems of the human organism (Aking, 2006). Important alterations occur in the cardiovascular and nervous systems, which are coupled to react dynamically to environmental demands (McEwen, 2003). Such adaptations to internal and external challenges, while leaving an imprint on body and brain, underlie healthy aging (Lipnitz and

Goldberger, 1992; Swanik, 1996). They are also reflected in brain-heart interactions – particularly in parasympathetic cardioregulation – that can be measured by resting heart rate variability (HRV).

HRV quantifies variations in the cardiac beat-to-beat (or RR) interval that can be measured by electrocardiogram (ECG). Phasic modulation of heart rate (HR) arises from both branches of the autonomic nervous system, the parasympathetic (PNS) and sympathetic (SNS). The PNS quickly reduces HR while the SNS slowly increases it. Some HRV measures represent parasympathetic (i.e., vagal) influences on the heart more

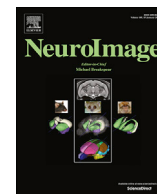
* Corresponding author. Department of Neurology, Max Planck Institute for Human Cognitive and Brain Sciences, Leipzig, Germany.
E-mail address: dkumral@ch.mpg.de (D. Kumral).

<https://doi.org/10.1016/j.neuroimage.2018.10.027>

Received 26 June 2018; Received in revised form 5 October 2018; Accepted 9 October 2018

Available online 10 October 2018

1053-8119/© 2018 Elsevier Inc. All rights reserved.



The age-dependent relationship between resting heart rate variability and functional brain connectivity



D. Kumral^{a,b,*}, H.L. Schaare^{a,c}, F. Beyer^{a,d}, J. Reinelt^a, M. Uhlig^{a,c}, F. Liem^a, L. Lampe^a, A. Babayan^a, A. Reiter^{e,a}, M. Erbey^b, J. Roebbig^a, M. Loeffler^f, M.L. Schroeter^{a,f,g}, D. Husser^h, A.V. Witte^a, A. Villringer^{a,b,d,f,i}, M. Gaebler^{a,b,f}

^a Department of Neurology, Max Planck Institute for Human Cognitive and Brain Sciences, Leipzig, Germany

^b MindBrainBody Institute at the Berlin School of Mind and Brain, Humboldt-Universität zu Berlin, Berlin, Germany

^c International Max Planck Research School NeuroCom, Leipzig, Germany

^d Subproject A1, Collaborative Research Centre 1052 “Obesity Mechanisms”, University of Leipzig, Leipzig, Germany

^e Lifespan Developmental Neuroscience, Technical University of Dresden, Dresden, Germany

^f LIFE – Leipzig Research Center for Civilization Diseases, University of Leipzig, Leipzig, Germany

^g Department of Cognitive Neurology, University of Leipzig, Leipzig, Germany

^h Department of Electrophysiology, Leipzig Heart Centre, University of Leipzig, Leipzig, Germany

ⁱ Center for Stroke Research Berlin, Charité – Universitätsmedizin Berlin, Berlin, Germany

ARTICLE INFO

Keywords:

Heart rate variability

Aging

Eigenvector centrality mapping

Brain structure

Voxel-based morphometry

Default mode network

ABSTRACT

Resting heart rate variability (HRV), an index of parasympathetic cardioregulation and an individual trait marker related to mental and physical health, decreases with age. Previous studies have associated resting HRV with structural and functional properties of the brain – mainly in cortical midline and limbic structures. We hypothesized that aging affects the relationship between resting HRV and brain structure and function. In 388 healthy subjects of three age groups (140 younger: 26.0 ± 4.2 years, 119 middle-aged: 46.3 ± 6.2 years, 129 older: 66.9 ± 4.7 years), gray matter volume (GMV, voxel-based morphometry) and resting state functional connectivity (eigenvector centrality mapping and exploratory seed-based functional connectivity) were related to resting HRV, measured as the root mean square of successive differences (RMSSD). Confirming previous findings, resting HRV decreased with age. For HRV-related GMV, there were no statistically significant differences between the age groups, nor similarities across all age groups. In whole-brain functional connectivity analyses, we found an age-dependent association between resting HRV and eigenvector centrality in the bilateral ventromedial prefrontal cortex (vmPFC), driven by the younger adults. Across all age groups, HRV was positively correlated with network centrality in the bilateral posterior cingulate cortex. Seed-based functional connectivity analysis using the vmPFC cluster revealed an HRV-related cortico-cerebellar network in younger but not in middle-aged or older adults. Our results indicate that the decrease of HRV with age is accompanied by changes in functional connectivity along the cortical midline. This extends our knowledge of brain-body interactions and their changes over the lifespan.

1. Introduction

Behavioral and physiological changes that occur with advancing age become manifest in the structure and function of multiple macro- and micro-systems of the human organism (Arking, 2006). Important alterations occur in the cardiovascular and nervous systems, which are coupled to react dynamically to environmental demands (McEwen, 2003). Such adaptations to internal and external challenges, while leaving an imprint on body and brain, underlie healthy aging (Lipsitz and

Goldberger, 1992; Swank, 1996). They are also reflected in brain-heart interactions – particularly in parasympathetic cardioregulation – that can be measured by resting heart rate variability (HRV).

HRV quantifies variations in the cardiac beat-to-beat (or RR) interval that can be measured by electrocardiogram (ECG). Phasic modulation of heart rate (HR) arises from both branches of the autonomic nervous system, the parasympathetic (PNS) and sympathetic (SNS). The PNS quickly reduces HR while the SNS slowly increases it. Some HRV measures represent parasympathetic (i.e., vagal) influences on the heart more

* Corresponding author. Department of Neurology, Max Planck Institute for Human Cognitive and Brain Sciences, Leipzig, Germany.
E-mail address: dkumral@cbs.mpg.de (D. Kumral).

than others (Thayer and Lane, 2007). HRV, typically acquired at rest, is known to decrease with age (De Meersman and Stein, 2007; Umetani et al., 1998). Preservation of autonomic function, as indexed by relatively increased HRV, has been related to longevity and healthy aging (Zulfikar et al., 2010). Higher HRV has also been associated with better health outcomes (Kemp and Quintana, 2013), for example, with lower risk for cardiovascular diseases (Liao et al., 1997; Thayer et al., 2010) and reduced overall mortality (Buccelletti et al., 2009). In older adults, HRV can indicate inter-individual differences in cognitive performance (Kim et al., 2006; Mahinrad et al., 2016; Zeki Al Hazzouri et al., 2014). Hence, resting HRV could be regarded as a biomarker of healthy aging.

Based on resting state fMRI (i.e., continuous fMRI recordings in the absence of overt task performance or experimental stimulation), spontaneous modulations of the blood oxygenation level dependent (BOLD) signal are used to quantify temporal correlations between brain regions to extract functional connectivity patterns. The number of functional networks in the resting brain is consistent across individuals (Damoiseaux et al., 2006), reliable across time (Shehzad et al., 2009; Zuo et al., 2010), and has been related to inter-individual differences in behavior and cognition (Adelstein et al., 2011; Mennes et al., 2011; Smith et al., 2015). Common ways to examine connectivity patterns of specific brain regions are seed-based functional connectivity analysis (SBCA) or independent component analysis (ICA; Margulies et al., 2010; for a review). Further, graph theory provides a powerful approach to investigate complex brain connectivity patterns (Bullmore and Sporns, 2009; Rubinov and Sporns, 2010). One commonly used measure is eigenvector centrality mapping (ECM). ECM can identify important network nodes (in this case: voxels) based on their functional connectivity (similar to Google's page rank algorithm) without the need to select specific seed regions *a priori* or specify the number of networks/components (Lohmann et al., 2010; Wink et al., 2012). Since ECM focuses on the integration of individual brain regions into the whole brain network, it is a useful whole-brain measure to assess the resting state architecture as it relates to an individual's physiology (García-García et al., 2015; Lohmann et al., 2010), psychology (Koelsch et al., 2013), or health/disease (Binnewijzend et al., 2014; Mueller et al., 2016).

Using such connectivity methods, brain networks associated with autonomic, affective, and cognitive regulation have been identified (Babo-Rebelo et al., 2016; Gould van Praag et al., 2017; Sakaki et al., 2016). One of those is the “central autonomic network” (CAN; Benarroch, 1993), which includes cortical midline structures such as the anterior cingulate cortex (ACC), orbitofrontal cortex (OFC), ventromedial prefrontal cortex (vmPFC), and subcortical areas like the insula, amygdala, and hypothalamus (Beissner et al., 2013; Thayer et al., 2009). With its connections to the sinoatrial node of the heart, via the stellate ganglia and vagus nerve (Beissner et al., 2013; Thayer et al., 2009), the CAN supports visceromotor and neuroendocrine responses that are critical for goal-directed behavior, adaptability, and health (Benarroch, 1993; Hagemann et al., 2003). The “neurovisceral integration model”, a framework to explain individual differences in resting vagal function (Kemp et al., 2017; Thayer et al., 2012), extends the role of the CAN in parasympathetic cardioregulation. According to this model, frontal and midbrain areas interact. In particular, the prefrontal cortex (PFC) inhibits subcortical regions and the ANS. Assuming this close interaction of the brain and the ANS in HR regulation, it has been suggested that inter-individual differences in HRV may reflect structural and functional differences in the brain (Thayer et al., 2012). Indeed, resting HRV has been associated with cortical thickness in the right anterior midcingulate cortex (aMCC) in a young sample (Winkelmann et al., 2017). A similar association between cortical thickness and the (rostral anterior) cingulate cortex was found in Yoo et al. (2017), which also included older subjects. The main result of the latter study was an age-invariant association between resting HRV and cortical thickness in ventral brain areas like the lateral OFC (Yoo et al., 2017) (Carnevali et al., 2018 for a review). Another recent study in individuals between 20 and 60 years found a negative correlation between resting HRV and gray matter volume

(GMV) in limbic structures such as the insula, amygdala, and parahippocampal gyrus (Wei et al., 2018). Similar brain regions have also been related to HRV in functional neuroimaging studies (Holzman and Bridgett, 2017; Mather and Thayer, 2018; Thayer et al., 2012); both task-based (e.g., BOLD: Critchley et al., 2000; regional cerebral blood flow; rCBF: Gianaros et al., 2004; meta-analyses: Beissner et al., 2013; Thayer et al., 2012) and under resting state conditions (Chang et al., 2013; Jennings et al., 2016; Sakaki et al., 2016). In these studies, activation and connectivity in the medial prefrontal cortex (mPFC), ACC, and posterior cingulate cortex (PCC) have most consistently been associated with HRV and parasympathetic cardioregulation.

Here, we investigated brain-heart interactions across the adult lifespan by combining measures of brain structure and function with the assessment of resting HRV. So far, the only fMRI study that investigated heart-brain interactions on functional connectivity across the adult lifespan included 17 younger and 18 older subjects and restricted their analyses to *a priori* defined regions-of-interest (Sakaki et al., 2016). Across all subjects, higher HRV was related to stronger functional connectivity between the right amygdala and medial prefrontal regions, while age group differences were found in HRV-related connectivity between the right amygdala and lateral prefrontal regions. The main aims of this study were to examine (i) the relationship between resting HRV, brain structure, and functional connectivity as well as (ii) its dependence on age in a large sample of healthy adults across the lifespan. Based on structural and functional findings (reviewed above), we hypothesized that the neural correlates of resting HRV are age-dependent. To detect HRV-related structural alterations, we used voxel-based morphometry (VBM) (Ashburner and Friston, 2000). To assess HRV-related changes in the functional architecture across the whole brain, we used ECM as a data-driven approach, which allows the characterization of whole-brain network architecture without requiring *a priori* assumptions (Lohmann et al., 2010). To further explore age-dependent ECM-derived whole-brain connectivity patterns, we also implemented an exploratory SBCA (for more details see *Methods*).

2. Methods

2.1. Participants

Data from two studies were used: (I) the “Leipzig Research Centre for Civilization Diseases” (LIFE; Loeffler et al., 2015) and (II) the “Leipzig Study for Mind-Body-Emotion Interactions” (LEMON; Babayan et al. in revision).

LIFE is a large population-based cohort study from Leipzig, Germany (Loeffler et al., 2015). From the sample of LIFE subjects with MRI data ($n = 2667$), we selected healthy subjects between the ages of 20 and 80 years. We applied strict exclusion criteria in three categories: i) health-related criteria; participants were excluded if they reported any medication intake except vitamin food supplements, any past or present cardiovascular health problems, diagnoses, or surgeries, any other medical history and/or diagnosis, in a medical interview. ii) ECG-related criteria (see details on ECG acquisition below); if a subject had more than one ECG recording, we used the first acquired ECG file that was collected on the same day as the MRI acquisition. Otherwise, we selected the ECG recording that was temporally closest to MRI acquisition. Regarding data quality, we excluded data with unrepairable signal artifacts or problems regarding R-peak detection. We also omitted data with any abnormal ECG signal (e.g., supraventricular extrasystoles) after visual inspection as well as subjects with extreme HRV values based on Tukey's (1977) criterion of 3 interquartile ranges (IQR) above the LIFE sample median ($N = 14$, Median: 30.13, IQR: 29.76). iii) MRI-related criteria; we excluded subjects with incidental findings (e.g., brain tumor, multiple sclerosis, or stroke) on T1-weighted and/or fluid-attenuated inversion recovery (FLAIR) images. We further excluded subjects based on rs-fMRI quality assessment, for example with faulty preprocessing (e.g., during denoising) or excessive head motion (criterion: mean framewise

displacement (FD) > 0.6 mm; Power et al., 2015, 2012).

LEMON is a cross-sectional sample of healthy younger and older subjects from Leipzig, Germany, who had never participated in another “psychological or MRI research”-related study, did not report any neurological disorders, head injury, any medication affecting the cardiovascular and/or central nervous system, alcohol or other substance abuse, hypertension, pregnancy, claustrophobia, chemotherapy and malignant diseases, current and/or previous psychiatric disease (Babayán et al. in revision). The LEMON sample comprised 171 eligible subjects divided into two age groups (young: 20–35 years, old: 59–77 years). Similar to the exclusion criteria mentioned above, subjects with incomplete data (N = 38), incidental findings in MRI (FLAIR, T2-weighted, T1-weighted, SWI) (N = 7), or psychoactive drug intake (e.g., tetrahydrocannabinol) determined by urine test (N = 9) were excluded. Two subjects were discarded due to the HRV outlier criterion mentioned above (LEMON sample Median: 40.62, IQR: 39.82) and five subjects due to excessive head motion (mean FD > 0.6 mm; Power et al., 2015, 2012). To increase the statistical power and the comparability, we pooled the two samples and divided them into three age groups: young (20–35 years from LIFE and LEMON), middle-aged (35–60 years from LIFE), and old (60–80 years from LIFE and LEMON). Details are provided in Table 1. The participant characteristics separately for each sample and comparing the samples can be found in Supplementary Tables 1–5.

All participants provided written informed consent approved by the ethics committee of the medical faculty at the University of Leipzig, Germany. Both studies were in agreement with the Declaration of Helsinki.

2.2. ECG collection and HRV analysis

LIFE sample. Ten seconds of a standard medical 12-lead resting ECG were acquired using a Page-Writer TC50 ECG system (Philips Medical Systems, Amsterdam, Netherlands) in supine position. The subjects did not receive an explicit instruction before the ECG acquisition. We used lead I (from Einthoven's triangle) for the analysis. R-peaks were automatically detected using the findpeaks function in Matlab 9 (The Math-Works, Inc., Natick, Massachusetts) or Kubios 2.2 (Tarvainen et al., 2014). The ECG data for each subject was manually checked for physiological or computational artifacts like supraventricular extrasystoles or faulty peak detection, respectively. From RR interval time series (i.e., tachograms), we calculated the root mean square of successive differences (RMSSD) of adjacent RR intervals (Task Force of the European Society of Cardiology and the North American Society of Pacing Electrophysiology, 1996; Munoz et al., 2015; Nussinovitch et al., 2011a, 2011b).

LEMON sample. Four minutes of resting ECG were acquired using a Biopac MP35 amplifier with the acquisition software AcqKnowledge

version 4.0 (Biopac Systems Inc., http://www.biopac.com, Goleta, CA, USA) and three disposable electrodes on the thorax: the reference electrode was attached near the right collarbone, the measuring electrode on the left-hand side of the body on the same level as the 10th rib, and the ground electrode on the right hip bone. The subjects were instructed to think about daily routines, relax, and breathe at a comfortable rate in sitting position. The peak detection and RMSSD calculation were performed using Kubios 2.2 (Tarvainen et al., 2014).

RMSSD values of our sample were natural log-transformed to obtain normally distributed data (Shapiro-Wilk tests; W = 0.99, p = 0.12). In the following, log-transformed RMSSD will be referred to as “HRV”.

2.3. MRI acquisition

Brain imaging for both datasets was performed on the same 3T Siemens Magnetom Verio MR scanner (Siemens Medical Systems, Erlangen, Germany) with a standard 32-channel head coil. In both samples, subjects were instructed to keep their eyes open and not to fall asleep during the acquisition period.

LIFE sample. The structural T1-weighted images were acquired using a generalized auto-calibrating partially parallel acquisition technique (Griswold et al., 2002) and the Alzheimer's Disease Neuroimaging Initiative standard protocol with the following parameters: inversion time (TI) = 900 ms, repetition time (TR) = 2.3 ms, echo time (TE) = 2.98 ms, flip angle (FA) = 9°, band width = 240 Hz/pixel, field of view (FOV) = 256 × 240 × 176 mm³, voxel size = 1 × 1 × 1 mm³, no interpolation. T2*-weighted functional images were acquired using an echo-planar-imaging (EPI) sequence with the following parameters: TR = 2000 ms, TE = 30 ms, FA = 90°, FOV = 192 × 192 × 144 mm³, voxel size = 3 mm × 3 mm, slice thickness = 4 mm, slice gap = 0.8 mm, 300 vol, duration = 10.04 min. A gradient echo field map with the sample geometry was used for distortion correction (TR = 488 ms, TE 1 = 5.19 ms, TE 2 = 7.65 ms).

LEMON sample. The structural image was recorded using an MP2RAGE sequence (Marques et al., 2010) with the following parameters: TI 1 = 700 ms, TI 2 = 2500 ms, TR = 5000 ms, TE = 2.92 ms, FA 1 = 4°, FA 2 = 5°, band width = 240 Hz/pixel, FOV = 256 × 240 × 176 mm³, voxel size = 1 × 1 × 1 mm³. The functional images were acquired using a T2*-weighted multiband EPI sequence with the following parameters: TR = 1400 ms, TE = 30 ms, FA = 69°, FOV = 202 mm, voxel size = 2.3 × 2.3 × 2.3 mm³, slice thickness = 2.3 mm, slice gap = 0.67 mm, 657 vol, multiband acceleration factor = 4, duration = 15.30 min. A gradient echo field map with the sample geometry was used for distortion correction (TR = 680 ms, TE 1 = 5.19 ms, TE 2 = 7.65 ms).

Table 1

Participant characteristics for each age group. For continuous variables, data is provided in means and standard deviations (in parenthesis). One-way ANOVAs were used to detect age group differences.

	Young (20-35 years) (N = 140)	Middle (35-60 years) (N = 119)	Old (60-80 years) (N = 129)	df	F-value	Eta-squared (η ²)
Age (years)	26.01 (4.17)	46.39 (6.25)	66.88 (4.68)			
Sex	38 F/102 M	36 F/83 M	50 F/79 M		4.38 ^a	
Resting HRV (RMSSD in ms)	53.35 (27.11)	32.77 (21.01)	27.27 (22.99)	385	43.01***	0.18
Mean HR (1/min)	64.38 (9.62)	62.93 (10.01)	66.24 (10.44)	385	3.41*	0.02
RR interval (ms)	952.56 (137.06)	977.87 (149.75)	928.32 (148.53)	385	3.62*	0.02
mean FD (mm)	0.18 (0.05)	0.28 (0.10)	0.31 (0.11)	385	82.61***	0.30
BMI (kg/m ²)	23.58 (3.03)	26.51 (3.62)	26.54 (3.57)	382	33.34***	0.15
WHR	0.86 (0.07)	0.92 (0.08)	0.95 (0.08)	381	47.64***	0.20
SBP (mmHg)	122.08 (11.42)	126.55 (13.74)	138.76 (18.2)	381	45.45***	0.20
DBP (mmHg)	71.23 (7.33)	78.21 (9.11)	80.00 (10.44)	381	35.47***	0.16
TMT A (s)	24.95 (7.79)	30.33 (12.73)	40.01 (13.54)	384	58.48***	0.23
TMT B (s)	57.72 (17.89)	71.40 (39.04)	95.15 (45.09)	382	45.73***	0.20

*p < 0.05; **p < 0.01; ***p < 0.001, 2-tailed.

^a Kruskal-Wallis-Test.

2.4. MR data preprocessing and analysis

Structural MRI. We analyzed structural brain alterations on the T1-weighted 3D image using VBM (Ashburner and Friston, 2000) as implemented in SPM12 (Wellcome Trust Centre for Neuroimaging, UCL, London, UK) and the Computational Anatomy Toolbox (CAT12: <http://dbm.neuro.uni-jena.de/cat/>), running on Matlab 9.3 (Mathworks, Natick, MA, USA). In the LEMON sample before the preprocessing, we removed the background noise from MP2RAGE on the computed uniform images via masking (Streitbürger et al., 2014). The preprocessing steps consisted of segmentation, bias-correction, and normalization using high-dimension Diffeomorphic Anatomical Registration Through Exponentiated Lie Algebra (DARTEL; Ashburner, 2007) with the template from 550 healthy controls of all ages in the IXI Dataset (<http://www.brain-development.org>) in MNI space. We then applied a 12-parameter affine registration and nonlinear transformation to correct for image size and position. The voxel size was resampled to $1.5 \times 1.5 \times 1.5$ mm and smoothed using an 8-mm Gaussian kernel. For each subject, whole-brain GMV was calculated. An absolute threshold mask of 0.05 was specified in the analyses to cover the whole brain. For quality assessment, we visually inspected the segmentation quality and image homogeneity with the CAT12 toolbox. One participant from the middle-aged group was excluded because of MRI inhomogeneities.

Functional MRI. Preprocessing was implemented in Nipype (Gorgolewski et al., 2011), incorporating tools from FreeSurfer (Fischl, 2012), FSL (Jenkinson et al., 2012), AFNI (Cox, 1996), ANTs (Avants et al., 2011), CBS Tools (Bazin et al., 2014), and Nitime (Rokem et al., 2009). The pipeline comprised the following steps: (I) discarding the first five EPI volumes to allow for signal equilibration and steady state, (II) 3D motion correction (FSL mcflirt), (III) distortion correction (FSL fugue), (IV) rigid body co-registration of functional scans to the individual T1-weighted image (FreeSurfer bbrgister), (V) denoising including removal of 24 motion parameters (CPAC, Friston et al., 1996), motion, signal intensity spikes (Nipype rapidart), physiological noise in white matter and cerebrospinal fluid (CSF) (CompCor; Behzadi et al., 2007), together with linear and quadratic signal trends, (VI) band-pass filtering between 0.01 and 0.1 Hz (Nilearn), (VII) spatial normalization to MNI152 standard space (3 mm isotropic) via transformation parameters derived during structural preprocessing (ANTS). (VIII) The data were then spatially smoothed with a 6-mm FWHM Gaussian kernel.

The reproducible workflows containing all implementation details for our datasets can be found here: LIFE; https://github.com/fliem/LIFE_RS_preprocessing, LEMON; <https://github.com/NeuroanatomyAndConnectivity/pipelines/releases/tag/v2.0>.

Eigenvector Centrality Mapping (ECM). In ECM, each voxel in the brain receives a centrality value that is larger if the voxel is strongly correlated with many other voxels that are themselves central (Lohmann et al., 2010). Higher EC values thus indicate stronger connectedness of the respective area (Lohmann et al., 2010; Wink et al., 2012). ECM is computationally efficient, enables connectivity analysis at the voxel level, and does not require initial thresholding of connections (Lohmann et al., 2010). Here, the fast ECM implementation was used (Wink et al., 2012). We restricted our ECM analysis to GM, which we extracted with a mask from the tissue priors in SPM12 by selecting voxels with a GM tissue probability of 20% or higher. The resulting mask contained ~63,000 voxels covering the entire brain.

Exploratory Seed-based Functional Connectivity Analysis (SBCA). To further explore the connectivity patterns of significant age-dependent centrality changes across the whole brain, ECM was complemented by SBCA. Regions detected in ECM can be used as seeds in a subsequent SBCA to investigate intrinsic functional connectivity patterns (Taubert et al., 2011). A bilateral vmPFC seed was created by binarizing the significant ECM findings (MNI coordinates: $[x = 0, y = 57, z = -6]$, cluster size $k = 62$). Time series were extracted and averaged across all voxels of the seed. For each subject, a correlation between the time series of the seed and every other voxel in the brain was calculated using 3dfim+

(AFNI). The resulting correlation maps were Fisher r -to- z transformed using 3dcalc (AFNI).

Statistical analyses for fMRI. Statistical analyses were carried out using the general linear model (GLM) approach implemented in SPM12. For all analyses, we used resting HRV as the variable of interest and age, sex, study, and either total intracranial volume (TIV, for VBM analysis) or in-scanner head motion (mean FD; Power et al., 2015, 2012 for ECM and SBCA) as covariates of no interest. We performed a one-way ANOVA with three age groups (young, middle, and old) as between-subject factor and calculated the interaction effect between HRV and age group. Based on the significant results of the ANOVA, we computed pairwise group differences using independent t -tests. Using one-sample t -tests, we further tested the main effect of HRV across all subjects and for each age group separately.

As additional controls, (1) both samples were analyzed separately (for more details see Supplementary Table 7), (2) HRV analyses were repeated using resting HR – instead of HRV – as variable of interest and age, sex, study, and either TIV (for VBM) or mean FD (for ECM and SBCA) as covariates of no interest, as well as (3) the effect of age on EC maps – controlling for sex, study, and mean FD (Long et al., 2017; Zuo et al., 2012).

For each statistical analysis, a positive and a negative contrast were computed. Only results surviving whole-brain family-wise error (FWE) correction at $p < 0.05$ (cluster-level) with a voxel-level threshold of $p < 0.001$ were considered significant. All (unthresholded) statistical maps are available at NeuroVault (Gorgolewski et al., 2015) for detailed inspection in 3D (<http://neurovault.org/collections/TELEUIIY>).

2.5. Potential confounding factors for HRV

Sex. As HRV has been reported to differ between sexes (Koenig and Thayer, 2016; Voss et al., 2015; Thayer et al., 2015), we analyzed sex differences in HRV per age group in a 2 (sex) \times 3 (age group) ANOVA.

Smoking. Since smoking has a short- and long-term impact on HRV (Felber Dietrich et al., 2007; Hayano et al., 1990), we examined potential effects of smoking status on HRV. To this end, we classified subjects into three groups (smokers: $N = 75$, former smokers: $N = 84$, and non-smokers: $N = 220$, [no info available: $NA = 9$]). We used a 2 (sex) \times 3 (smoking) ANOVA to test the mean differences between the groups using sex as additional between-subjects factor.

Blood Pressure. Systolic blood pressure (SBP) and diastolic blood pressure (DBP) were measured in a seated position using an automatic oscillometric blood pressure (BP) monitor (LIFE sample; OMRON 705IT, LEMON sample; OMRON M500) after a resting period of 5 min. While in the LIFE sample three consecutive BP measurements were taken from the right arm in intervals of 3 min, in the LEMON sample measurements were taken from participants' left arms on three separate occasions within two weeks. In each sample, all available measurements per participant were averaged to one SBP and one DBP value.

Anthropometric measurements. Subjects' heights and weights were taken according to a standardized protocol by trained study staff. Body mass index (BMI; in kg/m^2) was calculated by dividing the body weight by the square of the body height, while waist to hip ratio (WHR) was calculated as waist circumference measurement divided by hip circumference measurement (Huxley et al., 2010). As a control, all analyses on the association between HRV and the brain across the age groups were repeated with BP and BMI as additional covariates of no interest.

Cognition. Previous studies have related resting HRV to cognitive performance (Hansen et al., 2004; Mahinrad et al., 2016; Zeki Al Hazzouri et al., 2014). The latter is often assessed using the Trail Making Test (TMT), which measures executive function, processing speed, or mental flexibility (Reitan, 1955; Reitan and Wolfson, 1995). By drawing lines, subjects sequentially connect numbers and/or letters while their reaction times are recorded. In the first part of the test (TMT-A) the targets are all numbers (1, 2, 3, etc.), while in the second part (TMT-B), participants need to alternate between numbers and letters (1, A, 2, B, etc.). In both

TMT A and B, the time to complete the task quantifies the performance and lower scores indicate better performance.

For cognition, BP, and anthropometric measurements, we assessed age-group differences statistically using one-way ANOVAs and then tested their association with HRV using Spearman correlations for each age group. To determine statistical significance, we used a two-sided α -level of 0.05. Statistical analyses were conducted using R version 3.3.2 (R Core Team, 2016).

3. Results

Details about the demographic, anthropometric, cardiovascular, and cognitive characteristics of the 388 participants can be found in Table 1. The age groups differed significantly on all variables (Table 1). Compared to population-based norms (Hobert et al., 2011; Then et al., 2014; Tombaugh, 2004), our sample shows higher TMT scores, indicating cognitive health.

Note. HRV = heart rate variability; RMSSD = root mean square of successive differences; HR = heart rate, FD = framewise displacement; BMI = body mass index; WHR = waist to hip ratio; SBP = systolic blood pressure; DBP = diastolic blood pressure; TMT = trail making test.

There was a significant main effect of age group ($F(2,382) = 63.552$, $p = 2 \times 10^{-16}$, $\eta^2 = 0.182$), no significant main effect of sex ($F(1,382) = 0.187$, $p = 0.666$), and no significant age group \times sex

interaction on HRV ($F(2,382) = 0.233$, $p = 0.792$). HRV did not differ as a function of smoking status (main effect smoking group: $F(2,373) = 1.241$, $p = 0.290$, main effect of sex: $F(1,373) = 0.473$, $p = 0.492$; smoking group \times sex interaction: $F(2,373) = 0.606$, $p = 0.546$).

HRV was negatively correlated with age ($\rho = -0.210$, $p = 0.010$), BMI ($\rho = -0.207$, $p = 0.020$), and DBP ($\rho = -0.231$, $p = 0.012$) in the middle-aged individuals. No significant associations were found between HRV and mean FD, SBP, WHR, TMT A, or TMT B in any of the age groups (Supplementary Table 6).

Voxel-based Morphometry (VBM). There was no significant association between HRV and GMV across all subjects. Also, an ANOVA did not yield a significant age group \times HRV interaction on GMV. While an exploratory one-sample *t*-test in the middle-aged group indicated a significant HRV-related increase of GMV in the left cerebellum (MNI coordinates: [-15, -87, -51], $k = 1540$, $T = 3.92$, $p_{FWE} = 0.004$), there were no significant effects of HRV on GMV for younger and older adults. Control analyses that included BP and BMI as covariates of no interest did not change the results (<https://neurovault.org/collections/TELEUIIY/>). Additional analyses using resting HR as covariates of interest did not show any significant VBM results neither across all age groups, nor in each age group (<https://neurovault.org/collections/TELEUIIY/>).

Eigenvector Centrality Mapping (ECM). A significant effect of age group on the relation between resting HRV and EC was detected in the bilateral

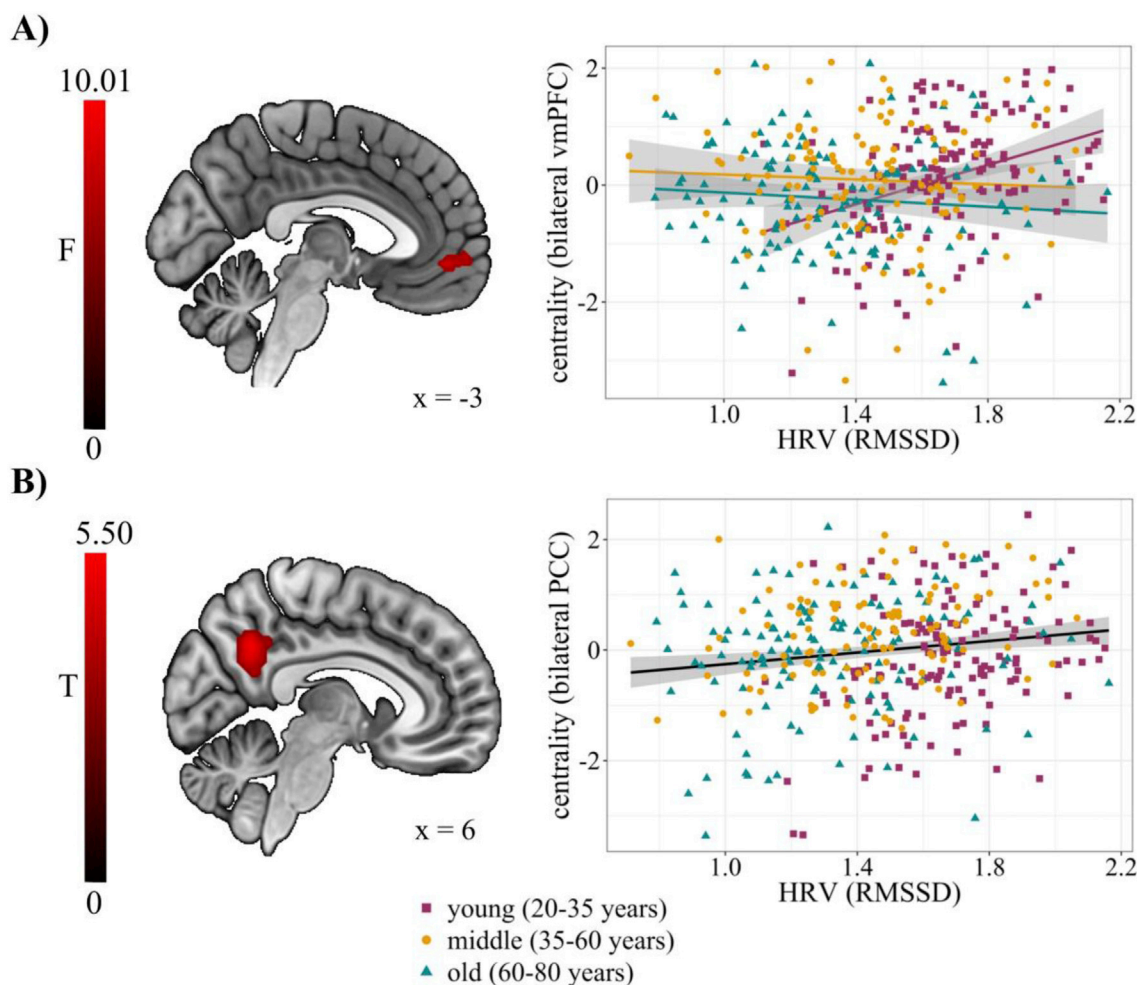


Fig. 1. Association between resting heart rate variability (HRV), measured as root mean square of successive differences (RMSSD), and eigenvector centrality (EC). **A)** The interaction between age group and HRV was significant in the bilateral ventromedial prefrontal cortex (vmPFC; MNI coordinates: [0, 57, -6], $k = 62$, $F = 10.79$, $p_{FWE} = 0.006$), displayed at $x = -3$. **B)** An increased EC in the bilateral posterior cingulate cortex (PCC; MNI coordinates [6, -54, 36], $k = 204$, $T = 5.29$, $p_{FWE} < 0.001$) across all age groups, displayed at $x = 6$. Threshold: $p < 0.001$ at the voxel and $p < 0.05$ with family-wise error (FWE) correction at the cluster level.

vmPFC (MNI coordinates: [0, 57, -6], k = 62, F = 10.79). The resulting beta values for each age group are plotted in Fig. 1A, suggesting that younger adults show a stronger positive association between HRV and EC in the bilateral vmPFC than middle-aged and older individuals (Table 2). This was supported by post-hoc two-sample t-tests, which indicated that the correlation between HRV and EC in the bilateral vmPFC was significantly stronger for young > old and young > middle-age subjects (Table 2). A one-sample t-test across all subjects showed increased EC with higher HRV in the bilateral PCC (Fig. 1B). The negative contrast did not yield any significant results. In separate one-sample t-tests for each age group, we found HRV-dependent EC increases in the right vmPFC, bilateral PCC, and superior frontal gyrus (SFG), as well as HRV-dependent EC decreases in the left superior occipital gyrus (SOG) including the cuneus and calcarine sulcus in the group of young subjects. Our data did not show any significant positive or negative correlation with HRV in the groups of middle-aged and old subjects that were correctable for multiple comparisons. The complete ECM results are presented in Table 2.

Control analyses that included BP and BMI as covariates of no interest did not change the results (<https://neurovault.org/collections/TELEUIIY/>). Resting HR – instead of HRV – was not significantly associated with functional brain centrality, neither across all age groups, nor in each age group separately (<https://neurovault.org/collections/TELEUIIY/>). The association between age and EC is shown in Supplementary Figure 1.

Exploratory Seed-based Functional Connectivity Analysis (SBCA). In the additional exploratory SBCA, a significant effect of age group on the relation between resting HRV and whole-brain bilateral vmPFC connectivity was found in the bilateral cerebellum, right superior parietal lobe

(SPL), left middle occipital gyrus (MOG), inferior occipital gyrus (IOG), and left SFG extended to the supplementary motor area (SMA). The beta values from the right cerebellum for each age group are plotted in Fig. 2A, suggesting that younger adults show stronger functional connectivity between the bilateral vmPFC and right cerebellum than middle-aged and older individuals (Table 3). The post-hoc two-sample t-tests similarly indicated that higher HRV levels were significantly correlated with stronger functional connectivity between the bilateral vmPFC and cerebellum, right SPL, left MOG, left post-central gyrus, and left SMA for the contrasts of young > old and young > middle (Table 3). A one-sample t-test in the overall sample, to assess the association between HRV and bilateral vmPFC connectivity, showed an increased functional connectivity with the left middle frontal gyrus (MFG) extending to the dorso-lateral prefrontal cortex (DLPFC) (Fig. 2B). Separate one-sample t-tests for each age group showed no significant association for the middle-aged and older subjects but an increased vmPFC connectivity in distributed brain regions including the bilateral cerebellum, bilateral MOG, and the right SMA for the young subjects. We did not observe any significant negative correlations, neither in the overall sample nor in each age group. Control analyses that included BP and BMI as covariates of no interest did not change the results (<https://neurovault.org/collections/TELEUIIY/>). The complete SBCA results are presented in Table 3.

4. Discussion

In the present study, we assessed the relationship between parasympathetic cardio-regulation (indexed by HRV) and brain structure (using VBM) as well as whole-brain resting state functional connectivity (using ECM and SBCA) in a large sample of healthy young, middle-aged,

Table 2

Brain regions that show significant increases or decreases in eigenvector centrality with resting heart rate variability (HRV). Threshold: p < 0.001 at the voxel and p < 0.05 with family-wise error (FWE) correction at the cluster level.

	Regions	H	cluster size k (Voxel)	MNI coordinates			FWE	z	F/T-value
				x	y	z			
ANOVA	Ventromedial prefrontal cortex	R/L	62	0	57	-6	0.006	4.03	10.79
				-3	48	-6		3.76	9.63
				0	60	3		3.49	8.53
Across age groups (+)	Posterior cingulate cortex/precuneus	R/L	204	6	-54	36	<0.001	5.29	5.39
				-9	-57	33		4.04	4.09
				-12	-51	45		3.35	3.38
Young (+)	Ventromedial prefrontal cortex	R	316	0	57	-6	<0.001	5.07	5.16
				6	51	9		4.89	4.98
				15	60	15		4.22	4.16
	Posterior cingulate cortex/precuneus	R/L	167	6	-57	27	<0.001	4.46	4.52
				-9	-54	18		3.72	3.75
				-9	-60	27		3.70	3.74
Superior frontal gyrus	R/L	240	15	33	48	0.002	4.50	4.56	
			15	48	39		4.32	4.37	
			-6	36	48		4.24	4.29	
Young (-)	Superior occipital gyrus	L	129	-6	-96	3	<0.001	4.63	4.70
				-15	-99	-3		4.24	4.29
				0	-84	-3		3.71	3.76
Middle (+)	n.s								
Middle (-)	n.s								
Old (+)	n.s								
Old (-)	n.s								
Young > Old	Ventromedial prefrontal cortex	R/L	131	0	57	-6	<0.001	4.45	4.51
				0	60	3		4.01	4.05
				-3	45	-8		3.62	3.65
Young < Old	n.s								
Middle > Young	n.s								
Middle < Young	Ventromedial prefrontal cortex	R/L	85	3	45	-6	0.005	4.09	4.13
				-12	48	-9		4.06	4.11
				6	45	15		3.58	3.61
Old > Middle	n.s								
Old < Middle	n.s								

Note. R = right, L = left, H = hemisphere, ANOVA = analysis of variance, MNI = Montreal Neurological Institute, n.s = not significant.

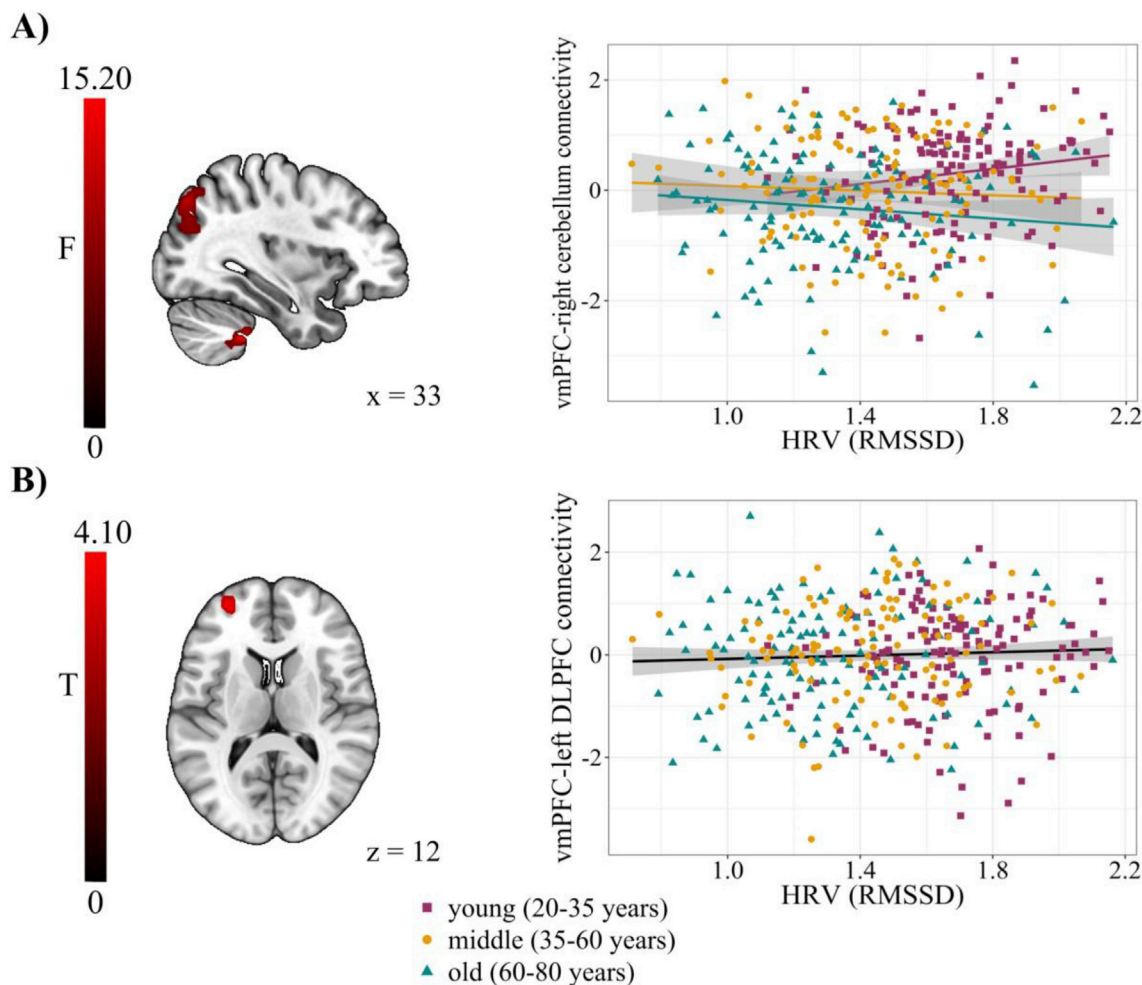


Fig. 2. Association between resting heart rate variability (HRV), measured as root mean square of successive differences (RMSSD), and brain function in an exploratory seed-based functional connectivity analysis originating from the bilateral ventromedial prefrontal cortex (vmPFC). **A)** The interaction between age group and HRV was significant in the right cerebellum (MNI coordinates [33, -42, -45], $k = 46$, $F = 15.19$, $p_{FWE} < 0.001$), displayed at $x = 33$. **B)** An increased functional connectivity in the right dorsolateral prefrontal cortex (DLPFC; MNI coordinates [-30, 54, 12], $k = 67$, $T = 4.10$, $p_{FWE} = 0.032$) was found across all age groups, displayed at $z = 12$. Threshold: $p < 0.001$ at the voxel and $p < 0.05$ with family-wise error (FWE) correction at the cluster level.

and older participants. We used an optimally healthy sample for a given age range in terms of both physical (e.g., Janssen et al., 2002) and cognitive health (e.g., Hobert et al., 2011; Tombaugh, 2004). We found the frequently observed age-related decrease in resting HRV (Almeida-Santos et al., 2016; Voss et al., 2015) to be accompanied by age-dependent and age-invariant alterations in brain function. Specifically, higher HRV was linked to stronger network centrality in several brain regions, particularly along the cortical midline. In the PCC, this correlation was present in all age groups while in the vmPFC, network centrality was related to higher HRV in young but not in middle-aged and old adults. These findings support the view that altered HRV during aging may have a functional brain component associated with it.

4.1. Age-dependent association of resting HRV with functional connectivity

Given the relationship between HRV and age (Almeida-Santos et al., 2016; Voss et al., 2015), HRV and brain structure (Wei et al., 2018), as well as HRV and brain function (Sakaki et al., 2016), we hypothesized the neural correlates of resting HRV to be also age-dependent. Our results confirm that the relationship between HRV and network centrality at rest differs between age groups. Evidence is accumulating that alterations of intrinsic brain activity are a key feature of normal brain aging (Damoiseaux et al., 2008). Age-dependent intrinsic connectivity alterations in

the DMN have been found not only in healthy aging (Ferreira and Busatto, 2013) but also in age-related pathologies, for example, in individuals with a high familial risk for depression (Posner et al., 2016) and in young APOE- $\epsilon 4$ carriers (Filippini et al., 2009), which is a possible biomarker for Alzheimer's dementia (Kanekiyo et al., 2014). Our finding that resting HRV is related to increased network centrality in medial frontal regions in the young but not in the middle-aged or old age group could be interpreted in the framework of the functional plasticity hypothesis of cognitive aging (Greenwood, 2007). According to this hypothesis, the structural vulnerability – particularly of prefrontal cortex – leads to an age-related functional reorganization (e.g., Grady, 2012; for a review). The changes in the resting state network architecture around the vmPFC that are related to parasympathetic cardioregulation could thus represent altered cardiovascular control with advancing age and concomitant network reorganization.

In addition to the age-dependent association of resting HRV with functional brain network centrality in medial frontal regions, we also found an HRV-related bilateral medial parietal cluster in the PCC that was independent of age. Both vmPFC and PCC are central nodes of the CAN (Benarroch, 1993) and the DMN (Greicius et al., 2003; Uddin et al., 2009) and have been related to self-generated or internally directed mental processes like thoughts and feelings (Andrews-Hanna et al., 2014; Raichle et al., 2001). The medial frontal (e.g., vmPFC) and medial

Table 3

Brain regions that show resting heart rate variability-related connectivity with the bilateral ventromedial prefrontal cortex (vmPFC) in an exploratory seed-based functional connectivity analysis. Thresholds: $p < 0.001$ at the voxel and $p < 0.05$ with family-wise error (FWE) correction at the cluster level.

	Regions	H	cluster size k (Voxels)	MNI coordinates			FWE	z	F/T- value
				x	y	z			
ANOVA	Cerebellum	R	46	33	-42	-45	0.049	4.91	15.19
	Superior parietal lobe	R	203	24	-75	51	<0.001	4.48	12.94
				33	-78	45		4.34	12.25
				36	-75	30		3.82	9.88
	Middle occipital gyrus	L	57	-33	-84	30	0.021	4.24	11.74
				-39	-66	24		3.31	7.84
	Inferior occipital gyrus		60	-33	-69	-6	0.016	3.85	9.97
				-42	-63	-3		3.76	9.61
				-51	-69	-15		3.62	9.03
	Cerebellum	L	61	-30	-60	-30	0.015	3.83	9.91
-33				-66	-21	3.59		8.91	
-39				-72	-18	3.58		8.87	
Superior frontal gyrus extended to supplementary motor area	R/ L	71	0	15	66	0.007	3.73	9.47	
			0	3	57		3.6	8.96	
			9	12	57		3.53	8.66	
Across age groups (+)	Middle frontal gyrus extended to dorsolateral prefrontal cortex	L	67	-30	54	12	0.032	4.06	4.10
				-36	54	3		3.54	3.57
				-18	51	3		3.39	3.42
Young (+)	Cerebellum	R	131	33	-42	-45	0.001	5.06	5.15
				42	-60	-48		4.68	4.75
				36	-63	-39		3.29	3.31
	Cerebellum	L	116	-12	-57	-54	0.002	4.6	4.67
				-21	-69	-54		4.2	4.25
				-15	-48	-51		4.09	4.14
	Middle occipital gyrus	R	163	39	-75	42	<0.001	4.46	4.52
				30	-69	51		4.15	4.20
				21	-78	51		3.63	3.67
	Middle occipital gyrus	L	131	-39	-66	24	0.001	4.31	4.37
-33				-84	30	3.94		3.98	
-39				-60	12	3.47		3.50	
Cerebellum	R	63	18	-75	-18	0.04	4.13	4.18	
			27	-81	-18		3.68	3.72	
			18	-84	-15		3.64	3.67	
Cerebellum	L	102	-33	-81	-21	0.005	4.13	4.18	
			-30	-60	-30		3.7	3.74	
			-21	-90	-15		3.59	3.62	
Supplementary motor area	R	87	3	6	54	0.01	3.77	3.81	
			0	15	69		3.68	3.72	
			9	12	57		3.59	3.63	
Young (-)	n.s								
Middle (+)	n.s								
Middle (-)	n.s								
Old (+)	n.s								
Old (-)	n.s								
Young > Old	Cerebellum	R	67	33	-42	-45	0.032	4.59	4.66
				15	-48	-51		3.63	3.67
				27	-57	-45		3.41	3.44
	Inferior occipital gyrus	L	237	-33	-69	-6	<0.001	4.41	4.47
				-42	-63	-3		4.33	4.38
				-39	-72	-18		4.14	4.19
	Superior parietal lobe	R	275	24	-78	51	<0.001	4.31	4.37
				36	-75	45		4.21	4.26
				36	-75	27		3.95	4.00
	Middle occipital gyrus	L	140	-27	-84	27	0.001	4.30	4.35
-36				-66	24	3.89		3.93	
-39				-60	12	3.62		3.65	
Superior frontal gyrus extended to supplementary motor area	R/ L	147	-3	3	57	0.001	3.99	4.04	
			12	6	63		3.72	3.75	
			3	12	66		3.61	3.65	
Postcentral gyrus	R	72	42	-6	30	0.024	3.87	3.91	
			54	6	24		3.69	3.73	
			54	0	33		3.53	3.56	
Superior frontal gyrus extended to supplementary motor area	R/ L	73	3	-18	60	0.022	3.62	3.66	
			-3	-36	69		3.56	3.59	
			3	-9	69		3.29	3.31	
Young < Old	n.s								
Middle > Young	n.s								
Middle < Young	Cerebellum	R	189	33	-42	-45	<0.001	4.99	5.08
				42	-60	-48		4.60	4.67

(continued on next page)

Table 3 (continued)

Regions	H	cluster size k (Voxels)	MNI coordinates			FWE	z	F/T- value
			x	y	z			
Superior parietal lobe	R	270	18	−45	−51	<0.001	4.34	4.40
			27	−72	51			
			33	−78	45			
			36	−75	30			
Cerebellum	L	239	−12	−57	−54	<0.001	4.74	4.82
			−15	−45	−51			
			−12	−39	−45			
Middle occipital gyrus	L	76	−33	−84	30	0.019	4.59	4.66
			−45	−72	27			
Cerebellum	R/ L	313	−30	−60	−30	<0.001	4.27	4.32
Superior frontal gyrus extended to supplementary motor Area	L	109	12	−69	−21	0.003	4.18	4.23
			18	−78	−18			
			0	15	66			
			15	9	69			
Old > Middle	n.s							
Old < Middle	n.s							

Note. R = right, L = left, H = hemisphere, ANOVA = analysis of variance, MNI = Montreal Neurological Institute.

parietal components (e.g., PCC and precuneus) of CAN and DMN have been particularly implied in parasympathetic functioning (Beissner et al., 2013; Benarroch, 1993). In addition, prefrontal visceral structures (Price, 2007, 1999) respond to heartbeats (Babo-Rebelo et al., 2016; Park et al., 2014) and modulate HR or HRV (Makovac et al., 2017; Van Eden and Buijs, 2000). It is plausible that in the absence of external stimulation, brain function (i.e., activity and connectivity) in CAN and DMN is predominantly allocated to the “internal milieu”, that is, to monitoring and regulating bodily signals (e.g., the parasympathetic “rest-and-digest”). Fittingly, the PCC has been found active in tasks that involved the assessment of self-relevance (Yu et al., 2011) as well as self-location and body ownership (Guterstam et al., 2015), while the vmPFC was related to processing bodily information (Gusnard et al., 2001), autonomic control (Critchley et al., 2011), and cardiovascular arousal (Wong et al., 2007).

Using the cluster that showed a significant interaction in the centrality analyses, the exploratory SBCA similarly showed an age-dependent relationship between resting HRV and functional brain connectivity. Specifically, we found stronger functional connectivity between the bilateral vmPFC and a widespread set of brain regions including the bilateral cerebellum, bilateral occipital gyrus, right SPL, and bilateral SFG extending to the SMA in young but not in middle-aged or older adults. These results extend the ECM findings by suggesting additional cortico-cerebellar regions might be involved in the modulation of visceral processes. In line with this interpretation, activation in the cerebellum has been connected to the regulation of visceral responses (Demirtas-Tatlidede et al., 2011), fear conditioning (Leaton, 2003; Sacchetti et al., 2002), feeding (Tataranni et al., 1999), as well as the coordination and control of cardiovascular activities (Bradley et al., 1991; Ghelarducci and Sebastiani, 1996). Furthermore, autonomic activity during cognitive and motor tasks was positively associated with activation in the cerebellum and, among other regions, the SMA and dorsal ACC (Critchley et al., 2003).

Despite previous evidence of the relationship between GMV and vagally-mediated HRV in CAN regions (Wei et al., 2018), using whole-brain VBM analysis, we only found a significant GMV change related with resting HRV in the cerebellum for the middle-aged group. Notably, in the study by Wei et al. (2018), reduced GM volume in the cerebellum was associated with HR (but not HRV) in healthy middle-aged individuals. However, using resting HR, we were also not able to replicate the previous findings (Wei et al., 2018). The divergent results could be due to different measurement parameters (e.g., MRI sequence parameters) but also to different effect size or statistical power (for more details see *Limitations*).

Finally, while our study investigated the neural correlates of resting

HRV, previous studies investigated the neural correlates of HR at rest and HR changes with stimulation or tasks (e.g., Beissner et al., 2013 for a review). Our additional analyses using resting HR as covariate of interest did not show significant associations with brain structure or function. This suggests that resting HRV and resting HR (as they are differentially influenced by the branches of the ANS) have different neural components at rest.

4.2. Physiological and psychophysiological interpretations of HRV

The most fundamental (purely physiological) understanding of the role of the ANS – and particularly the PNS – is to ensure visceral and cardiovascular functioning or bodily homeostasis by allowing rapid adaptive behavioral and physiological reactions in ever-changing environments, or by disengagement and relaxation in resting moments (“rest-and-digest”; e.g., Cannon, 1929). More psychophysiological interpretations of ANS function have extended this view to cognitive, affective, and social phenomena. For example, the neurovisceral integration model takes higher HRV to facilitate physiological, cognitive, socio-emotional, and behavioral flexibility or adaptation (Smith et al., 2017; Thayer and Lane, 2000; Thayer and Ruiz-Padial, 2006). It explicitly links the brain and the rest of the body by assuming that the PFC – and particularly the vmPFC – tonically inhibits the amygdala, which affects autonomic function, thereby linking both nervous systems to inhibitory or self-regulatory processes (Holzman and Bridgett, 2017; Kemp et al., 2017; Thayer et al., 2012). Convergently, resting HRV has recently been associated with vmPFC activation during a dietary self-control task in young adults (Maier and Hare, 2017).

5. Limitations

There are a number of limitations that should be considered in the interpretation of our results. The study design is cross-sectional and does not allow us to infer the directionality of the association between resting HRV and the brain. Additionally, our health criteria also allowed inclusion of subjects with higher BMI (>25 kg/m²) or untreated/undiagnosed hypertension (SBP > 140 mmHg, DBP > 90 mmHg). This makes it difficult to disentangle HRV-related influences from other bodily/cardiovascular influences, which are also physiologically related (BMI: Molfino et al., 2009; BP: Singh et al., 1998). However, control analyses that accounted for BP and BMI showed very similar results of the association between resting HRV and the brain. Although psychological interpretations of a single physiological marker like resting HRV are intrinsically limited, previous studies have associated HRV with different

trait or state levels of, for example, executive control (Capuana et al., 2014), stress (Sin et al., 2016), and emotion regulation (Williams et al., 2015). For a psychological interpretation of our finding that the association between HRV and functional connectivity at rest is age-dependent, similar analyses on task-related parasympathetic and neural activity could be helpful. The samples differed significantly, for example in resting HRV (young subjects), sex distribution, sample size, BP, and MRI/ECG acquisition parameters (Supplementary Table 1, Tables 4 and 5). Although we accounted for within- and between-sample variance in the second-level GLM, these differences may still have influenced our results (e.g., for structural MRI; Streitbürger et al., 2014). Further, we calculated the RMSSD using 10 s of ECG data, which has been shown to be a valid measurement (Munoz et al., 2015; Nussinovitch et al., 2011a, 2011b). Nevertheless, ECG data recorded over longer periods (e.g., 24-h) can complement this “ultra-short” evaluation of parasympathetic function. Finally, although ECM is a relatively new measure that has certain advantages (see above and Lohmann et al., 2010; Wink et al., 2012), studies using other measures of functional connectivity could complement our findings on the association of parasympathetic cardioregulation and functional brain connectivity.

6. Conclusion

In this cross-sectional study, we examined the association of resting HRV with brain structure and functional connectivity in different age groups of healthy adults. Our main findings are correlations between resting HRV and brain network architecture in the PCC across all age groups and in the vmPFC in young but not in middle-aged or older subjects. These support the view that the well-known HRV decrease with age may have a functional brain network component along the cortical midline. Consistent with the role of these areas in affective, cognitive, and autonomic regulation, our results provide a comprehensive picture of the differential effect of aging on heart-brain interactions. These findings emphasize the importance of parasympathetic cardioregulation in healthy aging.

Financial disclosures

The authors declare no conflict of interest.

Acknowledgments

This study was supported by LIFE Leipzig Research Center for Civilization Diseases at the University of Leipzig funded by the European Union, European Regional Development Fund, and the Free State of Saxony. The authors would like to thank all volunteers for their participation in one of the two studies. Further, we thank all researchers, technicians and students who planned, collected, entered and curated data, used in this manuscript.

Appendix A. Supplementary data

Supplementary data related to this article can be found at <https://doi.org/10.1016/j.neuroimage.2018.10.027>.

References

- Adelstein, J.S., Shehzad, Z., Mennes, M., DeYoung, C.G., Zuo, X.N., Kelly, C., Margulies, D.S., Bloomfield, A., Gray, J.R., Castellanos, F.X., Milham, M.P., 2011. Personality is reflected in the brain's intrinsic functional architecture. *PLoS One* 6. <https://doi.org/10.1371/journal.pone.0027633>.
- Almeida-Santos, M.A., Barreto-Filho, J.A., Oliveira, J.L.M., Reis, F.P., da Cunha Oliveira, C.C., Sousa, A.C.S., 2016. Aging, heart rate variability and patterns of autonomic regulation of the heart. *Arch. Gerontol. Geriatr.* 63, 1–8. <https://doi.org/10.1016/j.archger.2015.11.011>.
- Andrews-Hanna, J.R., Smallwood, J., Spreng, R.N., 2014. The default network and self-generated thought: component processes, dynamic control, and clinical relevance. *Ann. N. Y. Acad. Sci.* 1316, 29–52. <https://doi.org/10.1111/nyas.12360>.
- Arking, R., 2006. The biology of aging: observations and principles. *The Biology of Aging Observations Principles*. <https://doi.org/10.1080/03601270701498491>.
- Ashburner, J., 2007. A fast diffeomorphic image registration algorithm. *Neuroimage* 38, 95–113. <https://doi.org/10.1016/j.neuroimage.2007.07.007>.
- Ashburner, J., Friston, K.J., 2000. Voxel-based morphometry—the methods. *Neuroimage* 11, 805–821. <https://doi.org/10.1006/nimg.2000.0582>.
- Avants, B.B., Tustison, N.J., Song, G., Cook, P.A., Klein, A., Gee, J.C., 2011. A reproducible evaluation of ANTs similarity metric performance in brain image registration. *Neuroimage* 54, 2033–2044. <https://doi.org/10.1016/j.neuroimage.2010.09.025>.
- Babayan, A., Erbey, M., Kumral, D., Reinelt, R. D., Reiter, A. M. F., Röbbig, J., Schaare, L. H., Uhlig, M., et al., A Mind-brain-body Dataset of MRI, EEG, Cognition, Emotion, and Peripheral Physiology in Young and Old Adults. (in revision).
- Babo-Rebelo, M., Wolpert, N., Adam, C., Hasboun, D., Tallon-Baudry, C., 2016. Is the cardiac monitoring function related to the self in both the default network and right anterior insula? *Philos. Trans. R. Soc. B Biol. Sci.* 371 <https://doi.org/10.1098/rstb.2016.0004>, 20160004.
- Bazin, P.L., Weiss, M., Dinse, J., Schäfer, A., Trampel, R., Turner, R., 2014. A computational framework for ultra-high resolution cortical segmentation at 7 Tesla. *Neuroimage* 93, 201–209. <https://doi.org/10.1016/j.neuroimage.2013.03.077>.
- Behzadi, Y., Restom, K., Liu, J., Liu, T.T., 2007. A component based noise correction method (CompCor) for BOLD and perfusion based fMRI. *Neuroimage* 37, 90–101. <https://doi.org/10.1016/j.neuroimage.2007.04.042>.
- Beissner, F., Meissner, K., Bar, K.-J., Napadow, V., 2013. The autonomic brain: an activation likelihood estimation meta-analysis for central processing of autonomic function. *J. Neurosci.* 33, 10503–10511. <https://doi.org/10.1523/JNEUROSCI.1103-13.2013>.
- Benarroch, E.E., 1993. The central autonomic network: functional organization, dysfunction, and perspective. *Mayo Clin. Proc.* 68, 988–1001. [https://doi.org/10.1016/S0025-6196\(12\)62272-1](https://doi.org/10.1016/S0025-6196(12)62272-1).
- Binnewijzend, M.A.A., Adriaanse, S.M., Van der Flier, W.M., Teunissen, C.E., de Munck, J.C., Stam, C.J., Scheltens, P., van Berckel, B.N.M., Barkhof, F., Wink, A.M., 2014. Brain network alterations in Alzheimer's disease measured by Eigenvector centrality in fMRI are related to cognition and CSF biomarkers. *Hum. Brain Mapp.* 35, 2383–2393. <https://doi.org/10.1002/hbm.22335>.
- Bradley, D.J., Ghelarducci, B., Spyer, K.M., 1991. The role of the posterior cerebellar vermis in cardiovascular control. *Neurosci. Res.* 12, 45–56. [https://doi.org/10.1016/0168-0102\(91\)90099-K](https://doi.org/10.1016/0168-0102(91)90099-K).
- Buccelletti, E., Gilardi, E., Scaini, E., Galiuto, L., Persiani, R., Biondi, a, Basile, F., Silveri, N.G., 2009. Heart rate variability and myocardial infarction: systematic literature review and metanalysis. *Eur. Rev. Med. Pharmacol. Sci.* 13, 299–307.
- Bullmore, E., Sporns, O., 2009. Complex brain networks: graph theoretical analysis of structural and functional systems. *Nat. Rev. Neurosci.* 10 <https://doi.org/10.1038/nrn2618>, 312–312.
- Cannon, W.B., 1929. Organization for physiological homeostasis. *Physiol. Rev.* 9, 399–431. <https://doi.org/10.1152/physrev.1929.9.3.399>.
- Capuana, L.J., Dywan, J., Tays, W.J., Elmers, J.L., Witherspoon, R., Segalowitz, S.J., 2014. Factors influencing the role of cardiac autonomic regulation in the service of cognitive control. *Biol. Psychol.* 102, 88–97. <https://doi.org/10.1016/j.biopsycho.2014.07.015>.
- Carnevali, L., Koenig, J., Sgoifo, A., Ottaviani, C., 2018. Autonomic and brain morphological predictors of stress resilience. *Front. Neurosci.* 12, 1–13. <https://doi.org/10.3389/fnins.2018.00228>.
- Chang, C., Metzger, C.D., Glover, G.H., Duyn, J.H., Heinze, H.J., Walter, M., 2013. Association between heart rate variability and fluctuations in resting-state functional connectivity. *Neuroimage* 68, 93–104. <https://doi.org/10.1016/j.neuroimage.2012.11.038>.
- Cox, R.W., 1996. AFNI: software for analysis and visualization of functional magnetic resonance images. *Comput. Biomed. Res.* 29, 162–173. <https://doi.org/10.1006/cbmr.1996.0014>.
- Critchley, H.D., Corfield, D.R., Chandler, M.P., Mathias, C.J., Dolan, R.J., 2000. Cerebral correlates of autonomic cardiovascular arousal: a functional neuroimaging investigation in humans. *J. Physiol.* 523 (Pt 1), 259–270. <https://doi.org/10.1111/j.1469-7793.2000.t01-1-00259.x>.
- Critchley, H.D., Mathias, C.J., Josephs, O., O'Doherty, J., Zanini, S., Dewar, B.K., Cipolotti, L., Shallice, T., Dolan, R.J., 2003. Human cingulate cortex and autonomic control: converging neuroimaging and clinical evidence. *Brain* 126, 2139–2152. <https://doi.org/10.1093/brain/awg216>.
- Critchley, H.D., Nagai, Y., Gray, M.A., Mathias, C.J., 2011. Dissecting axes of autonomic control in humans: insights from neuroimaging. *Auton. Neurosci. Basic Clin.* 161, 34–42. <https://doi.org/10.1016/j.autneu.2010.09.005>.
- Damoiseaux, J.S., Beckmann, C.F., Arigita, E.J.S., Barkhof, F., Scheltens, P., Stam, C.J., Smith, S.M., Rombouts, S.A.R.B., 2008. Reduced resting-state brain activity in the “default network” in normal aging. *Cerebr. Cortex* 18, 1856–1864. <https://doi.org/10.1093/cercor/bhm207>.
- Damoiseaux, J.S., Rombouts, S.A.R.B., Barkhof, F., Scheltens, P., Stam, C.J., Smith, S.M., Beckmann, C.F., Raichle, M.E., 2006. Consistent Resting-state Networks across Healthy Subjects.
- De Meersman, R.E., Stein, P.K., 2007. Vagal modulation and aging. *Biol. Psychol.* 74, 165–173. <https://doi.org/10.1016/j.biopsycho.2006.04.008>.
- Demirtas-Tatlidede, A., Freitas, C., Pascual-Leone, A., Schmahmann, J.D., 2011. Modulatory effects of theta burst stimulation on cerebellar nonsomatic functions. *Cerebellum* 10, 495–503. <https://doi.org/10.1007/s12311-010-0230-5>.
- Felber Dietrich, D., Schwartz, J., Schindler, C., Gaspoz, J.-M., Barthélémy, J.-C., Tschopp, J.-M., Roche, F., von Eckardstein, A., Brändli, O., Leutenberger, P.,

- Gold, D.R., Ackermann-Lieblich, U., 2007. Effects of passive smoking on heart rate variability, heart rate and blood pressure: an observational study. *Int. J. Epidemiol.* 36, 834–840. <https://doi.org/10.1093/ije/dym031>.
- Ferreira, L.K., Busatto, G.F., 2013. Resting-state functional connectivity in normal brain aging. *Neurosci. Biobehav. Rev.* 37, 384–400. <https://doi.org/10.1016/j.neubiorev.2013.01.017>.
- Filippini, N., MacIntosh, B.J., Hough, M.G., Goodwin, G.M., Frisoni, G.B., Smith, S.M., Matthews, P.M., Beckmann, C.F., Mackay, C.E., 2009. Distinct patterns of brain activity in young carriers of the APOE-4 allele. *Proc. Natl. Acad. Sci. Unit. States Am.* 106, 7209–7214. <https://doi.org/10.1073/pnas.0811879106>.
- Fischl, B., 2012. FreeSurfer. *Neuroimage* 62, 774–781. <https://doi.org/10.1016/j.neuroimage.2012.01.021>.
- Friston, K.J., Williams, S., Howard, R., Frackowiak, R.S.J., Turner, R., 1996. Movement-related effects in fMRI time-series. *Magn. Reson. Med.* 35, 346–355. <https://doi.org/10.1002/mrm.1910350312>.
- García-García, I., Jurado, M.A., Garolera, M., Marqués-Iturria, I., Horstmann, A., Segura, B., Pueyo, R., Sender-Palacios, M.J., Vernet-Vernet, M., Villringer, A., Junqué, C., Margulies, D.S., Neumann, J., 2015. Functional network centrality in obesity: a resting-state and task fMRI study. *Psychiatry Res. Neuroimaging.* 233, 331–338. <https://doi.org/10.1016/j.psychres.2015.05.017>.
- Ghelarducci, B., Sebastiani, L., 1996. Contribution of the cerebellar vermis to cardiovascular control. *J. Auton. Nerv. Syst.* 56, 149–156. [https://doi.org/10.1016/0165-1838\(95\)00068-2](https://doi.org/10.1016/0165-1838(95)00068-2).
- Gianaros, P.J., Van Der Veen, F., Jennings, J.R., 2004. Regional cerebral blood flow correlates with heart period and high-frequency heart period variability during working-memory task: implications for the cortical and subcortical regulation of cardiac autonomic activity. *Psychophysiology* 41, 521–530. <https://doi.org/10.1111/j.1469-8986.2004.00179.x>.
- Gorgolewski, K., Burns, C.D., Madison, C., Clark, D., Halchenko, Y.O., Waskom, M.L., Ghosh, S.S., 2011. Nipype: a flexible, lightweight and extensible neuroimaging data processing framework in Python. *Front. Neuroinf.* 5, 13. <https://doi.org/10.3389/fninf.2011.00013>.
- Gorgolewski, K.J., Varoquaux, G., Rivera, G., Schwarz, Y., Ghosh, S.S., Maumet, C., Sochat, V.V., Nichols, T.E., Poldrack, R.A., Poline, J.-B., Yarkoni, T., Margulies, D.S., 2015. NeuroVault.org: a web-based repository for collecting and sharing unthresholded statistical maps of the human brain. *Front. Neuroinf.* 9. <https://doi.org/10.3389/fninf.2015.00008>.
- Gould van Praag, C.D., Garfinkel, S.N., Sparasci, O., Mees, A., Philippides, A.O., Ware, M., Ottaviani, C., Critchley, H.D., 2017. Mind-wandering and alterations to default mode network connectivity when listening to naturalistic versus artificial sounds. *Sci. Rep.* 7, 45273. <https://doi.org/10.1038/srep45273>.
- Grady, C., 2012. The cognitive neuroscience of ageing. *Nat. Rev. Neurosci.* 13, 491–505. <https://doi.org/10.1038/nrn3256>.
- Greenwood, P.M., 2007. Functional plasticity in cognitive aging: review and hypothesis. *Neuropsychology* 21, 657–673. <https://doi.org/10.1037/0894-4105.21.6.657>.
- Greicius, M.D., Krasnow, B., Reiss, A.L., Menon, V., 2003. Functional connectivity in the resting brain: a network analysis of the default mode hypothesis. *Proc. Natl. Acad. Sci. Unit. States Am.* 100, 253–258. <https://doi.org/10.1073/pnas.0135058100>.
- Griswold, M.A., Jakob, P.M., Heidemann, R.M., Nittka, M., Jellus, V., Wang, J., Kiefer, B., Haase, A., 2002. Generalized autocalibrating partially parallel acquisitions (GRAPPA). *Magn. Reson. Med.* 47, 1202–1210. <https://doi.org/10.1002/mrm.10171>.
- Gusnard, D.A., Akbudak, E., Shulman, G.L., Raichle, M.E., 2001. Medial prefrontal cortex and self-referential mental activity: relation to a default mode of brain function. *Proc. Natl. Acad. Sci. Unit. States Am.* 98, 4259–4264. <https://doi.org/10.1073/pnas.071043098>.
- Guterstam, A., Björnsdotter, M., Gentile, G., Ehrsson, H.H., 2015. Posterior cingulate cortex integrates the senses of self-location and body ownership. *Curr. Biol.* 25, 1416–1425. <https://doi.org/10.1016/j.cub.2015.03.059>.
- Hagemann, D., Waldstein, S.R., Thayer, J.F., 2003. Central and autonomic nervous system integration in emotion. *Brain Cognit.* 52, 79–87. [https://doi.org/10.1016/S0278-2626\(03\)00011-3](https://doi.org/10.1016/S0278-2626(03)00011-3).
- Hansen, A.L., Johnsen, B.H., Sollers, J.J., Stenvik, K., Thayer, J.F., 2004. Heart rate variability and its relation to prefrontal cognitive function: the effects of training and detraining. *Eur. J. Appl. Physiol.* 93, 263–272. <https://doi.org/10.1007/s00421-004-1208-0>.
- Hayano, J., Yamada, M., Sakakibara, Y., Fujinami, T., Yokoyama, K., Watanabe, Y., Takata, K., 1990. Short- and long-term effects of cigarette smoking on heart rate variability. *Am. J. Cardiol.* 65, 84–88. [https://doi.org/10.1016/0002-9149\(90\)90030-5](https://doi.org/10.1016/0002-9149(90)90030-5).
- Hoibt, M.A., Niebler, R., Meyer, S.I., Brockmann, K., Becker, C., Huber, H., Gaenslen, A., Godau, J., Eschweiler, G.W., Berg, D., Maetzler, W., 2011. Poor trail making test performance is directly associated with altered dual task prioritization in the elderly - baseline results from the trend study. *PLoS One* 6. <https://doi.org/10.1371/journal.pone.0027831>.
- Holzman, J.B., Bridgett, D.J., 2017. Heart rate variability indices as bio-markers of top-down self-regulatory mechanisms: a meta-analytic review. *Neurosci. Biobehav. Rev.* 74, 233–255. <https://doi.org/10.1016/j.neubiorev.2016.12.032>.
- Huxley, R., Mendis, S., Zheleznyakov, E., Reddy, S., Chan, J., 2010. Body mass index, waist circumference and waist:hip ratio as predictors of cardiovascular risk: a review of the literature. *Eur. J. Clin. Nutr.* 64, 16–22. <https://doi.org/10.1038/ejcn.2009.68>.
- Janssen, I., Katzmarzyk, P.T., Ross, R., 2002. Body mass index, waist circumference, and health risk. *Arch. Intern. Med.* 162, 2074. <https://doi.org/10.1001/archinte.162.18.2074>.
- Jenkinson, M., Beckmann, C.F., Behrens, T.E.J., Woolrich, M.W., Smith, S.M., 2012. Fsl. *Neuroimage* 62, 782–790. <https://doi.org/10.1016/j.neuroimage.2011.09.015>.
- Jennings, J.R., Sheu, L.K., Kuan, D.C.H., Manuck, S.B., Gianaros, P.J., 2016. Resting state connectivity of the medial prefrontal cortex covaries with individual differences in high-frequency heart rate variability. *Psychophysiology* 53, 444–454. <https://doi.org/10.1111/psyp.12586>.
- Kanekiyo, T., Xu, H., Bu, G., 2014. ApoE and Aβ in Alzheimer's disease: accidental encounters or partners? *Neuron*. <https://doi.org/10.1016/j.neuron.2014.01.045>.
- Kemp, A.H., Koenig, J., Thayer, J.F., 2017. From psychological moments to mortality: a multidisciplinary synthesis on heart rate variability spanning the continuum of time. *Neurosci. Biobehav. Rev.* <https://doi.org/10.1016/j.neubiorev.2017.09.006>.
- Kemp, A.H., Quintana, D.S., 2013. The relationship between mental and physical health: insights from the study of heart rate variability. *Int. J. Psychophysiol.* 89, 288–296. <https://doi.org/10.1016/j.ijpsycho.2013.06.018>.
- Kim, D.H., Lipsitz, L.A., Ferrucci, L., Varadhan, R., Guralnik, J.M., Carlson, M.C., Fleisher, L.A., Fried, L.P., Chaves, P.H.M., 2006. Association between reduced heart rate variability and cognitive impairment in older disabled women in the community: women's Health and Aging Study I. *J. Am. Geriatr. Soc.* 54, 1751–1757. <https://doi.org/10.1111/j.1532-5415.2006.00940.x>.
- Koelsch, S., Skouras, S., Jentschke, S., 2013. Neural correlates of emotional personality: a structural and functional magnetic resonance imaging study. *PLoS One* 8, e77196. <https://doi.org/10.1371/journal.pone.0077196>.
- Koenig, J., Thayer, J.F., 2016. Sex differences in healthy human heart rate variability: a meta-analysis. *Neurosci. Biobehav. Rev.* 64, 288–310. <https://doi.org/10.1016/j.neubiorev.2016.03.007>.
- Leaton, R., 2003. Fear and the cerebellum. *Mol. Psychiatr.* 8, 461–462. <https://doi.org/10.1038/sj.mp.4001286>.
- Liao, D., Cai, J., Rosamond, W., Barnes, R., Hutchinson, R., Whitsel, E., Rautaharju, P., Heiss, G., 1997. Cardiac autonomic function and incident coronary heart disease: a population-based case-cohort study the ARIC study. *Am. J. Epidemiol.* 145, 696–706. <https://doi.org/10.1093/aje/145.8.696>.
- Lipsitz, L.A., Goldberger, A.L., 1992. Loss of 'complexity' and aging: potential applications of fractals and chaos theory to senescence. *JAMA, J. Am. Med. Assoc.* 267, 1806–1809. <https://doi.org/10.1001/jama.1992.03480130122036>.
- Loeffler, M., Engel, C., Ahnert, P., Alfermann, D., Arelin, K., Baber, R., Beutner, F., Binder, H., Brähler, E., Burkhardt, R., Ceglarek, U., Enzenbach, C., Fuchs, M., Glaesmer, H., Girlich, F., Hagendorff, A., Häntzsch, M., Hegerl, U., Henger, S., Hensch, T., Hinz, A., Holzendorf, V., Husser, D., Kersting, A., Kiel, A., Kirsten, T., Kratzsch, J., Krohn, K., Luck, T., Melzer, S., Netto, J., Nüchter, M., Raschpichler, M., Rauscher, F.G., Riedel-Heller, S.G., Sander, C., Scholz, M., Schönknecht, P., Schroeter, M.L., Simon, J.-C., Speer, R., Stäker, J., Stein, R., Stöbel-Richter, Y., Stumvoll, M., Tarnok, A., Teren, A., Teupser, D., Then, F.S., Tönjes, A., Treudler, R., Villringer, A., Weissgerber, A., Wiedemann, P., Zachariae, S., Wirkner, K., Thiery, J., 2015. The LIFE-Adult-Study: objectives and design of a population-based cohort study with 10,000 deeply phenotyped adults in Germany. *BMC Publ. Health* 15, 691. <https://doi.org/10.1186/s12889-015-1983-z>.
- Lohmann, G., Margulies, D.S., Horstmann, A., Pleger, B., Lepsien, J., Goldhahn, D., Schloegl, H., Stumvoll, M., Villringer, A., Turner, R., 2010. Eigenvector centrality mapping for analyzing connectivity patterns in fMRI data of the human brain. *PLoS One* 5, e10232. <https://doi.org/10.1371/journal.pone.0010232>.
- Long, X., Benischek, A., Dewey, D., Lebel, C., 2017. Age-related functional brain changes in young children. *Neuroimage* 155, 322–330. <https://doi.org/10.1016/j.neuroimage.2017.04.059>.
- Mahinrad, S., Jukema, J.W., Van Heemst, D., MacFarlane, P.W., Clark, E.N., De Craen, A.J.M., Sabayan, B., 2016. 10-Second heart rate variability and cognitive function in old age. *Neurology* 86, 1120–1127. <https://doi.org/10.1212/WNL.0000000000002499>.
- Maier, S.U., Hare, T.A., 2017. Higher heart-rate variability is associated with ventromedial prefrontal cortex activity and increased resistance to temptation in dietary self-control challenges. *J. Neurosci.* 37, 446–455. <https://doi.org/10.1523/JNEUROSCI.2815-16.2017>.
- Makovac, E., Garfinkel, S., Bassi, B., Macaluso, E., Cercignani, M., Calcagnini, G., Mattei, E., Mancini, M., Agalliu, D., Cortelli, P., Caltagirone, C., Critchley, H., Bozzali, M., 2017. Fear processing is differentially affected by lateralized stimulation of carotid baroreceptors. *Cortex* 99, 200–212. <https://doi.org/10.1016/j.cortex.2017.07.002>.
- Margulies, D.S., Böttger, J., Long, X., Lv, Y., Kelly, C., Schäfer, A., Goldhahn, D., Abushai, A., Milham, M.P., Lohmann, G., Villringer, A., 2010. Resting developments: a review of fMRI post-processing methodologies for spontaneous brain activity. *Magn. Reson. Mater. Phys. Biol. Med.* 23, 289–307. <https://doi.org/10.1007/s10334-010-0228-5>.
- Marques, J.P., Kober, T., Krueger, G., van der Zwaag, W., Van de Moortele, P.F., Gruetter, R., 2010. MP2RAGE, a self bias-field corrected sequence for improved segmentation and T1-mapping at high field. *Neuroimage* 49, 1271–1281. <https://doi.org/10.1016/j.neuroimage.2009.10.002>.
- Mather, M., Thayer, J.F., 2018. How heart rate variability affects emotion regulation brain networks. *Curr. Opin. Behav. Sci.* 19, 98–104. <https://doi.org/10.1016/j.cobeha.2017.12.017>.
- McEwen, B.S., 2003. Interacting mediators of allostasis and allostatic load: towards an understanding of resilience in aging. *Metabolism* 52, 10–16. [https://doi.org/10.1016/S0026-0495\(03\)00295-6](https://doi.org/10.1016/S0026-0495(03)00295-6).
- Mennes, M., Zuo, X.N., Kelly, C., Di Martino, A., Zang, Y.F., Biswal, B., Castellanos, F.X., Milham, M.P., 2011. Linking inter-individual differences in neural activation and behavior to intrinsic brain dynamics. *Neuroimage* 54, 2950–2959. <https://doi.org/10.1016/j.neuroimage.2010.10.046>.
- Molfino, A., Fiorentini, A., Tubani, L., Martuscelli, M., Fanelli, F.R., Laviano, A., 2009. Body mass index is related to autonomic nervous system activity as measured by

- heart rate variability. *Eur. J. Clin. Nutr.* 63, 1263–1265. <https://doi.org/10.1038/ejcn.2009.35>.
- Mueller, K., Arelin, K., Möller, H.E., Sacher, J., Kratzsch, J., Luck, T., Riedel-Heller, S., Villringer, A., Schroeter, M.L., 2016. Serum BDNF correlates with connectivity in the (pre)motor hub in the aging human brain—a resting-state fMRI pilot study. *Neurobiol. Aging* 38, 181–187. <https://doi.org/10.1016/j.neurobiolaging.2015.11.003>.
- Munoz, M.L., Van Roon, A., Riese, H., Thio, C., Oostenbroek, E., Westrik, I., De Geus, E.J.C., Gansevoort, R., Lefrandt, J., Nolte, I.M., Snieder, H., 2015. Validity of (Ultra-)Short recordings for heart rate variability measurements. *PLoS One* 10, 1–15. <https://doi.org/10.1371/journal.pone.0138921>.
- Nussinovitch, U., Elishkevitz, K.P., Kammer, K., Nussinovitch, M., Segev, S., Volovitz, B., Nussinovitch, N., 2011a. The efficiency of 10-second resting heart rate for the evaluation of short-term heart rate variability indices. *PACE - Pacing Clin. Electrophysiol.* 34, 1498–1502. <https://doi.org/10.1111/j.1540-8159.2011.03178.x>.
- Nussinovitch, U., Elishkevitz, K.P., Katz, K., Nussinovitch, M., Segev, S., Volovitz, B., Nussinovitch, N., 2011b. Reliability of ultra-short ECG indices for heart rate variability. *Ann. Noninvasive Electrocardiol.* 16, 117–122. <https://doi.org/10.1111/j.1542-474X.2011.00417.x>.
- Park, H.-D., Correia, S., Ducorps, A., Tallon-Baudry, C., 2014. Spontaneous fluctuations in neural responses to heartbeats predict visual detection. *Nat. Neurosci.* 17, 612–618. <https://doi.org/10.1038/nn.3671>.
- Posner, J., Cha, J., Wang, Z., Talati, A., Warner, V., Gerber, A., Peterson, B.S., Weissman, M., 2016. Increased default mode network connectivity in individuals at high familial risk for depression. *Neuropsychopharmacology* 41, 1759–1767. <https://doi.org/10.1038/npp.2015.342>.
- Power, J.D., Barnes, K.A., Snyder, A.Z., Schlaggar, B.L., Petersen, S.E., 2012. Spurious but systematic correlations in functional connectivity MRI networks arise from subject motion. *Neuroimage* 59, 2142–2154. <https://doi.org/10.1016/j.neuroimage.2011.10.018>.
- Power, J.D., Schlaggar, B.L., Petersen, S.E., 2015. Recent progress and outstanding issues in motion correction in resting state fMRI. *Neuroimage* 105, 536–551. <https://doi.org/10.1016/j.neuroimage.2014.10.044>.
- Price, J.L., 2007. Definition of the orbital cortex in relation to specific connections with limbic and visceral structures and other cortical regions. In: *Annals of the New York Academy of Sciences*, pp. 54–71. <https://doi.org/10.1196/annals.1401.008>.
- Price, J.L., 1999. Prefrontal cortical networks related to visceral function and mood. In: *Annals of the New York Academy of Sciences*, pp. 383–396. <https://doi.org/10.1111/j.1749-6632.1999.tb09278.x>.
- Raichle, M.E., MacLeod, A.M., Snyder, A.Z., Powers, W.J., Gusnard, D.A., Shulman, G.L., 2001. A default mode of brain function. *Proc. Natl. Acad. Sci. Unit. States Am.* 98, 676–682. <https://doi.org/10.1073/pnas.98.2.676>.
- R Core Team, 2016. *R: A Language and Environment for Statistical Computing*. R Foundation for Statistical Computing, Vienna, Austria.
- Reitan, R.M., 1955. Certain differential effects of left and right cerebral lesions in human adults. *J. Comp. Physiol. Psychol.* 48, 474–477.
- Reitan, R.M., Wolfson, D., 1995. Category test and trail making test as measures of frontal lobe functions. *Clin. Neuropsychol.* 9, 50–56. <https://doi.org/10.1080/13854049508402057>.
- Rokem, A., Trumpis, M., Perez, F., 2009. Nitime: time-series analysis for neuroimaging data. In: *Proc. 8th Python Sci. Conf. (SciPy 2009)* 1–8.
- Rubinov, M., Sporns, O., 2010. Complex network measures of brain connectivity: uses and interpretations. *Neuroimage* 52, 1059–1069. <https://doi.org/10.1016/j.neuroimage.2009.10.003>.
- Sacchetti, B., Baldi, E., Lorenzini, C.A., Bucherelli, C., 2002. Cerebellar role in fear-conditioning consolidation. *Proc. Natl. Acad. Sci. Unit. States Am.* 99, 8406–8411. <https://doi.org/10.1073/pnas.112660399>.
- Sakaki, M., Yoo, H.J., Nga, L., Lee, T.-H., Thayer, J.F., Mather, M., 2016. Heart rate variability is associated with amygdala functional connectivity with MPFC across younger and older adults. *Neuroimage* 139, 44–52. <https://doi.org/10.1016/j.neuroimage.2016.05.076>.
- Shehzad, Z., Kelly, A.M.C., Reiss, P.T., Gee, D.G., Gotimer, K., Uddin, L.Q., Lee, S.H., Margulies, D.S., Roy, A.K., Biswal, B.B., Petkova, E., Castellanos, F.X., Milham, M.P., 2009. The resting brain: unconstrained yet reliable. *Cerebr. Cortex* 19, 2209–2229. <https://doi.org/10.1093/cercor/bhn256>.
- Sin, N.L., Sloan, R.P., McKinley, P.S., Almeida, D.M., 2016. Linking daily stress processes and laboratory-based heart rate variability in a national sample of midlife and older adults. *Psychosom. Med.* 78, 573–582. <https://doi.org/10.1097/PSY.0000000000000306>.
- Singh, J.P., Larson, M.G., Tsuji, H., Evans, J.C., O'Donnell, C.J., Levy, D., 1998. Reduced heart rate variability and new-onset hypertension: insights into pathogenesis of hypertension: the Framingham Heart Study. *Hypertension* 32, 293–297. <https://doi.org/10.1161/01.HYP.32.2.293>.
- Smith, R., Thayer, J.F., Khalsa, S.S., Lane, R.D., 2017. The hierarchical basis of neurovisceral integration. *Neurosci. Biobehav. Rev.* 75, 274–296. <https://doi.org/10.1016/j.neubiorev.2017.02.003>.
- Smith, S.M., Nichols, T.E., Vidaurre, D., Winkler, A.M., Behrens, T.E.J., Glasser, M.F., Ugurbil, K., Barch, D.M., Van Essen, D.C., Miller, K.L., 2015. A positive-negative mode of population covariation links brain connectivity, demographics and behavior. *Nat. Neurosci.* 18, 1565–1567. <https://doi.org/10.1038/nn.4125>.
- Streitbürger, D.P., Pampel, A., Krueger, G., Lepsius, J., Schroeter, M.L., Mueller, K., Möller, H.E., 2014. Impact of image acquisition on voxel-based-morphometry investigations of age-related structural brain changes. *Neuroimage* 87, 170–182. <https://doi.org/10.1016/j.neuroimage.2013.10.051>.
- Swank, A.M., 1996. Physical dimensions of aging. *Med. Sci. Sports Exerc.* 28, 398–399. <https://doi.org/10.1097/00005768-199603000-00018>.
- Tarvainen, M.P., Niskanen, J.-P., Lipponen, J.A., Ranta-Aho, P.O., Karjalainen, P.A., 2014. Kubios HRV—heart rate variability analysis software. *Comput. Methods Progr. Biomed.* 113, 210–220. <https://doi.org/10.1016/j.cmpb.2013.07.024>.
- Task Force of the European Society of Cardiology and the North American Society of Pacing and Electrophysiology, 1996. Heart rate variability: Standards of measurement, physiological interpretation, and clinical use. *Circulation* 93, 1043–1065.
- Tataranni, P.A., Gautier, J.F., Chen, K., Uecker, A., Bandy, D., Salbe, A.D., Pratley, R.E., Lawson, M., Reiman, E.M., Ravussin, E., 1999. Neuroanatomical correlates of hunger and satiation in humans using positron emission tomography. *Proc. Natl. Acad. Sci. U. S. A* 96, 4569–4574. <https://doi.org/10.1073/pnas.96.8.4569>.
- Taubert, M., Lohmann, G., Margulies, D.S., Villringer, A., Ragert, P., 2011. Long-term effects of motor training on resting-state networks and underlying brain structure. *Neuroimage* 57, 1492–1498. <https://doi.org/10.1016/j.neuroimage.2011.05.078>.
- Thayer, J.F., Ahs, F., Fredrikson, M., Sollers, J.J., Wager, T.D., 2012. A meta-analysis of heart rate variability and neuroimaging studies: implications for heart rate variability as a marker of stress and health. *Neurosci. Biobehav. Rev.* 36, 747–756. <https://doi.org/10.1016/j.neubiorev.2011.11.009>.
- Thayer, J.F., Lane, R.D., 2007. The role of vagal function in the risk for cardiovascular disease and mortality. *Biol. Psychol.* 74, 224–242. <https://doi.org/10.1016/j.biopsycho.2005.11.013>.
- Thayer, J.F., Lane, R.D., 2000. A model of neurovisceral integration in emotion regulation and dysregulation. *J. Affect. Disord.* 61, 201–216. [https://doi.org/10.1016/S0165-0327\(00\)00338-4](https://doi.org/10.1016/S0165-0327(00)00338-4).
- Thayer, J.F., Ruiz-Padial, E., 2006. Neurovisceral integration, emotions and health: an update. *Int. Congr. Ser.* 1287, 122–127. <https://doi.org/10.1016/j.ics.2005.12.018>.
- Thayer, J.F., Sollers, J.J., Friedman, B.H., Koenig, J., 2015. Gender differences in the relationship between resting heart rate variability and 24-hour blood pressure variability. *Blood Press.* 7051, 1–5. <https://doi.org/10.3109/08037051.2016.1090721>.
- Thayer, J.F., Sollers, J.J., Labiner, D.M., Weinand, M., Herring, A.M., Lane, R.D., Ahern, G.L., 2009. Age-related differences in prefrontal control of heart rate in humans: a pharmacological blockade study. *Int. J. Psychophysiol.* 72, 81–88. <https://doi.org/10.1016/j.ijpsycho.2008.04.007>.
- Thayer, J.F., Yamamoto, S.S., Brosschot, J.F., 2010. The relationship of autonomic imbalance, heart rate variability and cardiovascular disease risk factors. *Int. J. Cardiol.* 141, 122–131. <https://doi.org/10.1016/j.ijcard.2009.09.543>.
- Then, F.S., Luck, T., Lupp, M., Arelin, K., Schroeter, M.L., Engel, C., Löffler, M., Thiery, J., Villringer, A., Riedel-Heller, S.G., 2014. Association between mental demands at work and cognitive functioning in the general population – results of the health study of the Leipzig research center for civilization diseases (LIFE). *J. Occup. Med. Toxicol.* 9, 23. <https://doi.org/10.1186/1745-6673-9-23>.
- Tombaugh, T.N., 2004. Trail Making Test A and B: normative data stratified by age and education. *Arch. Clin. Neuropsychol.* 19, 203–214. [https://doi.org/10.1016/S0887-6177\(03\)00039-8](https://doi.org/10.1016/S0887-6177(03)00039-8).
- Tukey, J.W., 1977. *Exploratory Data Analysis*. Addison-Wesley, Reading, MA.
- Uddin, L.Q., Kelly, A.M.C., Biswal, B.B., Castellanos, F.X., Milham, M.P., 2009. Functional connectivity of default mode network components: correlation, anticorrelation, and causality. *Hum. Brain Mapp.* 30, 625–637. <https://doi.org/10.1002/hbm.20531>.
- Umetani, K., Singer, D.H., McCraty, R., Atkinson, M., 1998. Twenty-four hour time domain heart rate variability and heart rate: relations to age and gender over nine decades. *J. Am. Coll. Cardiol.* 31, 593–601. [https://doi.org/10.1016/S0735-1097\(97\)00554-8](https://doi.org/10.1016/S0735-1097(97)00554-8).
- Van Eden, C.G., Buijs, R.M., 2000. Functional neuroanatomy of the prefrontal cortex: autonomic interactions. *Prog. Brain Res.* 126, 49–62. [https://doi.org/10.1016/S0079-6123\(00\)26006-8](https://doi.org/10.1016/S0079-6123(00)26006-8).
- Voss, A., Schroeder, R., Heitmann, A., Peters, A., Perz, S., 2015. Short-term heart rate variability - influence of gender and age in healthy subjects. *PLoS One* 10, e0118308. <https://doi.org/10.1371/journal.pone.0118308>.
- Wei, L., Chen, H., Wu, G.R., 2018. Heart rate variability associated with grey matter volumes in striatal and limbic structures of the central autonomic network. *Brain Res.* 1681, 14–20. <https://doi.org/10.1016/j.brainres.2017.12.024>.
- Williams, D.P., Cash, C., Rankin, C., Bernardi, A., Koenig, J., Thayer, J.F., 2015. Resting heart rate variability predicts self-reported difficulties in emotion regulation: a focus on different facets of emotion regulation. *Front. Psychol.* 6, 1–8. <https://doi.org/10.3389/fpsyg.2015.00261>.
- Wink, A.M., de Munck, J.C., van der Werf, Y.D., van den Heuvel, O.A., Barkhof, F., 2012. Fast eigenvector centrality mapping of voxel-wise connectivity in functional magnetic resonance imaging: implementation, validation, and interpretation. *Brain Connect.* 2, 265–274. <https://doi.org/10.1089/brain.2012.0087>.
- Winkelmann, T., Thayer, J.F., Pohlack, S., Nees, F., Grimm, O., Flor, H., 2017. Structural brain correlates of heart rate variability in a healthy young adult population. *Brain Struct. Funct.* 222, 1061–1068. <https://doi.org/10.1007/s00429-016-1185-1>.
- Wong, S.W., Masse, N., Kimmerly, D.S., Menon, R.S., Shoemaker, J.K., 2007. Ventral medial prefrontal cortex and cardiovascular control in conscious humans. *Neuroimage* 35, 698–708. <https://doi.org/10.1016/j.neuroimage.2006.12.027>.
- Yoo, H.J., Thayer, J.F., Greening, S., Lee, T.-H., Ponzio, A., Min, J., Sakaki, M., Nga, L., Mather, M., Koenig, J., 2017. Brain structural concomitants of resting state heart rate variability in the young and old: evidence from two independent samples. *Brain Struct. Funct.* <https://doi.org/10.1007/s00429-017-1519-7>.
- Yu, C., Zhou, Y., Liu, Y., Jiang, T., Dong, H., Zhang, Y., Walter, M., 2011. Functional segregation of the human cingulate cortex is confirmed by functional connectivity based neuroanatomical parcellation. *Neuroimage* 54, 2571–2581. <https://doi.org/10.1016/j.neuroimage.2010.11.018>.
- Zeki Al Hazzouri, A., Haan, M.N., Deng, Y., Neuhaus, J., Yaffe, K., 2014. Reduced heart rate variability is associated with worse cognitive performance in elderly

- Mexican Americans. *Hypertension* 63, 181–187. <https://doi.org/10.1161/Hypertensionaha.113.01888>.
- Zulfiqar, U., Jurivich, D.A., Gao, W., Singer, D.H., 2010. Relation of high heart rate variability to healthy longevity. *Am. J. Cardiol.* 105, 1181–1185. <https://doi.org/10.1016/j.amjcard.2009.12.022>.
- Zuo, X.-N., Di Martino, A., Kelly, C., Shehzad, Z.E., Gee, D.G., Klein, D.F., Castellanos, F.X., Biswal, B.B., Milham, M.P., 2010. The oscillating brain: complex and reliable. *Neuroimage* 49, 1432–1445. <https://doi.org/10.1016/j.Neuroimage.2009.09.037>.
- Zuo, X.N., Ehmke, R., Mennes, M., Imperati, D., Castellanos, F.X., Sporns, O., Milham, M.P., 2012. Network centrality in the human functional connectome. *Cerebr. Cortex* 22, 1862–1875. <https://doi.org/10.1093/cercor/bhr269>.

7.2.5 Acute Psychosocial Stress Alters Thalamic Network Centrality. Reinelt, Uhlig et al., NeuroImage (2019)

NeuroImage 199 (2019) 680–690



Contents lists available at ScienceDirect

NeuroImage

journal homepage: www.elsevier.com/locate/neuroimage



Acute psychosocial stress alters thalamic network centrality



Janis Reinelt^{a,*}, Marie Uhlig^{a,b,1}, Karsten Müller^a, Mark E. Lauckner^{a,f}, Deniz Kumral^{a,g}, H. Lina Schaare^{a,b}, Blazej M. Baczkowski^{a,b,c}, Anahit Babayan^a, Miray Erbey^{a,g,h}, Josefina Roebbig^a, Andrea Reiter^{a,c,i}, Yoon-Ju Bae^d, Juergen Kratzsch^d, Joachim Thiery^d, Talma Hendler^j, Arno Villringer^{a,g}, Michael Gaebler^{a,g}

^a Department of Neurology, Max Planck Institute for Human Cognitive and Brain Sciences, Leipzig, Germany

^b International Max Planck Research School NeuroCon, Leipzig, Germany

^c Institute of Psychology, University of Leipzig, Leipzig, Germany

^d Institute for Laboratory Medicine, Clinical Chemistry and Molecular Diagnostics (ILM) of the Medical Faculty at the University of Leipzig, Leipzig, Germany

^e Lifespan Developmental Neuroscience, Technische Universität Dresden, Dresden, Germany

^f Charité – Universitätsmedizin Berlin, Berlin, Germany

^g MindBrainBody Institute at the Berlin School of Mind and Brain, Humboldt-Universität zu Berlin, Berlin, Germany

^h International Max Planck School on the Life Course, Max Planck Institute for Human Development, Berlin, Germany

ⁱ Max Planck UCL Centre for Computational Psychiatry and Ageing Research, London, United Kingdom

^j School of Psychological Science, Department of Physiology and Pharmacology and Psychiatry, Faculty of Medicine, Sagol School of Neuroscience, Tel Aviv University, Tel Aviv, Israel

ARTICLE INFO

Keywords:
Resting-state fMRI
Eigenvector centrality mapping
Stress
Cortisol
Thalamus
TSST

ABSTRACT

Acute stress triggers a broad psychophysiological response that is adaptive if rapidly activated and terminated. While the brain controls the stress response, it is strongly affected by it. Previous research of stress effects on brain activation and connectivity has mainly focused on pre-defined brain regions or networks, potentially missing changes in the rest of the brain. We here investigated how both stress reactivity and stress recovery are reflected in whole-brain network topology and how changes in functional connectivity relate to other stress measures.

Healthy young males ($n = 67$) completed the Trier Social Stress Test or a control task. From 60 min before until 105 min after stress onset, blocks of resting-state fMRI were acquired. Subjective, autonomic, and endocrine measures of the stress response were assessed throughout the experiment. Whole-brain network topology was quantified using Eigenvector centrality (EC) mapping, which detects central hubs of a network.

Stress influenced subjective affect, autonomic activity, and endocrine measures. EC differences between groups as well as before and after stress exposure were found in the thalamus, due to widespread connectivity changes in the brain. Stress-driven EC increases in the thalamus were significantly correlated with subjective stress ratings and showed non-significant trends for a correlation with heart rate variability and saliva cortisol. Furthermore, increases in thalamic EC and in saliva cortisol persisted until 105 min after stress onset.

We conclude that thalamic areas are central for information processing after stress exposure and may provide an interface for the stress response in the rest of the body and in the mind.

1. Introduction

A typical response to stress involves changes in subjective experience (Hellhammer and Schubert, 2012), in the brain's functional connectivity and activity (van Coort et al., 2017), and in the autonomic nervous as well as the endocrine system (Allen et al., 2017). Through these changes, the acute stress response enables adequate reactions to a stressor. It is

therefore highly adaptive, especially if rapidly activated and rapidly terminated (McEwen and Gianaros, 2011; Steptoe and Kivimäki, 2013). Moreover, an efficient neural processing of stressors is crucial for adapting to future occurrences of similar stressors (Peters et al., 2017). Insufficient initialization or delayed termination of the stress response ("delayed stress recovery") constitute a major risk factor for mental (Fanelli et al., 2012; Hermans et al., 2014; Pittenger and Duman, 2008)

* Corresponding author. Max Planck Institute for Human Cognitive and Brain Sciences, Stephanstr. 1A, 04108, Leipzig, Germany.

E-mail address: reinelt@chm.gpg.de (J. Reinelt).

¹ shared first authors.

<https://doi.org/10.1016/j.neuroimage.2019.06.005>

Received 18 December 2018; Received in revised form 29 May 2019; Accepted 3 June 2019

Available online 5 June 2019

1053-8119/© 2019 Published by Elsevier Inc.



Acute psychosocial stress alters thalamic network centrality

Janis Reinelt^{a,*}, Marie Uhlig^{a,b,1}, Karsten Müller^a, Mark E. Lauckner^{a,f}, Deniz Kumral^{a,g},
H. Lina Schaare^{a,b}, Blazej M. Baczowski^{a,b,c}, Anahit Babayan^a, Miray Erbey^{a,g,h},
Josefin Roebbig^a, Andrea Reiter^{a,e,i}, Yoon-Ju Bae^d, Juergen Kratzsch^d, Joachim Thiery^d,
Talma Hendler^j, Arno Villringer^{a,g}, Michael Gaebler^{a,g}

^a Department of Neurology, Max Planck Institute for Human Cognitive and Brain Sciences, Leipzig, Germany

^b International Max Planck Research School NeuroCom, Leipzig, Germany

^c Institute of Psychology, University of Leipzig, Leipzig, Germany

^d Institute for Laboratory Medicine, Clinical Chemistry and Molecular Diagnostics (ILM) of the Medical Faculty at the University of Leipzig, Leipzig, Germany

^e Lifespan Developmental Neuroscience, Technische Universität Dresden, Dresden, Germany

^f Charité – Universitätsmedizin Berlin, Berlin, Germany

^g MindBrainBody Institute at the Berlin School of Mind and Brain, Humboldt-Universität zu Berlin, Berlin, Germany

^h International Max Planck School on the Life Course, Max Planck Institute for Human Development, Berlin, Germany

ⁱ Max Planck UCL Centre for Computational Psychiatry and Ageing Research, London, United Kingdom

^j School of Psychological Science, Departments of Physiology and Pharmacology and Psychiatry, Faculty of Medicine, Sagol School Neuroscience, Tel Aviv University, Tel Aviv, Israel



ARTICLE INFO

Keywords:

Resting-state fMRI
Eigenvector centrality mapping
Stress
Cortisol
Thalamus
TSST

ABSTRACT

Acute stress triggers a broad psychophysiological response that is adaptive if rapidly activated and terminated. While the brain controls the stress response, it is strongly affected by it. Previous research of stress effects on brain activation and connectivity has mainly focused on pre-defined brain regions or networks, potentially missing changes in the rest of the brain. We here investigated how both stress reactivity and stress recovery are reflected in whole-brain network topology and how changes in functional connectivity relate to other stress measures.

Healthy young males ($n = 67$) completed the Trier Social Stress Test or a control task. From 60 min before until 105 min after stress onset, blocks of resting-state fMRI were acquired. Subjective, autonomic, and endocrine measures of the stress response were assessed throughout the experiment. Whole-brain network topology was quantified using Eigenvector centrality (EC) mapping, which detects central hubs of a network.

Stress influenced subjective affect, autonomic activity, and endocrine measures. EC differences between groups as well as before and after stress exposure were found in the thalamus, due to widespread connectivity changes in the brain. Stress-driven EC increases in the thalamus were significantly correlated with subjective stress ratings and showed non-significant trends for a correlation with heart rate variability and saliva cortisol. Furthermore, increases in thalamic EC and in saliva cortisol persisted until 105 min after stress onset.

We conclude that thalamic areas are central for information processing after stress exposure and may provide an interface for the stress response in the rest of the body and in the mind.

1. Introduction

A typical response to stress involves changes in subjective experience (Hellhammer and Schubert, 2012), in the brain's functional connectivity and activity (van Oort et al., 2017), and in the autonomic nervous as well as the endocrine system (Allen et al., 2017). Through these changes, the acute stress response enables adequate reactions to a stressor. It is

therefore highly adaptive, especially if rapidly activated and rapidly terminated (McEwen and Gianaros, 2011; Steptoe and Kivimäki, 2013). Moreover, an efficient neural processing of stressors is crucial for adapting to future occurrences of similar stressors (Peters et al., 2017). Insufficient initialisation or delayed termination of the stress response (“delayed stress recovery”) constitute a major risk factor for mental (Faravelli et al., 2012; Hermans et al., 2014; Pittenger and Duman, 2008)

* Corresponding author. Max Planck Institute for Human Cognitive and Brain Sciences, Stephanstr. 1A, 04103, Leipzig, Germany.

E-mail address: reinelt@cbs.mpg.de (J. Reinelt).

¹ shared first authors.

and physical health (Stephoe and Kivimäki, 2013). Although it is largely acknowledged that brain networks orchestrate the overall stress response and adaptability (Hermans et al., 2014), it remains unclear what circuit guides it (Peters et al., 2017).

Stress-driven changes in the activation and functional connectivity of the brain have been reported in several regions relevant to emotional processing, autonomic control, thoughts, and memory (van Oort et al., 2017). For example, seed-based connectivity analysis of resting-state data acquired after stress exposure showed an increased connectivity of the amygdala – using the averaged time course of bilateral amygdala seeds (Quaedflieg et al., 2015; van Marle et al., 2010) – with multiple regions, including the parahippocampal gyrus and the medial prefrontal cortex (Quaedflieg et al., 2015) as well as the dorsal anterior cingulate (van Marle et al., 2010). Persistent amygdala-hippocampus connectivity, between a bilateral hippocampus seed and amygdala regions, was also related to prolonged subjective stress (Vaisvaser et al., 2013). In another study, elevated connectivity between a bilateral amygdala seed and the posterior cingulate cortex, the ventromedial prefrontal cortex (vmPFC), and the frontal pole until 60 min after stressor offset was found (Veer et al., 2011).

While these studies have shown connectivity changes between predefined subcortical seed regions and the rest of the brain, this region-of-interest (ROI) approach may have missed connectivity between other regions in the brain that are relevant for stress processing. To our knowledge, only two studies so far have investigated neural effects of acute stress at the whole-brain level: Using an independent component approach, which requires a priori definition of the number of components or networks, Hermans et al. (2011) found increased connectivity in regions of the salience network, including anterior insula, inferotemporal cortex, amygdala, and thalamus. Through a pharmacological intervention, blocking either β -adrenergic receptors or cortisol synthesis, the authors could also relate stress-induced connectivity increases to endocrine changes. In another study, Maron-Katz et al. analysed whole-brain functional connectivity using a parcellation-based univariate analysis to show an increased coupling of the thalamus with regions in the frontal, parietal, and temporal lobes after subjects were exposed to a stressful arithmetic task (Maron-Katz et al., 2016). Another study, in which stress was induced through a stressful arithmetic task in the MRI, used the graph-based metrics of “network efficiency” in 106 literature-derived ROIs and of “betweenness centrality” in 12 ROIs (in hippocampus, amygdala, and mPFC) to find a stress-related decrease in “flow of information” (Wheelock et al., 2018).

We here aimed to expand the scope on the stress response in terms of modalities (including psychological, bodily, and brain measures), time (longer sampling period until 105 min after onset of the intervention), and space (voxel-level connectivity analysis), compared to previous stress studies. We chose the Trier Social Stress Test (TSST) as a naturalistic stressor with pronounced, lasting effects on subjective, autonomic, and endocrine stress measures (Allen et al., 2014). To closely control for the study procedure – and particularly for physical activity (standing, walking), which is known to influence endocrine and autonomic parameters (Het et al., 2009) – the so-called “placebo TSST” was chosen as a control intervention (Het et al., 2009). This control procedure involves the same sequence of standing, sitting, talking, and calculating as the TSST but without the social stress of a committee. To investigate stress-related changes in functional network topology, Eigenvector centrality (EC) mapping (ECM) was applied (Lohmann et al., 2010). ECM is an exploratory and data-driven whole-brain approach that allows the quantification of the importance of network nodes with a voxel-wise resolution and without the need to preselect specific ROIs. In contrast to other centrality measures (e.g., [within-module] degree centrality), EC uses all correlations of the adjacency matrix, that is, it not only regards direct connections but integrates information about all linked regions. To maximally capture the large-scale effects of stress on brain functional connectivity (Hermans et al., 2014), the whole-brain approach of ECM was chosen. Voxels and regions with high EC can be considered

“influential hubs” within a network, which facilitate functional integration and are essential to network resilience under stress perturbation (Joyce et al., 2010; Rubinov and Sporns, 2010).

In this study, we aimed to (1) investigate stress reactivity in the brain and hypothesized immediate stress-driven effects on whole-brain network topology, based on previous findings of functional connectivity changes after stress (Hermans et al., 2014; van Oort et al., 2017). We also aimed to (2) explore the association between neural stress reactivity and other dimensions of the stress response, expecting a correlation with subjective stress ratings as well as with autonomic (heart rate and its variability) and – particularly – endocrine stress markers (i.e., cortisol) (Hermans et al., 2014). Finally, we aimed to (3) characterize the time course of stress-induced brain connectivity alterations by extending the sampling window to the point at which stress-related changes in functional connectivity are assumed to recover (i.e., 60–90 min after stress onset or approximately 40–70 min after stress offset; Hermans et al., 2014).

2. Methods

2.1. Participants

Male participants between 18 and 35 were recruited via leaflets, online advertisements, and from a database at the Max Planck Institute for Human Cognitive and Brain Sciences in Leipzig, Germany. We limited the sample to male participants, since the female reproductive cycle impacts stress hormone levels (Childs et al., 2010). Prior to the stress study, participants were tested according to the protocol of the MPI-Leipzig Mind-Brain-Body database that comprised cognitive testing, blood screening, anthropometric measurements, structural and resting-state functional MRI scans, resting-state electroencephalography (EEG), self-report questionnaires, and a structured clinical interview (for details, cf. Babayan et al., 2019; Mendes et al., 2019). A pre-screening was conducted via telephone with the following exclusion criteria: smoking, excessive alcohol or drug consumption, past or present enrolment in a psychology study programme, no previous exposure to the TSST or similar stress experiments, regular medication intake, history of cardiovascular, psychiatric, or neurological diseases, or body mass index higher than 27 kg/m². For magnetic resonance imaging (MRI), standard MRI exclusion criteria additionally applied (e.g., tattoos, irremovable metal objects such as retainers or piercings, tinnitus, or claustrophobia). For details, cf. Babayan et al. (2019) and Mendes et al. (2019). 67 participants were included in the study and randomly assigned to either the TSST (n = 33) or the control group (n = 34). Written informed consent was obtained from all participants. The study was approved by the ethics committee at the Medical Faculty of the University of Leipzig (number 385-1417112014). Participants received a financial compensation for their participation.

2.2. Procedure

For an overview of the whole procedure, see Fig. 1. Appointments were scheduled at the same time of day (11:45 am) to control for diurnal fluctuations of hormones (e.g., cortisol). Participants were asked to get at least 8 h of sleep before the day of the experiment, to get up no later than 9 am, to have a normal breakfast, and then refrain from eating until their appointment. Additionally, participants were asked not to exercise or to consume stimulant drinks like coffee or black tea before their study appointment, since caffeine intake may alter the hypothalamic-pituitary-adrenal axis response (al'Absi et al., 1998) and resting-state measures (Rack-Gomer et al., 2009). The experimental staff was blind to the participant's group assignment before the intervention, after which they did not communicate with the participant (until the second anatomical scan). Throughout the experiment, there were fifteen time points (T0-T14) at which saliva samples and subjective measures were collected and 14 time points (T1-T14) at which blood samples were collected. After a short

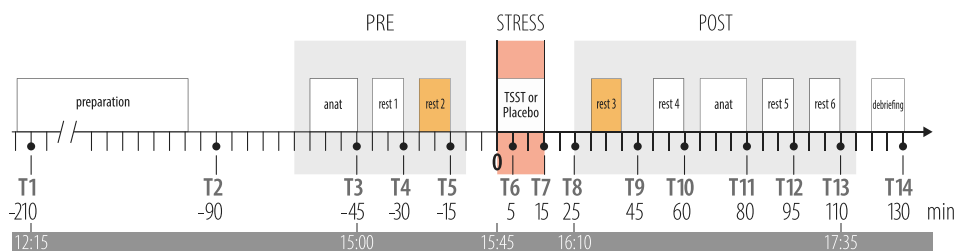


Fig. 1. Experimental design. Between-subject design with one group ($n = 33$) undergoing the Trier Social Stress Test (TSST) and the other ($n = 34$) a “placebo” TSST. Six 8-min blocks of resting-state fMRI were acquired: two before (*rest1*, *rest2*) and four after the intervention (*rest3*–*rest6*). During resting-state fMRI, participants were instructed to fixate a crosshair. Psychometric ratings, saliva, and blood samples were acquired at 14 time points throughout the experiment (T1–T14). The hours indicate the time at which important sampling points were scheduled. Heart rate was recorded inside and outside the scanner. The resting-state blocks before (*rest2*) and after (*rest3*) the intervention (labelled in orange) were used for the analysis of stress reactivity. White boxes labelled “anat” represent sequences of cerebral blood flow (pulsed arterial spin labelling; results reported elsewhere) and high-resolution anatomical image acquisition (MP2RAGE). The grey boxes indicate phases in the MRI. The TSST and the control condition took place outside of the scanner.

period of familiarisation to the experimental environment, signing consent forms, and receiving instructions, participants chewed on a first Salivette swab (Sarstedt AG & Co. KG, Nümbrecht, Germany) while they answered questions about their current subjective experiences (T0). The second psychometric and saliva sample were acquired together with the first blood sample, after participants were equipped with an intravenous catheter and the portable electrocardiography (ECG) device (T1, 210 min before TSST onset). Participants then gave a urine sample before they had a 15-min break, during which they received a standardised lunch. Participants then filled out self-report trait questionnaires (see below and Table S2) and rested for 30 min, before sampling instance T2 followed (90 min before TSST onset). Afterwards, participants completed the pre-intervention scanning session, consisting of a quin pilot (to plan details like the slice positioning of the subsequent image acquisition), a pulsed arterial spin labelling (pASL) scan (the results of which will be reported elsewhere), a high-resolution anatomical scan (MP2RAGE), and two resting-state (RS) scans (T2*-weighted EPI). While participants were in the MRI, they completed two more sampling instances: T3 between the MP2RAGE and the first RS scan (45 min before TSST onset) as well as T4 between the two successive RS scans (30 min before TSST onset). After the baseline RS scan (*rest2*, 25 min before TSST onset), sampling instance T5 followed in the MRI (15 min before TSST onset). Participants were then brought to the testing room, where they underwent either the TSST or the “placebo” TSST (cf. Next section and supplementary material for details). During the intervention, there were two sampling instances: T6 (+5 min after TSST onset) and T7 (+15 min after TSST onset). Following the intervention, participants were brought back to the MRI, where sampling instance T8 (+25 min after TSST onset) followed. The post-intervention scan protocol consisted of a second quin pilot, two RS scans (*rest3*, +30 min after TSST onset, and *rest4*, +50 min after TSST onset), a second pASL scan, a second high-resolution anatomical scan (MP2RAGE), again followed by two RS scans (*rest5*, +85 min after TSST onset, and *rest6*, +105 min after TSST onset). Between the sequences, there were sampling instances T9 (+45 min after TSST onset), T10 (+60 min after TSST onset), T11 (+80 min after TSST onset), T12 (+95 min after TSST onset), and T13 (+110 min after TSST onset). For the sampling instances between the scans, participants stayed within the MRI bore and the scanner bed was not moved. The Salivette was placed inside the participant’s mouth through the bore opening close to his head. Blood drawing inside the scanner was accomplished through a tube attached to the intravenous catheter. Following the last RS scan, participants left the

MRI and completed a post-event processing questionnaire (Fehm et al., 2008), the results of which will be presented elsewhere. In the end, participants were brought to a separate room, where they were debriefed. The experiment ended with final sampling instance T14 (+130 min after TSST onset).

2.3. Stress and control intervention

To elicit a pronounced stress response, which is required for the study of its time course (Linden et al., 1997), we chose the Trier Social Stress Test (TSST) as one of the strongest and most naturalistic stressors applicable in humans (Kirschbaum et al., 1993). To tightly control for physical and cognitive load, the “placebo” TSST was selected as the control task (Het et al., 2009; Kirschbaum et al., 1993). A detailed description of both conditions can be found in the supplementary material. After participants in the TSST group had finished the mental arithmetics, they were told that another task would follow in the MRI; to maximize and extend the psychological and physiological effects of the TSST. They were then brought back to the scanning area in the company of the experimenter and the committee members. After *rest4* (+60 min after TSST onset), they were told that no additional task would follow and that they could relax.

2.4. Psychometric data

Throughout the experiment, subjective ratings were collected at 15 time points (T0–T14, see Fig. 1). Except for the first two (T0, T1), all sampling instances followed the same procedure: questionnaires were presented with OpenSesame 3.1.2 (Mathôt et al., 2011) on a laptop screen (outside the scanner) or on the MRI screen (inside the scanner). Participants answered the questionnaires with the laptop keyboard (outside the scanner) or an MRI-compatible button box (inside the scanner). Subjective experience was measured using an affect grid (Killgore, 1998), the state trait anxiety questionnaire (STAI, state subscale, Grimm et al., 2009; Spielberger, 1983), the “current mood scale” (“Aktuelle Stimmungsskala” (Dalbert, 1992), and a set of individual questions (e.g., “How stressed do you feel right now?”), which were answered using visual analogue scales (VAS) with sliding bars from 0 (“not at all”) to 100 (“very much”). For details cf. Table S1.

In addition to the psychometric assessment of subjective state measures, participants completed self-report trait questionnaires during the

relaxation period prior to the first MRI measurement (between T1 and T2). These included the Trier Inventory of Chronic Stress (Schulz and Schlotz, 1999), the Perceived Stress Scale (Klein et al., 2016), and questions regarding individual sportive activity and sleep quality (for details cf. Table S2).

For the analysis of subjective experience, we focused on the measures most relevant to subjective stress and used in previous stress studies (e.g. Allen et al., 2014; Hellhammer and Schubert, 2012): That is, anxiety and subjective stress at each sampling time point were quantified using the STAI sum score and the VAS value of the question “How stressed do you feel right now?”, respectively. Results of other psychometric measures will be reported elsewhere.

2.5. Autonomic data

To measure heart rate (HR) and its variability (HRV), electrocardiography (ECG) and photoplethysmography (PPG) were recorded. Outside the MRI, a 1-channel ECG was recorded (at 250 Hz) using a BioHarness3 (Zephyr, Annapolis, Maryland, US) strap attached to the participants' chests at the height of the xiphoid process. Inside the MRI, ECG was recorded (at 1000 Hz) using an MR-compatible BrainAmp ExG MR amplifier (Brain Products GmbH, Gilching, Germany) with Power-Pack battery, SyncBox synchronization interface and the acquisition software BrainVision Recorder (Version 1.20). To reduce artifacts related to breathing (i.e., movement of the thorax), three electrodes were placed on the participants' backs (adjacent to cervical spine c7, above the coccyx, and 15 cm below the left armpit). Also in the MRI, PPG was recorded (at 1000 Hz) using an OXY100C pulse oximeter module with TSD123A finger clip transducer and a BIOPAC MP150 system with the acquisition software AcqKnowledge (Version 4.0, BIOPAC Systems Inc., Goleta, CA, USA).

For the analysis of HR and HRV, the time series were binned into intervals of 3 min. This resulted in two intervals per RS scan and one interval for each phase of the TSST (“anticipation”, “interview”, “arithmetic”). For ECG data acquired during RS fMRI, gradient artefacts were removed using a self-built template-based subtraction method in Matlab (Nierhaus et al., 2013). For ECG and PPG data, peaks were automatically detected and – if needed – manually corrected (less than 1% of peaks) upon visual inspection using Matlab's *findpeaks* function or Kubios 2.2 (Tarvainen et al., 2014). For each interval, either PPG or ECG data were used for HR/V analysis: For data acquired in the MRI, the PPG data was used unless when missing (in total 37 intervals) or when the number of faulty, manually uncorrectable peaks (due to wrong detection and/or artefacts) exceeded 5% (in total 40 intervals); then, the ECG data for that interval were analysed instead. The heart period (average interbeat interval length in ms or inverse HR) was determined for each interval and HRV was quantified as root mean square of successive differences (RMSSD), indexing parasympathetic cardio-regulation (e.g. Berntson et al., 1997).

2.6. Endocrine data

In parallel to the subjective ratings, blood and saliva samples were obtained at 14 time points throughout the procedure (T1–T14, also see Fig. 1). While participants were responding to the questionnaires, saliva was sampled with a Sarstedt Salivette (duration: at least 2 min). During the subjective sampling, the experimenter acquired blood samples (serum and plasma, Sarstedt Monovette) from the intravenous catheter in the left or right cubital vein. Samples were centrifuged and aliquoted for the quantitative analysis. Cortisol concentrations in saliva were determined using Liquid chromatography-tandem mass spectrometry (LC-MS/MS) at the Institute for Laboratory Medicine, Clinical Chemistry and Molecular Diagnostics, University of Leipzig, following the protocol described in (Gaudl et al., 2016). For a different focus of the study, other endocrine markers in blood and serum were measured (results reported in Bae et al., 2019).

2.7. Neuroimaging data

Magnetic resonance imaging (MRI) was performed on a 3 T S MAGNETOM Verio (Siemens, Erlangen, Germany) scanner using a 32-channel Siemens head-coil. High resolution structural MR images were acquired using an MP2RAGE sequence: sagittal acquisition orientation, one 3D volume with 176 slices, repetition time (TR) = 5000 ms, TE = 2.92 ms, T11 = 700 ms, T12 = 2500 ms, FA1 = 4°, FA2 = 5°, pre-scan normalization, echo spacing = 6.9 ms, bandwidth = 240 Hz/pixel, FOV = 256 mm, voxel size = 1 mm isotropic, GRAPPA acceleration factor 3, slice order = interleaved, duration = 8 min 22 s (Marques et al., 2010). Six blocks (see Fig. 1) of 8-min RS fMRI (336 vol) were acquired using a T2*-weighted echo planar imaging (EPI) sequence: axial acquisition orientation, phase encoding = A >> P, voxel size = 2.3 mm isotropic, FOV = 202 mm, imaging matrix = 88 x 88, 64 slices with 2.3 mm thickness, TR = 1400 ms, TE = 30 ms, flip angle = 69°, echo spacing = 0.67 ms, bandwidth = 1776 Hz/pixel, partial fourier 7/8, no pre-scan normalization, multiband acceleration factor = 4, 336 vol, slice order = interleaved, duration = 7 min 50 s. During each RS scan, participants were instructed to lie still with their eyes open and to loosely fixate a low-contrast crosshair. Before each RS scan, a pair of gradient echo non-EPI scans (TR = 0.68 s, TE1 = 5.19 ms, TE2 = 7.65 ms, flip angle = 60°, voxel size = 2.3 mm isotropic, FOV = 202 mm, 64 slices) and two sets of spin echo EPI scans (TR = 2.2 s, TE = 50 ms, flip angle = 90°, multiband factor = 4, voxel size = 2.3 mm isotropic, FOV = 202 mm, 64 slices, phase encoding = AP, 3 vol/PA, 3 vol) were acquired for field map and reverse phase encoding distortion correction, respectively. FMRIB Software Library FSL (Smith et al., 2004) was used for all preprocessing steps except for spatial transformations, which were performed with Advanced Normalization Tools (ANTs; Avants et al., 2011). To ensure a standardised and reproducible procedure, the complete pipeline (https://github.com/NeuroanatomyAndConnectivity/pipelines/tree/master/src/lzd_lemmon) was implemented in Nipype (Gorgolewski et al., 2011). Preprocessing of the RS data fMRI comprised: discarding the first 5 vol, realignment, distortion correction, denoising (motion parameters and physiological noise), co-registration to the T1-weighted high resolution image, high pass filtering (0.01 Hz), spatial smoothing with a 6 mm full-width-at-half-maximum (FWHM) kernel, and normalisation to standard space (MNI152). A detailed description of the preprocessing pipeline can be found in the supplementary material.

Quality reports for all RS scans were created using a customized Nipype workflow described in Mendes et al. (2019) and are available at https://github.com/NeuroanatomyAndConnectivity/pipelines/tree/master/src/lzd_lemmon. Quality assessment (QA) included the calculation of motion parameters such as framewise displacement (calculated as the sum of the absolute values of the six realignment parameters), and the visual assessment of co-registration quality, and temporal signal-to-noise (tSNR). Each individual's scan quality scores were compared to the group-level distribution and for each scan, the QA report was visually inspected to ensure adequate data quality (cf. “Data availability”).

2.7.1. Eigenvector centrality mapping

To assess stress-related changes in the topology of whole-brain functional connectivity, Eigenvector centrality (EC) mapping (ECM; Lohmann et al., 2010) was used. The graph-analytic metric EC quantifies the importance of individual nodes (here: voxels) within a network (Joyce et al., 2010; Rubinov and Sporns, 2010), that is, high EC indicates that a node is highly connected to other nodes of the network, which are themselves highly connected. ECM allows an exploratory whole-brain approach independent from predefined seed regions (Lohmann et al., 2010). Voxelwise ECMs were calculated (for each RS scan) using the fast ECM algorithm (Wink, de Munck, van der Werf, van den Heuvel and Barkhof, 2012).

2.8. Statistical analysis

2.8.1. Data availability

From the analysis of the MRI data, six participants were excluded: four due to excessive head movement (criterion: at least one volume with >2.3 mm [voxel length] of framewise displacement; Power et al., 2012) in the RS scans immediately before (*rest2*) or after (*rest3*) the intervention, one participant aborted the scan, and one participant was excluded because of an incidental finding that was discovered after the data acquisition was completed. Imaging data from 29 participants in the stress and 32 participants in the control group were analysed. From the analysis of EC, psychometric, autonomic, and endocrine data using linear mixed models, an additional participant in the stress group was excluded because of a cortisol increase below 1.5 nmol/l, which is considered a non-responder (Miller et al., 2013). For the correlations between brain measures and subjective or autonomic stress markers within the stress group, participants with missing data points at either *rest2* or *rest3* were excluded: None for psychometric data (total $n = 28$) and three for HR/VP analysis due to mis-sampled ECG/PPG data (total $n = 26$).

For the endocrine data, two single missing sampling time points (T8, in the stress group) were imputed with the mean of the values before and after the missing value. In total, cortisol data from 28 participants were analysed.

2.8.2. Group-level analysis of EC maps

Differential effects of the intervention on both groups were analysed using a “flexible factorial” model in SPM12 (Wellcome Trust Centre). ECMs from *rest2* (immediately before the intervention) and *rest3* (immediately after the intervention, i.e., +30 min after its onset) were entered into a model including the factors *pre-post* (*rest2*, *rest3*; within-subject), *group* (stress, control; between-subject), and *subject*. We defined contrasts which tested the interaction of *time point* and *group*, as well as the simple effect of *time point*, within the stress and the control group, respectively. To specify stress-related EC changes, the ECMs of the time point by group interaction and of the simple effect of time point in the stress group were overlaid using FSLmaths. The resulting mask was binarized and used to extract EC values from all participants and scans (*rest1* to *rest6*), which were then correlated with psychometric, endocrine, and autonomic data.

All maps were corrected for multiple comparisons using a cluster-level family wise error (FWE) correction (Nichols and Hayasaka, 2003) with a threshold of $p < 0.005$ (uncorrected) at the voxel-level and of $p < 0.05$ (FWE-corrected) at the cluster-level (Bansal and Peterson, 2018; Mueller et al., 2017). The cluster extent (k_E) threshold was set using the tool SPM_ClusterSizeThreshold (Phillips, 2016), yielding a cluster extent threshold of $k_E = 251$. To investigate the network of stress-related EC changes, an exploratory seed-based functional connectivity was performed (cf. Supplement for methods and results).

2.8.3. Linear mixed models of stress measures

To investigate the time courses of EC values and other (i.e., psychometric, autonomic, and endocrine) measures across all RS scans (*rest1* to *rest6*), linear mixed models (Baayen, R Harald, 2008; Brown et al., 2014) were computed using the function *lmer* of the package *lme4* (version 1.1–13; Bates et al., 2015) in R 3.0.2 (R Core Team, 2008). To test whether the measures of interest were specifically influenced by stress (i.e., the interaction of *RS-scan* and *group*), the model included the respective measure as the outcome variable and *RS-scan* as well as *group* as fixed effects. To correct for differences in baseline values, these were included (average values during *rest2*) as a fixed effect. To control for the repeated measures, “participant” was included as a random intercept. Significance of the full model was determined by comparing it to a reduced model without the interaction of *RS-scan* and *group* using a likelihood ratio test (R function *anova* with argument *test* set to “Chisq”; Dobson and Barnett, 2018; Forstmeier and Schielzeth, 2011). In case of a significant difference between the full and the reduced model, post-hoc

least-squares means tests, adjusted for multiple comparisons using Tukey’s method, were performed with the R-package *emmeans* (version 1.1.2.; Lenth et al., 2018). Prior to analyses, the data were inspected, the required assumptions were tested, and parametric variables were *z*-transformed (see supplementary material for details).

2.8.4. Correlations between brain measures and other stress markers

To analyse the relationship between stress-related changes in EC values and the other (psychometric, autonomic, and endocrine) stress markers, their deltas were computed by subtracting *rest2* values from *rest3* values and correlated using Spearman’s rank correlation (due to the non-normality of EC values; Shapiro-Wilk test: $W(29) = 0.87$, $p = 0.002$) in R 3.0.2 (R Core Team, 2008). As psychometric (state anxiety, subjective stress) and endocrine (salivary cortisol) stress markers were not acquired during the fMRI sequence but before and after each RS scan, the two values were averaged before the delta between *rest2* and *rest3* was created. For the heart rate data, the two 3-min intervals during the RS scans were averaged before the correlation.

3. Results

The stress and the control group did not differ significantly in age, hours of sleep before the day of the experiment, average sportive activity per week, or self-reported chronic stress (see Table S5).

3.1. Psychometric, autonomic, and endocrine results

In response to the TSST, the stress group showed significantly different reactions in psychometric (state anxiety and subjective stress), autonomic (HR and HRV), and endocrine (salivary cortisol) stress markers compared to the control group (Fig. 2).

3.1.1. State anxiety and subjective stress

For state anxiety (STAI) scores, there was a significant interaction between *RS-scan* and *group* ($\chi^2(5) = 27.62$, $p < 0.001$). Post-hoc tests showed significant group differences at *rest3* (+35 min, t-ratio (272.59) = -3.13 ; $p < 0.01$; stress > control group), and *rest6* (+105 min, t-ratio (272.59) = 2.20; $p < 0.05$; control > stress group). For subjective stress (VAS “stressed”), there was a significant interaction between *RS-scan* and *group* ($\chi^2(5) = 15.19$, $p < 0.01$). Post-hoc tests did not show significant group differences at *rest3* (+35 min, t-ratio (303.44) = -1.57 ; $p = 0.11$) but at *rest6* (+105 min, t-ratio (303.44) = 2.60; $p < 0.01$; control > stress group).

3.1.2. Heart rate and heart rate variability

For HR changes, there was a significant interaction between *RS-scan* and *group* ($\chi^2(5) = 74.94$, $p < 0.001$). Post-hoc tests revealed significant group differences (stress > control group) in HR at *rest3* (+35 min, t-ratio (180.67) = -7.96 ; $p < 0.0001$), *rest4* (+55 min, t-ratio (180.67) = -5.4 ; $p < 0.0001$), *rest5* (+90 min, t-ratio (180.67) = -3.87 ; $p < 0.001$), and *rest6* (+105 min, t-ratio (184.36) = -4.48 ; $p < 0.0001$). For HRV measured as RMSSD changes, there was a significant interaction between *RS-scan* and *group* ($\chi^2(5) = 15.68$, $p < 0.01$). Post-hoc tests revealed significant group differences (control > stress group) in RMSSD at *rest3* (+35 min, t-ratio (220.13) = 2.95; $p < 0.01$) and *rest6* (+105 min, t-ratio (223.84) = 2.24; $p < 0.05$).

3.1.3. Saliva cortisol

For saliva cortisol there was a significant *RS-scan* by *group* interaction ($\chi^2(5) = 183.62$, $p < 0.001$) driven by significant group difference (stress > control group) for all RS scans after stress exposure, at *rest3* (+35 min, t-ratio (232.35) = -12.64 ; $p < 0.0001$), *rest4* (+55 min, t-ratio (232.35) = -11.75 ; $p < 0.0001$), *rest5* (+90 min, t-ratio (232.35) = -7.75 ; $p < 0.0001$), and *rest6* (+105 min, t-ratio (232.35) = -6.48 , $p < 0.0001$).

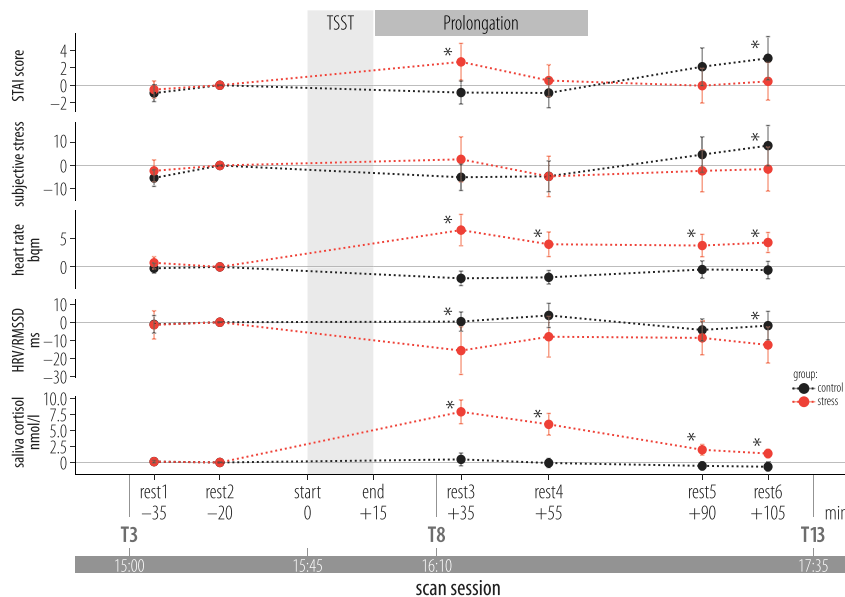


Fig. 2. Mean time courses of state anxiety (STAI), subjective stress (VAS, “stressed”), heart rate (HR, in beats per minute, bpm), heart rate variability (HRV, as root mean square of successive differences, RMSSD, in ms), and saliva cortisol (in nmol/l), plotted over the six resting-state (RS) scans (baseline-corrected with the values of *rest2*). Timing relative to TSST (start, end, darker grey area). The lighter grey area highlights the time when participants in the stress group were still expecting another task (see section 2.3). After *rest4* (+60 min after TSST onset), they were told that no additional task would follow and that they could relax. The hours indicate the time at which important sampling points were scheduled. Linear mixed models show significant *RS-scan* by *group* interactions for all five measures. For visualization purposes and to be comparable to the brain measure of Eigenvector centrality, the values were down-sampled by taking the mean per RS scan. See Fig. S1 for the time courses over all 14 time points. Error bars: 95% confidence interval. * = $p < .05$.

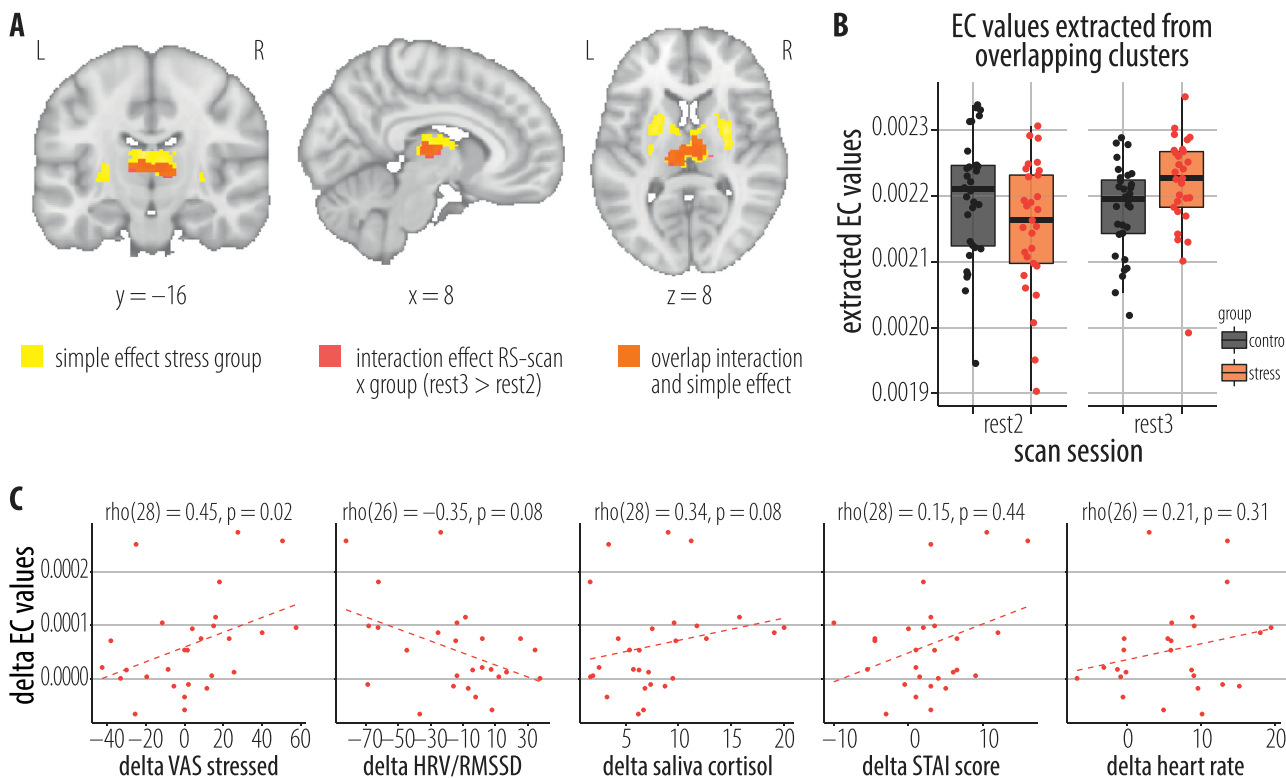


Fig. 3. Changes in Eigenvector centrality (EC) after an acute stressor and their association with other stress markers. **(A)** Significant clusters of increased EC, *rest2* (20 min before the stressor) < *rest3* (+35 min after the stressor). The overlap between the *RS-scan* by *group* interaction and the simple effect of *RS-scan* in the stress group (which almost completely overlaps the cluster of the simple effect) was located in the bilateral thalamus. Threshold: $p < 0.005$ (uncorrected) at the voxel and $p < 0.05$ (FWE-corrected) at the cluster level. **(B)** Box plots (horizontal bar: median; whiskers: 1.5 interquartile range; dots: data from individual participants) of the extracted EC values from the overlap of simple and interaction effect depicted in (A) plotted for *rest2* and *rest3* in the stress (red) and control (black) group. **(C)** Stress-related EC increases in the subcortical cluster (overlap simple and interaction effect) significantly correlated (Spearman's rank correlation on deltas between *rest3* and *rest2*) with other stress measures in the stress group: (top left) positively with subjective stress (visual analogue scale, VAS, “How stressed do you feel right now?”), (top middle) negatively with heart rate variability (HRV, measured as root mean squared successive differences, RMSSD, in ms), and (top right) positively with saliva cortisol (in nmol/l) but not with (bottom left) state anxiety (STAI) or (bottom right) heart rate. Dashed lines support visual estimation.

3.2. Neuroimaging results

The interaction of *pre-post* (*rest2*, *rest3*) and *group* (stress, control) was

significant in subcortical and frontal clusters. In the stress group (compared to the control group), EC in a subcortical cluster around the bilateral thalamus (peak MNI coordinate: [−6, −26, 2], $T = 4.14$,

$p_{FWE} = 0.011$, $k_E = 335$; see Fig. 3A, see Table 1), increased from pre-stress (*rest2*, 20 min before TSST onset) to post-stress (*rest3*, +35 min after TSST onset). Significant clusters of increased EC in the simple effect in the stress group overlapped with the clusters of the interaction effect and showed a wider extension to bilateral putamen and caudate nucleus (MNI coordinate: [−26, 12, −6], $T = 5.24$, $p_{FWE} < 0.001$, $k_E = 545$; and MNI coordinate: [28, 14, −8], $T = 4.5$, $p_{FWE} < 0.001$, $k_E = 1336$, respectively, see Table 1). The simple effect in the stress group also showed a significant cluster of increased EC in the bilateral cerebellum

Table 1
Stress-related increases in subcortical Eigenvector centrality.

Contrast	cluster/ extent (n voxels)	Region	Peak Voxel coordinates (MNI)			T max
			x	y	z	
			Interaction stress vs. control (<i>pre-post</i> by group)	Cluster 1/ 335	Thalamus	
		Maximum 1	−6	−26	2	4.14
		Maximum 2	8	−14	6	3.86
		Maximum 3	−4	−16	8	3.69
		Maximum 4	18	−20	6	3.44
		Maximum 5	4	−4	4	2.94
Simple effect in stress group (<i>rest2 < rest3</i>)	Cluster 1/ 1336	Thalamus				
		Maximum 1	28	14	−8	4.50
		Maximum 2	28	6	−2	4.32
		Maximum 3	−8	−18	8	4.29
		Maximum 4	28	0	8	4.19
		Maximum 5	10	0	18	4.16
		Maximum 6	−4	−16	16	4.08
		Maximum 7	−6	−20	10	3.89
		Maximum 8	28	−10	10	3.87
		Maximum 9	16	0	18	3.70
		Maximum 10	12	−4	14	3.68
		Maximum 11	26	4	−10	3.67
	Cluster 2/ 766	Cerebellum				
		Maximum 1	−16	−72	−24	4.28
		Maximum 2	−36	−62	−28	4.26
		Maximum 3	−44	−70	−14	4.03
		Maximum 4	−6	−70	−34	3.90
		Maximum 5	−16	−48	−24	3.82
		Maximum 6	−38	−58	−40	3.76
		Maximum 7	−24	−60	−30	3.66
		Maximum 8	−32	−70	−24	3.37
		Maximum 9	−10	−56	−28	3.34
		Maximum 10	−32	−76	−30	3.32
		Maximum 11	−18	−66	−32	3.26
	Cluster 3/ 545	Putamen				
		Maximum 1	−26	12	−6	5.24
		Maximum 2	−26	2	−2	4.44
		Maximum 3	−22	6	6	3.92
		Maximum 4	−26	0	6	3.89
		Maximum 5	−18	8	20	3.60
		Maximum 6	−26	−16	6	3.50
		Maximum 7	−12	14	14	3.22
		Maximum 8	−32	−8	−4	3.19
		Maximum 9	−28	−10	14	2.95
		Maximum 10	−30	−10	−14	2.77
		Maximum 11	−8	10	12	2.74

(MNI coordinate: [−16, −72, −24], $T = 4.28$, $p_{FWE} < 0.001$, $k_E = 766$, see Table 1). Furthermore, the interaction contrast for testing the decrease of EC within the stress group revealed a significant cluster in the frontal pole (MNI coordinate: [8, 62, −4], $T = 4.18$, $p_{FWE} = 0.005$, $k_E = 374$, see Table 1). However, this did not overlap with any simple effect. The simple effect in the control group showed a significant EC increase in a cluster around the left lateral temporal pole (MNI coordinate: [30, −30, −32], $T = 5.27$, $p_{FWE} < 0.05$, $k_E = 276$, see Table 1) and a decrease in occipital cluster (MNI coordinate: [4, −88, 8], $T = 5.22$, $p_{FWE} < 0.001$, $k_E = 1427$, see Table 1). Both clusters did not overlap with significant clusters in the interaction analysis.

The exploratory seed-based analysis yielded widespread connectivity increases between the thalamic cluster and parietal as well as temporal regions in the stress group (cf. Fig. S3), including bilateral hippocampus and amygdala.

3.3. Associations between stress measures

For delta values (*rest3-rest2*) in the stress group, EC showed a significant positive correlation with both subjective stress ($\rho(28) = 0.45$, $p = 0.02$). The positive correlation between saliva cortisol and EC showed a non-significant trend ($\rho(28) = 0.34$, $p = 0.08$). Similarly, the negative correlation between HRV/RMSSD and EC showed a non-significant trend ($\rho(26) = -0.35$, $p = 0.08$) (see Fig. 3C). No significant correlations were found between EC and STAI scores ($\rho(28) = 0.15$, $p = 0.44$) or between EC and heart rate ($\rho(26) = 0.21$, $p = 0.31$).

3.4. Time courses of subcortical eigenvector centrality

EC time courses of subcortical clusters in the stress and the control group are shown in Fig. 4. The full model that included the *RS-scan* by *group* interaction and the null model (without the interaction term) differed significantly (likelihood ratio test: $\chi^2(5) = 18.46$, $p < 0.01$). Post-hoc tests showed significantly higher EC values in the stress than in the control group at *rest3* (+35 min; t-ratio (312.18) = −3.40; $p < 0.001$) and *rest4* (+55 min; t-ratio (312.18) = −2.49; $p < 0.05$). Qualitatively, EC values decreased at 50 min after stressor onset (*rest4*) but then increased again at 85 min (*rest5*) to stay elevated (at least) until 105 min after stress onset (*rest6*). At *rest5* and *rest6*, subcortical EC values in the control group showed a similar increase.

4. Discussion

In this study, we investigated functional brain network topology in response to an acute psychosocial stressor and during the recovery from it. Eigenvector centrality (EC) mapping was used to identify brain hubs involved in stress processing, which were subsequently related to subjective, autonomic, and endocrine stress markers. First, our results show that the TSST elicits strong subjective, autonomic, and endocrine stress responses, as previously described (for a review see Allen et al., 2014). Second, we found an immediate, stress-driven change in whole-brain network topology: EC increased in a cluster peaking in the thalamus, which was connected to regions across the whole brain. This EC increase was more pronounced in participants who also showed stronger stress-related changes in subjective (VAS stressed) as well as – to a lesser extent – autonomic (HRV), and endocrine (saliva cortisol) measures. Third, and different from our expectations based on Hermans et al. (2014), the stress-driven elevation of EC did not recover within 105 min after stress onset. EC values did decrease at 50 min after stressor onset (*rest4*) but then increased again (at least) until the 105 min after stressor onset (*rest6*).

Stress-related changes in brain network topology indicate that thalamic connectivity may be important to information processing immediately after stress exposure. Especially in the immediate aftermath of stress exposure, when the organism is in a hypervigilant state (van

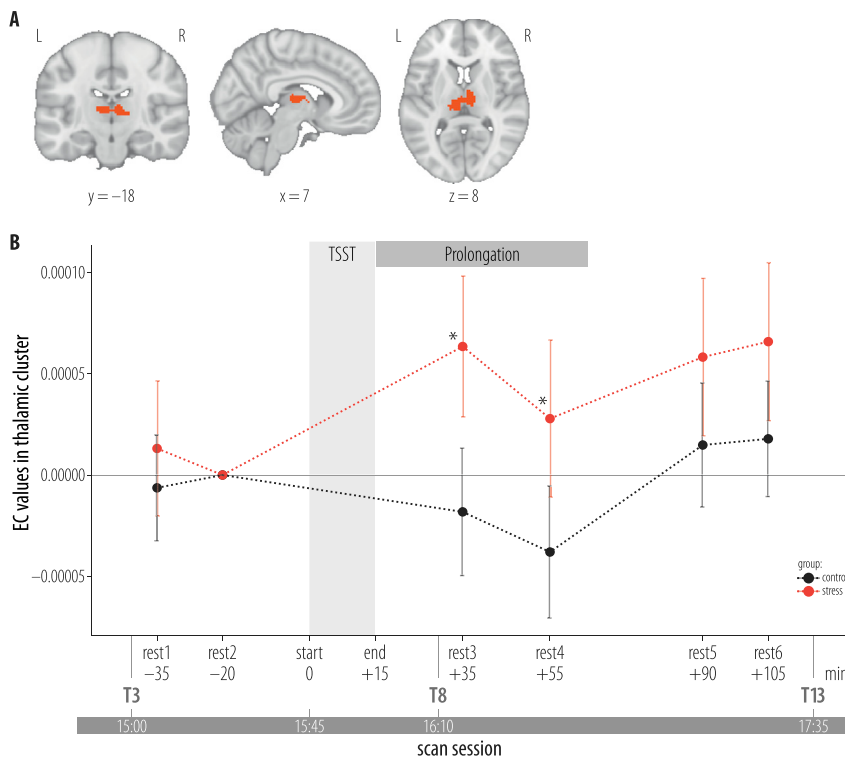


Fig. 4. Thalamic Eigenvector centrality (EC) plotted over the six resting-state (RS) scans. (A) Overlap of the RS-scan by group interaction and the simple effect in the stress group (incl. *rest2* and *rest3*), from which EC values were extracted. (B) Baseline-corrected (with the value at *rest2*) mean EC values in the cluster shown in A for the six RS scans. Timing relative to TSST onset (start, end, darker grey area). The lighter grey area indicates the time when participants in the stress group were still expecting another task (see section 2.3). After *rest4* (+60 min after TSST onset), they were told that no additional task would follow and that they could relax. The hours indicate the time at which important sampling points were scheduled. There was a significant RS-scan by group interaction ($\chi^2(5) = 18.46$, $p < 0.01$) with significant group differences (stress > control group) at *rest3* (+35 min, t -ratio (312.18) = -3.4 ; $P_{\text{corr}} < 0.001$) and *rest4* (+55 min, t -ratio (312.18) = -2.49 ; $P_{\text{corr}} < 0.05$).

Marle et al., 2010), adequate behaviour requires focused resource allocation (e.g., energy supply to brain regions that process relevant information; Hermans et al., 2014). Increased centrality in the thalamus supports its essential role for the control of functional network balance and resource allocation (Garrett et al., 2018; Hwang, Bertolero, Liu, & D'Esposito, 2017). With its extensive structural and functional connectivity, the thalamus is a central relay for sensory signals ascending to the cortex and for trans-thalamic cortico-cortical communication (Sherman and Guillery, 2002). Thalamic nuclei thereby modulate the transfer of information in accord with current attentional and motor or behavioral demands (Sherman and Guillery, 2002; Wolff and Vann, 2019). Beyond being a relay, the thalamus actively and dynamically gates salient inputs by minimizing the importance of currently irrelevant ones (Wolff and Vann, 2019, for review). Activation in the – particularly paraventricular – thalamus has recently been shown to represent salient stimulus features like aversiveness, novelty, and surprise (Zhu et al., 2018). With its inputs from the hypothalamus and brainstem, it also receives information about the homeostatic or arousal state of the organism; and its activation but also its connectivity with cortical regions have been linked to learning processes that underlie behavioral flexibility (Wolff and Vann, 2019; Zhu et al., 2018).

Increased centrality in the thalamus might therefore reflect an increased arousal or alertness (Lohmann et al., 2010; Schiff, 2008) to support the anticipation and processing of salient stimuli (Greenberg et al., 2015; Zhu et al., 2018). The extent of stress effects on brain connectivity is also visible in the results of our exploratory seed-based analysis, showing stress-driven connectivity increases between the thalamic cluster and widespread parietal and temporal regions. Previous studies have shown stress-driven changes in thalamic activation (Dedovic et al., 2014; Fan et al., 2015; Gianaros et al., 2008; Koric et al., 2012; Pruessner et al., 2008; Sinha et al., 2016; Sinha et al., 2004) as well as an increased thalamo-cortical integration with widespread consequences for cortical activity (Maron-Katz et al., 2016) after stressor exposure. While previous stress studies have often also found activation or connectivity changes in the thalamus (but less often discuss them), we did not find significant centrality changes in regions prominent in the stress

literature, like the PFC, the amygdala, the hippocampus, or the hypothalamus. To all these regions, the thalamus is strongly connected (Wolff and Vann, 2019; Zhu et al., 2018) and thalamic EC changes in our study may represent connectivity with these regions (cf. the results of the exploratory seed-based functional connectivity analysis; Fig. S3).

Our results also relate these regions to stress markers beyond the brain: stress-related brain changes in the thalamus were more pronounced in participants with stronger stress responses in subjective stress and – to a lesser extent – peripheral measures (saliva cortisol and heart rate variability). These findings align with evidence that relates thalamic function not only to emotional processing (Barrett, 2016; Kober et al., 2008; Lee et al., 2012; Lee and Shin, 2016; Penzo et al., 2015; Timbie and Barbas, 2015; Wang et al., 2005) but also to homeostatic regulation (Åhs et al., 2009; Cechetto and Shoemaker, 2009; Jaferi and Bhatnagar, 2006; M. M. Suárez and Perassi, 1997; M. Suárez, Maglianesi and Perassi, 1998; Wager et al., 2009; Zhu et al., 2018), showing thalamic involvement for example in the endocrine adaptation to repetitive stressors (Jaferi and Bhatnagar, 2006), respiratory control (Cechetto and Shoemaker, 2009), and parasympathetic cardioregulation (Åhs et al., 2009; Wager et al., 2009). That EC changes were not significantly correlated with changes in STAI scores or HR may suggest that EC alterations are relevant for more stress-specific (VAS, cortisol) and parasympathetic (HRV) than for general anxiety (STAI) or sympathetic (HR) aspects of the stress response.

Besides emotions and homeostasis, our findings can be related to uncertainty. While uncertainty is a crucial component of the TSST and other stressors (de Berker et al., 2016; Koolhaas et al., 2011), according to the free energy principle, the brain constantly tries to match predictions and the environment with the goal of minimizing uncertainty (Friston, 2010; Peters et al., 2017). Thalamic regions – as part of a basal ganglia-thalamo-cortical loop – have been involved in the cognitive processing of uncertainty (Grinband et al., 2006) and in the coordination of “higher” cortical regions (e.g., in prefrontal, insular, and parietal cortices) with the goal to adapt to uncertain environments through probabilistic inferential learning (Mestres-Missé et al., 2017). In general, learning from (stressful) experiences is crucial to reduce uncertainty – and stress – in future situations (de Berker et al., 2016; Peters et al.,

2017). An adaptive stress response thus enables and involves neural plasticity to support these learning processes (Regev and Baram, 2014).

Hallmark of an adaptive stress response is an adequate cortisol response, which, in synergy with other neuroendocrine transmitters, supports rapid behavioural choices but also promotes longer-term neural recovery and higher cognitive functions (Joëls et al., 2013). We thus speculate that our findings can be interpreted as indirect evidence that thalamic are involved in stress-based learning processes (Wolff and Vann, 2019; Zhu et al., 2018). However, as we did not measure such processes, we cannot directly test their relation to the observed EC changes in the thalamus.

Based on the model by Hermans et al. (2014), we anticipated the functional connectivity changes to resemble the time course of the endocrine stress response, increasing immediately after stress exposure and then decaying over time. In the stress group, EC values increased immediately after stress exposure (*rest3*) and decayed during *rest4* (+50 min). However, in both groups, they then increased (again) until the end of the experiment. This pattern may reflect a more general (i.e., group-independent) state (e.g., exhaustion, boredom, annoyance) towards the end of the 6-h experimental procedure. The psychometric measures of stressfulness and exhaustion, which show a similar time course as the EC values in both groups (Fig. 2), support this interpretation. It has been reported that an MRI scan itself can be perceived as stressful (Muehlhan et al., 2011) and the procedure during a RS fMRI acquisition may share some characteristics with the TSST: for example, the participant's "performance" is monitored and recorded by a team of specialists trying to remain and interact in a neutral fashion. Thus, it is conceivable that the observed effects on the neural level are a superposition of two different effects: stress induced by the TSST and the expectation of another task, specific to the stress group and with a clear cortisol response, and exhaustion/boredom/annoyance in both groups, caused by the overall length of the experiment. For the last scan (*rest6*), the control group reported significantly higher state anxiety and subjective stress than the stress group (while the autonomic and endocrine stress markers did not "flip"). This illustrates that physiological and subjective stress measures can – and often do – dissociate (D. Hellhammer, Stone, Hellhammer and Broderick, 2010; J. Hellhammer and Schubert, 2012).

There are several limitations that should be considered when interpreting the findings of our study: we only included young, healthy, male participants. While this allowed us to investigate stress-induced changes using a multimodal approach without confounds like the impact of the ovarian cycle, the generalisability of our results has to be tested in studies with more heterogeneous samples. To sample female participants at the same phase of the ovarian cycle would have been beyond the resources of our study as self-reports or (single) assessments of physiological parameters (e.g., body temperature, hormone concentrations) are unreliable and, for example, highly influenced by day-to-day fluctuations (cf. Barth et al., 2016). Our study design cannot disentangle the aspects of increased thalamic centrality that are due to more general changes in alertness or arousal from those that are stress-specific. That there is a stress-specific component is suggested by the association of EC increases with dedicated stress markers like subjective stress or - to a lesser extent saliva cortisol and by the absence of a group difference in self-reported alertness (non-significant *RS-scan* by *group* interaction in a linear mixed model of the mood scale's sleepiness component; Dalbert, 1992; Fig. S2). Although the TSST's strong and long lasting effect was crucial for our research question, it does not include a parametric modulation of the stressor (e.g., by varying levels of uncertainty; de Berker et al., 2016), which would provide a more fine-grained analysis of the association between stress-inducing uncertainty and, for example, thalamic network centrality. In addition, the functional significance of centrality changes could be confirmed by including a task after the stressor, which allows, for example, the measurement of attentional performance. Please note that our results show the network hubs based on EC across voxels - but not regions - in the brain. Treating each voxel as an independent unit

might bias the results because of the different size of different brain regions. However, atlas-based network analyses depend on prior assumptions about functional brain topology, which can also bias the results (de Reus & van den Heuvel, 2013).

In this study, we show stress-driven changes in whole-brain functional network topology without a priori definition of seed regions or network masks. By acquiring data from different stress systems over an extended time after stressor onset, it was possible to not just multimodally investigate immediate stress effects but also their time courses during recovery. We identified thalamic regions to be centrally involved in the neural response to acute stress, underlying stress-related connectivity changes across the whole brain. Changes in thalamic centrality were also related to subjective as well as – to a lesser extent – to autonomic and endocrine stress measures. The importance of the thalamus supports the hypothesis that acute stress shifts resources towards a state of heightened saliency processing. The thalamus may thus be a target for future research – also investigating stress-related psychopathology, such as post-traumatic stress disorder (Yin et al., 2011), depression (Greicius et al., 2007), addiction (Everitt and Robbins, 2013), or schizophrenia (Giraldo-Chica and Woodward, 2017; Howes et al., 2017). Of particular importance is also the role of stress resilience (Brown et al., 2014), which requires studying the time course of the brain's response to stress and its association with peripheral stress markers. In conclusion, our findings suggest thalamic connectivity to play a central role for the processing of stress and to constitute a nexus for stress responses in the rest of the body and in the mind.

Funding

This research did not receive any specific grant from funding agencies in the public, commercial, or not-for-profit sectors.

Acknowledgments

The authors would like to thank Dr. Ilya Veer and Dr. Robert Nadon for helpful methodological discussions. MG was funded by the German Federal Ministry of Education and Research (grant no. 13GW0206B).

Appendix A. Supplementary data

Supplementary data to this article can be found online at <https://doi.org/10.1016/j.neuroimage.2019.06.005>.

References

- Åhs, F., Sollers, J.J., Furmark, T., Fredrikson, M., Thayer, J.F., 2009. High-frequency heart rate variability and cortico-striatal activity in men and women with social phobia. *Neuroimage* 47 (3), 815–820. <https://doi.org/10.1016/j.neuroimage.2009.05.091>.
- al'Absi, M., Lovallo, W.R., McKey, B., Sung, B.H., Whitsett, T.L., Wilson, M.F., 1998. Hypothalamic-pituitary-adrenocortical responses to psychological stress and caffeine in men at high and low risk for hypertension. *Psychosom. Med.* 60 (4), 521–527.
- Allen, A.P., Kennedy, P.J., Cryan, J.F., Dinan, T.G., Clarke, G., 2014. Biological and psychological markers of stress in humans: focus on the trier social stress test. *Neurosci. Biobehav. Rev.* 38, 94–124. <https://doi.org/10.1016/j.neubiorev.2013.11.005>.
- Allen, A.P., Kennedy, P.J., Dockray, S., Cryan, J.F., Dinan, T.G., Clarke, G., 2017. The trier social stress test: principles and practice. *Neurobiol. Stress* 6, 113–126. <https://doi.org/10.1016/j.ynstr.2016.11.001>.
- Avants, B.B., Tustison, N.J., Song, G., Cook, P.A., Klein, A., Gee, J.C., 2011. A reproducible evaluation of ANTs similarity metric performance in brain image registration. *Neuroimage* 54 (3), 2033–2044. <https://doi.org/10.1016/j.neuroimage.2010.09.025>.
- Baayen, R. Harald, 2008. *Analyzing Linguistic Data: A Practical Introduction to Statistics Using R*. Cambridge University Press.
- Babayán, A., Erbey, M., Kumral, D., Reinelt, J.D., Reiter, A.M.F., Röbbig, J., et al., 2019. A mind-brain-body dataset of MRI, EEG, cognition, emotion, and peripheral physiology in young and old adults. *Sci. Data* 6, 180308. <https://doi.org/10.1038/sdata.2018.308>.
- Bae, Y.J., Reinelt, J., Netto, J., Uhlig, M., Willenberg, A., Ceglarek, U., et al., 2019. Salivary cortisone, as a biomarker for psychosocial stress, is associated with state anxiety and heart rate. *Psychoneuroendocrinology* 101, 35–41. <https://doi.org/10.1016/j.psyneuen.2018.10.015>.

- Bansal, R., Peterson, B.S., 2018. Cluster-level statistical inference in fMRI datasets: the unexpected behavior of random fields in high dimensions. *Magn. Reson. Imag.* 49, 101–115. <https://doi.org/10.1016/j.mri.2018.01.004>.
- Barrett, L.F., 2016. The theory of constructed emotion: an active inference account of interoception and categorization. *Soc. Cognit. Affect Neurosci.* nsw154 <https://doi.org/10.1093/scan/nsw154>.
- Barth, C., Steele, C.J., Mueller, K., Rekkas, V.P., Arélin, K., Pampel, A., et al., 2016. In-vivo dynamics of the human Hippocampus across the menstrual cycle. *Sci. Rep.* 6, 32833. <https://doi.org/10.1038/srep32833>.
- Bates, D., Mächler, M., Bolker, B., Walker, S., 2015. Fitting linear mixed-effects models using lme4. *J. Stat. Softw.* 67 (1), 1–48. <https://doi.org/10.18637/jss.v067.i01>.
- Berntson, G.G., Bigger, J.T., Eckberg, D.L., Grossman, P., Kaufmann, P.G., Malik, M., et al., 1997. Heart rate variability: origins, methods, and interpretive caveats. *Psychophysiology* 34 (6), 623–648.
- Brown, V.M., LaBar, K.S., Haswell, C.C., Gold, A.L., Mid-Atlantic MIRECC Workgroup, McCarthy, G., Morey, R.A., 2014. Altered resting-state functional connectivity of basolateral and centromedial amygdala complexes in posttraumatic stress disorder. *Neuropsychopharmacology: Official Publication of the American College of Neuropsychopharmacology* 39 (2), 351–359. <https://doi.org/10.1038/npp.2013.197>.
- Cechedo, D.F., Shoemaker, J.K., 2009. Functional neuroanatomy of autonomic regulation. *Neuroimage* 47 (3), 795–803. <https://doi.org/10.1016/j.neuroimage.2009.05.024>.
- Childs, E., Dlugos, A., De Wit, H., 2010. Cardiovascular, hormonal, and emotional responses to the TSST in relation to sex and menstrual cycle phase. *Psychophysiology* 47 (3), 550–559. <https://doi.org/10.1111/j.1469-8986.2009.00961.x>.
- Dalbert, C., 1992. Subjektives Wohlbefinden junger Erwachsener: theoretische und empirische Analysen der Struktur und Stabilität. [Young adults' subjective well-being: theoretical and empirical analyses of its structure and stability.]. *Z. Differ. Diagn. Psychol.* 13 (4), 207–220.
- de Berker, A.O., Rutledge, R.B., Mathys, C., Marshall, L., Cross, G.F., Dolan, R.J., Bestmann, S., 2016. Computations of uncertainty mediate acute stress responses in humans. *Nat. Commun.* 7 (1). <https://doi.org/10.1038/ncomms10996>.
- de Reus, M.A., van den Heuvel, M.P., 2013. The parcellation-based connectome: limitations and extensions. *Neuroimage* 80, 397–404. <https://doi.org/10.1016/j.neuroimage.2013.03.053>.
- Dedovic, K., Duchesne, A., Engert, V., Lue, S.D., Andrews, J., Efanov, S.I., et al., 2014. Psychological, endocrine and neural responses to social evaluation in subclinical depression. *Soc. Cognit. Affect Neurosci.* 9 (10), 1632–1644. <https://doi.org/10.1093/scan/nst151>.
- Dobson, Annette J., Barnett, Adrian G., 2018. *An Introduction to Generalized Linear Models*.
- Everitt, B.J., Robbins, T.W., 2013. From the ventral to the dorsal striatum: devolving views of their roles in drug addiction. *Neurosci. Biobehav. Rev.* 37 (9 Pt A), 1946–1954. <https://doi.org/10.1016/j.neubiorev.2013.02.010>.
- Fan, Y., Pestke, K., Feeser, M., Aust, S., Pruessner, J.C., Böker, H., et al., 2015. Amygdala–Hippocampal connectivity changes during acute psychosocial stress: joint effect of early life stress and oxytocin. *Neuropsychopharmacology* 40 (12), 2736–2744. <https://doi.org/10.1038/npp.2015.123>.
- Faravelli, C., Lo Sauro, C., Godini, L., Lelli, L., Benni, L., Pietrini, F., et al., 2012. Childhood stressful events, HPA axis and anxiety disorders. *World J. Psychiatr.* 2 (1), 13–25. <https://doi.org/10.5498/wjp.v2.i1.13>.
- Fehm, L., Hoyer, J., Schneider, G., Lindemann, C., Klusmann, U., 2008. Assessing post-event processing after social situations: a measure based on the cognitive model for social phobia. *Anxiety Stress Coping* 21 (2), 129–142. <https://doi.org/10.1080/10615800701424672>.
- Forstmeier, W., Schielzeth, H., 2011. Cryptic multiple hypotheses testing in linear models: overestimated effect sizes and the winner's curse. *Behav. Ecol. Sociobiol.* 65 (1), 47–55. <https://doi.org/10.1007/s00265-010-1038-5>.
- Friston, K., 2010. The free-energy principle: a unified brain theory? *Nat. Rev. Neurosci.* 11 (2), 127–138. <https://doi.org/10.1038/nrn2787>.
- Garrett, D., Epp, S., Perry, A., Lindenberger, U., 2018. Local temporal variability reflects functional network integration in the human brain: on the crucial role of the thalamus. *BioRxiv*. <https://doi.org/10.1101/184739>.
- Gaudl, A., Kratzsch, J., Bae, Y.J., Kiess, W., Thiery, J., Ceglarek, U., 2016. Liquid chromatography quadrupole linear ion trap mass spectrometry for quantitative steroid hormone analysis in plasma, urine, saliva and hair. *J. Chromatogr. A* 1464, 64–71. <https://doi.org/10.1016/j.chroma.2016.07.087>.
- Gianaros, P.J., Sheu, L.K., Matthews, K.A., Jennings, J.R., Manuck, S.B., Hariri, A.R., 2008. Individual differences in stressor-evoked blood pressure reactivity vary with activation, volume, and functional connectivity of the amygdala. *J. Neurosci.* 28 (4), 990–999. <https://doi.org/10.1523/JNEUROSCI.3606-07.2008>.
- Giraldo-Chica, M., Woodward, N.D., 2017. Review of thalamocortical resting-state fMRI studies in schizophrenia. *Schizophr. Res.* 180, 58–63. <https://doi.org/10.1016/j.schres.2016.08.005>.
- Gorgolewski, K., Burns, C.D., Madison, C., Clark, D., Halchenko, Y.O., Waskom, M.L., Ghosh, S.S., 2011. Nipype: a flexible, lightweight and extensible neuroimaging data processing framework in python. *Front. Neuroinf.* 5, 13. <https://doi.org/10.3389/fninf.2011.00013>.
- Greenberg, T., Carlson, J.M., Rubin, D., Cha, J., Mujica-Parodi, L., 2015. Anticipation of high arousal aversive and positive movie clips engages common and distinct neural substrates. *Soc. Cognit. Affect Neurosci.* 10 (4), 605–611. <https://doi.org/10.1093/scan/nsu091>.
- Greicius, M.D., Flores, B.H., Menon, V., Glover, G.H., Solvason, H.B., Kenna, H., et al., 2007. Resting-state functional connectivity in major depression: abnormally increased contributions from subgenual cingulate cortex and thalamus. *Biol. Psychiatry* 62 (5), 429–437. <https://doi.org/10.1016/j.biopsych.2006.09.020>.
- Grimm, S., Ernst, J., Boesiger, P., Schuepbach, D., Hell, D., Boeker, H., Northoff, G., 2009. Increased self-focus in major depressive disorder is related to neural abnormalities in subcortical-cortical midline structures. *Hum. Brain Mapp.* 30 (8), 2617–2627. <http://doi.org/10.1002/hbm.20693>.
- Grinband, J., Hirsch, J., Ferrera, V.P., 2006. A neural representation of categorization uncertainty in the human brain. *Neuron* 49 (5), 757–763. <https://doi.org/10.1016/j.neuron.2006.01.032>.
- Hellhammer, D., Stone, A., Hellhammer, J., Broderick, J., 2010. Measuring stress. *Encycl. Behav. Neurosci.* 2, 186–191.
- Hellhammer, J., Schubert, M., 2012. The physiological response to Trier Social Stress Test relates to subjective measures of stress during but not before or after the test. *Psychoneuroendocrinology* 37 (1), 119–124. <https://doi.org/10.1016/j.psychoneu.2011.05.012>.
- Hermans, E.J., Henckens, M.J.A.G., Joëls, M., Fernández, G., 2014. Dynamic adaptation of large-scale brain networks in response to acute stressors. *Trends Neurosci.* 37 (6), 304–314. <https://doi.org/10.1016/j.tins.2014.03.006>.
- Het, S., Rohleder, N., Schoofs, D., Kirschbaum, C., Wolf, O.T., 2009. Neuroendocrine and psychometric evaluation of a placebo version of the 'trier social stress test'. *Psychoneuroendocrinology* 34 (7), 1075–1086. <https://doi.org/10.1016/j.psychoneu.2009.02.008>.
- Howes, O.D., McCutcheon, R., Owen, M.J., Murray, R.M., 2017. The role of genes, stress, and dopamine in the development of schizophrenia. *Biol. Psychiatry* 81 (1), 9–20. <https://doi.org/10.1016/j.biopsych.2016.07.014>.
- Hwang, K., Bertolero, M.A., Liu, W.B., D'Esposito, M., 2017. The human thalamus is an integrative hub for functional brain networks. *J. Neurosci.* 37 (23), 5594–5607. <https://doi.org/10.1523/JNEUROSCI.0067-17.2017>.
- Jaferi, A., Bhatnagar, S., 2006. Corticosterone can act at the posterior paraventricular thalamus to inhibit hypothalamic-pituitary-adrenal activity in animals that habituate to repeated stress. *Endocrinology* 147 (10), 4917–4930. <https://doi.org/10.1210/en.2005-1393>.
- Joëls, M., Pasricha, N., Karst, H., 2013. The interplay between rapid and slow corticosteroid actions in brain. *Eur. J. Pharmacol.* 719 (1–3), 44–52. <https://doi.org/10.1016/j.ejphar.2013.07.015>.
- Joyce, K.E., Laurienti, P.J., Burdette, J.H., Hayasaka, S., 2010. A new measure of centrality for brain networks. *PLoS One* 5 (8), e12200. <https://doi.org/10.1371/journal.pone.0012200>.
- Killgore, W.D., 1998. The Affect Grid: a moderately valid, nonspecific measure of pleasure and arousal. *Psychol. Rep.* 83 (2), 639–642. <https://doi.org/10.2466/pr0.1998.83.2.639>.
- Kirschbaum, C., Pirke, K.-M., Hellhammer, D.H., 1993. The 'trier social stress test' – a tool for investigating psychobiological stress responses in a laboratory setting. *Neuropsychobiology* 28 (1–2), 76–81.
- Klein, E.M., Brähler, E., Dreier, M., Reinecke, L., Müller, K.W., Schmutz, G., et al., 2016. The German version of the Perceived Stress Scale - psychometric characteristics in a representative German community sample. *BMC Psychiatry* 16, 159. <https://doi.org/10.1186/s12888-016-0875-9>.
- Kober, H., Barrett, L.F., Joseph, J., Bliss-Moreau, E., Lindquist, K., Wager, T.D., 2008. Functional grouping and cortical-subcortical interactions in emotion: a meta-analysis of neuroimaging studies. *Neuroimage* 42 (2), 998–1031. <https://doi.org/10.1016/j.neuroimage.2008.03.059>.
- Koolhaas, J.M., Bartolomucci, A., Buwalda, B., de Boer, S.F., Flügge, G., Korte, S.M., et al., 2011. Stress revisited: a critical evaluation of the stress concept. *Neurosci. Biobehav. Rev.* 35 (5), 1291–1301. <https://doi.org/10.1016/j.neubiorev.2011.02.003>.
- Koric, L., Volle, E., Seassau, M., Bernard, F.A., Mancini, J., Dubois, B., et al., 2012. How cognitive performance-induced stress can influence right VLPFC activation: an fMRI study in healthy subjects and in patients with social phobia. *Hum. Brain Mapp.* 33 (8), 1973–1986. <https://doi.org/10.1002/hbm.21340>.
- Lee, S., Ahmed, T., Lee, S., Kim, H., Choi, S., Kim, D.-S., et al., 2012. Bidirectional modulation of fear extinction by mediodorsal thalamic firing in mice. *Nat. Neurosci.* 15 (2), 308–314. <https://doi.org/10.1038/nn.2999>.
- Lee, S., Shin, H.-S., 2016. The role of mediodorsal thalamic nucleus in fear extinction. *J. Anal. Sci. Technol.* 7 (1). <https://doi.org/10.1186/s40543-016-0093-6>.
- Lenth, R., Singmann, H., Love, J., Buerkner, P., Herve, M., 2018. *Emmeans: Estimated Marginal Means, Aka Least-Squares Means (Version 1.1.3)*. Retrieved from. <https://CRAN.R-project.org/package=emmeans>.
- Linden, W., Earle, T.L., Gerin, W., Christenfeld, N., 1997. Physiological stress reactivity and recovery: conceptual siblings separated at birth? *J. Psychosom. Res.* 42 (2), 117–135. [https://doi.org/10.1016/S0022-3999\(96\)00240-1](https://doi.org/10.1016/S0022-3999(96)00240-1).
- Lohmann, G., Margulies, D.S., Horstmann, A., Pleger, B., Lepsien, J., Goldhahn, D., et al., 2010. Eigenvector centrality mapping for analyzing connectivity patterns in fMRI data of the human brain. *PLoS One* 5 (4), e10232. <https://doi.org/10.1371/journal.pone.0010232>.
- Maron-Katz, A., Vaisvaser, S., Lin, T., Hendler, T., Shamir, R., 2016. A large-scale perspective on stress-induced alterations in resting-state networks. *Sci. Rep.* 6 (1). <https://doi.org/10.1038/srep21503>.
- Marques, J.P., Kober, T., Krueger, G., van der Zwaag, W., Van de Moortele, P.-F., Gruetter, R., 2010. MP2RAGE, a self bias-field corrected sequence for improved segmentation and T1-mapping at high field. *Neuroimage* 49 (2), 1271–1281. <https://doi.org/10.1016/j.neuroimage.2009.10.002>.
- Mathôt, S., Schrei, D., Theeuwes, J., 2011. OpenSesame: an open-source, graphical experiment builder for the social sciences. *Behav. Res. Methods* 44 (2), 314–324. <http://doi.org/10.3758/s13428-011-0168-7>.
- McEwen, B.S., Gianaros, P.J., 2011. Stress- and allostasis-induced brain plasticity. *Annu. Rev. Med.* 62 (1), 431–445. <https://doi.org/10.1146/annurev-med-052209-100430>.

- Mendes, N., Oligschläger, S., Lauckner, M.E., Golchert, J., Huntenburg, J.M., Falkiewicz, M., et al., 2019. A functional connectome phenotyping dataset including cognitive state and personality measures. *Sci. Data* 6, 180307. <https://doi.org/10.1038/sdata.2018.307>.
- Mestres-Missé, A., Trampel, R., Turner, R., Kotz, S.A., 2017. Uncertainty and expectancy deviations require cortico-subcortical cooperation. *Neuroimage* 144 (Pt A), 23–34. <https://doi.org/10.1016/j.neuroimage.2016.05.069>.
- Miller, R., Plessow, F., Kirschbaum, C., Stalder, T., 2013. Classification criteria for distinguishing cortisol responders from nonresponders to psychosocial stress: evaluation of salivary cortisol pulse detection in panel designs. *Psychosom. Med.* 75 (9), 832–840. <https://doi.org/10.1097/PSY.0000000000000002>.
- Muehlhan, M., Lueken, U., Wittchen, H.-U., Kirschbaum, C., 2011. The scanner as a stressor: evidence from subjective and neuroendocrine stress parameters in the time course of a functional magnetic resonance imaging session. *Int. J. Psychophysiol.* 79 (2), 118–126. <https://doi.org/10.1016/j.ijpsycho.2010.09.009>.
- Mueller, K., Jech, R., Hoskocová, M., Ulmanová, O., Uργοšik, D., Vymazal, J., Růžicka, E., 2017. General and selective brain connectivity alterations in essential tremor: a resting state fMRI study. *NeuroImage. Clinical* 16, 468–476. <https://doi.org/10.1016/j.nicl.2017.06.004>.
- Nichols, T., Hayasaka, S., 2003. Controlling the familywise error rate in functional neuroimaging: a comparative review. *Stat. Methods Med. Res.* 12 (5), 419–446. <https://doi.org/10.1191/0962280203sm341ra>.
- Nierhaus, T., Gundlach, C., Goltz, D., Thiel, S.D., Pleger, B., Villringer, A., 2013. Internal ventilation system of MR scanners induces specific EEG artifact during simultaneous EEG-fMRI. *Neuroimage* 74, 70–76. <https://doi.org/10.1016/j.neuroimage.2013.02.016>.
- Penzo, M.A., Robert, V., Tucciarone, J., De Bundel, D., Wang, M., Van Aelst, L., et al., 2015. The paraventricular thalamus controls a central amygdala fear circuit. *Nature* 519 (7544), 455–459. <https://doi.org/10.1038/nature13978>.
- Peters, A., McEwen, B.S., Friston, K., 2017. Uncertainty and stress: why it causes diseases and how it is mastered by the brain. *Prog. Neurobiol.* 156, 164–188. <https://doi.org/10.1016/j.pneurobio.2017.05.004>.
- Phillips, C., 2016. *SPM Cluster Size Threshold Estimation* [Matlab]. Retrieved from: https://github.com/CyclotronResearchCentre/SPM_ClusterSizeThreshold (Original work published 2016).
- Pittenger, C., Duman, R.S., 2008. Stress, depression, and neuroplasticity: a convergence of mechanisms. *Neuropsychopharmacology: Off. Publ. Am. Coll. Neuropsychopharmacol.* 33 (1), 88–109. <https://doi.org/10.1038/sj.npp.1301574>.
- Power, J.D., Barnes, K.A., Snyder, A.Z., Schlaggar, B.L., Petersen, S.E., 2012. Spurious but systematic correlations in functional connectivity MRI networks arise from subject motion. *Neuroimage* 59 (3), 2142–2154. <https://doi.org/10.1016/j.neuroimage.2011.10.018>.
- Pruessner, J.C., Dedovic, K., Khalili-Mahani, N., Engert, V., Pruessner, M., Buss, C., et al., 2008. Deactivation of the limbic system during acute psychosocial stress: evidence from positron emission tomography and functional magnetic resonance imaging studies. *Biol. Psychiatry* 63 (2), 234–240. <https://doi.org/10.1016/j.biopsych.2007.04.041>.
- Quaedflieg, C.W.E.M., van de Ven, V., Meyer, T., Siep, N., Merckelbach, H., Smeets, T., 2015. Temporal dynamics of stress-induced alternations of intrinsic amygdala connectivity and neuroendocrine levels. *PLoS One* 10 (5), e0124141. <https://doi.org/10.1371/journal.pone.0124141>.
- Rack-Gomer, A.L., Liau, J., Liu, T.T., 2009. Caffeine reduces resting-state BOLD functional connectivity in the motor cortex. *Neuroimage* 46 (1), 56–63. <https://doi.org/10.1016/j.neuroimage.2009.02.001>.
- R Development Core Team, 2008. *R: A language and environment for statistical computing*.
- Regev, L., Baram, T.Z., 2014. Corticotropin releasing factor in neuroplasticity. *Front. Neuroendocrinol.* 35 (2), 171–179. <https://doi.org/10.1016/j.yfrne.2013.10.001>.
- Rubinov, M., Sporns, O., 2010. Complex network measures of brain connectivity: uses and interpretations. *Neuroimage* 52 (3), 1059–1069. <https://doi.org/10.1016/j.neuroimage.2009.10.003>.
- Schiff, N.D., 2008. Central thalamic contributions to arousal regulation and neurological disorders of consciousness. *Ann. N. Y. Acad. Sci.* 1129 (1), 105–118. <https://doi.org/10.1196/annals.1417.029>.
- Schulz, P., Schlotz, W., 1999. Trierer Inventar zur Erfassung von chronischem Sre (TICS): skalenkonstruktion, teststatistische Überprüfung und Validierung der Skala Arbeitsüberlastung. [The Trier Inventory for the Assessment of Chronic Stress (TICS). Scale construction, statistical testing, and validation of the scale work overload.]. *Diagnostica* 45 (1), 8–19. <https://doi.org/10.1026//0012-1924.45.1.8>.
- Sherman, S.M., Guillery, R.W., 2002. The role of the thalamus in the flow of information to the cortex. *Phil. Trans. Biol. Sci.* 357 (1428), 1695–1708. <https://doi.org/10.1098/rstb.2002.1161>.
- Sinha, R., Lacadie, C.M., Constable, R.T., Seo, D., 2016. Dynamic neural activity during stress signals resilient coping. *Proc. Natl. Acad. Sci. Unit. States Am.* 113 (31), 8837–8842. <https://doi.org/10.1073/pnas.1600965113>.
- Sinha, R., Lacadie, C., Skudlarski, P., Wexler, B.E., 2004. Neural circuits underlying emotional distress in humans. *Ann. N. Y. Acad. Sci.* 1032 (1), 254–257. <https://doi.org/10.1196/annals.1314.032>.
- Smith, S.M., Jenkinson, M., Woolrich, M.W., Beckmann, C.F., Behrens, T.E.J., Johansen-Berg, H., et al., 2004. Advances in functional and structural MR image analysis and implementation as FSL. *Neuroimage* 23 (Suppl. 1), S208–S219. <https://doi.org/10.1016/j.neuroimage.2004.07.051>.
- Spielberger, C.D., 1983. *Manual for the State-Trait Anxiety Inventory STAI (Form Y) ("Self-Evaluation Questionnaire")*. Retrieved from: <http://ubir.buffalo.edu/xmlui/handle/10477/1873>.
- Steptoe, A., Kivimäki, M., 2013. Stress and cardiovascular disease: an update on current knowledge. *Annu. Rev. Public Health* 34 (1), 337–354. <https://doi.org/10.1146/annurev-publichealth-031912-114452>.
- Suárez, M.M., Perassi, N.I., 1997. Influence of anterodorsal thalamic nuclei on ACTH release under basal and stressful conditions. *Physiol. Behav.* 62 (2), 373–377.
- Suárez, M., Maglianesi, M.A., Perassi, N.I., 1998. Involvement of the anterodorsal thalamic nuclei on the hypophysoadrenal response to chronic stress in rats. *Physiol. Behav.* 64 (1), 111–116.
- Tarvainen, M.P., Niskanen, J.-P., Lipponen, J.A., Ranta-Aho, P.O., Karjalainen, P.A., 2014. Kubios HRV—heart rate variability analysis software. *Comput. Methods Progr. Biomed.* 113 (1), 210–220. <https://doi.org/10.1016/j.cmpb.2013.07.024>.
- Timbie, C., Barbas, H., 2015. Pathways for emotions: specializations in the amygdalar, mediodorsal thalamic, and posterior orbitofrontal network. *J. Neurosci.: Off. J. Soc. Neurosci.* 35 (34), 11976–11987. <https://doi.org/10.1523/JNEUROSCI.2157-15.2015>.
- Vaisvaser, S., Lin, T., Admon, R., Podlipsky, I., Greenman, Y., Stern, N., et al., 2013. Neural traces of stress: cortisol related sustained enhancement of amygdala-hippocampal functional connectivity. *Front. Hum. Neurosci.* 7. <https://doi.org/10.3389/fnhum.2013.00313>.
- van Marle, H.J.F., Hermans, E.J., Qin, S., Fernández, G., 2010. Enhanced resting-state connectivity of amygdala in the immediate aftermath of acute psychological stress. *Neuroimage* 53 (1), 348–354. <https://doi.org/10.1016/j.neuroimage.2010.05.070>.
- van Oort, J., Tendolcar, I., Hermans, E.J., Mulders, P.C., Beckmann, C.F., Schene, A.H., et al., 2017. How the brain connects in response to acute stress: a review at the human brain systems level. *Neurosci. Biobehav. Rev.* 83, 281–297. <https://doi.org/10.1016/j.neubiorev.2017.10.015>.
- Veer, I.M., Oei, N.Y.L., Spinhoven, P., van Buchem, M.A., Elzinga, B.M., Rombouts, S.A.R.B., 2011. Beyond acute social stress: increased functional connectivity between amygdala and cortical midline structures. *Neuroimage* 57 (4), 1534–1541. <https://doi.org/10.1016/j.neuroimage.2011.05.074>.
- Wager, T.D., van Ast, V.A., Hughes, B.L., Davidson, M.L., Lindquist, M.A., Ochsner, K.N., 2009. Brain mediators of cardiovascular responses to social threat, Part II: prefrontal-subcortical pathways and relationship with anxiety. *Neuroimage* 47 (3), 836–851. <https://doi.org/10.1016/j.neuroimage.2009.05.044>.
- Wang, J., Rao, H., Wetmore, G.S., Furlan, P.M., Korczykowski, M., Dinges, D.F., Detre, J.A., 2005. Perfusion functional MRI reveals cerebral blood flow pattern under psychological stress. *Proc. Natl. Acad. Sci. Unit. States Am.* 102 (49), 17804–17809. <https://doi.org/10.1073/pnas.0503082102>.
- Wellcome Trust Centre. (n.d.). SPM12 - Statistical Parametric Mapping - by Members & Collaborators of the Wellcome Centre for Human Neuroimaging. Retrieved from <https://www.fil.ion.ucl.ac.uk/spm/software/spm12/>
- Wheelock, M.D., Rangaprakash, D., Harnett, N.G., Wood, K.H., Orem, T.R., Mrug, S., et al., 2018. Psychosocial stress reactivity is associated with decreased whole-brain network efficiency and increased amygdala centrality. *Behav. Neurosci.* 132 (6), 561–572. <https://doi.org/10.1037/bne0000276>.
- Wink, A.M., de Munck, J.C., van der Werf, Y.D., van den Heuvel, O.A., Barkhof, F., 2012. Fast eigenvector centrality mapping of voxel-wise connectivity in functional magnetic resonance imaging: implementation, validation, and interpretation. *Brain Connect.* 2 (5), 265–274. <https://doi.org/10.1089/brain.2012.0087>.
- Wolff, M., Vann, S.D., 2019. The cognitive thalamus as a gateway to mental representations. *J. Neurosci.: Off. J. Soc. Neurosci.* 39 (1), 3–14. <https://doi.org/10.1523/JNEUROSCI.0479-18.2018>.
- Yin, Y., Jin, C., Hu, X., Duan, L., Li, Z., Song, M., et al., 2011. Altered resting-state functional connectivity of thalamus in earthquake-induced posttraumatic stress disorder: a functional magnetic resonance imaging study. *Brain Res.* 1411, 98–107. <https://doi.org/10.1016/j.brainres.2011.07.016>.
- Zhu, Y., Nachtrab, G., Keyes, P.C., Allen, W.E., Luo, L., Chen, X., 2018. Dynamic salience processing in paraventricular thalamus gates associative learning. *Science* 362 (6413), 423–429. <https://doi.org/10.1126/science.aat0481>.

7.2.6 Neural Control of Vascular Reactions: Impact of Emotion and Attention. Okon-Singer et al., Journal of Neuroscience (2014)

The Journal of Neuroscience, March 19, 2014 • 34(12):4251–4259 • 4251

Behavioral/Cognitive

Neural Control of Vascular Reactions: Impact of Emotion and Attention

Hadas Okon-Singer,^{1,2,3} Jan Mehnert,^{2,4,5} Jana Hoyer,² Lydia Hellrung,² Herma Lina Schaare,² Juergen Dukart,^{2,6,7} and Arno Villringer^{2,3,4}

¹Department of Psychology, University of Haifa, 3498838 Haifa, Israel, ²Department of Neurology, Max Planck Institute for Human Cognitive and Brain Sciences, 04103 Leipzig, Germany, ³Mind Brain Institute at Berlin School of Mind and Brain, Humboldt-University, 10099 Berlin, Germany, ⁴Charité University Hospital, 10117 Berlin, Germany, ⁵Machine Learning Group, Berlin Institute of Technology, 10587 Berlin, Germany, ⁶Laboratoire de Recherche en Neuroimagerie, Département des Neurosciences Cliniques, Centre Hospitalier Universitaire Vaudois, Université de Lausanne, 1011 Lausanne, Switzerland, and ⁷F. Hoffmann-La Roche, pRED, Pharma Research and Early Development, DTA Neuroscience, 4070 Basel, Switzerland

This study investigated the neural regions involved in blood pressure reactions to negative stimuli and their possible modulation by attention. Twenty-four healthy human subjects (11 females; age = 24.75 ± 2.49 years) participated in an affective perceptual load task that manipulated attention to negative/neutral distractor pictures. fMRI data were collected simultaneously with continuous recording of peripheral arterial blood pressure. A parametric modulation analysis examined the impact of attention and emotion on the relation between neural activation and blood pressure reactivity during the task. When attention was available for processing the distractor pictures, negative pictures resulted in behavioral interference, neural activation in brain regions previously related to emotion, a transient decrease of blood pressure, and a positive correlation between blood pressure response and activation in a network including prefrontal and parietal regions, the amygdala, caudate, and mid-brain. These effects were modulated by attention; behavioral and neural responses to highly negative distractor pictures (compared with neutral pictures) were smaller or diminished, as was the negative blood pressure response when the central task involved high perceptual load. Furthermore, comparing high and low load revealed enhanced activation in frontoparietal regions implicated in attention control. Our results fit theories emphasizing the role of attention in the control of behavioral and neural reactions to irrelevant emotional distracting information. Our findings furthermore extend the function of attention to the control of autonomous reactions associated with negative emotions by showing altered blood pressure reactions to emotional stimuli, the latter being of potential clinical relevance.

Introduction

Threatening stimuli prototypically facilitate adaptive motor behavior and activate the autonomic nervous system, affecting heart rate and blood pressure (Lang et al., 2000). These vascular responses can aggravate when the threatening situation develops into stress for the organism. It has been shown that, among healthy subjects, those with higher blood pressure responses are more likely to subsequently develop hypertension (Matthews et al., 2004). It is therefore highly relevant to identify neural mechanisms for the vascular response and potential ways to modulate it.

Studies on the neural underpinnings of vascular response to stress identified brain areas known to be associated with emotion processing, including the amygdala, insula, and cingulate (Gian-

aros and Sheu, 2009). These pioneer studies used intermittent blood pressure measurements between functional neuroimaging and were therefore limited to longer-lasting “stress periods.” Recent technical developments (Gray et al., 2009), however, on which we build here, allow for simultaneous recording of blood pressure during fMRI to match neural activity associated with brief (threatening) events closely to blood pressure changes.

Regarding potential ways to modulate emotion-related autonomic responses, a crucial question concerns the degree to which reactions to emotional stimuli are affected by cognitive mechanisms. A debate exists on whether processing of emotional items depends on allocation of sufficient attention to them (see Pessoa et al., 2002 and Evans et al., 2011 for similar effects on attention bias to drug-related cues in drug-addicts). Recent models propose that projections from frontoparietal regions to amygdala modulate reactions to emotional stimuli (cf. Pessoa, 2009; Pourtois et al., 2013). Conversely, it has been suggested that although attention influences emotion processing, it may not affect neural activation related to defensive motor responses (Pichon et al., 2012). If the latter were coupled to autonomic responses, this would mean that (action-related) vascular responses to emotional stimuli could occur independently of attention to them.

Motivated by these considerations, the aims of this study were to identify neural regions involved in blood pressure responses to emo-

Received Feb. 18, 2013; revised Jan. 17, 2014; accepted Jan. 20, 2014.

Author contributions: H.O.-S., J.H., and A.V. designed research; H.O.-S. performed research; J.M., L.H., and J.D. contributed unpublished reagents/analytic tools; H.O.-S., J.M., and L.S. analyzed data; H.O.-S., J.M., J.H., L.S., J.D., and A.V. wrote the paper.

We thank Bettina Johst, Andre Pampel, and Joran Lejoson for technical support, Heike Schmidt and Stephan Liebig for help with the graphics, and Noga Cohen for helpful comments on previous versions of this manuscript.

The authors declare no competing financial interests.

Correspondence should be addressed to Hadas Okon-Singer, University of Haifa, Mount Carmel, 3498838 Haifa, Israel. E-mail: hadasos@psy.haifa.ac.il.

DOI:10.1523/JNEUROSCI.0747-13.2014

Copyright © 2014 the authors 0270-6474/14/344251-09\$15.00/0

Neural Control of Vascular Reactions: Impact of Emotion and Attention

Hadas Okon-Singer,^{1,2,3} Jan Mehnert,^{2,4,5} Jana Hoyer,² Lydia Hellrung,² Herma Lina Schaare,² Juergen Dukart,^{2,6,7} and Arno Villringer^{2,3,4}

¹Department of Psychology, University of Haifa, 3498838 Haifa, Israel, ²Department of Neurology, Max Planck Institute for Human Cognitive and Brain Sciences, 04103 Leipzig, Germany, ³Mind Brain Institute at Berlin School of Mind and Brain, Humboldt-University, 10099 Berlin, Germany, ⁴Charité University Hospital, 10117 Berlin, Germany, ⁵Machine Learning Group, Berlin Institute of Technology, 10587 Berlin, Germany, ⁶Laboratoire de Recherche en Neuroimagerie, Département des Neurosciences Cliniques, Centre Hospitalier Universitaire Vaudois, Université de Lausanne, 1011 Lausanne, Switzerland, and ⁷F. Hoffmann-La Roche, pRED, Pharma Research and Early Development, DTA Neuroscience, 4070 Basel, Switzerland

This study investigated the neural regions involved in blood pressure reactions to negative stimuli and their possible modulation by attention. Twenty-four healthy human subjects (11 females; age = 24.75 ± 2.49 years) participated in an affective perceptual load task that manipulated attention to negative/neutral distractor pictures. fMRI data were collected simultaneously with continuous recording of peripheral arterial blood pressure. A parametric modulation analysis examined the impact of attention and emotion on the relation between neural activation and blood pressure reactivity during the task. When attention was available for processing the distractor pictures, negative pictures resulted in behavioral interference, neural activation in brain regions previously related to emotion, a transient decrease of blood pressure, and a positive correlation between blood pressure response and activation in a network including prefrontal and parietal regions, the amygdala, caudate, and mid-brain. These effects were modulated by attention; behavioral and neural responses to highly negative distractor pictures (compared with neutral pictures) were smaller or diminished, as was the negative blood pressure response when the central task involved high perceptual load. Furthermore, comparing high and low load revealed enhanced activation in frontoparietal regions implicated in attention control. Our results fit theories emphasizing the role of attention in the control of behavioral and neural reactions to irrelevant emotional distracting information. Our findings furthermore extend the function of attention to the control of autonomous reactions associated with negative emotions by showing altered blood pressure reactions to emotional stimuli, the latter being of potential clinical relevance.

Introduction

Threatening stimuli prototypically facilitate adaptive motor behavior and activate the autonomic nervous system, affecting heart rate and blood pressure (Lang et al., 2000). These vascular responses can aggravate when the threatening situation develops into stress for the organism. It has been shown that, among healthy subjects, those with higher blood pressure responses are more likely to subsequently develop hypertension (Matthews et al., 2004). It is therefore highly relevant to identify neural mechanisms for the vascular response and potential ways to modulate it.

Studies on the neural underpinnings of vascular response to stress identified brain areas known to be associated with emotion processing, including the amygdala, insula, and cingulate (Gian-

aros and Sheu, 2009). These pioneer studies used intermittent blood pressure measurements between functional neuroimaging and were therefore limited to longer-lasting “stress periods.” Recent technical developments (Gray et al., 2009), however, on which we build here, allow for simultaneous recording of blood pressure during fMRI to match neural activity associated with brief (threatening) events closely to blood pressure changes.

Regarding potential ways to modulate emotion-related autonomic responses, a crucial question concerns the degree to which reactions to emotional stimuli are affected by cognitive mechanisms. A debate exists on whether processing of emotional items depends on allocation of sufficient attention to them (see Pessoa et al., 2002 and Evans et al., 2011 for similar effects on attention bias to drug-related cues in drug-addicts). Recent models propose that projections from frontoparietal regions to amygdala modulate reactions to emotional stimuli (cf. Pessoa, 2009, Pourtois et al., 2013). Conversely, it has been suggested that although attention influences emotion processing, it may not affect neural activation related to defensive motor responses (Pichon et al., 2012). If the latter were coupled to autonomic responses, this would mean that (action-related) vascular responses to emotional stimuli could occur independently of attention to them.

Motivated by these considerations, the aims of this study were to identify neural regions involved in blood pressure responses to emo-

Received Feb. 18, 2013; revised Jan. 12, 2014; accepted Jan. 20, 2014.

Author contributions: H.O.-S., J.H., and A.V. designed research; H.O.-S. performed research; J.M., L.H., and J.D. contributed unpublished reagents/analytic tools; H.O.-S., J.M., and L.S. analyzed data; H.O.-S., J.M., J.H., L.H., L.S., J.D., and A.V. wrote the paper.

We thank Bettina Johst, Andre Pampel, and Jöran Lepsien for technical support; Heike Schmidt and Stephan Liebig for help with the graphics; and Noga Cohen for helpful comments on previous versions of this manuscript.

The authors declare no competing financial interests.

Correspondence should be addressed to Hadas Okon-Singer, University of Haifa, Mount Carmel, 3498838 Haifa, Israel. E-mail: hadasos@psy.haifa.ac.il.

DOI:10.1523/JNEUROSCI.0747-13.2014

Copyright © 2014 the authors 0270-6474/14/344251-09\$15.00/0

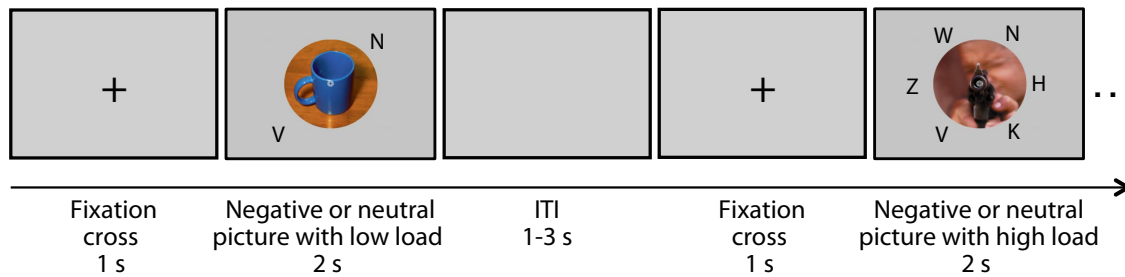


Figure 1. Examples of low-load and high-load trials. In each trial, a fixation cross was presented for 1 s, followed by presentation of a target letter (i.e., “X” or “N”) with either one (i.e., low load) or five (i.e., high load) distracting letters. Simultaneously to the letters, a distracting picture, either neutral or negative, appeared. The valence of the picture was independent of the load condition. ITI, Intertrial interval.

tional stimuli and to elucidate whether and how attention modulates these neural processes and the associated vascular response.

Our study builds on an affective perceptual load task that we previously established to assess the impact of attention on emotion processing (Okon-Singer et al., 2007). Participants discriminate a target letter among few (low load) or many (high load) distractor letters, whereas they are asked to ignore simultaneously presented distractor pictures that are emotionally negative or neutral. Using this paradigm, we investigated whether attention affects behavioral, neural, and vascular reactions to irrelevant emotional distractors in healthy individuals. In the low-load condition, negative pictures were hypothesized to deteriorate task performance, to activate regions implicated in emotion processing (amygdala, anterior insula, orbitofrontal cortex, visual areas), and to transiently decrease blood pressure (Minati et al., 2009; Dan-Glauser and Gross, 2011). In high load (reduced attention) these reactions were hypothesized to be attenuated. Finally, we expected activations related to enhanced perceptual load in frontoparietal and primary visual regions.

Materials and Methods

Subjects

Twenty-four healthy subjects (11 females; mean age = 24.75 ± 2.49 years) without any history of neurological, psychiatric, vascular, or cardiologic diseases volunteered to participate in the study in return for payment. The study was approved by the local ethics committee and all subjects gave informed consent before the experiment. All subjects were right handed according to the Edinburgh Handedness Inventory (Oldfield, 1971) and all fell in the normal range of anxiety and stress as assessed by the German version of the Spielberger State-Trait Anxiety Inventory (Laux et al., 1981) and the Trier Inventory of Chronic Stress (Schulz and Schlotz, 1999), respectively.

Due to technical problems, the behavioral data of five subjects was not recorded, so the behavioral analysis is based on 19 subjects (11 females). In addition, after technical challenges involved in recording blood pressure continuously and noninvasively inside the MRI scanner, the blood pressure measurement of eight of the initial 24 subjects contained $>40\%$ signal dropout (caused by slight movements of the subjects resulting in signal loss and low-pressured attachment of blood pressure sensors; see further details regarding data preprocessing in the “Blood pressure preprocessing” section). Therefore, we performed two types of analyses (see details in “Data analysis” below): (1) analysis of the fMRI data, without correlating them to the blood pressure measures, was performed to examine the neural correlates of the interaction between attention and emotion and was based on fMRI data acquired from all 24 participants (the fMRI data were not affected by the signal dropouts); and (2) analyses correlating the fMRI data with the blood pressure measurements, which had to be conducted based on 16 participants (nine females) due to the signal dropouts and unreliable blood pressure data from eight subjects and include both a parametric modulation analysis and an analysis with a continuous blood pressure regressor (see details in the “Correlation

with blood pressure: parametric modulation analysis” and the “Correlation with continuous blood pressure” sections).

Stimuli and design

Stimuli pictures (distractors) were modified, color real-life photos from the International Affective Picture System (IAPS; Lang et al., 2008). To avoid differences in complexity between the pictures, we modified the original IAPS pictures using clipping and, where necessary, magnification. The emotional valence and arousal levels of the modified pictures were judged by a sample of 41 (20 males, mean age = 26.0 ± 4.6 years) healthy volunteers. For the current experiment, 80 negative and 80 neutral pictures were chosen based on the valence scores of the modified pictures. We did not examine possible differences in the blood pressure response to subtypes of pictures, such as aggressive compared with disgusting images. Visual features were further matched between negative and neutral pictures. *t* tests showed no difference in luminance, contrast, or dominant spatial frequency between the negative and the neutral pictures (all *t*-values <0.53 , all *p*-values >0.6). Furthermore, the content of the pictures (i.e., people, objects, or scenes) was similar across conditions.

Figure 1 describes the order of events in an experimental trial. Each trial started with a fixation cross shown for 1 s, followed by a negative or a neutral picture in the center of the screen for 2 s. The picture was presented as a circular shape and was surrounded by either two (i.e., low perceptual load; 50% of the trials) or six (i.e., high perceptual load) letters presented in an imaginary circle. The letters always included a target letter (i.e., “X” or “N”) and one or five distracting letters. Participants were asked to ignore the picture and discriminate the target letter. They were asked to press different buttons in the response box allocated to indicate either “X” or “N” using the index and middle finger of their right (dominant) hand. They were requested to respond as fast and accurately as possible. Before the fMRI session, subjects performed a short practice session outside the scanner to familiarize them with the task. The experiment was presented in short blocks separated by “null trials” to control for habituation and expectancy effects. The trials were presented in a pseudorandomized order, with the criteria that no more than three consecutive short blocks of the same emotional valence (i.e., negative or neutral) were presented. The reason for using a block design was to maximize the vascular reactivity and neural reactions to the task. Block designs are known to produce more robust effects in fMRI compared with event-related designs (Friston et al., 1999).

Data acquisition

fMRI acquisition. fMRI acquisition was performed on a 3T scanner (Siemens). All images were acquired using a 12-channel head coil. Functional images were acquired using a gradient-echo EPI sequence (FOV 19.2 cm, matrix size 64×64 , voxel size $3 \times 3 \times 4$ mm³, TR/TE/FA = 2000/30/90, 30 axial slices of 3 mm with an interslice gap of 1 mm). Anatomical scans were acquired in a separate session using a T1-weighted 3D MP-RAGE sequence (FOV 256 \times 240 mm², spatial resolution $1 \times 1 \times 1.5$ mm³). Geometric distortions were characterized by a B0 field-map scan. The field-map scan consisted of gradient-echo readout (24 echoes, inter-TE 0.95 ms) with a standard 2D phase encoding. The B0

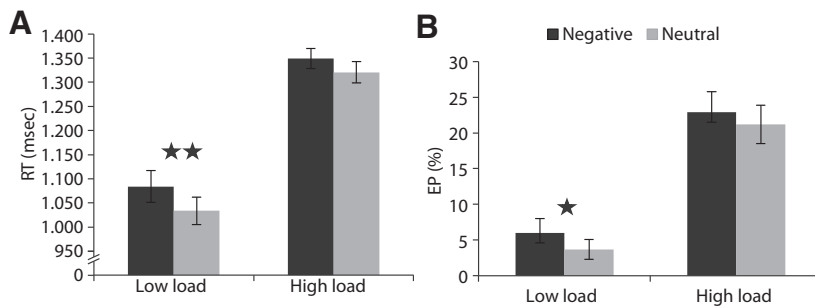


Figure 2. Analysis of RT and EP in the perceptual load task revealed that in the low-load condition, negative distractor pictures resulted in longer RT (*A*) and reduced accuracy (*B*) compared with neutral distractor pictures. In the high-load condition, these differences were not significant. Error bars indicate SD.

Table 1. RT and EP analysis in the perceptual load task

	Mean	SD	<i>t</i> test	<i>p</i> -value
RT (msec)				
Low load				
Negative	1083.9	33.1	2.96	0.008
Neutral	1033.59	28.5		
High load				
Negative	1349.1	21.1	1.17	0.25
Neutral	1320.4	22.2		
EP (error %)				
Low load				
Negative	6.0	2.0	2.37	0.029
Neutral	3.7	1.4		
High load				
Negative	22.9	2.9	0.9	0.37
Neutral	21.2	2.7		

In the low-load condition, negative distractor pictures resulted in slower RT and higher EP compared with neutral distractor pictures. These differences were not significant in the high-load condition.

Table 2. Blood pressure reaction in response to distractor pictures and different load conditions in the perceptual load task

	Mean	SD	<i>F</i> test	<i>p</i> -value
Low load				
Negative	−0.48	1.29	4.34	0.055
Neutral	0.403	1.66		
High load				
Negative	−0.12	1.71	1.59	0.22
Neutral	−0.78	1.35		

In the low-load condition, blood pressure was lower after negative compared with neutral distractor pictures. The difference between negative and neutral distractor pictures was not significant in the high-load condition. Blood pressure changes are reported as a change from mean baseline from 1 s before the beginning of each block to the onset of the first picture in the block.

field was obtained by a linear fit to the unwrapped phases of all odd echoes.

Blood pressure acquisition. Blood pressure was continuously recorded simultaneously to fMRI acquisition using an MR-compatible biophysical measurement system (CareTaker unit; Empirical Technologies/Biopac Systems; <http://www.biopac.com/>). Given the high correlation between their time courses ($r = 0.9219$), further analyses were conducted only on systolic blood pressure because systolic blood pressure has been shown to have higher reactivity to stress (Krantz and Manuck, 1984; Sherwood et al., 1990; Swain and Suls, 1996) and other stimuli (Gravlee and Brockschmidt, 1990) compared with diastolic blood pressure.

An arterial pulse signal was measured noninvasively via a small plastic device that was sensitive to pressure and attached firmly to the L brachial artery. The signal was transformed in real-time to systolic and diastolic blood pressure values using a Pulse Decomposition Analysis (PDA) algorithm (Baruch et al., 2007; Baruch et al., 2011). In short, the PDA algorithm uses the temporal structure of the pressure pulse to extract

features highly correlated with diastolic and systolic blood pressure. The assumption is that the pressure pulse consists of a main, leading pressure component and two following components rising from reflections of the first one. The temporal delay between the first and the third pressure component in combination with their amplitudes are thereby highly correlated with systolic and diastolic blood pressure. Notably, the algorithm calculates neither diastolic nor systolic blood pressure from the mean arterial pressure.

After calibration with individual blood pressure readings from a blood pressure cuff (Biopac Systems), the pulse decomposition analysis algorithm was used to track blood pressure by analyzing the timing and ampli-

tudes of the primary L ventricular ejection pulse and arterial pulse reflections in the upper arm. To avoid movement artifacts, subjects responded to the task using the index and middle fingers of their right hand while the blood pressure device was attached to their left arm. To ensure subject safety, only plastic MR-compatible parts of the system entered the scanner room and the data were transferred using a transducer, Bluetooth dongle, USB D/A converter and cables, and an INISO optically isolated input adapter. Data were sampled at a 500 Hz sampling rate. To maintain sufficient pressure, an automatic blood pressure calibration unit was used and, if necessary, air was pumped into the plastic device attached to the subjects (e.g., in instances in which small movements of the subject affected the blood pressure pad connection to the artery). The data were acquired via the CareTaker blood pressure software module and transferred to AcqKnowledge software (BioPac Systems), which also saved triggers at the onset of each picture onset to allow for the synchronization with the fMRI data.

Data preprocessing

fMRI preprocessing. Functional data were processed and analyzed using Statistical Parametric Mapping software (SPM8; Wellcome Department of Imaging Neuroscience, London, United Kingdom) with MATLAB 7.11.0 software (MathWorks). Preprocessing included the following steps: removal of the first 10 s (first five repetitions) to achieve a scanner steady state, motion correction using realignment to the first volume, geometric distortions correction using a field map, and slice timing correction to the middle slice. Functional and anatomical images were normalized to Montreal Neurological Institute (MNI) space. Images were then spatially smoothed with an 8 mm full-width at half-maximum Gaussian kernel and a high-pass filter of 1/128 Hz was applied.

Blood pressure preprocessing. The systolic blood pressure raw data were corrected for clearly visible artifacts (when pressure went below 3 SDs from its mean) using a linear interpolation between the last corrected blood pressure value before the artifacts occurrence and the first value afterward. Subjects for whom >40% of the data had to be interpolated were excluded from any further analysis, resulting in 16 subjects being used for analyses of blood pressure data. Within these 16 subjects, 3.1% (SD = 5.9%) of the data were interpolated (25.3/0.3 max/min in individuals). For the parametric modulation analysis, we calculated one value for systolic blood pressure in each block. These values were based on an average of the values from 3 s after the first picture onset in a block to 5 s after the end of the block (based on Gray et al., 2009 and James et al., 2013) minus a baseline based on the values of the second before the block onset (i.e., period of −1 to zero when zero is the first stimulus onset in a block). These values were used in the analysis of the blood pressure responses and for the parametric analysis with the fMRI data. For the analyses of the relation of neural activation to blood pressure fluctuations, we prepared a continuous regressor for systolic pressure that was based on one blood pressure value for each TR.

Data analysis

Behavioral data analysis. The analyses of behavioral data included reaction time (RT) and accuracy (error percentage; EP) and was performed

Table 3. Brain regions activated during the perceptual load task

Side	Region	MNI coordinates			t-value	Voxels
		x	y	z		
Regions that exhibited enhanced activation for negative vs neutral pictures						
R	Middle frontal gyrus	42	5	34	5.58	21
R	Inferior frontal gyrus	48	20	22	5.49	24
R	Inferior frontal gyrus	51	32	4	5.77	44
L	Superior frontal gyrus	−3	53	28	5.20	8
L	Inferior frontal gyrus	−36	23	1	6.53	106
L	Orbito-frontal cortex	−27	17	−17	5.40	10
R	Lateral occipital cortex	51	−70	7	9.89	681
L	Fusiform gyrus	−39	−49	−17	7.94	603
R	Amygdala	21	−4	−14	5.70	13
L	Amygdala	−21	−4	−14	5.75	24
R	Brainstem	9	−28	−8	5.53	11
R	Cerebellum	21	−76	−44	5.10	5
L	Cerebellum	−18	−76	−41	6.50	50
Regions that exhibited enhanced activation for neutral vs negative pictures						
R	Temporal lobe/lateral ventricle	18	−37	13	5.58	7
L	Temporal lobe	−27	−46	1	5.38	9
Regions that exhibited enhanced activation in the low-load vs the high-load condition						
	Medial frontal gyrus	0	47	−20	5.43	35
L	Superior medial frontal gyrus	−9	56	28	5.30	11
R	Middle temporal gyrus	57	−64	−5	7.02	64
R	Middle occipital gyrus	27	−94	−2	5.42	14
R	Hippocampus	21	−7	−17	5.13	5
L	Hippocampus	−24	−13	−17	5.94	47
Regions that exhibited enhanced activation in the high-load vs the low-load condition						
R	Middle frontal gyrus	33	47	19	7.75	180
L	Middle frontal gyrus	−33	50	13	6.43	47
L	Middle frontal gyrus	−24	2	49	5.61	20
R	Inferior frontal gyrus	30	26	−5	7.41	122
R	Supplementary motor area	18	11	64	5.38	8
L	Supplementary motor area	−9	14	46	6.11	87
R	Inferior parietal lobule	42	−52	49	5.71	121
L	Superior parietal gyrus	−24	−61	49	7.34	309
L	Lingual gyrus	−9	−79	−5	10.54	1449
L	Insula/Inferior frontal gyrus	−33	20	−2	6.71	82
Regions that exhibited enhanced activation for negative vs neutral pictures in the low-load condition						
R	Inferior frontal/orbitofrontal gyrus	36	29	−11	4.97	6
R	Middle temporal gyrus	51	−70	7	8.16	217
L	Middle temporal gyrus	−48	−61	4	6.32	210
R	Inferior temporal gyrus	42	−40	−14	6.54	69
L	Fusiform gyrus	−39	−49	−17	5.27	11
L	Insula	−36	23	1	5.95	35
L	Cerebellum	−18	−76	−41	5.33	8
Similar contrast: amygdala examination using a small volume correction ($p < 0.05$ FWE corrected)						
R	Amygdala	18	−4	−11	4.30	58
L	Amygdala	−18	−7	−14	4.69	70
Regions that exhibited enhanced activation for neutral vs negative pictures in the low-load condition						
R	Caudate	21	−34	13	5.67	13
Regions that exhibited enhanced activation for negative vs neutral pictures in the high-load condition						
R	Fusiform gyrus	39	−49	−20	5.87	47
L	Fusiform gyrus	−39	−49	−17	5.46	27
R	Middle occipital gyrus	51	−73	1	5.73	16
L	Middle occipital gyrus	−42	−79	−2	5.11	7
No regions exhibited enhanced activation for neutral vs negative pictures in the high-load condition						

The table shows left (L) and right (R) regions that were activated in the corresponding analyses. For each region, the t-values for voxels of peak activation and their corresponding cluster sizes were derived from a whole-brain group analysis (see text for details). The table includes only clusters of at least five voxels.

using SPSS (version 18, <http://www-01.ibm.com/software/analytics/spss/>). For the RT analysis, only correct responses were included. Extreme responses (i.e., >3 SDs from the mean of the specific condition) were excluded. Mean RTs and EP data were used in a two-way factorial ANOVA with the factors valence (negative/neutral pictures) and load (low/high) as within-subjects effects.

Blood pressure responses. Similar to the analysis of the behavioral data, the analysis of the blood pressure responses was also performed using SPSS (version 18, <http://www-01.ibm.com/software/analytics/spss/>). As described above, for each subject, we calculated one value for systolic

blood pressure in each block. These values were used in a two-way factorial ANOVA with the factors valence (negative/neutral pictures) and load (low/high) as within-subjects effects.

fMRI analysis of the task conditions. To examine the effect of the task on neural activation, whole-brain voxelwise general linear model analyses were conducted on the first level. The analysis was based on a block design similar to the analyses of the behavioral performance and the blood pressure reaction. Regressors modeling stimulus events were locked to the first stimulus onset in each experimental block and convolved with a canonical hemodynamic response function (HRF). The

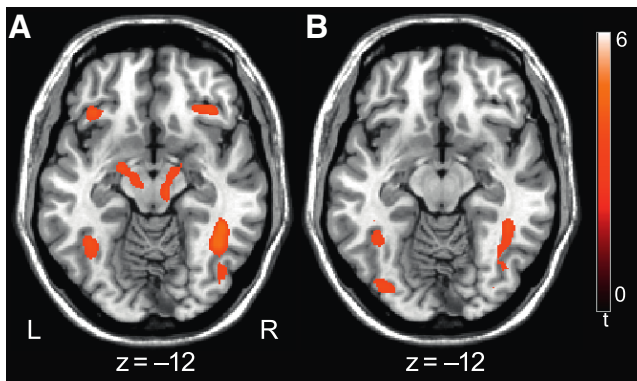


Figure 3. Neural regions that revealed enhanced activation in the perceptual load task when contrasting negative (in red) and neutral (in blue) distractor pictures in the low-load (A) and high-load (B) conditions. Results were thresholded at $p < 0.05$ FWE corrected.

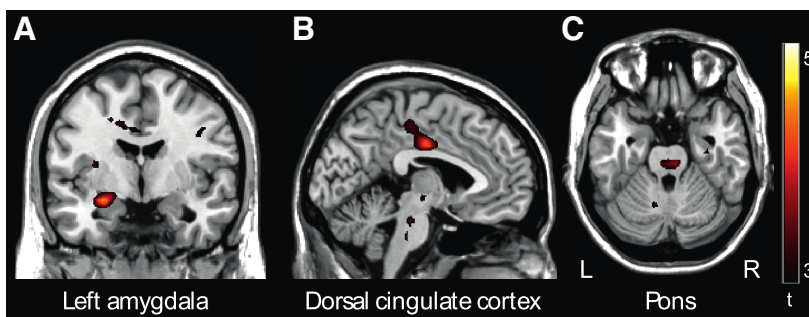


Figure 4. Neural regions that revealed enhanced positive correlation with changes in blood pressure in the low-load condition when contrasting negative and neutral pictures. Results were thresholded at $p < 0.001$ uncorrected. A, Coronal section. B, Sagittal section. C, Horizontal section.

analysis model included the task conditions and six motion realignment nuisance regressors. A factorial design was applied with emotion (negative/neutral) and load (low/high) as within-subjects factors. The individual maps of activation were entered into a group analysis computed with random effects controlling for voxelwise multiple comparisons using a familywise error rate (FWE) threshold of $p < 0.05$ (Friston et al., 1996). In addition, based on our hypothesis that the amygdala would be involved in the reaction to emotional stimuli, we specifically analyzed this region as a region of interest (ROI). The coordinates for the amygdala analysis were based on a recent meta-analysis of reactions to emotional items (amygdala left: $-20, -6, -17$; right: $22, -3, -17$; Sabatinelli et al., 2011). Considering the small size of the amygdala (1500 mm^3 ; Amunts et al., 2005), we used a small volume correction using 8-mm-radius sphere based on a formula for radius calculation for a spherical shape. Subjects were included as a between-subjects factor to correct for individual differences in activation. The group level model further included a nuisance regressor of sex (Sacher et al., 2012). To examine early and later effects of attention on the reaction to the emotional distractors, we further plotted the time course of regions that were related to the task's reactions. Coordinates for the ROIs were chosen based on Table 3. We examined regions that are important based on previous literature related to emotional processing and/or emotion control (Sabatinelli et al., 2011). We chose cortical and subcortical regions to investigate the potential differences in their time courses. Therefore, the following regions were chosen: bilateral amygdala, L middle frontal gyrus, and right inferior frontal gyrus. To avoid overlapping responses between trials, the time courses are based on averages of the first trial in each experimental block. Analyses were performed using rfxplot toolbox for SPM using the Peri-Stimulus Time Histogram option (Gläscher, 2009).

Correlation with blood pressure: parametric modulation analysis. To examine possible differences between the task conditions in the activation of neural regions that are related to systolic blood pressure, we

conducted a parametric modulation analysis model in SPM. On the individual level, the statistical model included the task conditions as regressors (as mentioned in fMRI analysis of the task conditions, above), a blood pressure parameter for each condition and experimental block, and the six movement realignment parameters. Contrast maps were computed on the first level for each parameter (i.e., negative/neutral pictures \times low/high load). These contrast maps were entered in factorial analysis on the group level, with a general factor of subjects and sex as a covariate, similarly to previous analyses described above (see "fMRI analysis of the task conditions" section). An analysis based on a FWE-corrected p -value yielded very few regions of activation, probably due to the relatively low number of remaining subjects after excluding subjects with many signal dropouts. Therefore, we report results based on a p -value of 0.001.

Correlation with continuous blood pressure. To examine possible relation between neural activation of and blood pressure fluctuations, we conducted an analysis with a continuous blood pressure regressor in SPM. Similarly to the other analyses, we focused on systolic blood pressure. The individual-level statistical model included the systolic blood pressure continuous regress, the task regressor, and six motion realignment parameters as covariates of no-interest. A regression analysis at the first level was followed by a one-sample t test at the group level computed with random effects modeling sex as a covariate of no-interest, similarly to previous analyses described above (see "fMRI analysis of the task conditions" section). Similarly to the parametric modulation analysis, we report results based on a p -value of 0.001.

Results

Behavioral performance

Separate analyses were performed for RT and EP. The ANOVA revealed a main effect of valence due to longer RTs after presentation of negative pictures compared with neutral pictures ($F_{(1,18)} = 5.12, p = 0.03$). The same trend in EP did not reach significance ($F_{(1,18)} = 2.93, p = 0.1$). In addition, RTs were longer and EP was higher in the high-load compared with the low-load condition ($F_{(1,18)} = 172.7, p = 0.001$ and $F_{(1,18)} = 90.6, p = 0.001$ for RT and EP, respectively). The interaction between load and valence was not significant ($F_{(1,18)} = 1.39, p = 0.25$ and $F_{(1,18)} = 0.08, p = 0.7$ for RT and EP, respectively). However, based on our a priori hypotheses, we further examined the difference between negative and neutral picture trials in the low-load and high-load conditions separately. As expected, the difference between negative and neutral pictures was significant in the low-load condition ($t_{18} = 2.96, p = 0.008$ and $t_{18} = 2.37, p = 0.029$, for RT and EP, respectively). In the high-load condition, the difference between negative and neutral pictures was not significant ($t_{18} = 1.17, p = 0.25$ and $t_{18} = 0.9, p = 0.37$, for RT and EP, respectively; Fig. 2, Table 1).

Blood pressure responses

An ANOVA revealed an interaction between load and valence ($F_{(1,15)} = 7.35, p = 0.01$). *Post hoc* analyses revealed that this interaction resulted from an opposite pattern between low and high load: in the low load, systolic blood pressure responses were lower when negative pictures were presented, compared with neutral pictures ($F_{(1,15)} = 4.34, p = 0.055$). In contrast, in the high-load condition, systolic blood pressure responses did not differ significantly between negative and neutral pictures ($F_{(1,15)} = 1.59, p = 0.22$; Table 2). The main effects of load and valence were not significant (all $f < 1.08$; all $p > 0.3$).

Table 4. Brain regions activated during the perceptual load task in correlation with blood pressure changes

Side	Region	MNI coordinates			t-value	Voxels
		x	y	z		
Regions that exhibited enhanced correlation with blood pressure for negative vs neutral pictures ($p < 0.001$ uncorrected)						
L	Supplementary motor area	−9	−22	49	3.72	11
L	Postcentral gyrus	−21	−40	70	4.16	12
L	Middle temporal cortex	−42	−7	−20	3.60	6
L	Insula/caudate	−33	−37	22	4.04	7
L	Amygdala	−27	−4	−17	3.56	7
R	White matter	24	−16	37	3.91	19
No regions exhibited enhanced correlation with blood pressure for neutral vs negative pictures						
No regions exhibited enhanced correlation with blood pressure for the low-load vs the high-load condition						
Regions that exhibited enhanced correlation with blood pressure for the high-load vs the low-load condition						
R	Anterior cingulate cortex	18	38	16	4.41	79
L	Precentral gyrus	−54	2	28	3.31	8
L	Caudate	−24	14	22	3.30	5
L	White matter	−18	17	34	4.39	33
Regions that exhibited enhanced correlation with blood pressure for negative vs neutral pictures in the low-load condition						
R	Middle frontal gyrus	36	8	34	3.70	15
R	Lateral prefrontal cortex	42	23	40	3.57	5
L	Lateral prefrontal cortex	−42	47	16	3.47	6
R	Inferior frontal gyrus/Insula	54	26	1	3.70	6
L	Supplementary motor area	−9	−22	49	3.79	13
R	Dorsal cingulate	21	−16	40	5.20	374
R	Posterior cingulate	21	−46	34	4.75	61
L	Superior parietal gyrus	−18	−40	70	3.99	12
L	Superior parietal gyrus	−27	−43	64	3.60	5
L	Inferior parietal cortex	−57	−46	37	3.51	17
L	Inferior parietal cortex	−42	−58	37	3.55	16
L	Insula	−39	−22	10	4.09	45
R	Parahippocampal gyrus	30	−19	−20	4.11	29
L	Amygdala	−27	−4	−14	4.57	9
R	Putamen	21	8	−11	3.62	86
L	Putamen	−30	5	−11	4.68	28
R	Midbrain	9	−10	−8	4.48	21
R	Midbrain	6	−25	−26	3.78	17
R	Cerebellum	33	−76	−38	3.97	17
No regions exhibited enhanced correlation with blood pressure for neutral vs negative pictures in the low-load condition. In the high-load condition, no regions exhibited enhanced correlation with blood pressure either for negative vs neutral pictures or for neutral vs negative pictures						
Regions that exhibited a correlation with continuous blood pressure						
R	Superior frontal gyrus	18	14	46	4.90	13
R	Frontal pole	27	65	19	4.57	10
L	Frontal pole	−39	56	10	5.12	13
L	Frontal pole	−6	68	16	4.28	5
L	Prefrontal cortex (bilateral)	−6	−7	67	7.12	352
L	Precentral gyrus	−21	−25	55	5.65	126
L	Cingulate gyrus	−6	−4	46	4.40	19
R	Parietal cortex	42	−49	31	4.13	5
R	Hippocampus	36	−19	−14	4.47	10
L	Cerebellum	−21	−31	−29	4.92	5
L	Cerebellum	−9	−55	−50	7.03	71
R	Cerebellum	9	−58	−50	5.47	14

Table shows left (L) and right (R) regions that were activated in the corresponding analyses. For each region, the t-values for voxels of peak activation and their corresponding cluster sizes were derived from a whole-brain group analysis (see text for details). The table includes only clusters of at least five voxels.

Neural responses to the task

Table 3 depicts the brain regions that were found in the whole brain analysis ($p < 0.05$, FWE corrected) of the perceptual load task when contrasting load, valence, and their interaction. In relation to our main hypothesis regarding attention, in the low-load condition, higher activation was revealed after negative pictures compared with after neutral pictures in the bilateral amygdala, the bilateral medial temporal cortex, the right inferior frontal cortex and the left insula: brain regions implicated in emotion processing. In the high-load condition, the difference between negative and neutral pictures was restricted to only a few vision brain regions (Fig. 3, Table 3).

Further examination of the time courses of several ROIs reveals clear differences between the amygdala and prefrontal regions (see Fig. 5). Although activation in bilateral amygdala was higher for negative compared with neutral distracting pictures, and in general higher in the low-load compared with the high-load condition, activation in prefrontal regions was higher during the high-load compared with the low-load condition. These activation patterns are consistent with the suggestion that attention resources had an impact on the neural response to distracting pictures. Additionally, they suggest that top-down control processes originating in frontoparietal regions might have affected the reduced neural responses during the high-

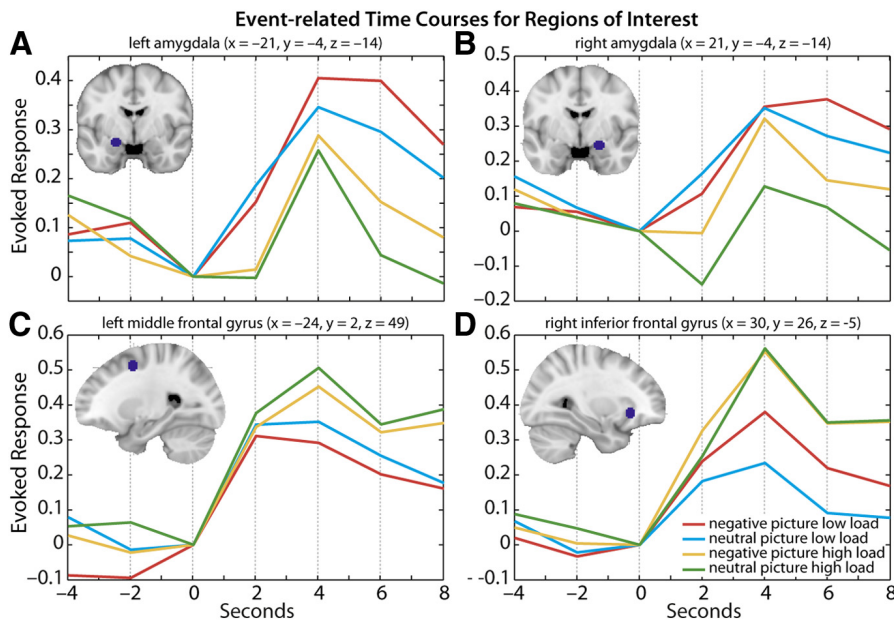


Figure 5. Time courses of fMRI-BOLD activations in the following ROIs: bilateral amygdala (**A**, **B**), left middle frontal gyrus (**C**), and right inferior frontal gyrus (**D**). The plots are based on activation in a 6 mm sphere surrounding the coordinates. To avoid overlapping responses, the time courses are based on the first trials in the relevant block for each condition (see text for details).

load condition. Please note that our block design did not allow averaging of all the trials. Therefore, these time courses are based on an average of only the first trial in each block, yielding eight trials per condition for each subject. Furthermore, comparison of the timing between different regions is problematic because the HRF is known to differ between neural sites (Neumann et al., 2003).

Neural correlates of blood pressure: modulation by task conditions

Table 4 depicts the neural regions that correlated with changes in systolic blood pressure in the different task conditions. In the low-load condition, comparison of the neural regions related to systolic blood pressure responses to negative pictures compared with neutral pictures revealed activation in the bilateral lateral prefrontal cortex, the right dorsal and posterior cingulate, the left superior and inferior parietal cortex, the bilateral insula, the left amygdala, the bilateral putman, and the bilateral midbrain and cerebellar regions (Fig. 4, Table 4).

Neural correlates of blood pressure fluctuations

Table 4 shows the neural regions that positively correlated with changes in systolic blood pressure during the fMRI acquisition. This analysis revealed activation in bilateral frontal pole, bilateral prefrontal cortex, the right parietal cortex, the left cingulate cortex, the right hippocampus, and bilateral cerebellum.

Discussion

Using an affective perceptual load task, we found that in the low-load condition—when attention was available for processing distractor pictures—negative (compared with neutral) pictures deteriorated performance in the central task, activated brain regions known to be involved in emotion processing, and decreased blood pressure; we furthermore found a positive correlation between blood pressure response and activation in prefrontal and parietal regions, amygdala, caudate, and the midbrain. These effects were modulated by attention: behavioral and neural re-

sponses to highly negative distractor pictures were smaller or diminished, as was the negative blood pressure response when the central task involved high perceptual load. Furthermore, comparing the high-load and low-load conditions revealed enhanced activation in frontoparietal regions.

The finding of stronger behavioral interference of irrelevant pictures in the low-load condition confirms our previous results using the same task (Okon-Singer et al., 2007). The activation of amygdala, insula, orbitofrontal, visual, and cerebellar areas for negative pictures and the reduced activation in the high-load condition is also highly consistent with our hypothesis and previous findings. Subsequently, we discuss the results concerning the main aims of our study, the blood pressure response to emotion stimuli and the involved neural regions and the influence of attention on these responses. Finally, we speculate about clinical implications and suggest future studies.

Blood pressure response to emotional stimuli and involved brain areas

Emotions are strongly linked to physiological reactions via modulation of the autonomic system. Most previous fMRI investigations on neural correlates of blood pressure responses have either measured vascular responses at the end of stress-evoking blocks (Gianaros et al., 2006) or used replica protocols to correlate vascular responses measured outside the scanner with neural responses acquired with fMRI (Gianaros et al., 2012). Here, we measured blood pressure simultaneously to fMRI (pioneered by Gray et al., 2009) so the results represent neural and vascular responses to brief emotional stimuli. Furthermore, this design allows investigating the interaction between various mental processes occurring simultaneously. We cannot rule out possible influences of other factors, such as familiarity, and although we believe our results reflect neural activity that preceded vascular reactivity, it is possible that blood pressure responses themselves also influenced the measured neural activity.

Our finding of an early blood pressure decrease to negative stimuli is consistent with results showing heart rate deceleration and blood pressure decrease when viewing unpleasant pictures (Lang et al., 1993; Minati et al., 2009; Dan-Glauser and Gross, 2011; Wangelin et al., 2011). Blood pressure responses during emotional stimuli correlated with activity in bilateral lateral prefrontal cortex, the right dorsal and posterior cingulate cortex, the left insula, the left amygdala, midbrain, and cerebellar regions. These regions, which are known to be key players in emotion generation and regulation, are consistent with a meta-analysis of studies investigating neural correlates of vascular responses to stress (Gianaros and Sheu, 2009), and were shown to reduce the sensitivity of the arterial baroreflex during stress (Gianaros et al., 2012). Interestingly, these areas were related to blood pressure responses to emotional stimuli, but not to spontaneous fluctuations of blood pressure, pointing to recruitment of a neural network involved in vascular reactions associated with emotion.

Notably, BOLD signal in these areas correlated positively with blood pressure, which decreased with negative picture observa-

tion. Although we did not have the spatial resolution to parcel different amygdala subareas, it is tempting to speculate that different amygdala subareas are responsible for the blood pressure response and the overall response to negative pictures. Analogously, different amygdala subregions were shown to mediate valence-related and attention/predictiveness effects during emotional processing (Gamer et al., 2010; Boll et al., 2013).

Related to our study, there is recent work on neural correlates of peripheral autonomic activity in other settings: James et al. (2013) recorded muscle sympathetic nerve activity simultaneously to fMRI at rest. BOLD activity covaried with muscle sympathetic nerve activity in bilateral dorsolateral prefrontal cortex, precuneus, posterior cingulate cortex, hypothalamus, left insula, and left cerebellum (for review, see Macefield et al., 2013). Henderson et al. (2012) recorded skin sympathetic nerve activity simultaneously with fMRI during presentation of arousing pictures. Skin sympathetic nerve activity was positively related to activation in the right amygdala, bilateral thalamus, right nucleus accumbens, bilateral pons, and right cerebellum and negatively related to activation in the left orbitofrontal cortex, left frontal cortex, and right precuneus (see also Brown et al., 2012). Gray et al. (2009) measured cardiovascular responses to electric shocks administered at different time points of the cardiac rhythm simultaneously with fMRI. Their results imply that a network including the amygdala, insula, and brainstem is related to vascular reactions to painful stimuli. Although direct comparison between these studies and the current study is difficult due to methodological differences, we also found a relation to the amygdala only when examining blood pressure in response to the task and not during rest. All studies point to the involvement of frontal, limbic, midbrain, and cerebellar regions in the regulation of autonomous activity. Recent developments in autonomic signal acquisition simultaneously with fMRI may provide better differentiation of the neural networks regulating different autonomic systems in response to emotional stimulation and at rest.

Influence of attention on behavioral, neural, and blood pressure reaction to emotional stimuli

In our study, attention influenced behavioral and neural responses to negative pictures and there was an interaction between emotional valence and attention on the blood pressure response. Emotion theories typically consider both limbic-mediated projections to sensory areas related to the emotional salience of the stimulus and frontoparietal-mediated projections related to emotion regulation (Ochsner et al., 2012). Consistent with these models, we find modulation of neural responses due to the affective value of distracting pictures and allocation of attention. During low load, negative (compared with neutral) pictures led to higher activations in the amygdala, insula, orbitofrontal, visual, and cerebellar areas. These activations were reduced at high load. Furthermore, comparison of high and low load across picture types revealed enhanced activation in the middle and inferior frontal cortex, intraparietal lobule, and superior parietal lobule.

It is as yet unclear, however, whether these modulatory factors interact. Several studies support the notion that neural reactions to emotional stimuli depend on an interaction between “evaluative” and “control” projections (Pessoa et al., 2002; Van Dillen and Derks, 2012; for review, see Okon-Singer et al., 2012 and Jordan et al., 2013), but there are also conditions in which no interaction was found. For example, Gläscher et al. (2007) found attention and emotion not to interact; rather, their data indicated a “multiplicative gain effect of emotional salience.” Additionally, in invasive amygdala recordings, there was an early attention-

independent amygdala response preceding top-down attentional control effects (Pourtois et al., 2010; for review, see Pourtois et al., 2013). The 2 s picture presentation in our study would allow for both early control mechanisms and later top-down control; The frontoparietal activations that we found when comparing high and low load across picture types and the accordingly differential BOLD time courses given in Figure 5 suggest involvement of top-down cortical regions. Levens and Phelps (2010) showed that bilateral inferior frontal gyrus (found in our study when comparing high and low load across picture types) mediates interference resolution for both neutral and emotional items, whereas the left anterior insula and the right orbitofrontal cortex (found in our study when comparing negative and neutral distractors in low load) are specifically related to emotional distraction (see also Levens et al., 2011). Overall, we believe that at current levels of evidence, conclusions regarding the exact control mechanisms should be taken cautiously.

Implications, open questions, and perspectives

We believe that our approach provides a suitable setting for systematically studying the relationship among behavioral, neural, and physiological parameters during emotion processing. For example, it is not clear yet why the initial “negative” vascular response to emotional stimuli changes toward a later “positive” vascular response when threat continues (i.e., the “fight or flight” response). The underlying mechanisms are of potential clinical relevance because it has been shown that, among healthy, normotensive individuals, those in the upper quartile of blood pressure reaction to psychological stressors carry a higher risk of later developing hypertension (Matthews et al., 2004). In a similar vein, it has been suggested that “exaggerated” cardiovascular responses to stressors are mediated by abnormal brain structure, function, and connectivity (Gianaros et al., 2009a; Gianaros et al., 2009b) and that such neural abnormality may precede hypertension (Jennings and Zanstra, 2009). Our finding that attention modulates blood pressure response to emotional stimuli is consistent with the effect of emotion regulation on autonomic reactions (Dan-Glauser and Gross, 2011). These findings may provide a basis for preventive strategies for individuals at risk of developing hypertension. Further studies may elucidate neural factors predisposing individuals to vascular overreactions (i.e., at risk to develop hypertension) and enable the development of measures (e.g., emotion regulation, meditation) to prevent such vascular “overreactions.”

References

- Amunts K, Kedo O, Kindler M, Pieperhoff P, Mohlberg H, Shah NJ, Habel U, Schneider F, Zilles K (2005) Cytoarchitectonic mapping of the human amygdala, hippocampal region and entorhinal cortex: intersubject variability and probability maps. *Anat Embryol (Berl)* 210:343–352. [CrossRef Medline](#)
- Baruch M, Kwon KW, Abdel-Rahman E, Isaacs R (2007) The structure of the radial pulse—a novel noninvasive ambulatory blood pressure device. *Stud Health Technol Inform* 125:40–42. [Medline](#)
- Baruch MC, Warburton DE, Bredin SS, Cote A, Gerdt DW, Adkins CM (2011) Pulse decomposition analysis of the digital arterial pulse during hemorrhage simulation. *Nonlinear Biomed Phys* 5:1. [CrossRef Medline](#)
- Boll S, Gamer M, Gluth S, Finsterbusch J, Büchel C (2013) Separate amygdala subregions signal surprise and predictiveness during associative fear learning in humans. *Eur J Neurosci* 37:758–767. [CrossRef Medline](#)
- Brown R, James C, Henderson LA, Macefield VG (2012) Autonomic markers of emotional processing: skin sympathetic nerve activity in humans during exposure to emotionally charged images. *Front Physiol* 3:394. [CrossRef Medline](#)

- Dan-Glauser ES, Gross JJ (2011) The temporal dynamics of two response-focused forms of emotion regulation: Experiential, expressive, and autonomic consequences. *Psychophysiology* 48:1309–1322. [CrossRef Medline](#)
- Evans DE, Craig C, Oliver JA, Drobos DJ (2011) The smoking N-back: a measure of biased cue processing at varying levels of cognitive load. *Nicotine Tob Res* 13:88–93. [CrossRef Medline](#)
- Friston KJ, Zarahn E, Josephs O, Henson RN, Dale AM (1999) Stochastic designs in event-related fMRI. *Neuroimage* 10:607–619. [CrossRef Medline](#)
- Friston KJ, Holmes A, Poline JB, Price CJ, Frith CD (1996) Detecting activations in PET and fMRI: levels of inference and power. *Neuroimage* 4:223–235. [CrossRef Medline](#)
- Gamer M, Zurowski B, Büchel C (2010) Different amygdala subregions mediate valence-related and attentional effects of oxytocin in humans. *Proc Natl Acad Sci U S A* 107:9400–9405. [CrossRef Medline](#)
- Gianaros PJ, Sheu LK, Remo AM, Christie IC, Critchley HD, Wang J (2009a) Heightened resting neural activity predicts exaggerated stressor-evoked blood pressure reactivity. *Hypertension* 53:819–825. [CrossRef Medline](#)
- Gianaros PJ, Greer PJ, Ryan CM, Jennings JR (2006) Higher blood pressure predicts lower regional grey matter volume: Consequences on short-term information processing. *Neuroimage* 31:754–765. [CrossRef](#)
- Gianaros PJ, Hariri AR, Sheu LK, Muldoon MF, Sutton-Tyrrell K, Manuck SB (2009b) Preclinical atherosclerosis covaries with individual differences in reactivity and functional connectivity of the amygdala. *Biol Psychiatry* 65:943–950. [CrossRef Medline](#)
- Gianaros PJ, Sheu LK (2009) A review of neuroimaging studies of stressor-evoked blood pressure reactivity: emerging evidence for a brain-body pathway to coronary heart disease risk. *Neuroimage* 47:922–936. [CrossRef Medline](#)
- Gianaros PJ, Onyewuenyi IC, Sheu LK, Christie IC, Critchley HD (2012) Brain systems for baroreflex suppression during stress in humans. *Hum Brain Mapp* 33:1700–1716. [CrossRef Medline](#)
- Gläscher J (2009) Visualization of group inference data in functional neuroimaging. *Neuroinformatics* 7:73–82. [CrossRef Medline](#)
- Gläscher J, Rose M, Büchel C (2007) Independent effects of emotion and working memory load on visual activation in the lateral occipital complex. *J Neurosci* 27:4366–4373. [CrossRef Medline](#)
- Gravlee GP, Brockschmidt JK (1990) Accuracy of four indirect methods of blood pressure measurement, with hemodynamic correlations. *J Clin Monit* 6:284–298. [CrossRef Medline](#)
- Gray MA, Rylander K, Harrison NA, Wallin BG, Critchley HD (2009) Following one's heart: Cardiac rhythms gate central initiation of sympathetic reflexes. *J Neurosci* 29:1817–1825. [CrossRef Medline](#)
- Henderson LA, Stathis A, James C, Brown R, McDonald S, Macefield VG (2012) Real-time imaging of cortical areas involved in the generation of increases in skin sympathetic nerve activity when viewing emotionally charged images. *Neuroimage* 62:30–40. [CrossRef Medline](#)
- Jordan AD, Dolcos S, Dolcos F (2013) Neural signatures of the response to emotional distraction: a review of evidence from brain imaging investigations. *Front Hum Neurosci* 7:200. [CrossRef Medline](#)
- James C, Macefield VG, Henderson LA (2013) Real-time imaging of cortical and subcortical control of muscle sympathetic nerve activity in awake human subjects. *Neuroimage* 70:59–65. [CrossRef Medline](#)
- Jennings JR, Zanstra Y (2009) Is the brain the essential in hypertension? *Neuroimage* 47:914–921. [CrossRef Medline](#)
- Krantz DS, Manuck SB (1984) Acute psychophysiologic reactivity and risk of cardiovascular disease: a review and methodologic critique. *Psychol Bull* 96:435–464. [CrossRef Medline](#)
- Lang PJ, Greenwald MK, Bradley MM, Hamm AO (1993) Looking at pictures—affective, facial, visceral, and behavioral reactions. *Psychophysiology* 30:261–273. [CrossRef Medline](#)
- Lang PJ, Davis M, Ohman A (2000) Fear and anxiety: animal models and human cognitive psychophysiology. *J Affect Disord* 61:137–159. [CrossRef Medline](#)
- Lang PJ, Bradley MM, Cuthbert BN (2008) International affective picture system (IAPS): affective ratings of pictures and instruction manual. Technical Report A-8. Gainesville, FL: University of Florida.
- Laux L, Glanzmann P, Schaffner P, Spielberger CD (1981) Das State-Trait-Angstinventar. Theoretische Grundlagen und Handanweisung [in German]. Weinheim: Beltz Test.
- Levens SM, Phelps EA (2010) Insula and orbital frontal cortex activity underlying emotion interference resolution in working memory. *J Cogn Neurosci* 22:2790–2803. [CrossRef Medline](#)
- Levens SM, Devinsky O, Phelps EA (2011) Role of the left amygdala and right orbital frontal cortex in emotional interference resolution facilitation in working memory. *Neuropsychologia* 49:3201–3212. [CrossRef Medline](#)
- Macefield, V.G., James, C., and Henderson, L (2013) Identification of sites of sympathetic outflow at rest and during emotional arousal: Concurrent recordings of sympathetic nerve activity and fMRI of the brain. *Int J Psychophysiology*.
- Matthews KA, Katholi CR, McCreath H, Whooley MA, Williams DR, Zhu S, Markovitz JH (2004) Blood pressure reactivity to psychological stress predicts hypertension in the CARDIA study. *Circulation* 110:74–78. [CrossRef Medline](#)
- Minati L, Jones CL, Gray MA, Medford N, Harrison NA, Critchley HD (2009) Emotional modulation of visual cortex activity: a functional near-infrared spectroscopy study. *Neuroreport* 20:1344–1350. [CrossRef Medline](#)
- Neumann J, Lohmann G, Zysset S, von Cramon DY (2003) Within-subject variability of BOLD response dynamics. *Neuroimage* 19:784–796. [CrossRef Medline](#)
- Ochsner KN, Silvers JA, Buhle JT (2012) Functional imaging studies of emotion regulation: a synthetic review and evolving model of the cognitive control of emotion. *Ann N Y Acad Sci*, 1251:E1–E24. [CrossRef Medline](#)
- Okon-Singer H, Tzelgov J, Henik A (2007) Distinguishing between automaticity and attention in the processing of emotionally significant stimuli. *Emotion* 7:147–157. [CrossRef Medline](#)
- Okon-Singer H, Lichtenstein-Vidne L, Cohen N (2013) Dynamic modulation of emotional processing. *Biol Psychol* 92:480–491. [Medline](#)
- Oldfield RC (1971) The assessment and analysis of handedness: the Edinburgh inventory. *Neuropsychologia* 9:97–113. [CrossRef Medline](#)
- Pessoa L (2009) How do emotion and motivation direct executive control? *Trends Cogn Sci* 13:160–166. [CrossRef Medline](#)
- Pessoa L, McKenna M, Gutierrez E, Ungerleider LG (2002) Neural processing of emotional faces requires attention. *Proc Natl Acad Sci U S A* 99:11458–11463. [CrossRef Medline](#)
- Pichon S, de Gelder B, Grèzes J (2012) Threat prompts defensive brain responses independently of attentional control. *Cereb Cortex* 22:274–285. [CrossRef Medline](#)
- Pourtois G, Spinelli L, Seeck M, Vuilleumier P (2010) Temporal precedence of emotion over attention modulations in the lateral amygdala: Intracranial ERP evidence from a patient with temporal lobe epilepsy. *Cogn Affect Behav Neurosci* 10:83–93. [CrossRef Medline](#)
- Pourtois G, Schettino A, Vuilleumier P (2013) Brain mechanisms for emotional influences on perception and attention: what is magic and what is not. *Biol Psychol* 92:492–512. [CrossRef Medline](#)
- Sabatinielli D, Fortune EE, Li Q, Siddiqui A, Krafft C, Oliver WT, Beck S, Jeffries J (2011) Emotional perception: meta-analyses of face and natural scene processing. *Neuroimage* 54:2524–2533. [CrossRef Medline](#)
- Sacher, J., Neumann, J., Okon-Singer, H., Gotowiec, S., and Villringer, A (2012) Sexual dimorphism in the human brain: evidence from neuroimaging. *Magn Reson Imaging*.
- Schulz P, Schlotz W (1999) Das Trierer Inventar zur Erfassung von chronischem Streß (TICS): Skalenkonstruktion, teststatistische Überprüfung und Validierung der Skala Arbeitsüberlastung [in German]. *Diagnostica* 45:8–19. [CrossRef](#)
- Sherwood A, Dolan CA, Light KC (1990) Hemodynamics of blood pressure responses during active and passive coping. *Psychophysiology* 27:656–668. [CrossRef Medline](#)
- Swain A, Suls J (1996) Reproducibility of blood pressure and heart rate reactivity: a meta-analysis. *Psychophysiology* 33:162–174. [CrossRef Medline](#)
- Van Dillen LF, Derks B (2012) Working memory load reduces facilitated processing of threatening faces: an ERP study. *Emotion* 12:1340–1349. [CrossRef Medline](#)
- Wangelin BC, Löw A, McTeague LM, Bradley MM, Lang PJ (2011) Aversive picture processing: effects of a concurrent task on sustained defensive system engagement. *Psychophysiology* 48:112–116. [CrossRef Medline](#)

Erklärung über die eigenständige Abfassung der Arbeit

Hiermit erkläre ich, dass ich die vorliegende Arbeit selbstständig und ohne unzulässige Hilfe oder Benutzung anderer als der angegebenen Hilfsmittel angefertigt habe. Ich versichere, dass Dritte von mir weder unmittelbar noch mittelbar eine Vergütung oder geldwerte Leistungen für Arbeiten erhalten haben, die im Zusammenhang mit dem Inhalt der vorgelegten Dissertation stehen, und dass die vorgelegte Arbeit weder im Inland noch im Ausland in gleicher oder ähnlicher Form einer anderen Prüfungsbehörde zum Zweck einer Promotion oder eines anderen Prüfungsverfahrens vorgelegt wurde. Alles aus anderen Quellen und von anderen Personen übernommene Material, das in der Arbeit verwendet wurde oder auf das direkt Bezug genommen wird, wurde als solches kenntlich gemacht. Insbesondere wurden alle Personen genannt, die direkt an der Entstehung der vorliegenden Arbeit beteiligt waren. Die aktuellen gesetzlichen Vorgaben in Bezug auf die Zulassung der klinischen Studien, die Bestimmungen des Tierschutzgesetzes, die Bestimmungen des Gentechnikgesetzes und die allgemeinen Datenschutzbestimmungen wurden eingehalten. Ich versichere, dass ich die Regelungen der Satzung der Universität Leipzig zur Sicherung guter wissenschaftlicher Praxis kenne und eingehalten habe.

.....18.12. 2019.....

Datum

...Lina Schaare.....

Unterschrift

Lebenslauf

– nicht elektronisch veröffentlicht –

– nicht elektronisch veröffentlicht –

Publikationen

Journal articles

- 2019 Reinelt, J.; Uhlig, M.; Mueller, K.; Lauckner, M.; Kumral, D.; **Schaare, H. L.**; Baczkowski, B.; Babayan, A.; Erbey, M.; Röbbing, J. et al.: Acute psychosocial stress alters thalamic network centrality. *NeuroImage* 199, pp. 680 - 690 (2019)
- Schaare, H. L.**; Kharabian, S.; Beyer, F.; Kumral, D.; Uhlig, M.; Reinelt, J.; Reiter, A.; Lampe, L.; Babayan, A.; Erbey, M. et al.: Association of peripheral blood pressure with gray matter volume in 19- to 40-year-old adults. *Neurology* 92 (8), pp. e758 - e773 (2019)
- Babayan, A.; Erbey, M.; Kumral, D.; Reinelt, J.; Reiter, A.; Röbbing, J.; **Schaare, H. L.**; Uhlig, M.; Anwender, A.; Bazin, P.-L. et al.: A mind-brain-body dataset of MRI, EEG, cognition, emotion, and peripheral physiology in young and old adults. *Scientific Data* 6 (2019)
- Mendes, N.; Oligschläger, S.; Lauckner, M.; Golchert, J.; Huntenburg, J. M.; Falkiewicz, M.; Ellamil, M.; Krause, S.; Baczkowski, B.; Cozatl, R. et al.: A functional connectome phenotyping dataset including cognitive state and personality measures. *Scientific Data* 6 (2019)
- Kumral, D.; **Schaare, H. L.**; Beyer, F.; Reinelt, J.; Uhlig, M.; Liem, F.; Lampe, L.; Babayan, A.; Reiter, A.; Erbey, M. et al.: The age-dependent relationship between resting heart rate variability and functional brain connectivity. *NeuroImage* 185, pp. 521 - 533 (2019)
- 2014 Okon-Singer, H.; Mehnert, J.; Hoyer, J.; Hellrung, L.; **Schaare, H. L.**; Dukart, J.; Villringer, A.: Neural control of vascular reactions: Impact of emotion and attention. *The Journal of Neuroscience* 34 (12), pp. 4251 - 4259 (2014)

Conference presentations

- 2018 Beyer, F.; Kharabian, S.; **Schaare, H. L.**; Villringer, A.; Witte, A. V.: Investigating a structural network linked to development and aging with quantitative T1 imaging. Poster presented at the 31st meeting of the European College of Neuropsychopharmacology (ECNP), Barcelona, Spain (2018)
- 2017 Beyer, F.; **Schaare, H. L.**; Kharabian, S.; Kratzsch, J.; Thiery, J.; Loeffler, M.; Schroeter, M. L.; Villringer, A.; Witte, A. V.: Metabolic obesity profiles and gray matter tissue loss in older individuals. Poster presented at the 23rd Annual Meeting of the Organization for Human Brain Mapping (OHBM), Vancouver, BC, Canada (2017)
- Schaare, H. L.**; Kharabian, S.; Beyer, F.; Kumral, D.; Uhlig, M.; Reinelt, J.; Reiter, A.; Babayan, A.; Erbey, M.; Röbbing, J. et al.: Modulation of brain structure by resting blood pressure variations in young adults. Poster presented at the 23rd Annual Meeting of the Organization for Human Brain Mapping, Vancouver, BC, Canada (2017)
- 2016 Dähne, S.; Huntenburg, J. M.; Babayan, A.; Erbey, M.; Kumral, D.; Reinelt, J.; Reiter, A.; Röbbing, J.; **Schaare, H. L.**; Margulies, D. S. et al.: Detecting resting-state networks using scalable multi-subject spatial canonical correlation analysis. Poster presented at the 22nd Annual Meeting of the Organization for Human Brain Mapping (OHBM), Geneva, Switzerland (2016)
- 2015 **Schaare, H. L.**; Mueller, K.; Babayan, A.; Erbey, M.; Gaebler, M.; Kumral, D.; Reinelt, J.; Reiter, A.; Röbbing, J.; Okon-Singer, H. et al.: Higher blood pressure is associated with lower regional grey matter density in healthy, young adults. Poster presented at the International Society for Autonomic Neuroscience Meeting 2015, Stresa, Italy (2015)
- 2014 **Schaare, H. L.**; Rohr, C.; Mueller, K.; Margulies, D. S.; Pampel, A.; Erbey, M.; Gaebler, M.; Reinelt, J.; Reiter, A.; Röbbing, J. et al.: Less grey matter density in young adults' frontal lobes is associated with higher blood pressure. Poster presented at the 4th IMPRS NeuroCom Summer School, London, United Kingdom (2014)

- Schaare, H. L.**; Rohr, C.; Schäfer, A.; Huntenburg, J. M.; Margulies, D. S.; Pampel, A.; Erbey, M.; Reinelt, J.; Reiter, A.; Röbbing, J. et al.: Resting-state functional connectivity associated with blood pressure. Poster presented at the 20th Annual Meeting of the Organization for Human Brain Mapping (OHBM), Hamburg, Germany (2014)
- Erbey, M.; Nierhaus, T.; **Schaare, H. L.**; Röbbing, J.; Reiter, A.; Villringer, A.: Neurocognitive correlates of the positivity effect. Poster presented at the Life Spring Academy 2014, University of Virginia, Charlottesville, VA, USA (2014)
- 2013 **Schaare, H. L.**; Hoyer, J.; Mehnert, J.; Lepsien, J.; Villringer, A.; Okon-Singer, H.: Neural correlates of vascular reactivity to emotion and its interaction with attention. Poster presented at the 43rd Annual Meeting of the Society for Neuroscience (SfN 2013), San Diego, CA, USA (2013)
- Schaare, H. L.**; Villringer, A.; Okon-Singer, H.: Effects of attention on vascular reactivity and neural activation to emotional information. Poster presented at the 53rd Annual Meeting of the Society for Psychophysiological Research, Florence, Italy (2013)
- Schaare, H. L.**; Hoyer, J.; Mehnert, J.; Lepsien, J.; Villringer, A.; Okon-Singer, H.: Neural correlates of vascular reactivity. Poster presented at the 3rd IMPRS NeuroCom Summer School, Leipzig, Germany (2013)
- Schaare, H. L.**; Villringer, A.; Okon-Singer, H.: Can attention modulate blood pressure? Continuous non-invasive blood pressure recordings during fMRI of an emotional spatial attention task. Poster presented at the Mind-Brain Symposium, Berlin, Germany (2013)

Danksagung

Diese Dissertation ist nur dank der Unterstützung vieler wunderbarer Menschen zustande gekommen, denen ich an dieser Stelle gerne danken möchte.

Arno Villringer gebührt der größte Dank für den unendlichen Zuspruch und das Vertrauen, das er mir über die gesamte Zeit entgegengebracht hat. Beides hat mich durch bessere und schlechtere Tage der letzten Jahre bis hierher manövriert. Ich schätze mich sehr glücklich, über unsere bisherige Zusammenarbeit, die vor allem durch Arnos offene und wohlgesinnte Art geprägt war.

Danke, Hadas Okon-Singer, Jana Hoyer, Christiane Rohr und Jan Mehnert, für die Unterstützung als die Doktorarbeit noch in ihren Kinderschuhen steckte und für die Ur-Motivation, die mich immer noch antreibt, das Gehirn und den Blutdruck besser verstehen zu wollen. Im weiteren Verlauf hat es mir besonders viel Spaß gemacht mit Anahit Babayan, Michael Gaebler, Deniz Kumral, Janis Reinelt, Marie Uhlig, Andrea Reiter, Maria Blöchl, Shahrzad Kharabian, Mark Lauckner und Navot Naor zusammenzuarbeiten.

Für mich war und ist das MPI CBS und darin vor allem die Neurologie, ein besonderer Ort zum Forschen und Arbeiten, dessen Atmosphäre durch die täglichen Mühen bestimmter Mitarbeiter*innen besonders geprägt wird. Conny Ketscher, Birgit Mittag und Ramona Menger sind die leuchtenden Fixsterne der Abteilung und hatten immer Zeit, einen guten Rat und ein Lächeln für mich auf Lager. Herr Deubel und Toni haben mir mit ihren Kochkünsten unzählige Stunden Mittagessensplanung abgenommen, wofür ich ihnen überaus dankbar bin. Danke auch an Maria Paerisch, André Pampel, Jöran Lepsien, Karsten Müller, Heike und Kerstin von der Grafik, das Bibliotheksteam, die EDV, und alle anderen Institutsmitarbeiter, die mir in den letzten Jahren immer wieder weitergeholfen haben. Ich möchte mich auch vielmals bei der IMPRS NeuroCom für die Aufnahme in das Graduiertenprogramm bedanken und für alles, was ich dadurch lernen und erleben durfte.

Ich habe während der Doktorarbeitszeit sehr viele kluge, lustige und liebe Kolleg*innen kennengelernt, die das Institut zu einem zweiten Zuhause gemacht haben und von denen mittlerweile viele gute Freund*innen geworden sind. Mit Maike, Elli und Maria sind die Stunden am Institut (und darüber hinaus) wie im Flug vergangen und Arbeit hat sich nie wie welche angefühlt. Ich vermisse es, euch jeden Tag zu sehen. Domi, Norman und Christopher waren meine Vorbilder, wenn es darum ging, unermüdlich und gefasst zu bleiben, wenn nichts nach Plan lief. Außerdem sind die drei die nettesten Menschen. Marie-Theres ist für jemanden wie mich, die quasi wurzellos ist, wegen der vielen geteilten

Erinnerungen, die wir über all die Jahre gemeinsam sammeln konnten, unverzichtbar. Und natürlich möchte ich auch meine Institutsfamilie, das Awefice, nennen. Frauke, Filip, Janis, Marie und Samyogita, dass wir zusammengewürfelt wurden, ist so ein glücklicher Zufall gewesen. Ich möchte mir nicht vorstellen, wie die Zeit ohne das Awefice und unsere Traditionen verlaufen wäre und hoffe, dass wir auch in Zukunft Mittel und Wege finden gemeinsam Weihnachtslieder zu singen.

Zu guter Letzt möchte ich mich bei Marie-Louisa, Henning, Armin, Tante Rosi, Matthias und dem Rest meiner Familie für ihre Geduld und Unterstützung bedanken.

Ihr alle wart – manche von Anfang bis Ende, andere etappenweise, aber alle wichtig – und habt einen entscheidenden Anteil an dieser Arbeit geleistet. Dafür möchte ich euch von Herzen danken!